

PROCEEDINGS OF THE FIFTH  
INTERNATIONAL SYMPOSIUM ON

CLEANING TECHNOLOGY IN  
SEMICONDUCTOR DEVICE  
MANUFACTURING

Editors

**Jerzy Ruzyllo**  
The Pennsylvania State University  
University Park, Pennsylvania, USA

**Richard E. Novak**  
SubMicron Systems, Inc.  
Allentown, Pennsylvania, USA

Co-editors

**Charlotte M. Appel**  
Texas Instruments  
Dallas, Texas, USA

**Takeshi Hattori**  
Sony Corporation  
Atsugi, Japan

**Marc Heyns**  
IMEC  
Leuven, Belgium

ELECTRONICS DIVISION

Proceedings Volume 97-35



THE ELECTROCHEMICAL SOCIETY, INC.,  
10 South Main St., Pennington, NJ 08534-2896

**Copyright 1998 by The Electrochemical Society, Inc.  
All rights reserved.**

**This book has been registered with Copyright Clearance Center, Inc.  
For further information, please contact the Copyright Clearance Center,  
Salem, Massachusetts.**

**Published by:**

**The Electrochemical Society, Inc.  
10 South Main Street  
Pennington, New Jersey 08534-2896, USA**

**Telephone (609) 737-1902  
Fax (609) 737-2743  
e-mail: [ecs@electrochem.org](mailto:ecs@electrochem.org)  
Web site: <http://www.electrochem.org>**

**ISBN 1-56677-188-9**

**Printed in the United States of America**

## PREFACE

The Fifth International Symposium of Cleaning Technology in Semiconductor Device Manufacturing was held during the Fall Meeting of the Electrochemical Society in Paris in September 1997. This series of symposia was initiated in 1989 during the Society Fall Meeting in Hollywood, Florida. Since then, recognition of the "ECS Cleaning Symposia", reflected by both number of participants as well as quality of papers presented, continues to grow systematically. This trend clearly corresponds to the still increasing need for the improved surface preparation methods of the semiconductor industry.

We are very pleased that all papers presented during the symposium in Paris are included in this volume. The papers are divided into several sections with the most voluminous one devoted to wet cleaning. The number of papers in this section clearly indicates that wet wafer cleaning technology will remain a workhorse of surface preparation procedures in IC manufacturing for years to come. It also testifies to the fact that much research and development is still needed not only to improve performance of wet cleans, but also to optimize these operations with the reduction of use of chemicals and deionized water as the prime objective. Besides general aspects of wet cleaning technology papers in this part of the proceedings are concerned with issues such as control of metallic contaminants in liquid chemistries, SC-1 chemistry, HF-last processes, and increasingly common use of ozonated water in wafer cleaning operations.

The papers presented in the section on gas-phase cleaning technology reflect the current status quo which suggests that breakthroughs are needed in order to assure for this process mode a place in the mainstream of the future IC manufacturing. As usual, a number of papers presented during the symposium are concerned with a key issue of characterization and monitoring of wafer cleaning operations. A separate section devoted to the problems of resist stripping responds to the growing tendency to consider resist stripping as an integral part of the wafer cleaning sequence. Compared to previous symposia in this series a relatively smaller number of papers are included in the section covering specifically particle removal issues. The main reason for this is that various issues related to this key aspect of wafer cleaning technology are considered in the numerous other papers included in this volume. Finally, some important topics in the area of surface cleaning in back-end-of-line processing are represented in the last section of this volume.

We would like to take this opportunity to thank all symposium authors and participants who turned this symposium into a very informative and productive meeting. In particular, we would like to thank our colleagues who assisted us in editing this volume and who chaired the symposium sessions. Moreover, our thanks are due to the invited speakers for their excellent contributions and to all the participants for their encouragement and support which makes us look toward the next symposium in this series in the Fall of 1999 with great enthusiasm and great expectations.

Jerzy Ruzyllo  
Richard E. Novak



## TABLE OF CONTENTS

PREFACE	iii
<b>WET CLEANING - General</b>	<b>1</b>
KEY ISSUES IN WET CHEMICAL CLEANING OF SILICON SURFACES - T. Hattori (INVITED)	3
PERFORMANCE OF "DDC": DILUTED DYNAMIC CLEAN BEFORE 4.5 nm GATE OXIDE - F. Tardif, T. Lardin, B. Sandrier, P. Boelen, R. Matthews, I. Kashkoush, and R. Novak	15
MINIMIZING SULFUR CONTAMINATION AND RINSE WATER VOLUME REQUIRED FOLLOWING A SULPHURIC ACID/HYDROGEN PEROXIDE CLEAN BY PERFORMING A CHEMICALLY BASIC CLEAN - P. Clews, G.C. Nelson, C.A. Matlock, P.J. Resnick , and C.L.J. Adkin	23
STATE-OF-THE ART DRYING TECHNIQUES FOR SEMICONDUCTOR WET BENCHES - G.W. Gale, W.A Syverson, and J.A. Brigante	31
THE EFFECTS OF OXYGEN PASSIVATION OF SILICON BY WET CLEANING PROCESSES ON CONTAMINATION AND DEFECTS - S.L. Nelson	38
WET CHEMICALLY PASSIVATED SILICON SURFACES: ELECTRONIC PROPERTIES CORRELATED TO THE SURFACE MORPHOLOGY - H. Angermann, W. Henrion, A. Roseler, J.T. Zettler, M. Rebien, and H.Flietner	46
WAFER CLEANING BY WATER AND GAS MIXTURE WITH HIGH VELOCITY - I. Kanno, N. Yokoi, and K. Satoh	54
SURFACE PREPARATION USING ANHYDROUS FLUORIDE AND AQUEOUS H <sub>2</sub> O PRIOR TO LOW TEMPERATURE EPITAXIAL SILICON DEPOSITION - D.C. Frystak, R. Wise, P. Grothe, J. Barnett, B. Fowler, and R. Carpio	62
THE EVALUATION OF ULTRASONIC DAMAGE CAUSED BY BATCH TYPE WAFER CLEANING SYSTEM - A. Onishi, A. Chiyokawa, and A. Tomozawa	71

THE EVALUATION OF ULTRASONIC DAMAGE CAUSED BY SINGLE WAFER CLEANING SYSTEM - A.Tomozawa, H. Kinoshita, Y. Sakata, A. Ohnishi, Y. Harada, and N. Hiraoka	79
<b>WET CLEANING - Metallic Contaminants</b>	87
OPTIMIZED RINSING FOR LOW METALLIC CONTAMINATION - L.M. Loewenstein and P.W. Mertens	89
INTERACTION AMONG CONTAMINANT METALS IN WET CLEANING PROCESSES - Y. Hayami, Y. Okui, H. Ogawa, and S. Fujimura	97
SURFACE COMPLEXATION OF METALS: A PREDICTIVE MODEL BASED ON METAL COORDINATION CHEMISTRY - T.Q. Hurd, A.L.P. Rotondaro, J. Sees, A. Misra, and C. Appel	105
Fe REMOVAL IN SC2 SOLUTIONS - S. Dhanda, R.P. Chiarello, C.R. Helms, and P. Gupta	113
PROTECTION OF HF BATHS AGAINST NOBEL METAL CONTAMINATION - S.Kunz, S.Marthon, and F. Tardif	120
ELECTROCHEMICAL AND RADIOCHEMICAL STUDY OF COPPER CONTAMINATION MECHANISM FROM HF SOLUTIONS ONTO SILICON SUBSTRATES - V. Bertagna, F. Rouelle, and M. Chemla	128
REMOVAL OF Cu FROM Si WAFER SURFACES USING DILUTE HF-HCl SOLUTIONS - S. Dhanda, R.P. Chiarello, C.R. Helms, and P. Gupta	136
PASSIVATION OF Cu PARTICLES ON Si SUBSTRATE BY FOM(HF+O <sub>3</sub> - UPW) SOLUTION - H. Morita, J.-D. Joo, R. Messoussi, K. Kawada, J.-S. Kim, and T. Ohmi	143
THE EFFECT OF SURFACE DAMAGE DUE TO Si INPLANTATION ON ADSORPTION AND DESORPTION OF Cu ON Si SURFACE - J.-S. Kim, H. Morita, J.-D. Joo, and T. Ohmi	151

<b>WET CLEANING - SC-1 Chemistry</b>	159
OPTIMIZATION OF DILUTE SC1 - P. Boelen, T. Lardin, B. Sandrier, R. Matthews, I. Kashkoush, R. Novak, and F. Tardif	161
THE ROLE OF MEGASONIC ENERGY IN PARTICULATE REMOVAL FROM SILICON SUBSTRATES IN DILUTE SC1 CHEMISTRY- I. Kashkoush, E. Brause, R. Grant, and R. Novak	168
QUANTITATIVE MODELING OF H <sub>2</sub> O <sub>2</sub> DECOMPOSITION IN SC1 - P. Mertens, M. Baeyens, G. Moyaerts, H. Okorn-Schmidt, R. Vos, R. De Waele, Z. Hatcher, W. Hub, S. De Gendt, M. Knotter M. Meuris, and M. Heyns	176
THE ROLE OF THE PEROXIDE ANION AS AN OXIDIZER IN SC-1 SOLUTIONS - S. Verhaverbeke and J.Parker	184
<b>WET CLEANING - HF Last Process</b>	193
CHARACTERIZATION OF HF-LAST CLEANED Si FOR GATE OXIDES - J.S. Jeon, J.S. Glick, A. Jafarpour, and B. Ogle (INVITED)	195
OPTIMIZATION OF ETCHING UNIFORMITY AND REPEATABILITY IN DILUTED HF - E. Bellandi, M.Alessandri, A. Tonti, F. Pipia, K. Wolke, M. Schenkl, M. Geomini, and L.F.T. Kwakman	207
H-TERMINATION ON Ge (100) AND Si (100) BY DILUTED HF DIPPING AND BY ANNEALING IN H <sub>2</sub> - M. Sakuraba, T. Matsuura, and J. Murota	213
IN-LINE MONITORING OF HF-LAST CLEANING OF IMPLANTED AND NON-IMPLANTED SILICON SURFACES BY NON-CONTACT SURFACE CHARGE MEASUREMENTS - E. Kondoh, M.-A. Trauwaert, M. Heyns, and K. Maex	221
<b>WET CLEANING - Ozonated Water</b>	229
THE BEHAVIOR OF OZONE IN WET CLEANING CHEMICALS - J.-G. Park and J.-H. Han	231

EFFICIENCY OF OZONE DISSOLUTION INTO AMBIENT TEMPERATURE RINSE BATHS - K. Wolke, M. Schenkl, M. Alessandri, and E. Bellandi	239
EFFICIENCY OF OZONATED DI WATER IN REMOVING ORGANIC CONTAMINATION - C. Kenens, S. De Gendt, D.M. Knotter, L.M. Loewenstein, M. Meuris, W. Vandervorst, and M.M. Heyns	247
CONTAMINATION REMOVAL BY SINGLE-WAFER SPIN CLEANING WITH REPETITIVE USE OF OZONATED WATER IN DILUTE HF - T. Osaka, A. Okamoto, H. Kuniyasu, and T. Hattori	256
DIRECT REPLACEMENT CLEANING TECHNOLOGY BASED ON OZONATED WATER USING A SINGLE PROCESSING TANK - Y. Fukazawa, K. Miyazaki, and Y. Ogawa	264
OPTIMIZATION OF OZONIZED DI RINSE FOR HF LAST PRE-GATE CLEAN - L. Li, W. Lee, T. Gilton, and F. Gonazalez	272
COMPARISON OF CLEANING EFFICIENCIES OF NOBEL METALS ON Si SURFACES BETWEEN O <sub>3</sub> -UPW AND SPM - J.-D. Joo, J.-S. Kim, H. Morita, and T. Ohmi	280
<b>GAS - PHASE CLEANING</b> 289	
Fe REMOVAL EFFECTS OF SILICON CHLORIDES (SiCl <sub>x</sub> ) DURING UV/Cl <sub>2</sub> DRY CLEANING - R. Sugino, Y. Okui, M. Shigeno, S. Ohkubo, K. Takasaki, and T. Ito	291
THE MECHANISM OF COPPER REMOVAL FROM A BARE SILICON SURFACES WITH ULTRAVIOLET EXCITED CHLORINE - A. Lawing, H. Sawin, and T. Fayfield	299
HYDROGEN PLASMA CLEANING OF OXIDE PATTERNED Si WAFERS FOR LOW TEMEPARATURE Si EPITAXY - H.-K. Yuh, J.-W. Park, K.-H. Hwang, E. Yoon, and K.-W. Whang	307
EFFECTS CONTROLLING INITIATION AND TERMINATION OF GAS-PHASE CLEANING REACTIONS - J. Staffa, S. Fakhouri, M. Brubaker, P. Roman, and J. Ruzylo	315
DRY CLEANING FOR DEEO SUBMICRON VIAS - A.L.P. Rotondaro, D.B. Aldrich, P.B. Smith, and C. Appel	322

CLEANING OF SiO <sub>2</sub> BULK LAYERS WITH SUCCESSIVE PROCESSING OF POLY-Si CVD AND UV/Cl <sub>2</sub> - R. Sugino, Y. Tada, T. Ito, Y. Okui, and J.Sakuma	328
VAPOR PHASE CLEANING OF Cu, Fe, AND Na FROM WAFER SURFACES USING 1,1,1,5,5,5-HEXAFLURO-2,4-PENTANEDIONE - S.E. Beck, E.A. Robertson, M.A. George, D.A. Moniot, J.L. Waskiewicz, D.A. Bohling, K.M. Young, and A.A. Badowski	336
DRY PROCESS FOR THE DEFINITION OF SUB 0.1μm W/TiN GATES - A.L.P. Rotondaro, H.Yang, J.C. Hu, R. Kraft, G. Brown, and C. Appel	344
THERMOPHORESIS ASSISTED CRYOGENIC AEROSOL CLEANING OF WAFERS - N. Narayanswami	350
ON THE GENERATION OF CRYOGENIC AEROSOLS FOR WAFER PROCESSING - N. Narayanswami	357
COMPARISON OF PROCESS EMISSIONS DURING C <sub>3</sub> F <sub>8</sub> AND C <sub>2</sub> F <sub>6</sub> PECVD CLEANING USING EXTRACTIVE FTIR - L. Zazzera, B. Reagen, and A. Cheng	365
<b>CHARACTERIZATION AND MONITORING</b>	<b>375</b>
ELECTROCHEMICAL DETECTION OF IRON CONTAMINATION DURING SILICON WAFER CLEANING - E.A. Kneer, S. Raghavan, and J.S. Jeon	377
CHARACTERIZATION OF EVAPORATION IN A PURGED SYSTEM - M. Olim	385
APPLICATIONS OF NON-INVASIVE AC-SURFACE PHOTOVOLTAGE MONITORING IN INTEGRATED CIRCUIT CLEANING - K. Torek, W. Lee, D. Palsulich, L. Weston, and F. Gonzalez	392
MONITORING OF NOBLE METALS IN HF BASED CHEMISTRIES USING μ-PCD, SPV, SCI, and SCP - A. Danel, U. Straube, G. Kamarinos, E. Kamieniecki, and F. Tardif	400
DETERMINATION OF NATIVE OXIDE REMOVAL IN CLUSTER COMPATIBLE DRY CLEANING SYSTEMS USING A SURFACE PHOTOVOLTAGE TECHNIQUE - M. Brubaker, J. Staffa, P. Roman, S. Fakhouri, and J. Ruzylo	408

IN-LINE X-RAY PHOTOELECTRON SPECTROSCOPY FOR ANHYDROUS HYDROGEN FLUORIDE CLEANING OPTIMIZATION - B. Froeschle, F. Glowacki, A. Bauer, I. Kasko, R. Oechsner, and C. Schneider	415
CHARACTERIZATION OF SILICON OXIDE ETCHING IN HF VAPOR PROCESSES - Y.-P. Han, S. Lawing , and H. Sawin	423
SURFACE ANALYSIS OF CLUSTERED DRY CLEANING OF RESIDUE FROM AN ICP OXIDE ETCH - A. Lawing, Y.-P. Han, and H. Sawin	431
IN-SITU SURFACE ANALYSES OF Si(111) ELECTRODES IN FLUORIDE CONTAINING SOLUTIONS DURING CURRENT OSCILLATIONS - S.Rauscher, O. Nast, H. Jungblut, and H.J. Lewerenz	439
NATURAL HYDROCARBON DEPOSITION ON SILICON WAFERS AND REMOVAL AS MEASURED BY IMS - E. Ollier, S. Marthon, G. Quagliotti, and F. Tardif	447
EVALUATION OF Si SURFACE CONDITIONS BY THE USE OF A SURFACE PHOTOVOLTAGE TECHNIQUE - M.-A. Trauwaert, K. Kenis, M. Caymax, P.W. Mertens, M.M. Heyns, J. Vanhellemont, D. Graf, and P. Wagner	455
CONTROL OF QUALITY OF SURFACE BY THE SELECTIVE WETTING METHOD - V.V. Bakovets	463
<b>RESIST STRIPPING</b>	469
PHOTORESIST STRIPPING USING OZONE/DEIONIZED WATER CHEMISTRY - I.I. Kashoush, R.Matthews, and R. Novak	471
MASS TRANSFER IN DI:O <sub>2</sub> RESIST STRIPPING - K. Christenson, S. Nelson, M.Olim, and G. Nelson	480
ROOM TEMPERATURE PHOTORESIST REMOVAL PROCESS BY USING KF/H <sub>2</sub> O <sub>2</sub> /H <sub>2</sub> O - S.Omae, T. Jizaimaru, S. Ojima, and T. Ohmi	488
ALTERNATIVE METHODS FOR RESIST STRIPPING -J. Wei and S. Verhaverbeke	496
EVALUATION OF POST-ASHED PHOTORESIST CLEANING USING OXIDIZING CHEMISTRIES - P. Resnick, and C. Matlock	505

ORGANIC CONTAMINATION ON SILICON WAFER SURFACES IN PROCESSING ENVIRONMENT - M.Tanishima and N. Abe	513
<b>PARTICLES</b>	521
PARTICLE REMOVAL EFFICIENCY OF DILUTED HF SOLUTIONS - M. Alessandri, E. Bellandi, F. Pipia, B. Crivelli, K. Wolke, and M. Schenkl	523
PARTICLE AND METALLIC IMPURITIES REMOVAL BY USING NEW SPIN CLEANER BASED ON UCT CLEANING CONCEPT - K. Kawada, M. Nakamori, and H. Morita, S. Okano, T. Nitta, and T. Ohmi	528
ANALYSIS FOR ADSORPTION BEHAVIOR OF PSL PARTICLES BY USING ATOMIC FORCE MICROSCOPY - A. Kawai, H. Horiguchi,Y. Tatehaba, K. Shimada, and E. Andoh	536
AGGRESSIVE SC-1 PARTICLE REMOVAL TECHNIQUES IN A SPRAY PROCESSOR AND THEIR EFFECTS ON OTHER METRICS - S.M. Smith and K. Christenson	544
$\text{Si}_3\text{N}_4$ PARTICLE REMOVAL EFFICIENCY STUDIES -J.Q. Liu, C. Lee, J. M. Rosamilia, T. Boone, and G.S. Higashi	552
ADHESION ENERGY OF POLYSTYRENE AND SUBSTRATE IN FUNCTION WATER - Y. Tatehaba, K. Shimada, E. Ando, and A. Kawai	560
<b>BACK-END-OF-LINE CLEANING</b>	567
CORROSION OF ALUMINUM ALLOYS DURING DRYING OF METALLIZED WAFERS - R. Vos, M. Meuris, P. Mertens, M. Heyns, and Z. Hatcher (INVITED)	569
NOVEL WET ETCHEs FOR SALICIDE STRIP PROCESSING - S. O'Brien	579

<b>POST METAL ETCH POLYMER REMOVAL PROCESS: THE ELIMINATION OF AN INTERMEDIATE RINSE STEP - S.W. Graham</b>	<b>587</b>
<b>MOBILE ION CONTAMINATION AND DEFECT REDUCTION ON A POST-METAL ETCH CLEAN PROCESS - K.E. Mautz</b>	<b>594</b>
<b>APPLICABILITY OF HF SOLUTIONS FOR CONTACT HOLE CLEANING ON TOP OF TiSi<sub>2</sub> - M. Baklanov, E.Kondoh, S. Vanhaelemeersch, and K. Maex</b>	<b>602</b>
<b>THE FORMATION AND REMOVAL OF RESIDUE FORMED DURING TiN FLUOROCARBON PLASMA ETCHING - Y.B. Kim, T. Conard, D. Vanhaeren, M.Baklanov, S. Vanhaelemeersch, W. Vandervorst, and K. Maex</b>	<b>610</b>
<b>A UNIQUE CHEMISTRY TO CLEAN SIDEWALL POLYMERS FORMED BY PLASMA ETCHING OF VIA AND METAL LAYERS OF INTEGRATED CIRCUIT FABRICATION - K. Honda, D. Perry, J. O'Neil, R. Molin, G.Hansen, V. Leon, D. Petersen, and L. Roberson</b>	<b>617</b>
<b>POST W CMP CLEANING - I. Constant, S. Marthon, T. Lardin, C. David, M.N. Jacquemond, and F.Tardif</b>	<b>626</b>
<b>EVALUATION OF NON-CONTACT POST-CMP CLEANING PROCESS UTILIZING SPLIT-LOT POLISHING AND CLEANING COMPARISONS - B. Fraser, M.B. Olesen, T. Phan, and B.Morrison</b>	<b>634</b>
<b>AUTHOR INDEX</b>	<b>643</b>
<b>SUBJECT INDEX</b>	<b>647</b>

## FACTS ABOUT THE ELECTROCHEMICAL SOCIETY, INC.

The Electrochemical Society, Inc., is an international, nonprofit, scientific, educational organization founded for the advancement of the theory and practice of electrochemistry, electrothermics, electronics, and allied subjects. The Society was founded in Philadelphia in 1902 and incorporated in 1930. There are currently over 7000 scientists and engineers from more than 60 countries who hold individual membership; the Society is also supported by more than 100 corporations through Patron and Sustaining Memberships.

The Technical activities of the Society are carried on by Divisions and Groups. Local Sections of the Society have been organized in a number of cities and regions.

Major international meetings of the Society are held in the Spring and Fall of each year. At these meetings, the Divisions and Groups hold general sessions and sponsor symposia on specialized subjects.

The Society has an active publications program which includes the following:

**Journal of The Electrochemical Society** - The Journal is a monthly publication containing technical papers covering basic research and technology of interest in the areas of concern to the Society. Papers submitted for publication are subjected to careful evaluation and review by authorities in the field before acceptance, and high standards are maintained for the technical content of the Journal.

**Interface** - Interface is a quarterly publication containing news, reviews, advertisements, and articles on technical matters of interest to Society Members in a lively, casual format. Also featured in each issue are special pages dedicated to serving the interests of the Society and allowing better communication between Divisions, Groups, and Local Sections.

**Meeting Abstracts (formerly Extended Abstracts)** - Meeting Abstracts of the technical papers presented at the Spring and Fall Meetings of the Society are published in serialized softbound volumes.

**Proceedings Series** - Papers presented in symposia at Society and Topical Meetings are published from time to time as serialized Proceedings Volumes. These provide up-to-date views of specialized topics and frequently offer comprehensive treatment of rapidly developing areas.

**Monograph Volumes** - The Society has, for a number of years, sponsored the publication of hardbound Monograph Volumes, which provide authoritative accounts of specific topics in electrochemistry, solid state science, and related disciplines.

For more information on these and other Society activities, visit the ECS Home Page at the following address on the World Wide Web:

<http://www.electrochem.org>.



## **WET CLEANING - General**



# **Key Issues in Wet Chemical Cleaning of Silicon Surfaces**

**Takeshi Hattori**

SONY Corporation, Atsugi 243-8585, Japan

## **ABSTRACT**

The following three key issues in wet chemical cleaning of silicon surfaces for pre-oxidation/deposition are discussed with special emphasis on the future prospects of this technology. (1) Limitation of immersion-type wet cleaning due to contamination brought by to-be-cleaned wafers, (2) clean wafer drying after wet cleaning, and (3) prevention of organic adsorption on the silicon surfaces after wafer drying.

## **INTRODUCTION**

Scrupulous maintenance of clean wafer surfaces throughout the wafer processing cycle is essential to obtain high yields in the manufacture of semiconductor devices. As a result, wet chemical cleaning to remove contaminants from the wafer surfaces is the most repetitively applied processing step in any LSI fabrication sequence. Over the past 25 years, immersion-type wet cleaning with essentially unchanged chemistry has been used in the semiconductor industry worldwide. In this paper, some key issues in the wet chemical cleaning of silicon surfaces for pre-oxidation/deposition will be discussed with special emphasis on the future prospects of this technology.

## **WET CLEANING**

### **Influence of Initial Wafer Cleanliness on Metal Removal Efficiency in Immersion SC-1 Cleaning: Limitation of Immersion-Type Wet Cleaning**

Rigorous wet cleaning is known to be effective in reducing contaminants from wafer surfaces [1][2], but this is only true if the immersion-type wet bench being widely used in the semiconductor industry uses very pure wet chemicals and deionized water and if the wafer carriers [3][4] and cleaning baths [5] as well as the ambient air are clean. Even in such an ultra clean environment, metallic contaminants brought into the bath of an immersion-type wet bench by the to-be-cleaned wafers themselves will dissolve and accumulate in the chemical solution, though the particles brought into the bath are filtered out by a circulating particle-filtering system equipped in the wet bench. Such kinds of metallic impurities incorporated into the fresh solution by the to-be-cleaned wafers themselves may limit the effectiveness of the metal-removal efficiency even if ultraclean chemicals are used and, even if these chemicals are disposed of after each cleaning [6].

We have investigated here the influence of initial metal concentration on the wafer surfaces on metal-removal efficiency in immersion cleaning using the SC-1 solution widely used in the industry, which employs a NH<sub>4</sub>OH/H<sub>2</sub>O<sub>2</sub>/H<sub>2</sub>O mixture, and to clarify the limitations of immersion-type wet cleaning in terms of the metallic contamination removal efficiency. Although the SC-1 solution is generally recognized as the most effective chemical for particle removal, it can also remove metallic contaminants with varying degrees of efficiency, depending on the type of metallic element. The surface concentration of two typical heavy metals, Fe and Cu, on silicon surfaces before and after ultrapure SC-1 cleaning was compared for various levels of initial wafer surface Cu or Fe concentration and also for different numbers of wafers simultaneously immersed in the bath. The SC-1 solution was prepared by mixing deionized water with an H<sub>2</sub>O<sub>2</sub> solution (30%) and an NH<sub>4</sub>OH solution (30%). The blend ratio used was NH<sub>4</sub>OH : H<sub>2</sub>O<sub>2</sub> : H<sub>2</sub>O = 1:2:7. The Fe and Cu concentrations in the SC-1 solution were both less than 0.02 ppb, the detection limit of atomic absorption spectrometry. The solution temperature was kept at 60°C throughout the experiments. The treatment time was 10 min. The bath volume was  $1.3 \times 10^4 \text{ cm}^3$  including the volume circulated in the particle filtration system. The SC-1 treatment was followed by water rinsing and drying.

Figure 1 (a) shows the surface concentration of Fe on silicon wafers after SC-1 cleaning, with the initial surface concentration of  $1.4 \times 10^{13} \text{ atoms/cm}^2$  for various numbers of 125-mm wafers simultaneously immersed in the bath. As can be seen, even though the initial Fe concentration is the same for the wafers used for this experiment, the surface concentration after SC-1 cleaning varied with the number of contaminated wafers simultaneously immersed in the bath. As shown in Fig. 1(b), for the initial Fe concentration of  $1.0 \times 10^{12} \text{ atoms/cm}^2$  the concentration after cleaning has a lower value than that for  $1.4 \times 10^{13} \text{ atoms/cm}^2$  with the same number of wafers. In both Fig. 1(a) and (b), as the number of wafers immersed in the bath increases, the higher the surface concentration becomes after cleaning. The experimental results indicate that the concentration after cleaning depends not only on the initial wafer cleanliness but also on the number of wafers treated at the same time. This suggests that when intentionally contaminated wafers are immersed in an ultrapure SC-1 solution whose impurity concentration is negligible, the level of wafer-surface metal contamination after the cleaning treatment depends on the total amount of metallic impurities brought by the wafers themselves into the solution. For Cu contamination, as shown in Fig. 2, the initial surface contamination of as high as  $5 \times 10^{14} \text{ atoms/cm}^2$  can be reduced to a level below  $1 \times 10^{10} \text{ atoms/cm}^2$  by SC-1 cleaning. Thus, Cu can be reduced much more effectively than Fe. As with Fe, Cu concentration on the wafer after SC-1 cleaning increases as the number of wafers treated at the same time increases.

It is known that the final surface impurity concentration on the wafer is in equilibrium with the final impurity concentration of the SC-1 solution after cleaning [7]. So, the final impurity concentration of the solution can be estimated if the initial surface impurities can be assumed to be dissolved into the solution during cleaning [6]. The Fe and Cu concentrations calculated on the wafer surfaces after cleaning were essentially consistent with those measured and shown in Figs. 1 and 2.

In our experiment, the impurity concentration on the silicon surface was dominated not by the purity of the chemical but by the impurities brought by the wafers themselves into the chemical. Ryuta et al., on the other hand, have reported [7], [8] that the initial surface concentration does not influence the surface concentration after the cleaning treatment. But this is only true if a comparatively dirty chemical solution with 0.1 ppb of Fe is used, in which case the surface concentration is governed by only the chemical impurities and thus cannot be lowered to a level below  $10^{11}$  Fe atoms/cm<sup>2</sup>. In the past, purer chemicals have been sought to improve metal removal efficiency, but after reasonably pure chemicals have been obtained, the metal removal efficiency will be dominated by the contamination brought by the wafers themselves.

In immersion-type wet cleaning where the chemical solution is repetitively used before disposal, as the number of 25-wafer lots subjected to the cleaning treatment increases, the impurity concentration of the chemical solution increases due to the incorporation of metallic contaminants into the chemical from the wafers, thus the final surface impurity concentration becomes gradually greater as the number of lots subjected to immersion cleaning increases. The variation in the surface metal concentration calculated on our 125-mm diameter wafers due to immersion in SC-1 solution repetitively used is shown in Fig. 3. In the calculation, the amount of metallic impurities carried out of the chemical and adsorbed onto the wafer surfaces is taken into consideration. After the cleaning of 20 wafer-lots, the surface Cu concentration can still be reduced below  $1 \times 10^{10}$  atoms/cm<sup>2</sup>, while surface Fe contamination can be only slightly reduced.

A very similar calculated result is obtained for 300-mm diameter wafers, as shown in Fig. 4. In this case, the bath volume is assumed to be  $5.0 \times 10^4$  cm<sup>3</sup>. If the bath volume is reduced in order to save chemicals and water as well as to reduce the footprint of the wet station, the surface metal concentration will increase.

To prevent or reduce the detrimental effect of contamination brought into the solution during immersion-type wet cleaning by the to-be-cleaned wafers, the following procedures are recommended.

- (1) Brush or water-jet scrubbing of dirty wafer back-surfaces before immersion-type cleaning, for most of the metallic contaminants on the back-surfaces take the form of particles. (See Fig. 5 for a typical result.)
- (2) Scrubbing of wafer front-surfaces between each comparatively dirty wafer processing step and subsequent immersion-type cleaning.
- (3) Adding chelating agents to the solution in order to prevent metal adsorption onto the silicon surfaces, if the residue of these organic agents does not have a detrimental effect on the silicon surface and the device characteristics. (See Fig. 6 for a typical result.)
- (4) Disposing of chemical solutions after each cleaning cycle and using only fresh chemicals.

However, strictly speaking, even if the chemicals are disposed of after immersion-type wet cleaning, the surface metallic contamination is still dominated by the amount of impurities brought into the fresh solution by the wafers themselves. In order to meet

further stricter wafer-cleanliness requirements in the future, a new cleaning method in which fresh chemicals are continuously supplied, such as single-wafer spin cleaning [9], will have to be employed.

## WAFER DRYING AFTER WET CLEANING

### Evaluation of the Amount of Adsorbing IPA and Residual Water on Silicon Surfaces Using Various Drying Methods

In the aqueous processing of silicon wafers, drying after water rinsing is a critical step in terms of the prevention of both watermark (or drying spot) formation and particle adhesion. While centrifugal spin drying has been widely used for many years, the vapor drying method using isopropyl alcohol (IPA) is preferred for the reduction of both watermarks and particle adhesion in most advanced production lines. The thermal design of the equipment and the purity of the solvent are extremely important to achieve good results [1]. Recently, in order to completely eliminate the formation of watermarks on the wafer surface, various new *in-situ* drying techniques employing IPA vapor have been or will be put on the market. Figure 7 compares the features of these techniques employing IPA vapor.

The amount of IPA and wafer residue remaining on the surface of silicon wafers after drying using different drying methods was evaluated using gas chromatography-mass spectrometry following thermodesorption (TD-GC/MS) and thermal desorption spectrometry (TDS), respectively.

As a result, the amount of IPA adsorbing on the surface of the silicon wafers dried using the Marangoni method and the IPA Direct-Displacement method was found to be approximately 1/20 and 1/5, respectively, of the amount on wafers dried using the conventional IPA vapor drying method. This phenomenon is likely due to the difference in the concentration of IPA vapor in the atmosphere surrounding the to-be-dried wafers. The amount of IPA adsorbing on the silicon surfaces did not desorb after exposure to the ambient air for many hours at room temperature or after nitrogen was blown against the silicon surface. On the other hand, the amount of water adsorbed on the surface of the silicon wafers dried using the three drying methods employing IPA was almost the same and was much smaller than the amount adsorbing onto the surface of wafers dried using the conventional spin-drying method.

The new wafer drying methods employing IPA can effectively prevent watermark formation with much less residual water and IPA adsorbing on the surface of silicon wafers, but the prevention of particle adhesion on the surface is a big challenge for these new methods, particularly during drying after oxide-film etching and rinsing, or HF-last process [10] [11].

## WAFER STORAGE AFTER DRYING

### Prevention of Organic Adsorption on the Silicon Surface after Drying

Not only particulate and metallic contamination but also trace organic contamination adsorbing on the surface of silicon wafers has been found to have an increasingly detrimental impact on the performance and yield of semiconductor products. It has been shown that such organic contaminants have deleterious effects on the gate oxide integrity (GOI) [12], but this is strongly dependent on the atmosphere in which the wafers are inserted into the oxidation furnace. While contaminated wafers are being loaded in a nitrogen atmosphere, the GOI can be degraded. This shows that organic contaminants will reside on the surface as carbon contamination in the nitrogen ambient, while they are oxidatively degraded and evaporated in an ambient containing oxygen. Organic contaminants can have a more deleterious effect in chemical vapor deposition (CVD) where the employment of an oxidizing ambient cannot be used. Organic adsorption onto substrate surfaces must be prevented before CVD to eliminate film thickness deviation due to variable incubation time in thin film deposition [13] as well as to avoid the degradation of the integrity of gate oxides on which polycrystalline silicon is chemically deposited. Therefore, in order to prevent the adsorption of organic contaminants onto silicon surfaces both before gate oxidation and before CVD, it is necessary to determine the origin of the contaminants by the identifying organic compounds adsorbing on the surface of the silicon wafer.

When silicon wafers are exposed after wet cleaning and drying to the atmosphere in regular cleanrooms, gaseous organic molecules in the air easily adsorb onto the wafer surfaces in a short time[14]. Major organic molecules in the cleanroom air are volatiles outgassing from polymeric materials. In fact, polymeric materials are found almost everywhere in cleanrooms[15]. Dioctyl phthalate, a plasticizer for plastic materials, outgasses from panels made of polyvinylchloride materials and even from HEPA filters because of its being used for trapping tests of filters, while low-molecular cyclosiloxane outgasses from sealants. Furthermore, phosphoric acid esters outgas from prefilters in cleanrooms as well as covering materials of electric cables for process equipment. The organic volatiles outgassing from these polymeric materials can be easily adsorbed on silicon surfaces. In order to avoid the adsorption of airborne organics onto silicon surfaces, wafers should be stored in plastic boxes, which are usually made of polypropylene and/or polycarbonate materials. However, while wafers are stored in such boxes to protect them from airborne contaminants, organic volatiles outgassing from the plastic material adsorb onto the wafer surfaces [4][15][16].

#### Organic Contaminants Adsorbing on the Silicon Wafers

We have analyzed organic contaminants on the surface of silicon wafers stored in various types of plastic boxes supplied by the major silicon-wafer vendors without wafer cleaning using gas chromatography-mass spectrometry following thermodesorption (TD-GC/MS). Organic volatiles outgassing from the materials which compose these plastic boxes were also analyzed using head-space gas chromatography-mass spectrometry (HS-GC/MS).

Figure 8 shows a typical example of the gas chromatogram of organic contaminants adsorbing on the surface of the silicon wafer stored in a plastic box. Chemical structures of the organic compounds identified from the mass spectra are also shown in the figure. A large amount of 2,6-di-t-butyl-2,5-cyclohexadiene-1,4-dione and 2,6-di-t-butyl-4-methylene-2,5-cyclohexadiene-1-one, corresponding to the two adjacent peaks in the middle of the chromatogram as well as a large amount of dibutyl phthalate (DBP) and small amounts of many types of aliphatic hydrocarbons were detected on this wafer. The former two aromatic hydrocarbons, found on the wafer are known as oxidizing products of BHT. This suggests that BHT, which had outgassed from the boxes, would have adsorbed onto the wafer surface. The DBP detected on the wafer surface must be a result of the adsorption of DBP outgassing from the box material onto the wafer.

It should be noted that major organic compounds adsorbing on the surface of silicon wafers stored in plastic boxes are additives, such as antioxidants, plasticizers, and crosslinking agents outgassing in small quantities, rather than aliphatic hydrocarbons, such as unpolymerized monomers and oligomers, outgassing in large quantities from the plastic material [4]. Organic additives such as BHT and DBP, with comparatively low vapor pressures and/or high dipole moments, have polar groups such as  $>\text{C}=\text{O}$  and  $-\text{OH}$ , thus that these additives are apt to adsorb on the surface of the native oxide on the silicon substrate which has polar groups such as  $-\text{OH}$  and  $-\text{O}$ , even if the quantity of these additives' outgassing is very small. On the other hand, aliphatic hydrocarbons do not have polar groups and have comparatively high vapor pressures, so that these are difficult to adsorb on the surface of the native silicon dioxide, although the quantity of outgassing is comparatively large. In other words, if the quantity of outgassing organics is small, this does not necessarily mean that the quantity of the organics adsorbing on the silicon surfaces is small [4].

#### Removal of Organic Contaminants by Wet Cleaning

It has been shown [4] that these trace organic contaminants on silicon surfaces can be completely removed using ozonized water and/or dilute HF. Ozonized water has the highest oxidation potential of the chemicals used, thus it is able to oxidatively degrade organics. On the other hand, dilute HF is capable of removing the organic contaminants by lifting off the thin native oxide on which the organic contaminants are adsorbed.

#### Prevention of Organic Adsorption after Organic Removal

However, wafer storage in plastic boxes after wet cleaning prior to oxidation or CVD results in the re-adsorption of organic volatiles onto silicon surfaces, even though the organic contaminants have been removed by wet cleaning. After all organic contamination is completely removed by wet cleaning, the silicon wafers were stored for one month in plastic boxes whose interior was continuously purged with nitrogen or oxygen. As a result, only aliphatic hydrocarbons were detected on the wafer exposed to the nitrogen atmosphere in the nitrogen purged box, while additives such as BHT and DBP, in addition to the aliphatic hydrocarbons, were detected on the wafer exposed to ambient oxygen, as is shown in Fig. 9. Additionally, it was found that the amount of organic additives adsorbing on the silicon surfaces stored in a plastic box without oxygen purging (in an air ambient without hermetic sealing) was the same as that with oxygen purging. The TDS pyrogram and the XPS Si2p spectrum for the wafers before and after

storing in a nitrogen or oxygen purged box suggest that hydrogen termination was broken and a native-oxide layer grew on the silicon wafers stored in the oxygen atmosphere for one month, while native oxides did not grow with hydrogen termination on the silicon wafer stored in the nitrogen atmosphere.

The organic additives outgassing from plastic boxes have polar groups such as  $>\text{C}=\text{O}$  and  $-\text{OH}$ . On the other hand, several layers of water molecules may have already adsorbed on the native oxide in the form of hydrogen bonding, under normal conditions. Thus, the organic additives adsorb on the polar group of water molecules,  $\text{H}-\text{O}-\text{H}$ , with hydrogen bonding, as shown in Fig. 10(a). In contrast, because the hydrogen-terminated surface is non-polar due to the absence of a native oxide as shown in Fig. 10 (b), organic additives outgassing from the plastic box are less easily adsorb onto a hydrogen terminated surface kept in a nitrogen atmosphere. On the other hand, large quantities of organic contaminants are adsorbed onto the surface of an ozonized-water-treated wafer even in a nitrogen atmosphere, due to the presence of a chemical oxide with polar groups on the surface.

It has also been found that residual fluorine on silicon surfaces after cleaning of the silicon wafers with aqueous HF as well as anhydrous HF accelerates the adsorption of organic contamination onto the silicon surfaces[17]. The amount of a typical organic contaminant, BHT, adsorbing on a silicon surface as a function of the storage time in a plastic box after HF cleaning with/without DI water rinse is shown in Fig. 11. The acceleration of organic adsorption is due to the electrostatic force of attraction between the polar groups of organic compounds and the residual fluorine on the silicon surface.

## SUMMARY AND CONCLUSIONS

Three key issues in the wet chemical cleaning of silicon surfaces have been discussed.

(1) When contaminated silicon wafers are immersed in an ultrapure cleaning solution in which the impurity concentration is negligible, the level of wafer-surface metallic contamination after cleaning depends on the amount of metallic impurities brought into the solution by the to-be-cleaned wafers themselves. Even if the chemicals are disposed of after each wafer cleaning, the surface metal contamination is still dominated by the amount of impurities brought into the fresh solution by the wafers themselves. Much more attention should, therefore, be paid to wafer-carried contamination rather than the purity of reasonably clean chemicals. From this viewpoint, wafer scrubbing after a dirty process but before immersion-type wet cleaning is preferable. In order to meet future stricter wafer-cleanliness requirements, new cleaning methods where fresh chemicals are continuously supplied, such as single-wafer spinning cleaning, will have to be employed.

(2) New wafer drying methods employing IPA can effectively prevent watermark formation with much less residual water as well as IPA adsorbing on the silicon surfaces, but the prevention of particle adhesion on the surface is a big challenge for these new methods. Further revisions are expected with a view to lower cost, higher performance, and environmental friendliness.

(3) As semiconductor device geometries continue to shrink, trace volatile organic contamination adsorbing on the surface of silicon wafers has an increasingly detrimental impact on product performance and yield. The adsorption of the organic contaminants on the silicon surfaces can be inhibited by preventing the growth of native oxides after DHF cleaning and subsequent sufficient water rinsing. On the other hand, plastic materials which contain a smaller amount of additives should be used for wafer storage boxes to prevent the adsorption of organic contaminants onto the silicon surface.

## REFERENCES

- [1] T. Hattori, in *Proceedings of the 2nd International Symposium on Ultra Clean Processing of Silicon Surfaces (UCPSS'94)*, p.13, Academische Coöperatief, Leuven, Belgium (1994).
- [2] T. Hattori, in *Contamination Control and Defect Reduction in Semiconductor Manufacturing III, PV94-9*, p.3, the Electrochemical Society Proceedings Series, Pennington, NJ (1994).
- [3] T. Hattori, S.Koyata, M.Funada, and H. Mishima, *Microcontamination*, **9** (12), 17 (1991).
- [4] K. Saga and T. Hattori, *J. Electrochem Soc.*, **143**, 3279 (1996).
- [5] M. Watanabe, I. Kanno, and T. Ohmori, in *Proceedings of ISSM'94*, p.99 (1994).
- [6] T. Osaka and T. Hattori, *IEEE Trans. on Semiconductor Manufacturing*, to be published (1998).
- [7] Y. Ryuta, T. Yoshimi, H. Kondo, H. Okubo, and Y. Shimanuki, *Japan J. Appl. Phys.*, **3**, 2338 (1992).
- [8] J. Ryuta, T. Yoshimi, I. Takahashi, C. Okada, H. Kobayashi, G. Maeda, and T. Shinjoji, in *Extended Abstracts of the Electrochemical Society Fall Meeting*, Chicago, **95-2**, p.688 (1995).
- [9] T. Osaka, and T. Hattori, in *Cleaning Technology in Semiconductor Device Manufacturing V*, J. Ruzylo and, R. E. Novak Editors, to be published (1998).
- [10] T. Sato, F. Mieno, S. Kuzuya, and T. Kawamoto, *Proceedings of the ISSM'96*, p.349, Ultra Clean Society, Tokyo (1996).
- [11] K. Asada, H. Iwamoto, T. Hashiguchi, Y. Okamoto, T. Minami, K. Ueno, and S. Kitahara, in *Proceedings of the ISSM'97*, San Francisco, to be published (1997).
- [12] S. R. Kasi, M. Liehr, P. A. Thiry, H. Dallaporta, and M. Offenberg, *Appl. Phys. Lett.*, **59**, 108 (1991).
- [13] K. Saga, and T. Hattori, *J. Electrochem. Soc.*, **144**, L253 (1997).
- [14] A. J. Muller, L. A. Psota-kelty, J. D. Sinclair, and W. Morrison, in *Semiconductor Cleaning Technology/1989*, J. Ruzylo and R. E. Novak, Editors, **PV90-9**, p.204, The Electrochemical Society Proceedings Series, Pennington, NJ (1989).
- [15] K. J. Budde and W. J. Holzapfel, and M. M. Bayer, *J. Electrochem. Soc.*, **142**, 888 (1995)
- [16] W. Storm, W. Vandervorst, J. Alay, M. Meuris, A. Opdebeek, M. M. Heyns, in *Proceedings of the 2nd International Symposium on Ultra Clean Processing of Silicon Surfaces*, p.367, Academische Coöperatief Leuven, Belgium (1994).
- [17] K. Saga and T. Hattori, *J. Electrochem. Soc.*, **144**, L250 (1997).

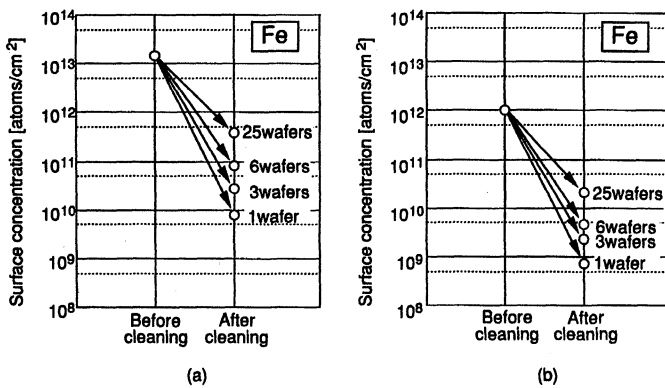


Fig.1. Fe concentration on the surface of 125-mm silicon wafers before and after SC-1 cleaning for different numbers of wafers with the same initial surface concentration of (a)  $1.4 \times 10^{13}$  atoms/cm<sup>2</sup> and (b)  $1 \times 10^{12}$  atoms/cm<sup>2</sup> simultaneously immersed in the chemical solution.

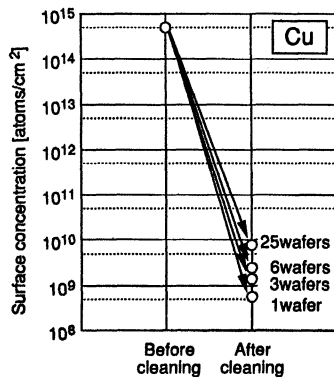


Fig.2. Cu concentration on the surface of 125-mm silicon wafers before and after SC-1 cleaning for different numbers of wafers with the same initial surface concentration of  $5 \times 10^{14}$  atoms/cm<sup>2</sup> simultaneously immersed in the SC-1 solution.

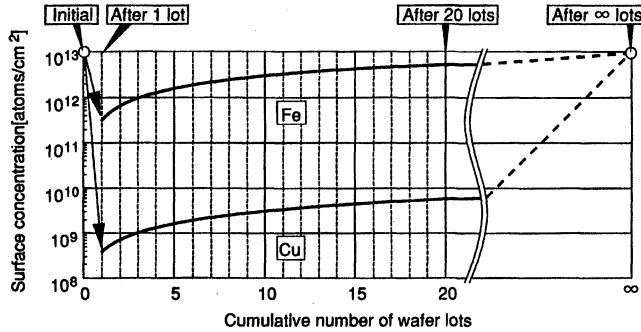


Fig.3. Wafer-surface metal concentration calculated on 125-mm wafer surfaces as a function of the cumulative number of 25 wafer lots subjected to SC-1 immersion cleaning.

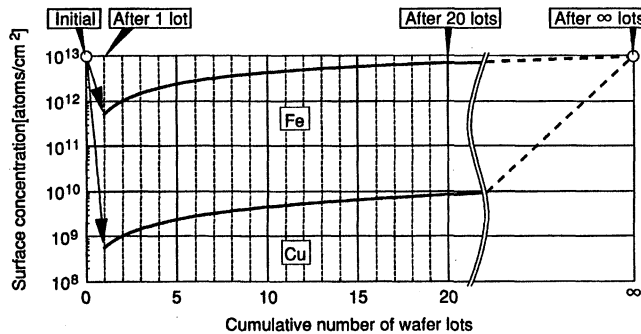
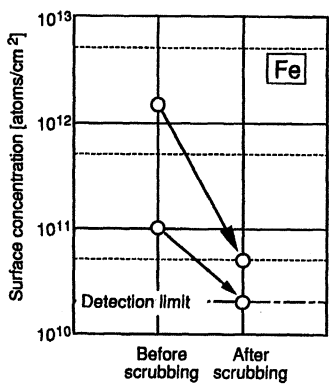
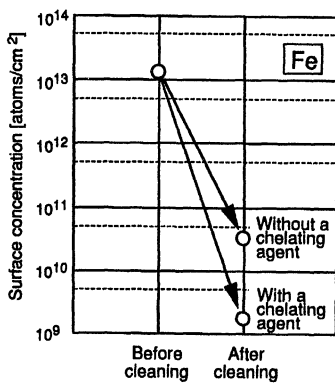


Fig.4. Wafer-surface metal concentration calculated on 300-mm wafer surfaces as a function of the cumulative number of 25 wafer lots subjected to SC-1 immersion cleaning.



**Fig.5.** Iron contamination on the back-surface of silicon wafers before and after brush scrubbing of the back-surfaces. The concentration was measured using TXRF in the same areas of the wafer back-surface before and after the scrubbing.



**Fig.6.** Fe contamination on the surface of silicon wafers before and after wet chemical cleaning in a SC-1 solution with and without a chelating agent.

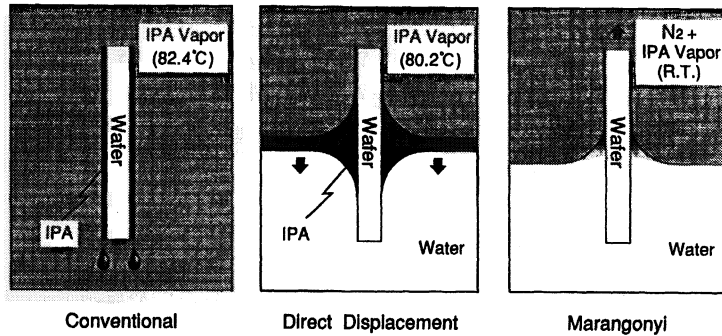


**Fig 7.** Various water drying methods employing IPA vapor

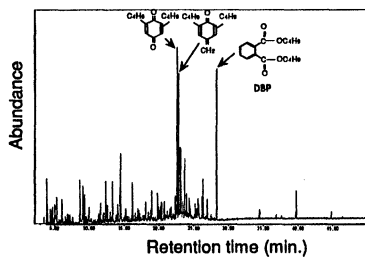


**Fig.8.** Typical gas chromatogram for organic contaminants adsorbing on the surface of a silicon wafer stored in a plastic box.

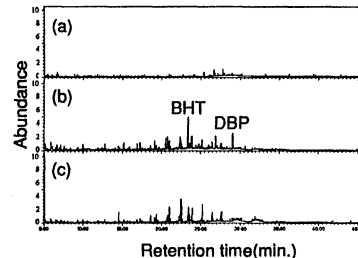


**Fig.9 .** Gas chromatograms of organic contaminants adsorbing on the surface of silicon wafers (a) just after DHF immersion, (b) stored in a plastic box purged with oxygen after DHF immersion, and (c) stored in a plastic box purged with nitrogen after DHF immersion.

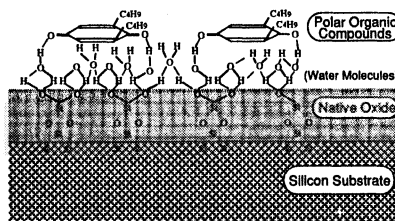


**Fig.10(a)** Model for adsorption of organic contaminants on a silicon surface covered with native oxide.

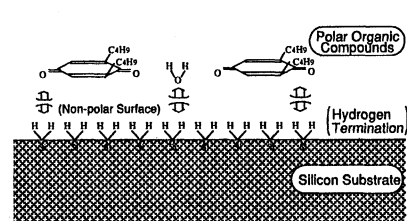


**Fig.10(b)** Model for relationship between polar organic compounds and the hydrogen-terminated silicon surface.

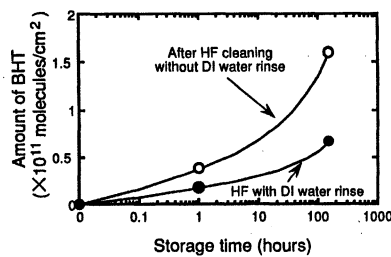


**Fig.11**  
Amount of BHT adsorbing on the surface of silicon wafers vs. storage time in the plastic box after HF cleaning.

## **PERFORMANCE OF "DDC" : DILUTED DYNAMIC CLEAN BEFORE 4.5 nm GATE OXIDE**

F. Tardif<sup>(1)</sup>, T. Lardin<sup>(1)</sup>, B. Sandrier<sup>(1)</sup>

P. Boelen<sup>(2)</sup>, R. Matthews<sup>(2)</sup>, I. Kashkoush<sup>(2)</sup> and R. Novak<sup>(2)</sup>

(1) : Gressi-Leti-CEA/G, 17 rue des Martyrs , 38054 Grenoble Cedex 09, France

(2) : SubMicron Systems Inc., 6330 Hedgewood Dr. 150, Allentown, PA 18106 USA

The "DDC" : Diluted Dynamic Clean which uses only diluted chemicals at room temperature is optimized here for pre-gate cleaning applications. The dissolved O<sub>3</sub> process is investigated in terms of smoothing effect, hydrocarbon removal efficiency and added particle reduction. The acidification of the DI water initially implemented to prevent Fe contamination is proved to be efficient as well for Zn, Al, Ca and Na. The optimized DDC gives as good electrical performances as a conventional RCA for 4.5 nm gate oxides and drastically reduces the consumption of chemicals.

### **INTRODUCTION**

In order to reduce the cost and environmental impact of cleaning processes in IC manufacturing, two alternatives now seem to be emerging. The first approach consists in diluting the conventional RCA. This solution is probably more attractive for the very conservative IC industry and has to be carefully studied. Nevertheless it does present some limitations mainly linked to the necessary relatively high process temperature which consumes the major part of chemicals by evaporation. The use of diluted chemicals at room temperature represents the other alternative and enables new technological concepts to be envisaged. The previously exposed<sup>(1)</sup> Diluted Dynamic Clean : "DDC" using HF, HCl and O<sub>3</sub> constitutes an interesting solution as it cuts the cycle time by a factor 2 and reduces the chemical consumption by more than a decade compared to the conventional SPM+HF+RCA. The DDC process adapted to pre-gate cleaning is here optimized and tested on a 4.5 nm gate oxide test vehicle including PBL lateral isolation. The electrical results are compared with those obtained with the conventional RCA process.

### **DILUTED DYNAMIC CLEAN CONCEPT**

The main idea consists in using a conventional quartz overflow rinsing tank in which small amounts of O<sub>3</sub> or HCl (but other reactives can also be used) are injected alternately or together into the continuous flow of DI water. Both the process and associated rinsing are performed alternately in this same bath. The first consequence is that the space usually occupied by the rinsing bath is saved. As the quantity of chemicals is negligible, the overflow can still be connected directly to the drain, thus the wafers always see fresh ultrapure reactants. Since for environmental considerations IC manufacturing has to limit its fluoride wastes, another bath dedicated to HF-based chemistries completes the whole concept. This bath comprises a conventional HF recirculated/filtered bath including an oxygen desorption device and a chemical purifier to remove noble metals. The DDC concept is constituted by the association of the two baths as represented in figure 1.

## LATEST DEVELOPMENTS ON DDC PROCESSES

The DDC process has to be adapted for each technological application because the requirements and the materials present on the wafer can be different. The full DDC process optimized for pre-gate cleaning is given in figure 2. A first optional O<sub>3</sub> treatment performed in bath "2" removes both hydrocarbons and noble metals. Then the sacrificial oxide and the ionic contamination are removed in the "%" solution composed of 1%HF acidified with 1%HCl (bath "1"). The wafers are then transferred into the dynamic bath "2" where the last traces of HF are eliminated before injection of O<sub>3</sub> which grows a chemical oxide under the particles. The particles are then eliminated in the "%" solution by under-etching mechanism. Then the wafers are rinsed in the dynamic bath before injection of O<sub>3</sub> necessary to grow the final passivation oxide. As there is no more acidic treatment after these 2 final treatments, gaseous traces of HCl are continuously injected as well during these steps in order to prevent any wafer recontamination. The proposed recipe used in this study takes less than 30 minutes instead of more than one hour for a conventional SPM/HF/RCA process. The consumptions of chemicals actually measured on the advanced SubMicron wet bench installed at Leti show that this DDC recipe consumes 8 to 40 times less chemicals (according to the throughput : respectively 7200 and 1200 wafers/day) and about 3 times less DI water than the conventional RCA recipe (bath lifetime : 24 h). The latest improvements achieved in the DDC process are exposed hereafter.

### Hydrocarbon removal

Figure 3 shows "natural hydrocarbon" removal efficiency by 6 ppm O<sub>3</sub> compared to different CARO 3/1 processed at different temperatures. The hydrocarbons were deposited by exposing the wafers 3 months in a state of the art class 10 clean room. The measurements were performed by a thermal desorption chamber coupled with an IMS (Ion Mobility Spectrometer from PCP inc.-USA). Hydrocarbons presenting a reduced mobility of 1.82 cm<sup>2</sup>/V.s were tested here. These types of species are removed with the same efficiency in CARO as in O<sub>3</sub>. Figure 4 shows that the removal efficiency kinetics of all the different hydrocarbons present on the same wafers is faster in the case of higher O<sub>3</sub> concentrations. The use of 20 ppm of O<sub>3</sub> in the first DDC step enables the process time to be reduced to 5 minutes.

### Oxide removal

Diluted HF is required to better control the oxide overetch. In the DDC process the roughening effects caused by diluted HF based mixtures is reduced by adjunction of 1% HCl in order to reduce the pH and by the presence of a degassifier in the bath recirculating loop to continuously decrease the dissolved oxygen content<sup>(2)</sup>. If the Silicon is not protected for example by an oxide layer, traces of noble metals can oxidize the surface leading to heavy yield loss. The most dangerous elements revealed by the electrical surface degradation as detected by μ-PCD are : Ag followed by Au, Cu and Pt (see figure 5). The kinetics is enhanced when the HF is more diluted<sup>(3)</sup>. The addition of a strong oxidant such as H<sub>2</sub>O<sub>2</sub> in HF<sup>(4),(5)</sup> continuously removes the just deposited metal but leaves the even more dangerous associated roughness. Processing the wafers in the dark in order to limit the available carriers necessary for the oxidation mechanism in certain cases reduces only the kinetics<sup>(6)</sup>. Acidification of HF by HCl is not efficient for this purpose<sup>(7)</sup>. Removal of noble metals in an HF bath therefore seems to be the only solution. Adding a Chempure™ from Millipore purifier in the recirculating loop before the filter was evaluated<sup>(8)</sup>. As seen in figure 6, a 10 ppb spike of Cu contamination is rapidly eliminated to an acceptable

concentration level. This is a very encouraging result but progress still has to be achieved especially for Ag.

### Metallic removal

In the DDC process the metallic removal is performed with the above defined % bath which was previously proved to eliminate major impurities in less than 30"(2). This treatment is in fact often naturally performed during the necessary sacrificial oxide overetch. Noble metals (verified for Ag and Cu) are removed with the hydrocarbons by the first step of DDC : 5 minutes in O<sub>3</sub> since the bath does not contain Cl<sup>-</sup> ions<sup>(1)</sup>. It is important then to avoid any risk of re-contamination during the next cleaning steps. Even if the DI water plants usually produce very pure water some contamination peaks can occur for example during the shift of new ion exchange resins. Unfortunately, due to the low ionic strength and the relatively high pH of the DI water, transfer from the water to the substrate is very high, sometimes even higher than in SC1 especially for Ca and Cu<sup>(9)</sup>. A 50 ppt contamination level in the rinsing bath leads to a measurable deposition of some 10<sup>10</sup> at/cm<sup>2</sup>. Injection of 0.01% of HCl had in the past proved its efficiency to reduce the consequences of an Iron contamination experience actually lived at Leti (see figure 7). As represented in figure 8, 0.01% HCl (pH=2.6) is finally valid for other contaminants as well. The results were obtained by intentionally adding contaminants in a static bath initially filled with DI water containing less than 10 ppt of contaminants. The same results were obtained for Na.

### Particle removal

Particle removal in diluted chemistry performed at room temperature is still the main challenge. From T. Ohmi<sup>(10)</sup> it is possible to remove particles with the "FPMS" solution based on the complementary effects of underetching by dHF and oxidizing by H<sub>2</sub>O<sub>2</sub>. The roughening effect is controlled by addition of a surfactant which then has to be removed with dissolved O<sub>3</sub>.

The particle removal process proposed in DDC uses 2-step cleaning : O<sub>3</sub> followed by a dHF/HCl dip. The O<sub>3</sub> concentration drives the oxidation kinetics<sup>(11)</sup> and consequently both the process time and the DI water consumption. This is why it is interesting to theoretically use a high O<sub>3</sub> concentration. Nevertheless this assumption is limited in practice on initially hydrophobic wafers by the particle deposition caused by the O<sub>3</sub> desorption in the bath. Indeed, as concluded by Roustan et al<sup>(12)</sup>, Henry's law is obeyed for dissolution of O<sub>3</sub> in water : the ozone solubility is controlled by the temperature and the O<sub>3</sub> partial pressure in the gaseous phase. Major O<sub>3</sub> adsorption devices use the principle represented in figure 9. When the gaseous phase is eliminated in the debubbler the system desorbs the O<sub>3</sub> back to create a new gas phase in order to equilibrate the dissolved concentration. This mechanism generates a large number of microscopic bubbles (Champagne effect) which create a gas/liquid interface propitious to particle deposition<sup>(13)</sup> especially in the case of hydrophobic wafers. As demonstrated in figure 9 this behaviour is enhanced by a high O<sub>3</sub> concentration (distance from the thermodynamic equilibrium). As the bubbles arise preferentially on the horizontal parts of the carrier-supports they pollute the parts of the wafers vertically above the supports (see figure 10). When the debubbler effect is partially limited, a few big bubbles are to be found in the bath instead of thousands of microscopic ones. As shown in figure 9, the presence of a few big bubbles can finally lead to a lower particle deposition. Nevertheless, as we did not obtain sufficiently reproducible results by reducing the dedubbler efficiency, we chose for the time being to still keep a low O<sub>3</sub> concentration of 3 ppm for hydrophobic wafers. When the O<sub>3</sub> concentration is fixed, it is then necessary to optimize the process times of the 2-step cleaning : O<sub>3</sub> and HF. As demonstrated in figure 11

for both  $\text{SiO}_2$  and  $\text{Al}_2\text{O}_3$  particles a minimum of 10 minutes has to be spent in the  $\text{O}_3$  bath before the underetching step. Using these conditions for the first step, the particle removal efficiency kinetics in 1%HF acidified or not with 1%HCl is shown in figure 12. The use of the "%" solution : 1%HF+1%HCl enables the etching time to be reduced drastically to 1 minute and consequently limits the detrimental etchings (locos edges for example). This behaviour was previously attributed to the sign change of the substrate Zeta potential<sup>(1)</sup>. The particle removal efficiency obtained with this 2-step cleaning is quite high, but it is still slightly lower than a conventional SC1 with megasonics.

The first tests with megasonics in the % solution showed that no degradation of the surface occurs in terms of roughness. But megasonics have not yet achieved a clear advantage from the particle removal point of view. Other tests are in progress.

#### **Final passivation before gate oxidation**

The good oxide integrity systematically obtained with 3 ppm  $\text{O}_3$  performed in dynamic mode could be related to a Silicon smoothing effect. Indeed as shown in figures 13 and 14,  $\text{O}_3$  drastically reduces the average surface roughness (RMS) and the high peaks which are even more detrimental for thin oxide integrity as shown by numerical simulations<sup>(14)</sup>. This effect has already been demonstrated in the past for the other strong oxidant cleaning : CARO<sup>(2)</sup>. This smoothing effect kinetics is probably enhanced by a higher  $\text{O}_3$  concentration as indicated by figures 13 and 14 for which 3 and 20 ppm  $\text{O}_3$  were used respectively. Nevertheless, today the  $\text{O}_3$  concentration has to be reduced to 3 ppm for the final passivation step in order to minimize particle addition.

### **ELECTRICAL RESULTS ON 4.5 nm GATE OXIDE**

Tests were performed on SGS Thomson base wafers (8" p 14-22  $\Omega\text{.cm}$  (100) CZ and epi) including a PBL lateral isolation. Before the 4.5 nm gate oxide growth, the wafers were cleaned with a conventional CARO/HF/RCA (referenced as "RCA" in figures 15 and 16) or the DDC process described in figure 2. Another process guaranteeing the well proved robustness of the RCA and the better passivation proposed in DDC was tested as well. Figure 15 shows that as expected DDC gives as good average EBD on big capacitors as the other cleanings in the case of dry HCl performed at 800°C. DDC gave an even better robustness in the case of the WET oxidation performed at 750°C. Figure 16 again shows that DDC gives as good intrinsic QBD as the other cleaning recipes. No differences could be identified between epi and CZ wafers in this test. The good DDC performances were obtained on wafers representative of today's production. The next step will consist in comparing DDC and RCA cleanings in terms of robustness on initially dirty and rough substrates.

### **CONCLUSION**

The DDC concept using existing wet bench technology and a diluted chemistry performed at room temperature represents one of the most interesting ways of reducing the cleaning costs and environmental impact. The performances of the DDC process adapted for pre-gate cleaning gave as good results as the conventional RCA-based chemistry on a 4.5 nm oxide with a reduction of chemicals by a factor 8 to 40 according to the throughput and a cycle time cut by a half.

## ACKNOWLEDGEMENTS

The authors would like to thank D. Levy and K. Barla from SGS Thomson for their active contribution and JL. Di Maria from Leti who performed the electrical tests.

## REFERENCES

1. F. Tardif, T. Lardin, P. Boelen, R. Novak, I. Kashkoush, UCPSS'96, Antwerp, 1996
2. F. Tardif, T. Lardin, C. Paillet, J.P. Joly, A. Fleury, P. Patruno, D. Levy, K. Barla, ECS Fall meeting, Chicago, October 1995.
3. F. Tardif, JP. Joly, A. Courteaux, U. Straube, A. Danel and G. Kamarinos, ECS Fall meeting, Paris, September 1997
4. H. Morinaga, T. Ohmi, Electrochem. Soc. Proc. Vol 95-20, p. 257.
5. T. Shimomo and M. Tsuji, Extended Abstracts of Electrochem. Soc. Meeting, Vol.91-1, p. 278, Washington DC, (1991).
6. I. Teerlinck, H.F. Schmidt et al., Electrochem. Soc. Proc. Vol 95-20, p. 284.
7. I. Teerlinck, P.W. Mertens, H.F. Schmidt, M. Meuris, M.M. Heyns, J. Electrochem. Soc., Vol. 143, p. 3323, (1996).
8. S. Kunz, S. Marthon and F. Tardif, ECS Fall meeting, Paris, September 1997
9. L. Mouche, F. Tardif and J. Derrien, J. Electrochem.Soc., Vol. 142, N° 7, July 1995
10. T. Ohmi, J. Electrochem.Soc., Vol. 143, N° 9, September 1996
11. T. Isagawa, M. Kogure, T. Imaoka, T. Ohmi, International Conference on Solid State Devices and Materials, Tsukuba, p. 193-195, 1992
12. M. Roustan, J. Mallevialle, Ozonation Manual for Water and Wastewater Treatments, Chapter 9, page 47, Edited by W.J. Masschelein, J. Wiley, 1982
13. AFM. Leenars, "Particles on surfaces I", Edited by K.L. Mittal, Plenum press
14. MCV. Lopes, S. G. dos Santos F. and C. M. Hasenack, J. Electrochem. Soc., Vol 143, N°. 3, March 1996

This work was carried out within the GRESSI consortium between CEA-LETI and France Télécom-CNET

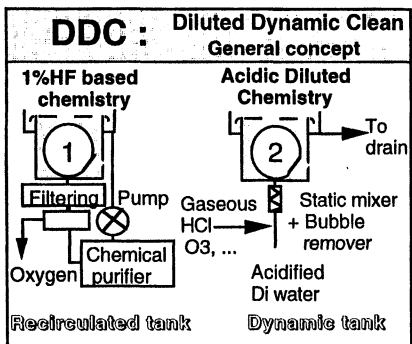


Figure 1: "DDC" : Diluted Dynamic Clean concept.

Process (20 °C)	Time (min.)	Goal
O <sub>3</sub> 20 ppm	5	CHx + noble metals
% : 1%HF+1%HCl	+ 0.5 overetch	Sac. Ox. + metals
Rinse	1	Rinse
O <sub>3</sub> 3 ppm	10	Particle removal
% : 1%HF+1%HCl	1	
Rinse 0.01% HCl	1	Rinse
O <sub>3</sub> 3 ppm 0.01% HCl	7	Final Passivation
Total :	26.5	

Figure 2 : Full DDC process adapted to pre-gate cleaning including protections against noble metals and DI water contamination peaks.

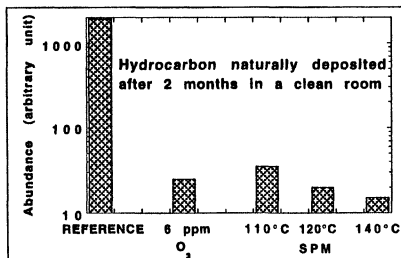


Fig 3 : "Natural" hydrocarbon removal efficiency as measured by IMS (process time : 10 min.).

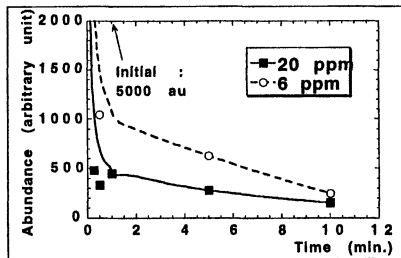


Figure 4 : Impact of O<sub>3</sub> concentration on hydrocarbon removal kinetics

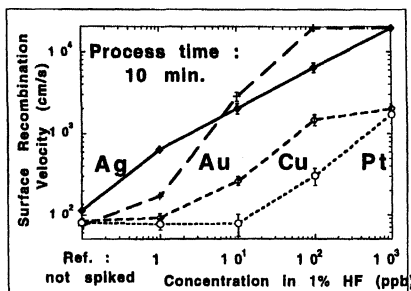


Fig 5 : Surface Recombination Velocity as measured by  $\mu$ -PCD on wafers dipped in a contaminated 1% HF bath.

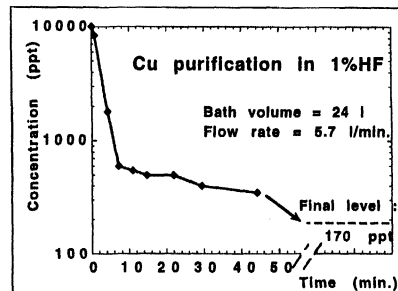


Figure 6 : Cu elimination in 1% HF after an initial spike of 10 ppb using a Chempure<sup>TM</sup> purifier from Millipore

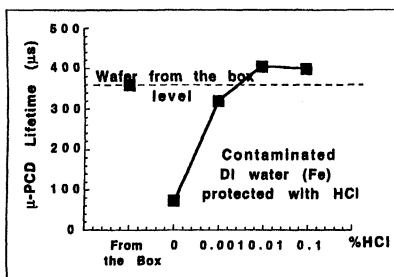


Figure 7 : Fe contamination reduction in DI water as measured by  $\mu$ -PCD.

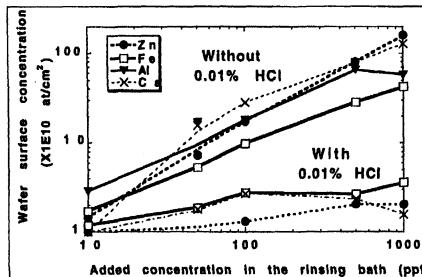


Figure 8 : Contamination reduction in DI water as measured by TXRF and VPD-ICPMS (Al)

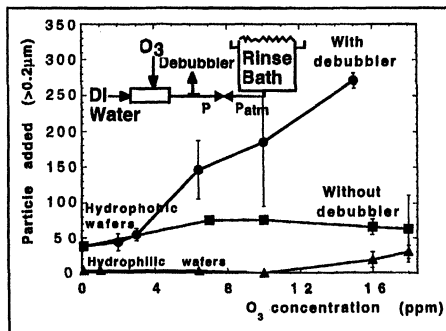


Figure 9 : Added particles in O<sub>3</sub> bath with or without a debubbler : "Champagne effect".

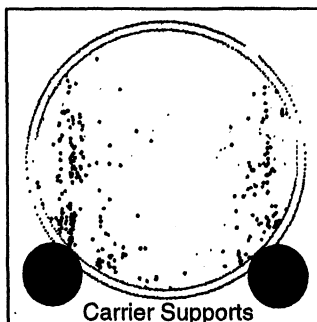


Figure 10 : Particle deposition map using the debubbler

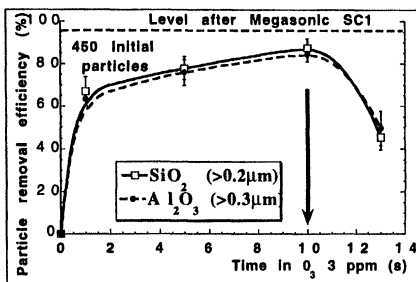


Figure 11 : Particle removal efficiency as a function of the  $O_3$  process time followed by a 3 min. 1% HF dip.

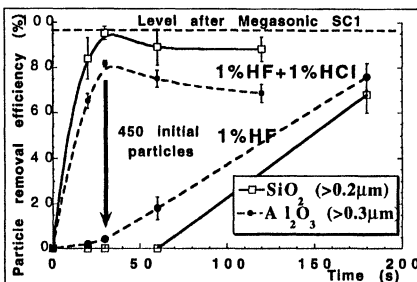


Figure 12 : Particle removal efficiency as a function of the HF process time. Previous treatment : 10 min. 3 ppm  $O_3$

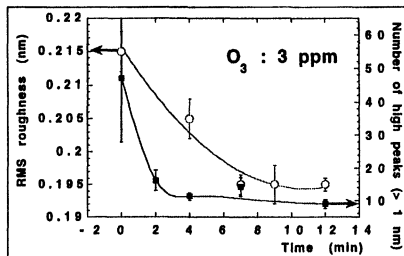


Fig 13 : Smoothing effect of 3 ppm  $O_3$  in water both on the average roughness and in terms of high peak ( $>1\text{ nm}$ ) reduction.

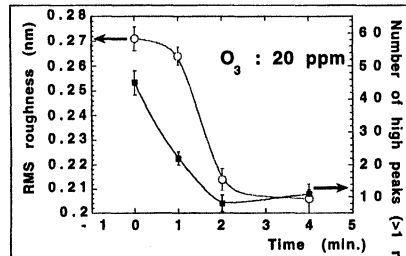


Figure 14 : Smoothing effect of 20 ppm in water on average roughness

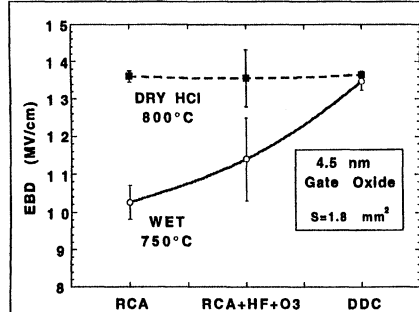


Fig 15 : RCA and DDC performances in terms of EBD obtained on 4.5 nm gate oxides

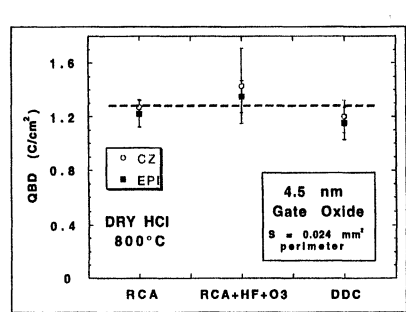


Figure 16 : RCA and DDC performances in term of QBD obtained on 4.5 nm gate oxides.

**MINIMIZING SULFUR CONTAMINATION AND RINSE WATER VOLUME  
REQUIRED FOLLOWING A SULFURIC ACID/HYDROGEN PEROXIDE  
CLEAN BY PERFORMING A CHEMICALLY BASIC RINSE\***

**P. J. Clews, G. C. Nelson, C. A. Matlock<sup>a</sup>, P. J. Resnick, C. L. J. Adkins**  
*Sandia National Laboratories, Albuquerque, NM 87185*

**ABSTRACT**

Sulfuric acid hydrogen peroxide mixtures (SPM) are commonly used in the semiconductor industry to remove organic contaminants from wafer surfaces. This viscous solution is very difficult to rinse off wafer surfaces. Various rinsing conditions were tested and the resulting residual contamination on the wafer surface was measured. The addition of small amounts of a chemical base such as ammonium hydroxide to the rinse water has been found to be effective in reducing the surface concentration of sulfur and also mitigates the particle growth that occurs on SPM cleaned wafers. The volume of room temperature water required to rinse these wafers is also significantly reduced.

**INTRODUCTION**

Sulfuric acid/hydrogen peroxide mixtures (SPM), also commonly referred to as a piranha clean, are widely used in the semiconductor industry for removing organic contamination from wafer surfaces. This viscous mixture is difficult to rinse off the wafer surface even when using copious amounts of water. Conservation of water in semiconductor fabrication is becoming an important issue, especially in areas that do not have abundant water supplies. Reducing the amount of water required for wet processing can significantly reduce the cost-of-ownership of wet processing equipment. The residual contamination remaining on the wafer surface after a SPM clean results in particle growth on the wafer surface after the wafers have been stored in the clean room environment for a period of time. The mechanism for particle growth and the composition of these particles are not well understood. Some researchers suggest that the particles are formed when residual acid on the wafer surface reacts with moisture from the air. Over time the residual acid grows large enough to be detected as particles [1] Other researchers suggest that contamination is trapped in the SPM chemical oxide, diffuses to the wafer surface

---

\* This work was performed at Sandia National Laboratories, a multiprogram laboratory operated by Sandia Corporation, a Lockheed Martin company, for the U. S. Department of Energy under contract number DE-AC04-94AL85000. This work was funded through a cooperative research and development agreement with SEMATECH.

<sup>a</sup> Present address: FSI International, Surface Conditioning Division, Chaska, MN 55318

and coalesces forming micro-crystals during storage. Given enough time, most of the contaminants diffuse to the surface and a simple water rinse step can remove it preventing further particle formation [2].

Methods to eliminate or significantly reduce particle growth on SPM cleaned wafers are also reported in the literature [1-5]. These methods are effective but they require hot deionized (DI) rinse water, addition of HF to the SPM tank, or additional processing tanks so wafers can be exposed to HF, SC1 or IPA solutions after the SPM clean to remove the contamination. The objective of this study was to: 1) better understand the particle growth that occurs on SPM cleaned wafers; 2) minimize the amount of rinse water required to rinse SPM cleaned wafers; and 3) minimize the amount of sulfur contamination remaining on the wafer surface after the SPM clean.

In previous work [6] we demonstrated that megasonic power applied during the rinse step following a SPM clean removes particles added during the clean but does not aid in the removal of sulfur (S) contamination from the wafer surface or eliminate the time-dependent SPM particle growth. We also demonstrated that SPM particle growth correlates with the relative amount of sulfur contamination on the wafer surface after a SPM clean. Higher sulfur concentration on wafers cleaned in SPM is correlated with faster particle growth.

In this paper we present information on the shape and composition of the SPM particles and wafer storage conditions that alter the growth rate of these particles. We also present additional rinsing experiments that investigate the effects of extended rinse times and adding chemicals to the rinse water. We demonstrate that addition of a chemically basic material to the rinse water reduces the amount of water required to rinse SPM cleaned wafers and also reduces the amount of sulfur contamination remaining on the wafer surface following a SPM clean. As a result, the time dependent SPM particle growth is mitigated. Based on our results we suggest a mechanism for SPM particle growth.

## EXPERIMENTAL DETAILS

Rinsing studies were performed using 6-inch n-type (100) bare silicon wafers and 100 Å thermally oxidized silicon wafers. The contact angle of the thermal oxide and silicon wafers was altered prior to the SPM clean by processing these wafers through either a 100:1 HF dip, a 64:4:1 ( $H_2O:H_2O_2:NH_4OH$ ) SC-1 clean, a 5:1:1 ( $H_2O:H_2O_2:HCl$ ) SC-2 clean, or a combination of these chemistries. A full cassette of wafers was cleaned in a 5:1 or 10:1 ( $H_2SO_4:H_2O_2$ ) SPM solution at 95°C for 10 minutes. The SPM temperature and time were constant for all experiments. Wafers were rinsed in a Verteq Turbo Sunburst Quick Dump Rinse (QDR) tank. The rinsing parameters used for each experiment are described in the experimental results section. Bulk resistivity of the water

was monitored during the rinsing process. The ambient rinse water temperature for all experiments was approximately 25°C. Light point defect (LPD) measurements were made to monitor particle growth on these wafers using a Tencor SFS-6200. Wafers were measured periodically until the SFS-6200 failed to scan the entire wafer. The SFS-6200 will fail to scan a wafer if light scattering from particles or haze on the wafer surface overwhelms the PMT at a given gain setting. Time of Flight Secondary Ion Mass Spectroscopy (TOF-SIMS) and/or Total Reflectance X-Ray Fluorescence Spectroscopy (TXRF) measurements were taken to compare LPD growth with the amount of sulfur left on the wafer surface. These data were used to evaluate the effectiveness of the rinse step [6].

## EXPERIMENTAL RESULTS

### Composition and Shape of SPM-Derived Particles

Scanning electron microscopy (SEM) images of SPM-derived particles (particles which are formed from residual SPM contamination) are shown in Figure 1. The morphology of the SPM-derived particles depends on the concentration of H<sub>2</sub>O<sub>2</sub> in the SPM solution. Particles derived from 10:1 SPM are crystalline but the 5:1 SPM-derived particles have no distinct shape. In order to obtain these images, the samples had to be carbon coated. TOF-SIMS negative and positive ion image maps of the SPM-derived particles, shown in Figure 2, indicate that the particles are composed of SO<sub>x</sub><sup>-</sup> and NH<sub>4</sub><sup>+</sup>.

### Effect of Wafer Storage Environment on SPM-Derived Particle Growth

Altering the storage conditions of SPM cleaned wafers can drastically alter the particle growth behavior. Data in Table I indicate that wafers stored in a very humid environment (storage box with small amount of DI water in the bottom) do not exhibit particle growth for as long as two weeks after the SPM clean. However, once the humid wafers are exposed to the cleanroom air, particles begin to grow very quickly. Although wafers stored in humid environments do not exhibit particle growth, we speculate that the reaction to form SPM-derived particles is still occurring, but the particulate matter is dissolved in the monolayers of water present on the wafer surface. When the wafers are removed from the humid environment, excess moisture evaporates and the particles form. Wafers cleaned and rinsed at the same time as the wafers stored in the humid environment but stored in the normal cleanroom air (in an open cassette) exhibited particle growth and failed the SFS-6200 scan less than 24 hours after the SPM clean. Wafers stored in a closed storage box, with no water in the bottom of the box, took longer to fail the SFS-6200 scan than the wafers stored in the open cassette. This indicates that SPM-derived particle growth depends on cleanroom air exposure.

**Table I: Effect of Wafer Storage Environment on SPM-Derived Particle Growth**

Storage Condition	X = Time to Fail SFS-6200 Scan (> 0.13μm)
Open cassette	15 < X < 22 hours
Closed storage box	41 < X < 112 hours
Humid storage box	> two weeks
Humid wafers moved to dry storage box	2 < X < 5 hours after move

**Extended Rinse Times**

The TXRF and SFS-6200 data shown in Figure 3 indicate that extended room temperature rinse times do not eliminate SPM-derived particle growth on bare silicon wafers. Wafers from this 5:1 SPM clean were removed from the rinse bath after 10 minutes and after 20 hours of total rinse time. Room temperature rinse water was flowing into the QDR during the entire 20 hour rinse.

**Addition of Chemicals to the Rinse Water**

The extended rinse time data presented above and megasonic rinse data presented in prior work [6] indicate that the sulfur contamination remaining on silicon wafer surfaces after a SPM clean is chemically bound to the wafer surface. A chemical reaction is required to break the sulfur/silicon bond so that the sulfur contamination can be removed from the wafer surface. The TOF-SIMS particle image maps, shown in Figure 2, indicate that SPM-derived particles are composed of  $\text{NH}_4^+$  and  $\text{SO}_x^-$ . This knowledge led to the discovery that adding small amounts of  $\text{NH}_4\text{OH}$  directly to the SPM wafer rinse water significantly reduces SPM-derived particle growth. The addition of ammonium salts such as ammonium chloride and ammonium persulfate did not reduce SPM-derived particle growth; however, the addition of KOH, or another chemically basic material, to the room temperature rinse water did.

Figure 4 shows plots of the number of LPDs measured on 5:1 SPM cleaned wafers which were rinsed using either the standard rinse process or with the addition of KOH or  $\text{NH}_4\text{OH}$  to the rinse water. Sulfur concentration on these wafers is shown in Figure 5. All runs illustrated in these figures were performed on a full boat of wafers and were rinsed with approximately 60 liters of room temperature water. Wafers were rinsed for 5 dump cycles to remove most of the acid before the KOH or  $\text{NH}_4\text{OH}$  was added to the rinse water. The pH of the rinse water after the addition of KOH or  $\text{NH}_4\text{OH}$  was 10.4. Only 5 ml of  $\text{NH}_4\text{OH}$  and 3 g of KOH was added to the rinse water for these runs. Wafers were stored on a shelf and exposed directly to the cleanroom air to accelerate particle growth rate. Wafers rinsed using the standard process had significantly higher sulfur

concentration on the wafer surface than the wafers which were rinsed with NH<sub>4</sub>OH or KOH. The standard rinsed wafers failed the SFS-6200 scan one day after the SPM clean. The KOH and NH<sub>4</sub>OH rinsed wafers were still passing the SFS-6200 scan 3 weeks after the clean. The KOH wafers have a higher initial count because they were rinsed in a different ("KOH contaminated") wet bench. A slight increase in the number of LPDs on the NH<sub>4</sub>OH rinsed wafers appeared after 3 weeks of storage.

#### SPM-Derived Particle Growth Mechanism

Mechanisms for SPM-derived particle growth have been suggested in the literature [1-3]. The data presented above do not support these theories. Another mechanism is suggested here [6]. Ammonia gas in the cleanroom air absorbs into the monolayer of water present on the wafer surface forming ammonium hydroxide. The hydroxide ion reacts with the silicon surface, breaks the sulfur/silicon bond and ammonium sulfate particles form on the wafer surface. In humid environments, the ammonium sulfate remains dissolved in the monolayers of water on the wafer surface. When the wafers are removed from the humid environment, excess moisture evaporates and the particles appear. If hydroxide ions are introduced into the rinse water, this same reaction takes place except the ammonium sulfate can be removed by the water during the rinse step.

#### SUMMARY

Sulfur contamination tenaciously adheres to the silicon wafer surface after a SPM clean. Resistivity is not a good indication for rinse endpoint for SPM cleaned wafers because the contaminant is bound to the wafer surface and therefore cannot contribute to the conductivity of the water. Megasonic power applied during the room temperature rinse step of SPM cleaned wafers is not effective in removing SPM contamination. Room temperature rinse times as long as 20 hours do not eliminate SPM particle growth on bare silicon wafers. Scanning electron microscopy images of particles formed after SPM cleaning indicate the shape of the particles depends on the concentration of H<sub>2</sub>O<sub>2</sub> in the SPM solution. Particles formed from 10:1 SPM are crystalline but the particles from 5:1 SPM are amorphous. TOF-SIMS negative and positive ion image maps of the SPM particles indicate the SPM particles are composed of SO<sub>x</sub><sup>-</sup> and NH<sub>4</sub><sup>+</sup>. The addition of small amounts of a chemical base such as ammonium hydroxide (e.g., sufficient to achieve pH = 10) to the SPM rinse water has been found to be effective in reducing the surface concentration of sulfur and mitigates SPM induced particle growth. The volume of room temperature water required to rinse SPM wafers can be significantly reduced by removing the majority of the sulfuric acid with a quick dump rinse step, followed by the addition of enough ammonium hydroxide to the rinse water to make the solution basic, and finally completing the rinse process with room temperature ultra pure rinse water. Additional process tanks to perform the SC1 clean or dilute HF dip are not needed. The

water need not be heated, obviating energy-intensive heaters. Commercially available quartz equipment may be used to reprocess the H<sub>2</sub>SO<sub>4</sub>. Few chemicals are required which reduces the cost of both chemicals and waste disposal. Most important, the amount of water required for rinsing SPM cleaned wafers is reduced, and residual sulfur contamination is diminished. As a result, SPM derived particle growth is mitigated. Rinse tanks commonly used in semiconductor manufacturing can be easily modified to incorporate this rinsing technique.

#### ACKNOWLEDGMENTS

The authors thank Verteq for supplying the rinse tank used in these experiments. They also thank Kurt Christenson, FSI International; Steven Verhaverbeke and Chris McConnell, CFM Technologies; Bill Syverson and Rick Gaylord, IBM Corporation; Mark Hall Santa Clara Plastics; Tom Nicolosi Verteq; Russ Parker, Hewlett Packard; Robert Donovan, Sandia National Laboratories, for helpful discussions of the rinsing results.

#### REFERENCES

- [1] Hall, R. M., J.J. Rosato, P.G. Lindquist, T. Jarvis, T. Parry, J.D. Kelly, R.N. Walters. In *Proceedings of Semiconductor Pure Water and Chemicals Conference 1995*, M.K. Balazs (Ed), 101-112 (1995).
- [2] Rotondaro, L. P., H.F. Schmidt, M. Meuris, M.M. Heyns, C. Claeys and J. Mulready. *Proceedings of the Second International Symposium on Ultra-Clean Processing of Silicon Surfaces*, 301 (1994).
- [3] Fleming, M. Jr., W. Syverson, and E. White. "Reduction of Foreign Particulate Matter on Semiconductor Wafers", IBM Corporation, US Patent #5,294,570, March 15, 1994.
- [4] Verhaverbeke, S., R. Messoussi, and T. Ohmi. *Proceedings of the Second International Symposium on Ultra-Clean Processing of Silicon Surfaces*, 201 (1994).
- [5] Li, L., E. Grieger, K. Griffiths, S. Byrne, and R.C. Hawthorne, *Proceedings of the 188<sup>th</sup> Electrochemical Society Meeting*, Chicago, (1995).
- [6] Clews, P. J., G.C. Nelson, C.A. Matlock, P.J. Resnick, C.L.J. Adkins, and N.C. Korbe. *Proceedings of the 188<sup>th</sup> Electrochemical Society Meeting*, Chicago, (1995).

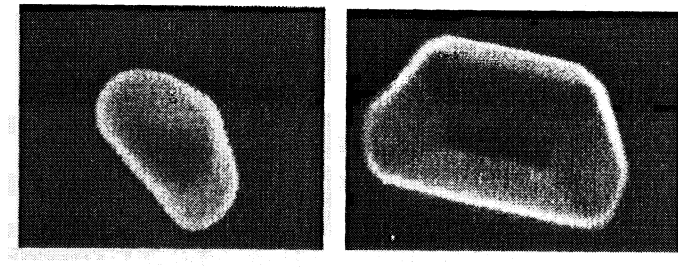


**Figure 1:** SEM image of SPM-Derived particles.

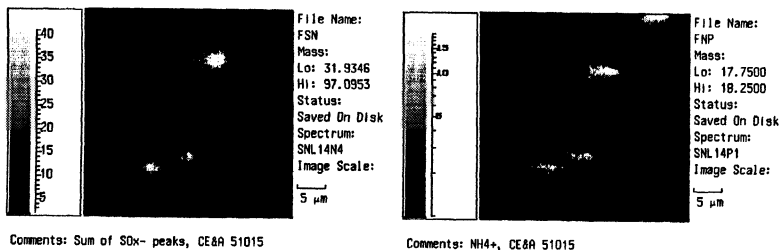


**Figure 2:** TOF-SIMS ion image map of SPM-Derived particles.

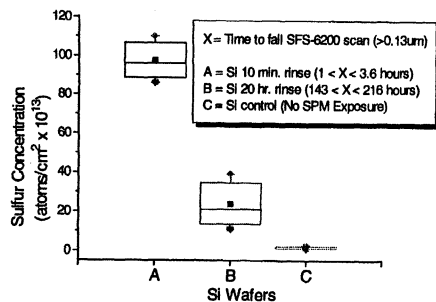


**Figure 3:** Box plot of TXRF S contamination levels measured on wafers processed through a 5:1 SPM and rinsed for a) 10 min. rinse; b) 20 hour rinse; c) Si control wafer not exposed to SPM solution.

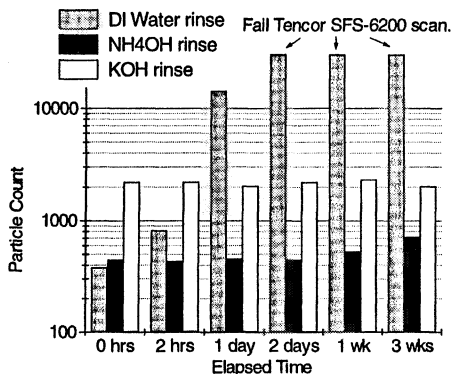


**Figure 4:** LPD average counts per wafer vs. elapsed time following a 5:1 SPM clean and rinse process. Wafers were rinsed using a) standard DI water rinse; addition of b) NH<sub>4</sub>OH or c) KOH to the rinse water.

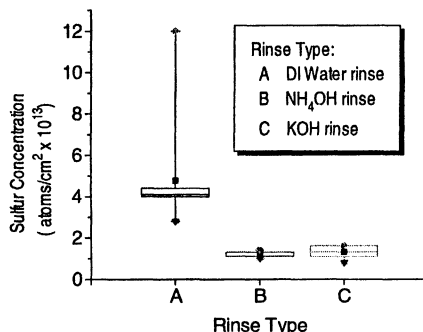


**Figure 5:** Surface sulfur concentration following basic and DI water rinsing. Wafers were rinsed using a) standard DI water rinse; addition of b) NH<sub>4</sub>OH or c) KOH to the rinse water.

## STATE-OF-THE-ART DRYING METHODS FOR SEMICONDUCTOR WET BENCHES

Glenn W. Gale, William A. Syverson, and Jeffrey A. Brigante  
*IBM Microelectronics, Essex Junction, VT 05452 USA*

### ABSTRACT

Current techniques for drying wafers in semiconductor manufacturing wet benches are evaluated and compared. Three different centrifugal spin dryers and two IPA-type dryers (Marangoni and 100% IPA vapor) are investigated. Results comparing a Marangoni dryer to a spin dryer indicate that the former provides superior particle performance. Additionally, stains are observed on spin-dried wafers containing hydrophobic surfaces after HF-last processing but are not seen on similar wafers processed by IPA-type dryers. The stains are removed by a brief HF etch followed by a Marangoni dry.

### INTRODUCTION

Wet processing in semiconductor manufacturing has experienced remarkable technology advancements in recent years. New and purer chemistries have been developed, megasonics and vapor phase processing have been used successfully, and there is improved understanding of interactions between process chemistries and wafer surfaces. A vitally important aspect of modern wet cleaning and etching is wafer drying, which significantly influences the post-process surface states of wafers because it is the final step they see in the process. Essentially, the goal of a wafer-drying process is to remove water from the substrate without evaporating it; when water evaporates, any solids in the water remain on the wafer as surface contamination.

Centrifugal spin drying of wafer batches has been used successfully for many years; wafer batches are spun at speeds approaching 1000 RPM or more, with hot nitrogen introduced into the drying chamber. However, there have been some problems associated with this technique. First, the dynamics of the drying chamber and process can introduce some inconsistencies in performance across the wafer batch. Also, following a spin dry, a very thin film of water remains on the wafers. This film is not visible to the naked eye because its thickness is less than half the wavelength of visible light (1). The water film thickness  $h(t)$  decreases from its initial value  $h_0$  (determined by the withdrawal speed from the final rinse bath) during the dry, as shown in equation 1 (2)

$$h(t) = h_0 [1 - (4\omega^2 \rho h_0^2 t / 3\eta)]^{1/2} \quad [1]$$

where  $\omega$  is the rotational speed in RPM,  $\rho$  is the liquid density,  $\eta$  is the liquid viscosity and  $t$  is time. Figure 1 shows the theoretical film thickness as a function of time for a film of 10 $\mu\text{m}$  initial thickness during spin-drying. Even after 10 minutes at 1000 RPM a liquid film approximately 0.3 $\mu\text{m}$  thick remains on the wafers; solid residues will remain after the film evaporates. There may also be evaporation during the drying process itself. Recently, drying residues have been a particular concern on hydrophobic Si surfaces following hydrofluoric acid (HF-last) processing (3,4).

When using a technique called Marangoni drying, far thinner water films remain on the wafers (1). The technique uses a small amount of vapor of a low surface tension organic liquid such as 2-propanol (IPA) in a nitrogen ambient at room temperature. While the wafer batch is slowly drawn upward from a water bath through this ambient, the water-soluble organic is dissolved into the water so that its concentration in the water is higher in the meniscus near the wafer surface than in the region midway between wafers. This concentration gradient leads to a Marangoni flow of water away from the wafer surface, leaving it dry.

## PARTICLE REMOVAL EXPERIMENTS

Performance data were compared for two wet benches that were identical except that one used a Marangoni dryer and the other a spin dryer, for both hydrophilic and hydrophobic wafers. Both wet benches have been in use for approximately one year. Wafers were run through the following process sequence on the wet benches once a day, with pre- and post-particle counts taken at  $\geq 0.16\mu\text{m}$  using a 3mm edge exclusion:

1. Dilute SC1 ( $\text{H}_2\text{O}/\text{H}_2\text{O}_2/\text{NH}_4\text{OH}$ )
2. Jet Rinse
3. Dilute SC2 ( $\text{H}_2\text{O}/\text{H}_2\text{O}_2/\text{HCl}$ )
4. Jet Rinse
5. Final Rinse
6. Dry (spin or Marangoni)

On average, the Marangoni dryer has demonstrated significantly better performance for particle addition at 0.16 $\mu\text{m}$  (3mm edge exclusion) on average for an SC1/SC2 process. The data in Table 1 represent daily manufacturing test runs for the last 50 days, with the highest and lowest data points ignored in each case.

Table 1. Particle performance of spin-dryer and Marangoni dryer.

50-slot cassette	POINTS	Spin Dry		Marangoni	
		Avg	Std Dev	Avg	Std Dev
Slot #50	48	55.1	90.4	12.9	16.8
Slot #1	48	3.1	21.6	5.5	27.9

### DRYING STAIN EXPERIMENTS

Experiments were performed to assess the drying performance after HF-last processing using wafers with arrays of high aspect ratio trenches (>10:1) with a TEOS mask (Figure 2). The wafers were given a 5nm etch in HF, then rinsed and dried using different dryers. The etch removed only a small percentage of the thick TEOS film, but was sufficient to expose the bare silicon within the trenches. The wafers were then inspected using bright and dark fields at 100-500X using a Polyvar optical microscope. Wafers dried with a Marangoni dryer appeared clean, whereas wafers dried using spin dryers had stains of varied sizes and shapes. The stains tended to appear from the edge of the wafer to about the midpoint between center and edge. They were located in open areas between the trench arrays, and most easily visible using bright-field optics. The stains appeared to stop at the edges of trench arrays. Several different types of stains were observed:

- Type 1: Large, approximately circular stains with more concentrated regions of precipitate near the edges of the stain (spin dryers #1 and #3).
- Type 2: Long, narrow streaks along array edges; many had "heads" at the end pointing toward wafer edges (spin dryers #1, #2 and #3).
- Type 3: Small stains in a line, resembling a series of drips (spin dryers #1, #2 and #3).
- Type 4: Large stains in "clamshell" shapes, with striations on the sides closer to the center of the wafers (spin dryer #2).
- Type 5: Large, circular stains with more concentrated circular regions of precipitate (resembling a "bullseye") in the centers (spin dryer #2).

Figure 3 shows a Type 1 stain from spin dryer #1 against the edge of a trench array. The size scale of the stain is on the order of 100µm. Figure 4 shows a Type 2 stain from spin dryer #2 and indicates that the water streak was moving toward the edge of the wafer (right side of the picture) until it stopped at the edge of the trench array. Finally, Figure 5 shows a Type 4 stain, also from spin dryer #2; the stains stop at the edge of trench arrays because the surface under the stains is TEOS (hydrophilic) whereas the dense array structure tends to be hydrophobic.

A wafer was also run through a 5nm etch in a plug flow type processor with an IPA dry. Drying stains were not observed on this wafer. When the stained wafers were run through a 5nm etch followed by a Marangoni dry, the stains were completely removed.

The experiments demonstrated that the Marangoni dryer works well for HF-last processing where bare silicon is exposed. Furthermore, ESCA analysis revealed no residual organics from IPA after Marangoni drying. Finally, TXRF analysis comparing the two dryers after SC1/SC2 processing in otherwise identical wet benches indicated that both dryers perform without adding metals. The TXRF data shown in Table II represent a control (no processing) wafer and wafers run through spin and Marangoni dryers. The incoming wafers had some Cu and Zn contamination, as seen in the control wafer data, but this was removed.

Table II. TXRF data comparison for spin and Marangoni dry ( $\times 10^{10}$  atoms/cm $^2$ ).

Sample	S	Cl	K	Ca	Ti	Mn	Fe	Ni	Cu	Zn
Control	---	---	---	---	---	---	---	---	---	---
Spin Dry	196	78	19	39	2	1	2	<4	13	30
Marangoni	205	79	20	37	1	3	2	<7	0	1
	209	65	19	33	2	1	1	<5	<DL	4

## DISCUSSION

Wafers with large areas of exposed bare silicon, such as high aspect ratio trenches, are vulnerable to drying stains after HF-last processing. Other studies have concluded (3-5) that the stains can be traced to the rinse after HF. The rinse, essentially saturated with dissolved oxygen which can slightly etch exposed Si (even at ambient temperature), results in the formation of a hydrated silicon oxide (silicic acid (5)) in the film of rinse water adjacent to the wafer surfaces. During the dry step the water comes out of the trenches. During a spin dry, the water film is thinned as previously described. As the water film thins and the silicon oxide remains in the film, the silicon oxide concentration increases and eventually precipitates can form. As the water evaporates, the precipitated silicon oxide remains on the wafer surface.

## CONCLUSION

This study compared spin and IPA-type dryers relative to the formation of large-scale drying stains on wafers with large areas of exposed bare silicon subjected to HF-last processing. At the magnifications used, drying stains were always observed on centrifugally dried wafers but never observed on Marangoni-dried wafers. Stains were also not observed on wafers dried

in a 100% IPA vapor dry. The results indicate that for wet benches the Marangoni dry process, because it avoids evaporation of water on the wafer surface, does not have the drying stain problem. Alternatives for HF processing in the presence of bare Si include reoxidizing the surface using an SC1-type process or ozonated rinse, but such techniques are not always valid options if a truly bare silicon surface is required.

#### ACKNOWLEDGEMENTS

The authors wish to acknowledge Ed Adams, Hiro Akatsu, Rick Amos, Russ Arndt, Bill Bowers, Jim Elliott, Pegs Gibson, Klaus Penner, and Klaus Wolke for their assistance and/or useful discussions regarding this work.

#### REFERENCES

1. Marra, J., and Huethorst, J. A. M., *Langmuir*, **7**, 2748 (1991).
2. Meyerhofer, D., *J. Appl. Phys.*, **49**, 3993 (1978).
3. MacKinnon, S., *Proceedings, Microcontamination '94*, 174 (1994).
4. Park, J., and Pas, M. F., *J. Electrochem. Soc.*, **142**, 6, 2028 (1995).
5. Watanabe, M., Hamano, M., and Harazono, M., *Mat. Sci. Eng.*, **B4**, 401 (1989).

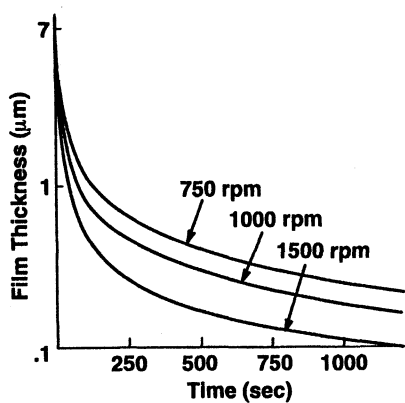


Figure 1. Film thickness remaining on spin-dried wafer as a function of dry time at various rotational speeds.

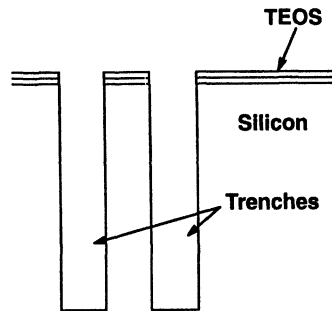


Figure 2. Cross section of the structures used on drying stain test wafers.

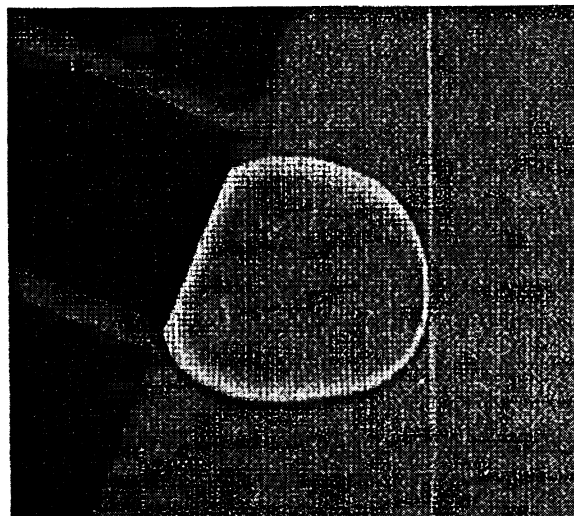


Figure 3. A type 1 stain from spin dryer #1; the size scale of the stain is on the order of 100  $\mu\text{m}$ .

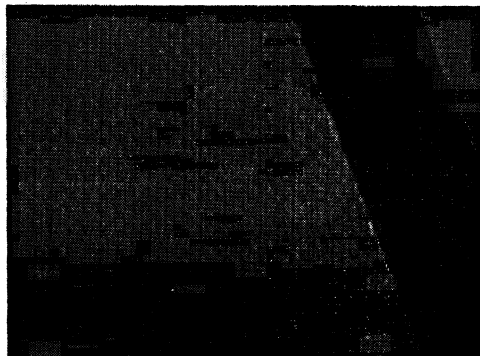


Figure 4. A type 2 stain from spin dryer #2.

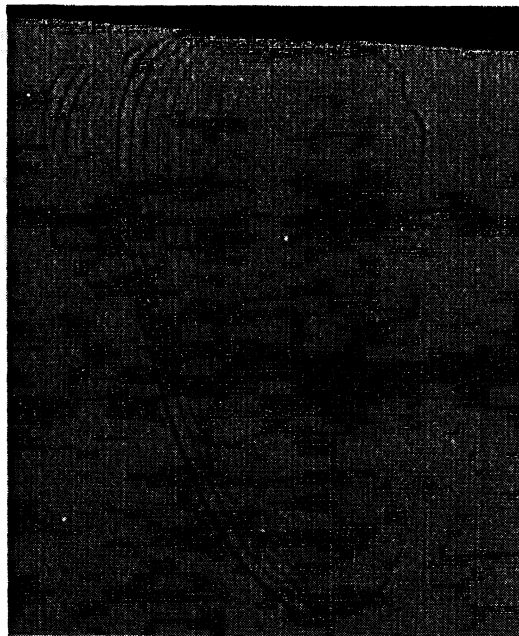


Figure 5. A type 4 stain from spin dryer #2. The edge of the wafer is to the right (out of the picture).

# THE EFFECTS OF OXYGEN PASSIVATION OF SILICON BY WET CLEANING PROCESSES ON CONTAMINATION AND DEFECTS

S. L. Nelson  
FSI International  
322 Lake Hazeltine Drive, Chaska, MN 55318-1096, USA

High-concentration ozonated water is used to grow a thin layer of oxide on a silicon surface after a dilute hydrofluoric acid (HF) step. The thickness of this oxide layer can be measured using an ellipsometer. After characterization of the effects of ozonated water dispense time and ozone concentration on the oxide thickness, the degree of oxygen passivation of the silicon can be controlled. The oxide thickness, which is a measure of the degree of oxygen passivation, was found to be an important property of the silicon surface. Experiments were performed using an ozonated water process that passivates the silicon surface as completely as possible with oxygen. These results were compared with processes that result in incomplete oxygen passivation of the silicon surface. It was found that the degree of oxygen passivation of the silicon surface affects the susceptibility of the surface to particle contamination and the susceptibility of the surface to organic contamination.

## INTRODUCTION

It is well documented that the cleanliness of process chemicals and DI water are very important to minimizing the contamination of silicon wafers by a wet cleaning processes (1). Also important is the implementation of each individual step in the cleaning process. Parameters of a step that can affect the contamination on the surface include the condition of the surface upon exposure to the chemical, the type of chemical used, the chemical mixture, chemical concentration, temperature, and exposure time. Often there are two or more requirements for a step in the cleaning process. An example would be a step that removes particle contamination while at the same time not depositing particle or metallic contamination. For an ozonated water step after a dilute HF step, these parameters must be optimized so that the chemical state of the surface is stable and the contamination of the silicon surface is minimized. To determine the optimal implementation for an ozonated water step after a dilute HF step, the effect of ozone concentration and ozone dispense time on the growth of a stable layer of silicon oxide will be discussed. Then the effect that the silicon oxide layer thickness has on particle contamination and organic contamination will also be shown.

## EXPERIMENTAL

The experiments for this paper were performed in an FSI MERCURY® MP acid spray processor using 150-mm wafers. The machine was programmed to dispense 90 seconds of sulfuric acid and hydrogen peroxide (SPM) 4:1, followed by 120 seconds of 0.5 volume % HF, and then ozonated water ( $O_3$ ). Cold DI water rinses were performed before each of the chemical steps and a hot (95° C) DI water rinse and a spin dry were the last steps performed. All these steps occur in an uninterrupted sequence inside a single process chamber that has an inert nitrogen gas environment.

The ozone generator in these experiments uses a dielectric discharge tube to generate ozone gas. The ozone gas is then dissolved into DI water in a Teflon® contactor that results in dissolved ozone concentrations that can be varied from 1.0 ppm up to 50.0 ppm by changing the ozone gas concentration. The ozonated water is plumbed to the MERCURY MP at one of the manifold flow systems so that the flow of ozonated water into the process chamber is controlled to 1500 cc/min. The temperature of the DI water into which the ozone is dissolved is 22° C.

## ANALYTICAL TECHNIQUES

A RUDOLPH FOCUS ellipsometer was used to measure the thickness of the oxide layer that is grown on the silicon. Five points were measured on each sample and the average and standard deviation were calculated. The optical constants that were used for these measurements were fixed: substrate index of refraction = 3.858, substrate extinction coefficient = 0.018, and film index of refraction = 1.462. All measurements were made within five minutes after removing the wafers from the process chamber to minimize the effect that organic contamination has on ellipsometry. New prime wafers were used to minimize the effect that surface microroughness has on ellipsometry.

The number of light point defects on the silicon surface was measured with a TENCOR 6200 particle counter. Test wafers were placed in slots 1, 5, 10, 15, 20, and 25 of a cassette with filler wafers in the remaining slots of the cassette. The number of particles added by the cleaning process was calculated by subtracting the pre measurement from the post measurement for each wafer. The average number of particles added and the standard deviation were calculated for each run. Particles were measured and reported at greater than or equal to 0.15  $\mu m$  diameter.

The amount of carbon contamination on the silicon surface was measured with an AUGER spectrometer. The spectra from the samples are reported after they have been differentiated. The accuracy of these measurements as shown by the error bars was taken to be 20% of the reading.

## RESULTS AND ANALYSIS

### Degree of Oxygen Passivation

After an HF step, the native oxide layer on the surface has been removed and the surface is passivated with no more than a mono-layer of hydrogen (2). A measurement of the oxide thickness for a surface prepared in this way is shown in figure 1 as zero minutes ozone dispense time. The non-zero measurement is due to a combination of surface microroughness, adsorbed hydrocarbon contamination, and error in the optical constant values. Starting from this hydrogen-passivated surface, an oxide layer begins to grow immediately when ozonated water is dispensed onto the surface. Figure 1 shows that the higher the dissolved ozone concentration, the faster the rate of oxidation because more ozone molecules are available to react with the surface. Due to the mechanism of low-temperature oxide growth, explained by the Cabrera-Mott oxidation model, the oxide will only grow to about 10 Å thickness at room temperature or about three monolayers of silicon oxide (3)(4). At this point the silicon surface is passivated as completely as possible with oxygen and any additional ozone dispense has no effect on the surface. The mechanism of oxidation is not strong enough to overcome the activation energy barrier for the oxide to continue growing. This oxide layer will be stable unless the temperature of the wafers is increased in the presence of an oxidizing gas or liquid. Using a 10.0 ppm concentration of dissolved ozone, a 10-minute dispense time is required to completely passivate the silicon surface. Using a 50.0 ppm concentration of dissolved ozone, a 2-minute dispense time is required to completely passivate the silicon surface.

### Surface Energy

A measure of the relative energy of a surface is the contact angle of a water drop that is placed on the surface. The contact angle is an indicator of the equilibrium between the surface area of the drop and the solid/liquid repulsive force. The contact angle of a water drop on a hydrogen-terminated surface was measured to be 72 degrees. A drop, of a given volume, with a 72-degree contact angle has a small surface area, so the relative Gibbs free energy of the silicon surface will be high. Figure 2 shows that as the degree of oxygen passivation of the surface is increased, the contact angle of a water drop on the surface decreases. A drop, of the same volume, with a low contact angle has a large surface area, so the relative Gibbs free energy of the silicon surface will be low. Figure 2 shows that between the extremes of hydrogen-termination and oxygen-passivation there is a good correlation between the contact angle of a drop on the surface and the thickness of the oxide that is grown on the surface. Ellipsometry is a better technique for measuring the oxygen-passivated surface because it has a higher sensitivity. Contact angle is better for measuring the hydrogen-terminated surfaces because it has a higher sensitivity.

### Particle Contamination

Figure 3 shows that the average number of particles added to six wafers per run over a total of 14 runs is  $2.2 \pm 6.9$  at  $0.15 \mu\text{m}$  particle size on 150-mm wafers. The cleaning process used to generate this data is an SPM\HF\O<sub>3</sub> process with a 10-minute ozone step, using 10.0 ppm dissolved-ozone concentration. The particle-added data appears to be stable from run to run and the distribution can be modeled by a gaussian function, allowing statistical tests to be performed. The information in figure 3 is summarized in figure 4 as the data point on the far right side of the graph. Information from three similar data sets for processes having 1-minute, 3-minute, and 5-minute ozone steps and 10.0-ppm, dissolved-ozone concentration is also included, ordered from left to right in the graph. The effect of the different ozonated-water dispense times is that the surface has different degrees of oxygen passivation, as shown on the x-axis of figure 4. The trend in the data shows that as the silicon surface is passivated more completely with oxygen, the average number of particles added by the process is lower. A statistical t-test shows that, with greater than 99% confidence, the 10-minute ozone dispense added fewer particles than the 3-minute ozone dispense. The same test shows that, with greater than 95% confidence, the 10-minute ozone dispense added fewer particles than the 5-minute ozone dispense. The data also shows that the standard deviation of the particle contamination is reduced by improving the oxygen passivation of the surface.

There are several possible explanation for this data. During the dry step, if the relative Gibbs free energy of the surface is low, fewer islands of water will form that will leave behind a particle when they evaporate. The relative Gibbs free energy of the surface may instead affect the zeta potential of the surface when it is being rinsed and results in fewer particles being added during the final rinse. Last, if the relative Gibbs free energy of the surface is reduced, the van der Waals force that holds particles to the surface may be reduced, resulting in fewer particles remaining after the process is complete.

### Organic Contamination

The atomic concentration of carbon adsorbed on the surface of wafers that have been processed in an SPM\HF\O<sub>3</sub> process and then placed in a polypropylene single-wafer storage container was measured using AUGER spectroscopy. The wafers were processed in the order: 10-minute ozone step, 5-minute ozone step, 1-minute ozone step. These wafers were measured in the same order so that each wafer was in the storage box for the same period of time, 2 hours. Because the wafers were initially clean and the SPM step in the process removes organic contamination, any difference in the samples will be due to re-adsorption of organic contamination from the cleanroom environment (5) or from the wafer storage box (6). Figure 5 shows that a completely passivated silicon surface is much less susceptible to carbon contamination. Figure 6 shows the actual

differentiated AUGER spectra for two of the samples; the top sample has been passivated as completely as possible with oxygen and the bottom sample has an incomplete oxide-passivation layer. A possible explanation for this data is that when the relative Gibbs free energy of the surface is reduced, the sticking coefficient of organics on the surface may also be reduced. The result will be a lower adsorption rate and a lower equilibrium concentration of organics on the surface.

## CONCLUSIONS

Ozone gas dissolved in DI water is used to grow a thin layer of oxide on the silicon surface. The surface can be oxidized as completely as possible in 2 minutes using a concentration of 50-ppm ozone. The silicon surface that is completely passivated with oxygen using an ozonated water process will be stable because the silicon will not continue to oxidize. The data in this paper has shown that the more complete the oxygen passivation of the silicon surface and the lower the relative Gibbs free energy of the surface, the surface susceptibility to particle contamination and organic contamination is proportionally reduced.

## REFERENCES

1. R. P. Donovan and V. B. Menon, *Handbook of Semiconductor Wafer Cleaning Technology*, W. Kern, Editor, p. 167-170, Noyes Publications, Park Ridge, NJ (1993).
2. H. Bender, S. Verhaverbeke, and M. M. Heyns, *J. Electrochem. Soc.*, **141**, 3128 (1994).
3. S. L. Nelson, R. T. Fayfield, K. K. Christenson, and B. E. Deal, *Proceedings of the Third International Symposium on Ultra Clean Processing of Silicon Surfaces/1996*, M. Heyns, M. Meuris, and P. Mertens, Editors, p. 287, ACCO, Leuven, Belgium (1996).
4. F. P. Fehlner, *Low Temperature Oxidation: The Role Of Vitreous Oxides*, p. 149-156, Wiley Interscience, New York (1986).
5. A. J. Muller, L. A. Psota-Kelty, H. W. Krautter, J. D. Sinclair, F. A. Stevie, E. P. Martin, P. M. Kahora, and A. K. Nanda, *Proceedings of the Symposium on Contamination Control and Defect Reduction in Semiconductor Manufacturing II/1994*, R. Novak, T. Ito, D. N. Schmidt, and D. Reedy, Editors, *PV 94-3*, p. 143, The Electrochemical Society, Pennington, NJ (1994).
6. K. Saga, and T. Hattori, *Proceedings of the Third International Symposium on Ultra Clean Processing of Silicon Surfaces/1996*, M. Heyns, M. Meuris, and P. Mertens, Editors, p. 299, ACCO, Leuven, Belgium (1996).

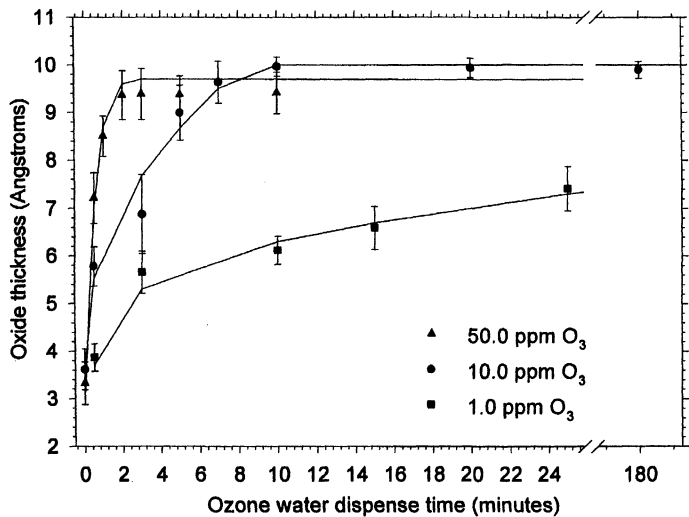


Figure 1: Shows the final oxide thickness and the oxidation kinetics for three different dissolved ozone concentrations. 22° C, <100>, Arsenic doped, 10-14 ohm-cm.

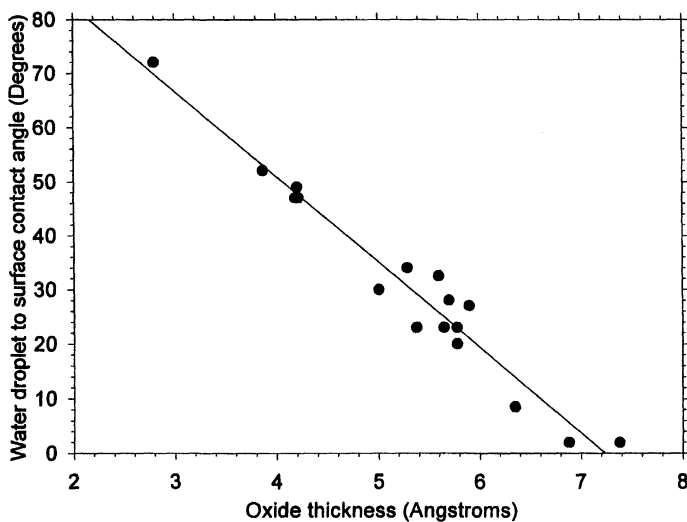


Figure 2: Shows the correlation between surface energy as measured by the water drop contact angle and the degree of oxygen passivation

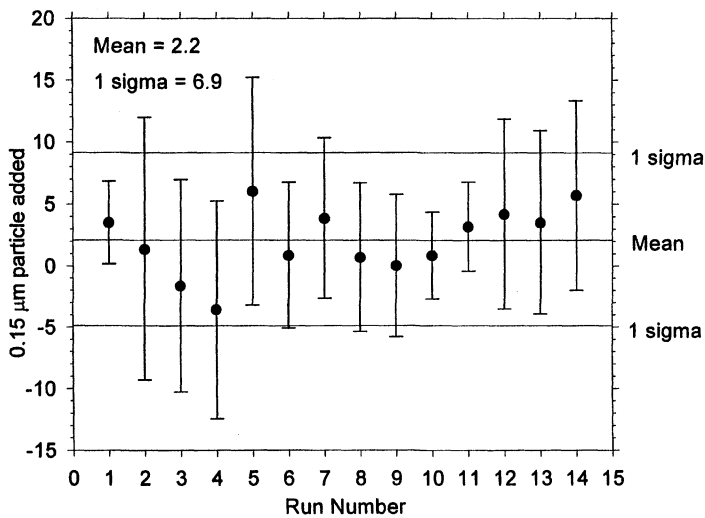


Figure 3: Shows the results of particle contamination,  $\geq 0.15 \mu\text{m}$ , for a process using 10.0-ppm ozonated water, 10-minute dispense time. Average of six wafers.

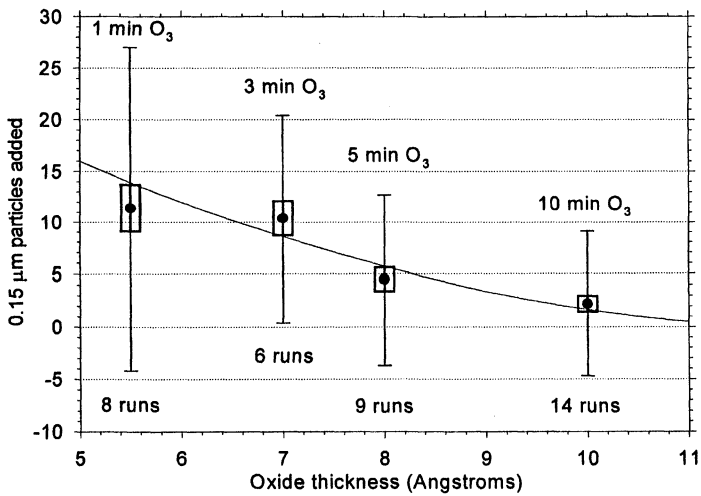


Figure 4: Shows the effect of improved oxygen passivation of the silicon surface on the particle contamination. O<sub>3</sub> concentration of 10.0-ppm. Error bar is 1 sigma standard deviation. Error box is RMS error of the mean.

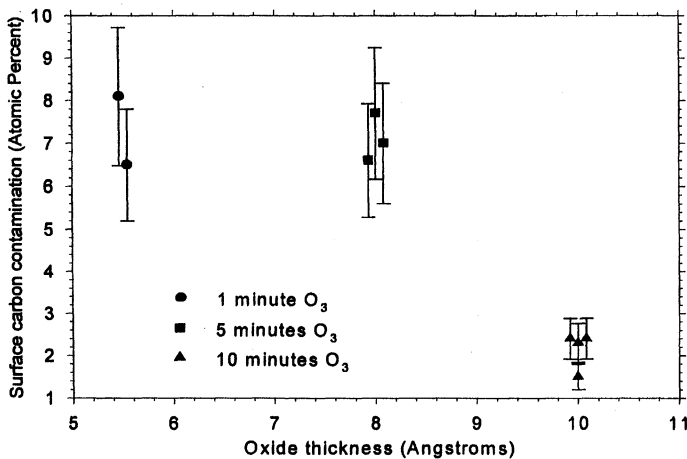


Figure 5: Shows the percentage of carbon on the silicon surface for three different degrees of oxygen passivation using ozonated water.

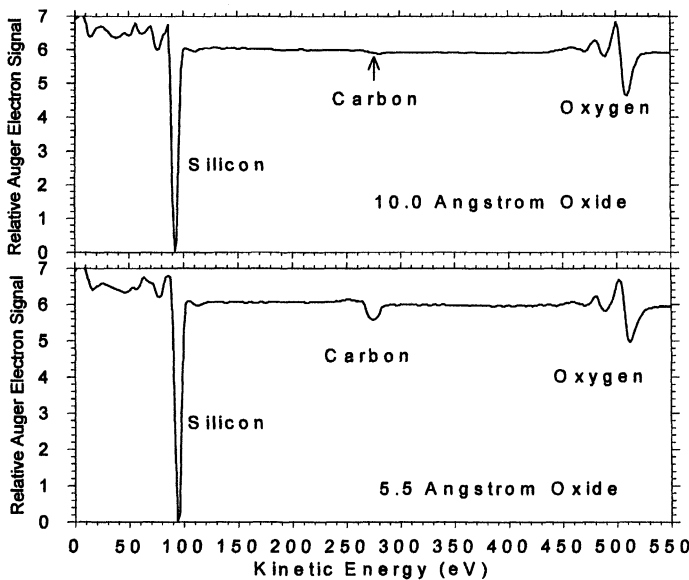


Figure 6: The differentiated AUGER spectra for a silicon surface with a compete oxide passivation layer (top) and an incomplete oxide passivation layer (bottom).

# WET CHEMICALLY PASSIVATED SILICON SURFACES: ELECTRONIC PROPERTIES CORRELATED TO THE SURFACE MORPHOLOGY

H. Angermann<sup>1</sup>, W. Henrion<sup>1</sup>, A. Röseler<sup>2</sup>, J.-T. Zettler<sup>3</sup>, M. Rebien<sup>1</sup>, H. Flietner<sup>1</sup>

<sup>1</sup> Hahn-Meitner-Institut, Abt. Photovoltaik; Rudower Chaussee 5, D-12489 Berlin, Germany

<sup>2</sup> Institut für Spektrochemie und Spektroskopie, Rudower Chaussee 5, D-12489 Berlin, Germany

<sup>3</sup> Institut für Festkörperphysik, Techn. Universität Berlin, Hardenbergstr. 36, D-10623 Berlin, Germany

By combining SPV and SE measurements monitoring the preparation process, a correlation was established between the morphological structure of the chemically cleaned Si-surface and the resulting density and energetic distribution of interface states. By applying a special Hydrogen-termination procedure, very smooth Si (111) surfaces were obtained, which were characterised by an intrinsic surface state distribution and a low surface state density  $D_{it,min} \approx 1.5 \times 10^{10} \text{ cm}^{-2} \text{ eV}^{-1}$ . The changing number of Si-H bonds on a Si(111) surface during native oxidation in air was detected by a characteristic structure in the IR ellipsometric spectra at  $2082 \text{ cm}^{-1}$ . Because only a single reflection is necessary, FT-IR ellipsometry is capable of routinely sensing the extent of H-termination of standard wafers. By hot water treatment of H-terminated surfaces, thin passivating oxide layers up to  $15\text{\AA}$  thickness were prepared.

## INTRODUCTION

Wet chemical treatments are conventionally used in semiconductor processing to remove particles, organic, and metallic contaminants. In order to prepare thin silicon hetero-structures with excellent electronic properties it is necessary to start the subsequent deposition or oxidation with microscopically smooth, chemically and electronically passivated surfaces. The electronic properties of Si interfaces are defined by the density and the character of interface states. These interface states originate from dangling bond (DB) defects, localised in an interlayer only a few Å thick. Therefore, they are strongly influenced by the chemical integrity and the morphological structure of the surface prior to preparation. Wet chemical passivation methods can be classified into two groups according to the underlying passivation mechanisms: the surface passivation (i) by Hydrogen (H)-termination and (ii) by thin chemical oxide layers prepared under carefully optimised conditions.

In this paper we report on the combined monitoring of electronic, chemical, and morphological interface properties during different wet chemical pre-cleaning treatments. By simultaneous surface photo voltage (SPV) and spectroscopic ellipsometry (SE) measurements, we established a correlation between the morphological structure of the chemically cleaned Si-surface and the resulting density and energetic distribution of interface states. We utilised the large-signal field-modulated SPV technique for contactless measurement of the surface band-bending ( $Y$ ) and of the energetic distribution of surface states ( $D_{it}(E)$ ).

Ultraviolet-visible (UV-VIS) Spectroscopic ellipsometry is a surface-sensitive and non-destructive method for detecting roughness and submonolayer coverage during processing of silicon surfaces (1). Compared to UV-VIS SE, infrared (IR)-SE has the

general advantage that vibrational modes can be directly observed through characteristic, energetically sharp structures in the measured spectra. As recently shown, the degree of H-bonds on a H-terminated Si(111) surface during the initial phase of oxidation can be measured by sensing the Si-H vibrational resonance by Fourier-Transform (FT)-IR ellipsometry (2). In contrast to the former Attenuated Total Reflection (ATR) work (3), the FT-IR SE utilises only a single reflection for sensing the Si-H vibrational resonance and can therefore be used for standard wafer characterisation.

## EXPERIMENTAL

Using polished p- and n-type Si(111) and Si(100) wafer, we started the preparation of Hydrogen-terminated Si-surfaces by the conventional RCA cleaning (4). After removing the native oxide, the wafers were chemically reoxidized by applying three different procedures: (i) deionised water at 80° C for 120 minutes, (ii) boiling solution of H<sub>2</sub>SO<sub>4</sub>:H<sub>2</sub>O<sub>2</sub> (1:1) for 10 minutes - a standard procedure described by Chabal (5), and (iii) RCA II solution at 80° C for 10 minutes. Finally, the Hydrogen-termination was completed by placing the wafers into pure Ammoniumfluorid solution (40%, pH = 7.8) for 6.5 min.

H-terminated atomically smooth samples were additionally treated (5 to 600 sec) in HF (48%) solution for preparing a set of samples with a systematic and well defined increase in surface roughness. To investigate the native oxidation of H-terminated surfaces, the samples have been stored in clean-room air (temperature 25 °C, humidity about 50%). Wet chemical oxide layers on H-terminated surfaces were prepared in deionised water (18 MΩcm resistivity, at 80° C) with exposition times ranging from 2 to 440 min.

The UV-VIS SE was carried out ex-situ immediately after preparation using a commercial spectroscopic ellipsometric system (Woollam Co., Inc (6)) in the 3.2 - 4.5 eV photon energy range. The angle of incidence was 77 ± 0.02°. As usual, the directly measured complex reflectivity ratio has been transformed to the complex effective dielectric function  $\langle\epsilon\rangle$  by assuming a three-media model consisting of ambient, rough layer and bulk silicon. The rough surface was modelled by the Bruggemann effective medium approximation, assuming a mixture of 50% bulk Si (7) and 50% voids. The thickness of native oxides on previously H-terminated surfaces was derived from a fitting procedure of a SiO<sub>2</sub> layer on top of a Si bulk material that uses the SiO<sub>2</sub> and Si bulk dielectric function data from (8). For the infrared region (400-4000 cm<sup>-1</sup>), a photometric ellipsometer was used (9), which is coupled to a FT-Spectrometer (BRUKER IFS55) set to a resolution of 4 cm<sup>-1</sup>. From four polariser settings the  $|\rho| = \tan(\Psi)$  and  $\arg(\rho) = \Delta$  spectra are calculated. The angle of incidence was 65 ° and the MCT-detector output was corrected for the non-linearity. For a precise measurement of  $\Delta$  in the range of 0° ≤  $\Delta$  ≤ 360° and to reduce depolarisation effects due to reflections from the sample backside, a reflection retarder (KR55-Prism) with approximately 90° retardation (10) was used.

We applied the pulsed field modulated SPV for contactless measurements of the surface potential using a mica foil dielectric spacer in the same experimental configuration as described in (13). The SPV measurements were performed under flowing dry N<sub>2</sub>. A pulsed laser diode (150 ns, wavelength λ = 904 nm and power P = 150 W) was used for flashing

the sample. From a large-signal photovoltage pulse the surface potential was obtained.  $D_{it}(E)$  was determined from a series of photovoltage pulses measured with different field voltages between the transparent electrode and the wafer (11).

## ELECTRONIC PROPERTIES OF THE Si/SiO<sub>2</sub> INTERFACE

The minimal values of the density of interface states  $D_{it,min}$  influencing the electronic interface properties (ranging from  $10^{10}\text{eV}^{-1}\text{cm}^{-2}$  to  $10^{14}\text{eV}^{-1}\text{cm}^{-2}$ ) are typically at least several orders of magnitude less than that of surface atoms (12). Our recently reported results demonstrated that the SPV technique is sufficiently sensitive to determine the surface band-bending Y and the energetic distribution of the interface states  $D_{it}(E)$  on chemically treated silicon surfaces (13).

The continuous energetic distribution of rechargeable interface states as determined by SPV methods can be separated into several groups of states. Following the dangling bond model for the Si/SiO<sub>2</sub> interface (14), two groups of intrinsic states,  $U_T$  resulting from strained ( $\text{Si}_3\equiv\text{Si}-\text{Si}\equiv\text{Si}_3$ ) bonds and  $U_M$  resulting from DB defect centres back-bonded only to silicon ( $\text{Si}_3\equiv\text{Si}-$ ), give rise to U-shaped distributions. DB defects correlated to Si atoms of different state of oxidation,  $\text{Si}^{+1}$  ( $\text{Si}_2\text{O}\equiv\text{Si}-$ ) and  $\text{Si}^{+2}$  ( $\text{SiO}_2\equiv\text{Si}-$ ), additionally form Gaussian distributions of extrinsic states  $P_L$  and  $P_H$  in the lower and upper half of the gap, respectively. After chemical etching, silicon surface states originate from DB defects with different back-bond configurations. The saturation of dangling bonds by Hydrogen removes these surface states and replaces them by adsorbate-induced states influencing the surface band-bending.

## RESULTS AND DISCUSSION

### Surface State Density on H-Terminated Surfaces Correlated to the Surface Roughness

On conventionally cleaned and etched surfaces we observed a high surface state density, resulting from surface roughness and unintentionally grown native oxides (2). Various chemical treatments using HF and NH<sub>4</sub>F solutions have been developed to dissolve the native oxide completely and to passivate the surface with hydrogen (5). In order to investigate the influence of the chemical reoxidation process on the final surface state density, different treatments have been applied.

Fig. 1 shows the  $D_{it}(E)$  distributions on the differently prepared surfaces and the imaginary part of the effective dielectric function  $\langle\varepsilon_2\rangle$  obtained by simultaneous SE measurements on the same samples. The magnitude of  $\langle\varepsilon_2\rangle$  at the E<sub>2</sub> bulk critical point energy of approximately 4.24 eV can be taken here as a measure of the smoothness of the surface. Successfully H-terminated surfaces are characterised by an intrinsic like surface state distribution and very low surface state densities. The minimal values of the surface state distribution ( $D_{it,min}$ ) after different treatments were found to be strongly influenced by the effective surface roughness  $\langle d_r \rangle$ . The lowest value  $D_{it,min} < 1.5 \times 10^{10} \text{ cm}^{-2} \text{ eV}^{-1}$  was obtained

on the smoothest, hot water pre-treated H-terminated Si(111) surface (curve a). On Si(100), generally higher values of  $\langle d_r \rangle$  and  $D_{it,min}$  ( $3 \times 10^{11} \text{ cm}^{-2} \text{ eV}^{-1}$ ) were found (curve d), resulting from the anisotropic etching behaviour of the NH<sub>4</sub>F solution.

#### Surface State Distribution on HF-Treated Surfaces Correlated to the Surface Roughness

In order to further elucidate the correlation between the effective roughness and  $D_{it,min}$ , we systematically increased the roughness of a very smooth H-terminated Si(111) n-type surface by an additional HF treatment of varying duration. In Fig. 2 the resulting surface state density  $D_{it,min}$  is plotted versus the measured effective surface roughness  $\langle d_r \rangle$ . Obviously, after HF-treatment the density of surface states increases stepwise when the surface roughness  $\langle d_r \rangle$  exceeds one, two and three monolayers.

The surface state distributions and the corresponding SE data measured on HF (48%) treated p-type Si (111) surfaces after different exposure times (ranging from a few seconds to three minutes) are shown in Fig. 3. The surface state density  $D_{it,min}$  on HF-treated p-type surfaces was found to be also strongly dependent on the remaining surface roughness after different HF treatment times. Moreover, the energetic distribution of surface states changed when the surface roughness increased. While the flat H-terminated surface is characterised by an U-shaped intrinsic-like surface state distribution, on HF (48%) treated surfaces a group of extrinsic states additionally appears as soon as the surface roughness exceeds two monolayer. These extrinsic states  $P_L$ , forming Gaussian distributions in the lower half of the forbidden gap, are caused by DB defects correlated to Si atoms of low state of oxidation, Si<sup>+1</sup>. The occurrence of oxygen back-bonded Si DB defects indicates that the atomically rough surface is not completely H-terminated. We regard the competition between reactions of various nucleophilic components (H<sub>2</sub>O and OH<sup>-</sup>) of the HF solution, resulting in Si-OH groups on the surface, to be the reason for the appearance of these defects. Our results suggest that these reactions cause extrinsic states and take place preferentially at crystallographic defects when the surface roughness increases.

#### Change of Interface State Distribution During Native Oxide Growth in Air

SPV, FT-IR and UV-VIS SE measurements were performed to monitor the native oxidation of the previously H-terminated surface in air. As recently reported the Si-H bonds on successfully H-terminated surfaces can be directly detected by IR-SE measurement (2). The bond vibrational stretching resonance causes a dispersion like structure  $\delta_{max}$  in the  $\Delta$  spectrum and a minimum in the  $\tan \Psi$  spectrum at  $2082 \text{ cm}^{-1}$  (Fig. 4a, b). These features can be modelled by a Lorentz oscillator at  $2050 \text{ cm}^{-1}$  that represents the IR dielectric properties of the H-terminated surface by assuming an anisotropic surface layer with an effective thickness of 0.2 nm (Fig. 4c). Fig. 5 shows the decrease of the relative number  $N_{rel} = \delta / \delta_{max}$  of the Si-H oscillators (proportional to the number of Si-H bonds on the surface) and the increasing effective thickness  $\langle d_{ox} \rangle$  of the native oxide film as a function of storage time in air.  $\langle d_{ox} \rangle$  was derived from UV-VIS SE measurements on the same sam-

ple. The reduction in the number of Si-H bonds during the initial phase of oxidation complementary to native oxide growth is clearly shown.

Fig. 6 shows  $D_{it}$  (E) curves obtained by the SPV measurements on the same previously H-terminated surface immediately after preparation and during storage in air correlated to the effective oxide coverage  $\langle d_{ox} \rangle$ . As detected by the characteristic U-shaped distribution (curve 1), the successfully prepared H-terminated surface is dominated by intrinsic defects. During the first 24 h storage in air, when according to the IR-SE data the hydrogen coverage is reduced to less than 50% and the effective oxide coverage reaches around 50% of a monolayer, the surface state distribution shows a weak increase of intrinsic defect states by a factor of about 4 (curve 2). The surface state distribution changes drastically when the effective native oxide thickness exceeds one monolayer. An increasing density of intrinsic states and an additional appearance of extrinsic states  $P_L$  are to be observed after 48 h, when the hydrogen coverage decreases and the  $\langle d_{ox} \rangle$  exceeds one monolayer (3). During further native oxide growth the density of these states caused by the  $Si^{+1}$  DB defects decreases while the  $P_H$  group correlated to the  $Si^{+2}$  DB defects additionally appears (4). The native oxide grown in air causes such a high surface state density  $D_{it,min} > 10^{12} eV^{-1} cm^{-2}$  that the wafer can not be used successfully for further preparation of thin hetero-structures.

#### The Change of Interface State Distribution During Oxidation in Hot Water

Wet chemical methods conventionally used to prepare thin native oxide layers are mainly based on  $H_2O_2$  containing solutions which increase the silicon surface micro-roughness as a side effect to the  $H_2O_2$  decomposition. As recently shown, they result in high values of positive surface charge and high surface state densities (15). To avoid both, micro-roughness and contaminated native oxides, we started the preparation of thin passivating oxide layers on very smooth H-terminated surfaces applying a hot water treatment. The thicknesses of the oxide films ranging from 0 to 17 Å were derived from UV-VIS SE measurements as described in (15). Simultaneously SPV measurements (Fig. 7) show the changing densities of the extrinsic states during layer by layer oxide growth. The evolution of extrinsic defects correlated to the oxide growth (a) and the corresponding shift of surface band bending Y (b) are shown in Fig. 8. The initial phase of oxidation is characterised by a drastic increase of the density of intrinsic states and the appearance of a group of extrinsic states below mid-gap. Later on, when the second monolayer is formed, the density of these states below midgap decreases while another group of Gaussian distributed states additionally appears in the upper part of the gap. During further oxidation, these extrinsic defects also decrease and finally an again nearly intrinsic final surface state distribution is to be found. The interface state density  $D_{it,min}$  of about  $4 \times 10^{11} cm^{-2} eV^{-1}$  after the hot water oxidation was found to be significantly lower than that of conventionally wet chemically oxidised surfaces and of thermally prepared oxide layers in the thickness range below 3 nm (15). We assume the very slow oxide growth on the atomically flat H-terminated surface to result in a well ordered interface already during the formation of the first monolayers.

## SUMMARY

The influence of preparation-induced surface roughness and the hydrogen and oxide coverage on electronic properties of H-terminated Si surfaces was investigated by the combination of two surface sensitive techniques SE and SPV. It was shown that the density of states on H-terminated surfaces strongly depends on the atomic scale surface roughness after NH<sub>4</sub>F- and HF-treatments, respectively. By applying a special wet chemical oxidation pre-treatment, very smooth Si (111) surfaces, characterised by an intrinsiclike surface state distribution and a very low surface state density  $D_{it,min} < 1.5 \times 10^{10} \text{ cm}^{-2} \text{ eV}^{-1}$  were prepared.

Simultaneous FT-IR SE, UV-VIS SE, and SPV measurements yielded detailed information on the evolution of intrinsic and extrinsic interface states during the initial oxidation of previously H-terminated Si(111) surfaces. The evolution of dangling bond defects was correlated to the change of hydrogen coverage and the oxide growth on an atomic scale. As shown by these experiments, the surface electronic properties change drastically by the appearance of extrinsic states after an initial storage time in air when the Hydrogen coverage disappears and the effective native oxide thickness exceeds one monolayer. The density of extrinsic states can be significantly reduced by wet chemical oxidation of H-terminated surfaces on carefully optimised conditions. The results of these systematic investigations have been successfully used for the wet chemical oxide preparation by a hot water treatment yielding a passivation layer up to 15 Å thickness with surface state densities of about  $4 \times 10^{11} \text{ cm}^{-2} \text{ eV}^{-1}$ .

## REFERENCES

1. E. A. Irene, Thin Solid Films **233**, 96 (1993).
2. H. Angermann, W. Henrion, M. Rebien, D. Fischer, J.-T. Zettler and A. Röseler, in Sec. Int. Conf. on Spectroscopic Ellipsometry ( ICSE - 2/1997), to be publ. in Thin Solid Films.
3. G. S. Higashi, Y. J. Chabal, G. W. Trucks, and K. Raghavachari, Appl. Phys. Letters **56** (7), 656 (1990).
4. W. Kern, Surf. Sci. **31**, 207 (1970).
5. Y. A. Chabal, G.S. Higashi, K. Raghavachari, and V. A. Burrows, J. Vac. Sci. Technol. A7 (3), 2104 (1989).
6. J.A.Woollam and P.G. Snyder, Material Science and Engineering **B5**, 279 (1990).
7. T. Yasuda and D. E. Aspnes, Applied Optics, **33**, 7436 (1994).
8. B. Brixner, in Handbook of Optical Constants of Solids, E. D. Palik, Editor, Academic Press, New York (1985).
9. A. Röseler, Infrared Spectroscopic Ellipsometry, p. 15, 93, Akademie-Verlag Berlin, (1990).
10. A. Röseler, J. Opt. Soc. Am. (A) **9/7**, 1124 (1992).
11. K. Heilig, Solid State Electron. **27** (4), 395 (1984).
12. W Flüssel, M. Schmidt, H. Angermann, G. Mende and H. Flietner, Nucl. Instr. And Meth. A **377** 177 (1996).
13. H. Angermann, K. Kliefoth, and H. Flietner, Appl. Surf. Sci. **104/105**, 107 (1995).
14. H. Flietner, Material Science Forum Vol. **185- 188**, 73 (1995).
15. H. Angermann, W. Henrion, M. Rebien, K. Kliefoth, D. Fischer and J.-T. Zettler, Microelectronics Engineering **36**, (1997).

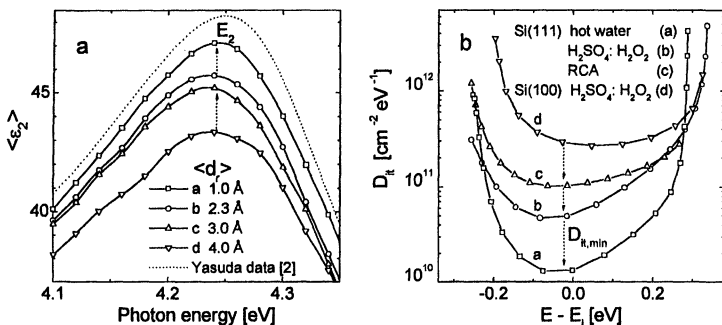


**Fig. 1** Imaginary part of the effective dielectric function  $\langle\epsilon_2\rangle$  (a) and surface state distribution  $D_{it}(E)$  (b) for differently pre-treated H-terminated Si(111) and Si(100) surfaces

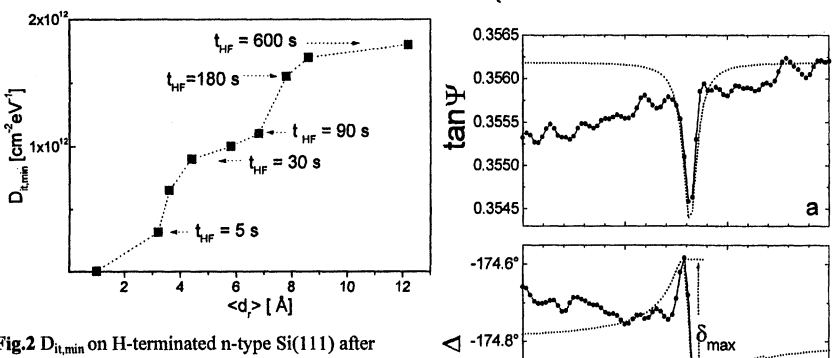


**Fig. 2**  $D_{it,min}$  on H-terminated n-type Si(111) after different HF-treatment times correlated to the effective surface roughness  $\langle d \rangle$ .

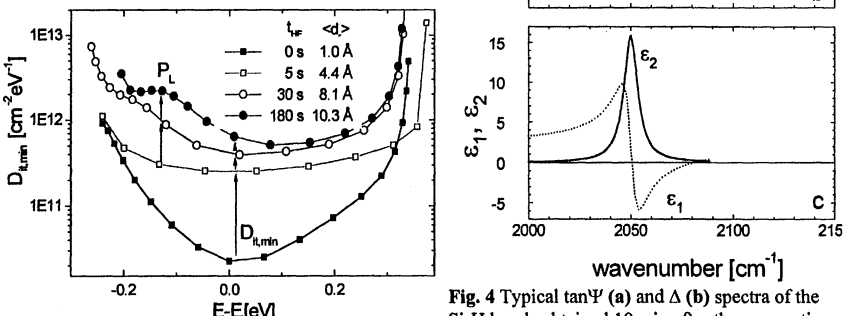


**Fig. 3** Surface state distribution  $D_{it}(E)$  for p-type Si(111) surfaces after 5, 30 and 180 sec treatment times in HF

**Fig. 4** Typical  $\tan\Psi$  (a) and  $\Delta$  (b) spectra of the Si-H bonds obtained 10 min after the preparation of the H-terminated surface. The  $\epsilon$  spectrum of the best fit Lorentz oscillator is given in (c).

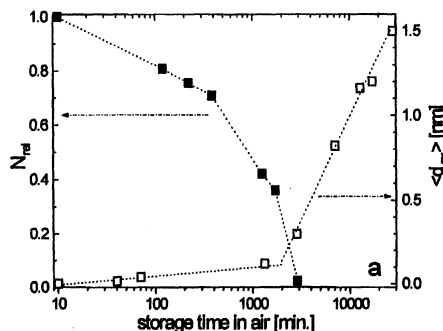


Fig. 5 Change of the relative number of Si-H bonds (filled squares) and the effective oxide thickness (open squares)

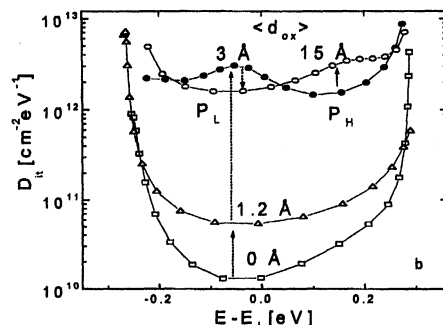


Fig. 6 Change of the interface state distribution  $D_{\text{it}}$  ( $E$ ) of a H-terminated surface (1) after 24 h (2), 48 h (3), and 21 d (4) storage time in air

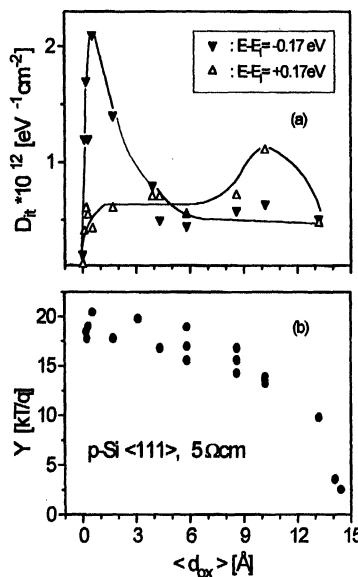


Fig. 8 Change of the extrinsic states  $P_L$  ((a) filled triangles) and  $P_H$  ((a) open triangles) correlated to the oxide growth and corresponding shift of surface band bending (b)

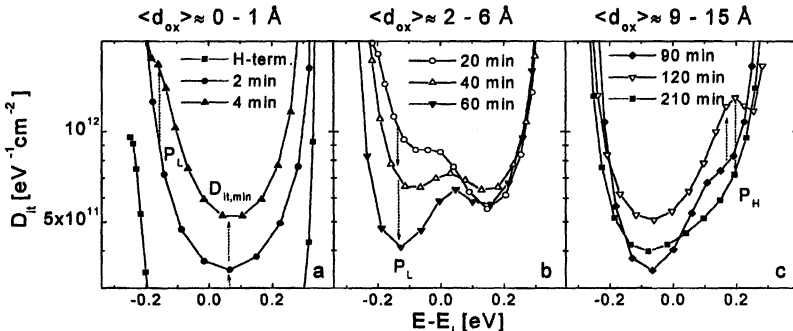


Fig. 7 Change of  $D_{\text{it}}$  ( $E$ ) of H-terminated Si(111) surface during hot water oxidation: the initial phase (a), the formation of the second monolayer (b) and the formation of the final Si/SiO<sub>2</sub> interface (c)

## WAFER CLEANING BY WATER AND GAS MIXTURE WITH HIGH VELOCITY

I.Kanno, N.Yokoi, and K.Sato

ULSI Laboratory, MITSUBISHI ELECTRIC Corp.

Mizu hara 4-1, Itami, Hyogo, 664, Japan

A novel single wafer cleaning method using fine water droplets has been developed, called "M-jet scrubber". Water droplets are generated by mixing water and gas in a jet nozzle, and are jetted onto a wafer surface at high velocity to remove particulate contaminants from a wafer. It was confirmed that the M-jet scrubber was more effective than conventional cleaning methods in removing fine particles and etching residual polymers without damage to Al patterns, and, by using in combination with a chemical solution, in removing particles tightly adhering to a wafer after W etch-back. A model of the cleaning mechanism for the M-jet scrubber is proposed, in which the particle removal force of the M-jet scrubber is more than ten times greater than that of a conventional megasonic scrubber.

### INTRODUCTION

In recent LSI fabrication processes, the wafer surface cleaning technology is becoming more important. The basic concept in reducing the trouble concerned with particles is to avoid generating them or to prevent them from sticking to wafers. Efforts are also necessary to remove particles from wafers efficiently with less damage to devices. An immersion-type wet cleaning such as RCA cleaning has the problem that the contaminants are transported from wafer to wafer in the bath(1),(2). A single wafer cleaning can solve this problem.

We have developed a new single wafer cleaning method using fine water droplets, which aims at efficiently removing submicron particles and other contaminants from wafers(3). We call this method "M-jet scrubber". In this method, water droplets are jetted onto a wafer surface at high velocity, and remove contaminants on a wafer. The particle removal efficiency of the M-jet scrubber is higher than that of conventional cleaning methods, especially for finer particles.

## OUTLINE OF THE M-JET SCRUBBER

The main components of the M-jet scrubber apparatus are shown in Fig. 1. Fine droplets are generated when liquid (water or chemicals) and carrier gas (dry air or N<sub>2</sub>) are mixed in a jet nozzle. The droplets are accelerated by high velocity gas, and jet onto a wafer surface. These droplets are about 10  $\mu\text{m}$  in diameter. The jetting speed varies from 50 to 330 m/s ( $\approx$  sonic speed) depending on the carrier gas flow rate. Fresh chemicals are also added from a different nozzle onto a wafer surface to increase removal efficiency.

## M-JET PERFORMANCE

The M-jet scrubber was basically evaluated by comparing its removal efficiency to those of other conventional cleaning methods. Polystyrene latex (PSL) particles of various sizes were used in the evaluation. The Si wafers were intentionally contaminated by dipping in water, which contains PSL particles of a certain size. The wafers were subsequently heated at 120°C for 1 min so that the partially molten particles adhered tightly to the wafers. A megasonic scrubber and a high pressure water jet were both used to remove the PSL particles. Fig. 2 compares the removal efficiency of the M-jet scrubber with those of other cleaning methods as a function of the PSL particle size. The M-jet scrubber removes particles smaller than 1  $\mu\text{m}$  almost completely. On the other hand, the megasonic scrubber and the high pressure water jet do not remove those particles. The jetting speed of the M-jet scrubber was varied between 50 and 330 m/s. The removal efficiency of the M-jet scrubber varied depending upon the jetting speed. This indicates that the impact of the water droplets upon a wafer can be controlled by changing the jetting speed. Such a control of the impact makes it possible to adjust the removal force so as to remove particles without device damage.

There are many possible applications of the M-jet scrubber in LSI processes. One of these applications is the removal of the residue after reactive ion etching in Al wiring. The residue, which can not be removed by a megasonic scrubber, consists of mixtures originating from etching gas, etched metals, silicon oxides, and photo-resists. Fig. 3 shows the scanning electron microscope photographs before and after the M-jet scrubber treatment in the etching residue removal. The M-jet scrubber removes most of the residue effectively. The impact of water droplets does not cause any damage to the Al patterns.

In LSI processes, a large amount of particles are generated when a W film is etched back to fabricate plugs. Another application of the M-jet scrubber is particle removal after W etch-back. Table I compares the particle removal efficiency of various cleaning methods applied to wafers after W etch-back. The M-jet scrubber removes finer particles as well as larger particles, while the removal efficiency of a megasonic scrubber decreases as the particle size becomes smaller. This result is in good agreement with Fig.2. When the particles chemically adhere to a wafer, a chemical solution is necessary to lift them off. HF/H<sub>2</sub>O<sub>2</sub>/H<sub>2</sub>O (FPM) was used as the solution. This solution etches underlying silicon oxide film to lift the particles off. The removal efficiency of the FPM spraying was higher for smaller particles. The combination of the chemical solution spraying and the M-jet scrubbing is expected to lead to high efficiency removal because it provides both chemical and physical effects. The result of FPM spraying followed by the water M-jet scrubbing is also shown in Table I. This combination effectively removes most of the particles.

One of the recent issues concerning Si wafer cleaning processes is contamination on back surfaces. The back surface of a wafer is more contaminated by contact with transfer systems or stages of process equipment than the front surface. Our apparatus can be used to remove contaminants on both sides of a wafer. Fig.4 represents the removal efficiency of the M-jet scrubber for metallic contaminants on back surfaces by comparing metallic impurity concentrations measured by total reflection X-ray fluorescence (TRXRF) before and after cleaning. The removal efficiency was evaluated using wafers which had been processed in a chemical-vapor-deposition (CVD) chamber. The back surface of the wafer before cleaning by the M-jet scrubber was contaminated with metallic impurities whose concentrations were more than  $10^{12}$  atoms/cm<sup>2</sup>. The metallic concentrations are reduced by an order of one or two by the M-jet scrubber without chemical solutions, which is equal to the performance of conventional RCA cleaning. The metallic contaminants, which are considered to adhere to the back surfaces as particles, are effectively removed by the physical force of the M-jet scrubber. Fig.5 shows the result of another cleaning experiment of back surfaces. This experiment was performed on wafers processed using equipment with vacuum-holding transfer systems. For particles with diameter larger than 0.12  $\mu\text{m}$ , the M-jet scrubber achieved higher removal efficiency than a conventional megasonic scrubber. The M-jet scrubber effectively removes fine particles smaller than 0.3  $\mu\text{m}$ , which are hardly removed at all with a megasonic scrubber.

## MECHANISMS OF PARTICLE REMOVAL

Fig.6 schematically shows a possible model for the cleaning mechanism of the M-jet scrubber. This model is based upon a combination of fluid mechanics and rain erosion of materials caused by the impact of highly accelerated droplets(4). When a droplet impacts on a wafer surface, reflected a shock-wave within the droplet generates pressure, which results in a radial flow along the surface. The pressure and the radial flow apply continuous external force (removal force) to particles. The impulsive pressure is described as follows;

$$P = \frac{1}{2} \alpha \frac{\rho_L C_L V_o}{1 + (\rho_L C_L / \rho_s C_s)} \quad [1]$$

where  $\rho_L$ ,  $\rho_s$  are the densities of liquid and a substrate, respectively,  $C_L$ ,  $C_s$  are the sonic velocities in the liquid and in the substrate, respectively,  $\alpha$  is the decay coefficient, which has no dimension. The velocity  $V_f$  of the radial flow is specified as follows;

$$V_f = (\alpha C_L V_o)^{1/2} \quad [2]$$

The removal force applied to a spherical particle whose diameter is  $d$  can be calculated using either Eq.[3] or [4], which give the same value.

$$F = C_D \left( \frac{\pi d^2}{4} \right) P \quad [3]$$

$$F = C_D \left( \frac{\pi d^2}{4} \right) \left( \frac{\rho_L V_f^2}{2} \right) \quad [4]$$

In Eqs.[3] and [4],  $C_D$  is the drag coefficient.

Assuming that the velocity of droplets, impact angle measured from a wafer surface, the decay coefficient, and the drag coefficient are 330 m/s, 60°, 0.28, and 0.47, respectively, the removal force applied to a particle with a diameter of 1  $\mu\text{m}$  is  $2 \times 10^{-5}$  N.

The cleaning mechanism of a megasonic scrubber, which applies supersonic oscillation at a frequency larger than 1 MHz to a wafer through water from an aperture, can be similarly modeled. The model of the megasonic scrubber is also based upon a combination of fluid mechanics and erosion. Assuming that the wafer size, the rotating speed, the frequency , and the amplitude are 8", 2000 rpm, 1.6 MHz, and 0.07  $\mu\text{m}$ , the removal force applied to a particle with a diameter of 1  $\mu\text{m}$  is estimated to be  $8 \times 10^{-7}$  N.

Fig.7 shows the removal force calculated according to the mechanism described above as a function of the diameter of the spherical particles. In Fig.7, the surface tension force and van der Waals force in the air and in the water which are generally used as adhesion forces of particles are also shown. The external force applied to a particle in the cleaning process is determined by fluid velocity, the drag coefficient and the projected area of the particle. Hence, a particle becomes harder to remove as the diameter becomes smaller because the external force decreases in proportion to the square of the diameter. According to the models described above, the minimum size of particles which can be removed by the M-jet scrubber, whose removal force is larger by an order of one or more than that of a megasonic scrubber, is estimated to be smaller by an order of one than that of particles which can be removed by a megasonic scrubber. The result of PSL particle removal shown in Fig.2 is in agreement with this estimation.

## CONCLUSION

We have developed a novel technique to remove finer particles or tightly sticking contaminants from Si wafers. This method, the M-jet scrubber, provides higher particle removal efficiency than other conventional cleaning methods, removes etching residue without damage to Al patterns, and, combined with a chemical solution application, removes particles almost completely after W etch-back. A model for the cleaning mechanism of the M-jet scrubber is also proposed to show that the M-jet scrubber can remove finer particles than a conventional megasonic scrubber. This model has been confirmed to be adequate by an experiment to remove PSL particles. In LSI fabrication, the M-jet scrubber can be widely used as a powerful tool to reduce contaminants on Si wafers.

## REFERENCES

1. M.Watanabe, I.Kanno, and T.Ohmori, Proceedings of ISSM'94, p.99-102(1994).
2. T.Osaka and T.Hattori, Proceedings of ISSM'96, p.204-207(1994).
3. I.Kanno, Journal of Japan Air Cleaning Association, vol.33, no.5, p.241-247(1996).
4. Japan Society of Corrosion Engineering: Erosion & Corrosion, p.46-50, Shokabo, Tokyo(1987)

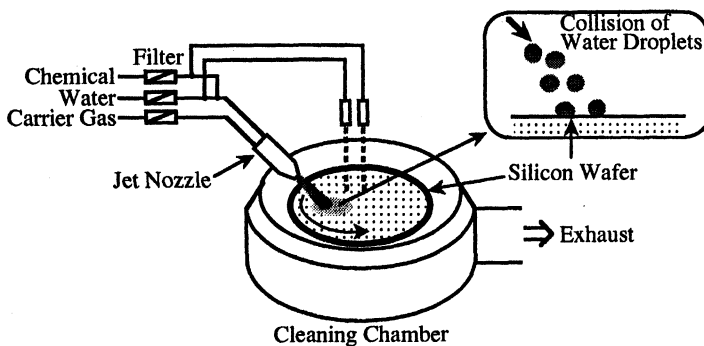


Fig.1 Main construction of M-jet scrubber

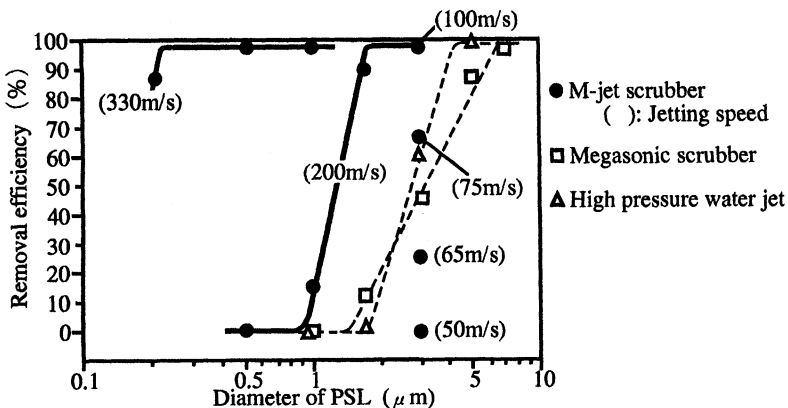


Fig.2 Removal efficiency dependence on PSL size

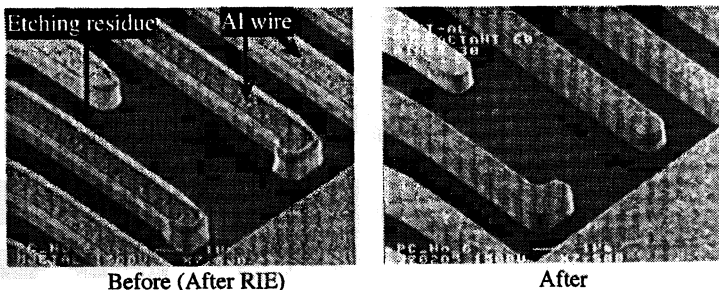


Fig.3 RIE residue removal by M-jet scrubber

Table I Particle removal efficiency after W etch-back for various particle sizes

Cleaning conditions		M-jet (used water)	FPM spraying + M-jet (used water)	FPM spraying	Megasonic scrubber
Removal rate (%)	>0.2μm	44%	91%	32%	22%
	>0.3μm	44%	84%	50%	34%
	>0.7μm	42%	75%	13%	50%

FPM spraying : HF/H<sub>2</sub>O<sub>2</sub>/H<sub>2</sub>O = 0.5%/30%/69.5%, 0.5 L/min, 60s

M-jet (used water) : Jetting speed = 275m/s, 60s, Water flow rate=0.2 L/min

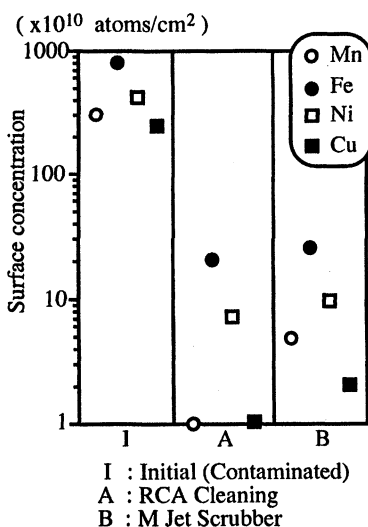


Fig.4 TRXRF measurements of back surface contamination cleaning

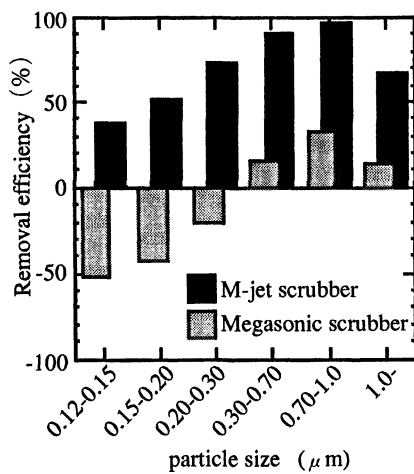


Fig.5 Particle removal efficiency of back surface for various particle sizes

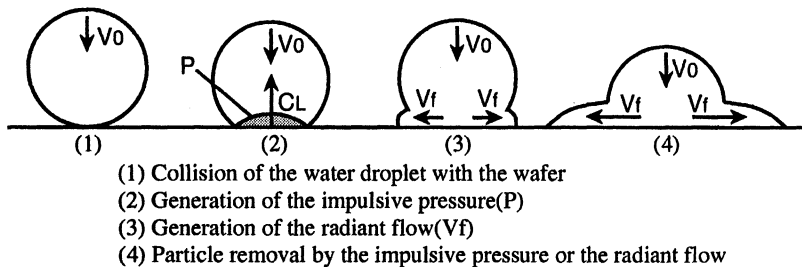


Fig.6 Particle removal model for M-jet scrubber

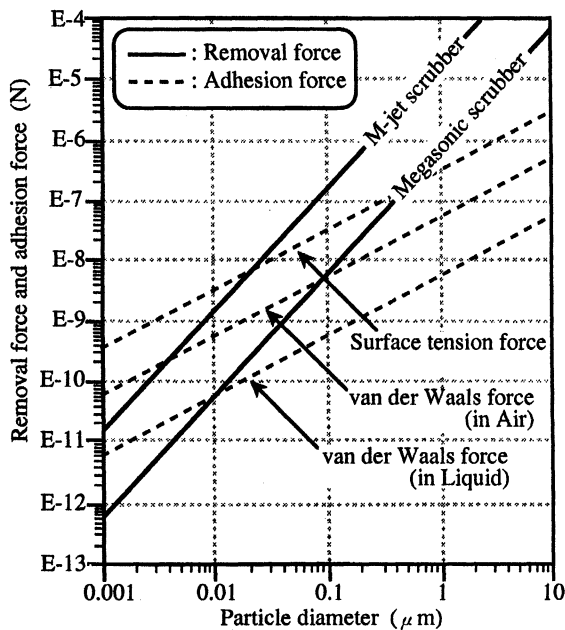


Fig.7 The relationship between removal force and adhesion force as a function of particle size

# SURFACE PREPARATION USING ANHYDROUS HYDROGEN FLUORIDE AND AQUEOUS H<sub>2</sub>O PRIOR TO LOW TEMPERATURE EPITAXIAL SILICON DEPOSITION

David C. Frystak<sup>1</sup>, Rick Wise<sup>1</sup>, Phil Grothe<sup>2</sup>,  
Joel Barnett<sup>2</sup>, Burt Fowler<sup>3</sup>, Ron Carpio<sup>3</sup>

<sup>1</sup>Texas Instruments, Semiconductor Process and Device Center,  
13570 N. Central Expressway, MS 3701, Dallas, TX 75243

<sup>2</sup>FSI International, Chaska, MN 55318

<sup>3</sup>SEMATECH, Austin, TX 78741

## ABSTRACT

A true HF-last cleanup which enables the deposition of epitaxial silicon at reduced temperature has been developed. The process is activated by dispensing anhydrous hydrogen fluoride into a single wafer process chamber during a water spin rinse cycle. This process was found to leave lower amounts of bonded oxygen on the silicon surface relative to other types of treatments. High quality epitaxial films have been deposited at 850°C with a 950°C hydrogen pre-bake using this surface preparation method. The films were free of oxygen contamination at the epi/substrate interface as measured using SIMS and contained 0.014 light point defects per square centimeter. The electrical yield of diode devices formed in these films was equivalent to that of high temperature epi films. Clustering this pre-epi cleanup process with the epi deposition reduced the oxygen and carbon contamination at the film/substrate interface which would otherwise be present as a result of exposure to room air and extended hold time in the vacuum loadlock of the cluster tool.

## INTRODUCTION

Reducing the thermal budget of the epitaxial silicon deposition process used in semiconductor device manufacturing is desirable for various reasons. Schemes incorporating the use of low temperature epi deposition can be used to suppress arsenic autodoping thereby enhancing device performance [1]. It is expected that the formation of slip defects on 300mm wafers and boron autodoping of ultra-thin epi layers will further necessitate the need to reduce the thermal budget of the epi process. Lowering the

thermal budget can also potentially lead to a general reduction in the production cost of epi wafers.

Improving the silicon surface preparation step which precedes the epitaxial silicon deposition process enables the lowering of the thermal budget of the epi process. Historically, a high temperature hydrogen bake performed in the epi reactor just prior to deposition has been required to reduce the oxide present on the silicon surface which would otherwise form defects in the epi layer [2]. Reducing the temperature and duration of this bake requires that the pre-clean remove this oxide and leave the silicon surface passivated against oxide regrowth. The wafer transfer time and transfer ambient encountered between the pre-clean and the epi deposition process must also be controlled to minimize contamination of the passivated silicon surface via spontaneous native oxidation or impurity adsorption.

A true HF-last cleanup which enables the deposition of epitaxial silicon at reduced temperature has been developed. The process, from this point forward referred to as the anhydrous HF-Rinse process or simply the HF-Rinse, is activated by dispensing anhydrous hydrogen fluoride (aHF) into a single wafer process chamber during a water spin rinse cycle. The wafer is subsequently spin dried in a nitrogen ambient. Elimination of the water rinse step prevents undesirable oxide formation and contamination of the silicon surface which can occur during this process. This HF-Rinse process is performed in a single wafer cleanup reactor which is connected to a cluster tool platform hosting a single wafer epi reactor thereby facilitating automated transfer of the product wafers in a controlled ambient between the cleanup and the epi processes. Such a configuration allows each wafer to be cleaned just prior to the epi process thereby eliminating the effects of contamination associated with storage time.

## EXPERIMENTAL

A diagram of the single wafer cleanup reactor used in this evaluation, an FSI Excalibur® MVP system, is presented in Fig. 1. The reactor is capable of performing an aHF/H<sub>2</sub>O-vapor oxide etch prior to the HF-Rinse process. The process can be used to remove either chemical/native oxide or thermal oxide. The configuration of the cleanup module on the cluster tool platform is illustrated in Fig. 2 which also shows the proximity of the epi reactor.

Four different surface preparation methods, summarized in Table I, were investigated. All results were compared directly with the wet HF process of record, case 1 in Table I. The experimental HF-Rinse process, case 4 in Table I, is a modification of the HF-vapor oxide etch process, case 2 in Table I, which was designed to remove a thermal oxide film prior to gate oxidation. The combination of HF-Rinse with subsequent H<sub>2</sub>O rinse, case 3, was also investigated. Details of the HF-Rinse process sequence are summarized in Table II. The silicon wafers used in all experiments were p-type, (100) oriented and 150 mm in diameter. The silicon surface was typically passivated with a chemical oxide layer

prior to the pre-epi cleanup treatment. The influence of process variables such as the use of the HF-vapor etch (Yes/No), the use of aHF during the water rinse (HF-Rinse, Yes/No), the use of a subsequent water rinse (Yes/No), and method of wafer transport to the epi reactor (clustered/non-clustered) were explored in the course of developing the HF-Rinse process [3]. The level settings of the HF-Rinse step were set to maximize the surface hydro-phobicity as determined by water droplet contact angle and minimize the surface light point defect (LPD) density. Process characterization, see Fig. 3, consisted of X-ray photoelectron spectroscopy (XPS) and attenuated total-reflectance Fourier Transform infrared spectroscopy (ATR-FTIR) following cleanup and LPD measurements as well as secondary ion mass spectroscopy (SIMS) and diode leakage following either polysilicon or epi deposition and device formation.

Table I. Pre-Epi Cleanup Test Matrix.

CASE	NAME	DESCRIPTION
1	Wet-HF	HF+H <sub>2</sub> O_Rns+IPA_Dry
2	HF-Vapor	aHF/HCl/H <sub>2</sub> O_Vpr+H <sub>2</sub> O_Rns+Spin_Dry
3	HF-Rinse+H <sub>2</sub> O-Rns	aHF/HCl/H <sub>2</sub> O_Vpr+HF_Rns+H <sub>2</sub> O_Rns+Spin_Dry
4	HF-Rinse	aHF/HCl/H <sub>2</sub> O_Vpr+HF_Rns+Spin_Dry

Table II. Dual Side HF-Rinse Process: Front-side Process Conditions.

Step	Description	Chemistry	aHF flow (sccm)	Time (sec)	Other
1	HF-VprEtch	aHF/HCl/H <sub>2</sub> O-Vpr	200	5	
2	HF-Rinse	aHF + H <sub>2</sub> O liquid	500	10	
3	H <sub>2</sub> O Rinse	H <sub>2</sub> O	N/A	4 to 7	Optional
4	Spin_Dry	N <sub>2</sub>	N/A	13	3000 rpm
5	Wfr Xfer to Epi	N/A	N/A		

## RESULTS

Ex-situ XPS was used to measure the concentration of oxygen and fluorine remaining on the silicon surface following the cleanup process. An oxygen concentration of 1-3 atomic percent was obtained using conventional wet HF processing (Fig. 4, case 1) while the fluorine concentration was found to be at or below the detection limit of the XPS instrument. Variations in HF concentration and wafer drying method did not significantly impact the results. The HF-Vapor (case 2) and HF-Rinse+H<sub>2</sub>O-Rinse (case 3) processes were found to be less effective in producing an oxide free silicon surface with 7% and 4% oxygen coverage respectively. Difficulties in wetting the silicon surface in part limit the ability of the HF-Vapor deglaze process to remove trace oxide. The subsequent water rinse following the HF-Rinse process is known to lead to silicon oxidation via hydrolysis

[4]. A 0.8-2.0% oxygen concentration was obtained using the HF-Rinse process (case 4) which was slightly better than that of the wet HF process. The fluorine content, higher following the HF-Rinse process due to the absence of H<sub>2</sub>O rinsing, was found to be an acceptable surface passivation element under the conditions of process clustering where wafers are transferred to the epi process in a controlled ambient thus limiting exposure to oxidizing species.

The fluorine content could be, as previously noted, reduced with a water rinse following the HF-Rinse process, Fig. 5, but at the expense of increasing the content of bonded oxygen on the surface. Rinsing for as little as 3-7 seconds brings the fluorine levels down to 0.3 percent while the oxygen content increases to 3-4 percent. This known phenomena is primarily a result of oxidation reactions occurring at the fluorine sites on the silicon surface [4,5].

Additional characterization of the pre-epi cleanup processes was performed using polysilicon encapsulated SIMS. Samples were transferred from cleanup to the poly dep process, either in cluster mode or conventionally in the case of wet HF processing, where the surfaces were then encapsulated with a polysilicon layer. SIMS depth profiling was then used to measure the impurity content at the polysilicon/crystal silicon interface. This approach eliminates some of the difficulties in separating process and ambient induced contamination encountered with ex-situ XPS. The oxygen trend, Fig. 6, was similar to that observed using XPS; the HF-Rinse process was found to be superior to the wet HF process. The HF-Rinse treated samples also had the lowest amount of carbon and fluorine at the interface. It should be noted that process clustering also contributed to the HF-Rinse results. The other two processes, cases 2 and 3, were much less reproducible and yielded greater amounts of oxygen at the poly/substrate interface.

The impact of the pre-epi cleanup was also characterized using the ATR-FTIR technique. The abundance of SiH<sub>3</sub> and SiH bonds relative to SiH<sub>2</sub> is presented in Fig. 7 as a function of the cleanup treatment. The characteristics of a silicon surface following a high temperature hydrogen bake in the epi reactor, case 5, is included for reference. The reconstructed surface following the bake, the standard starting point for high quality epi, was virtually free of the tri-hydride species. The SiH<sub>3</sub> and SiH content following the HF-Rinse process was similar to that of the wet HF process. This indicated that a higher percentage of the surface was terminated with the more desirable SiH<sub>2</sub> structure relative to the alternative cleans, cases 2 and 3, which had greater amounts of tri-hydride and mono-hydride on the surface.

Substrate type was found to influence the performance of the HF-Rinse process. As mentioned previously, the ability to wet the surface of the substrate was identified as a factor influencing the quality of the oxide deglaze process. All of the results presented previously were obtained using silicon wafers with a thin chemical oxide layer passivating the surface. Repeating the XPS characterization using substrates with thermal oxide present, Fig. 8, indicated that better oxide removal and surface passivation could be obtained using the HF-Rinse process. These results suggest that having an oxide film in place prior to the HF-Rinse+CVD sequence could offer additional gains in interface quality.

The transfer between the pre-epi cleanup and the epi deposition process must be controlled in order to prevent contamination of the silicon surface. SIMS measurements of interfacial oxygen and carbon following wet HF cleanup and polysilicon deposition for two different transfer/hold times is presented in Fig. 9. A minimum time of 10 minutes was required to transfer samples from wet cleanup into the cluster tool loadlock and subsequently into the poly chamber for deposition. Extending the hold time in the nitrogen purged loadlock, 4 hours in this case, was sufficient to cause significant increases in oxygen and carbon at the film/substrate interface.

The HF-Rinse pre-epi cleanup process was ultimately integrated with a low temperature epi deposition process. A deposition temperature of 850°C, much higher than that of the polysilicon deposition, was used with and without a short 950°C hydrogen bake. The oxygen concentration at the epi/substrate interface was found to be below the detection limit of SIMS, 1E+12 atoms/cm<sup>2</sup>, following HF-Rinse and 850°C epi deposition, Table III, with no high temperature bake preceding the deposition. This result was superior to the wet HF process of record. Carbon and fluorine were also below the SIMS detection limit. The wet HF and HF-Rinse processes were equivalent in this respect with the addition of a 950°C bake and with negligible hold time. The additional hold time associated with processing larger batches of wafers in a production environment was found to increase the defect density associated with non-clustered, i.e. wet HF, cleans.

Table III. Monolayers of oxygen at film/substrate interface via SIMS.

CLEANUP	FILM TYPE ->	POLY	EPI	EPI
	H <sub>2</sub> BAKE ->	None	None	950 C
	DÉP ->	690 C	850 C	850 C
1	Wet HF	19.2%	8.0%	< 0.1%
2	HF-Vapor	43.6%	21.4%	Not Tested
3	HF-Rinse+H <sub>2</sub> O-Rinse	33.8%	3.0%	Not Tested
4	HF-Rinse	9.0%	< 0.1%	< 0.1%

The epi film defect density and diode yield obtained using the HF-Rinse process are summarized in Table IV. Despite the SIMS results, significantly different results were obtained as a result of the 950°C bake. Excellent low temperature epi defect density and diode yield, relative to 1100°C epi deposition, were obtained when using the bake. The defects in the films produced without the bake were not detected using SIMS depth profiling but could be detected as LPDs and also impacted device yield.

Table IV. Epi film characterization following HF-Rinse+Low Temp Epi Dep.

850C Epi	Epi LPD Density (#/cm <sup>2</sup> @ >0.136μm)	Relative Diode Yield
No Bake	1.420	72%
Bake	0.014	97%

The benefits of clustering the pre-epi cleanup with 850°C epi deposition were further demonstrated. A full factorial designed experiment with single wafer cleanup conditions and method of wafer transport to epi deposition as input variables was performed. Both the average oxygen and carbon concentration at the epi/substrate interface, Fig. 10, were found to be lower when the cleanup was clustered to the epi process. The importance of clustering on the preservation of the clean silicon surface is expected to become more important as the epi deposition temperature is lowered still further.

## SUMMARY

The HF-Rinse process effectively etches trace oxide and passivates the silicon surface. The HF-Rinse process is equivalent to or better than the wet HF process of record in this regard and is a safe/manufacturable method of performing true HF-last processing. Clustering this process with the epi deposition process improves process control by protecting the clean silicon surface from contamination. Good quality epi films have been formed using this process. Excellent light point defect density and device yield characteristics associated with clustered cleanup/ epi processes have been demonstrated.

## ACKNOWLEDGEMENTS

Many thanks to Norris Tidwell, Jana Julien, Tommy Gray, Lissa Magel, Ray Potts, Scott Johnson and Katherine Violette of Texas Instruments for their contributions to this project. The support provided by Fred Tapp of BOC Gases and Don See of Applied Materials is also gratefully acknowledged. A major portion of the funding for this work was provided by SEMATECH as part of Project E58.

## REFERENCES

1. R.L. Wise, F.S. Johnson, D.C. Frystak, K.E. Violette, N.E. Tidwell and E. Forrest, in The Proceedings of the Joint International Symposium on Chemical Vapor Deposition: CVD XIV and EUROCVD 11, The Electrochemical Society Proceedings Series, Pennington, NJ (to be published).
2. J.A. Friedrich, G.W. Neudeck and S.T. Liu, *Appl. Phys. Lett.*, **53**, 2544 (1988).
3. R. Wise, D. Frystak, J. Barnett, P. Grothe, B. Fowler and E. Forrest, in Thirteenth International Conference on Chemical Vapor Deposition/1996, T.M. Besmann, M.D. Allendorf, McD. Robinson and R.K. Ulrich, Editors, *PV 96-5*, p. 287, The Electrochemical Society Proceedings Series, Pennington, NJ (1996).

4. M. Hirose, T. Yasaka, K. Kanda, M. Takakura and S. Miyazaki, in Proceedings of the Second International Symposium on Cleaning Technology in Semiconductor Device Manufacturing/1991, J. Ruzyllo and R.E. Novak, Editors, PV 92-12, p. 1, The Electrochemical Society Proceedings Series, Pennington, NJ (1992).  
 5. G.J. Pietsch, Applied Physics A, **60**, 347 (1995).

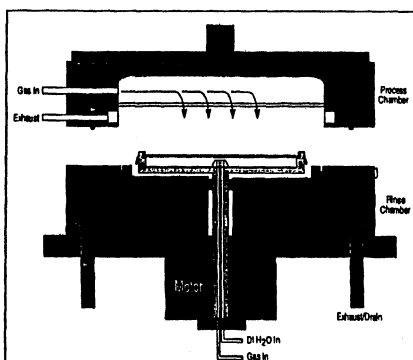


Fig. 1. Cross-sectional diagram of single wafer cleanup reactor.

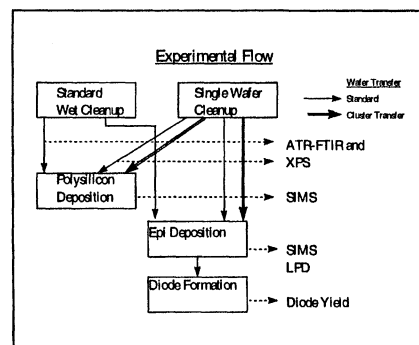


Fig. 3. Diagram illustrating experimental sequence.

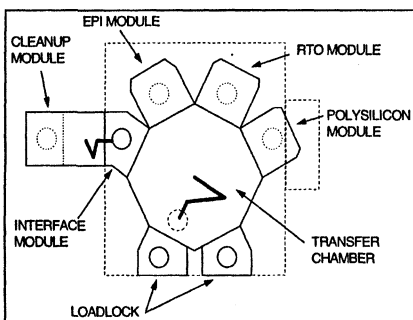


Fig. 2. Layout of single wafer cluster tool with cleanup module and epitaxial silicon deposition module.

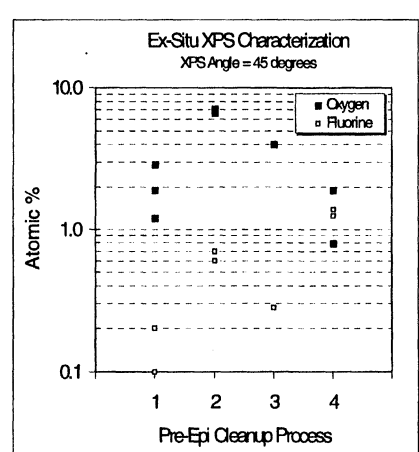


Fig. 4. Silicon surface characterization using XPS following various pre-epi cleanup treatments.

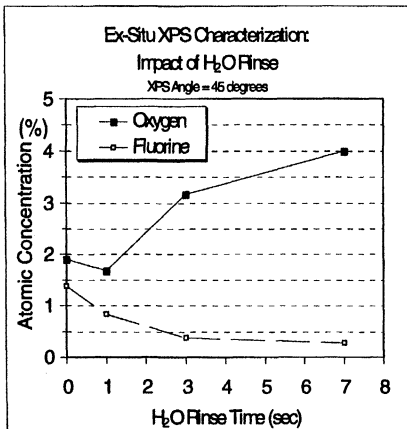


Fig. 5. Silicon surface characterization using XPS following the HF-Rinse pre-epi cleanup treatment demonstrating the impact of a subsequent water rinse.

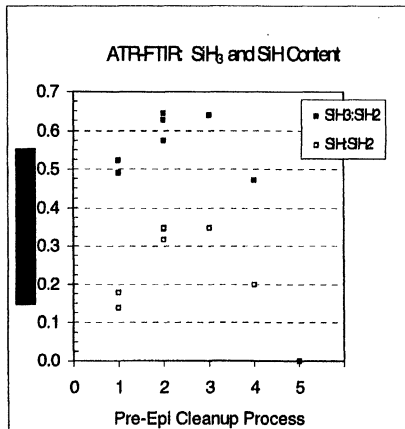


Fig. 7. Silicon surface characterization using ATR-FTIR following various pre-epi cleanup treatments.

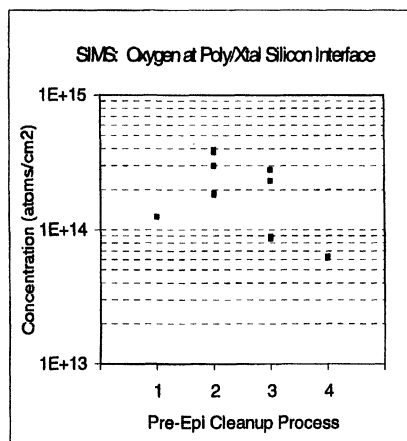


Fig. 6. Oxygen at the polysilicon/crystal silicon interface as a function of pre-epi cleanup treatment.

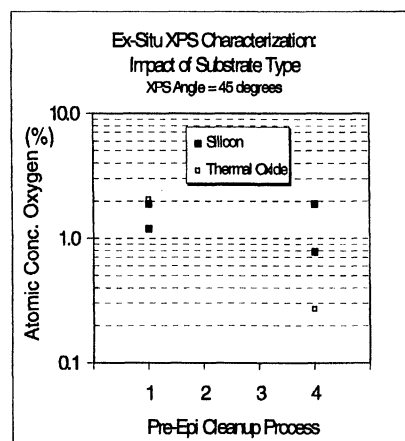


Fig. 8. Impact of substrate type on the effectiveness of oxide removal.

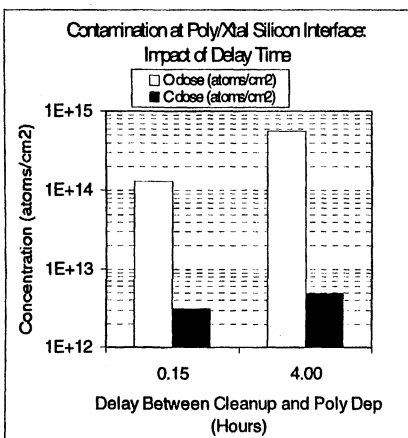


Fig. 9. Impact of delay time between pre-epi cleanup and deposition process.

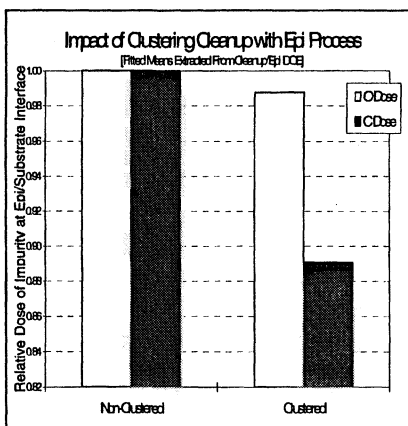


Fig. 10. Reduction in oxygen and carbon contamination of the exposed silicon surface during the time between cleanup and epi deposition as a result of process clustering.

## **THE EVALUATION OF ULTRASONIC DAMAGE CAUSED BY BATCH TYPE WAFER CLEANING SYSTEM**

**Akihiro Onishi, Akira Chiyokawa, Akihiro Tomozawa**  
**Takasaki Technical Center, Hitachi Microcomputer System LTD.**  
**1-1, Nishiyokote-machi, Takasaki-shi, Gunma-ken, 370, Japan**

Ultrasonic cleaning is applied to remove particles that adhere to a wafer during the manufacturing process, but it sometimes damages the semiconductor devices. The authors investigated ultrasonic cleaning by using a hydro-microphone, an oscilloscope, and a spectrum analyzer. They found that the degree of device damage depends on the maximum ultrasonic intensity. The change in the intensity over time depends on the method of intensity control used in a cleaning equipment. The maximum intensity of ultrasonic waves in an equipment can be only slightly controlled with the phase-control method. Measuring the frequency spectrum in a phase-control cleaning tub shows that many cavitation noises occur, even when the intensity control dial is set to low. However, an equipment using the amplitude-control method is superior for wafer cleaning because the maximum intensity of the equipment can be controlled more precisely.

### **INTRODUCTION**

Various particles, such as dust from the equipment and dust floating in the air, are generated and adhere to a wafer during the semiconductor manufacturing process. Because these particles reduce the production yield, several methods to remove them have been tried. One method is ultrasonic cleaning, but this can cause particles to break away physically and sometimes damages the devices. To prevent such damage, the intensity of ultrasonic waves in the equipment needs to be set appropriately. However, cleaning ability has been the main focus when evaluating the ultrasonic cleaning used in manufacturing, and the relationship between the intensity of ultrasonic waves and device damage have been rarely mentioned, even in research journals or documents. We believe that a simplified intensity measuring equipment is generally used to measure the intensity, except in advanced ultrasonic laboratories. In this paper, we concentrate on the device damage. We have investigated the relationship between ultrasonic intensity and the device damage, but found that a simplified intensity measuring equipment cannot clarify this relationship. Therefore, we used a sound measuring equipment that provides precise measurement and conducted a detailed analysis of the ultrasonic cleaning. Our methods and results are described here.

### **OVERVIEW OF ULTRASONIC CLEANING**

Figure 1 shows an overview of an ultrasonic cleaning equipment. The equipment consists of a quartz tub overflowing with pure water, a pure-water supply line, an ultrasonic cleaning tub with an oscillator at the bottom, and an

ultrasonic generator driving the oscillator. The generator dial is used to set the intensity of the ultrasonic waves. Wafers to be cleaned are placed on a resin cleaning jig and put into the quartz tub. The ultrasonic waves generated from the oscillator are transmitted into the quartz tub by the medium of the pure water. The sound pressure of the ultrasonic waves produces fine cavitations in the pure water. These cavitations produce impact waves when they burst, and the energy physically breaks away particles that were adhered to a wafer<sup>(1)</sup>.

Excessive cavitation energy causes cracks in the thin film deposited on a wafer and damages the devices. Figure 2 shows the distribution of damaged devices in a wafer when this occurs. The width of the striped pattern and the space between the stripes in Figure 2, is half the length of the ultrasonic waves. The length equals the interval between the sound pressure loops of the ultrasonic standing wave in a cleaning tub, and a great deal of cavitation occurs in these areas (2)-(5). However, the amount of cavitation that occurs is known to depend on the kind of the medium and its temperature even at the same sound pressure (intensity). Both the intensity of the ultrasonic waves and the amount of cavitation that occurs need to be determined to prevent device damage.

## MEASUREMENT METHOD

The measurement method used in this evaluation is shown schematically in Figure 3. The method uses a hydro-microphone as a sensor, and an oscilloscope and a spectrum analyzer in a measured-value display unit.

### Intensity Measurement Method

In the simple measurement method, an ultrasonic intensity indicator is used to easily measure ultrasonic intensity. The indicator has a probe with a sensor on the top and a measured-value indication meter. A piezo rubber for a pressure-sensitive electroacoustic element is used for the sensor, which converts the sound pressure in the ultrasonic cleaning tub to an electric signal. The intensity of the electrical signal is measured from its voltage, and there is about a 1-second response time for an input signal. Therefore, the intensity change cannot be measured within less than 1 second. To measure the intensity change more quickly, we used an oscilloscope and a hydro-microphone with a wide-sensitivity band. In this method, the change of intensity over time with millisecond intervals can be observed as a waveform. The intensity can then be read from the waveform amplitude.

### Cavitation Measurement Method

The cleaning effect in ultrasonic cleaning depends on the degree of cavitation, not on the intensity. Therefore, the cavitation should be measured, not only through the intensity, but also by other methods. A simple method is to evaluate the cavitation using a hole in aluminum foil. However, this method has disadvantages, such as limited accuracy, and contamination in the cleaning tub. We analyzed the frequency with the hydro-microphone and spectrum analyzer. In ultrasonic cleaning, frequency components other than a basic frequency appear. The frequency ( $nf$ ) is  $n$  times the basic frequency ( $f$ ), which is called the high

harmonics. When cavitation occurs, frequency components of  $nf/2$ ,  $nf/3$ , and  $nf/4$ , which are called the sub-harmonics, result from the cavitation noise (1), (6), (7). Therefore, when sub-harmonics in the measurement frequency band are observed, cavitation must be occurring. Using this method, we measured and compared equipment A, which had a low degree of device damage, and equipment B, which had a high degree of device damage. Table 1 lists the basic specifications of both equipments.

## MEASUREMENT RESULTS

### Intensity

Figure 4 shows the measured intensity. The change in the amplitude over time was small in equipment A, but the change in output values from equipment B was large and intermittent oscillation occurred. When the intensity control value for the oscillator was changed, the maximum amplitude in equipment A also changed. This is called the amplitude-control method. On the other hand, in equipment B, the maximum amplitude changed little, but the intermittent oscillation forms changed. This is called the phase-control method.

Figure 5 shows the relationship between the intensity control value for the oscillator and the intensity measured with the oscilloscope. In the amplitude-control method, the maximum intensity and the average intensity are equal. However, in the phase-control method, the maximum intensity is much larger than the average intensity because of the intermittent oscillation. Even if the average intensity is set equally in both equipments A and B, the maximum intensity in equipment B is much larger than in equipment A. In this case, the simplified intensity measuring equipment gives the intensity of both equipments as equal since the device measures only the average intensity. In equipment B, the setting dial value and the measured value are not proportional. In addition, the maximum intensity is difficult to control since the measured value becomes larger even if the dial is set to low.

Figure 6 shows the degree of device damage as a function of the maximum ultrasonic intensity. The dependency of the degree of device damage on the maximum intensity differs in equipments A and B is the same. Therefore, the degree of device damage depends on the maximum intensity. To avoid device damage, the maximum intensity should be optimized, and should be measured for intensity management.

### Cavitation

Figure 7 shows the measured cavitation. In equipment A, only high harmonics were observed when the oscillator setting was low, and when the setting was increased, the sub-harmonic intensity became larger. On the contrary, in equipment B, the sub-harmonic intensity was high when the setting was low. This suggests that more cavitation may occur in equipment B than equipment A, because cavitation depends on the maximum intensity. Therefore, in the phase-control method, a lot of cavitation may occur when the setting is low, so this method is not suitable for cleaning without device damage.

## CONCLUSION

From our measurements using the two types of equipment, for low and high levels of device damage, we found that:

1. The device damage depends on the maximum intensity at the millisecond levels.
2. The phase-control method is not suitable for wafer cleaning since the maximum intensity is difficult to control.
3. The evaluation of ultrasonic cleaning using a hydro-microphone, an oscilloscope, and a spectrum analyzer is an effective method.

## REFERENCES

1. Junichi Miyoshi, Ultrasonic Technology (new version), Nikkan Kogyo Shimbun, Sept., 1987.
2. Toshio Utsunomiya, Special Issue of Ultrasonic, Denshi Joho Tsushin Gakkai, p. 72 and pp. 346-488, Apr., 1989.
3. Shoji Dobashi, Glass Cleaner — Actual Selection, Development, Suitable Cleaning, and Technology (Materials), Software Giken Shuppan, Mar. 1984.
4. Yasuo Tarui, Ultra clean Technology for Precise Cleaning (Materials), Software Giken Shuppan, Apr., 1982.
5. Sadao Kanai, Surface Control and Precise Cleaning, No. 38, Kindai Henshu, Jul., 1988.
6. Katsuo Negishi, The 8th Symposium Lecture Draft for Basic and Application of Ultrasonic Electronics, Ouyou Butsuri Gakkai, Dec., 1987.
7. Katsuo Negishi, Proceedings of the 8th Symposium on Ultrasonic Electronics, JJAP, 27 Suppl 27-1, Ouyou Butsuri Gakkai, Jun., 1988.

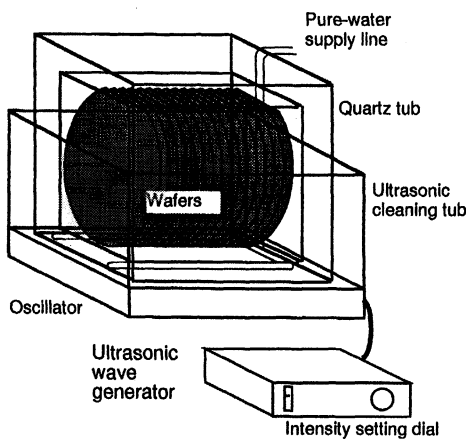


**Fig.1 Ultrasonic Cleaning Equipment**

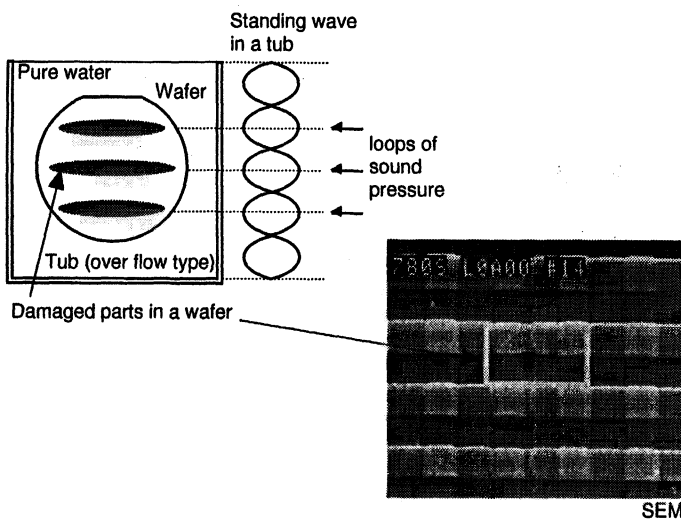


**Fig.2 Distribution of Damaged Devices In a Wafer**

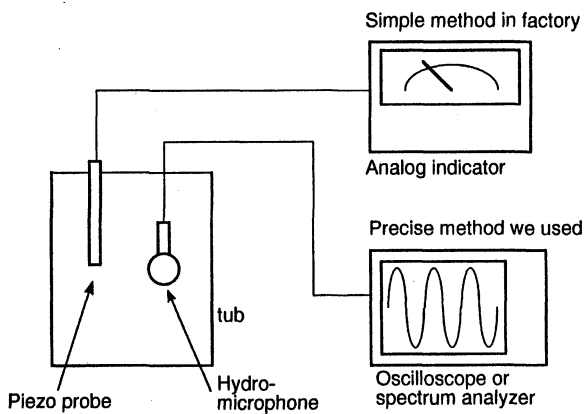


**Fig.3 Measurement Method**

**Table 1 Ultrasonic Cleaning Equipment Specifications**

Equipment	Frequency [kHz]	Max Output [W]	Power Control
A	26	300	amplitude control
B	26	600	phase control

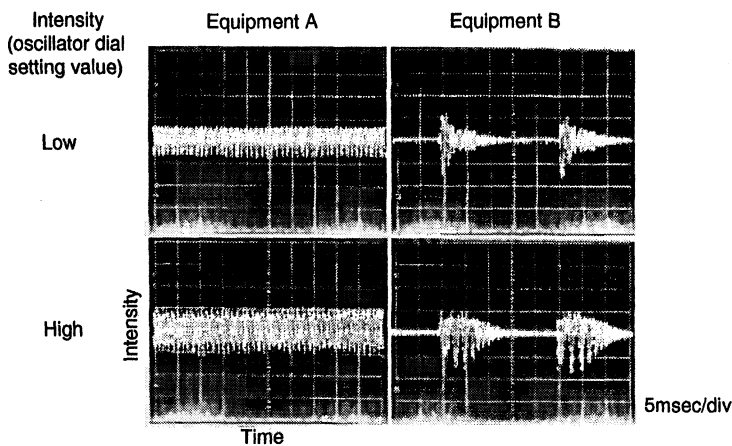


**Fig.4 Intensity Wave Forms**

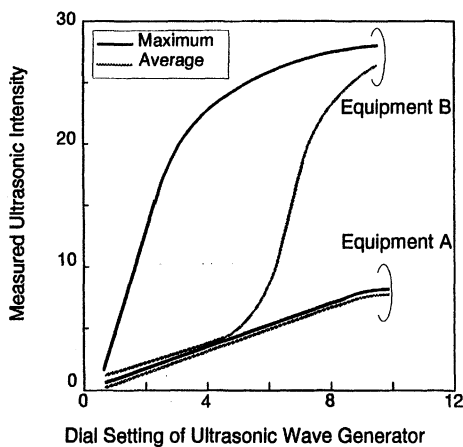


**Fig. 5 Dial Setting vs. Measured Ultrasonic Intensity**

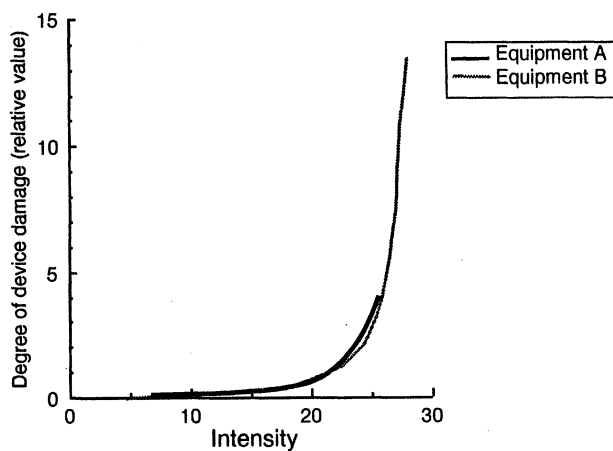


Fig. 6 Intensity vs. Device Damage

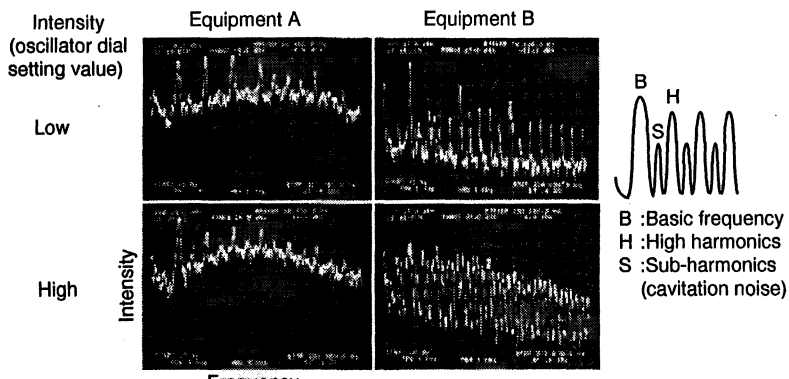


Fig. 7 Frequency Distributions

## THE EVALUATION OF ULTRASONIC DAMAGE CAUSED BY SINGLE WAFER CLEANING SYSTEM

A. Tomozawa, H. Kinoshita,  
Y. Sakata, A. Ohnishi,  
Y. Harada, \* N. Hiraoka \*\*

Takasaki Technical Center, Hitachi Microcomputer System LTD.  
1-1, Nishiyokote-machi, Takasaki-shi, Gunma-ken 370, Japan  
PRE-TECH Co. Ltd. \*  
2-1-14, Fuchuu-naka-machi, Fuchuu-shi, Tokyo 183, Japan  
Dainippon Screen MFG. Co. Ltd. \* \*  
322, Hadukashi-Furukawa-cho, Fushimi-ku, Kyoto 612, Japan

To remove particles from backside of Si wafers in semiconductor manufacturing line, single wafer scrubber machine having high-frequency ultrasonic water jet was applied. High-frequency ultrasonic is safe, but wafers were damaged on front-side surface during backside cleaning. Preparing various thicknesses of Si wafers, changing incident angle, and transmissivity of ultrasonic through Si was measured. Afterwards Si wafers with LSI patterns were prepared, influence of backside cleaning in various transmissivity value was investigated. The defect density of LSI patterns and ultrasonic transmissivity were closely related. We can understand the mechanism of damage, by using the theory of "oblique incident of ultrasonic waves to the plate". During ultrasonic backside cleaning, VLSI devices on the surface-side were destroyed by vibration of rinse water, caused by transmitted ultrasonic energy. But, these damages can be avoided by optimizing back rinse.

### INTRODUCTION

As the VLSI integration scale increases, it becomes more important to decrease particles on the wafer surface during fabrication of VLSI in the semiconductor manufacturing line. We found that some part of particle contamination is caused by *Recontamination*. During the batch-type-wet-cleaning process, such as RCA cleaning or water rinsing, particles coming off of the backside of the wafers are diffused into the etchant, and re-adhere to the front side of a neighbor wafer as shown in Fig.1 (1). Furthermore the backside contamination is caused by wafer transportation in previous process machines. Generally robot-systems having vacuum-chuck is used as wafer-transportation from a wafer cassette to a process chamber of a single wafer fabrication equipment. Inside the process chamber of such equipment, electrostatic-chuck or mechanical-chuck is used for holding a wafer. So many particles are adhered onto backside of wafers after processing of photo-litho or dry-etching (2). (These are single wafer systems.) Therefore it is necessary to clean backside of the wafer before batch type wet cleaning process.

To remove the particles from the backside of the wafers, the wafer scrubber

machine shown in Fig.2-a, having an ultrasonic water jet called D-Sonic, is applied (2). After ultrasonic backside cleaning, authors found that some VLSI devices which existed on the "opposite side" of the wafer that is the front-side of the wafer were destroyed. Poly-Si patterns of LSI were gone, and Al wirings were bending as shown in Fig.3-b. These defects were distributed focusing on the center of the wafers as shown in Fig.3-a.

Generally, it is well known that in low-frequency ( $20\sim 40$ kHz) ultrasonic bath type cleaning, damage and cleaning efficiency are closely related because of its cavitation phenomena. So in case of low-frequency, we must control the ultrasonic generation power, most carefully (3). On the other hand, in a high-frequency (around 1MHz) ultrasonic cleaning system, energy is divided smaller than cavitation threshold value (4). It is expected that there's no damage in mega-sonic cleaning process. Therefore some people say that megahertz-ultrasonic system is damageless. But actually, our wafers were damaged in a single wafer cleaning system using this *damageless-ultrasonic jet*. We analyzed this unexpected phenomenon that was ultrasonic damage through the Si wafer to the front-side surface.

## EXPERIMENTAL

Various thicknesses,  $250\mu m\sim 3mm$  of (100) Si wafers were used in the experiments, and ultrasonic transmissivity through Si wafers were measured. Measurement method is shown in Fig.4. The ultrasonic jet nozzle was immersed in the water vessel which is big enough to prevent the influence of reflection from the wall. (Actually, the ultrasonic water jet nozzle is used in the air as shown in Fig.2-b, but we must use it in the water to measure the sound pressure.) The frequency of ultrasonic wave is 1.567MHz. The maximum generation power of ultrasonic wave is 48W. The diameter of the nozzle is 4mm. Sound pressure was measured by a hidrophone probe. Si wafer was set between nozzle and probe. The distance between nozzle and wafer is 25mm, the same as the actual condition of the scrubber. Transmissivity is defined as the ratio of a sound pressure through Si wafer to the one without Si wafer. Transmissivity was measured in various incident angles,  $0\sim 75$ degrees, by changing angle of the Si wafer.

After these experiments, Si wafers with LSI patterns were prepared, and the backside wafer scrub process in various conditions of ultrasonic transmissivity were applied to them. Both of these back rinse conditions, without water, and with water, which was used as an anti-mist, were examined. After that treatment, to find out the defects of LSI patterns, "Pattern Defect Inspection System" was used. The relationship between ultrasonic transmissivity and defect density was investigated.

## RESULT AND DISCUSSION

The result of this experiment about transmissivity is shown in Fig.5~8. The change of transmissivity is complicated depending on Si thickness or incident angle as shown in Fig.5. According to the theory of ultrasonic transmission through thin film, transmissivity D is indicated by following equation on the assumption that the transverse wave component of ultrasonic transmission in Si is negligible.

$$D(t_{Si}, \theta) = \frac{4}{4\cos^2(\alpha) + N^2\sin^2(\alpha)} \quad [1]$$

where

$$\alpha = (2\pi t_{Si} / \lambda_{Si})\cos(\phi) \quad [1a]$$

$$N(t_{Si}, \theta) = \frac{\rho_{Si}C_{Si}\cos(\theta)}{\rho_w C_w \cos(\phi)} + \frac{\rho_w C_w \cos(\phi)}{\rho_{Si}C_{Si}\cos(\theta)} \quad [1b]$$

where  $\rho_{Si}$ ,  $t_{Si}$  are density, thickness of Si respectively,  $C_{Si}$ ,  $\lambda_{Si}$  are transmission speed, wave length of ultrasonic wave in Si respectively,  $\rho_w$  is density of water,  $C_w$  is transmission speed of ultrasonic wave in water and  $\theta$ ,  $\phi$  are incident angle in water, refractive angle in Si respectively (4).

In the case of incident angle  $\theta = 0$  ( i.e.  $\phi = 0$ ), that is perpendicular incidence, transmissivity is periodically changing depending on Si thickness, as shown in Fig.6. The transmissivity  $D_0$  of perpendicular incidence is shown as

$$D_0(t_{Si}) = \frac{4}{4\cos^2(\alpha_0) + N_0^2\sin^2(\alpha_0)} \quad [2]$$

where

$$\alpha_0 = 2\pi t_{Si} / \lambda_{Si} \quad [2a]$$

$$N_0(t_{Si}) = \frac{\rho_{Si}C_{Si}}{\rho_w C_w} + \frac{\rho_w C_w}{\rho_{Si}C_{Si}} \quad [2b]$$

From this equation, we can easily understand that transmissivity D reaches maximum value when  $t_{Si} / \lambda_{Si} = (2n) / 4$  and become minimum value when  $t_{Si} / \lambda_{Si} = (2n-1) / 4$ . Therefore  $\lambda_{Si}$  is calculated as

$$\lambda_{Si} = C_{Si} / f = 8433 \text{m/sec} / 1.567 \text{MHz} = 5424 \mu \text{m},$$

in Fig. 6, we can confirm that  $D_0$  has reached maximum at  $2700 \mu \text{m}$  of Si thickness that is  $\lambda_{Si} / 2$  and minimum at  $1360 \mu \text{m}$  that is  $\lambda_{Si} / 4$  (5).

In this case Si thickness at  $550 \mu \text{m}$  is selected because  $500 \sim 750 \mu \text{m}$  thickness Si wafers are ordinarily used in semiconductor manufacturing line,  $\theta$ -dependence of transmissivity is shown in Fig.7. Transmissivity is decreased with increasing incident angle  $\theta$ . This phenomenon was easily expected, because Si wafer thickness towards the direction of sound transmission is increased with  $\theta$ . But from 15 degrees of the angle, transmission D is suddenly increased and becomes

becomes maximum value around 30 degrees, and then goes down to original curve at 40 degrees. When decreasing Si thickness this tendency is expanded. The range of irregular points are broadened and peak value of D becomes higher. We can understand these phenomena by using the theory of "oblique incident of ultrasonic waves to the plate" (4). According to this theory, the maximum transmission is generated when (a) the longitudinal wave of incident ultrasonic sound in water, and (b) the transverse wave on Si surface caused by sound impact, are in phase as shown in Fig.8. This situation is shown as

$$\sin(\theta) = \frac{\lambda_w}{\lambda_{ss}} \quad [3]$$

where  $\theta$  is incident angle of ultrasonic wave that causes maximum transmission and  $\lambda_w$  is wave length of longitudinal ultrasonic wave in water, and  $\lambda_{ss}$  is wave length of transverse wave on Si surface. And this equation can be changed as

$$\sin(\theta) = \frac{V_w}{V_{ss}} \quad [4]$$

where  $V_w$  and  $V_{ss}$  are velocity of waves. The incident angle of bulk Si that causes maximum transmission is calculated as follows (5).

$$\theta = \arcsin(V_w/V_{ss}) = \arcsin(1483\text{m/sec} / 5843\text{m/sec}) = 14.7^\circ \quad [4a]$$

This is almost the same value as 15 degrees, that is the starting point of transmission increase, as mentioned before. The incident angle  $\theta$  of the starting point of transmission increase and that of maximum transmission value are represented in various thicknesses of Si in Fig.9. In spite of changing thickness, the angle of starting point for transmission increase is always at constant value, that is corresponding to maximum transmission of bulk Si. And when Si thickness is thin, under  $2000\mu\text{m}$ , incident angle  $\theta$  causing maximum transmission value become larger than that of bulk Si.

$V_{ss}$  also can be shown as

$$V_{ss} = \sqrt{(G/\rho)} \quad [5]$$

where,  $\rho$  is the density of Si and G is shear modulus of (100) bulk Si. We can speculate that the shear modulus of thin wafer Si ( $G_t$ ) becomes smaller than that of bulk Si ( $G_b$ ), then  $V_{ss}$  of wafer Si becomes smaller than that of bulk Si, and finally maximum transmission angle of wafer Si become bigger than that of bulk Si.

Next we measured the ultrasonic damage, using Al wiring patterned wafers in various transmissivity, with or without surface rinse water. The result of this experiment is shown in Fig. 10. The defect density of Al wiring pattern is directly proportional to the transmissivity of ultrasonic energy, and, without surface rinse water, there's no defect on the front side of the wafer, even in higher transmissivity

condition. This result shows that the Al wiring pattern on the surface side of a wafer is destroyed by the vibration of surface rinse water caused by transmitted ultrasonic energy from backside wafer cleaning.

## CONCLUSION

According to the result of these experiments, we can understand the mechanism of these unexpected phenomena. During ultrasonic water jet cleaning of backside of the wafer, the VLSI devices on the surface-side were destroyed by the vibration of water, caused by ultrasonic energy transmitted from backside cleaning jet. But, these damages can be avoided by optimum process conditions of incident angle and surface rinse. And manipulating this phenomena, we'll be able to offer a new machine, such as "the simultaneous both side single wafer cleaning system with oblique incident of high frequency ultrasonic waves".

## REFERENCES

- 1)Y. Sakata, A. Ohnishi, G. Kishi, S. Izumo, H. Kondou, A. Tomozawa : "The Particle Contamination during Wet Cleaning Process onto Various Wafer Surfaces", pp. 560-563, Proceedings on Semiconductor Cleaning Technology of the 188th Electrochemical Society Meeting, Chicago, October 8-13, 1995
- 2)K. Sugimoto, N. Hiraoka, M. Nonomura : "Scrub Cleaning Technology", Ultrasonic TECHNO, pp.24-27, Vol.3, 1996
- 3)A. Onishi, A. Chi yokawa, A. Tomozawa: "The Evaluation of Ultrasonic Damage(1) caused by Bath Type Wafer Cleaning System" Extended Abstracts Vol. 97-2, No.1932 of the 192th Electrochemical Society Meeting, Paris, August 30-September 5, 1997
- 4)J. Miyoshi, Y. Kikuchi, O. Yoshimoto : "Ultrasonic Technology Handbook", The Nikkan Kogyo Shimbun LTD, 1960
- 5)S. Iizumi: "Chronological Scientific Table", Maruzen Co. LTD, 1981

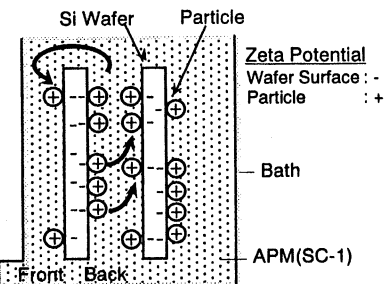


**Fig. 1 Particle Recontamination Mechanism  
in Bath Type Wafer Cleaning System**

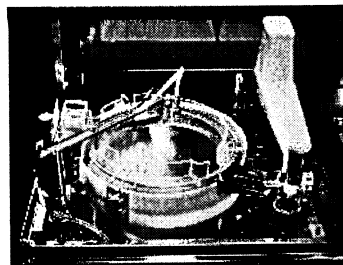


**Fig. 2-a Wafer Scrubber Machine  
with an Ultrasonic Water Jet**

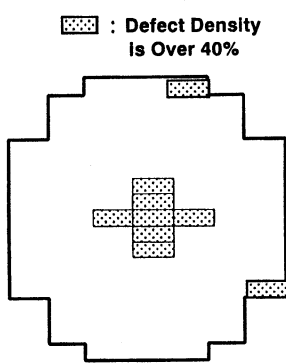


**Fig. 3-a Defect Distribution  
(Superimposition of 36 wafers)**

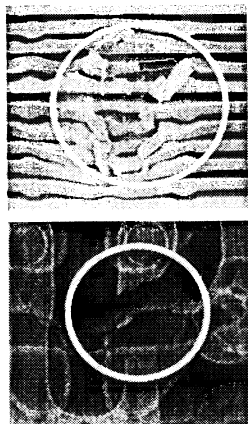


**Fig. 3-b Defect of AL Pattern  
and Poly Si Pattern**

(Fail chip are concentrated in the center of wafers.)

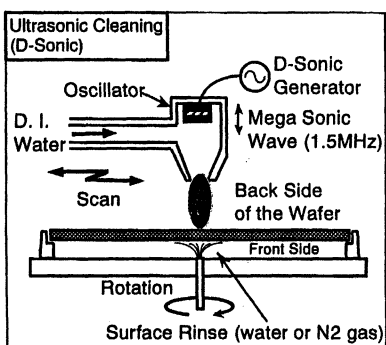


**Fig. 2-b Ultrasonic Cleaning Equipment (Single Wafer Type)**

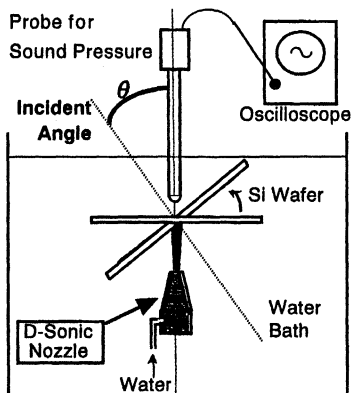


**Fig. 4 Measurement Method of Ultrasonic Transmissivity through Si Wafer**

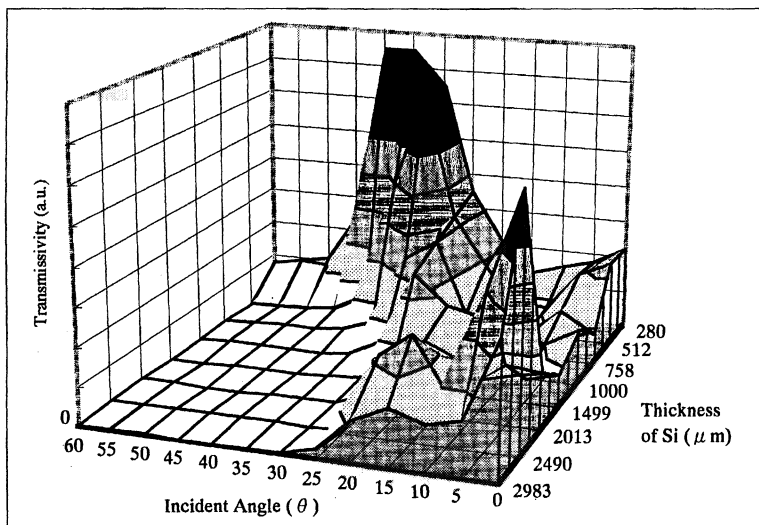


**Fig. 5 Ultrasonic Transmissivity through Si Wafer depending on Si Thickness or Incident Angle.**

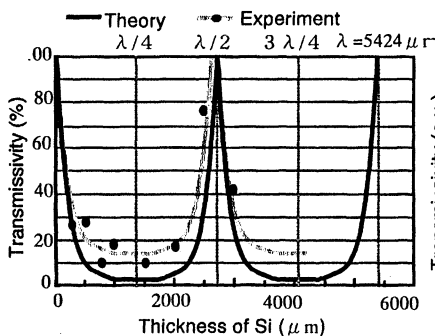


Fig. 6 Ultrasonic Transmissivity thr. Si (Perpendicular Incidence)

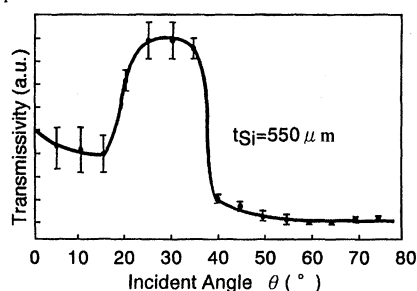


Fig. 7 Ultrasonic Transmissivity thr. Si (Oblique Incidence)

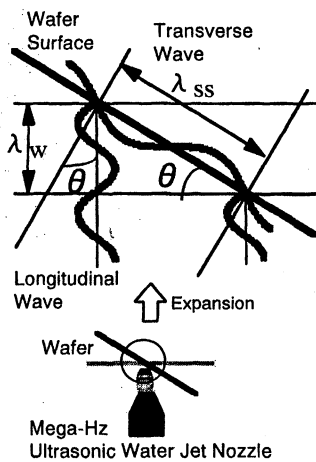


Fig. 8 The Agreement on Phase of Two Waves (Longitudinal Wave & Transverse Wave)

$$\text{Boundary Condition for Maximum Transmissivity} \quad \sin \theta = \frac{\lambda_w}{\lambda_{ss}}$$

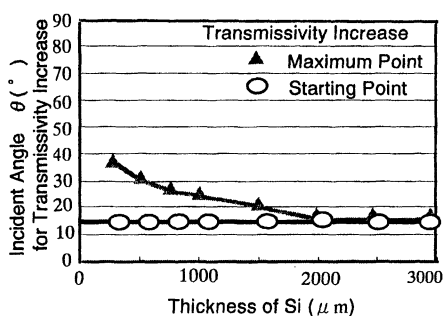


Fig. 9 The Incident Angle causing Maximum Ultrasonic Transmission

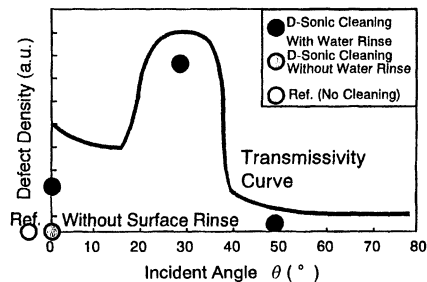


Fig. 10 Defect Density of Al Patterns on the Front side of the Wafer caused by Backside US Cleaning

## **WET CLEANING - Metallic Contaminants**



## OPTIMIZED RINSING FOR LOW METALLIC CONTAMINATION

Lee M. Loewenstein\* and Paul W. Mertens

IMEC, Kapeldreef 75, B-3001 Leuven, Belgium

\*On assignment from Texas Instruments, PO Box 650311, M/S 3701  
Dallas, Texas 75265

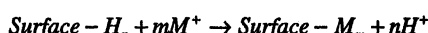
Acidifying the rinse solution after SC1 or SC2 cleaning prevents some metallic ions such as  $\text{Ca}^{2+}$  from contaminating the silicon wafer surface. We tested the effect of acidification with  $\text{HNO}_3$  over the range pH 4 - 6, in the presence of solute species  $\text{Ca}^{2+}$ ,  $\text{K}^+$  and  $\text{Fe}^{3+}$ . 2 ppb Ca at a pH=6, for instance, gives  $>10^{12}$  atoms/cm<sup>2</sup> of Ca on the wafer surface. The Ca contamination, however, can be reduced in direct proportion to  $[\text{H}^+]$ , while K and Fe are not affected. A model based on the chemical equilibria of the metallic species with the silicon dioxide surface agrees well with the observed behavior.

### INTRODUCTION

A major goal of wafer cleaning is to reduce surface metal contamination to as low a level as possible. The SC2 process chemistry is designed to remove metal from the silicon surface. Metal removal is largely a function of the acidic solution in which many metals are quite soluble. After processing in SC2 solution, however, the wafers are rinsed in water of near neutral pH. This places wafers again at risk of contamination by any residual metals present in the water. Even with state-of-the-art water purity, mid- $10^{10}$  atom/cm<sup>2</sup> levels of metals such as Ca on wafer surfaces are commonly seen. Reliance on ultrapure water can also lead to an unstable manufacturing environment, since fluctuations of metal contaminant concentrations in solution will have negative consequences on device performance and yield.

An alternative approach is to rinse the wafers with a very dilute acid instead of DI water. Fabry et al. have described that oxalic acid and carbon dioxide can reduce the level of iron contamination.<sup>1</sup> Our paper explores the effect of acidic rinsing on metal contamination of semiconductor surfaces. We test the effects of pH, T, time, and final clean type (SC1 or SC2) on contamination. The rinse solution is deliberately contaminated with known amounts of metals, Ca, K and Fe.

We develop a model of the silicon dioxide surface in equilibrium with metal and hydrogen ions:



In such a model, the surface concentration of a metal,  $\sigma_M$ , is given by an expression of the form:

$$\sigma_M = \frac{\text{const.} [M^+]^m}{[H^+]^n} \quad [2]$$

where  $m$  and  $n$  are integers. The metal concentration was fixed in this work, so we can only test the dependence on  $[H^+]$  here.

## EXPERIMENTAL

The experiment followed a screening design suggested by a commercial DOE software package<sup>2</sup>. Screening designs choose experimental trials along the edges of the design space, plus the centerpoint to determine the presence of curvature. Variables are shown in Table I.

*Table I. Rinsing process parameters.*

Variable	Unit	Range	Type
Final clean	-	SC1 or SC2	variable
log [HNO <sub>3</sub> ]	(mol/L)	-5.6 - -4.0	variable
OR temperature, T	°C	20 - 70	variable
OR time	min	6 - 31	variable
OR flow rate	(L/min)	3	fixed
K, Fe and Ca concentrations	(mol/L)	$5 \times 10^{-8}$	fixed

A manual wet bench was used for the immersions in SC1 and SC2 and for the metal-spiked final rinse process. The SC1 and SC2 immersions were performed separately in the same heated, recirculating bath. The cleaning solutions were circulated and filtered. The SC1 solution was prepared in a volume mixing ratio of 0.25:1:5 NH<sub>3</sub>:H<sub>2</sub>O<sub>2</sub>:H<sub>2</sub>O. The SC2 was prepared in a volume mixing ratio of 1:1:5 HCl:H<sub>2</sub>O<sub>2</sub>:H<sub>2</sub>O. The baths were heated to 50 °C. Wafers were processed for 10 min in the cleaning solutions. At the end of the immersion cleaning the wafers were lifted from the cleaning tank and excess cleaning chemicals allowed to drip off for a few seconds. The wafers were then put into the overflow rinse (OR) tank. Figure 1 contains a schematic of the experimental processing.

In some of the analysis to follow, the dimensionless turnover,  $\tau$ —given by  $\tau = \phi t / V$ , where  $t$  is the time,  $\phi$  the flow rate and  $V$  the tank volume—is used.

The feed line has a connection point used for spiking the UPW rinse water immediately before entering the actual rinse tank. A metering pump was connected to spike with a premixed solution of HNO<sub>3</sub> and metallic contaminants. Metal solutions (Merck AAS standard solutions) were mixed to give equimolar mixtures of Ca<sup>2+</sup>, K<sup>+</sup> and Fe<sup>3+</sup> at  $5 \times 10^{-8}$  mol/L, corresponding to 2 ppb Ca.

After the rinsing process was completed the wafers were immediately spun dry (Semitool) without any additional rinsing.

Wafers were evaluated for particles or metal surface contamination. The metal surface contamination was determined by VPD-DC-TXRF (vapor phase decomposition-droplet collection-total-reflectance X-ray fluorescence). Wafers were individually exposed to HF-vapor for 8-10 min. DC was performed with an automated scanner PAD-SCAN (GeMeTec) using a spiral pattern from wafer center to edge and back. Subsequently the droplet was dried under a heat lamp. TXRF measurements were performed with an Atomika TXRF8010. Particles were counted with the Surfscan 6400.

## RESULTS AND ANALYSIS

Table II contains the surface concentrations of metals and nonmetals measured by VPD-DC-TXRF in the columns marked *Expt*.

*Table II. Processing conditions in order of trials, and resulting surface concentrations of elements measured by VPD-DC-TXRF in units of  $10^{10}$  atoms/cm<sup>2</sup>, compared with model predictions.*

Trial	Final	pH	T	t	Ca		K		Fe		Zn	
	Clean		C	min	Expt	Model	Expt	Model	Expt	Model	Expt	Model
8	SC1	5.6	20	31	425	240	7.5	2.3	26.8	6.5	11	3.2
10	SC1	5.6	20	6	234	263	1.1	1.4	10.4	8.8	3.8	3.6
6	SC1	5.6	70	19	552	389	1.6	3.3	5.3	9.5	5.4	2.2
11	SC1	4.8	44	6	43.6	36.3	0	2.8	35.3	6.9	0.1	0.4
4	SC1	4.0	20	6	2.6	3.8	1.8	1.4	3.6	6.8	0	0.1
1	SC1	4.0	70	31	4.3	5.0	6.5	5.4	4.3	5.4	0.1	0.1
2	SC2	5.6	20	6	1.8	146	3.9	1.3	0	2.2	0	3.7
3	SC2	5.6	70	31	135	195	4.6	5.1	1.0	1.7	0.8	1.9
12	SC2	4.0	44	19	17.2	20.4	3.4	2.6	4.8	1.7	1.1	0.4
5	SC2	4.0	20	31	2.6	1.9	1.35	2.1	0.9	1.2	0.5	0.1
7	SC2	4.0	70	6	3.8	3.1	4.8	3.0	4.7	1.8	0.1	0.1
9	SC2	4.0	70	31	6.2	2.8	7.8	5.0	4.9	1.3	0.2	0.1
Control					6.6	2.6	0.2				3.1	

We transformed the metal surface concentration variables by taking their logarithms. Trial 2 was excluded from the analysis, as its inclusion resulted in extraordinary influence of this point in multiple responses. Possibly there was a larger carryover of liquid from the cleaning tank to the rinsing tank for this trial. The general effects are the same with or without this point.

Significant effects can be determined by comparing coefficients,  $a_i$ , with their standard deviations in Table III. Furthermore, comparison of the replicate and residual standard deviations indicates the presence of statistically unaccounted experimental variations, apparent particularly for Fe. The  $R^2$  values gives a measure of the total fit: Ca is fit relatively well, while the other metals show poorer fits.

*Table III. Coefficients and their standard deviations (SD) for surface concentration models using centered variables.*

		Ca		K		Fe		Zn	
	<i>i</i>	<i>a<sub>i</sub></i>	<i>b<sub>i</sub></i>	<i>a<sub>i</sub></i>	<i>b<sub>i</sub></i>	<i>a<sub>i</sub></i>	<i>b<sub>i</sub></i>	<i>a<sub>i</sub></i>	<i>b<sub>i</sub></i>
Constant	0	1.44	1.44	0.42	0.42	0.53	0.53	-0.34	-0.34
	SD	0.05	0.05	0.05	0.05	0.04	0.04	0.12	0.12
log [HNO <sub>3</sub> ]	1	-1.14	-0.92	-0.01	-0.01	-0.07	-0.06	-0.95	-0.77
	SD	0.07	0.05	0.06	0.05	0.05	0.04	0.15	0.13
1/T	2	-333.	-0.08	-751.	-0.19	-66.5	-0.02	444.	0.11
	SD	209.	0.05	199.	0.05	158.	0.04	492.	0.12
turnover	3	-0.01	-0.02	0.06	0.11	-0.03	-0.07	-0.01	-0.03
	SD	0.03	0.06	0.03	0.06	0.02	0.04	0.07	0.14
SCx	4	-0.13	-0.13	-0.01	-0.01	-0.31	-0.31	0.00	0.00
	SD	0.05	0.05	0.05	0.05	0.04	0.04	0.12	0.12
Repl. SD		0.23		0.26		0.40		0.54	
Res. SD		0.21		0.20		0.16		0.49	
R <sup>2</sup>		0.95		0.46		0.50		0.69	

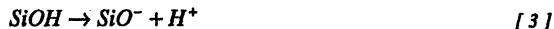
*Normalized* coefficients can be used to determine which effects are significant *over the range* of the experiment, as shown in Table III. The magnitude of the coefficients represent the effect of the variables over the experimental space. For each metal, we can easily see which variables are important. Significant effects can be determined by comparing coefficients with their standard deviations in Table III. Furthermore, comparison of the replicate and residual standard deviations indicates the presence of statistically unaccounted experimental variations, apparent particularly for Fe.

General effects were as follows: (1) The process variables had no effect on the level of particle deposition on the wafer. (2) The experiment produced significant effects on Ca deposition, in contrast to particle deposition. The most significant variable is *log\_Rinse\_HNO<sub>3</sub>*. The difference between the average high and average low [H<sup>+</sup>] has a negative effect on measured Ca. SC2 has a smaller negative effect on Ca. The effect of final clean is small and barely significant. The effects of the T and turnover number are insignificant. (3) Very little K was left on the wafer under any processing conditions. T has a significant effect on the surface concentration of K, which is not seen if a model linear in K is used. (4) Fe deposition was of very low magnitude, comparable to K. Only the final clean seems to have an effect on the surface Fe concentration. (5) Zinc was not deliberately added in this experiment, yet it appears consistently in the TXRF analysis. It probably came from one of the AAS solutions. Log [HNO<sub>3</sub>] is its only significant term.

Figure 2 shows several metal deposition responses to log [HNO<sub>3</sub>] and 1/T. The numbered contour levels are approximately one prediction standard deviation apart

## DISCUSSION

Most of the observations can be explained by a model of metal substitution for hydrogen at surface hydroxyl groups. We can understand the behavior of the metals with a simple model that relates a hypothetical surface species (represented by  $\text{SiO}^-$ ) to  $\text{H}^+$  and  $\text{M}^+$



From these equations we find

$$\log \sigma_{\text{SiOM}} = \log \frac{K_1 \sigma_{\text{SiOH}}}{K_2} + \log[\text{M}^+] - \log[\text{H}^+] \quad [5]$$

where  $[\text{H}^+]$  and  $[\text{M}^+]$  are volume concentrations, and  $\sigma_{\text{SiOH}}$  and  $\sigma_{\text{SiOM}}$  are surface concentrations.

If the active surface sites are initially protonated when the wafer is placed in solution, then  $\sigma_{\text{SiOH}}$  can be expressed by

$$\sigma_{\text{SiOH}} = \left( 1 + \frac{K_1}{[\text{H}^+]} + \frac{K_1 [\text{M}^+]}{K_2 [\text{H}^+]} \right)^{-1} \sigma_{\text{SiOH}}^o \quad [6]$$

where  $\sigma_{\text{SiOH}}^o$  is the original surface concentration of active sites,  $\text{SiOH}$ . In acidic solutions with low metal concentrations, when  $[\text{H}^+]$  is large and  $[\text{M}^+]$  is small, we can expect that

$$\sigma_{\text{SiOH}} \approx \sigma_{\text{SiOH}}^o \quad [7]$$

and thus that the first term of the above equation will be nearly constant.

If we include the  $T$  dependence of the equilibrium constant, we find

$$\log \sigma_{\text{SiOM}} = \text{Constant} - \Delta G/RT + \log[\text{M}^+] - n \log[\text{H}^+] \quad [8]$$

where  $\Delta G$  is the change in Gibbs free energy for the reaction.  $n=1$  or  $2$  (or some other integer) depending on the order of the reaction. In equilibrium, the turnover or flow rate would have no effect on surface concentration.

### Comparison of chemical and empirical models

Table III lists the coefficients,  $a_0-a_4$ , and their standard deviations, for the comparable model obtained in these experiments:

$$\log \sigma_{\text{Metal}} = a_0 + a_1(\log[HNO_3] - \log[HNO_3]_c) + a_2(1/T - 1/T_c) + a_3(t - t_c) + a_4 SCx \quad [9]$$

where  $T$  is the absolute temperature in K,  $t$  the number of turnovers, and  $SCx$ , the final clean ( $x=1$  or 2) having corresponding values of -1 and 1. From these equations we can see a correspondence between  $a_1$  and the coefficient of  $\log [H^+]$ . The coefficient  $a_2$  corresponds to  $-\Delta G/R$ . Since this is an equilibrium model,  $a_3$  should be 0, while  $a_4$  could be non-zero if the last cleaning process has an effect on  $\sigma_{SiOH}$ . Comparison of the coefficients with their standard deviations shows which ones are significant.

For Ca and Zn,  $n$  is approximately 1, while for K and Fe,  $n$  is nearly 0. These results suggest that Ca and Zn associate with the surface reactive sites in a 1:1 manner, not 1:2. A possible reason for this is that the attached Ca-OSi groups are charged +1. A model where the surface site is charged -2 and neutralized by an exchange of  $M^{2+}$  for  $2 H^+$  would not be able to account for the observed behavior.

### [HNO<sub>3</sub>] OR PH

Surface concentrations of Ca and Zn are strongly dependent on pH, as Figure 3—a plot of [9]—shows. Higher [HNO<sub>3</sub>] (lower pH) results in reduced surface metal contamination for Ca and Zn, but no significant difference for K and Fe.

Previous work from this laboratory<sup>3</sup> indicated a greater dependence of the amount of surface Fe on the pH than suggested here. Part of the difference could be related to that work removing metal from the surface, while this work looks at deposition onto the surface. Admittedly these are both aspects of the same chemical phenomenon, as the surface-solution approaches equilibrium, yet the situations are substantially different, since the previous work removed Fe from the wafer surface into a solution that was effectively free of Fe ions as the cleaning solution was flowed continuously through the process tank.

Another consideration that might account for this difference is the significantly lower pH of Reference 3 (pH=1-3) than that of this work (pH=4-6). In agreement with the present work, Reference 3 showed at its highest pH (3) that the removal efficiencies of Ca and Zn were significantly higher than Fe, at least at 20 C. Removal efficiencies at pH=3 and 20 C were approximately 88, 98 and 76% for these elements, respectively.

### TEMPERATURE

T was one of the least important variables, except for K contamination.

## TIME

Time or turnover had an effect on the level of contamination for Fe. As performed in this experiment, the turnover had several effects. One was to increase the time of exposure of the wafer to the metal ion contaminants in solution. Another effect, though, was to dilute any solution brought from the cleaning tank into the rinse tank. Thus, the pH of the rinse tank varied over time. Reference 3 is in reasonable agreement with this study as it showed, for Fe removal, negligible dependence on process time.

## FINAL CLEAN

SC2 final clean results in lower surface metal contamination than SC1. This is reasonable since SC2 last processing will lower the pH of the rinse tank for much of the rinse step.

## CONCLUSIONS

The experiment described here succeeded in measuring the effectiveness of a number of rinse parameters of preventing the deposition on the Si surface of metal contaminants, Ca, Fe and K. Ca deposition appears to be the most significant problem for deposition from contaminated solution at *neutral pH*. An acidic rinse is helpful in limiting the deposition of Ca, as well as other species such as Zn. Any acid which can promote the solubility of the metal ions according to the principals of the equations discussed above will help, provided that its counter ion does not itself form an insoluble metal-anion precipitate. One obviously would prefers an acid which does not itself constitute a contamination problem either due to particulates or its adherence to the wafer surface.

## REFERENCES

<sup>1</sup> L. Fabry, S. Pahlke, L. Kotz and Peter Blöchl, in *Proceedings of the Third International Symposium on Ultra-clean Processing of Silicon Surfaces* (Acco, Leuven, Belgium, 1996), p. 163.

<sup>2</sup> ECHIP, version 6, ECHIP Incorporated, Hockessin, DE.

<sup>3</sup> T.Q. Hurd, P.W. Mertens, L.H. Hall and M.M. Heyns in *Proceedings of the Second International Symposium on Ultra-clean Processing of Silicon Surfaces* (Acco, Leuven, Belgium, 1994), p. 41.

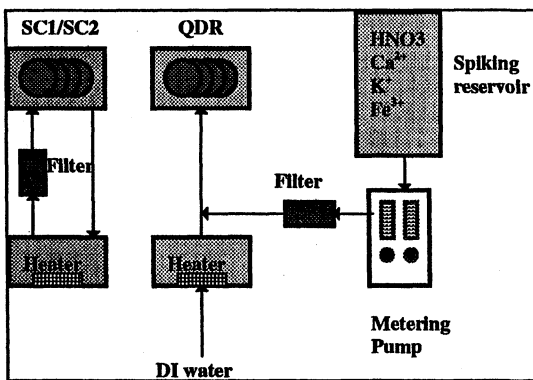


Figure 1. Schematic of experimental apparatus.

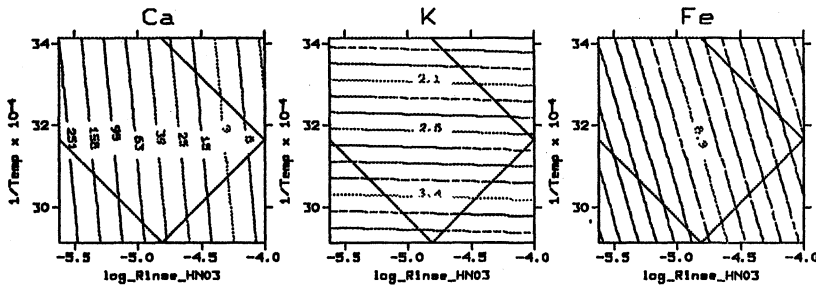


Figure 2. Response surface plot for Ca, K, and Fe deposition ( $10^{10}/\text{cm}^2$ ) versus  $\log [\text{HNO}_3]$  and  $1/T$ , for Final Clean=SC1, and Turnovers=3.

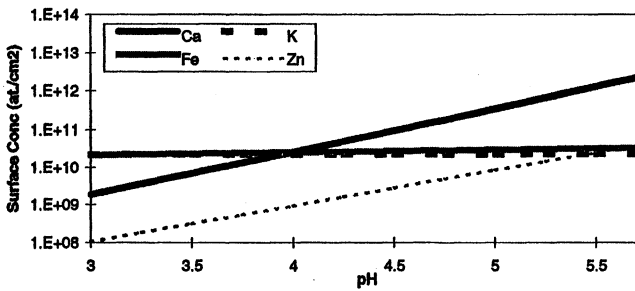


Figure 3. Calculated dependence of metal surface concentration on pH ( $T=20^\circ\text{C}$ ,  $t=5$ ).

# INTERACTION AMONG CONTAMINANT METALS IN WET CLEANING PROCESSES

Yuka Hayami, Yoshiko Okui, Hiroki Ogawa and Shuzo Fujimura\*

Process Development Division C850, Fujitsu Limited,  
1-1, Kamikodanaka 4-chome, Nakahara-Ku, Kawasaki, Kanagawa 211, JAPAN

\*Fujitsu Laboratory LTD., 10-1 Morinosato-Wakamiya,  
Atsugi, Kanagawa 243-01, JAPAN

Interaction among contaminant metals in wet cleaning processes was found. In particular, the Ni removal ratio in acid cleaning depended on the amount of aluminum (Al).

Two types of intentionally contaminated wafers prepared by IAP -method, one was contaminated by only Ni (single contamination) and another was contaminated by plural metal (multiple contamination), were treated in HNO<sub>3</sub>, SPM and DHF. Removal ability of metals in each solution was evaluated by ICP-MS and TXRF.

Ni on the wafers prepared by the single contamination was not removed effectively by the acid solutions, but it by the multiple contamination was removed effectively when certain amount Al was contained in SC-1 solution used for IAP -method. TXRF measurement shows that Ni on the wafers, on which it was removed effectively by acid solutions, distributed in the shallower part in vicinity of wafer surface than that on the wafers where it was not removed effectively by acid solutions. These suggest that removal ratio of Ni in acid cleaning depends on the difference of contaminant state of Ni caused by contamination circumstance.

## INTRODUCTION

Importance of cleaning technology is gradually increasing with increase in the influence of the technology upon the production yield of Ultra Large Scale Integration (ULSI) devices. In these days, one of the requirement for the cleaning technology is the removing contaminants such as particle, organic materials and metals. To satisfy this requirement, we must characterize adsorption and/or the desorption phenomena of contaminants in cleaning processing.

Many researchers has investigated the relationship between metallic contaminants and conventional cleaning solutions, for instance, the adsorption behavior of Al and Fe in SC-1 solution<sup>1,2)</sup> and that of Cu in DHF<sup>3)</sup>. Actually, SC-1 solution with chelating agent<sup>4)</sup> and DHF with H<sub>2</sub>O<sub>2</sub><sup>5)</sup> and ionized water<sup>6)</sup> were developed through analysis of behavior of contaminant metals in the solutions . However they has focused on the adsorption of the objective metal in SC-1 solution,

thus they used sample wafers that were immersed in chemical solutions with only one objective metal. Although Si-surface is contaminated simultaneously by several metallic contaminants in practical cleaning solutions used in actual ULSI fabrication processes, the interaction among those adsorbed metals has not been investigated except H. Okuda et al.<sup>7</sup>. Okuda et al. pointed out that the amount of Cu and Ni adsorbed on a Si surface in an SC-1 solution containing Cu, Ni and Fe was smaller than that adsorbed in an SC-1 solution containing each metal, independently. This indicates that the single contamination dose not reflect the practical contamination in which plural metallic contaminants attacked to the Si surface simultaneously. Thus we should not evaluate a new cleaning solution or process without consideration of the interaction among metals.

In this paper, we try to reveal the interaction among metallic contaminants by measuring the amount of metals on sample wafers, which were immersed in SC-1 solution containing several metallic contaminants (multiple contamination), after and before chemical treatment.

## EXPERIMENTAL

Sample wafers were 4-inch and 6-inch P-type Czochralski (CZ) Si (100) with a resistivity of 10  $\Omega\text{-cm}$ . We used P- and N-type Si wafers but did not detect significant differences between them in our experimental results. Thus, we discuss here the results of P-type silicon.

Figure 1 shows experimental procedure in this study. After conventional RCA cleaning, we intentionally contaminated sample wafers by immersing them into diluted SC-1 solution to which the standard solutions containing metals for atomic absorption spectroscopy (AAS) were added (=IAP Method). To evaluate the cleaning ability of solutions or processes, we have traditionally used test wafers which were intentionally contaminated by objective contaminants metals. Three methods<sup>8,9</sup> to prepare metallic contaminated wafers have reported, and in particular among them, immersion in alkaline hydrogen peroxide solution (IAP)<sup>10</sup> is the most commonly used. This is because, SC-1 solution, which is used for IAP-method, is one of the most widely used solution in practical ULSI fabrication processes for removing particles and organic contaminants. Thus, we used this technology in this study. Metallic contaminants intentionally added were aluminum (Al), calcium(Ca), cadmium (Cd), cobalt (Co), chromium (Cr), copper (Cu), iron (Fe), magnesium (Mg), manganese (Mn), sodium(Na), and nickel (Ni). We prepared two types of contamination circumstances. One is called single contamination in which sample wafers were immersed into SC-1 solution containing only Ni. Another one is called multiple contamination, in which sample wafers were contaminated by several metals at the same time in SC-1 treatment of one time.

After the above intentional contamination treatments, we immersed the sample wafers in several chemicals; diluted hydrofluoric acid (DHF), nitric acid ( $\text{HNO}_3$ ), sulfuric acid and hydrogen-peroxide mixture (SPM), hydrochloric acid and hydrogen-peroxide mixture (SC-2),etc.. To confirm the cleaning ability of these solutions, we etched the sample wafers by HF/ $\text{HNO}_3$  mixture before and after these acid cleanings and measured the amount of metals in the mixture by inductively coupled plasma mass spectrometry (ICP-MS). In addition, we analyzed wafer surfaces by total reflectance X-ray fluorescence (TXRF). The ICP-MS was SPQ6500 manufactured by SEIKO Instruments, Inc. and TXRF was TREX610 manufactured by

TECHNOS Ltd. We calculated removal ratio of metallic contaminants, especially that of Ni, from the difference of amount of metallic contaminants on the Si-wafer surface between before and after every chemical treatment.

Before this study, we tested accuracy of ICP-MS measurement by comparing the amount of metals measured by ICP-MS with that measured by TXRZF. This was because, there was a report indicating that Ni on Si surface couldn't be eliminated by HF/HNO<sub>3</sub> mixture<sup>11)</sup>. Figure 2 shows the result of the comparison of the measurement data between ICP-MS and TXRZF. Absolute numbers obtained by ICP-MS measurement are slightly different from those by TXRZF measurement but numerical relation between Ni and other metals is not different each other. Thus, ICP-MS is enough for measuring the residual Ni on the Si surface. However, we could not detect Al on the Si surface by TXRZF, since TXRZF signal from Al was disturbed by that from Si. Therefore ICP-MS was more convenient for the estimation of the amount of metals than TXRZF.

Moreover we analyzed how contaminant Ni distributed on and in the chemical oxide on the Si substrate by TXRZF with changing in incident angle of X-ray.

## RESULTS & DISCUSSION

The amount of Ni on the Si surface in the single contamination before and after acid cleaning are shown in Fig. 3. The amount of adsorbed Ni increases with increasing concentration of Ni in SC-1 solution. Though the amount of Ni on the sample of 100 ppb became about half contamination after acid cleaning, removal ratio of about 50 % was not enough for ULSI device fabrication processes. The amount of residual Ni on the other sample didn't change after SPM, HNO<sub>3</sub> and DHF treatment. (We obtained same results also by SC-2, HF/H<sub>2</sub>O<sub>2</sub> and HF/HCl/LDO<sup>12)</sup> treatment but dose not show here.)

Contaminant metals probably exist in or on the chemical oxide if sample wafers have been contaminated by IAP-method. However Ni was not eliminated even after chemical oxide had been completely etched off. Since Ni is not adsorbed on the Si surface in DHF solution, this result suggests that Ni detected here is not re-adsorbed but remained one. Acid solutions, which is widely used for surface cleaning, have been believed to have the ability to eliminate almost metals from Si-surface except only Cu in DHF solution. However the results of this experiment shows that Ni is not also removed by the acid solutions in the single contamination.

Figure 4 shows the amount of metals in the multiple contamination with 11 elements before and after HNO<sub>3</sub> or SPM treatment. Plural kind of contaminant metals were Ni, Al, Ca, Cd, Co, Cr, Cu, Fe, Na, Mg and Mn. Concentration of every metal in SC-1 solution was 1ppm. The amount of every metal decreased from about  $1 \times 10^{14}$  [atoms/cm<sup>2</sup>] to below  $1 \times 10^{11}$  [atoms/cm<sup>2</sup>] after both acid cleanings. In particular, the removal ratio of Ni was about 99.99%. In Fig. 4, moreover, the amount of Ni adsorbed in the multiple contamination is more than that in the single contamination (Fig. 3), though Ni concentration in SC-1 was the same. On the contrary, the amount of residual Ni after cleaning on the multiple contamination sample was less than that on the single contamination sample though treatment was the same solutions. These results suggest that the removal ability of metals in acid cleaning is independent of the initial amount of adsorbed metals.

Next, we prepared contaminated wafers with different combination of metals to investigate the dependence of removal ability of Ni on combination of contaminant metals in the multiple contamination. In the experiment of Fig. 4, the concentration of every metal in SC-1 solution was constant (1ppm). In this experiment, however, we controlled the amount of every kind of absorbed metals on sample wafers so as to be almost equal to about  $10^{12}$  [atoms/cm<sup>2</sup>]. Al, Ca, Cu, Fe and Ni was used. Then, concentration of metals in SC-1 solution was followed : Al = 0.83 ppb, Ca = 1ppm, Cu = 50ppb, Fe = 30ppb, Ni = 30ppb. Figure 5 shows the amount of residual metals before and after acid cleaning in the multiple contamination experiment using 5 elements. Only Ni was not removed from Si wafers though the other metallic contaminants were eliminated after acid cleaning. From Fig. 4 and Fig. 5, it is obvious that the ability of Ni removal depends on the combination of metals, i.e. the kind and number of each contaminant metal.

To clarify this interaction among metals, we have to reveal characteristics of each metal in the multiple contamination process, but 11 elements are too complicated to investigate. Thus, for simplifying the experiment, we selected following 6 elements as contaminants; Al, Cr, Cu, Fe, Mn and Ni. This was because these metals were well-known as the contaminant which sometimes caused contamination problem. Actually, in addition, they are commonly used for the material composing semiconductor device fabrication equipment. Concentration of the metals in SC-1 solution was 1ppm. Figure 6 shows the results of the multiple contamination experiment using theses 6 elements. The extent of decrease in each metal after acid cleaning in this experiment was almost the same as that in the experiment using 11 elements (Fig. 4).

To further investigate the influence of the kind of metals, we prepared the wafers contaminated by five metals except Al, and repeated the same cleaning. The reason of exclusion of Al is that Al is the most common contaminant in SC-1 solution. This result is shown in Fig. 7. In comparison of Fig. 7 with Fig. 6, the amount of residual Ni and Cu after the cleaning increased drastically by elimination of Al, though the amount of adsorbed Ni and Cu before acid cleaning increased slightly. Additionally, initial amount and removal ratio of Cr, Mn and Fe also somewhat changed. Thus, Al obviously influenced the amount of the other metals adsorbed on the Si surface in SC-1 solution and their removal ratio in acid cleaning. Therefore, the removal efficiency of Ni strongly depends on the existence of Al when contamination is caused by plural metal.

As it is shown in Fig. 5, however, Ni was not removed effectively when the amount of contaminant metals was small even under the existence of Al. Thus we investigated the dependence of the Ni removal ratio on the numerical relation between Ni and Al. Then we experimented with only Al and Ni. This result is shown in Fig. 8. The concentration values of Al and Ni in SC-1 solution are graduated at the horizontal axis. As demonstrated this figure, the initial amount of adsorbed Ni before cleaning depends on the concentration of Ni in SC-1 solution, however the amount of residual Ni after acid cleaning depends on the concentration of Al in SC-1 solution. Hence, after acid cleaning, the amount of residual Ni decreased to order of  $10^{11}$  [atoms/cm<sup>2</sup>] independent of the initial amount of adsorbed Ni in the SC-1 solution containing Al of 1ppm. On the other hand, in the SC-1 solution containing Al of 10ppb, the amount of Ni stayed at order of  $10^{13}$  [atoms/cm<sup>2</sup>] after acid cleaning. Therefore the removal efficiency of Ni strongly relates to the absolute concentration of Al in SC-1 solution. This result explains the reason that

Ni was not removed effectively by acid cleaning even under the existence of Al in Fig 5..

To prove the effect of Al in Ni removal, we tried to identify the location of Ni in vicinity of Si surface in TXRXF measurement. We observed contaminated wafers before acid cleaning which were used for the experiments of Fig.3, 5, 6 and 8. Figure 9 shows the angular dependence of fluorescence intensity from Ni on contaminated wafers after the single contamination and the multiple contamination in TXRXF observation. Ni on the sample wafers where Ni was removed effectively by the acid solution (Fig. 6 and 8) distributed in shallower part than that on the sample wafers where Ni was not removed so much by the acid solution (Fig. 3 and 5). From these observation results, removal ratio of Ni may be influenced by its distribution.

## CONCLUSION

We found the Ni removal ratio depended on contamination circumstance, moreover, on the combination of other metals in the multiple contamination. No acid solution without Si surface etching Si-surface such as HF/HNO<sub>3</sub> mixture eliminated Ni from Si-surface if sample wafers are contaminated by only Ni. The Ni removal ratio and the amount of residual Ni after acid cleaning strongly depends on the concentration of contaminant Al if sample wafers are contaminated by plural kind of metals including Al. However certain amount of Al is necessary to remove Ni effectively by acid solutions.

## ACKNOWLEDGMENTS

The authors would like to thank Dr. N. Awaji for helpful discussion, and Mr. Ojima for analysis using TXRZF.

## REFERENCE

- 1) W. Kern and D. A. Puotien: RCA Rev. 31 (1970) 187.
- 2) H. Hiratsuka et al. : Ext. Abst. The Electrochem Soc. Vol. 1991-2 p.619 (1991)
- 3) H. Morinaga et al. : J. Electrochem. Soc., Vol. 141, No. 10, p.2834 (1994)
- 4) H. Morinaga et al.: 1997 MRS spring meeting, San Francisco, p273 (1997)
- 5) T. Shimono et al. : IEICE Trans. on Electron., Vol. E75-C, No. 7, pp812-815 (1992)
- 6) H. Aoki et al.: Jpn. J. Appl. Phys. , 33, 5686 (1994)
- 7) H. Okuda et al.: Mat. Res. Soc. Proceeding, Vol. 259, p399 (1992)
- 8) H. Kondo et al.: Jpn. J. Appl. Phys., 31, L11-13 (1992)
- 9) M. Hourai et al.: Jpn. J. Appl. Phys., 27, L2261-2263 (1988)
- 10) Y. Mori et al.: ECS proceeding, PV-94-10, p258-269 (1994)
- 11) T. Hosoya et al.: J. Electrochem. Soc.; vol 132, p2436 (1985)
- 12) Y. Hayami et al.: Ext. Abst. Solid State Device and Material, Yokohama, p864-p865 (1996)

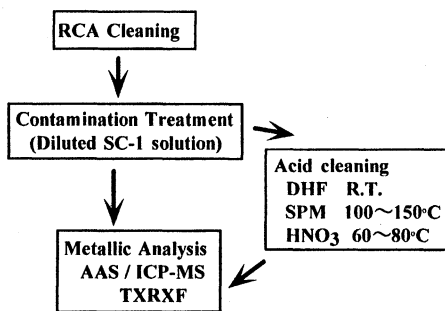


**Fig.1 Experimental procedure**

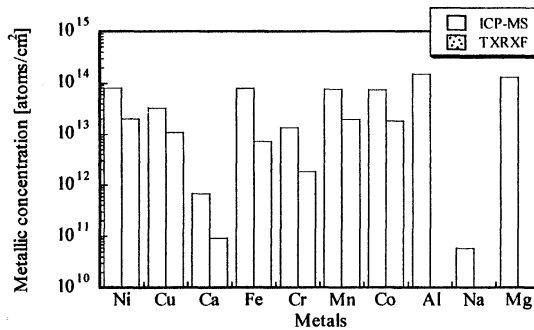


**Fig.2 The result of the comparison of the measurement data between ICP-MS and TXRZF**

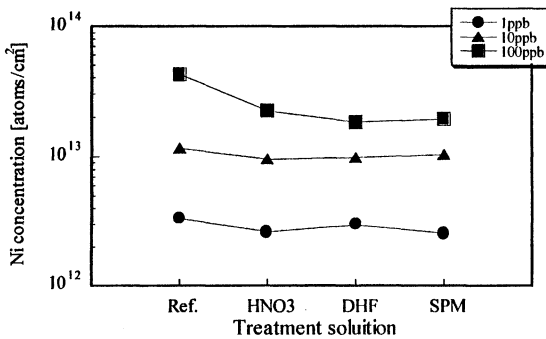


**Fig.3 The amount of Ni on the Si surface in the single contamination before and after acid cleaning**

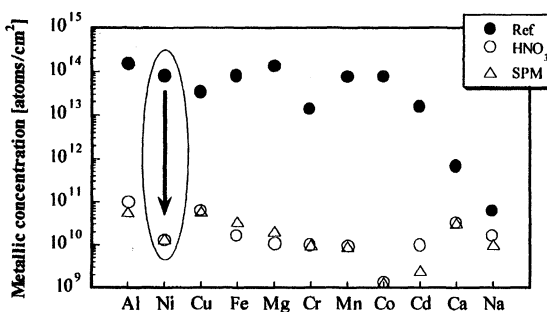


Fig.4 The amount of residual metals in the multiple contamination with 11 elements before and after  $\text{HNO}_3$ , SPM treatment

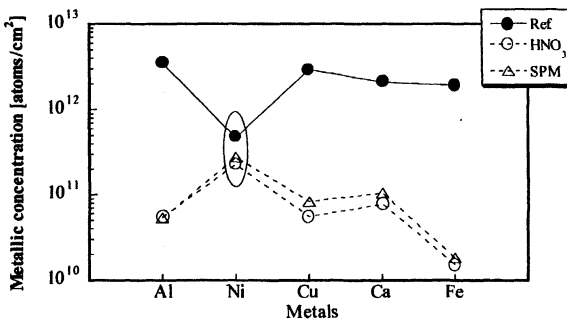


Fig.5 The amount of residual metals before and after acid cleaning in the multiple contamination experiment using 5 element

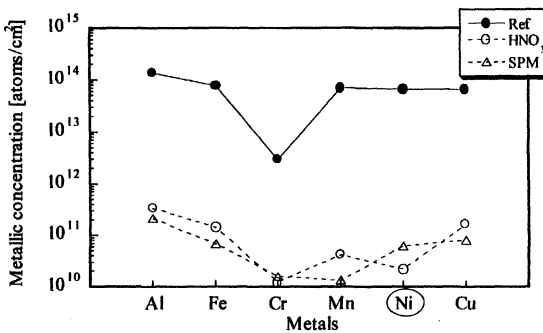
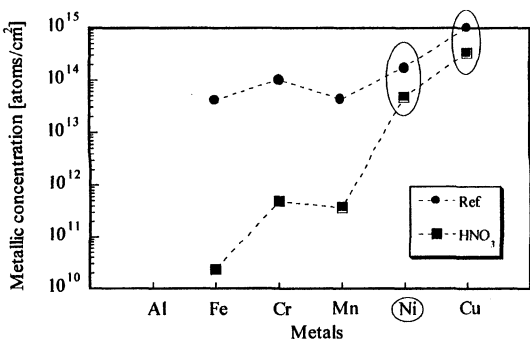
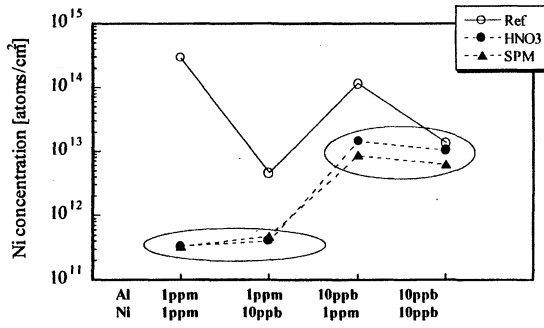


Fig.6 the result of the multiple contamination experiments using theses 6 elements



**Fig. 7** The amounts of residual metals in the multiple contamination with 5 elements before and after  $\text{HNO}_3$  treatment



**Fig. 8** The amount of Ni and Al in the multiple contamination before and after acid treatment

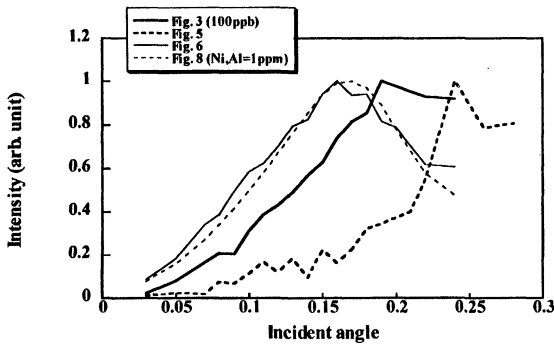


**Fig. 9** TXRF measurement

## **Surface Complexation of Metals: A Predictive Model Based on Metal Coordination Chemistry**

T.Q. Hurd, A.L.P. Rotondaro, J. Sees, A. Misra, C. Appel  
Texas Instruments, 13570 N Central, MS 3701, Dallas, TX 75243

### **ABSTRACT**

Various approaches to understanding and predicting adsorption metals onto oxidized silicon wafers have been put forward, with varying degrees of success, including ones based on electrochemical thermodynamics (ie Pourbaix diagrams) [1], solubility/precipitation [2], adsorption / desorption kinetics [3], and equilibrium thermodynamics [4]. This paper will explain the adsorption of metals at the silica surface in terms of the coordination chemistry of metal ions. A qualitative approach capable of predicting the robustness of chemical clean ups towards specific metals will be described. The conclusions based on this approach will be compared to original data as well as to data found in the literature.

### **INTRODUCTION**

In order to make improvements in cleaning and to meet the challenges of future generations of devices it is necessary to understand the chemistry of the metal ions both in solution as well as at the surface of the wafer. Various approaches to understanding and predicting adsorption phenomenon have been proposed, with varying degrees of success, including ones based on electrochemical thermodynamics (ie Pourbaix diagrams) [1], solubility/precipitation [2], adsorption / desorption kinetics [3], and equilibrium thermodynamics [4]. This paper will show that adsorption of metals at the silica surface can be adequately explained by the coordination chemistry of metal ions in aqueous solution. This approach leads not only to an understanding of the results of adsorption studies on common metals in the literature to date but also provides a straightforward way of predicting the adsorption behavior of new metals (Ba, Sr, Pt, Ru, Ta, etc...) that are now entering the fab due to the requirements of advanced device manufacturing.

### **ADSORPTION ON SILICA SURFACES**

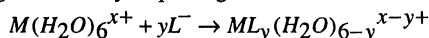
It is known that organic and inorganic acids will adsorb on silica surfaces. Various authors have successfully used complexation and ligand exchange to describe the observed absorption [5-11]. Stability constants have been determined for several different oxide surfaces, including silica. Work with organic acids has shown that the bonding at the surface can be inner sphere but this has not been shown decisively in the case of metals.[5,8] Successful models have been proposed based on the assumption of both inner and outer sphere mechanisms.[6,10] In the case of metals there are many difficulties associated with determining the exact mechanism controlling metal adsorption at the surface of silica. This is due to the fact that several phenomena, adsorption, hydrolysis and precipitation, converge in a very narrow pH range making it difficult, if

not impossible to separate them. This does not mean, however, that useful patterns cannot be found based on metal and silica reactivity.

The surface of silicon and metal oxides are covered by hydroxyl groups when in contact with aqueous solutions. These hydroxyl groups are able to pick up and release protons from solution resulting in the observed pH dependence of the surface charge. Silicon dioxide (silica) has weakly acidic hydroxyl groups on the surface as is evidenced by a point of zero charge (pzc) at pH ~2 and an estimated  $K_a$  of  $10^{-6.8}$  [12]. Thus the surface can act as an ion exchange or coordination site for both water and ions present in the solution [5,6,12].

### METAL IONS IN SOLUTION

When a metal ion is placed in aqueous solution it will stabilize its positive charge by surrounding itself with a hydration sphere of six water molecules. If other species (ligands) are present in the solution, especially Lewis bases, the metal can preferentially coordinate with the ligands thereby displacing the  $H_2O$  coordinated to the metal.

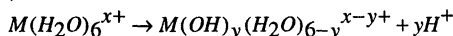


Stability constants for these reactions can be calculated from the equilibrium concentrations,

$$K_x = \frac{[ML_x]}{[M][L]^x} \quad (p,T,I = \text{constant})$$

( $p$  = pressure,  $T$  = temperature, and  $I$  = solution ionic strength). Such ligands can be monodentate (one reactive site per ligand) or, in the case of chelating agents, polydentate (multiple reactive sites per ligand). A sampling of stability constants is shown in Table 1.

A special case of the above occurs during the process of hydrolysis, in which the metal ejects a proton from its surrounding water sheath, acidifying the water and creating its own Lewis base ( $OH^-$ ) to coordinate to as shown:

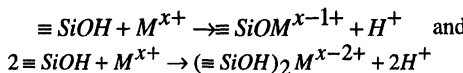


This process will repeat until the metal achieves thermodynamic equilibrium. The equilibrium condition of this reaction can be characterized by a hydrolysis stability constant, defined as,

$$K_{hx} = \frac{[H^+]^y [M(OH)_y(H_2O)_{6-y}^{x-y+}]}{[M(H_2O)_6^{x+}]} \quad (p,T,I = \text{constant})$$

The sequential ejection of protons can be characterized and the stepwise equilibrium constant assigned a subscript that denotes how many protons have been ejected (ie  $K_{h1}$ ,  $K_{h2}$ ,  $K_{h3}$ , etc...). The hydrolysis process has been well characterized for many metals and reliable tables of overall stability constants can be located in the literature [14,15]. These constants make it possible to calculate the hydrolytic speciation of a given metal over a wide pH range.

A similar approach can be taken when describing metal adsorption on the silica surface. Per reference 6 the reaction of a metal at the surface can be described as follows:



Stability constants for the surface complexes formed can be defined as follows:

$$K_{s1} = \frac{\{ \equiv SiOM^{x-1+} \}[H^+]}{\{ SiOH \}[M^{x+}]} \quad \text{and} \quad K_{s2} = \frac{\{ (\equiv SiOH)_2 M^{x-2+} \}[H^+]^2}{\{ \equiv SiOH \}^2 [M]}$$

$p, T, I = \text{constant}$ ,  $\{ \}$  indicates a surface concentration,  $[ ]$  indicates a solution concentration. It has been noted [6,13], that the  $\equiv Si(OH)_x$  ( $x=1,2$ ) groups covering the silica surface are chemically similar to the H-OH of water and thus a valuable guide as to how aggressively a metal will react with the silanol groups on the silica surface is provided by the metal's hydrolysis behavior. Simply put, the more readily hydrolyzable a metal is (with correspondingly larger  $K_{h1}$ ) the more readily it will coordinate to the silica surface. Metal ions with high charge/radius ratios will hydrolyze to a greater extent than those with smaller ratios, leading to the correlation that was previously observed [16]. The correlation between  $K_h$  and  $K_s$  has been reported several times in the past [6,13] and it was demonstrated with silica gel (at  $I = 1$ ) that the two types of stability constants were related by the equation:

$$\log K_{sx} = -0.09 + 0.62 \log K_{hx} \quad [6]$$

Thus, an inspection of hydrolysis constants for metals gives an immediate indication of how thermodynamically favorable its adsorption is relative to other given metals, assuming only  $H_2O$  is present. A simple comparison of  $K_{h1}$  values is sufficient.

Several general conclusions can be drawn from the equations cited above describing metal adsorption on silica surfaces. The first is that based on this model it would never be possible to have levels of metal adsorption larger than that surface concentration of  $SiOH$  which is  $4.6 - 5.5 \times 10^{14} \text{ cm}^{-2}$  [6,17]. The second is that two ways to drive the surface concentration down would be to increase  $[H^+]$  or to decrease  $[M^{x+}]$ . Thus the observed pH and metal concentration dependence of metal adsorption.

Strictly speaking,  $[M^{x+}]$  is the concentration of the free metal ion, not including any hydrolysis products. It is reasonable to assume that hydrolysis products of metals would form mixed complexes on the surface of the oxide (8-10). Contrary to reference 4 it does not seem necessary to assume that any particular hydrolysis product is dominant in the adsorption process as adsorption can be found all across the pH range, even where hydrolysis products are not formed. For the purpose of the discussion that follows it is assumed that  $[M^{x+}]$  refers to the free metal ion as well any of its hydrolysis products that are in solution.

One way in which to drive  $[M^{x+}]$  down is to add a competing ligand to the solution. If the ligand-metal complex is more stable than the silica-metal complex, then the ligand can effectively prevent the metal from adsorbing on the surface. A comparison of their stability constants with the hydrolysis constants or surface complex constants will indicate how effective they will be in preventing metal adsorption on silica.

Finally, in dealing with some of the new metals that are entering the wafer manufacturing process, it is necessary to look at how labile the metal is. Most 1<sup>st</sup> row transition metals are very labile and exchange ligands as fast a diffusion will permit. Others, in the 2<sup>nd</sup> and 3<sup>rd</sup> row can be very inert and even with a strong thermodynamic driving force can take hours, weeks, or years to exchange ligands (eg Ru) [18]. This can be critical when considering if a given metal will be removed from a wafer surface or if it will adsorb from solution.

The primary applicability of the complexation model is in the pH < 9 range although it can be applied across the entire pH range. At pH's > 9, the problem of silica dissolution grows with pH. It can be expected however, that the tendencies of a given metal to adsorb at lower pH's will remain the same relative to other metals and so this model can be profitably applied to SC1 solutions as well as SC2 or other acidic chemistries. Quantification of SC1 solutions may prove difficult but no doubt appropriate correction terms can be added.

The values of stability constants published in the literature for silica metal complexes are generally with solutions at ionic strengths of 1. This is not typical of wafer cleaning solutions and reduces the value of the published constants for quantitatively calculating actual surface coverage. Typically, under the conditions chosen by those who study silica gel complexation, the silanol concentration in solution is much greater than the metal ion concentration. In wafer cleaning, the exact opposite is true. The total number of silanol groups in the bath is much less than the total number of ions in solutions and the actual concentration of silanols only begins to approach that of the metal ions directly at the surface. An implication is that the published stability constants are almost certainly going to be skewed relative to what is observed in wafer cleaning. Our thesis is that this skewing should be relatively constant allowing for fruitful comparison.

### RESULTS AND DISCUSSION

Silicon wafers, CZ, p-type, <100>, 1-30 Ωcm, 150 mm diameter, were prepared by scribing and then cleaning the wafers with a HF-SC1-HCl sequence and in some cases were then thermally oxidized. The wafers were then dipped in various solutions, including some with chelating agents, that had been spiked with GFAA standard metal solutions. Except where noted, experiments were carried out at room temperature, with a dipping time of 10 minutes, a rinse time of 2 minutes followed by spin drying. Analysis was performed using VPD-DSE-TXRF (Vapor Phase Decomposition - Droplet Surface

Etching - TXRF), VPD-DSE-ICPMS, VPD-DSE-GFAA and/or HIBS (Heavy Ion Backscattering) as appropriate.

Figure 1 shows the concentration of  $\text{Fe}^{3+}$  remaining on thermal oxides following immersion in HCl solutions spiked with iron. The iron level shows a large increase in the region of pH 2-4 which is exactly the region where the first hydrolysis product begins to appear in significant amounts [8]. Comparing the  $\log K_1$  (from Table 1) for  $\text{Cl}^-$  (0.8) with the  $\log K_1$  for  $\text{OH}^-$  (11.0) shows that the  $\text{Cl}^-$  should negligibly interfere with the  $\text{Fe}^{3+}$  adsorption which is indeed the case.

Table 2 shows the adsorption of  $\text{Fe}^{3+}$  from SC1 solution. It can be seen that the adsorption level begins leveling off at  $\sim 2 \times 10^{13}$  at/cm<sup>2</sup> (compare with Figure 1). This same maximum has been reported for Fe (as well as Al and Zn) elsewhere in the literature [4, 19-23]. If it is assumed that the coordination complexes are a mixture of  $=\text{SiOM}$  and  $(=\text{SiO})_2\text{M}$ , then the maximum amount of metal adsorbed on the surface will never exceed low  $10^{14}$  / cm<sup>2</sup> values. The fact that it begins to level off in the  $10^{13}$  range indicates that either the adsorbed Fe is interfering with further adsorption [8] or that other metals not measured, most likely Al, are occupying the other available sites on the wafer. The rise in Fe on the wafer is first order in  $[\text{M}^{x+}]$  which is in agreement with the model.

This adsorption maximum is a good argument against precipitation or particle adsorption being dominant mechanism. Precipitation would result in higher quantities of metal as the only fundamental limitation would be the solubility of the metal, which is quite low for metal ions such as  $\text{Fe}^{3+}$ . Similarly, if the mechanism were dominated by particulate deposition, this upper ceiling should be broken at times, but in the literature, this has not been seen, even though such particles are known to exist [24] and no doubt deposit on the surface. Finally it has been shown [5, 6, 8-10, 25] that metal ions will adsorb on silica surfaces even when solubility is not an issue. This does not rule out the other mechanisms but relegates them to a secondary role in the adsorption process.

Table 3 shows the results of two experiments performed in SC1: first, of using a  $\text{H}_2\text{O}_2$  containing a polyphosphonic acid chelating agent [26,27], and second, of using EDTA to complex metals [23]. As can be seen, both chelating agents were effective in reducing the metal levels on the wafers. This is due to the high stability of the metal chelates that are formed resulting in a reduction in  $[\text{M}^{x+}]$ . EDTA stability constants can be compared in Table 1.

Table 4 shows the adsorption of Ba, Sr, Pt, and Ru from different solutions that were individually spiked to 1 and 10 ppb of each metal. The HF process was 2 minutes and the HCl solutions were heated to 50C. It should be noted that Ba and Sr, being alkaline earth metals would be expected to behave very similarly to Ca and this is indeed the case. In acid solutions their adsorption is low to <DL, while in SC1 they adsorb at levels that are similar for Ca (cf Table 2). Pt and Ru, on the other hand are known to readily

hydrolyze, even at low pH [26], which would argue in the favor of showing high adsorption. However, Pt and Ru are known to form very stable Cl<sup>-</sup> and NH<sub>3</sub> complexes and are, especially in the case of Ru, not very labile. The end result is that the metals do not adsorb readily from any of the solutions tested.

Table 5 shows the opposite situation, where Ba, Sr, Pt, and Ru are already on the wafers (spin deposited from stock acid solutions) and the various cleaning solutions are used to attempt to remove them. Sr and Pt are easily removed in all cases for basically the same reasons discussed above. Ru is poorly removed, no doubt due to its relative inertness to ligand exchange. Ba is the one real surprise, exhibiting low removal rates. This anomalous behavior will be the subject of further study.

**Conclusions:** Metal adsorption onto silicon oxide surfaces was shown to be understandable in the context of the hydrolysis and coordination chemistry of metals. It was shown that the tendency of a metal to adsorb to silica surfaces can be predicted by looking at the stability of its first hydrolysis product and comparing it to the stability of other coordination products that might form in the solution. A context and method was provided that not only gives valid interpretation for past results in the literature but also gives predictive capability when new metals are encountered. The relevant factors to consider are: 1) the tendency of the metal to hydrolyze, 2) the ratio of ionic charge to radius, 3) the presence and concentration of competing ligands in the solution, and 4) the lability of the metal in question. Future efforts toward quantification of metal removal from and adsorption onto oxidized silicon wafer surfaces can now be placed in a context of the chemical forces at work.

**Acknowledgements:** The assistance of Karine Kenis, Christian Wilms, Ann Opdebeeck, Don Dickson, and Bud Schmidt is gratefully acknowledged by all of the authors. Much of this work was performed under the joint TI-IMEC R&D program.

#### References:

1. G.J. Norga et al, *J. Electron. Mater.* **24** 397 (1995)
2. C.R. Helms et al, *ECS Proceedings* **94-7**, 26 (1994)
3. J. Ryuta et al, *Jpn. J. Appl. Phys.* **31** 2338 (1992)
4. Y. Mori et al, *J. Electrochem Soc* **142** 3104 (1995)
5. W. Stumm et al, *Croat. Chem. Acta* **53** (2) 291 (1980)
6. P.W. Schindler et al, *J. Colloid Sci.* **55** 469 (1976)
7. P.W. Schindler, *Metal Ions in Biological Systems* **18** 105 (1984)
8. R.O. James et al, *J. Colloid Sci.* **40** 42 (1972)
9. R.O. James et al, *J. Colloid Sci.* **40** 53 (1972)
10. R.O. James et al, *J. Colloid Sci.* **40** 65 (1972)
11. D.L. Dugger et al, *J. Phys. Chem.* **68** 757 (1964)
12. P. Schindler and H.R. Kamber *Helvetica Chimica Acta* **51** 1781 (1968)

13. S. Ahrland et al, *Acta Chem. Scand.* **14** 1059 (1960)
14. J. Kragten, *Atlas of Metal-Ligand Equilibria in Aqueous Solution* (John Wiley and Sons) 1978
15. L.G. Sillen et al, *Stability Constants of Metal Ion Complexes*. The Chemical Society, London (1964); *Supplement No. 1* (1971)
16. T.Q. Hurd et al, *ECS Proceedings* **95-20** 277 (1995)
17. R.K. Iler, *The Chemistry of Silica*, 665 (1979)
18. C.F. Baes, R.E. Mesmer, *The Hydrolysis of Cations* John Wiley and Sons, 1976
19. L. Mouché et al, *J. Electrochem. Soc.* **142** 2395(1995)
20. V. Penka et al, *Fres. Z. Anal. Chem.* **333** 568 (1989)
21. N. Fujino et al, *ECS Proceedings* **91-5** 301 (1991)
22. M. Hourai et al, *Jpn. J. Appl. Phys.* **27** L2361 (1988)
23. A. Misra et al, *TI internal report* (1996)
24. H. Lengweiler et al, *Helvetica Chimica Acta* **44** 805 (1961)
25. L. Lee , P.W. Mertens, *TI internal report* (1997)
26. I. Hayashida et al, *U.S. Patent #5,290,361*
27. Y. Sugihara et al, *U.S. Patent # 5,302,311*

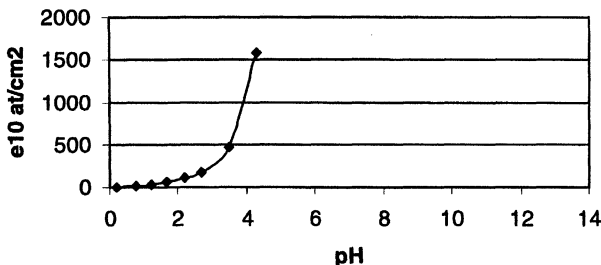


**Figure 1:** Iron concentration remaining on chemical and thermal oxide surfaces following 10 minute immersion in 100 ppb spiked HCl solutions of varying pH.

**Table 1.** Stability constants ( $\log K_1$ ) of metal complexes with  $\text{NH}_3$ ,  $\text{Cl}^-$ ,  $\text{OH}^-$ , and EDTA [12,13,25]. (Equilibria of reaction:  $\text{M} + \text{L} \rightarrow \text{ML}$ )

Complexant	$\text{Al}^{3+}$	$\text{Fe}^{3+}$	$\text{Zn}^{2+}$	$\text{Ca}^{2+}$	$\text{Ba}^{2+}$	$\text{Sr}^{2+}$	$\text{Pt}^{4+}$	$\text{Ru}^{3+}$
$\text{OH}^-$	9.7	11.4	4.8	1.4	0.8	0.6	↑	↑
$\text{Cl}^-$	-	0.8	-0.7	?	?	?	~16	↑
$\text{NH}_3$	-	~-0.6 <sup>a</sup>	2.3	-0.2	↓	↓	8.7b	↑
EDTA	16.1	25.1	16.5	10.7	7.8	8.6	?	?

<sup>a</sup>Based on mixed complex with CN

<sup>b</sup> $K_2$

**Table 2:** Fe<sup>3+</sup> adsorption on silicon oxide from SC1. Results in 10<sup>10</sup> at/cm<sup>2</sup>.

	<b>Control</b>	<b>+0.1 ppb</b>	<b>+1.0 ppb</b>	<b>+10 ppb</b>	<b>+100 ppb</b>
Fe	4.35	25.2	272	1509	2544
Ca	<0.7		3.1	18.3	160

**Table 3:** Effect of chelating agents on metal outplating. Results in 10<sup>10</sup> at/cm<sup>2</sup>.

<b>Solution</b>	<b>Fe</b>	<b>Ni</b>	<b>Cu</b>	<b>Zn</b>	<b>Ca</b>
SC1 + 1 ppb Fe	65.6	15.5	7.2	330	23.5
SC1+ 1 ppb Fe + Wako H <sub>2</sub> O <sub>2</sub>	1.2	1.0	3.7	1.9	6.9
SC1 + 1 ppm Fe, Ni, Cu, Zn, & Ca	1080	261	524	3520	142
SC1 + metals + 150 ppm EDTA	9.1	2.5	3.5	8.0	17

**Table 4:** Removal of spun on Ba, Sr, Pt, and Ru from thermal oxide in different solutions. Results in e10 at/cm<sup>2</sup> as measured by HIBS. (\*) indicates Br interference which can obscure metal scattering peak resulting in loss of precise quantification or inability to detect metal at all. Implies low level of metal in most cases)

<b>Metal</b>	<b>Pre</b>	<b>Post</b>			
		<b>1:1:5 SC1</b>	<b>0.49% HF</b>	<b>3.7% HCl</b>	<b>0.037% HCl</b>
Ba	121	14.6	11.7	30	33.8
Sr	170	3.9	5.1	*	5.3
Pt	189	<0.07	<0.07	<0.07	<0.07
Ru	433	52.9	71.3	72.0	50.4

**Table 5:** Adsorption of Ba, Sr, Pt, and Ru onto thermal oxide from various cleaning solutions spiked to 1 and 10 ppb. Results in e10 at/cm<sup>2</sup> as measured by HIBS.

(\* indicates Br interference which can obscure metal scattering peak resulting in loss of precise quantification or inability to detect metal at all. Implies low level of metal in most cases)

<b>Metal [ppb]</b>	<b>1:1:5 SC1</b>	<b>0.49% HF</b>	<b>3.7% HCl</b>	<b>0.037% HCl</b>
Ba	1	0.52	0.75	<0.18
	10	4.07	0.31	<0.16
Sr	1	2.61	*	*
	10	7.73	*	~2*
Pt	1	0.45	1.95	<0.06
	10	0.85	0.06	<0.07
Ru	1	~1.1*	*	<0.23
	10	~1.88	*	<0.20

## Fe REMOVAL IN SC2 SOLUTIONS

S. Dhanda, R. P. Chiarello, and C. R. Helms  
Solid State Laboratory, Stanford University, Stanford, CA 94305

P. Gupta  
Intel Corporation, Santa Clara, CA 95054

The efficiency and kinetics of Fe removal in SC2 mixtures were investigated as a function of key process variables. These variables included the temperature and composition of the SC2 mixture, the duration of the clean, and the starting Fe levels on the wafer surface. It was found that all of the above variables play an important role in the optimization of the SC2 step. The peroxide concentration in solution, and the temperature of the mixture, were found to be particularly important.

### INTRODUCTION

RCA based chemistries used in silicon wafer cleaning commonly employ both SC1 and SC2 cleans. The SC1 clean is effective for the removal of particles and organic material, but may often result in the deposition of metals onto the wafer surface. Removal of these metals prior to gate oxidation is imperative, and is commonly accomplished via cleaning in an HF-based chemistry,<sup>1,2,3</sup> or an acid-peroxide mixture such as SC2.<sup>4,5,6</sup> The SC2 mixture offers a low pH environment, additional oxidizing power, and excellent chloride complexing ability, all of which help in the removal of metals from the wafer surface.

Conventional SC2 cleans typically employ a 1:1:5 (HCl:H<sub>2</sub>O<sub>2</sub>:H<sub>2</sub>O) mixture, are performed at temperatures between 70 and 90°C, and wafer exposure times ranging from 5 to 20 minutes. Optimization of the composition, temperature and exposure time of the SC2 mixture are important for high metal removal efficiencies.

Previous investigations<sup>7,8,13</sup> have concentrated on optimizing the temperature and composition of SC2 mixtures, but the concurrent optimization of the SC2 clean with respect to temperature, composition and exposure time has not been systematically investigated.

Our study was designed to gain greater insight into the effects associated with varying the critical variables in an SC2 clean. Consequently, we measured surface metal contamination on wafer surfaces by varying the composition (by increasing or decreasing the HCl/H<sub>2</sub>O<sub>2</sub> ratio in solution) of the SC2 mixture, temperature of the SC2 bath, the wafer exposure time in SC2 and the level of metal contamination on the wafer surface.

## EXPERIMENT

6" p-type Cz wafers were treated using the process flow sequence shown in Figure 1. All wafers were initially cleaned using steps 1 through 4 before being exposed to Fe-contaminated SC1. Wafer surface contamination levels were varied by varying the amount of Fe contamination in the SC1 solution from 3 ppb to 3 ppm. The Fe levels on the wafer surface were subsequently measured using total x-ray reflectance fluorescence (TXRF). The contaminated wafers were then treated using SC2 solutions of various compositions and temperatures. TXRF measurements were made before and after exposure to the Fe-contaminated SC1 solution, and after treatment in SC2.

A conventional SC2 chemistry with a 1:1:5 composition was used as a starting point in our studies. The temperature of the mixture was varied from 25°C to 70°C to determine if elevated SC2 temperatures improved an SC2 mixture's effectiveness for removing Fe from the surface. The temperature of the SC2 mixture is also important in determining the half-life of an SC2 bath; lower temperatures translate into higher bath lives,<sup>9</sup> which implies less frequent replenishment of the SC2 bath, and therefore reduced costs from lower chemical usage. Dilute HCl chemistries also imply lower chemical usage by a reduction in the HCl content, and by the elimination of peroxide from the cleaning mixture. A similar argument applies to dilute SC2 mixtures. Comparing mixtures such as 1:1:5 and 1:0:5, as well as 0.1:0.1:5 (dilute SC2) and 0.1:0:5, helped determine the effect of peroxide on Fe removal efficiency. Similarly, comparing HCl solutions of varying degree of dilutions (such as 0.1:0:5 and 0.01:0:5) helped isolate the effect of HCl (in the absence of peroxide) on the extent of Fe removal. The SC2 mixtures, temperatures and other chemistries we studied are summarized in Table 1.

Table 1: Compositions and temperatures of SC2 and other solutions.

Clean	SC2 Composition (HCl:H <sub>2</sub> O <sub>2</sub> : H <sub>2</sub> O)	Temperature
Conventional SC2	1:1:5	25°C
		50°C
		70°C
Dilute HCl	1:0:5	25°C
		50°C
	0.1:0:5	70°C
	0.01:0:5	70°C
Dilute SC2	0.1:0.1:5	70°C

## RESULTS

Figure 2(a) shows Fe surface contamination plotted as a function of treatment time in the standard, 1:1:5, SC2 mixture at 70°C. The four sets of data represent four initial surface contamination levels of Fe. The solid lines represent the best fits to the data using a simple decaying exponential function. The only fit parameter was the time to reach steady state ( $\tau$ ). The curves were normalized using the initial Fe surface concentration. For each initial Fe surface contamination level we studied, a final Fe surface contamination level - equal to the TXRF detection limit - was obtained in approximately 10 - 20 seconds.

The kinetics of Fe removal in 1:1:5 mixtures at 25°C and 50°C are shown in Figures 2(b) and (c), respectively. In both cases a steady state value of  $\sigma_f$  was achieved in less than 50 seconds. However, unlike the treatment at 70 °C, for both of these temperatures the final Fe surface concentration was dependent on the initial Fe surface concentration. As seen in Figures 2(b) and (c) this indicates that the initial Fe surface contamination was not completely removed from the wafer surface. Specifically, for initial surface Fe contamination levels greater than  $10^{12} \text{ cm}^{-2}$ , complete removal of Fe from the wafer surface was not obtained using standard SC1 at 25 °C and 50 °C.

The kinetics of removal in dilute HCl mixtures (0.1:0.5, 0.01:0.5) at 70°C are shown in Figures 3(a) and (b). In both cases, the time taken to reach a steady state value was found to steadily increase with increasing  $\sigma_i$ , and was found to be as high as 150-300 seconds for initial surface concentrations above  $1 \times 10^{13} \text{ cm}^{-2}$ . From Figure 3(a) it can be seen that the removal of Fe was complete when using a more concentrated chemistry (0.1:0.5). For a more dilute chemistry (0.01:0.5) we found that the steady state value of  $\sigma_f \sim 4 \times 10^{10} \text{ cm}^{-2}$  was slightly above the detection limit. This may be attributed to the relatively high pH associated with such a dilute mixture.

Figures 4(a) and (b) show the Fe surface concentration plotted as a function of treatment time for 1:0:5 SC2 mixtures at 25 °C and 50 °C, respectively. At 50 °C, the Fe detection limit was reached in approximately 50 seconds. When we used the 1:0:5 SC2 mixture at 25°C, steady state was reached by 100 seconds and for initial surface contamination levels greater than  $10^{13} \text{ cm}^{-2}$ , significant amounts of Fe remained on the wafer surface even after 500 sec of treatment.

Figure 5 shows the surface Fe concentration plotted as a function of time for wafers treated using a 0.1:0.1:5, SC2 mixture at 70 °C. For all initial surface Fe concentrations we examined, a steady state Fe contamination level was reached within 100 seconds. For initial Fe surface contamination levels greater than or equal to  $10^{13} \text{ cm}^{-2}$ , a significant amount of Fe remained on the wafer surface after 500 seconds of treatment. The incomplete removal of Fe may be attributed to the reduced HCl concentration coupled with the presence of a strong oxidizing agent such as  $\text{H}_2\text{O}_2$ .<sup>10</sup>

## CONCLUSIONS

The efficacy of an SC2 clean depends on several parameters. These include the temperature and chemistry of the mixture, the duration of the clean, and the initial Fe (metal) level on the wafer surface. Further, there exists a complex dependence between these parameters, so that an attempt at optimizing the SC2 step via modification of only one of these variables, is not recommended. While an in-depth discussion of these interdependencies is beyond the scope of this work,<sup>10</sup> certain obvious inferences can be easily made.

Clearly, increasing the temperature serves to improve the removal efficiency, and in some cases even the rate of removal. The improvement in removal efficiency with temperature is especially evident for peroxide inclusive chemistries. The increase in temperature may be responsible for the efficient removal of iron silicate from the surface, leading to an increase in the removal efficiency.

A definitive trend is also observed with respect to hydrogen peroxide concentrations in solution. In general, an increase in peroxide concentration proves detrimental to the removal of Fe from the surface. While high temperatures coupled with high concentrations of HCl in solution (e.g. 1:1:5 SC2 at 70°C) prove effective in mitigating this detrimental effect, scaling down the HCl concentration must necessarily be accompanied by complete (or near complete) removal of peroxide in solution. Scaling down the concentration of HCl and H<sub>2</sub>O<sub>2</sub> in solution in this fashion is desirable since it results in lower costs. The potential problem of incomplete noble metal removal that may result from use of such a cleaning methodology can be avoided by ensuring that noble metal deposition<sup>11</sup> from a preceding HF clean is minimized. This may be achieved by using chemicals (HF solutions) that have intrinsically low noble metal levels, thus preventing the deposition of noble metals in the first place. Alternatively, innovative chemistries, such as the HF-HCl cleans,<sup>12</sup> may be used to mitigate this effect.

Another major finding is that SC2 cleans as currently implemented are "overdone" with respect to removal of Fe. The conventional RCA2 clean (1:1:5 SC2) is one which is still commonly employed by the semiconductor industry, and is often 10 minutes (or greater) in duration. In the case of high temperature chemistries with fairly high concentrations of HCl (e.g. 1:1:5 at 70°C), it is clear that such lengthy cleans are unnecessary, since the removal of Fe is complete in 10-20 seconds. Even dilute HCl chemistries at high temperatures completely remove Fe in less than 300 secs.

The importance of optimizing the temperature, the duration of the clean, and the chemistry is also strongly linked to the initial level of contaminant on the surface. So long as  $\sigma_i$  is below  $10^{12} \text{ cm}^{-2}$ , these variables are of little or no importance. The real value of optimizing cleans become evident, when excursions from normal contaminant levels occur in a cleaning sequence. In such cases, excessively high metal levels in an SC1 bath (due to an unforeseen contamination event) may lead to excessive metal deposition on the wafer surface, which may not be adequately removed in an unoptimized SC2 step.

Finally, we emphasize that these studies relate to Fe removal only and one must proceed with caution before extrapolating these results to other metals. It is likely however, that these trends are representative of other transition metals. We have performed preliminary studies which indicate that Zn behaves in a manner similar to Fe.

---

## REFERENCES

- <sup>1</sup> T. Shimono and M. Tsuji, "A New Cleaning Solution for Metallic Impurities on the Silicon Wafer Surface", Proceedings of the Second Symposium on Defects in Silicon II, Electrochem. Soc., 361 (1991).
- <sup>2</sup> R. Takizawa, T. Nakanishi, and A. Ohsawa, Jpn. J. Appl. Phys., **27**, 2210 (1988).
- <sup>3</sup> A. Ohsawa, R. Takizawa, K. Honda, T. Matsutani, and K. Imaoka, "Improvements of Trench Capacitor Characteristics by Pre-Oxidation Surface Cleaning with HNO<sub>3</sub>-HF-H<sub>2</sub>O Solution", IEEE IEDM Digest of Technical Papers, **35-1**, 726(1988).
- <sup>4</sup> W. Kern, J. Electrochem. Soc., **137**, 1887 (1990).
- <sup>5</sup> H. F. Schmidt, M. Meuris, P. W. Mertens, A. L. P. Rotondaro, M. M. Heyns, T. Q. Hurd and Z. Hatcher, "Physico Chemical Aspects of Hydrogen Peroxide Based Silicon Wafer Cleaning Solutions", Proc. Ultraclean Processing of Si Surfaces, 259 (1994).
- <sup>6</sup> C. R. Helms, H.-S. Park and S. Dhanda, "Fundamental Metallic Issues for Ultraclean Wafer Surfaces from Aqueous Solutions", Proc. Ultraclean Processing of Si Surfaces, 205 (1994).
- <sup>7</sup> O. J. Antilla and M. V. Tilli, J. Electrochem. Soc., **139**, 1751, 1992.
- <sup>8</sup> J. S. Glick, "Characterization of Deposition and Removal of Metallic Impurities of the RCA Standard Clean", Proc. Semiconductor Pure Water and Chemicals Conf., Santa Clara, 93 (1993).
- <sup>9</sup> T. Q. Hurd, P. W. Mertens, H. F. Schmidt, D. Ditter, L. H. Hall, M. Meuris and M. M. Heyns, "The Role of Hydrogen Peroxide in the SC2 Clean", Proc. Inst. Environmental Sci., 218 (1994).
- <sup>10</sup> S. Dhanda, R. P. Chiarello, C. R. Helms, P. Gupta, and B. B. Triplett, submitted for publication.
- <sup>11</sup> H. Morinaga, M. Suyama, M. Nose, S. Vehaverbeke, and T. Ohmi, "A Model for the Electrochemical Deposition and Removal of Metallic Impurities on Si Surfaces", IEICE Trans. Electron., **E79-C**, 343 (1996).
- <sup>12</sup> S. Dhanda, R. P. Chiarello, C. R. Helms, and P. Gupta, 192nd Electrochem. Soc Mtg.: Mtg Abstracts, **97-2**, 2210 (1997).

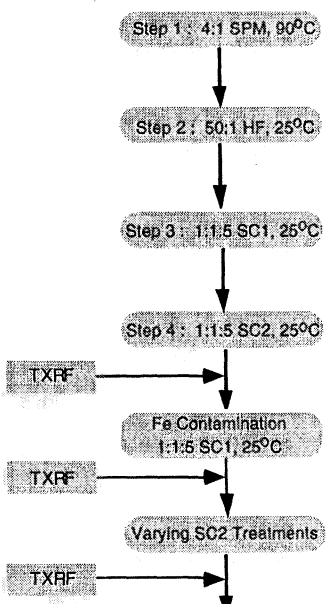


Figure 1: Process flow outlining the treatment of Fe-contaminated wafers in SC2 solutions of varying compositions and temperatures.

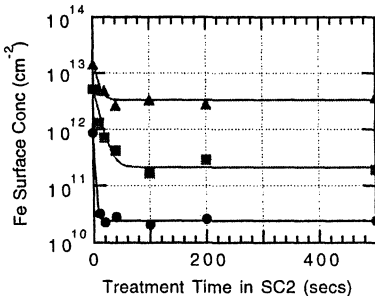
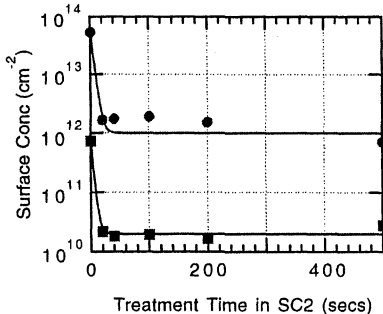
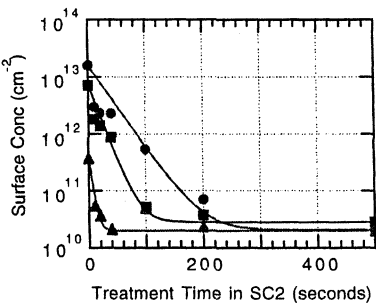
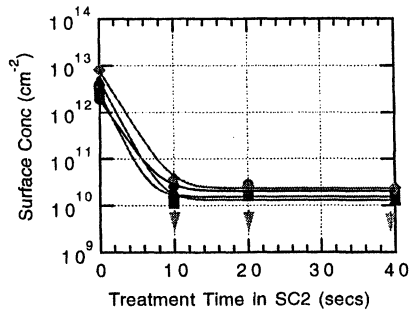


Figure 2. Kinetics of Fe removal in a (a) 1:1:5 SC2 mixture at 70°C. (b) 1:1:5 SC2 mixture at 50°C. (c) 1:1:5 SC2 mixture at 25°C.



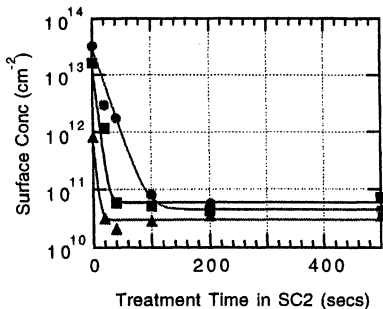


Figure 3. Kinetics of Fe removal in a  
(a) 0.1:0.5 SC2 mixture at 70°C. (b)  
0.01:0.5 SC2 mixture at 70°C.

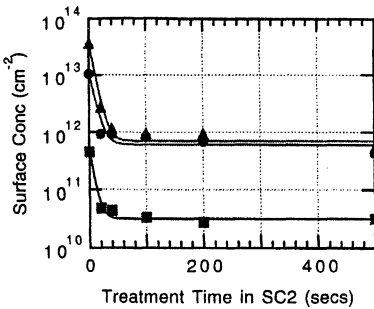


Figure 3. Kinetics of Fe removal in a  
(a) 0.1:0.5 SC2 mixture at 70°C.  
(b) 0.01:0.5 SC2 mixture at 70°C.

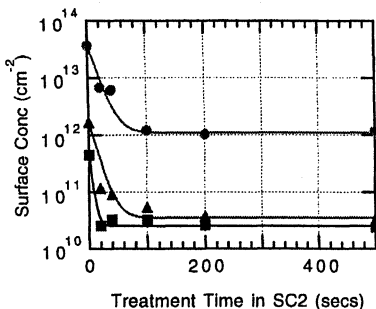


Figure 4. Kinetics of Fe removal in a  
(a) 1:0.5 SC2 mixture at 25°C. (b) 1:0.5  
SC2 mixture at 50°C.

## **PROTECTION OF HF BATHS AGAINST NOBLE METAL CONTAMINATION**

S. Kunz<sup>(1)</sup>, S. Marthon<sup>(2)</sup> and F. Tardif<sup>(2)</sup>

(1) : Millipore SA, BP 116, 67120 Molsheim, France

(2) : Gressi-Leti-CEA/G, 17 rue des Martyrs , 38054 Grenoble Cedex 09, France

Noble metals deposit electrochemically in HF. The impact of H<sub>2</sub>O<sub>2</sub> and light on the deposition behaviour of 1 to 1000 ppb of Cu and Ag from aqueous 1% HF solutions on silicon wafers is investigated. It is found by TXRF and AFM that under none of these conditions neither the deposition of the noble metals onto the silicon surface, nor the roughening of the silicon surface can be prevented. For 1 ppb Ag and 10 ppb Cu in 1% HF up to 10 nm high peaks of copper and silver and 6 nm deep holes are observed on the silicon surface. QBD measurements of 7 nm gate oxide show that only 10 ppb of either metal decreases the gate-oxide-integrity. Point-of-Use purification of diluted HF using a Millipore Chempure™ purifier can remove 98 % of the Cu, and 99.9 % of Pd, and Au contamination within a few bath turnovers and maintain contamination levels comparable to a fresh HF bath.

### **INTRODUCTION**

With the shrinkage of gate oxide thickness and device feature size, control of metal contamination during wet cleaning processes becomes increasingly important. In HF chemistry noble metals are particularly detrimental since they deposit onto the silicon surface due to their positive electrochemical potential (1). During the lifetime of a HF bath metal contamination gradually increases due to impurities which are brought into the bath by contaminated silicon substrates. Since the contamination buildup from conventional processing becomes the major source of contamination, using even higher grade chemicals can no longer be the answer to meet the increasing requirements with respect to metallic purity of HF baths in wafer processing (2). Additional contamination spikes can cause fatal damage to gate oxide integrity especially after a HF-last cleaning process.

In the literature, different approaches to diminish noble metal deposition in HF have been reported, such as adding H<sub>2</sub>O<sub>2</sub> (3), (4), adding surfactants (1), (5) adding complexing agents (6), or processing the wafers in the dark (7), (8). In order to guarantee constant and lowest possible metal contamination levels during the whole bath lifetime Point-of-Use (POU) purification is necessary.

In this study, the deposition behaviour of Ag and Cu in diluted HF under different chemical and photochemical conditions is investigated. The contaminated wafers are characterized by Total-reflection X-Ray Fluorescence (TXRF) and Atomic Force

Microscopy (AFM). In order to study the impact of noble metal contamination on the dielectric properties of the gate oxide, QBD measurements of intentionally contaminated wafers are performed. Finally, the removal efficiency of the POU-purifier with respect to Cu, Fe, Ag, Au and Pd in intentionally contaminated 1% HF is investigated.

## EXPERIMENTAL

In the experiments 100 mm diameter, CZ grown, p-type (B-doped), (100) silicon wafers (14-22 Ohm cm) were used. Prior to the HF step the wafers were cleaned in  $\text{H}_2\text{SO}_4/\text{H}_2\text{O}_2$  (3/1, 140°C, 10 minutes) followed by a 1 % HF dip at 20° C prepared with ULSI grade concentrated HF. After overflow rinsing the wafers were spin-dried. The 1% HF was either clean or intentionally contaminated with Cu or Ag (1-1000 w-ppb). The resulting surface concentrations were measured by TXRF. The surface roughness of the wafers after contamination was measured by AFM (tapping mode).

For the GOI measurements the wafers were subject to an RCA clean [ $\text{H}_2\text{SO}_4/\text{H}_2\text{O}_2$  (3:1), SC1 (0.25, 1, 5) , SC2 (1, 1, 5)]. The wafers were intentionally contaminated in a HF-last step for 2 minutes, with 1 to 1000 ppb of Ag or Cu. After overflow rinsing the wafers were spin-dried. The delay between HF-last and oxidation was less than 60 minutes to avoid degradation of the surface due to organic contamination. A 7 nm gate oxide was grown in a wet thermal process at 750°C.

A Millipore Chempure™ purifier was used as a POU ion exchange purifier. The device consists of a pleated UPE membrane cartridge in a polyethylene housing. It was plumbed in series with a 0.1 micron Millipore QuickChange™ particle filter in a recirculated HF bath (9). The metal concentration in the bath was measured by ICPMS. All the experiments except for the AFM measurements were performed in a class 10 environment.

## RESULTS

### Investigation of Noble Metal Deposition on Silicon by TXRF and AFM

In order to study the influence of light and strong oxidizing agents such as  $\text{H}_2\text{O}_2$  on the deposition behaviour of Cu and Ag the wafers were immersed in a solution of 1% HF which was intentionally contaminated with 100 ppb of Cu and Ag: i) under normal cleanroom illumination, ii) in the dark and iii) in 1%  $\text{HF}/\text{H}_2\text{O}_2$  (1/7) and normal cleanroom illumination for 10 minutes (fig.1). The blank was treated in clean 1% HF with cleanroom illumination.

Neither addition of  $\text{H}_2\text{O}_2$  nor processing in the dark diminished the measured Ag contamination of  $10^{14}$  atoms/cm<sup>2</sup>. Even though less Cu was deposited when  $\text{H}_2\text{O}_2$  was added or after contamination in the dark, the resulting contamination levels were always above  $10^{11}$  atoms/cm<sup>2</sup> compared to  $10^{10}$  atoms/cm<sup>2</sup> for the blank.

Under all deposition conditions the surface roughness, given as the Root Mean Square (RMS) of the surface profile, increased considerably (fig. 2). In the case of Cu the surface roughness doubled for all three deposition conditions. For Ag the surface roughness even increased up to 0.5-0.7 nm compared with 0.14 nm for the blank. It reached its maximum value when H<sub>2</sub>O<sub>2</sub> had been added.

Figure 3 shows the typical surface morphology of a silicon wafer after contamination with 100 ppb Cu or Ag in 1% HF obtained by AFM. Neither the wafers treated with HF/H<sub>2</sub>O<sub>2</sub> nor the wafers processed in the dark looked any different. Under all three contamination conditions and for both metals, Cu and Ag, the average surface roughness increased. Additionally up to 10 nm high peaks of deposited metal and 6 nm deep holes in the wafer surface were observed (10). This was valid also for contamination in 1% HF with 10 ppb Cu or 1 ppb Ag when the bath time was decreased to 2 minutes. For 1 ppb Cu and a 2 minutes bath time 1 nm high Cu deposits could still be observed. As the metal concentration in the HF was decreased the number density of the resulting metal peaks on the wafer decreased as well. But even for a metal concentration of 1 ppb up to 10 nm high metal peaks were still observed.

### **Electrical Tests**

The influence of Cu and Ag contamination in HF-last on the gate oxide integrity of 7 nm oxide was investigated. After an RCA clean the wafers were intentionally contaminated with 1 to 1000 ppb of Ag or Cu in HF-last. In figures 4 and 5 the infant breakdown, referred to as "pinholes" (< 10E-5 C/cm<sup>2</sup>), and the Mid BreakDown percentage (MBD) (10E-5 to 1.5 C/cm<sup>2</sup>) are shown.

The results show that only 10 ppb of either Cu or Ag clearly affected the Gate Oxide Integrity (GOI). Starting with 8 % for wafers treated in HF with no or 1 ppb of metal contamination the MBD increased to 21 % for 1000 ppb of copper. Additionally an increase of the infant breakdown was observed. Usually this is contributed to particle contamination prior to the gate oxidation. As depicted in figure 4 the infant breakdown increased with the Cu contamination in HF. This behaviour could be related to the observed big copper peaks which degrade the oxide and create pinholes. In the case of Ag, which deposited more uniformly, this effect was not observed (see figure 5). The MBD degradation could be attributed to the associated silicon roughness. Indeed Ag, which generated a particularly heavy roughness, degraded the oxide: 10 ppb increased the MBD to 80 %, 100 ppb leads to a nil yield.

Before gate oxidation the HF step, used to remove the sacrificial oxide, is often followed by a conventional RCA clean. This cleaning sequence is able to eliminate noble metals but not the roughening during the previous contaminated HF step. Figures 6 and 7 show that, as expected, the RCA restored only partially the surface. When a RCA was performed the dangerous noble metal concentrations were pushed to 1000 and 100 ppb for Cu and Ag respectively. From this point of view a RCA-last process is more robust than a HF-last process.

## **Point-of-Use Purification in 1 % HF**

To study the performance of the Chempure™ purifier after an accidental contamination of the bath, 8 ppb of Cu was spiked into a recirculated HF-bath, bypassing the purifier. After the solution was well mixed the flow was switched to the purifier. Samples were taken every 5 to 10 minutes and analyzed by ICPMS. Three turnovers after putting the purifier in-line the Cu concentration had fallen to 200 ppt and reached 170 ppt in equilibrium after 24 h of recirculation (fig. 8).

The corresponding graph for Fe<sup>3+</sup> is shown in figure 11. Before the contamination 130 ppt of Fe were measured in 1 % HF. Traces of Fe were always present due to extraction from the tank and the tubing. In this case 5 ppb of Fe was spiked into 1 % HF. After 3 bath turnovers through the purifier the remaining Fe concentration was diminished to 200 ppt resulting in a Fe contamination of 180 ppt after 24 hours.

The purifier was even more efficient in removing Au and Pd. In a single experiment 10 ppb of Au and Pd were added to 1 % HF (fig. 9). After 7 turnovers 20 ppt of Pd- and 40 ppt of Au-contamination were measured reaching a value of 10 ppt for both metals after 14 turnovers.

In order to simulate the performance of the purifier during the normal contamination build-up during the lifetime of a HF bath, four spikes of 1 ppb of Cu and Fe were consecutively added to 1 % HF (fig. 10). Samples were taken before and 30 minutes (7 turnovers) after each contamination spike. Before the contamination 0 ppt of Cu and 140 ppt of Fe (as extractable) were measured by ICPMS. As shown in figure 10, the purifier kept the Fe concentration constant at approximately 150 ppt even after 4 ppb had been added in total. In the case of Cu a linear dependence of the equilibrium concentration and the total added amount was observed, as it is predicted by the theoretical model (11), resulting in a remaining Cu contamination of 170 ppt after 4 ppb of Cu were added in total. The purifier did not remove Ag and Pt contamination.

## **DISCUSSION**

Neither addition of H<sub>2</sub>O<sub>2</sub> nor dark processing of the wafers could effectively protect against noble metal deposition in diluted HF. No influence on the Ag deposition was observed. Under all conditions the surface concentration could not be reduced to the blank level. Furthermore, an increase of surface roughness was observed even when hydrogen peroxide was added to the HF. Additionally to this increased average surface roughness up to 10 nm high metal depositions and 6 nm deep holes in the silicon surface were found by AFM.

As the electrical tests have shown 10 ppb of Cu or Ag in the HF-last bath could already drastically reduce the yields for 7 nm gate oxide. Ag is much more detrimental than Cu. The deposition of Cu seems to depend strongly on the initial surface state of each particular wafer. Even for 1000 ppb Cu in the 1% HF some wafers were found that showed the same QBD distribution as the reference treated in clean HF.

Even a RCA clean following the contamination in 1 % HF could not prevent the degradation of the gate oxide for high concentrations of Cu (1000 ppb) and Ag (100

ppb). AFM results show that the deposition of noble metals is accompanied by an increase of the surface roughness. For low metal concentrations the dielectric degradation of the gate oxide is dominated by defects created by the deposited noble metals whereas for high concentrations the associated surface roughening is sufficient to destroy the gate oxide.

Thus POU-purification seems to be the only way to efficiently prevent noble metal deposition in HF. The purifier is able to prevent the buildup of metal contamination during conventional processing and guarantees a constant bath quality during the whole bath lifetime at ppt contamination levels. It efficiently protects against noble metal spikes during wafer processing. After a contamination spike the purifier reached equilibrium in only a few turnovers and cleaned the HF with a removal efficiency of 97 % for Cu, 99 % for Fe and 99,9 % for Au and Pd. Reaching Sub-ppb levels in less than 2 turnovers it thus provides a "clean" bath for the next lot being processed. This enables the bath lifetime to be extended and can contribute to reducing costs-of-ownership and lower HF waste.

#### ACKNOWLEDGMENT

I would like to thank François Tardif and all members of the microelectronics division at LETI/Grenoble for their co-operation and help in the course of this work.

#### REFERENCES

1. H. Morinaga, M. Suyama, M. Nose, S. Verhaverbeke, T. Ohmi, IEICE Trans. Electron (electrochemical deposition and removal of metallic impurities on Si surfaces).
2. J.Sees, L. H. Hall, J. Electrochem. Soc., **142**, 1238, (1994).
3. H. Morinaga, T. Ohmi, Electrochem. Soc. Proc., **95-20**, 257.
4. T. Shimomo and M. Tsuji, Extended Abstracts of Electrochem. Soc. Meeting, **91**, 278, Washington DC, (1991).
5. M. Miyamoto, N. Kita, S. Ishida and T. Tatsuno, J. Electrochem. Soc., **141**, 2899, (1994).
6. I. Teerlinck, P. W. Mertens et al., Proc. of the 3rd Symposium on UCPSS, 21, (1996).
7. I. Teerlinck, P. W. Mertens, H. F. Schmidt, M. Meuris, M. M. Heyns, J. Electrochem. Soc., **143**, 3323, (1996).
8. I. Teerlinck, H. F. Schmidt et al., Electrochem. Soc. Proc., **95-20**, 284.
9. W. Fyen, L. Mouche, et al. Proc. of the 3rd Symp. on UCPSS, 131, (1996).
10. F. Tardif, T. Lardin, P. Boelen, R. Novak, I. Kashkoush, Proc. of the 3rd Symp. on UCPSS, 175, (1996).
11. B. Parekh, J. Zhaka, K. Gupta, B. Triplett, M. Tran., Solid State Technology, August 1996.

This work was carried out within the GRESSI consortium between CEA-LETI and France Télécom-CNET.

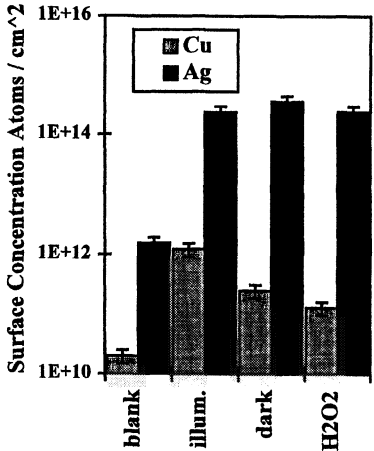


Fig.1: Influence of H<sub>2</sub>O<sub>2</sub> and dark processing on the deposition behaviour of Ag and Cu in 1 % HF (100 ppb, 10 min.) measured by TXRF.

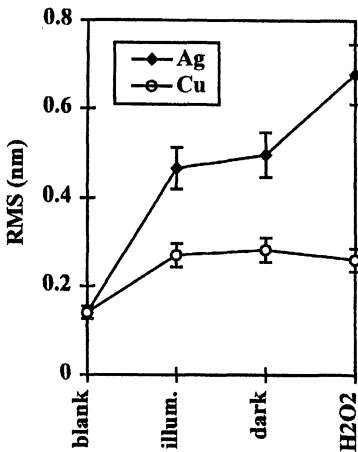


Fig.2: Influence of H<sub>2</sub>O<sub>2</sub> and dark processing on the surface roughness of silicon wafers (AFM tapping mode) treated in 1 % HF with 100 ppb of Ag or Cu (10 min.).

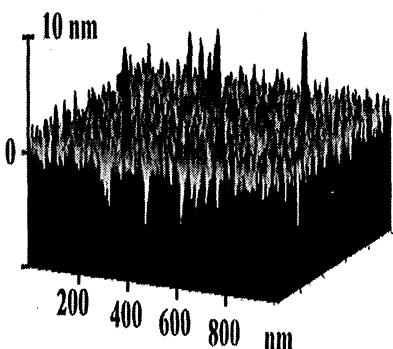


Fig.3: AFM plot of a silicon surface after 10 min. immersion in 1% HF/H<sub>2</sub>O<sub>2</sub> (7/1) containing 100 w-ppb of Ag.

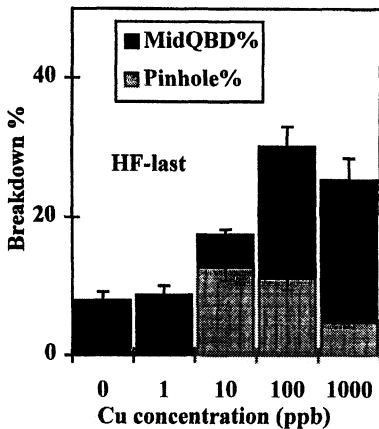


Fig.4: Breakdown for 0 to 1000 ppb of Cu in 1% HF, 2 minutes. Pinholes : < 1 E-5 C/cm<sup>2</sup>; Mid QBD: 1E-5 to 1.5 C/cm<sup>2</sup>.

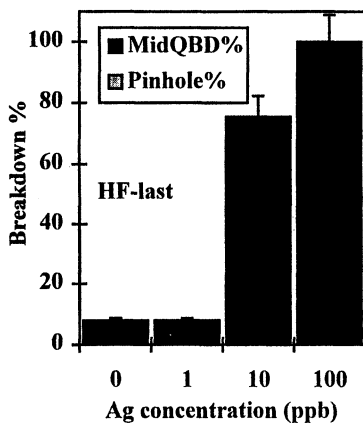


Fig.5: Breakdown for 0 to 100 ppb of Ag in 1% HF, 2 minutes. Pinholes: < 1 E-5 C/cm<sup>2</sup>; Mid QBD: 1E-5 to 1.5 C/cm<sup>2</sup>.

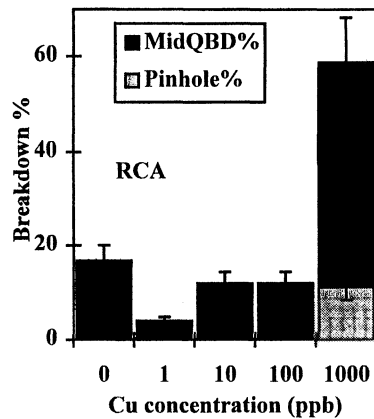


Fig.6: Breakdown for wafers treated in 1% HF with 0 to 1000 ppb of Cu, 2 minutes, followed by an RCA clean before oxidation. Pinholes: < 1E-5 C/cm<sup>2</sup>; Mid QBD: 1E-5 to 1.5 C/cm<sup>2</sup>.

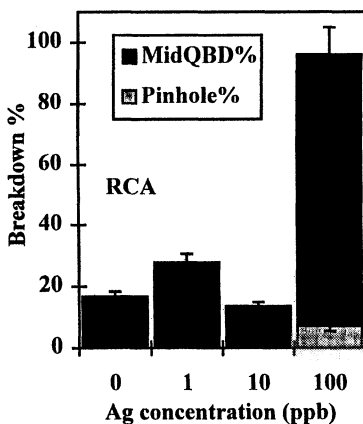


Fig.7: Breakdown for wafers treated in 1% HF with 0 to 100 ppb of Ag, 2 minutes, followed by an RCA clean before oxidation. Pinholes: < 1 E-5 C/cm<sup>2</sup>; Mid QBD: 1E-5 to 1.5 C/cm<sup>2</sup>.

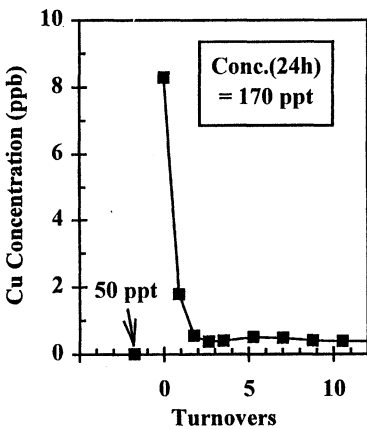


Fig.8: Cu concentration after spiking approximately 8 ppb Cu in 1 % HF vs. number of turnovers through the purifier (bath volume 24 liters, flowrate 5.7 l/min.).

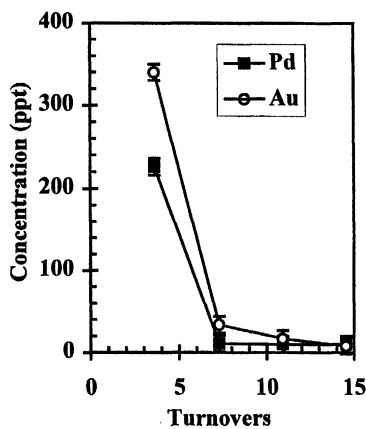


Fig.9: Au and Pd concentration after spiking 10 ppb of both metals in 1 % HF vs. number of turnovers through the purifier (bath volume 24 liters, flowrate 5.7 l/min.)

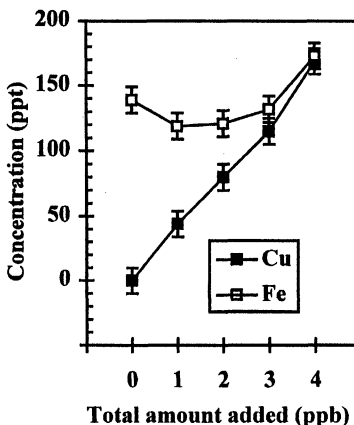


Fig.10: Low ppt performance of the purifier with Cu and Fe. Cu and Fe concentration after consecutively spiking 1 ppb of both metals in 1 % HF. Samples were taken 30 minutes or 7 turnovers after the spike.

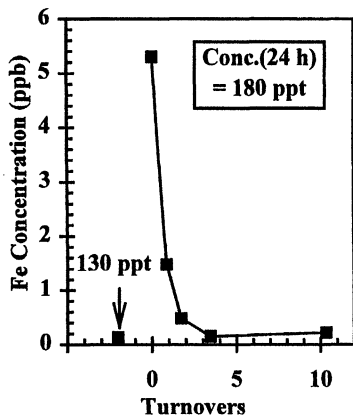


Fig.11: Fe concentration after spiking approximately 5 ppb Fe in 1 % HF vs. number of turnovers through the purifier (bath volume 24 liters, flowrate 5.7 l/min.).

## **ELECTROCHEMICAL AND RADIOCHEMICAL STUDY OF COPPER CONTAMINATION MECHANISM FROM HF SOLUTIONS ONTO SILICON SUBSTRATES.**

Valérie BERTAGNA, François ROUELLE and Marius CHEMLA

Université P. & M. Curie, 4 Place Jussieu, 75005, PARIS, FRANCE

The mechanism of contamination of silicon wafers from dilute HF solutions containing traces of metallic ion impurities, was investigated using a new electrochemical cell, which proved to act as a very efficient sensor for in situ characterization. Upon copper contamination, the open-circuit potential was observed to shift rapidly towards more positive values at a rate nearly proportional to the copper concentration. All potential/time curves tend to reach a plateau, while quantitative measurements using radioactive tracers revealed that copper ions were continuously reduced on the silicon surface.

Results led to the conclusion that copper nuclei act as a catalyst which enhances the cathodic activity for protons reduction. The model was supported by Atomic Force Microscopy (AFM) observations which showed the initiation of corrosion pits around the nuclei.

### **INTRODUCTION**

As the device dimensions are downsized, the surface conditioning of the silicon wafers utilized for the preparation of integrated circuits plays a role of increasing importance [1,2,3,4]. Because inorganic particles, metallic clusters and adsorbed organic compounds severely affect the electrical performances of devices [5, 6], it is necessary to clean these surfaces using wet processes called RCA cleaning established by Kern in 1970 [7]. Diluted hydrofluoric acid solution (DHF), which suppresses native or chemical silicon oxide, is included in this cleaning sequence. However, when this solution contains traces of noble metals such as copper, silicon wafers are contaminated during the native oxide removal step.

In the present work, we have associated, electrochemical and radioactivity measurements to study the mechanism of copper deposition on silicon wafers surfaces from DHF solutions containing traces of copper in the range of a few tens of ppb. The study was limited to deaerated DHF solutions, in the dark. This work, which demonstrates that electrochemical parameters are extremely sensitive to study silicon surface contamination by trace amounts of metallic ions, is a contribution to the silicon contamination process by metallic impurities in DHF solutions [8, 9].

## EXPERIMENTAL

We used two complementary investigation techniques.

Electrochemical methods -Firstly, silicon contamination was detected in-situ with electrochemical methods. These experiments were achieved with a home-built electrochemical cell [10-11], for reproducible open-circuit potential recordings by rigorous control of the oxygen content, exposure to light and purity of the chemicals. In our cell, presented in Fig. 1, the silicon wafer is in contact with a Teflon tube, filled with the electrolyte, and pressed between two polyvinyl plates. The whole cell is protected against room light by means of a closed cylinder made of black polyvinyl polymer. A special device [11] provides the feeding of the cell with beforehand dearated electrolyte by argon bubbling. The reference electrode was a saturated calomel electrode (SCE), connected to the electrolyte by means of a saturated KCl-agar salt bridge made of a Teflon tube. The electrochemical measurements were done with a Tacussel Radiometer Analytical PGS 201T potentiostat driven by an IBM PC computer using the Voltamaster software allowing for preselection of the experimental procedure.

Open circuit potential recording is quite interesting, because it is characteristic of the anodic and cathodic surface sites reactivity. Recently, it has gained high interest [14] because for a long time it was known to be not reproducible within a few hundreds of mV [12]. Cyclic voltammetry was used to investigate the silicon electrode anodic and cathodic reactions within a narrow potential range ( $\pm 250$  mV) to not induce porous silicon formation, and be as close as possible to the conditions where silicon wafers are simply immersed in DHF electrolyte.

Radioactive  $^{64}\text{Cu}$  indicator-The TXRF analysis technique was also used to quantify traces of contaminants on the wafers. But as this spectroscopy was very sensitive to surface roughness, the radioactivity analysis, has been a complementary method employed in this study. Moreover, we wanted to establish a correlation between each electrochemical potential measurements and the corresponding surface copper concentration on the same sample (surface less than  $4\text{ cm}^2$ ).

Experiments were undertaken according to activation analysis and radioactive isotope indicators [13]. Neutron activation of elemental metallic copper, leads mainly to  $^{64}\text{Cu}$ , a  $\beta^-$ ,  $\beta^+$  and  $\gamma$  emitter radioelement, with a half-life period of 12.6 hours.

In the first method, the silicon surface was contaminated in situ and exposed to a neutron flux ( $10^{14}$  neutrons/ $\text{cm}^2 \text{ s}$ ), in the Orphée nuclear reactor at the Saclay Nuclear Research Center (CENS). The main disadvantage of this method is that the bulk impurities and silicon itself are also activated. Only an excess surface contamination higher than  $3 \cdot 10^{12}$  atoms/ $\text{cm}^2$  is detected by activation analysis.

The second method consists in the use of  $^{64}\text{Cu}$  as a radioactive tracer, obtained by irradiation of a high purity copper wire, dissolved as  $\text{Cu}^{2+}$  ions in DHF to obtain a 1 ppm stock solution. This method is more convenient, because the radioactive emission concerns only  $^{64}\text{Cu}$  and because the lower limit of detection by this method is estimated to be  $2.10^{11}$  atoms/cm $^2$ .

Silicon wafers cleaning.-In our experiments, silicon wafers, 125 mm diameter and 625  $\mu\text{m}$  thickness, were purchased from MEMC Electronic Materials.

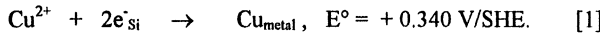
p-type wafers, boron doped, ( $5.10^{16}$  at.cm $^{-3}$ )  
n-type wafers, phosphorus doped, ( $2.10^{14}$  at.cm $^{-3}$ )

These ones, CZ-grown, (100) oriented, were mirror polished, for MOS applications, and their back side covered with a Ga-In alloy. Before each experiment, the silicon samples were cleaned with a mixture of  $\text{H}_2\text{SO}_4:\text{H}_2\text{O}_2$  (3:2, by volume) at 80°C during 10 minutes, then thoroughly rinsed with ultra pure water (UPW) and cleaned by a DHF solution to promote a hydrophobic H-terminated silicon surface.

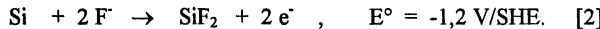
DHF solutions, 5% by volume, were obtained by mixing 40% HF SLSI grade (Sub Large Scale Integration, metal elements below 1 ppb) with UPW and deaerated by bubbling argon gas N60 grade. For the in-situ copper contamination experiments we used a deaerated 5% DHF stock solution, containing copper ions, with a 2 ppm concentration.

## RESULTS

In the previous models describing the copper plating onto silicon electrodes, the mechanism was supposed to involve electrons following the reaction on cathodic sites:



Moreover in a fundamental study of the silicon/DHF interface electrochemical properties [24], charge transfer reactions on cathodic sites result from the electrons generated by the corrosion process on anodic sites of the silicon substrate in DHF electrolytes.



We have obtained copper reduction kinetics, using open circuit potential (O.C.P.) measurements. The observed O.C.P.,  $\approx -650$  mV, was consistent with our previous results [14], indicating that the DHF solution was really pure, and Si substrate clean. Fig.2 shows five experimental results obtained for n-type substrates. The initial O.C.P. almost coincide, allowing the detection of any potential perturbation resulting from a change of the surface sites reactivity. Two minutes later, a small volume, 1 ml, of deaerated DHF solution containing copper traces was added so that the whole copper concentration in the electrochemical cell reaches 15 to 260 ppb. A reference curve for comparison with the results involving copper contaminant was obtained by simply adding 1 ml of deaer-

ated DHF. The graphs obtained in this set of experiments are presented in Fig. 2, in the case of n-type Si. The addition of trace amounts of copper contaminant induced a steep shift of the potential towards positive values, nearly proportional to the copper concentration and tend rapidly to a stable limiting value. From this result, the question arises whether the increase of the cathodic current should be assigned to the reduction of  $\text{Cu}^{2+}$  ions.

In order to separate the contribution of proton and copper reduction on cathodic sites, the previously contaminated silicon samples were rinsed with UPW in the cell, and then, the cell was filled again with deaerated DHF. Then, voltammetric curves were recorded (Fig. 3). These figures were found to behave identically as those obtained in the presence of trace amounts of copper impurities. We also noticed that anodic currents, responsible for the silicon substrate dissolution, are weakly dependent on copper contamination, while cathodic currents increase with surface copper concentration. The results suggest that the cathodic current is mainly correlated to the discharge of protons on copper nuclei which act as a catalyst.

Assuming that discharge cathodic current is nearly proportional to the deposited copper, what is the significance of the observed potential plateau exhibited on all curves on Fig. 2? Does it mean that the metal deposition ends after a short time following the ascending part of the graph? Radioactivity analysis was here very efficient because it enables the quantification of copper nuclei, and we noticed that the copper deposit grows continuously even after a few tens of minutes, suggesting that the open-circuit potentials are not directly correlated to the surface copper concentration. The first generated nuclei subsequently grow without any substantial enhancement of their catalytic properties.

The growth of the copper clusters has to involve electrons from electrochemical etching of the silicon substrate. Therefore we have completed the preceding experiments by studying the morphology of a silicon surface contaminated by copper with an atomic force microscope, AFM (Digital Instruments, Nanoscope III), working in tapping mode, in air. Copper atoms form small nuclei, often situated at the center of a corrosion pit as the result of the catalytic properties of copper cathodic sites (Fig. 4).

## DISCUSSION

Now, the general shape of the potential/time curves (Fig. 2) includes a rapid rise of potential followed by a plateau for which interpretation requires a closer analysis. Chyan et al. [15] experimental results demonstrated that the number of copper grains increases rapidly during the first minutes and then reaches a constant value. It follows that the continuous increase of the copper deposit should result from the growth of all nuclei without any change of their number.

Only one reaction occurs on the anodic sites, corresponding to the dissolution of elemental silicon following reaction (2), which generates electrons in the semiconductor.

On the other hand, these electrons are consumed on cathodic sites following three distinct paths:



From the computation of the radiotracer measurements, the contribution of the  $\text{Cu}^{2+}$  discharge to the overall cathodic current appears to be negligible. This conclusion could also be derived from the very weak concentration of  $\text{Cu}^{2+}$ , as compared to  $\text{H}^+$  species.

The expression for O.C.P.,  $E_r$ , suggests a discussion about the ascending part of the rest potential curves. This expression is:

$$E_r = \frac{\alpha E_1 + \beta E_2}{\alpha + \beta} + \frac{RT}{nF(\alpha + \beta)} \ln \frac{j_{0C}}{j_{0A}}, \quad [4]$$

where  $E_1$ ,  $E_2$ ,  $\alpha$  and  $\beta$  are respectively the equilibrium potentials and the transfer coefficients of the anodic and cathodic electrochemical reactions.  $j_{0A}$  and  $j_{0C}$  are the exchange current densities, characteristic of the rate the electronic transfer proceeds on anodic and cathodic sites. With the generation of the first copper nuclei,  $J_{0C}$  increases because of the electrocatalytic properties of small copper grains for protons reduction. Then, as AFM images show, corrosion pits are initiated around the grains of copper, increasing the anodic current. This behaviour is illustrated by the O.C.P. curve. The ascending part of the graph is associated to the generation of the first copper nuclei, which induce a strong hydrogen cathodic current, and the plateau to the generation of corrosion pits and anodic current.

Moreover, we assume, following to Chyan experimental results [16], that the number of nuclei remains constant and that their size grows with time. Under these conditions, the external area of the metal grains should increase following a  $t^{2/3}$  relation, which would result in a slowing down of the potential variation. However, in order to give an interpretation of the appearance of the potential plateau, despite the continuous increase of deposited copper, we suggest that the catalytic properties of metallic clusters for protons discharge decrease as the crystals size grows. This well known property of catalytic materials [17] would explain the appearance of a limiting constant value when the crystals growth result in the formation of large size particles with poor catalytic activity.

Finally, the high catalytic activity of metallic nuclei induces a rapid local corrosion of the substrate as a consequence of the formation of a short-circuited electrochemical cell. This phenomenon was illustrated using AFM microscopy working in the tapping mode. Fig. 4 shows a cross section of a Cu nucleus surrounded by a corrosion pit. The

high level of current density due to the protons reduction on Cu nuclei is responsible for a rapid dissolution of the substrate. The short-circuit current has to follow the minimal ohmic resistance lines (Fig. 4), in the solution as well as in the semiconductor and the current lines are focussed on the cathodic site whereas a corrosion pit is initiated nearby. This figure shows a striking illustration of this mechanism.

## CONCLUSION

Experimental investigations using a new electrochemical cell, along with radioactive tracer analyses, have successfully described the silicon behavior in copper contaminated DHF solutions, in the dark.

The mixed potential was considered as representing the relative activity of both cathodic and anodic sites distributed on the silicon surface. After an initial step where the first copper nuclei are formed, the catalytic properties of these particles promote a high cathodic current density due to protons discharge. During the growth of the copper grains, their catalytic properties decreased, which could explain the limiting plateau value of the rest potential. This interpretation was provided by radioactive measurements which revealed that contamination proceeded continuously with a nearly constant copper deposition rate during at least 30 minutes (in our experiments).

An important aspect of this work is that our electrochemical cell was established to be very sensitive to the presence of metallic traces in DHF solution and could be a powerful tool in the semiconductor industry for on-line monitoring of the cleaning solutions during chemical processing and of the surface defects of the wafers. Moreover, most of our results seem to indicate that the electrochemical properties of the high purity silicon substrate are more important than the electronic charge carriers characteristics for the behavior of the semiconductor/electrolyte interface.

## ACKNOWLEDGEMENTS

The authors express their thanks to Dr C. Plougonven, IBM Company, for fruitful discussions, and to MEMC Company for providing n- and p-doped silicon wafers. Technical assistance of Mrs Carrot, Laboratoire P. Sue at Saclay is warmly acknowledged.

## REFERENCES

1. D. N. Schmidt and D. Trestain, *The electrochemical society interface*, **5**, 24 (1996).
2. M. Meuris, S. Verhaverbeke, P. W. Mertens, M. M. Heyns, L. Hellemans, Y. Bruynseraeede and A. Philipossian, *Jpn. J. Appl. Phys.*, **31**, part 2, L1514-L1517 (1992).

3. M. Itano, T. Kesuka, M. Ishii, T. Unemoto, M. Kubo and T. Ohmi, J. Electrochem. Soc., **142**, 971 (1995).
4. M. Meuris, M. M. Heyns, P. W. Mertens, S. Verhaeverbeke and A. Philipossian, Microcontamination, **May**, 31, (1992).
5. K. Honda, A. Osaka and N. Toyokura, Appl. Phys. Lett., **45**, 270, (1984).
6. I.-W. Wu, M. Koyanagi, S. Holland, T. Y. Huang, J. C. Mikkelsen, R. H. Bruce and A. Chiang, J. Electrochem. Soc., **136**, 1638, (1989).
7. W. Kern and D. A. Puotinen, RCA Review, **31**, 187, (1970).
8. V. Bertagna, Thesis, University Pierre & Marie Curie, (1996).
9. V. Bertagna, F. Rouelle, G. Revel, M. Chemla, J. Electrochem. Soc., (in press).
10. V. Bertagna, F. Rouelle and M. Chemla, Analusis, **24**, 383, (1996).
11. V. Bertagna, F. Rouelle and M. Chemla, J. Applied Electrochem., (in press)
12. H. Föll, Appl. Phys. Lett., **45**, 1095, (1984).
13. G. Revel, Analusis, **12**, 506, (1984).
14. V. Bertagna, C. Plougonven, F. Rouelle and M. Chemla, J. Electrochem. Soc., **143**, 3532, (1996).
15. O.M.R. Chyan, J.J. Chen, Y. Chien, J. Sees, L. Hall, J. Electrochem. Soc., **143**, 92, (1996).
16. O.M.R. Chyan, J.J. Chen, H.Y. Chien, J. Wu, M. Liu, J.A. Sees and L.H. Hall, J. Electrochem. Soc., **143**, L 235, (1996).
17. G. C. Bond, Catalysis by metals, Academic Press, London, (1962).

## FIGURES

**Figure 1:**  
Electrochemical  
cell for reliable rest  
potential and  
voltammetric  
curves records  
on silicon  
materials.

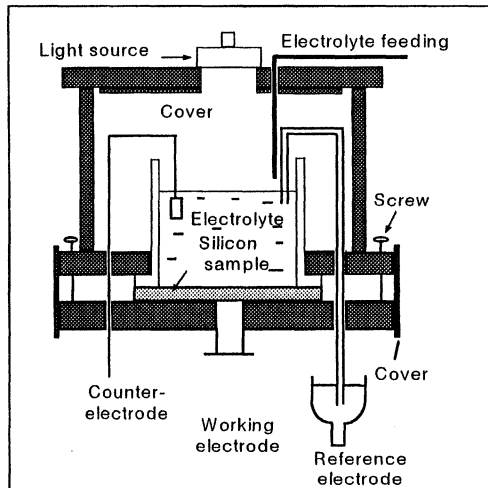


**Figure 2:** Open circuit potential versus time of n-type silicon, in the dark, in contact with a deaerated 5% DHF solution, upon addition of trace amounts of copper: 0 ppb (a), 15 ppb (b), 39 ppb (c), 74 ppb (d), 260 ppb (e).

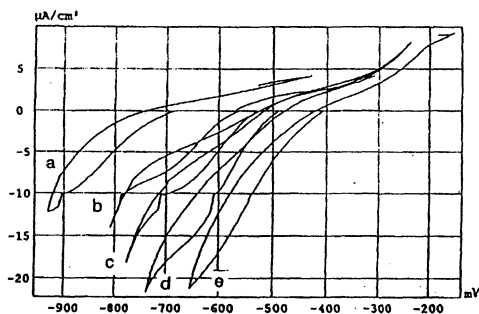
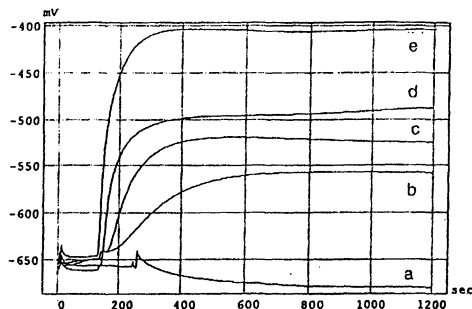
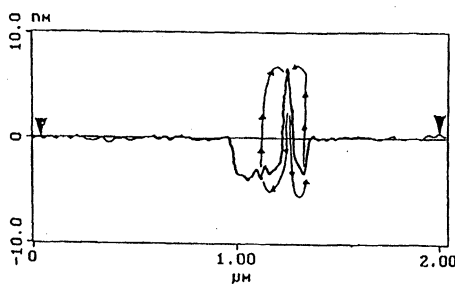


**Figure 3:** Voltammetric curves of n-type silicon samples, used in figure 1, after copper contamination in DHF solutions: 0 ppb (a), 15 ppb (b), 39 ppb (c), 74 ppb (d), 260 ppb (e).

**Figure 4:** Section profile around a copper nucleus, resulting from the contamination of a n-type silicon sample, in the dark, in a deaerated 5% DHF solution containing 100 ppb of  $\text{Cu}^{2+}$  ions.



# REMOVAL OF Cu FROM Si WAFER SURFACES USING DILUTE HF-HCl SOLUTIONS

S. Dhanda, R. P. Chiarello and C. R. Helms  
Solid State Lab, Stanford University, CA 94305

P. Gupta  
Intel Corporation, CA 95054

The deposition of Cu from dilute HF mixtures, and its effect on silicon surface microroughening is examined. The effect of adding small amounts of HCl to such a dilute HF mixture, is also examined. It is shown that the addition of HCl in fact suppresses the deposition of Cu from solution onto the wafer surface, without causing any additional microroughening, thus making a dilute HF-HCl based cleaning process a viable one.

## INTRODUCTION

Dilute HF solutions are frequently used to remove metals from silicon wafers. The process involves stripping off the native oxide (which in turn contains the imbedded metal impurities), by immersing the wafers in solutions containing 49 % w/w of hydrofluoric acid in water. While dilute HF solutions prove effective in removing most metals from the wafer surface, they also favor the deposition of noble metals (such as Cu, Ag and Au). These metals when present in large quantities in solution, deposit onto the silicon surface via a redox reaction, rendering any devices subsequently fabricated on such a wafer susceptible to failure.

The problem of noble metal deposition is often avoided by terminating a pre-gate oxidation cleaning sequence with an SC2 step, instead of a dilute HF clean. It is however, still a common practice to use a dilute HF clean as an intermediate step in the cleaning sequence. Thus, a typical sequence may involve a sulfuric peroxide clean, followed by an HF step, an SC1 step and finally an SC2 clean. While the SC2 chemistry does prove effective in removing any trace quantities of noble metals from the surface, it does not help prevent a possible secondary effect. The phenomenon in question is commonly referred to as "Metal Induced Pitting", and is described below.

Figure 1 outlines the process of noble metal deposition and removal during the course of an HF → SC1 → SC2 cleaning sequence. As shown in Figure 1a, noble metals present in an HF solution are deposited via a redox reaction onto the silicon surface. This process involves the displacement of a silicon atom from the surface, and its simultaneous replacement by an atom of the noble metal in question. Consequently, when

these wafers are cleaned in SC1, SC2 mixtures, the removal of the deposited (noble metal) impurities results in depressions or "pits" in the silicon surface (Figure 1b). On a macroscopic scale, these pits translate into surface roughness, which in turn degrades device performance.

Clearly, one way to mitigate any effects related to surface roughness, is to eliminate the deposition of noble metals onto the wafer surface in the first place. This chapter discusses a simple yet effective technique to achieve the same.

### HF-HCl Chemistries

Surface contaminants such as Cu, Au and Ag often prove to be the leading causes of device degradation.<sup>1,2,3,4</sup> Over time, advances in fluid purification have helped alleviate problems related to Au and Ag deposition, via elimination of these metals from the chemicals used in silicon cleaning (notably HF). Trace amount of Cu are however still found in HF solutions.

The addition of a powerful oxidizing agent (such as H<sub>2</sub>O<sub>2</sub>, O<sub>3</sub>), to a dilute HF solution, to prevent the deposition of Cu has been investigated by variety of experimenters.<sup>5,6</sup> The presence of the peroxide/ozone helps keep the copper in solution in its soluble oxidized form (Cu<sup>2+</sup>), thus preventing its deposition on the wafer surface via a redox process. In addition, the presence of an oxidizing agent helps maintain a hydrophilic surface, which mitigates the problem of particle addition often associated with HF last based chemistries.

Alternatively, the addition of a reagent which would facilitate the formation of soluble complexes with noble metals, could also help prevent their deposition. Given the propensity of noble metals to form soluble chloride complexes, the addition of a small amount of HCl to achieve the desired (high) solubilities, seems the logical choice.<sup>7</sup>

### EXPERIMENT

The experimental methodology adopted was as outlined in Figure 2. Bare silicon wafers were immersed in dilute HF and dilute HF-HCl solutions, contaminated with varying amounts of copper. The immersion times in each of these solutions were varied from 1 to 20 minutes. The contaminated wafers were rinsed, dried, and subsequently analyzed using TXRF to determine the amount of copper deposited from each of these solutions. The wafers from the splits were subsequently treated in SC1 and SC2 solutions to strip off any copper from the surface. AFM's were also performed on the wafers at critical points (as shown in the process flow), to ascertain which steps (if any) in the cleaning sequence were contributing to roughening of the silicon surface.

### Effect of HCl Addition

The build up of Cu on the wafer surface, in the absence of HCl (i.e. dilute HF only), is shown in Figure 3. The rate of build up varies with the amount of Cu in solution, with the build up being faster for higher concentrations of Cu in solution. Thus, for a dilute HF solution containing 5 ppm of Cu the kinetic curve has an exponential characteristic, while for a solution containing only 10 ppb of Cu, the build up is slower. The steady state surface values are also a function of the amount of copper in solution, with higher solution concentrations resulting in higher surface levels. Similar trends have also been observed by other experimenters.<sup>8</sup> Note that the saturation effect observed for deposition out of HF is different from that observed for deposition out of a BOE solution.<sup>9</sup> In the latter case, continuous build up of Cu on the surface occurs with time.

With the copper concentration in solution set at 10 ppb, a small amount of HCl was added to the dilute HF solution (1:1:50 :: HCl:HF:H<sub>2</sub>O). A dramatic reduction was observed in the surface Cu levels (Figure 4), when compared to the dilute HF (only) case (Figure 3). This is consistent with the earlier discussion, where it was predicted that the presence of chlorine in solution would prevent the deposition of Cu, due to the formation of the soluble CuCl<sub>2</sub> complex. However, for large amounts of Cu in solution (5 ppm), the amount of HCl added did not prove adequate in preventing the deposition of Cu onto the wafer surface (Figure 4).

### Atomic Force Microscopy Measurements

Atomic Force Microscopy (AFM) measurements were made on the wafers at various points in the processing sequence (as indicated in Table 1). A bare silicon wafer was used as a reference, to ascertain the effect that the processing sequence might have had on the original morphology.

In all cases it was found that little or no roughening of the wafer surface had occurred, when compared to the reference sample (Table 1). This result is not surprising when considering micrographs associated with low copper levels in solution. It is likely that the small amount of copper in solution (10 ppb), is not sufficient to cause pitting of the surface. The results for larger amounts of Cu in solution (5 ppm) are surprising, since it has been reported<sup>10,11</sup> that at such high concentrations, significant roughening occurs.

A possible explanation for this observed anomaly is that, the starting (reference) samples used were quite rough to begin with (RMS roughness ≈ 2.4 nm), as compared to those used by other investigators (RMS roughness ≈ 1 nm). Consequently, we may have been unable to distinguish between small changes in roughness, that may have been evident while using smoother reference wafers.

Table 1: RMS roughness values as measured by AFM, for varying surface treatments.

Contamination	Treatment Time	RMS Roughness	Comments
None	None	2.42 Å	Bare Wafer (Control Sample)
0 ppb Cu in HF	300 secs	2.31 Å	HF Control Sample (300 s)
10 ppb Cu in HF	300 secs	2.26 Å	
5 ppm Cu in HF	300 secs	2.40 Å	
0 ppb Cu in HF	1200 secs	2.23 Å	HF Control Sample (1200 s)
10 ppb Cu in HF	1200 secs	2.35 Å	
5 ppm Cu in HF	1200 secs	2.35 Å	
0 ppb Cu in HF	300 secs	2.30 Å	HF-HCl Control Sample (300 s)
10 ppb Cu in HF	300 secs	2.28 Å	
5 ppm Cu in HF	300 secs	2.40 Å	
0 ppb Cu in HF-HCl	1200 secs	2.32 Å	HF-HCl Control Sample (1200 s)
10 ppb Cu in HF-HCl	1200 secs	2.45 Å	
5 ppm Cu in HF-HCl	1200 secs	2.38 Å	

## DISCUSSION AND CONCLUSIONS

A significant amount of data exists, documenting the effects of copper deposition (especially microroughening) from dilute HF solutions. Almost all of these studies, however, focus on studying roughening associated with Cu levels greater than 1 ppm, in a dilute HF solution. While these studies are instructive in themselves, and help provide insight into the mechanisms leading to roughening of the surface, they lack direct applicability from a technological perspective. Excursions in wet processing, to the extent that copper levels in an HF bath reach values as high as 1 ppm seldom or never occur. Consequently, an HF based chemistry designed to provide extra process margin (to negate the effect of any accidental contamination), probably needs to account for excursions in the 10 ppb range.

Our experiments clearly show that a 1:1:50 HF-HCl clean proves extremely effective in keeping any copper off the surface, when contamination levels are in the 10 ppb range. Clearly, additional process margin can be "bought" by adding more HCl to a

dilute HF solution, if it so desired. Further, while the lack of good quality wafers prevented our studies from revealing any Cu induced roughening, it was also clear that the addition of HCl did not cause any additional roughening by itself, making the HF-HCl process a viable one.

---

## REFERENCES

- <sup>1</sup> T. Ohmi, T. Imaoka, I. Sugiyama, and T. Kezuka, J. Electrochem. Soc., **139**, 3317 (1992).
- <sup>2</sup> F. W. Kern Jr., M. Itano, I. Kawanabe, M. Miyashita, R. W. Rosenberg, and T. Ohmi, Proceedings of 11th Workshop in Ultra Clean Technology, 23 (1991).
- <sup>3</sup> M. Hourai, T. Naridomi, Y. Oka, K. Murakami, S. Sumita and N. Fujino, Jpn. J. Appl. Phys., **27**, L2361 (1988).
- <sup>4</sup> H. Wendt, H. Cerva, V. Lehmann and W. Pamler, J. Appl. Phys., **65**, 2402 (1989).
- <sup>5</sup> T. Shimono and M. Tsuji, "A New Cleaning Solution for Metallic Impurities on the Silicon Wafer Surface", Proceedings of the Second Symposium on Defects in Silicon-Defects in Silicon II, Proc. Electrochem. Soc., 361 (1991).
- <sup>6</sup> Y. Fukazawa, K. Sanpei, T. Nakijama, K. Takase, and K. Miyazaki, "An HF-O<sub>3</sub> Aqueous Solution for Silicon Wafer Cleaning", Proceedings of the Second International Symposium on Ultra-Clean Processing of Silicon Surfaces, 267-70 (1994).
- <sup>7</sup> W. C. Krusell and D. I. Golland, Proc. Electrochem. Soc., **90-9**, 23 (1990).
- <sup>8</sup> H. Morinaga, M. Suyama and T. Ohmi, "Mechanism of Metallic Particle Growth and Metal-Induced Pitting on Si Wafer Surface in Wet Chemical Processing", J. Electrochem. Soc., **141**, 2834 (1994).
- <sup>9</sup> H. G. Parks, J. B. Hiskey and K. Yoshinige, Proc. Mat. Res. Soc., **318**, 245 (1994).
- <sup>10</sup> H. Morinaga, M. Suyama, M. Nose, S. Vehaverbeke, and T. Ohmi, IEICE Trans. Electron., E79-C, 343 (1996).
- <sup>11</sup> O. M. R. Chyan, J-J. Chen, H. Y. Chien, J. Sees, and L. Hall, J. Electrochem. Soc., **143**, 92 (1996).

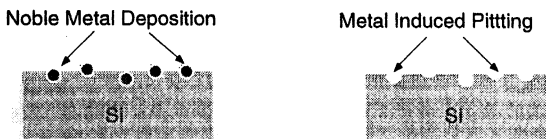


Figure 1: (a) Noble metal deposition from a dilute HF solution onto silicon (b) Expected surface morphology on subsequent removal via an SC1 → SC2 sequence.

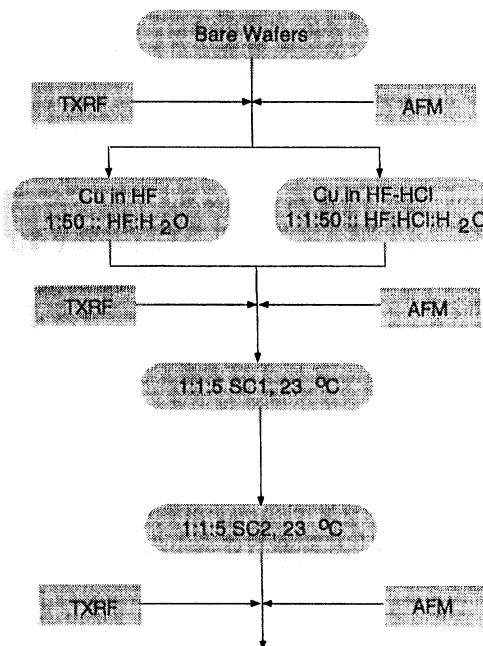


Figure 2: Process flow outlining the experimental methodology employed.

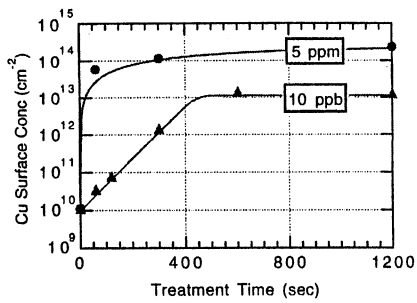


Figure 3: Rate of build up of Cu on the wafer surface. A 1:50 HF composition was used. The Cu levels in solution were also varied (10 ppb, 5 ppm).

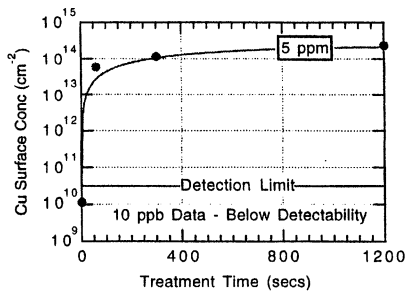


Figure 4: Rate of build up of Cu on the wafer surface. A 1:1:50 HF-HCl composition used. The Cu levels in solution were varied (10 ppb, 5 ppm)

# PASSIVATION OF Cu PARTICLES ON Si SUBSTRATE BY FOM(HF+O<sub>3</sub>-UPW) SOLUTION

HIROSHI MORITA\*, JAE-DONG JOO\*\*, ROCHDI MESSOUSSI\*\*\*,  
KAZUHIKO KAWADA, JONG-SOO KIM and TADAHIRO OHMI

Department of Electronics, Faculty of Engineering,  
Tohoku University, Sendai 980-77, Japan

## advanced address

\*Research & Development Division, Corporate Research & Development Center,  
Kurita Water Industries Ltd. 7-1, Wakamiya, Morinosato,  
Atsugi-City, Kanagawa, 243-01, Japan

\*\*PE Group, FAB Team II, Kihung Plant, Semiconductor Manufacturing Business,  
Samsung Electronics Co.,Ltd.San #24, Ningseo-Ri, Kihung-Eup,  
Yongin-City, Kyungki-Do, 449-900, Korea

\*\*\*Faculte des Sciences, Departement de Physique, Universite Ibn Tofail  
BP133, Kenitra, 12000, Morocco

We have investigated the removal efficiency of Cu contaminants from Si surface by ozonized ultrapure water(O<sub>3</sub>-UPW) based solutions. FOM(HF+O<sub>3</sub>-UPW) solution can not remove Cu contaminants unlike FPM(HF+H<sub>2</sub>O<sub>2</sub>) solution. It was speculated that metal Cu particle was passivated with insoluble CuF<sub>2</sub> when HF of 200ppm or more was added into O<sub>3</sub>-UPW. In case of using FPM solution, it is thought that F passivation may not occur because H<sub>2</sub>O<sub>2</sub> can not oxidize Cu particle on Si; therefore, Cu contaminants can be removed more effectively. Finally, it was confirmed that H<sub>2</sub>O<sub>2</sub> was essential in ultraclean technology(UCT) cleaning process for realization of a contamination free Si substrate.

## INTRODUCTION

For mass production of high quality devices, strictly parameter-controlled wet cleaning process is very important. We have already developed a total room temperature wet cleaning process, UCT cleaning process, of Si substrate(1) as shown in figure 1. That is an innovative process conducted at room temperature using very small amount of chemicals and UPW. O<sub>3</sub>-UPW(2,3), megasonic irradiation(MS) and low concentration surfactant are applied in this process. The most important step in the whole process is FPMS+MS treatment to remove particles, metallic

contaminants and native oxide on Si surface simultaneously. Oxidation process of impurities and Si surface by H<sub>2</sub>O<sub>2</sub> as an oxidizing agent and etching process of Si oxide by HF are successively progressed in this step(4).

It is well known that H<sub>2</sub>O<sub>2</sub> is a main component in some cleaning solutions such as SPM, APM(SC-1) and HPM(SC-2) which have been used in RCA cleaning process for past three decades(5). Oxidation potential of H<sub>2</sub>O<sub>2</sub> solution seems to be weaker than that of O<sub>3</sub>-UPW used in UCT cleaning process. Accordingly, H<sub>2</sub>O<sub>2</sub> can not replace O<sub>3</sub>-UPW, however, conversely O<sub>3</sub>-UPW can be used in some cleaning solutions instead of H<sub>2</sub>O<sub>2</sub>.

We tried to investigate whether FPM solution can be replaced with FOM(HF+O<sub>3</sub>-UPW) solution in this research. At the same time, cleaning efficiency of several solutions containing dissolved ozone was evaluated to understand the mechanism of Cu contaminants removal in more detail.

## EXPERIMENT

In this research, p-type CZ Si (100) wafers with resistivity of 5~15 Ω·cm were pre-cleaned by 4:1 SPM solution at 90°C for 10minutes and 0.5% DHF at 23°C for 1minute followed by a UPW rinse at 23°C for 10minutes and dried by N<sub>2</sub> gas blowing so that they have hydrophobic surfaces. The hydrophobic Si wafers were contaminated by dipping in DHF spiked with 1ppm CuCl<sub>2</sub> for 3minutes and post-rinsed in UPW for 10minutes. After Cu contamination onto Si wafer surface, the contaminated Si wafers were cleaned by dipping in various cleaning solutions for 5 minutes and rinsed by dipping in an overflowed UPW.

The cleaning solutions used in this work are O<sub>3</sub>-UPW containing only dissolved ozone of 4.7~5.3ppm, O<sub>3</sub>-UPW controlled in solution pH of 1~5 with small amount of H<sub>2</sub>SO<sub>4</sub>, O<sub>3</sub>-UPW mixed with HF of 10~5000ppm, H<sub>2</sub>O<sub>2</sub>-UPW containing only 0.5% H<sub>2</sub>O<sub>2</sub> and FPM solution mixed with 0.5% H<sub>2</sub>O<sub>2</sub> and HF. It has been reported that Cl<sup>-</sup> ion shows some special effect, e.g. making Cl-termination instead of H-termination(2) and forming some kinds of complexes with Cu(6). So, in this research, H<sub>2</sub>SO<sub>4</sub> was used in the cleaning solution as an acid to control pH without other affect. The dissolved ozone concentration in these cleaning solutions reduces by decomposition of itself. However, we think that the influence is negligible since the decomposition rate is less than about 20% in 5minutes which is the cleaning time in all solutions.

The Cu cleaning efficiency was evaluated by measuring Cu concentration on Si surface before and after cleaning by Total Reflection X-ray Fluorescence Spectroscopy (TRXRF), Technos TREX 610T, with an incident angle of 0.05° and an X-ray excitation condition of 30kV and 200mA. The detection limit of Cu on Si surface by this method is 1.8×10<sup>9</sup> atoms/cm<sup>2</sup>.

## RESULT

We measured the Cu concentration on Si surface before and after cleaning and the results were summarized in figure 2. First, in the case of O<sub>3</sub>-UPW, after cleaning Cu on Si surface reduced from the initial level of  $2.2 \times 10^{14}$  atoms/cm<sup>2</sup> to  $1.1 \times 10^{11}$  atoms/cm<sup>2</sup>. The Cu removal efficiency was improved slightly when H<sub>2</sub>SO<sub>4</sub> was added into O<sub>3</sub>-UPW for varying solution pH. On the other hand, we could improve the Cu removal efficiency by adding small amount of HF into O<sub>3</sub>-UPW, so called FOM solution, instead of H<sub>2</sub>SO<sub>4</sub>. However, it was decreased drastically when spiked HF concentration exceeded a critical value. With comparing to the case of O<sub>3</sub>-UPW mixture solution, Cu contaminants could not be removed at all by H<sub>2</sub>O<sub>2</sub>-UPW. Finally, Cu contaminants was removed below detection limit by FPM solution mixed with H<sub>2</sub>O<sub>2</sub>-UPW and HF showing the most effective cleaning efficiency in all cleaning solutions used in this research.

It is very interesting that FOM solution has a relationship between spiked HF concentration and Cu cleaning efficiency. Thus, we investigated the phenomenon in more detail as shown in figure 3. When around 100ppm-HF or less was added to O<sub>3</sub>-UPW, Cu removal efficiency was improved and residual Cu concentration after cleaning by this optimum FOM solution was reduced to  $4.0 \times 10^9$  atoms/cm<sup>2</sup> which is about 4% of that after cleaning by O<sub>3</sub>-UPW. However, Cu removal efficiency was decreased drastically when about 200ppm or more HF was added into O<sub>3</sub>-UPW. Moreover, Cu on Si surface was scarcely removed by FOM solution into which HF above 500ppm was added. From the result, it was recognized that the cleaning efficiency of FOM solution for Cu was completely different from that of FPM solution. Consequently, we concluded that FPM solution could not be substituted by FOM solution for cleaning of Cu on Si surface.

## DISCUSSION

In our previous research(2), it has been reported that Cu<sup>2+</sup> in solution can be electrochemically reduced by taking electron from Si and deposited on the Si surface in the form of metal Cu particle. According to the result, Cu on Si surface can be dissolved and removed in a solution having the pH value below 7 and higher oxidation-reduction(redox) potential than that of Cu<sup>2+</sup>.

Here, we discuss the removal mechanism of Cu contaminant from Si surface by some cleaning solutions used in this research.

### Cleaning by O<sub>3</sub>-UPW and acid added O<sub>3</sub>-UPW

In the case of cleaning by O<sub>3</sub>-UPW and acid added O<sub>3</sub>-UPW, Cu removal efficiency can be estimated by a state of Cu in aqueous solution as shown in pH-redox potential diagram(2, 7) of

figure 4. The more effective cleaning efficiency of acid added O<sub>3</sub>-UPW can be interpreted by the fact that addition of acid causes O<sub>3</sub>-UPW of the lower pH value and the higher redox potential and thus Cu<sup>2+</sup> in this acid added O<sub>3</sub>-UPW is electrochemically more stable than that in O<sub>3</sub>-UPW. On the other hand, the reason why Cu of a relatively high level,  $1.1 \times 10^{11}$  atoms/cm<sup>2</sup>, remains after cleaning by these solutions can be explained by the fact that Cu on Si surface can be dissolved and simultaneously included in chemical oxide grown during cleaning process.

#### Cleaning by H<sub>2</sub>O<sub>2</sub>-UPW

Figure 5 shows removal efficiency of Cu from Si surface and SiO<sub>2</sub> surface by H<sub>2</sub>O<sub>2</sub>-UPW. Cu on Si surface could not be removed while Cu on SiO<sub>2</sub> surface could be removed more effectively by H<sub>2</sub>O<sub>2</sub>-UPW. In the case of Cu contaminants on SiO<sub>2</sub> surface, more than 94% Cu was removed by H<sub>2</sub>O<sub>2</sub>-UPW. It can be estimated that oxidation potential of H<sub>2</sub>O<sub>2</sub> is less than critical value to oxidize metal Cu contacting to Si surface. These initial Cu contaminated wafers were prepared by dipping of hydrophobic Si wafers in Cu containing aqueous solution with or without HF.

The redox potential of H<sub>2</sub>O<sub>2</sub> containing solution can not be measured correctly because H<sub>2</sub>O<sub>2</sub> is decomposed rapidly on the surface of Pt electrode(2). In this experiment, therefore, the value could not be measured directly. From those results, however, it can be estimated that the potential of H<sub>2</sub>O<sub>2</sub>-UPW is slightly higher than isolated metal Cu by SiO<sub>2</sub> over Si substrate and lower than metal Cu contacting to Si which plays as a reducing agent for Cu<sup>2+</sup>.

#### Cleaning by FOM solution

We will discuss the interesting phenomenon that FOM solution has a relationship between spiked HF concentration and Cu cleaning efficiency in the point of the spiked HF concentration.

HF Concentration below 200ppm O<sub>3</sub>-UPW can remove metal Cu on the Si surface by oxidation, however, Cu included in SiO<sub>2</sub> can not be removed as previously mentioned. Therefore, it is recognized that the remaining Cu contaminants after cleaning by O<sub>3</sub>-UPW exist in SiO<sub>2</sub> layer produced by oxidation of Si. On the other hand, when small amount of HF is added in O<sub>3</sub>-UPW, Cu contaminants which exist near surface in Si oxide layer can be dissolved with Si oxide by slight etching by HF. So, Cu removal efficiency by this cleaning solution is superior to that by O<sub>3</sub>-UPW.

HF Concentration above 200ppm However, Cu removal efficiency was reduced drastically when HF concentration exceeded a critical value. It was found that the value was around 200ppm from this research.

In an attempt to confirm Cu contaminants after cleaning by FOM solution were remaining as particles or not, the Si surface was investigated by scanning electron microscope(SEM). Figure 6 shows a SEM image of the Si surface after cleaning by FOM solution mixed with 500ppm-HF and

5ppm-O<sub>3</sub>. Even though the solution had much higher redox potential than that of Cu, Cu particles remained on the surface. Thus it could be interpreted that the metal Cu particle can not be dissolved in the FOM solution including 500ppm-HF.

We, here, discuss the state of Cu particle surface in FOM solution containing HF of 200ppm or more. In this solution, a lot of Cu<sup>2+</sup> ions may surround the surface of Cu particle because metal Cu particle can be dissolved into Cu<sup>2+</sup> ions by oxidation of O<sub>3</sub>. Therefore, it is easily estimated that about 500ppm-CuF<sub>2</sub> can be produced by a reaction between Cu<sup>2+</sup> ions and 2F in FOM solution and that Cu particle surface in FOM solution must be covered and passivated by CuF<sub>2</sub>. This value is nearly equal to maximum soluble concentration of CuF<sub>2</sub>(470ppm) in aqueous solution at room temperature. Consequently, in figure 7, we suggest a CuF<sub>2</sub> passivation model that the surface of Cu particles is passivated by insoluble CuF<sub>2</sub> layer when more than 200ppm-HF was added into FOM solution. Moreover, it can be speculated that the contact point of metal Cu particle with Si surface is also covered with the CuF<sub>2</sub> passivation layer and that the passivated Cu particles can not be lifted from the surface by etching of SiO<sub>2</sub> layer. In addition, the CuF<sub>2</sub> passivation mechanism was confirmed by another experiment in which we investigated the Cu removal efficiency of O<sub>3</sub>-UPW containing KF instead of HF. The Cu removal behavior was almost same to that of FOM solution as shown in figure 8. From this result, it is confirmed that drastic reduction of Cu removal efficiency is caused by CuF<sub>2</sub> passivation produced in the mixture containing O<sub>3</sub> and F.

#### Cleaning by FPM solution

When H<sub>2</sub>O<sub>2</sub> instead of O<sub>3</sub> is used in the cleaning solution with HF, Cu contaminants are removed very well. As previously discussed, the oxidation potential of H<sub>2</sub>O<sub>2</sub> is stronger than those of Si and isolated metal Cu but weaker than that of metal Cu contacting with Si. And, it can be speculated that very high oxidizing potential of the solution is essential to occur CuF<sub>2</sub> passivation because the first step of this passivation reaction is surface oxidation, i.e. ionization, of Cu particles on Si substrate. Therefore, this passivation reaction can be occurred in only FOM solution not in FPM solution. In FPM solution, however, Si beneath metal Cu particle can be easily oxidized by H<sub>2</sub>O<sub>2</sub> in solution and the metal Cu particles can be lifted off by successive etching of HF in FPM solution. And thus, the Cu particles isolated from Si after lifting off can be oxidized and dissolved into FPM solution and re-adhesion of Cu<sup>2+</sup> ions onto Si surface can not occur. This is the reason why Cu contaminants can be perfectly removed in FPM solution.

## CONCLUSION

From this research, we recognized the mechanism of Cu contaminants removal from Si surface in more detail. Cu removal efficiency by O<sub>3</sub>-UPW or acid added O<sub>3</sub>-UPW solutions can be

easily understood from state of Cu shown in the pH-redox potential diagram. FOM solution can not remove Cu so effective as FPM solution. When very low concentration below 200ppm-HF is added in O<sub>3</sub>-UPW, Cu removal efficiency is improved comparing to O<sub>3</sub>-UPW. Small amount of HF can etch SiO<sub>2</sub> slightly. It is believed that Cu contaminants existing near surface in SiO<sub>2</sub> layer can be removed with SiO<sub>2</sub> layer in the FOM solution.

On the other hand, when HF of 200ppm or more is added in O<sub>3</sub>-UPW, Cu removal efficiency is drastically decreased. In this case, Cu particles on Si surface seem to be passivated by F with making insoluble CuF<sub>2</sub> layer. It was confirmed that Cu contaminants can not be removed by KF added O<sub>3</sub>-UPW. In HF added H<sub>2</sub>O<sub>2</sub> solution(FPM), however, Cu contaminants can be removed perfectly. From these results, CuF<sub>2</sub> passivation of metal Cu contaminants may occur only in case of using solution containing F (about 200ppm or more) and dissolved O<sub>3</sub> which can oxidize metal Cu contaminants on Si. On the other hand, H<sub>2</sub>O<sub>2</sub> used in FPM solution can not oxidize metal Cu contaminants on Si, however, it can oxidize isolated metal Cu. Therefore, CuF<sub>2</sub> passivation of Cu contaminants can not occur in FPM solution and thus Cu on Si surface can be perfectly removed by FPM solution. Finally, through this research, it was confirmed that FPM is essential in UCT cleaning process for realization of a contamination free Si substrate.

#### REFERENCES

1. T.Ohmi, J.Electrochem.Soc.,143,2957(1996).
2. H.Morinaga, M.Suyama, M.Nose, S.Verhaverbeke and T.Ohmi, IEICE Trans.Electron.,E79-C,343(1996).
3. H.Morita, J.S.Kim, T.Ohmi, in Proceedings of Semiconductor Pure Water and Chemicals Conference, p.215, Santa Clara(1996).
4. T.Shimono, M.Morita, Y.Muramatsu and M.Tsuji, in Proc.of 8th Workshop on ULSI Ultra Clean Technology,59(1990).
5. W.Karn and D.A.Puotinen, RCA Review,31,187(1970).
6. I.Teerlinck, P.W.Mertens, R.Vos, M.Meuris and M.M.Heyns, in Proceedings of Third International Symposium on Ultra Clean Processing of Silicon Surfaces, p.21, Acco Leuven, Antwerp(1996).
7. M.Pourbaix, "Atlas of Electrochemical Equilibria in Aqueous Solutions", Pergamon Press, London(1996).

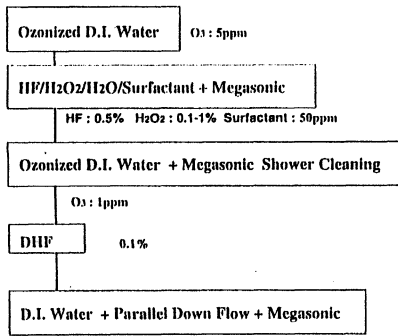


Figure 1 UCT cleaning process for Si substrate

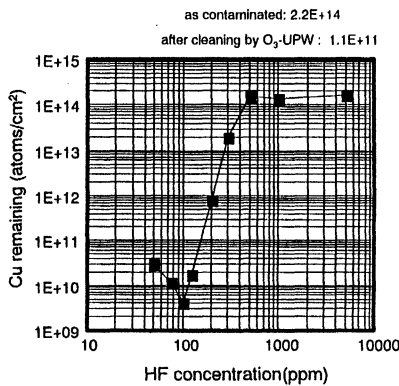


Figure 3 Dependence on HF concentration for Cu removal efficiency by FOM (HF+O<sub>3</sub>(5ppm)-UPW) solution

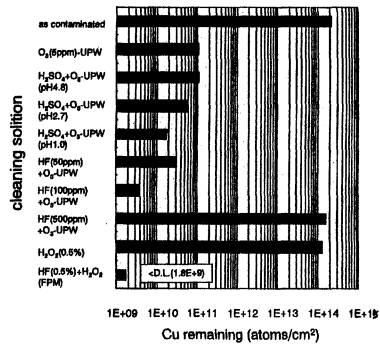


Figure 2 Cu contaminant removal efficiency of some cleaning solutions

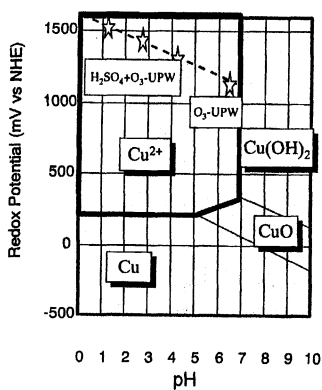


Figure 4 State of Cu in O<sub>3</sub> based cleaning solution on pH-redox potential diagram

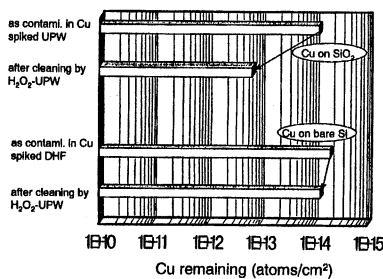


Figure 5 Cu removal efficiency of  $\text{H}_2\text{O}_2$ -UPW

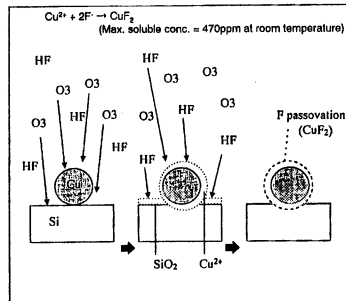


Figure 7 model of F passivation of Cu particle by FOM solution

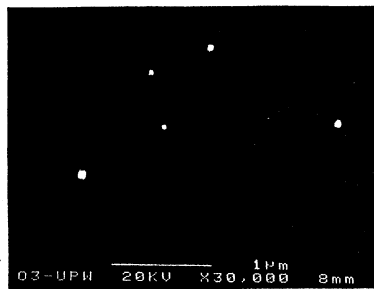


Figure 6 SEM image of Cu contaminated Si surface after cleaning by FOM (500ppm-HF + 5ppm-O<sub>3</sub>-UPW) solution

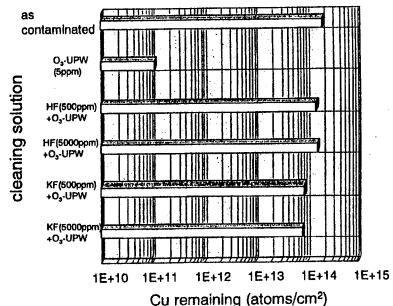


Figure 8 Cu removal efficiency of HF+O<sub>3</sub>-UPW (FOM) and KF+O<sub>3</sub>-UPW

# THE EFFECT OF SURFACE DAMAGE DUE TO Si IMPLANTATION ON ADSORPTION AND DESORPTION OF Cu ON Si SURFACE

Jong-Soo Kim, Hiroshi Morita\*, Jae-Dong Joo\*\*, and Tadahiro Ohmi

Department of Electronic Engineering, Graduate School of Engineering,  
Tohoku University, Sendai 980-77, Japan

\* Research & Development Division, Corporate Research & Development Center, Kurita  
Water Industries Ltd. 7-1, Wakamiya, Morinosato,  
Atsugi-City, Kanagawa, 243-01, Japan

\*\*PE Group, FAB Team II, Kiheung Plant, Semiconductor Manufacturing Business,  
Samsung Electronics Co., Ltd., San #24, Ningseo-Ri,  
Kiheung-Eup, Yongin-City, Kyungki-Do, 449-900, Korea

In this study, the effect of surface damage due to Si implantation into a single crystalline Si substrate on adsorption and desorption of Cu impurity was intensively investigated. The result of RHEED shows that the amount of implant-induced-damage increases with implantation fluence and that the surface damage can be nearly recovered by a N<sub>2</sub>-anneal at 1000°C for 30 minutes. In addition, the implant-induced-damage was characterized by AFM and displayed a crystalline lattice disorder not a macroscopic structure change. Using FTIR-ATR and XPS analysis, it was found that the implant-induced-damage deteriorated the hydrogen-termination property and chemical stability for oxidation of Si surface. Moreover, it was determined that the implant-induced-damage of the single crystalline Si surface deteriorates severely the Cu removal efficiency of various chemical cleaning solutions. It was very difficult to accomplish the metal contamination free Si surface following high fluence-implantation.

## INTRODUCTION

In ultra large scale integrated (ULSI) circuits manufacturing technology, the metal contamination has been known as a fatal factor in deterioration of device performance(1). The noble metals such Cu, Ag and Au that have higher electronegativity and oxidation-reduction (redox) potential than those of Si are hardly removed from Si surface(2). Among them, Cu is the easiest to be contaminated in device manufacturing processes, especially implantation, ashing and dry etch processes(3).

Ion implantation has been used as a key process for purpose of controlling shallow impurity doping in fine geometry device fabrication for the past three decades. However, ion implantation is known to induce damage to the crystalline lattice of Si substrate surface and the original crystalline Si substrate surface is turned into an amorphous layer when high fluences are implanted with above a critical dose(4).

In our previous research(5), it has been revealed that Cu adsorption and desorption behavior of single crystalline Si surface is different from that of amorphous Si surface. In this study, we intensively investigated the effect of surface damage due to Si implantation into a single crystalline Si substrate on adsorption and desorption of Cu through evaluation of surface characteristics for implantation-damaged Si surface.

## EXPERIMENT

Hydrophobic p-type (100) Cz Si wafers with a resistivity range of  $7\sim 15 \Omega \cdot \text{cm}$  were implanted with various  $\text{Si}^+$  ion dose levels,  $5.0 \times 10^{12}$ ,  $5.0 \times 10^{14}$  and  $5.0 \times 10^{15}$  ions/ $\text{cm}^2$ , at 60KeV accelerating voltage and each Si implanted sample was annealed in  $\text{N}_2$ -purged furnace at  $1000^\circ\text{C}$  for 30 minutes. Therefore, we could evaluate just the effect of surface damage on adsorption and desorption of Cu on Si surface and the recovery efficiency by post-heat treatment.

In order to investigate the adsorption and desorption behaviors of Cu on the damaged Si surfaces, the damaged Si wafers were dipped in ultrapure water (UPW) spiked with 1ppm  $\text{CuCl}_2$  for 3min. followed by post-UPW rinse for 10min. and cleaned by various chemical solutions such as sulfuric acid-hydrogen peroxide mixture (SPM), ozonized ultrapure water ( $\text{O}_3$ -UPW), hydrofluoric acid-hydrogen peroxide mixture (FPM), FPM with non-ionic surfactant (FPMS).

Firstly, Si implant-induced-surface damage on single crystalline Si surface is investigated by reflection high-energy electron diffraction (RHEED) and the microroughness due to Si crystalline lattice damage is evaluated by atomic force microscopy (AFM). Cu concentration on Si surfaces was measured by total reflection x-ray fluorescence spectroscopy (TRXRF) before and after cleaning. We also investigated hydrogen-termination behaviors on Si surfaces by fourier transform infrared reflectance-attenuated total reflection (FTIR-ATR) and effects of chemical oxidation and metal-induced-oxidation (MIO)(6) by x-ray photoelectron spectroscopy (XPS) in order to explain the mechanism for the dependence of the Cu adsorption and desorption on the amount of surface damage.

## RESULTS AND DISCUSSION

In Fig.1, RHEED pattern of the implantation fluence of  $5.0 \times 10^{15}$  ions/ $\text{cm}^2$  followed by no annealing shows that the implanted single crystalline Si surface was changed to

amorphous Si surface and that it was seemed to be recrystallized after post-N<sub>2</sub> annealing at 1000°C for 30 minutes. However, we could not distinguish the amounts of damage between the single crystalline Si surface and implanted Si surfaces with the fluence below than  $5.0 \times 10^{14}$  ions/cm<sup>2</sup> followed by no annealing.

As shown in Fig.2, the results of AFM image show almost same microroughness for all samples regardless of the implanted fluences and annealing conditions with just a little higher root-mean-square (RMS) value than that of the single crystalline Si surface. This implies that the Si implantation induces a crystalline lattice disorder not a macroscopic structure change on the single crystalline Si surface.

It has been reported that implanted Si substrate with relatively high ion fluences has a lot of crystalline defects(4) and that hydrogen-termination of Si surface is closely related to the amount of defect density, microroughness and surface oxidation kinetics(7). It would be expected that an ideal Si(100) surface is entirely covered with dihydride after removing silicon oxide from Si surface by diluted aqueous HF. The results of FTIR-ATR shown in Fig.3 show that implantation into Si surface with high fluence results in a more defective surface with accompanying by a broadening and weakening of dihydride mode. The Si surface implanted with varying the implantation fluence shows a same H-termination behavior regardless of HF concentration, 0.5~5.0%, included in diluted HF solution used for pre-treatment of Si surface. The results observed in Fig.3 clearly show that the higher implantation fluence causes a more amount of surface damage and deteriorates the H-termination characteristics.

It is well known that ideally H-terminated Si surface is characterized by a high chemical stability(7). XPS spectra obtained on the implanted Si surfaces after dipping in 0.5% diluted HF for 1 minute by followed with 10 minute-post UPW rinse are shown in Fig.4. The intensity of silicon oxide spectrum increases linearly with the implantation fluence regardless of the presence of post-annealing in N<sub>2</sub>-purged furnace at 1000°C for 30 minutes. Consequently, this results also show that the higher implantation fluence induce a chemically more unstable surface regardless of a post-annealing and that those are consistent with the results of RHEED and FTIR-ATR in Fig.1 and Fig.3.

According to the results above mentioned, it would be expected that the Cu adsorption and desorption behavior on implanted Si surfaces would be affected by the alternations of Si surface characteristics. The Cu cleaning efficiencies of various chemical solutions from implanted Si surfaces are shown in Fig.5. For this experiment, hydrophobic Si wafers were implanted with varying Si<sup>+</sup> ion fluence and a part of the samples were annealed in N<sub>2</sub>-purged furnace at 1000°C for 30 minutes. After that, both of the annealed and unannealed surface damaged Si wafers were contaminated by dipping in UPW spiked with 1 ppm CuCl<sub>2</sub> for 3 minutes followed by a post-UPW rinse for 10 minutes. These contaminated Si wafers were cleaned by using typical chemical solutions for microelectronics device manufacturing.

It was found that the surface damage due to implantation obviously affected both of adsorption and desorption of Cu. As for Cu adsorption behavior, contaminated Cu concentration on Si substrate shows a tendency to decrease as the amount of surface damage due to  $\text{Si}^+$  ion implantation increases regardless of the presence of post- $\text{N}_2$  annealing. According to our previous research(2,6), it has been revealed that metal Cu particle is grown on Si surface in Cu contaminated solution by redox reaction between  $\text{Cu}^{2+}$  ions in solution and Si of substrate and Brownian movement and that Cu particle growth is a main cause of Cu deposition with high concentration. Therefore, we can make an possible interpretation for this Cu deposition behavior as follows. The metal Cu particle growth is more severely hindered by two folds. The first is the reduction effect of redox reaction due to thicker oxide grown on damaged Si surface. And, the other one is the retardation of surface migration of metal Cu particle due to the stronger chemical interaction force. Confirming this idea, the SEM images of metal Cu particle grown on the damaged Si surfaces with different implantation fluences in Fig.6 show that the metal Cu particle size and density decrease when the implantation fluence increase regardless of the presence of a post-  $\text{N}_2$  anneal.

In the point of Cu removal efficiency, the recovery effect of surface damage on Cu removal efficiency after post- $\text{N}_2$  anneal is clearly shown with comparing to the case of unannealed Si wafers. However, the residual Cu concentration on  $\text{N}_2$  annealed Si surface after cleaning is higher than that on the controlled single crystalline Si surface when the implantation fluence is high. It can be, therefore, easily estimated that the implantation induced surface damage can not be recovered perfectly by the post- $\text{N}_2$  anneal. The implantation induced surface damage affects more severely on Cu cleaning efficiency in the case of unannealed Si wafer. The residual Cu concentration on the damaged and unannealed Si surface after cleaning by various chemical solutions increase with the amounts of surface damage. Moreover, Cu on the damaged and unannealed Si surface could be hardly removed after cleaning when the implantation fluence was  $5.0 \times 10^{15}$  ions/cm<sup>2</sup> although that could be reduced down the detection limit of  $2.0 \times 10^9$  ions/cm<sup>2</sup> when the implantation fluence was below  $5.0 \times 10^{12}$  ions/cm<sup>2</sup>.

As reported in our earlier researches(8,9), it is requested for one to remove Cu on single crystalline Si surface by wet cleaning process that first, Cu is dissolved in wet cleaning solution and the dissolved  $\text{Cu}^{2+}$  ions are kept from introducing in chemical oxide simultaneously grown during cleaning and readhering onto hydrophobic Si surface formed in the solution containing HF. From these results, it is estimated that more dissolved  $\text{Cu}^{2+}$  ions are included in chemical oxide simultaneously grown on the damaged Si surface in the typical dissolvable cleaning solutions such as  $\text{O}_3$ -UPW and SPM having no etching ability for both of Si and  $\text{SiO}_2$  substrates since chemical oxide is more easily grown on the damaged Si surface compared with the single crystalline Si surface. On the other hand, the implanted Si surface with higher fluence is characterized by the more active undangling Si bonds than those of the single crystalline Si surface in the solutions containing HF such as FPM and FPMS and thus we can easily imagine that more dissolved  $\text{Cu}^{2+}$  ions can readhere

onto the hydrophobic damaged Si surface formed in the solutions containing HF. Consequently, through this interpretation, it was found that the Si<sup>+</sup> ion implantation causes an implant-induced-damage on the Si substrate and alters the surface characteristics of the single crystalline Si into the worse. Moreover, the implant-induced-damage on the single crystalline Si surface deteriorates the Cu removal efficiency of various chemical cleaning solutions.

## CONCLUSION

The Si<sup>+</sup> ion implantation causes an implant-induced-damage on the single crystalline Si substrate. The result of RHEED analysis shows that the amount of damage due to implantation increases with implantation fluence and that the surface damage can be nearly recovered by a post N<sub>2</sub>-anneal at 1000°C for 30 minutes. The micro-structure of damaged Si surface was investigated by AFM and it was characterized by a crystalline lattice disorder not a macroscopic structure change on the single crystalline Si surface. The observed results of FTIR-ATR and XPS obviously show that the surface characteristics of damaged Si substrate was altered into the worse regardless of the presence of a post N<sub>2</sub>-anneal. The implant-induced-damage deteriorates the hydrogen-termination property and chemical stability for oxidation of Si surface. Moreover, the Cu cleaning efficiency of various chemical solutions was adversely affected by the implant-induced-damage on the single crystalline Si substrate and it was very difficult to realize the metal contamination free Si surface when high fluence-implantation was introduced.

## REFERENCE

1. T.Ohmi, T.Imaoka, I.Sugiyama, and T.Kenzuka, *J.Electrochem.Soc.*, 139, No.11, 3317, 1992.
2. H.Morinaga, M.Suyama, M.Nose, S.Verhaverbeke and T.Ohmi, *IEICE Trans.Electron.*, E79-C, 343, 1996.
3. N.Anzai, Y.Kureishi, S.Shimizu, and T.Nitta, in *Proceedings of 1st Workshop on ULSI Ultra Clean Technology*, p.75, 1989.
4. R.E.Hummel, Wei Xi, P.H.Holloway, and K.A.Jones, *J.Appl.Phys.*, Vol.63(8), 2591, 1988.
5. G.M.Choi, K.Sekine, H.Morita, and T.Ohmi, in *Extended Abstracts of the 1996 International Conference on Solid State Devices and Materials*, p.371, 1996.
6. J.S.Kim, H.Morita, J.D.Joo, and T.Ohmi, *J.Electrochem.Soc.*, 144, No.9, 3275, 1997.
7. G.S.Higashi, Y.J.Chabal, G.W.Trucks, and Krishnan Raghavachari, *Appl. Phys. Lett.*, 56(7), 656, 1990.
8. J.S.Kim, H.Morita, J.D.Joo, and T.Ohmi, *Abstract 583, p.751, The Electrochemical Society Extended Abstracts, Vol. 97-3, Montreal, Quebec, Canada, May 4-9, 1997.*
9. J.S.Kim, H.Morita, J.D.Joo, and T.Ohmi, *Materials Research Society 1997 Spring Meeting*, March 31-Apr.4, San Francisco, CA, Paper No. P7.7, 1997.

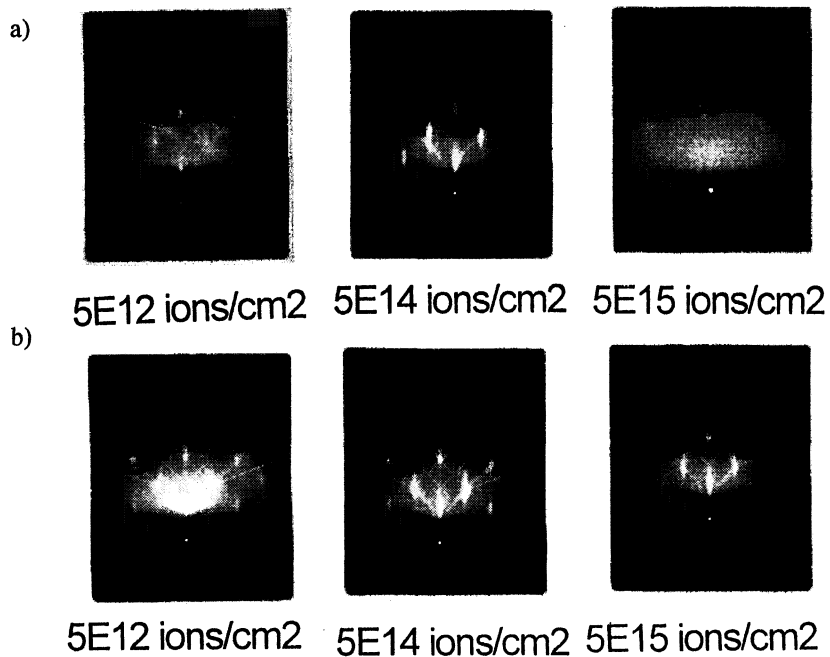


Fig.1 RHEED patterns of Si surface by Si ion implantation with different fluences of 5E12, 5E14 and 5E15 ions/cm<sup>2</sup> followed by a) No-anneal b) N<sub>2</sub>-anneal after contamination in ultrapure water spiked 1ppm CuCl<sub>2</sub> for 3min.

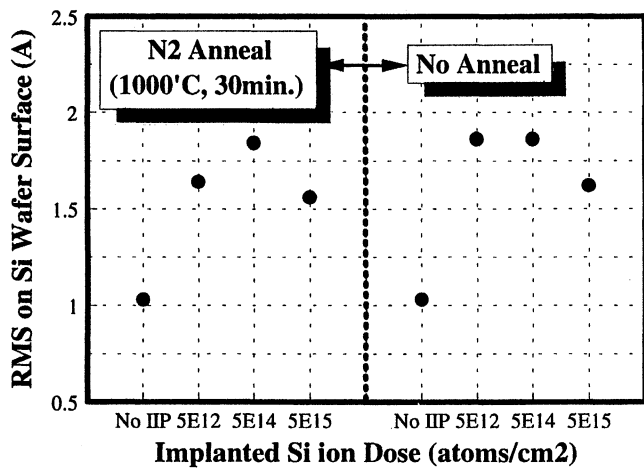


Fig.2 The AFM results of micro-roughness on damaged Si surface by Si ion implantation with different fluences of 5E12, 5E14 and 5E15 ions/cm<sup>2</sup> followed by N<sub>2</sub>-anneal (left hand) and No-anneal (right hand)

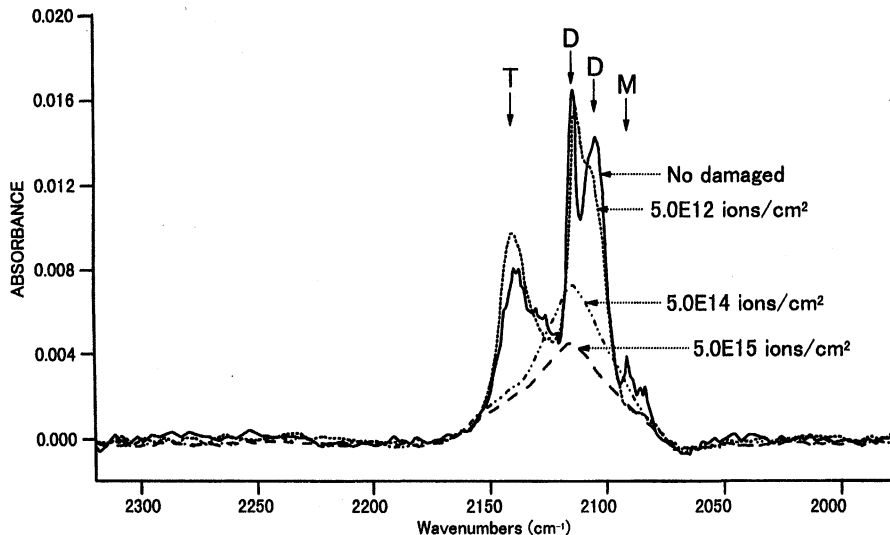


Fig.3 FTIR-ATR spectra of Si surface by Si ion implantation with different fluences of  $5E12$ ,  $5E14$  and  $5E15$  ions/ $\text{cm}^2$  after 5.0% DHF cleaning for 1min. followed by no post-UPW rinse

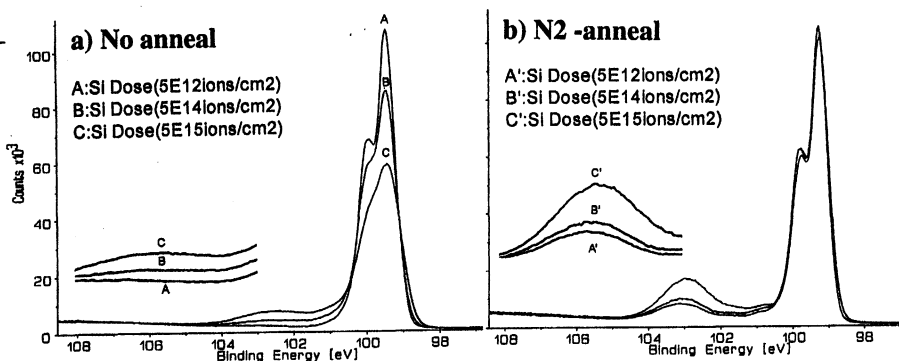


Fig.4 XPS spectra of Si surface by Si ion implantation with different fluences of  $5E12$ ,  $5E14$  and  $5E15$  ions/ $\text{cm}^2$  followed by a) No anneal b)  $N_2$ -anneal after 0.5% DHF cleaning for 1min. followed a post-UPW rinse for 10min.

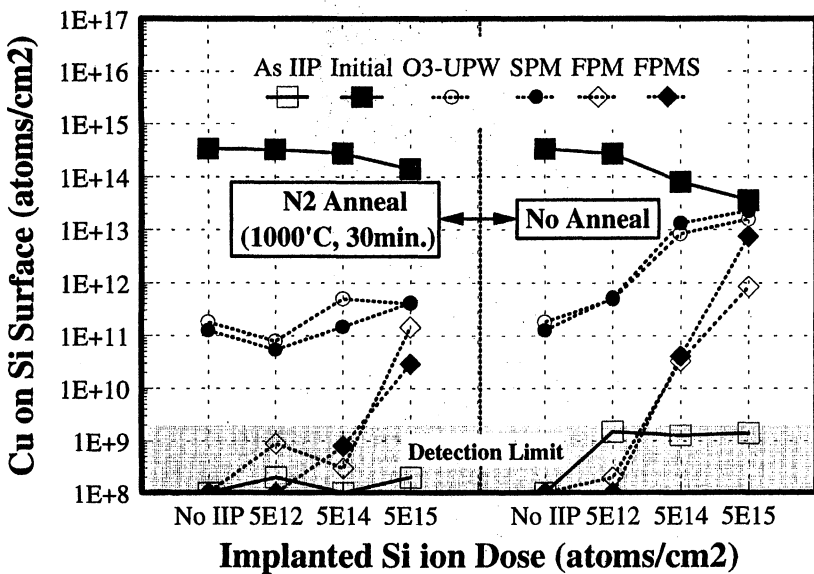


Fig.5 The cleaning efficiency of various chemical solutions for Cu on damaged Si surface with N<sub>2</sub>-anneal (left hand) and No-anneal (right hand) contaminated in UPW spiked with 1ppm CuCl<sub>2</sub> for 3min.

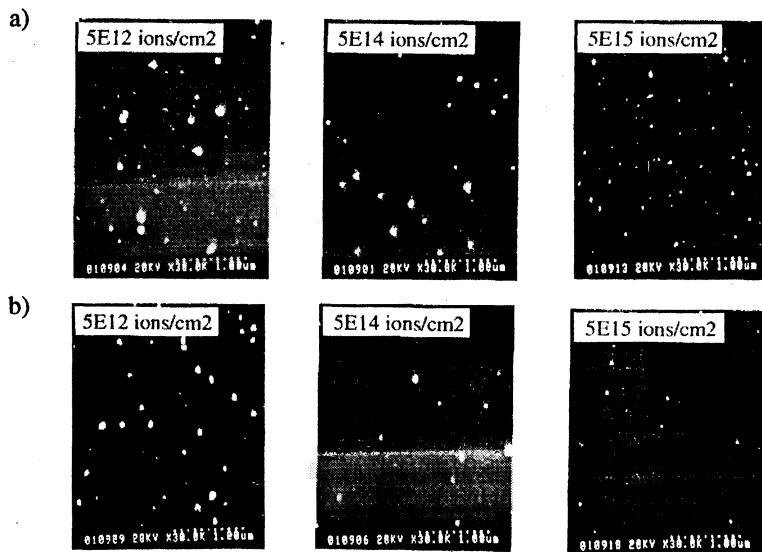


Fig.6 SEM photos of metal Cu particle on damaged Si surface with a) N<sub>2</sub>-anneal and b) No-anneal after contamination in ultrapure water spiked 1ppm CuCl<sub>2</sub> for 3min.

## **WET CLEANING - SC1 Chemistry**



## OPTIMIZATION OF DILUTE SC1

P. Boelen<sup>(1)</sup>, T. Lardin<sup>(2)</sup>, B. Sandrier<sup>(2)</sup>,  
R. Matthews<sup>(1)</sup>, I. Kashkoush<sup>(1)</sup>, R. Novak<sup>(1)</sup> and F. Tardif<sup>(2)</sup>

(1) : SubMicron Systems Inc., 6330 Hedgewood Dr. 150, Allentown, PA 18106 USA  
(2) : Gressi-Leti-CEA/G, 17 rue des Martyrs, 38054 Grenoble Cedex 09, France

In this paper the particle removal efficiency of different dilute SC1 mixtures, presenting a constant NH<sub>4</sub>OH/H<sub>2</sub>O<sub>2</sub> ratio (0.25/1), are evaluated. When the concentration is decreased the removal of SiO<sub>2</sub>, Al<sub>2</sub>O<sub>3</sub> and Si<sub>3</sub>N<sub>4</sub> particles decreases drastically, except if high power megasonic energy is used in conjunction. In these cases it is possible to reduce the chemical concentration drastically with an acceptable efficiency loss as a result. Chemical concentration reduction was verified to actually decrease the consumption of both NH<sub>4</sub>OH and H<sub>2</sub>O<sub>2</sub>.

### INTRODUCTION

The Standard RCA process<sup>(1)</sup> is one of the most widely used cleaning processes in IC manufacturing. The Standard Clean 1, so called "SC1", is used to remove particle contamination. This mixture is composed of ammonium hydroxide (NH<sub>4</sub>OH) and hydrogen peroxide (H<sub>2</sub>O<sub>2</sub>) diluted in ultra pure de-ionized water and used at temperatures varying from 40 to 80°C for up to 10 minutes. Recently, more stringent environmental requirements and general cost reducing factors in semiconductor manufacturing lead to a demand for an optimization and tighter control of all the process parameters in cleaning. Better cleaning performances with lower cost of ownership are therefore a must.

### EXPERIMENTAL

The experimental set-up consists of a heated and continuously filtered recirculation system and a quartz SC1 process tank which includes a 1 MHz/1600W phaser megasonic transducer and an in-situ chemical concentration control system, on a SubMicron Systems Corporation automated GAMA-1 wet station. The test wafers (CZ 200 mm, p-type, 14-22 Ohm.cm) are contaminated with different types of particles in order to obtain representative samples over the full Zeta potential range: particles of SiO<sub>2</sub>, Al<sub>2</sub>O<sub>3</sub> and Si<sub>3</sub>N<sub>4</sub>. All the wafers are pre-cleaned in a SC1 and then measured on a Tencor Surfscan 6200 from 0.16  $\mu$ m upwards. The maximum initial starting level is lower than 30 counts. The contamination procedure for SiO<sub>2</sub> and Al<sub>2</sub>O<sub>3</sub> particles consists of a dip in DI water in which SiO<sub>2</sub> or Al<sub>2</sub>O<sub>3</sub> commercial slurries are previously dispersed followed by a DI water rinse and spindry. The deposited particle level measured at 0.16  $\mu$ m is adjusted to 550  $\pm$  50 particles. The wafers with Si<sub>3</sub>N<sub>4</sub> particles are contaminated by dipping them in a static H<sub>3</sub>PO<sub>4</sub> etch bath, followed by a rinse and IPA dry. This yields total particle counts ranging

from 4000-5000 at sizes greater than 0.16  $\mu\text{m}$ . Six test wafers are used for each trial. These wafers are placed between dummy wafers in the process carrier.

The wafers are processed for 10 minutes in different SC1 solutions at 65 °C. In order to limit the evaporation of NH<sub>4</sub>OH and the decomposition of H<sub>2</sub>O<sub>2</sub> the process vessel was first filled with DI water and heated up to 65 °C. Then the reactives are injected and the test is performed 5 minutes afterwards. The dilution of the chemistry was achieved by varying the DI water volume ratio, which resulted in (0,25/ 1/ X) ratios, with X varying from 5 to 1000. The sequence was then further completed by a final rinse and an IPA dry.

The etch rate on Si wafers was determined by weighing the wafers on a high accuracy scale ( $\pm 0,01\text{mg}$ ), the consumed silicon was then calculated. The SOI (Silicon On Insulator) and SiO<sub>2</sub> wafers were measured with a Prometrix UV1050 Reflectometer.

## GENERAL CONSIDERATIONS

The particle removal mechanism in SC1 is based upon the separation of the particles from the substrate, followed by an electrostatic repulsion. H<sub>2</sub>O<sub>2</sub> oxidizes the silicon surface and forms a chemical oxide which protects the silicon surface from roughening effects caused by the anisotropic attack of an alkaline media. OH<sup>-</sup> species slowly etch this chemically grown oxide, this continuous undercutting action removes the particles. The alkaline pH induced by ammonia is sufficient to turn the Zeta potential of both the substrate and particles to negative values. The subsequent electrostatic repulsion prevents particle re-adhesion. It is now commonly accepted that the main criteria to obtain good particle removal efficiency on silicon consists to etch about 2 nm of equivalent thermal oxide<sup>(2)</sup>. The etch rate is considered to be a function of the OH<sup>-</sup> ion concentration and the temperature. The OH<sup>-</sup> concentration is driven by the partial neutralisation between the weak acid H<sub>2</sub>O<sub>2</sub> and the weak base NH<sub>4</sub>OH.

S. Verhaverbeke et al<sup>(3)</sup> calculated that after simplifications the OH<sup>-</sup> concentration a function of the square root of the NH<sub>4</sub>OH/H<sub>2</sub>O<sub>2</sub> ratio is. The etch rate on silicon and thermal oxide is here investigated for different SC1 mixtures. The NH<sub>4</sub>OH concentration was varied from 0,065 mol/l to 4,53 mol/l and the H<sub>2</sub>O<sub>2</sub> concentration was varied from 0,17 mol/l to 2,2 mol/l for each NH<sub>4</sub>OH concentration. On silicon the etch rate was measured in two different ways: by weight measurements for the bulk silicon wafers and by reflectometry for Silicon On Insulator (SOI) wafers. The etchrate of thermal oxide was measured by reflectometry. Figure 1 shows that the two measuring methods used for silicon are perfectly coherent. The etch rate is depending on both the NH<sub>4</sub>OH and H<sub>2</sub>O<sub>2</sub> concentration, but once passing a certain NH<sub>4</sub>OH concentration a maximum etch rate is reached. This saturation etch increases with decreasing H<sub>2</sub>O<sub>2</sub> concentration. The same behaviour was earlier reported by Kobayashi et al<sup>(4)</sup>, who demonstrated that the presence of H<sub>2</sub>O<sub>2</sub> directly inhibits the etch mechanisms (the presence of H<sub>2</sub>O<sub>2</sub> is more than just a pH reduction). This effect could be attributed to a buffering effect on the reaction kinetics: the presence of foreign species near the reaction sites slows down the diffusion of the active compounds.

In figure 2 the same data points are depicted but in function of the square root of the NH<sub>4</sub>OH/H<sub>2</sub>O<sub>2</sub> ratio. This shows the limitations of the above proposed model<sup>(3)</sup>, since there is only a linear relationship with the etch rate for the lower part of the curve.

Another interesting observation is the etch rate for thermal oxide. Figure 3 shows the etch rate is substantially lower on thermal oxide than on silicon. The etch rate is only driven by the NH<sub>4</sub>OH concentration and the H<sub>2</sub>O<sub>2</sub> concentration plays a negligible role in this

process. The different etch kinetic obtained with silicon and  $\text{SiO}_2$  could be explained by the cohesion of the thermal oxide compared to a chemical oxide.

Figure 4 shows the etch rate for a constant  $\text{NH}_4\text{OH}/\text{H}_2\text{O}_2$  ratio while the DI water dilution is increased. As expected the  $0,25/\text{I}/X$  ratios result in a constant etch rate, except for  $X=1000$ . Since we obtain constant etch rates, we should be able to obtain equal removal efficiencies for these ratios as well. It is clear from this data that the buffering effect of the  $\text{H}_2\text{O}_2$  is unexisting for the highly diluted ratios.

Figure 11 shows the impact of megasonic energy during the process on the etch rate, no effect was observed on silicon for DI water dilution ratios of  $X=5$  to 50.

With the above observations in mind the particle removal efficiency of different SC1 mixtures at  $65^\circ\text{C}$  was investigated, both with and without megasonics starting from one of the most commonly used ratios:  $0,25/1/5$  (0,25 volumes of  $\text{NH}_4\text{OH}$ , 1 of  $\text{H}_2\text{O}_2$ , 5 of DI water). We took care choosing this ratio as our starting point, since it is a ratio which shows a direct linear relationship between etch rate and the square root of the  $\text{NH}_4\text{OH}/\text{H}_2\text{O}_2$  ratio (figure 2).

## RESULTS

### **$\text{SiO}_2$ particles :**

As can be seen from figure 5 the particle removal efficiency drops very fast once the dilution is increased. On the other hand, when high energy megasonic power is used the removal efficiency is at a level greater than 95% until  $X=100$ . As shown in figure 6, at "ultra" dilute ratios the importance of the megasonic energy is even more obvious, with a removal efficiency greater than 80% for  $X=1000$ . This shows clearly that high removal efficiency can be obtained for very dilute chemistries.

### **$\text{Al}_2\text{O}_3$ particles :**

The wafers contaminated with  $\text{Al}_2\text{O}_3$  slurries are more difficult to clean. Only strong megasonics are able to give acceptable results. One can see on figure 7 and 8 an optimal dilution at  $X=20$  which was re-confirmed 3 times. No reason was still found to explain this strange but actual behaviour. In this case the use of diluted chemistries in conjunction with megasonics gives even better results than the conventional (0,25/1/5) recipe.

### **$\text{Si}_3\text{N}_4$ particles :**

It is well known that  $\text{Si}_3\text{N}_4$  particles from  $\text{H}_3\text{PO}_4$  chemistry are particles which are even more difficult to remove. As can be seen in figure 9, in spite of the high initial contamination level only 60% can be removed with the most concentrated recipe. The megasonics do not bring a decisive advantage in this case.

Except for the very particular case of nitride particles it is therefore possible and sometimes better to use dilute SC1 solutions. The dilution can be quite important in terms of process but is in practice limited by the regulation capability of the chemical concentration control system. Furthermore as depicted in figure 10 the chemical consumption, in order to maintain the nominal concentration, decreases at first very fast from  $X=5$  to 20 and then slower. For these two reasons we propose at first to use the  $0,25/1/20$  ratio.

## DISCUSSION AND CONCLUSIONS

The particle removal efficiency decreases drastically when the volume of DI water in the SC1 solution is increased. The explanation of this behaviour cannot be found just by taking the etch rate into account, but it could be attributed to the effects of the ionic strength of the liquid in between the particle and the substrate. The negative effect due to the dilution is almost entirely compensated by the addition of megasonic energy.

It is possible for the most important types of particles to reduce the chemical concentration drastically and still achieve an acceptable removal efficiency. A first relatively modest concentration reduction, down to the 0,25/1/20 ratio, would probably be necessary for the conservative IC industry. In this case the chemical consumption is actually decreased by a factor 3 both for NH<sub>4</sub>OH and H<sub>2</sub>O<sub>2</sub>. This represents a soft transition towards a more aggressive final dilution .

## REFERENCES

1. W. Kern, D.A Puiotinen, RCA revue vol 2, 1970
2. M. Meuris, M. Heyns, P. Mertens, S. Verhaverbeke and A. Philiposian, Microcontamination, May 1992.
3. S. Verhaverbeke, J. W. Parker and C. McConnel, ECS Chicago, October 1995
4. H. Kobayashi, J. Ryuta, T. Shingyouji, Y. Shimanuki, Jpn. J. Appl. Phys. Vol. 32, pp. L45 - L47, 1993

This work was carried out within the GRESSI consortium between CEA-LETI and France Télécom-CNET

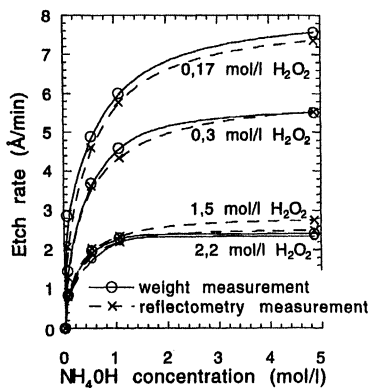


Figure 1: Etch rate of silicon in different SC1 solutions at 65°C.

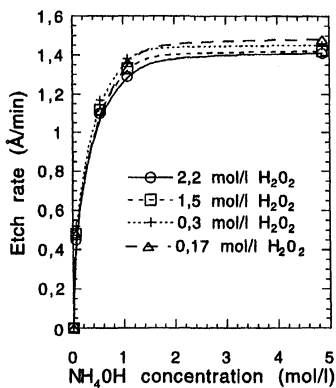


Figure 3: Etch rate of thermal oxide in different SC1 solutions at 65°C.

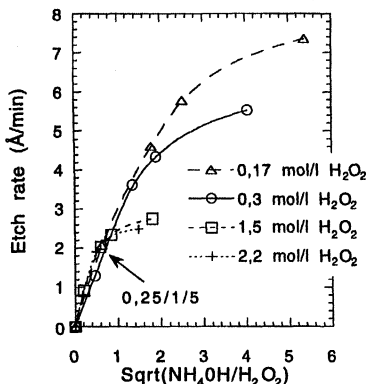


Figure 2 : Silicon etch rate for 65°C SC1 as a function of Sqrt(NH<sub>4</sub>OH/H<sub>2</sub>O<sub>2</sub>).

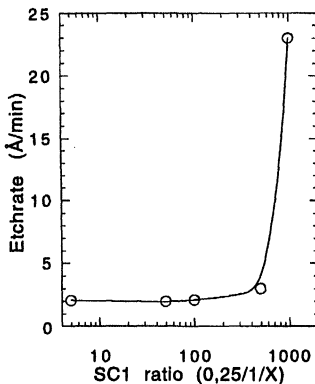


Figure 4: Silicon etch behaviour in 65°C SC1 solutions with a fixed NH<sub>4</sub>OH/H<sub>2</sub>O<sub>2</sub> ratio.

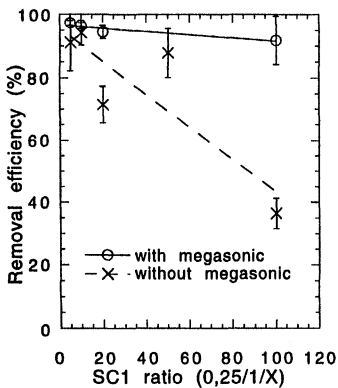


Figure 5 :  $\text{SiO}_2$  particle removal efficiency (CMP slurries measured at  $0.16 \mu\text{m}$ ) by SC1 ( $0,25/1/X$ )  $65^\circ\text{C}$  Scale :  $5 < X > 100$

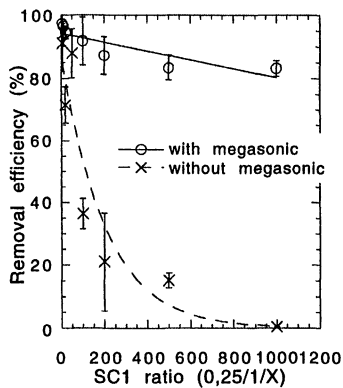


Figure 6 :  $\text{SiO}_2$  particle removal efficiency (CMP slurries measured at  $0.16 \mu\text{m}$ ) by SC1 ( $0.25,1,X$ )  $65^\circ\text{C}$  Scale :  $5 < X > 1000$

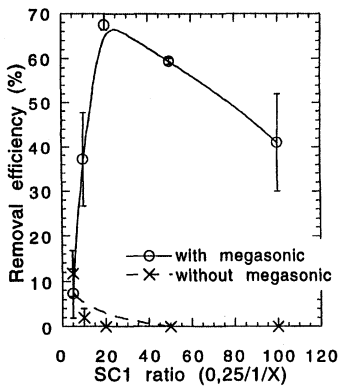


Figure 7 :  $\text{Al}_2\text{O}_3$  particle removal efficiency (measured at  $0.16 \mu\text{m}$ ) by SC1 ( $0.25,1,X$ )  $65^\circ\text{C}$  Scale :  $5 < X > 100$

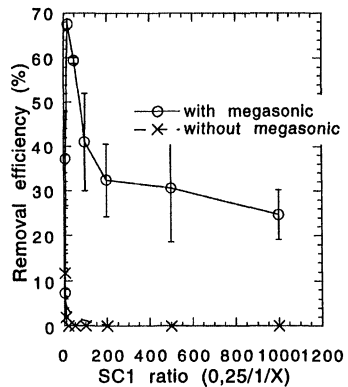


Figure 8 :  $\text{Al}_2\text{O}_3$  particle removal efficiency (measured at  $0.16 \mu\text{m}$ ) by SC1 ( $0.25,1,X$ )  $65^\circ\text{C}$  Scale :  $5 < X > 1000$

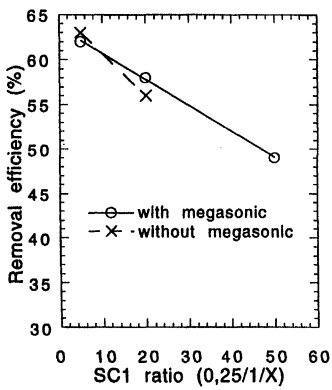


Figure 9 : Si<sub>3</sub>N<sub>4</sub> particle removal efficiency  
(From H<sub>3</sub>PO<sub>4</sub> bath measured at 0.16  $\mu$ m)  
by SC1(0.25,1,X) 65°C Scale : 5<X<50

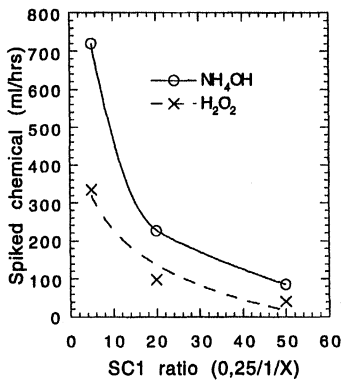


Figure 10 : Spiked chemicals versus  
(0,25,1,X) SC1 dilution. SC1 performed  
at 65°C (200 mm wafer bath)

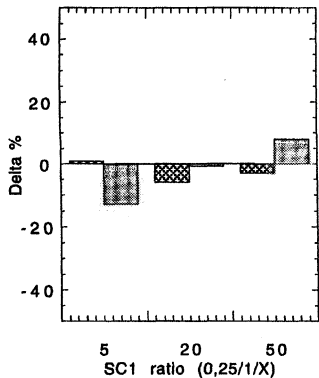


Figure 11: Differences in etchrate, expressed  
in Delta% for different SC1 ratios at 65°C with  
and without megasonic.

# THE ROLE OF MEGASONIC ENERGY IN PARTICULATE REMOVAL FROM SILICON SUBSTRATES IN DILUTE SC1 CHEMISTRY

Ismail Kashkoush, Eric Brause, Robert Grant, and Rich Novak

SubMicron Systems Corporation, 6330 Hedgewood Dr., #150, Allentown, PA 18106

The use of megasonic energy to enhance particulate removal from silicon surfaces in dilute SC1 solutions is demonstrated in this study. Ideal and "real world" particles were deposited on silicon wafers to challenge the SC1/megasonic particle removal system. Different dilute SC1 concentrations were used, e.g., 1:4:20, 1:10:120, and 1:1:100. Bath temperature was varied between 50 and 70 °C with megasonic energy kept constant at 800 W. Results showed that the megasonic energy enhanced the particle removal even in dilute solutions. The chemical concentrations were shown to be a significant factor and must be monitored or controlled in dilute SC1 solutions for particle removal to take place. A lower cost of ownership can be obtained from these techniques as a result of using dilute chemicals and extending current bath lives.

## INTRODUCTION

Surface contamination is considered to be a major problem in the semiconductor, aerospace, and pharmaceutical industries. The adhesion of contaminants to silicon substrates is largely responsible for the low yield in the manufacturing of VLSI and ULSI devices. Many methods for removing particles from silicon surfaces are currently used but the most common techniques are the wet chemical processes based on the hydrogen peroxide/ammonium hydroxide mixtures (SC1 or APM) [1,2]. The addition of megasonic energy during these processes has been proven to enhance particle removal. This paper presents the use of megasonics during dilute SC1 processes to enhance particle removal.

During an SC1 cleaning process, a cooperative and compensating action exists between the two chemical components.  $H_2O_2$  oxidizes the silicon and forms a chemical oxide; the formation of this oxide is limited by the diffusion of the oxidizing species. Ammonium hydroxide, conversely, slowly etches this chemically grown oxide. The result of these two processes is that a chemical oxide layer will continually be generated and removed. Particles are thus removed by this etching and undercutting action. Redeposition of particles onto the wafer surface is inhibited by the repulsion between the negatively charged silicon surface and the negative zeta potential that particles have in a SC1 solution. Particle removal efficiency can be increased by increasing the etch rate of  $SiO_2$ . The etch rate, in turn, can be increased by using greater concentrations of  $NH_4OH$ .

or by elevating the process temperature. However, too much NH<sub>4</sub>OH can cause surface roughness. Therefore, an optimal SC1 solution was suggested to have a low concentration of ammonium hydroxide and a low ratio of NH<sub>4</sub>OH/H<sub>2</sub>O<sub>2</sub> [3].

The continually increasing integration of advanced IC manufacturing requires tighter process control and specifications. In addition, more stringent environmental requirements are being mandated to reduce chemical and water consumption and waste. The use of megasonic energy has been applied to many wafer surface cleaning procedures as a means to enhance particle removal, reduce chemical concentrations, and shorten process times [4,5]. The acoustic waves need for cleaning are approximately 1 MHz and are generated from piezoelectric transducers. When megasonics is used in conjunction with SC1 solutions, particles of sizes 0.12  $\mu\text{m}$  or larger can be removed from the wafer surface.

The mechanism of particle removal consists of a combination of processes including acoustic streaming, acoustic cavitation, and radiation pressure [6,7]. However, the factors that affect particle removal effectiveness in SC1 solutions can be summarized as follows:

- 1) Concentration of Chemicals
- 2) Process time and temperature
- 3) Megasonic power and frequency
- 4) Contaminant size, shape, composition, and intensity (particle counts)
- 5) Surface conditions (i.e., hydrophobic, hydrophilic, bare silicon, oxide, nitride)

Particle removal efficiency increases with process time, temperature, ammonia concentration, megasonic input power and frequency [7,8]. However, careful attention must be paid to the wafer surface roughness and chemical consumption. The use of megasonics with dilute SC1 solutions can result in high particle removal efficiency with longer bath lives, resulting in a lower cost of ownership.

## EXPERIMENTAL SETUP

The experimental set-up consists of the process tank, pump, filters, IR heater, and conductivity sensor for concentration control. The megasonic system is equipped with 1 MHz/800 W pulsed generator in which the transducers are bonded to the bottom of the process tank assembly. Experiments were conducted in SubMicron Systems Corporation Class 1 Applications Laboratory, Allentown, PA, using a fully automated GAMA-1™ wafer processing wet station and utilizing an ICE-1™ in-situ chemical concentration control system. Field experiments were conducted under similar conditions.

Test wafers (p-type, <100>, 10-20  $\Omega\cdot\text{cm}$  resistivity bare silicon) were normalized to a background particle count of <10 at 0.20  $\mu\text{m}$  using a standard SC1 solution. The SC1 process removes any light organic materials on the wafer surface and produces clean

hydrophilic surfaces. Particle deposition was conducted by placing oxide wafers facing bare silicon wafers in 10:1 BOE (Buffered Oxide Etchant) solution at ambient temperature for 1 minute. Contamination occurred when  $\text{SiO}_2$  particles diffused through the solution and deposited onto the bare silicon. Wafers were then rinsed and dried in an IPA dryer. Another set of wafers were contaminated by atomizing suspended (in IPA)  $\text{SiO}_2$  and  $\text{Si}_3\text{N}_4$  particles onto the test wafers. Particle counts were taken for all contaminated wafers using a Tencor<sup>TM</sup> Surface Analysis System 6200.

Each particle test consisted of placing three test wafers in slots 1,13, and 25 of two cassettes. The remainder of the slots were filled with dummies. The cleaning process recipe consisted of the following sequence: SC1/Rinse/IPA dry. SC1 conditions were varied in dilution and temperature. The rinse cycle was performed as 2 quick dumps followed by 5 minute overflowing 18 MΩ.cm DIW, followed by a 5 minute IPA drying cycle. The dryer and rinse tank were previously qualified with particle addition limited to < 5 particles at 0.2  $\mu\text{m}$ . Post particle counts were then taken for the processed wafers.

The second set of experimental conditions involved wafers processed in a variety of different manufacturing environments. Contamination levels in photoresist stripping and pre and post epitaxial growth during silicon manufacturing were investigated. SC1/megasonic systems were designed to remove contaminants in these applications. The test conditions remained the same as previously discussed with results presented in the following section.

## RESULTS AND DISCUSSION

Results are presented graphically as initial particle counts versus the removed particles, particle  $\Delta$  (final counts - initial counts). The data is presented in this fashion for two reasons: First, the negative of the slope of the data fit line represents approximately the particle removal efficiency. Second, the intercept of this line ( $\Delta_0$ ) with the  $\Delta$ -axis represents the particles added to an ideal wafer (zero particle counts). This  $\Delta_0$  value provides a measure of the cleanliness of the process and/or equipment. Using these two parameters, the performance of a SC1/megasonic system can be easily evaluated and compared to other systems. The following sections show data collected on "prepared" as well as "real world" particle experiments.

### "Prepared" Particles

BOE contaminated wafers were cleaned using a 0.5:1:5 SC1 solution at 60 °C and 800 W. As can be observed in figure 1, a particle removal efficiency of 95% and  $\Delta_0$  of +35 was obtained. The experiment was repeated for a 0.25:1:5 SC1 @ 70 °C and 800 W process (see figure 2). Even though the NH<sub>4</sub>OH concentration was reduced 50%, the data showed a removal efficiency of 94% and  $\Delta_0$  of +23. The experiment was repeated again, this time using a 1:1:100 SC1 process at 70 °C and 800 W. A removal efficiency of 94% and  $\Delta_0$  of +41 was obtained even though the ammonia concentration had been decreased

5-fold (figure 3). These results indicate that high particle removal can be obtained at dilute chemistry.

Similar results were obtained when particles of different compositions were deposited on the wafer surface. Removal efficiency contours for  $\text{Si}_3\text{N}_4$  particles in 0.2:1:5 SC1 at 60 °C suggest that the higher the input power, the higher the particle removal at low  $\text{NH}_4\text{OH}$  concentrations (figure 4). When the experiments were performed for  $\text{SiO}_2$  particles, similar contour plots were obtained.

The effect of megasonic energy on the removal of  $\text{SiO}_2$  particles from 200 mm silicon substrates at 0.16  $\mu\text{m}$  is clearly shown in figure 5. For concentrated SC1 bath, the removal of the particles is mainly caused by chemical energy and slightly enhanced by the acoustic energy. As the concentration of ammonia decreases (less effect of chemical energy), the removal efficiency decreases as well, as can be seen from the dotted line in figure 5. However, with the aid of megasonic energy the effect of decreasing ammonia concentration did not impact the particle removal effectiveness, as shown by the solid line in figure 5. The same removal efficiency was maintained at approximately 98% even though the ammonia concentration was reduced 20 times. Similar results were obtained for more dilute chemistries [13].

#### "Real World" Particles

Wafers under a variety of typical manufacturing conditions were processed in megasonic SC1 systems. Particle removal results are shown in figure 6 for a post piranha process consisting of a  $\text{H}_2\text{SO}_4\text{-H}_2\text{O}_2\text{/Rinse/SC1/Rinse/Dry}$  sequence. Contamination occurred by insufficient rinsing after the  $\text{H}_2\text{SO}_4\text{-H}_2\text{O}_2$  process, resulting in high particle counts on the wafer surface (commonly known as light-point defects, or LPDs). These particle defects were described as time dependent surface haze [9] that results from poor rinsing after processing wafers in viscous acids e.g. phosphoric and sulfuric acids. This time dependent haze is usually sulfur (or phosphorous) and/or sulfur compounds (e.g., ammonium sulfate combined from traces of  $\text{NH}_3$  gas typically present in the cleanroom environment or in the wet bench itself). To reduce and/or eliminate these defects, an extended hot DIW rinse is normally used. The SC1/megasonic (0.5:1:5 at 50 °C and 800 W for 5 min) process was designed to enhance the particle performance in these situations. As shown in figure 6, the particle removal efficiency for this process is more than 98%. Implementation of the SC1/megasonic process not only gives good particle results but also can serve as a buffer in case of mis-processed wafers in a post-sulfuric rinse.

Another application of the dilute SC1/megasonic process was for a pre and post epitaxial process at the 0.13  $\mu\text{m}$  particle threshold. Wafers were processed in a 1:10:120 solution at 70 °C for 5 minutes. Figure 7 shows a removal efficiency of 94% and  $\Delta_0$  of +30 was obtained at 0.13  $\mu\text{m}$ . Similarly, a removal efficiency of 96% and  $\Delta_0$  of +25 was

obtained under the same conditions. Even at higher initial particle counts, a removal efficiency of 98% and  $\Delta_0 + 10$  particles was obtained. The increase in removal efficiency as the initial counts increase can be explained by the possible agglomeration of particles and the subsequent ease of removing a group of particles as compared to individual particles.

The increase in particle removal efficiency by high frequency sound waves in dilute SC1 solutions can be explained as follows: First, depending on the chemical ratios, dilute SC1 solutions normally have a pH value between 9.5 to 10.5. These pH values are required to achieve sufficient etch rates and negative zeta potentials in order for particle removal to take place [10-12]. Second, the speed of sound through liquids increases with solution density. The specific gravity of NH<sub>4</sub>OH and H<sub>2</sub>O<sub>2</sub> solutions is less than unity. At the same temperature and pressure, dilute SC1 solutions are more dense than concentrated SC1 solutions. This results in higher transmission efficiencies in dilute SC1 solutions as compared to concentrated SC1 solutions. In addition, the decomposition of H<sub>2</sub>O<sub>2</sub> introduces many fine bubbles into the process bath. These bubbles attenuate the transmission of sound waves, mask the surface of the wafer, and/or diffract or reflect sound waves from the wafer surface, leading to lower particle removals. In these situations, high particle removal can only occur by adding more ammonia and/or raising the temperature.

#### Concentration Control

The use of dilute SC1 solutions requires a more stringent means of monitoring and controlling chemical concentrations in order to obtain process stability. For many years, the RCA-based wafer processing had adopted the use of high concentration of chemicals at elevated process temperatures and long process times [4,5]. Due to the lack of chemical concentration control, the RCA-based cleaning solutions were typically replaced after fairly short periods of time (2-4 hours) in order to obtain any degree of process uniformity. Cleaning solutions can be used for longer intervals if an accurate and continuous control of chemical concentration is provided. In addition, the continuous monitoring of the SC1 solutions will allow more dilute chemicals to be used. The decreased consumption of chemicals (figure 8) will allow a lower cost of ownership.

Experiments were conducted to monitor the particle removal effectiveness in a dilute SC1 bath over 8 hours. Chemical concentrations were controlled by maintaining the solution conductivity using the ICE-1™ system available on the process bath (figure 9). As can be observed, the chemical concentration and conductivity were sustained in a narrow range. The initial and final particle counts on wafers processed in dilute 1:1:100 SC1 at 70 °C over a period of 8 hours are reported in figure 10. Little difference in removal effectiveness between the initial bath and at the end of the bath life was observed. Similar concentration control was observed when a 0.25:1:5 @ 70 °C SC1 bath was extended to 22 hours (figure 11).

Some experiments were conducted to investigate the effect of diluting the SC1 solutions on the wafer surface metallics. Results were obtained and tabulated in Table 1. It can be seen

also from Table 1 that cleaner surface (no metal contamination) can be obtained when dilute SC1 solutions are used. No Fe, Cu, Zn were detected on the test samples for those experiments. The need for a metal removal step (e.g. SC2) after SC1 step may not be required based on these findings. Even if that metal removal step has to be designed, it can be extremely dilute (e.g. 0.01% HCl by wt.).

## CONCLUSIONS

The use of megasonic energy to enhance particle removal efficiencies in dilute SC1 processes has been presented. Test results from different SC1 concentrations and particle size and compositions were reported. Results clearly indicate that megasonic energy enhances the particle removal process in dilute SC1 processes, even in solutions as dilute as 1:1:100 and 1:10:120. High particle removal efficiency was obtained when different particle sizes (0.13, 0.16, and 0.2  $\mu\text{m}$ ) and composition ( $\text{SiO}_2$  and  $\text{Si}_3\text{N}_4$ ) were used. Experiments also demonstrated the need for techniques of concentration control in order to obtain process stability and longer bath life. The use of megasonic energy and dilute chemicals can provide cleaner and smoother wafer surfaces (particles and metals), lower cost of ownership and more environmentally sound processes.

## REFERENCES

1. A. Schwartzman, A. Mayer, and W. Kern, *RCA Review*, 46, 1985, pp. 81.
2. W. Kern, *J. Electrochem. Soc.*, 137, 1887, 1990.
3. S. Verhaverbeke, J. Parker, and C. McConnell, *Electrochem. Soc. Proc.* Vol. 95-20, 1996, pp. 39-48.
4. I. Kashkoush, SMS Technical Report, June/July 1995.
5. I. Kashkoush, SMS Technical Report, Sept./October 1995.
6. I. Kashkoush and A. Busnaina, *Proc. 39<sup>th</sup> IES Annual Mtg.*, Las Vegas, NE, 1993.
7. G. Gale, A. Busnaina, and I. Kashkoush, *Semiconductor International*, August 1996, pp. 133-138.
8. A. Busnaina, I. Kashkoush, and G. Gale, *J. Electrochem. Soc.*, Vol. 142 (8), Aug. 1995, pp. 2812-2817.
9. W. Syverson and M. Fleming, *Electrochem. Soc. Proc.* Vol. 94-7, 1994, pp. 78-84.
10. D. Jan and S. Raghavan, *Electrochem. Soc. Proc.* Vol. 94-7, 1994, pp. 442-449.
11. W. Kern, *Handbook of Semiconductor Wafer Cleaning Technology*, Noyes, NJ, 1993.
12. T. Ohmi, *Electrochem. Soc. Proc.* Vol. 95-20, 1996, pp. 1-12.
13. P. Boelen, et. al., Optimization of Dilute SC1, this proceedings.

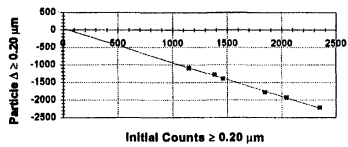


**Figure 1: Particle Removal in 0.5:1:5 @ 60°C Megasonic-assisted SC1 Process**

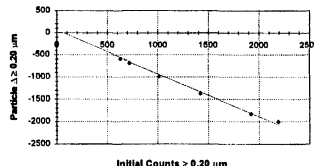


**Figure 2: Particle Removal in 0.25:1:5 @ 70°C Megasonic-assisted SC1 Process**

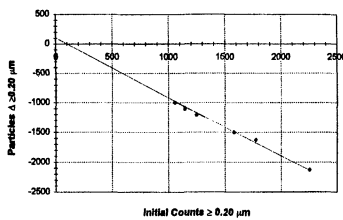


**Figure 3: Particle Removal in 1:1:100 @ 70°C Megasonic-assisted SC1 Process**

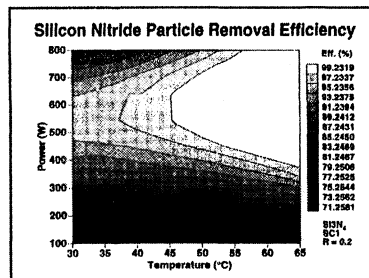


**Figure 4: Particle Removal in 0.2:1:5 @ 60°C Megasonic-assisted SC1 Process**

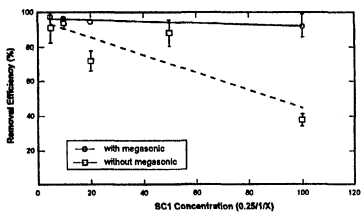


**Figure 5: Effect of Megasonic Energy on Particle Removal for Different Dilute SC1 Solutions [13]**

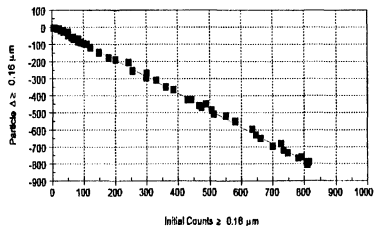


**Figure 6: Particle Removal in 0.5:1:5 @ 50°C Megasonic-assisted SC1 Process after H<sub>2</sub>SO<sub>4</sub>/H<sub>2</sub>O<sub>2</sub> Photoresist Stripping Process**

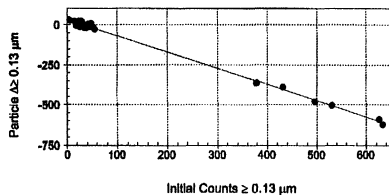


**Figure 7: Particle Removal in 1:10:120 @ 70°C Megasonic-assisted SC1 Process for Cleaning Post Epitaxial Growth Process**

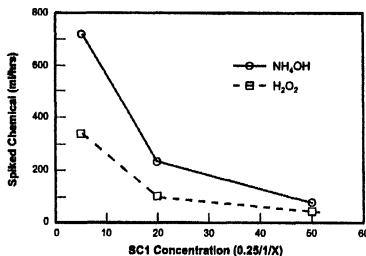


**Figure 8: Chemical Consumption per Hour for a 70°C SC1 Solution [13]**

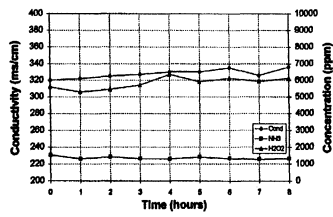


**Figure 9: Variation in Conductivity and Concentration over Time for a 1:1:100 SC1 @ 70°C**

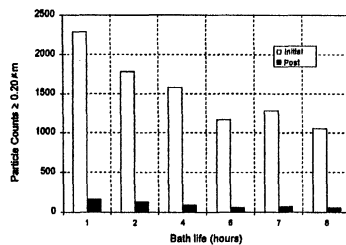


**Figure 10: Removal of  $\geq 0.20 \mu\text{m}$  Particles over an 8 Hour Bath Life for a 1:1:100 SC1 Solution @ 70°C**

## TXRF RESULTS FOR SC1 SOLUTION

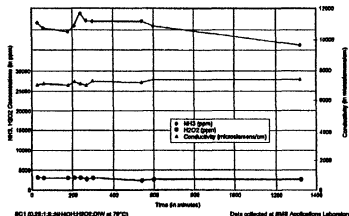


**Figure 11: NH<sub>3</sub>, H<sub>2</sub>O<sub>2</sub> Concentrations and Conductivity versus Time**

PROCESS    1:1:10 @ 50°C                  1:1:100 @ 70°C

Wafer	Fe	Cu	Zn	Fe	Cu	Zn
Control	BDL	BDL	BDL	BDL	BDL	BDL
Initial	39.8	BDL	42	BDL	BDL	BDL
After 1 hr.	53.4	BDL	47	BDL	BDL	BDL
After 2 hrs.	75.6	BDL	82	BDL	BDL	BDL
After 3 hrs.	39.4	BDL	43	BDL	BDL	BDL
After 4 hrs.	58	BDL	62	BDL	BDL	BDL
After 5 hrs.	27.9	BDL	33	BDL	BDL	BDL
After 6 hrs.	61.1	BDL	65	BDL	BDL	BDL
After 7 hrs.	45.5	BDL	52	BDL	BDL	BDL
After 8 hrs.	86.6	BDL	89	BDL	BDL	BDL
16 hrs.	63	BDL	69	BDL	BDL	BDL

BDL (Below Detection Limit of  $1.5 \times 10^{10}$  Atoms/cm<sup>2</sup>)

**Table I. Effect of SC1 Dilution on Wafer Surface Contamination**

## QUANTITATIVE MODELING OF H<sub>2</sub>O<sub>2</sub> DECOMPOSITION IN SC1

P.W. Mertens<sup>1</sup>, M. Baeyens<sup>1</sup>, G. Moyaerts<sup>2</sup>, H.F. Okorn-Schmidt<sup>1,3</sup>, R. Vos<sup>1</sup>, R. De Waele<sup>2</sup>, Z. Hatcher<sup>4</sup>, W. Hub<sup>5</sup>, S. De Gendt<sup>1</sup>, M. Knotter<sup>6</sup>, M. Meuris<sup>1</sup> and M.M. Heyns<sup>1</sup>

<sup>1</sup> IMEC, B-3001 Leuven, Belgium

<sup>2</sup> KHLim, B-3590 Diepenbeek, Belgium

<sup>3</sup> currently at IBM T.J. Watson Research Center, Yorktown Heights, NY 10598, USA

<sup>4</sup>Ashland Chemical, Columbus, OH 43216, USA

<sup>5</sup>Siemens, D-81739 München, Germany

<sup>6</sup> Philips, NL-5656 Eindhoven, The Netherlands

The effect of megasonic agitation, trace metallic contamination, temperature and *pH* on the kinetics of the H<sub>2</sub>O<sub>2</sub> decomposition in NH<sub>4</sub>OH/H<sub>2</sub>O<sub>2</sub>/H<sub>2</sub>O is studied. Quantitative experimental results and fitted models are presented.

### INTRODUCTION

The H<sub>2</sub>O<sub>2</sub> in NH<sub>4</sub>OH/H<sub>2</sub>O<sub>2</sub>/H<sub>2</sub>O cleaning mixture is known to be subject to decomposition [1]. This decomposition not only results in a gradual change of the composition of the cleaning mixture but has also been correlated with degradation of the silicon wafer surface integrity, particularly if made hydrophobic by an HF treatment [1–5]. Several experimental studies on the kinetics of the decomposition of H<sub>2</sub>O<sub>2</sub> in SC1-like cleaning solutions have been performed [3–6].

### EXPERIMENTAL TECHNIQUE

A technique has been developed to monitor the decomposition rate of H<sub>2</sub>O<sub>2</sub> in real time [3, 7]. The decomposition of H<sub>2</sub>O<sub>2</sub> follows the overall reactions:



Reaction (1) describes the H<sub>2</sub>O<sub>2</sub> decomposition itself while reaction (2) describes the subsequent O<sub>2</sub> degassification. It is further assumed that reaction (2) is not rate limiting in the overall decomposition process. Therefore, in the present study, the rate of the decomposition reaction is determined by measuring the rate at which O<sub>2</sub>(g) is generated. In order to obtain data representative for practical cleaning conditions, the pressure is kept as close as possible to the normal ambient pressure. Let *n* be the total number of moles H<sub>2</sub>O<sub>2</sub> dissolved in a sample of the SC1 liquid and *n*<sub>g</sub> be the number of moles O<sub>2</sub>, generated from decomposition. From the stoichiometry of the decomposition reaction it follows that a change in the number of moles of H<sub>2</sub>O<sub>2</sub> in the solution, Δ*n*, is related to a change in the number of moles O<sub>2</sub>(g) generated, Δ*n*<sub>g</sub>, as follows:

$$\Delta n = -2\Delta n_g \quad (3)$$

The measurement of the rate of O<sub>2</sub>(g) generation occurs with a dedicated set-up, schematically shown in Ref. [3]. A volume *V*<sub>1</sub> of the liquid SC1 solution under test is put in a vessel, denoted as “decomposition reactor”. The O<sub>2</sub>(g) generated is collected and fed to a second vessel, referred to as “gas filter”. In order to remove other gases than O<sub>2</sub>, such as NH<sub>3</sub>, the gas collected from the liquid under test is fed through a liquid trap in the second vessel.

The generation of O<sub>2</sub>(g) will give rise to a pressure increase  $\Delta p$  in the gas phase with total volume,  $V_g$ . If the pressure increase is kept small in comparison to the actual atmospheric pressure and if the ideal gas law approximation is applied to the gas volume one obtains:

$$\Delta n_g = \frac{V_g \Delta p}{RT} \quad (4)$$

where  $T$  is the absolute temperature of the gas phase. The change in the number of moles of H<sub>2</sub>O<sub>2</sub> in the liquid,  $\Delta n$ , can be rewritten in terms of the molar concentration of H<sub>2</sub>O<sub>2</sub> in the liquid,  $C$ :

$$\Delta n = V_l \Delta C \quad (5)$$

Substituting the expressions (4) and (5) in to the overall mass balance expression (3) and dividing by the time,  $\Delta t$ , elapsed during the pressure change,  $\Delta p$ , one obtains an expression for the rate of the H<sub>2</sub>O<sub>2</sub> decomposition:

$$\frac{\Delta C}{\Delta t} = -2 \frac{V_g}{V_l RT} \frac{\Delta p}{\Delta t} \quad (6)$$

In practice the measurements are performed as follows. The pressure,  $p$ , starts from ambient pressure and builds up to a small but fixed over pressure  $\Delta p$ , typically 20 (or 40) mbar. Once this over pressure is reached a valve is opened to reset the pressure to the ambient value and the process starts all over. A computer accurately registers the consecutive time intervals,  $\Delta t_i$ , required to reach this pressure increase. In this way the decomposition rate as a function of time is registered. Numerically integrating the decomposition rate over time, taking into account the initial peroxide concentration,  $C_i$ , thus yields the instantaneous H<sub>2</sub>O<sub>2</sub> concentration as a function of the age of the mixture. For practical reasons, the H<sub>2</sub>O<sub>2</sub> concentration,  $C$ , is normalized to its initial value,  $C_i$ , as

$$c_n = \frac{C}{C_i} \quad (7)$$

### METHOD OF DATA ANALYSIS

A simple description of the kinetics of the H<sub>2</sub>O<sub>2</sub> decomposition reaction (1) is given by the basic rate equation:

$$\frac{dc_n}{dt} = -k_n c_n^m \quad (8)$$

where  $k_n$  is the rate constant for the concentration normalized to  $C_i$  and  $m$  is the order of the reaction (1). The normalization, introduced in expression (7), makes the dimension of the rate constant order-independent. To analyse the experimental data it is useful to plot the log of the (normalized) decomposition rate versus the log of the (normalized) concentration, as is shown in Fig. 1. If the simple rate equation holds, the curve should be a straight line, with an intercept at  $c_n = 1$  of  $k_n$  and a slope  $m$ . Because of the normalization, shown in expression (7), the value of  $k_n$  equals the initial, (i.e. for  $c_n = 1$ ), decomposition rate.  $m$  is a parameter characterizing how the decomposition rate changes as the mixture evolves over time towards a lower H<sub>2</sub>O<sub>2</sub> concentration. From a practical standpoint, since  $k_n$  provides the decomposition rate of the fresh mixture, its value equals the H<sub>2</sub>O<sub>2</sub> spiking rate required to maintain  $C$  of the mixture constant at  $C_i$ .

Curve fitting is performed on the logarithms of the experimentally obtained values, in order to obtain more even weighting of all data. The normalization of the concentration to

its initial value results in fit parameters  $k_n$  and  $m$  that can be determined relatively independently. Because of this independence, in cases when too little decomposition has taken place to extract a meaningful value for  $m$ , still a good value for  $k_n$  can be obtained. In a comparative study on the decomposition rate in SC1 particularly the initial decomposition rate, which is given by  $k_n$  is of direct practical interest.

## EXPERIMENTAL CONDITIONS

Experiments were performed to generate information on different factors that affect the kinetics of the decomposition of  $H_2O_2$  in SC1 mixtures. The baseline SC1 mixture is obtained by mixing  $NH_4OH/H_2O_2/H_2O$  (with typical commercial w-concentrations (%):  $H_2O_2$  31.3,  $NH_3$  29.2 and  $(CH_3)_4NOH$  25) in a volume ratio (1/4/20). This corresponds to an initial  $H_2O_2$  concentration,  $C_{10}$ , of 1.63 mol/l and an initial  $NH_4OH$  concentration of 0.611 mol/l. The baseline temperature was chosen to be 70 °C resulting in a  $pH$  of 9.0 and no megasonic agitation was used, unless mentioned otherwise. The effect of different factors on the decomposition kinetics was investigated: megasonic agitation (300W) and the presence of trace amounts of different metals. In some experiments the base  $NH_4OH$  has been replaced by tetramethyl ammonium hydroxide (TMAH)  $(CH_3)_4NOH$ , keeping the  $pH$  and the initial molar  $H_2O_2$  concentration the same as in the corresponding  $NH_4OH$ -based mixture.

For studying the effect of traces of metallic contamination, individual SC1 mixtures are spiked with the metal of interest (see results). The  $H_2O_2$   $NH_4OH$  and  $(CH_3)_4NOH$  were of a grade with most metallic contaminants below 1 w-ppb, 0.1 w-ppb or in some critical cases even below 0.01 w-ppb. 1000 w-ppm AAS or ICP-MS standard metal solutions, obtained from Merck, were used for spiking in all the experiments. For all experiments a secondary solution is prepared by putting 1 vol-% of the original 1000 w-ppm solution of the metal under study, into a 5%  $HNO_3$  solution. Finally, the SC1 mixtures were prepared in the following sequence. At first the  $H_2O$  was heated. The appropriate amount of the secondary metal solution was then added. Subsequently  $H_2O_2$  and  $NH_4OH$  were added.

## RESULTS AND DISCUSSION

As can be seen in Fig. 2, the use of 300W megasonic agitation does not have a significant effect on the overall kinetics in case of an  $NH_4OH$ -based SC1 mixture containing 1 w-ppb Fe [6]. The megasonic agitation, however, suppresses the initial overshoot, characteristic for the measurement method and attributed to the bubble nucleation mechanism (reaction (2)).

Table 1 shows the results for 1 w-ppb of metal in SC1 at 70 °C for  $(NH_4OH/H_2O_2/H_2O)$  and for  $((CH_3)_4NOH/H_2O_2/H_2O)$ . It should be mentioned that the lower values of  $k_n$  obtained for some metals are not very accurate, because of limited measurement time. As can be seen from Table 1, different metals have a very different effect on the decomposition rate constant,  $k_n$ . Under the current conditions the metals that have the strongest effect on the decomposition rate are, in decreasing order of importance: Fe, Cu, W, Co and Bi. The addition of 1 w-ppb of Fe results in a 10 times larger decomposition reaction rate constant than the addition of an equal weight concentration of Cu, comparable to results reported for (1/1/5) mixtures at 30 °C [6]. Other metals such as Ti, Zn, Na and Cr have very little effect. Fe and Cu were also evaluated substituting the  $NH_4OH$  by a  $pH$ -equivalent concentration of TMAH. Fe yields the same decomposition kinetics in TMAH-based mixtures. In the presence of Cu, the initial decomposition rate is a factor of 2 higher in the TMAH-mixture than in the  $NH_4OH$ -mixture. The amine formation of Cu in the  $NH_4OH$ -mixture thus suppresses the catalytic effect by a factor of 2.

The typical values obtained for the order of the reaction in the experiments listed in Table 1 range from 0.5 to 1.5. Surprisingly these values are not integer numbers, possibly indicating simultaneous occurrence of different reaction paths in parallel. For Fe a value of approximately 1.5 is obtained consistently. A simple linear combination of a second and first order reaction rate would yield a curve with a kink. The first part (i.e. right of the kink) of the decomposition curve would have a slope  $m = 2$  the second part (i.e. left of the kink) having a unity slope. This is not observed (Fig. 1). If the initial transient, attributed to the bubble nucleation, is disregarded, the entire decomposition reaction kinetics nicely follows the slope  $m = 1.5$ , as is illustrated in Fig. 1. For Cu a value for  $m$  of approximately 1 is obtained in case of NH<sub>4</sub>OH-mixtures. As mentioned earlier, the values of  $m$  listed in Table 1 describe how the decomposition rate evolves with decreasing remaining peroxide concentration, but also with the age of the mixture. Therefore, also other changes in the mixture, such as e.g. the NH<sub>4</sub>OH-evaporation, can affect these fit values. Since TMAH is a lot less volatile than NH<sub>3</sub>, the data obtained for TMAH should be less affected by evaporation of the base. For Fe the evaporation does not seem to affect the value obtained for the order. For Cu a lower value for  $m$  is obtained with TMAH which could indicate that the higher value obtained in case of NH<sub>4</sub>OH is affected by evaporation (see below:  $pH$  dependence).

The order has also been determined, independent of the aging of the mixture, by analysing the initial decomposition rate for mixtures with different initial peroxide concentration but with the same NH<sub>4</sub>OH-concentration (Fig. 3). In agreement with eq. (7), the normalized initial H<sub>2</sub>O<sub>2</sub>-concentration is defined as  $c_{ni} = C_i/C_{i0}$ . Based on the general rate equation (8) one obtains:

$$k_n(c_{ni})|_{q_0, T_0} = k_n|_{c_{n0}, q_0, T_0} c_{ni}^m \quad (9)$$

$q$  stands for the metal concentration in the mixture and  $T$  is the absolute temperature.  $k_n|_{c_{n0}, q_0, T_0}$ , also abbreviated as  $k_{n0}$ , is the rate constant for the reference conditions:  $c_{n0} = 1$ ,  $q_0 = 1$  w-ppb and  $T_0 = 343.2$  K. Fitting the data, shown in Fig. 3, with expression (9), yields an  $m$ -value for Fe of 1.94 and for Cu of 0.74. Consistent with the results above, the value for Fe is higher than for Cu. Both values are slightly higher than those listed for the TMAH-mixture in Table 1. From a practical standpoint it is worth noticing that for low H<sub>2</sub>O<sub>2</sub>-concentration Cu will eventually result in a higher decomposition rate than Fe (Fig. 3).

The effect of metal concentration, in the range of 0.1 to 5 w-ppb, and temperature, in the range of 30 to 70 °C, on  $k_n$  has been measured (see Figs 4 and 5). The values for a clean solution, in Fig. 4, are calculated from the raw measurement data of Refs [4, 5]. Fig. 5 shows that the dependence on the metal concentration is linear, in agreement with Ref. [6] for the metal concentration range of interest. The experimental data are fit with the following expression,

$$k_n(q, T)|_{c_{n0}} = k_n|_{c_{n0}, q_0, T_0} \left( \frac{q}{q_0} \right)^r \exp \left[ -\frac{E_a}{R} \left( \frac{1}{T} - \frac{1}{T_0} \right) \right] \quad (10)$$

where  $E_a$  is the activation energy per H<sub>2</sub>O<sub>2</sub> and  $r$  is a fit parameter. The results are shown in Table 2. For the clean mixture, shown in Fig. 4, an activation energy of 93.0 kJ/mol is obtained, close to the value reported in Ref. [4].

In order to study the effect of the concentration of the caustic component, its concentration was varied, keeping the concentration of H<sub>2</sub>O<sub>2</sub> constant at 1.63 mol/l. Fig. 6 shows that  $k_n$  increases with increasing  $pH$ .

## REFERENCES

- [1] H.F. Schmidt, M. Meuris, P.W. Mertens, S. Verhaverbeke, M.M. Heyns, M. Kubota and K. Dillenbeck, in *IES 39th Annual Technical Meeting 1993 Proceedings* Vol. 1, (IES, Mount Prospect, Illinois, 1993) p. 238.
- [2] H.F. Schmidt, M. Meuris, P.W. Mertens, S. Verhaverbeke, M.M. Heyns, L. Hellemans, J. Snaauwaert and K. Dillenbeck, in *ECS-Proc. Vol. 94-7* (The Electrochemical Society, Pennington, NJ, 1994) p. 102.
- [3] H.F. Schmidt, M. Meuris, P.W. Mertens, A.L.P. Rotondaro, M.M. Heyns, T.Q. Hurd and Z. Hatcher, in *Proc. of the 2nd Internl Symp. on UCPSS* (Acco, Leuven, 1994) p. 259.
- [4] H.F. Schmidt, M. Meuris, P.W. Mertens, A.L.P. Rotondaro, M.M. Heyns, T.Q. Hurd and Z. Hatcher, in *Extd Abs. of the 1994 Internl Conf. on SSDM* (Acad. Soc. Japan, Tokyo, 1994) p. 419.
- [5] H.F. Schmidt, M. Meuris, P.W. Mertens, A.L.P. Rotandaro, M.M. Heyns, T.Q. Hurd and Z. Hatcher, *Jpn. J. Appl. Phys.* **34**, 727 (1995).
- [6] A. Philipposian and R. Wilkinson, in same as [3] p. 99.
- [7] T.Q. Hurd, P.W. Mertens, H.F. Schmidt, D. Ditter, L.H. Hall, M. Meuris and M.M. Heyns, in *IES 40th Annual Technical Meeting 1994 Proceedings* Vol. 1, (IES, Mount Prospect, Illinois, 1994) p. 218.

Table 1: Overview of experimental conditions and kinetic fit parameters,  $k_n$  and  $m$ , for  $\text{H}_2\text{O}_2$  decomposition in (1/4/20) SC1 and a  $((\text{CH}_3)_4\text{NOH}/\text{H}_2\text{O}_2/\text{H}_2\text{O})$  mixture with the same initial  $\text{H}_2\text{O}_2$  concentration (i.e.  $C_{10} = 1.63 \text{ mol/l}$ ) and the same initial  $pH$  (= 9.0). The metal weight concentration is 1 ppb except for the blank references. In absence of megasonic agitation at 70 °C.

Mt	$\text{NH}_4\text{OH}$ :		$(\text{CH}_3)_4\text{NOH}$ :	
	$k_{n0}$ ( $10^{-6} \text{ s}^{-1}$ )	$m$	$k_n$ ( $10^{-6} \text{ s}^{-1}$ )	$m$
blank	2.2		7.5	$2.2 \pm 0.8$
Na	3.5			
Mg	3.7			
K	7.5			
Ti	1.0			
Cr	3.2			
Fe	166.7	1.51	169.3	$1.50 \pm 0.02$
Co	10.2			
Cu	17.3	0.97	32.2	$0.45 \pm 0.02$
Zn	1.7			
Sr	6.2			
Ba	7.4			
W	11.7			
Pt	8.8			
Pb	4.6			
Bi	10.0			

Table 2: Overview of the fit parameters, obtained by fitting expression (10) to experimental data for the “normalised decomposition rate constant” in the case of different concentration of Fe or Cu in the (1/4/20) SC1 at different temperatures. In absence of megasonic agitation. The fit model using the fit parameters on the second and third row is depicted in figures 4 and 5.

Mt	$k_n$ ( $10^{-6}$ s $^{-1}$ )	$r$	$E_a$ (kJ/mol)
Fe	166.3	1.03	68.6
Fe	162.8	$\equiv 1$	68.1
Cu	17.6	$\equiv 1$	n/a

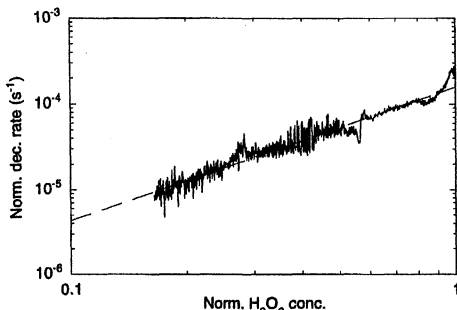


Figure 1: Normalized  $\text{H}_2\text{O}_2$  decomposition rate vs normalized  $\text{H}_2\text{O}_2$  concentration for (1/4/20) SC1 at 70 °C containing 1 w-ppb Fe.  $k_n = 166.7 \times 10^{-6} \text{ s}^{-1}$  and  $m = 1.51$ .

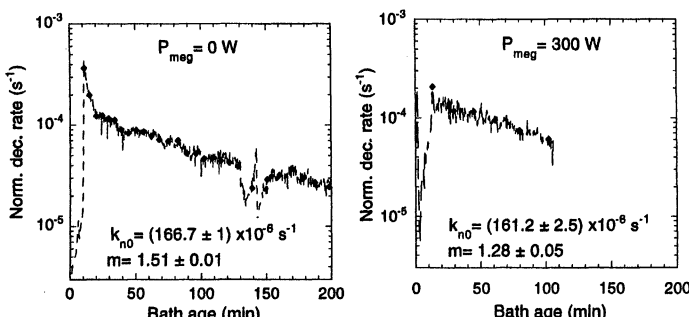


Figure 2: Effect of megasonic agitation on normalized  $\text{H}_2\text{O}_2$  decomposition rate versus age of the mixture for (1/4/20) SC1 at 70 °C containing 1 w-ppb Fe.

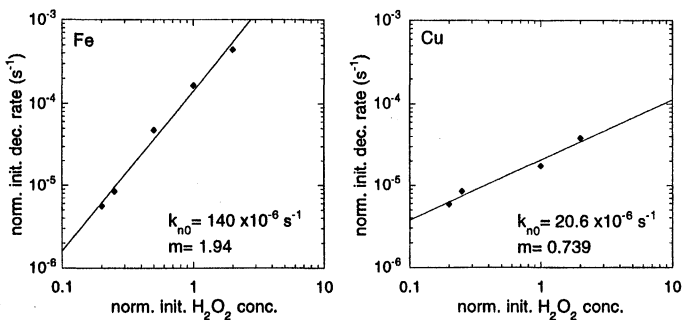


Figure 3: Effect of initial  $\text{H}_2\text{O}_2$  concentration on the initial decomposition rate both normalized to the initial  $\text{H}_2\text{O}_2$  concentration for the (1/4/20) mixture (i.e. 1.63 mol/l) for a constant  $\text{NH}_4\text{OH}$  concentration of 0.611 mol/l w-concentration of Fe or Cu of 1 ppb at 70 °C. The symbols show experimental data. The lines show the fit model according to equation (9).

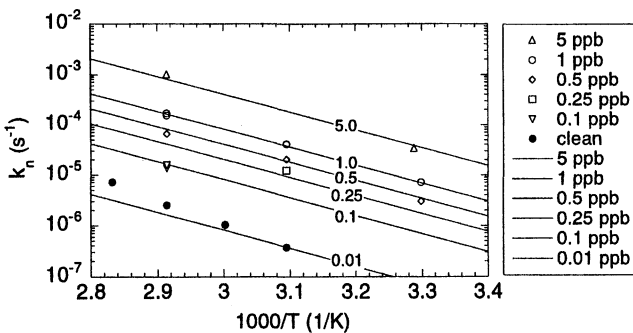


Figure 4: Effect of the temperature and of the Fe weight concentration on  $k_n$  for (1/4/20) SC1 solution. Symbols show experimental data obtained in the Fe weight concentration range of 0.1 to 5 ppb and the temperature range of 30 to 70 °C and in addition, data obtained for a "clean" reference solution in the temperature range of 50 to 80 °C. The lines show the fit model according to equation (10) using the values shown in the second row of Table 2.

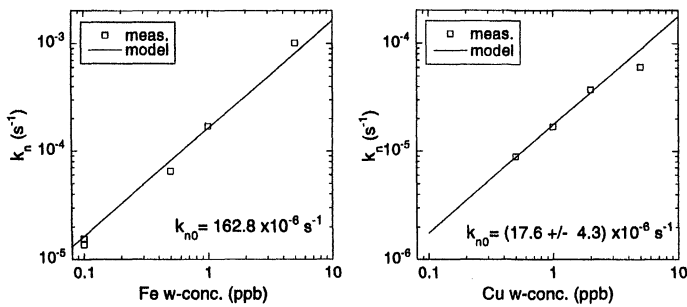


Figure 5: Effect of concentration of metal in the (1/4/20) SC1 solution at 70 °C on the decomposition kinetics. The symbols show experimental data. The lines show the fit model according to equation (10) using the values obtained for  $r \equiv 1$ , shown in Table 2.

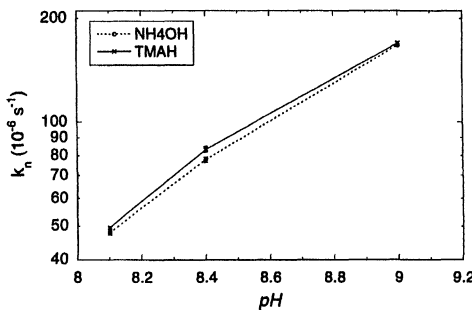


Figure 6:  $\text{H}_2\text{O}_2$  decomposition rate constant,  $k_n$ , measured for SC1-like mixtures with the same initial  $\text{H}_2\text{O}_2$  concentration,  $C_{10} = 1.63 \text{ mol/l}$ , but for two different caustic components,  $\text{NH}_4\text{OH}$  or  $(\text{CH}_3)_4\text{NOH}$ , at 70 °C and containing 1 w-ppb Fe, as a function of pH.

# THE ROLE OF THE PEROXIDE ANION AS AN OXIDIZER IN SC-1 SOLUTIONS

Steven Verhaverbeke, Ph.D. and Jennifer W. Parker, Ph.D.  
CFM Technologies, 1336 Enterprise Drive, West Chester, PA 19087

The oxidation reaction in SC-1 solutions is investigated. The oxidizer plays a major role in many of etching and cleaning applications of SC-1 solutions. The peroxide anion,  $\text{HO}_2^-$ , is shown to be the primary oxidant in these applications. The role that ammonium hydroxide plays in the SC-1 oxidation is to substantially increase this oxidant's concentration over that found in pure hydroxide solutions.

## INTRODUCTION

The RCA Standard Clean is the de-facto standard in the semiconductor industry for cleaning silicon wafers.[1] The RCA Standard Clean , developed by W. Kern and D. Puotinen in 1965 and published in 1970 [2], consists of two sequential steps: the Standard Clean 1 (SC-1) followed by the Standard Clean 2 (SC-2). The SC-1 solution, consisting of a mixture of Ammonium-Hydroxide/ Hydrogen-Peroxide/ Water, was developed to remove organic contamination as a result of the solvating action of ammonium hydroxide and the powerful oxidizing action of hydrogen peroxide.

SC-1 can also be used for surface etching. SC-1 will etch the following materials:  $\text{SiO}_2$ ,  $\text{Si}_3\text{N}_4$ , Si, Ti and TiN. Whether the SC-1 solution is used for cleaning or etching, the solution chemistry is similar.

## THE ROLE OF OXIDATION IN SC-1

In all applications of SC-1, some etching of the surface occurs. An overview of reported overall etching rates is given in Table I to indicate the order of magnitude of the etch rate for a given substance. In most of these etching reactions, the oxidation reaction plays a major role. For example in traditional cleaning applications, oxidation protects the silicon during wafer cleaning. Similarly, during the etching of silicon or  $\text{Si}_3\text{N}_4$ , the oxidation converts the substrate into  $\text{SiO}_2$  which can then be etched. Finally, when Ti and TiN are etched with SC-1, the oxidation reaction directly converts the Ti into soluble  $\text{TiO}^{4+}$  peroxide complexes. In this paper, the role of the oxidation reaction in two distinct SC-1 etching applications will be discussed: The case of the formation of an insoluble oxide will be considered and then the formation of a soluble oxide will be analyzed.

## SOLUTION CHEMISTRY

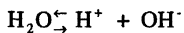
SC-1 solutions typically consist of mixtures of water with 31wt% hydrogen peroxide ( $\text{H}_2\text{O}_2$ ) and 29wt% ( $\text{NH}_4\text{OH}$ ) in ratios from 5:1:1 to 100:1:1. Three equilibrium reactions must be considered to analyze the chemistry of SC-1 solutions:



$$\text{where, } K_b = [\text{NH}_4^+][\text{OH}^-]/[\text{NH}_4\text{OH}] \quad (1)$$



$$\text{where, } K_a = [\text{HO}_2^-][\text{H}^+]/[\text{H}_2\text{O}_2] \quad (2)$$



$$\text{where, } K_w = [\text{OH}^-][\text{H}^+]/[\text{H}_2\text{O}] \quad (3)$$

The values of the equilibrium constants  $K_b$ ,  $K_a$ , and  $K_w$  as a function of temperature are given in Table II. The decomposition of hydrogen peroxide is not considered in this model, since most semiconductor applications of SC-1 are relatively short (i.e., around 5 minutes), and the amount of decomposition is limited in such a time frame.

The oxidizing species in SC-1 solutions is often assumed to be  $\text{H}_2\text{O}_2$ . In this work, however, two possible oxidizing species are considered:  $\text{H}_2\text{O}_2$  and  $\text{HO}_2^-$ .  $\text{HO}_2^-$  results from the dissociation of  $\text{H}_2\text{O}_2$  and its concentration can be calculated by solving the equilibrium reactions given by equations 1-3. Since the dissociation constant,  $K_a$ , for hydrogen peroxide is so low, in SC-1 solutions, peroxide remains relatively undissociated and  $[\text{H}_2\text{O}_2]$  can be expressed by:

$$[\text{H}_2\text{O}_2] \approx c_{\text{H}_2\text{O}_2} \quad (4)$$

where  $c_{\text{H}_2\text{O}_2}$  is the initial hydrogen peroxide concentration, assuming no dissociation given in mole/liter.

In contrast, the peroxide anion is produced by the equilibrium balance given in equation 2 and its concentration is affected by the presence of a base (i.e.,  $\text{NH}_4\text{OH}$ ). The equilibrium concentration for  $\text{HO}_2^-$  is approximated by [7]:

$$[\text{HO}_2^-] \approx \sqrt{\frac{K_a \cdot K_b}{K_w}} \sqrt{c_{\text{H}_2\text{O}_2} \cdot c_{\text{NH}_3}} \quad (5)$$

where  $c_{\text{H}_2\text{O}_2}$  and  $c_{\text{NH}_3}$  are the initial, undissociated concentrations of hydrogen peroxide and ammonia in the SC-1 solution.

It is interesting to recognize the difference in concentrations of oxidizing species (i.e.,  $\text{H}_2\text{O}_2$  and  $\text{HO}_2^-$ ) between SC-1 solutions and pure hydrogen peroxide solutions. In pure hydrogen peroxide solutions, the concentration of the  $\text{H}_2\text{O}_2$  is still described by equation. In contrast, the equilibrium of hydrogen peroxide (i.e., equation 2) is no longer shifted as a result of the presence of a base, and the peroxide anion concentration in pure  $\text{H}_2\text{O}_2$  solutions is given by:

$$[\text{HO}_2^-] = \sqrt{K_a [\text{H}_2\text{O}_2]} \approx \sqrt{K_a c_{\text{H}_2\text{O}_2}} \quad (6)$$

Thus, in SC-1 solutions the presence of ammonium hydroxide does not

significantly alter  $[\text{H}_2\text{O}_2]$ . In contrast,  $[\text{HO}_2^-]$  increases by the factor  $\sqrt{\frac{K_b}{K_w}} c_{\text{NH}_3}$ , as a result

of the ammonium hydroxide. Using the values given in Table 1,  $\sqrt{\frac{K_b}{K_w}}$  is on the order of

11,000 to 40,000 depending on the temperature. The fact that the equilibrium

concentrations of  $\text{HO}_2^-$  vary significantly in the presence or absence of a base allows for determination of the primary oxidizing species in SC-1 solutions.

### SC-1 IN TRADITIONAL CLEANING APPLICATIONS.

The hydrogen peroxide in SC-1 oxidizes the bare silicon (i.e., at the silicon/oxide interface). The oxide that is formed is insoluble, and so remains on the wafer surface until it is attacked by  $\text{OH}^-$  from the ammonia hydroxide in the aqueous solution at the boundary between the oxide and the aqueous solution (i.e., the wafer surface). Figure 1 is a schematic illustration of the overall SC-1 cleaning process.

#### Concentration Dependence of Oxide Growth

Oxide growth in pure hydrogen-peroxide solutions provides a simplified model of the reactions occurring in SC-1 solutions[10, 11] Figure 2 shows data of oxide growth in three different concentrations of hydrogen peroxide from Graef et al.[10] and Ryuta et al. [11] (Note the logarithmic time scale). This data clearly shows that the oxide growth thickness is not linear with time, but rather is a function of the square root of time.

The oxidation rate in SC-1 solutions is much higher than in pure peroxide solutions. Ryuta et al. [11] found that the final oxide thickness in SC-1 after a short exposure time (i.e., 1-2 minutes) is similar to an exposure of 50 minutes in pure  $\text{H}_2\text{O}_2$  at 90 °C. Recalling the differences in the concentration of the peroxide molecule and the peroxide anion between pure hydrogen peroxide solutions and SC-1 indicates why such a change in growth rate can occur. If the peroxide molecule is the primary oxidant, then no change in oxidant concentration and, therefore, no change in growth rate is anticipated. If, however, the peroxide anion,  $\text{HO}_2^-$ , is the principle oxidant, then a substantial increase in oxidant concentration is found in SC-1 solutions compared to pure  $\text{H}_2\text{O}_2$  solutions, correlating to large increase in growth rate.

The data in Figure 2 can be numerically differentiated to analyze the actual oxide growth rate. Figure 3a shows the oxidation rate as function of time for three different concentrations of hydrogen peroxide. Figure 3b shows the same data when it has been normalized by  $\sqrt{\text{H}_2\text{O}_2}$ . The data all falls on the same line within experimental error. If the oxidation is proportional to  $\text{HO}_2^-$  then according to equation (6), the oxidation rate should depend on  $\sqrt{\text{H}_2\text{O}_2}$ . These results further indicate that  $[\text{HO}_2^-]$  is the predominant oxidizing species. If on the other hand the data is normalized to the undissociated hydrogen peroxide, then the curves diverge drastically.

#### Time Dependence of Oxide Growth

Previously, we modeled the oxidation reaction at the silicon/oxide interface assuming only Fickian diffusion and found that models based only on diffusive flux cannot quantitatively describe the data shown in figure 2 [8]. Although the initial part of the growth curve can be fit with equations that follow the Deal-Grove model, these equations predict both much faster growth after 100 seconds and continued oxide growth after 10,000 seconds. Data in the literature indicate that no significant oxide growth is

found after 10,000 seconds. In fact, the data suggest that the maximum thickness for chemical oxides is 9 Å, whether the oxide is produced in SC-1 or pure peroxide solutions. Since the oxide growth ceases in pure hydrogen peroxide solutions as well as in SC-1 solutions, some other transport limitation must be active.

Stoneham and Tasker [12] studied the effect of image charges on the growth of oxide films. These authors found that the polarization energies associated with localized charges near the interface between oxides and silicon can directly affect the transport of charged species. The presence of localized charges at the interface provides a motive force that affects the transport by diffusion, over short distances. Figure 4 schematically illustrates the effect of image charges on transport. Because this force is electrostatic, it is active only over a short distance. As the oxide thickness grows, the image charge is unable to facilitate transport of the ionic species, and oxidation is minimized. The oxide growth follows the simple form:

$$g_{\text{image charge}} = \frac{dt_{\text{ox}}}{dt} = \frac{\Pi}{t_{\text{ox}}} \left( 1 - \frac{\Lambda}{t_{\text{ox}}} \right) \quad (7)$$

where,  $\Pi$ = fitting term including concentration dependency

$\Lambda$ = fitting term describing force resulting from image charge.

$\Lambda$  may have either sign, but for inward anion motion (i.e., toward the metal)  $\Lambda$  is negative. The data for a 1 wt% hydrogen peroxide solution was fit with equation 7. The best fit is obtained with:

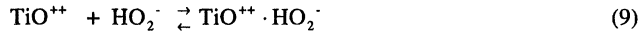
$$g_{\text{image charge, 1\% H}_2\text{O}_2} = \frac{dt_{\text{ox}}}{dt} = \frac{0.00123808}{t_{\text{ox}}} \left( 1 + \frac{0.0633044}{t_{\text{ox}}} \right) \quad (8)$$

The result of this fit shows that the sign of  $\Lambda$  is negative, indicating that an anion is the active oxidative species in the growth of the oxide film. The effect of the image charge motive force is to attract  $\text{HO}_2^-$  to the silicon/oxide interface in preference to  $\text{H}_2\text{O}_2$ . As a consequence of this electrostatic force, the ratio of  $[\text{HO}_2^-]/[\text{H}_2\text{O}_2]$  is significantly higher at the active interface than it is in solution, allowing  $\text{HO}_2^-$  to be the primary oxidant.

Analysis of the concentration and time dependence of the oxidation occurring in SC-1 solutions on wafers indicates that the principle oxidant is the peroxide anion.

#### ETCHING REACTIONS OF Ti AND TiN

Titanium readily forms orange peroxy-titanate complexes with hydrogen peroxide. These complexes are extremely soluble in water, consequently titanium dissolves rapidly in solutions containing hydrogen peroxide. Again considering SC-1 and pure hydrogen peroxide solutions, Ti and TiN are first oxidized by either hydrogen peroxide itself, or the peroxide anion,  $\text{HO}_2^-$ . The oxidation reactions of both metals with both oxidants are given in Table III. Once  $\text{TiO}^{4+}$  is produced, it reacts further, with either oxidant, to form peroxy-titanate complexes. For example,



with,  $K_{\text{HO}_2^-} = \frac{[\text{TiO}^{++} \cdot \text{HO}_2^-]}{[\text{TiO}^{++}][\text{HO}_2^-]} = 10^{12.29}$  at 18 °C [6],  
and



with,  $K_{\text{H}_2\text{O}_2} = \frac{[\text{TiO}^{++} \cdot \text{H}_2\text{O}_2]}{[\text{TiO}^{++}][\text{H}_2\text{O}_2]} = 10^{3.71}$  at 25 °C [6] .

The relative values of the equilibrium constants,  $K_{\text{HO}_2^-}$  and  $K_{\text{H}_2\text{O}_2}$ , show that the peroxide complex that forms with  $\text{HO}_2^-$  is highly favored over that produced with  $\text{H}_2\text{O}_2$ , despite the smaller amount of  $\text{HO}_2^-$ . In a solution of pure hydrogen peroxide,  $[\text{TiO}^{++} \cdot \text{HO}_2^-]/[\text{TiO}^{++} \cdot \text{H}_2\text{O}_2]$  is greater than  $3 \times 10^6$ . This ratio will only increase in SC-1 since  $[\text{HO}_2^-]$  increases by the factor  $\sqrt{\frac{K_b}{K_w} c_{\text{NH}_3}}$ .

Dissolution reactions (i.e., Equations (9) and (10)) are frequently the rate limiting steps in similar etching reactions. Then as a first approximation, the reactions can be modeled as first order reactions with the oxidants  $\text{H}_2\text{O}_2$  and  $\text{HO}_2^-$ . First order models of equations (9) and (10) require the assumption that the Ti or TiN concentration remains constant throughout the reaction, a reasonable approximation for these surface reactions. If  $\text{H}_2\text{O}_2$  is the primary oxidant, then the etch rate can be written as:

$$r_{e_{\text{H}_2\text{O}_2}} = k_{\text{H}_2\text{O}_2} [\text{H}_2\text{O}_2] \equiv k_{\text{H}_2\text{O}_2} c_{\text{H}_2\text{O}_2} \quad (11)$$

Equation (11) suggests that the etch rate is independent of  $\text{NH}_4\text{OH}$ . Similarly, if  $\text{HO}_2^-$  is the primary oxidant, then the reaction rate can be written as:

$$r_{e_{\text{HO}_2^-}} = k_{\text{HO}_2^-} [\text{HO}_2^-] \equiv k'_{\text{HO}_2^-} \sqrt{c_{\text{H}_2\text{O}_2} \cdot c_{\text{NH}_3}} \quad (12)$$

where  $k_{\text{H}_2\text{O}_2}$  and  $k_{\text{HO}_2^-}$  are reaction rate constants, and  $k'_{\text{HO}_2^-} = (k_{\text{HO}_2^-}) \sqrt{\frac{K_a K_b}{K_w}}$ .

Since equations (11) and (12) have only one unknown at any given temperature (i.e., the rate constants), the etch rate can be determined for all other  $\text{NH}_4\text{OH}$  and  $\text{H}_2\text{O}_2$  concentrations by using one actual data point. Using published Ti and TiN etch rate data from O'Brien et al. [4] and Philipossian and Magana [5], equations (11) and (12) were solved for TiN at 55 °C and  $c_{\text{NH}_4\text{OH}}=0.026$  mole/l and  $c_{\text{H}_2\text{O}_2}=2$  mole/l. The etch rate was then calculated over normal operating ranges. A comparison of these two theoretical models with O'Brien et al.'s data [4] shows that the model based on a first order reaction

with  $\text{HO}_2^-$  reflects the empirical data very well. The empirical data has similar functionality with respect to ammonium-hydroxide and hydrogen-peroxide as predicted by equation (12). Additionally, once the rate constant was determined using the data of O'Brien et al., the etch rates predicted by equation (12) are within 20% of the published data in the concentration ranges used for industrial applications. In contrast, assuming a first order reaction with  $\text{H}_2\text{O}_2$  indicates that the ammonia concentration does not influence the etch rate; a result that is in clear discrepancy with the empirical data. The comparison of these two theoretical models with published data indicates that  $\text{HO}_2^-$  is the predominant oxidant for the SC-1 reactions with Ti and TiN.

### Selectivity Issues

The first order model of the etch rate of Ti and TiN given by equation (12) is useful for determining the selectivity of the etching process. In industrial applications, preferential etching of Ti or TiN over  $\text{SiO}_2$  is frequently important. The etch rate of  $\text{SiO}_2$  is dependent on  $[\text{OH}^-]$  [13], whereas the etch rate of Ti and TiN is dependent on  $[\text{HO}_2^-]$ .

Using the equation as published by the authors earlier [13], the selectivity at any given temperature can be determined as follows :

$$\text{Selectivity} \left( \frac{\text{Ti}}{\text{SiO}_2} \right) \propto c_{\text{H}_2\text{O}_2} \quad (14)$$

Therefore, the selectivity is directly proportional to the initial, undissociated  $\text{H}_2\text{O}_2$  concentration which does not change as a function of temperature. Increasing the peroxide concentration leads to greater selectivity (i.e., Ti or TiN is etched faster than  $\text{SiO}_2$ ). The selectivity of Ti and TiN versus  $\text{SiO}_2$  also can be calculated as a function of temperature : [7]

$$\frac{\text{Selectivity Ti vs SiO}_2 \text{ at } t}{\text{Selectivity Ti vs SiO}_2 \text{ at } 25^\circ\text{C}} = \frac{K_a}{K_w} \quad (15)$$

Equation (15) is plotted in Figure 5 for identical SC-1 solutions; selectivity of Titanium over  $\text{SiO}_2$  is shown as a function of temperature. At lower temperatures, Ti or TiN is preferentially etched while higher temperatures lead to lower selectivity.

Similarly the selectivity of Ti and TiN versus  $\text{TiSi}_2$  etching can be considered. According to O'Brien et al. [4], the etch rate of  $\text{TiSi}_2$  is directly proportional to the initial undissociated  $\text{NH}_4\text{OH}$  concentration. Although it is not very well understood why the  $\text{TiSi}_2$  etch rate is only dependent on the  $\text{NH}_4\text{OH}$  concentration, such dependency could result from a second order reaction with  $\text{HO}_2^-$  and  $\text{OH}^-$ . The product of  $[\text{HO}_2^-]$  and  $[\text{OH}^-]$  is directly proportional to  $c_{\text{NH}_4\text{OH}}$ . (Note: The functional dependency on  $c_{\text{NH}_4\text{OH}}$  cannot result from etching by the  $\text{NH}_4^+$  ion since  $[\text{NH}_4^+]$  has a functional dependence on  $[\text{H}_2\text{O}_2]$  and  $[\text{NH}_4\text{OH}]$  that is similar to  $[\text{HO}_2^-]$ .) If such a second order reaction is responsible for  $\text{TiSi}_2$  etching, then the etch rate can be written as :

$$r_{\text{TiSi}_2} = A_{\text{TiSi}_2} [\text{HO}_2^-] [\text{OH}^-] e^{-\frac{E_{\text{TiSi}_2}}{kT}} \quad (16)$$

Substitution of the respective expressions for  $[\text{HO}_2^-]$  and  $[\text{OH}^-]$  yields:

$$r_{\text{TiSi}_2} = A_{\text{TiSi}_2} K_b c_{\text{NH}_3} e^{\frac{-E_{\text{TiSi}_2}}{kT}} \quad (17)$$

The selectivity of Ti/TiN versus  $\text{TiSi}_2$  at any given temperature is, therefore, expressed by :

$$\text{Selectivity} \left( \frac{\text{Ti}}{\text{TiSi}_2} \right) \propto \sqrt{\frac{K_a}{K_b K_w} \frac{c_{\text{H}_2\text{O}_2}}{c_{\text{NH}_3}}} \quad (18)$$

In order to get a high selectivity of Ti/TiN etching versus  $\text{TiSi}_2$  etching, the absolute concentrations are not important, only the ratio of hydrogen peroxide to ammonium hydroxide. However, it is important to remember that some  $\text{NH}_4\text{OH}$  is necessary to increase the  $[\text{HO}_2^-]$  over that found in pure hydrogen-peroxide solutions, so that Ti and TiN etching occurs at a reasonable rate. Assuming that the activation energies of the two etching processes are not dramatically different, the temperature dependency of the selectivity of the Ti versus  $\text{TiSi}_2$  can be determined from Equation (18). These results are shown in Figure 6. Once again selectivity for Ti or TiN etching is favored at low temperatures.

## CONCLUSIONS

In this paper, the oxidation reaction in SC-1 solutions is investigated. The oxidizer plays a major role in many of the etching and cleaning applications of SC-1 solutions. Different oxidizers are modeled and  $\text{HO}_2^-$  is found to be the primary oxidizer. Finally, some industrial implications of these results are discussed.

## REFERENCES

1. W. Kern, J. Electrochem. Soc. **137**, 1887 (1990).
2. W. Kern, J. and D. Puotinen, RCA Rev. **31**, 187 (1970).
3. M. Watanabe, M. Harazono, Y. Hiratsuka and T. Edamura, Proceedings of the Electrochemical Society, PV **83-8**, 488, (1983).
4. S. O' Brien, I. Goldwasser, and D. Prinslow. Proceedings of the Third International Symposium on Ultra Clean Processing of Silicon Surfaces, 205,(1996).
5. A. Philipposian and J. Magana, Proceedings of the Second International Symposium on Ultra Clean Processing of Silicon Surfaces, 275,(1994).
6. Perrin, D.D, IUPAC Chemical Data Series No 29., Pergamon Press, N.Y. 1982.
7. S. Verhaeverbeke and J.W. Parker and C.F. McConnell, The Science and Technology of Semiconductor Surface Preparation, MRS, Pittsburgh, PA 1977, to be published.
8. S. Verhaeverbeke, J.W. Parker and C.F. McConnell, in "Proceedings of the Third International Symposium on Ultra Clean Processing of Silicon Surfaces," (Acco, Leuven, Belgium, 1996), p. 153.
9. S. Rigo, Silica Films on Silicon, in "Instabilities in Silicon Devices," Volume 1, ed. G. Barbottin and A. Vapaille, North Holland, 1986, p. 57.
10. Graef, D. et al., ASSIST Progress Report 2, Esprit Basic Research Action 6108 European Union, Brussels, 1995.
11. Ryuta, I. Takabashi, C. Okada, H. Koabayashi, G. Maeda, and T. Shigyouji, ECS, **95-2**, 688 (1995).
12. Stoneham, A.M. and P.W. Tasker, **55 No. 2**, 237, 1987.
13. S. Verhaeverbeke and J.W. Parker, and C.F. McConnell, in "Cleaning Technology in Semiconductor Device Manufacturing IV," (The Electrochemical Society, Pennington, NJ, 1996), p39.

Table I . SC-1 etch rates as measured and reported in the literature [2,3,4]

Substrate	Etch Rate
PSG	60
Thermal SiO <sub>2</sub>	5
Silicon	8
Si <sub>3</sub> N <sub>4</sub>	2
TiN	320
TiSi <sub>2</sub>	11.8
Ti	300

Table II: The pK (pK= - logK) values for the equilibrium constants Kb, Ka, and Kw expressed in molarity as a function of temperature. [4]

Temp	pKw	pKb	pKa
25	13.99	4.75	11.620
30	13.84	4.74	11.550
35	13.69	4.73	11.340
40	13.54	4.73	11.297
45	13.41	4.73	11.25
50	13.28	4.72	11.21
55	13.15	4.73	11.16
60	13.03	4.74	11.12
65	12.92	4.73	11.08
70	12.81	4.73	11.03
75	12.71	4.73	10.99
80	12.61	4.73	10.95

Table III: Oxidation Reactions of Ti and TiN in SC-1 Solutions.

Metal	Oxidant	Reaction
Ti	H <sub>2</sub> O <sub>2</sub>	$Ti + 2H_2O_2 \rightarrow TiO^{++} + 2OH^- + H_2O$
Ti	HO <sub>2</sub> <sup>-</sup>	$Ti + 2HO_2^- + H_2O_2 \rightarrow TiO^{++} + 4OH^-$
TiN	H <sub>2</sub> O <sub>2</sub>	$TiN + 3H_2O + H_2O_2 \rightarrow TiO^{++} + 3OH^- + NH_4OH$
TiN	HO <sub>2</sub> <sup>-</sup>	$TiN + HO_2^- + 4H_2O \rightarrow TiO^{++} + 4OH^- + NH_4OH$

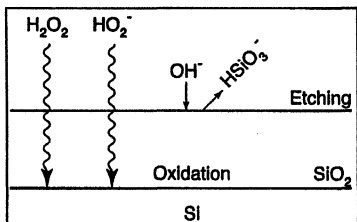


Figure1: Schematic of SC-1 Cleaning

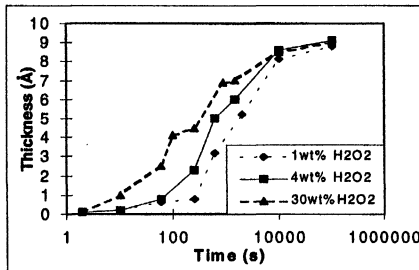


Figure 2: Oxide thickness as a function of time in H<sub>2</sub>O<sub>2</sub> solutions for 25 °C.[data taken from ref. 10,11]

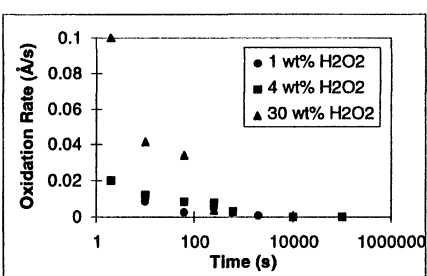


Figure 3a: Oxidation rate as a function of time.

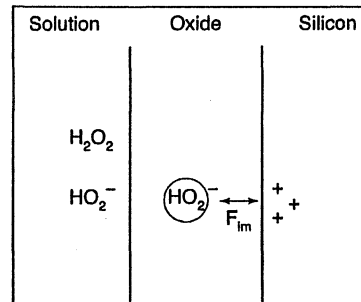


Figure 4: Schematic of Image Charge Transport.

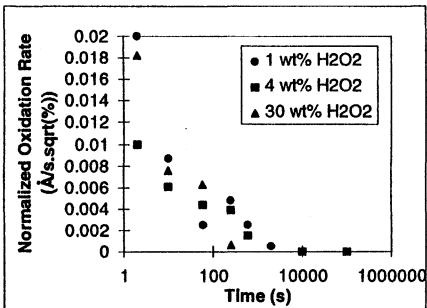


Figure 3b: Normalized (by  $\sqrt{\text{wt\% H}_2\text{O}_2}$ ) oxidation rate as a function of time.

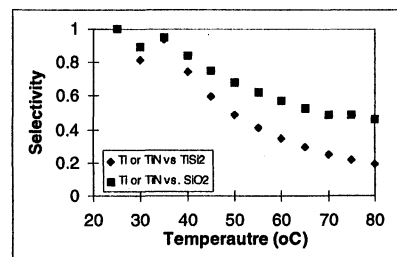


Figure 5. Selectivity of Ti or TiN etching versus SiO<sub>2</sub> and TiSi<sub>2</sub> etching in SC-1 solutions as a function of temperature.

## **WET CLEANING -HF Last Process**



# CHARACTERIZATION OF HF-LAST CLEANED Si FOR GATE OXIDES

Joong S. Jeon, Jeff S. Glick, Amir Jafarpour, and Bob Ogle

Advanced Micro Devices  
Sunnyvale, CA 94088-3453

Guangming Li and Srini Raghavan

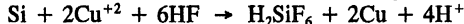
Department of Materials Science and Engineering  
University of Arizona  
Tucson, AZ 85721

## ABSTRACT

For the preparation of ultrathin gate oxides, HF-last pre-gate oxide cleaning methods were reviewed and characterized as one of pre-gate oxide cleaning techniques in terms of cleaning performances. The resulting cleaning efficiency was comparable to that of conventional standard RCA type cleaning. HF last cleaning combined with an IPA drying process demonstrated effective particle removals. It was found that HF-last cleaning improves charge-to-breakdown values of capacitors slightly. It was also observed that illumination increases Cu deposition on n-type and p-type Si wafers in dilute HF solutions. More Cu was deposited on Si surface in HF solutions than in SC1 solutions.

## I. INTRODUCTION

It has been shown that HF-last cleaning results in surfaces with low metallic contamination levels and yields hydrogen terminated Si surfaces which are stable against oxidation in room air [1,2]. However, HF-last cleaned surfaces are very susceptible to contamination by particles and noble metals such as Cu and Au. Thus, HF-last cleaning as a pre-gate oxide cleaning is still in dispute. It is known now that wafer drying methods play important roles in particle contaminations on HF-last cleaned hydrophobic surfaces. Also, copper ions present in HF solutions are known to deposit and contaminate Si surfaces in the HF immersion step by an electrochemical process [3-5] in which  $\text{Cu}^{+2}$  is reduced to Cu, and Si is oxidized to  $\text{Si}^{+4}$  according to the following equation :



To improve HF-last cleaning procedures, several HF based cleaning solutions were proposed. It has been shown that the addition of IPA into HF solutions is effective in reducing particulate contamination, and the addition of HCl or H<sub>2</sub>O<sub>2</sub> is found to be beneficial to prevent deposition of metallic contaminants, especially noble metals [6-8]. Also, treatment of HF-last cleaned wafers in ozonated water before drying steps, and H<sub>2</sub>SO<sub>4</sub>/O<sub>3</sub> or H<sub>2</sub>SO<sub>4</sub>/H<sub>2</sub>O<sub>2</sub> mixture replacing conventional SC1 and SC2 solutions have been introduced in connection with HF-last cleaning [9]. In addition, several noncontact instruments using surface photovoltages have been introduced to monitor HF-last cleaned or oxidized surfaces [10].

Conventional RCA cleaning processes induce approximately 10 Å thick chemical oxide which has lower density and has lower breakdown voltages than thermal oxide. As the thickness of gate oxide progressively decreases, the fraction of chemical oxide in thin gate thermal oxides increases significantly. Thus, this work was initiated to prepare ultrathin gate oxides with lower fractions of native oxides using a variety of HF-last cleaning techniques. For this work, Si samples were cleaned using HF-last cleaning recipes and dried with either a spin dryer or IPA dryer. The characterization of HF-last cleaning was focused on cleaning performances by (1) the measurements of metallic and particulate contamination levels as well as interface trap density and minority carrier diffusion length, (2) the evaluation of metallic contamination removal using challenge wafers intentionally contaminated with metallic ions in SC1 and HF solutions, (3) the evaluation of particle removal performance of HF-last cleaning recipes with dilute SC1, (4) the investigation of Cu deposition on n- and p-type wafers in the dark or under illumination, and (5) the evaluation of HF-last cleaning effect on gate oxide ( $t_{ox} < 50\text{\AA}$ ) integrity in terms of charge-to-breakdown values.

## II. MATERIALS AND EXPERIMENTAL PROCEDURES

All wafers, 200 mm p(100), used for this work were precleaned with a standard RCA cleaning process before experiments using commercially available cleaning tools. Unless otherwise specified, wafers were dried with an IPA dryer. Cleaning recipes used for HF-last cleaning are prepared with and without SC2 cleaning steps as follows:

- (1) Recipe HFL: HF - SC1 - SC2 - HF - Dry
- (2) Recipe NOSC2HFL: HF - SC1 - HF - Dry
- (3) Recipe Std. RCA: HF - SC1 - SC2 - Dry
- (4) Recipe SC1L: HF - SC1 - Dry

Std. RCA and SC1-last cleaning recipes were also prepared as reference cleaning recipes. Wafers cleaned using the above recipes were characterized in terms of metallic and particulate contaminations and surface charge as well as minority carrier diffusion length to evaluate cleaning efficiency. Challenge wafers for metallic contaminant deposition and removal tests were prepared. These wafers were intentionally contaminated with metals such as Cu, Al and Fe, etc. by conditioning them in metallic ion added SC1 (1:1:5 of

$\text{NH}_4\text{OH}:\text{H}_2\text{O}_2:\text{H}_2\text{O}$ ) solutions at 50°C. Also, for the investigation of surface states on metallic removal efficiency, wafers were contaminated by dipping in dilute HF solutions which had the same amount of metallic ions as SC1 solutions. The surface metallic contamination levels after cleaning were analyzed by a VPD-ICP MS technique.

For particle removal experiments, wafers contaminated with "natural" particles (less than 40/wafer) in a Fab. environment were used without any intentional particulate contaminations. The particles larger than 0.20  $\mu\text{m}$  were counted using an INSPEX (TPC 8530). Test wafers cleaned with a SC1-last cleaning recipe were prepared as reference samples for particle removal experiments.

For the characterization of Cu contamination in dilute HF (50:1) solutions, two different types of Si substrates were prepared: n(100) and p(100) Si wafers with resistivities of 20 to 50  $\Omega\text{cm}$  and 6 to 8  $\Omega\text{cm}$ , respectively. To investigate the effect of light on the extent of Cu depositions in HF solutions, experiments were performed both under illumination and in the dark conditions. For experiments under illumination condition, a 100 W tungsten lamp was placed 1 ft above HF solution container, while for experiments in the dark, the wafers were immersed in the dark and conditioned in the container inside a covered box in the dark with room light turned off. The resulting Cu deposition levels after conditioning in 10 ppb Cu containing 50:1 dilute HF solutions for 30 min were measured by a TXRF technique.

For the characterization of gate oxides prepared by Std. RCA and HF-last cleaning recipes, after oxidation, the interface trap density and oxide charge were measured by a surface charge analyzer (SCA, SemiTest Inc.). Minority carrier diffusion length and surface charge were also measured by a surface photovoltage (SPV) equipment (Semiconductor Diagnostics, Inc.). The oxide thickness including native oxides after cleaning was measured with an Optiprobe (Therma-Wave 2600). Gate oxide integrity was also analyzed for capacitors (area: 0.01  $\text{mm}^2$ ) with about 35 $\text{\AA}$  and 45 $\text{\AA}$  thick ultrathin gate oxides by the measurements of charge-to-breakdown values. The charge-to-breakdown was determined with a constant-current stress method using a current density of 200  $\text{mA}/\text{cm}^2$ .

### III. RESULTS AND DISCUSSION

The metallic contamination levels after cleaning using different cleaning recipes are shown in Fig. 1. It may be seen from this figure that no significant differences are found in the residual metallic contamination levels between HF-last and Std. RCA cleaned samples. Even without SC2 step in a HF-last cleaning sequence, low metallic levels were measured. As shown in Fig. 1, after HF-last cleaning, very low levels of Cu, below  $0.1 \times 10^{10}$  atoms/ $\text{cm}^2$ , were found, and slightly higher levels of Fe were measured compared to that of a sample cleaned with a Std. RCA cleaning recipe. This

low level of Cu contamination may due to the high purity of chemicals used for cleaning. Residual Al of about 2 to  $3 \times 10^{10}$  atoms/cm<sup>2</sup> levels was found on all samples cleaned with Std. RCA and HF-last cleaning recipes. After SC1-last cleaning, approximately  $50 \times 10^{10}$  atoms/cm<sup>2</sup> of Al and Fe were measured, and slightly high levels of other metallic contaminants were also found. It is well known that these contaminants are deposited on silicon surfaces in alkaline SC1 solutions due to the low solubility of these hydroxides in high pH solutions.

Fig. 2 shows the surface charge and minority carrier diffusion length values measured by a SPV technique before and after oxidation for wafers cleaned with different cleaning recipes. Before oxidation, the wafers cleaned with HF-last cleaning recipes showed higher surface charge and diffusion length values compared to Std. RCA cleaned wafers. This may be due to the difference in surface structures. In the case of SC1-last cleaned wafers contaminated with metallic contaminants, mainly Al and Fe, a similar diffusion length value and a lower surface charge value than those of Std. RCA cleaned samples were found. This low surface charge may be due to metallic contaminants inducing negative charges [11]. After oxidation (35 Å thick oxide), surface charge increased and diffusion length decreased significantly due to dissociated interstitial Fe as a recombination center. In contrast, wafers cleaned with Std. RCA and HF-last cleaning recipes revealed opposite behaviors.

Fig. 3 shows interface trap density and oxide charge measured by a surface charge analyzer. SC1-last cleaned samples were found to have lower oxide charge and higher trap density compared to other samples. HF-last cleaned samples showed oxide charges similar to Std. RCA cleaned samples. However, these samples were measured to have slightly higher interface trap density values than that of Std. RCA cleaned sample.

The particle count measurements before and after cleaning using 5 different cleaning recipes for wafers contaminated with an average number of 25 particles are shown in Fig. 4. As a reference, particle count data for wafers cleaned with a SC1 last cleaning recipe is also included. After a Std. RCA cleaning and SC1-last cleaning, an average of 8 and 13 particles/wafer were removed, respectively. In the case of HF-last cleaning recipes, it was noticed that average 7 and 5 particles/wafer were removed for the recipes of NOSC2HFL and HFL with an IPA drying process, respectively. This performance is very comparable to that of Std. RCA cleaning. It may be seen from this figure that the particulate contamination levels for HF-last cleaned hydrophobic samples are dependent on drying methods. When a spin dryer was used, thousands of particles were found on each wafer as shown in Fig. 4.

The number of particles removed or added as a function of the number of initial particles on wafers for three different cleaning recipes is shown in Fig. 5. As reported in other literature, particle addition rather than removal occurred for wafers which

initially had low numbers (i.e., below 10) of particles. Interestingly, all three curves were found to have nearly same slopes of  $\approx 0.5$ , and HF-last cleaning without SC2 step showed slightly better particle removal performance compared to the recipe of HF-last cleaning with SC2. With results of excellent particle removal performance for HF-last cleaning without SC2 step, two new cleaning recipes [(2) and (3)] with various dilution ratio of SC1 solutions were prepared as follows:

- (1) Recipe NOSC2HFL: HF-SC1 (1:1:5 of  $\text{NH}_4\text{OH}:\text{H}_2\text{O}_2:\text{H}_2\text{O}$ )-HF-Dry
- (2) Recipe DNOSC2HFL: HF-SC1 (1:4:20 of  $\text{NH}_4\text{OH}:\text{H}_2\text{O}_2:\text{H}_2\text{O}$ )-HF-Dry
- (3) Recipe VDNOSC2HFL: HF-SC1 (1:1:20  $\text{NH}_4\text{OH}:\text{H}_2\text{O}_2:\text{H}_2\text{O}$ )-HF-Dry

The particle removal/addition measurement results for above recipes are shown in Fig. 6. It can be seen from this figure that as the SC1 solution is diluted (less  $\text{NH}_4\text{OH}$  and  $\text{H}_2\text{O}_2$ ), the slopes of removal/addition lines become less steep and the crossover point moved to larger particle numbers indicating less effective particle removal performance. On the contrary, it has been shown that the removal efficiency for particles (nitrides and HF dip wafers) was affected slightly by  $\text{NH}_4\text{OH}$ , but not by  $\text{H}_2\text{O}_2$  [12].

For the investigation of metallic deposition and removal for different surface conditions, Si wafers were intentionally contaminated in two different kinds of solutions. Fig. 7 (a) and (b) shows metallic contamination levels on wafers contaminated in SC1 and diluted HF solutions containing metallic ions. It also shows metallic contamination levels after cleaning using three different HF-last cleaning recipes including dilute SC1 solutions. It is clearly seen that higher levels of Al, Fe, Ca and Zn are found on wafers conditioned in SC1 solutions compared to the wafers conditioned in diluted HF solutions. In contrast, higher levels ( $\approx 20\text{E}10$  atoms/cm<sup>2</sup>) of Cu are found on wafers contaminated in HF solutions than wafers conditioned in SC1 solutions indicating an electrochemical Cu deposition on bare Si surfaces. In SC1 solutions, less amount of Cu was measured possibly due to the chemical oxide layer hindering electron exchanges between Cu ions and Si atoms necessary for electrochemical Cu deposition. It has been also proposed that in the presence of Fe in SC1 solutions, less amount of Cu is deposited due to the interference of Fe on Cu deposition [13].

In an attempt to investigate the effect of surface states (i.e., oxide or bare surface) on the removal of metallic contaminants, these wafers were cleaned with three different cleaning recipes. Although HF-last cleaning recipes with dilute SC1 were not very effective in removing particles as shown in Fig. 6(b), contaminants such as Al and Fe deposited on Si surfaces in SC1 solutions were easily removed by HF-last cleaning as shown in Fig. 7(a). However, these contaminants deposited on hydrophobic Si wafers in HF solutions were hardly removed. These results indicate that most of these contaminants in SC1 are deposited on the top of oxide surfaces. Thus, metallic contaminants deposited in SC1 solutions could be removed by etching chemical oxides. It was also found that Cu deposited in HF is not easily removed by HF-last cleaning, and high levels of residual Cu after cleaning are found compared to that of wafers contaminated in SC1 solutions. It appears that for the effective removal of metallic

deposits on bare Si surface, acid and oxidizing agents are needed.

The amounts of Cu deposition on n-type and p-type wafers in dilute HF are shown in Fig. 8. It also shows the effect of light illumination on Cu deposition. It may be seen from this figure that no significant difference was found in Cu deposition between n-type and p-type wafers. However, light illumination enhanced Cu deposition by nearly one order of magnitude for both p-type and n-type of Si wafers.

As mentioned earlier, Cu deposition is an electrochemical reaction requiring charge transfers. Thus, deposition rate will be determined by the supply of charges. Fig. 9 shows energy level diagrams for Si with reducible species after aligning Fermi levels in solutions. In p-type Si wafers, the Fermi level of Si ( $E_{F,p} = 4.91$  eV) is lower than the redox potential of reducing species ( $E_{H+/H2} = 4.50$  eV). Band bending would then be present close to the silicon surface at a silicon/solution interface, and the silicon surface would be depleted of majority carriers (holes). Both conduction and valence bands would bend down as shown in Fig. 9. Thus, in the absence of illumination, the reaction rate may be expected to be small. While under illumination condition, many electron-hole pairs will be generated. This would provide sufficient carriers for redox reactions in solution. Therefore, under illumination, both the silicon dissolution rate and the amount of Cu deposition may be expected to increase significantly as shown in Fig. 8. In the case of n-type Si wafers, the Fermi level ( $E_{F,n} = 4.36$  eV) is higher than  $E_{H+/H2}$  (4.50 eV). When the Fermi levels and electrochemical potential of reducible species align, the Si surface would be depleted and both valence and conduction band would bend up (Fig. 9). The reaction rate for hydrogen reduction would then be slowed by the scarcity of electrons provided by silicon. Under illumination, as discussed for p-type Si wafers, reaction rate would be significantly improved.

Fig. 10 shows the effect of pre-gate oxide cleaning on charge-to-breakdown for capacitors with 35 Å and 45 Å thick gate oxides. The native oxide layer after cleaning was measured to be approximately 7.7 Å and 1.6 Å for Std. RCA and HF-last cleaned wafers, respectively. However, after oxidation for a 35 Å thick oxide layer, for example, the thicknesses of oxide layer was found to be 35.7 Å for Std. RCA and 35.3 Å for HF-last pre-gate oxide cleaned wafers. The removal of chemical oxide nearly did not affect the thickness of resulting thermal oxides. However, as shown in Fig. 10, small improvements in Charge-to-breakdown were observed for both 35 Å and 45 Å thick gate oxide capacitors.

#### IV. CONCLUSIONS

HF-last cleaning demonstrated very comparable cleaning performances to Std. RCA cleaning in terms of residual metallic and particulate contaminations as well as oxide charge and minority carrier diffusion length. It was observed that HF-last cleaning

slightly improves charge-to-breakdown of capacitors with 35Å and 45Å thick gate oxides. HF-last cleaning using IPA dryer showed effective particle removal. However, HF-last cleaning with dilute SC1 solutions degraded particle removal performances. The amount of metallic contaminant deposition, especially Cu deposition, depends on the types of solution and also Si surface properties. More Al and Fe were deposited on Si surfaces in SC1 solutions, while more Cu was found on wafers dipped in HF solutions. Light illumination enhanced Cu deposition on both n-type and p-type Si wafers by nearly one order of magnitude. This effect could be explained by band diagrams.

## REFERENCES

- [1] T. Takahagi, I. Nagai, A. Ishitani, H. Kuroda, and Y. Nagasawa, *J. Appl. Phys.*, **64**(7), 3516, 1988.
- [2] S. Verhaverbeke, J. Alay, P. Mertens, M. Meuris, M. Heyns, W. Vandervorst, M. Murrell, and C. Sofield, *Mat. Res. Soc. Symp. Proc.*, **259**, 391, 1992.
- [3] J. S. Jeon, S. Raghavan, H. G. Parks, J. K. Lowell, and I. Ali, *J. Electrochem. Soc.*, **143**, 2870, 1996.
- [4] G. Li, E. Kneer, B. Vermeire, H. Parks, J. S. Jeon and S. Raghavan, submitted to *J. Electrochem. Soc.*, 1997.
- [5] I. Teerlinck, P. W. Mertens, H. F. Schmidt, M. Meuris, and M. M. Heyns, *J. Electrochem. Soc.*, **143**, 3323, 1996.
- [6] S. Verhaverbeke, M. Meuris, M. Schackers, L. Haspeslagh, P. Mertens, M. M. Heyns, R. De Blank, and A. Philipossian, *Symp. on VLSI Tech. Digest of Tech. Papers*, p. 22, 1992.
- [7] I. Oki, H. Shibayama, and A. Kagisawa, *ECS PV 94-7*, 206, The Electrochemical Society, 1994.
- [8] F. Tardif, T. Lardin, C. Paillet, JP Joly, B. Beneyton, P. Patruno, D. Levy, K. Barla, and W. Sivert, *Microelectronic Engineering*, **28**, 121, 1995.
- [9] S. Verhaverbeke, H. F. Schmidt, M. Meuris, P. W. Mertens, M. M. Heyns, C. Werkhoven, R. De Blank, and A. Philipossian, Technical Conference, Semicon/Europe, '93, Geneva, Switzerland, 1993.
- [10] J. Ruzyllo, P. Roman, J. Staffa, I. Kashkoush, and E. Kamieniecki, *SPIE*, **2876**, 162, 1996.
- [11] H. Shimizu and C. Munakata, *Appl. Phys. Lett.*, **62**(3), 276, 1993.
- [12] K. K. Christenson, S. M. Smith, C. Bode, and K. Johnson, *ECS PV 95-20*, 597, The Electrochemical Soc., 1995.
- [13] H. Okuda, J. Ryuta, E. Morita, and Y. Shimanaki, *Mat. Res. Soc. Symp. Proc.*, **259**, 399, 1992.

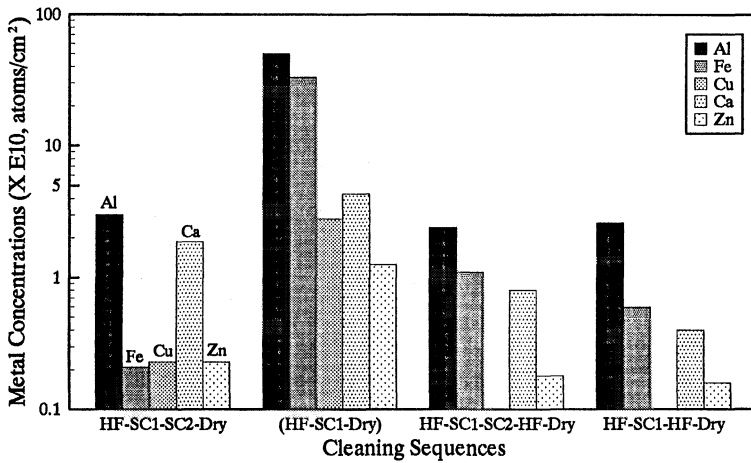


Fig. 1, Residual metallic contamination levels after cleaning using different cleaning recipes.

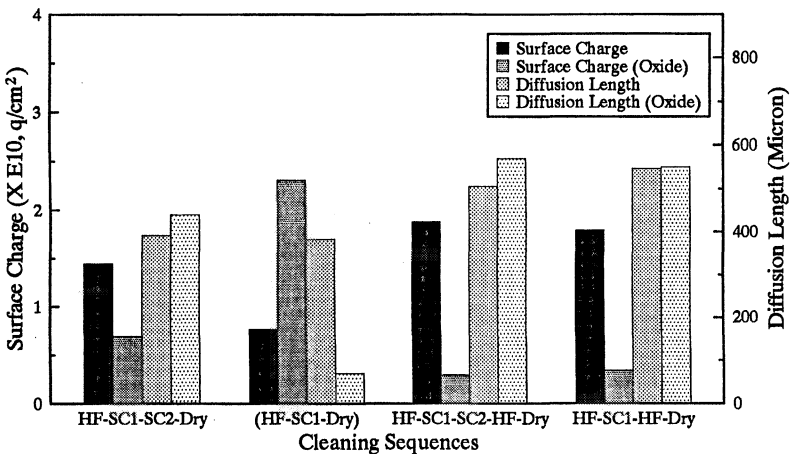


Fig. 2, Surface charge and diffusion length of Si wafers before and after oxidation for wafers cleaned with different cleaning recipes.

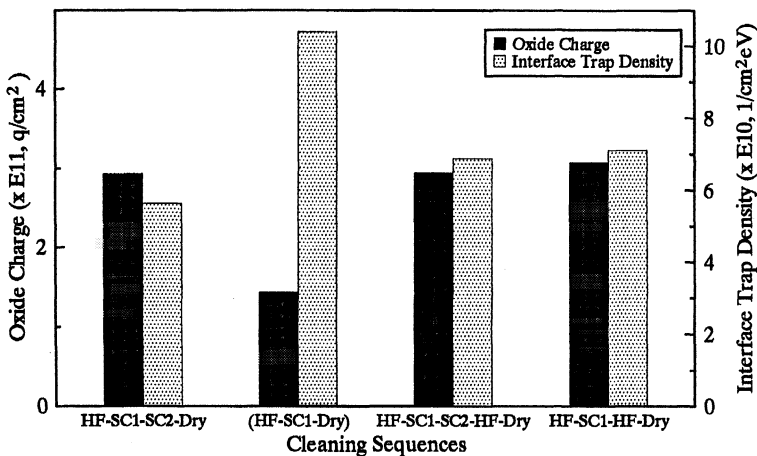


Fig. 3. Oxide charge and interface trap density of oxidized wafers after cleaning using different cleaning recipes.

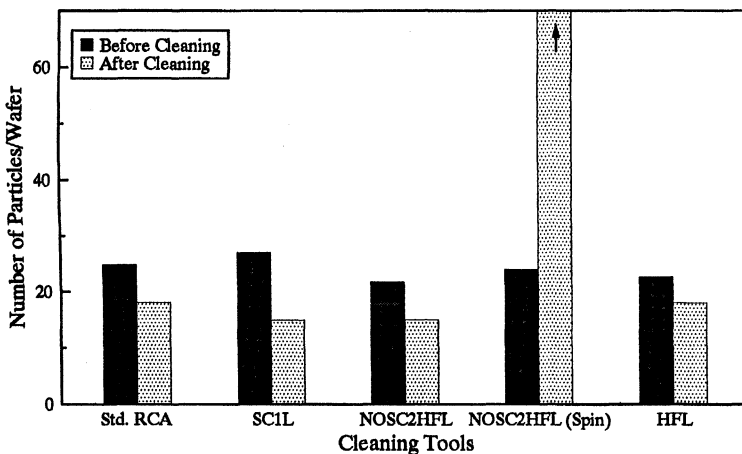


Fig. 4. Average number of particles before and after cleaning using different cleaning recipes.

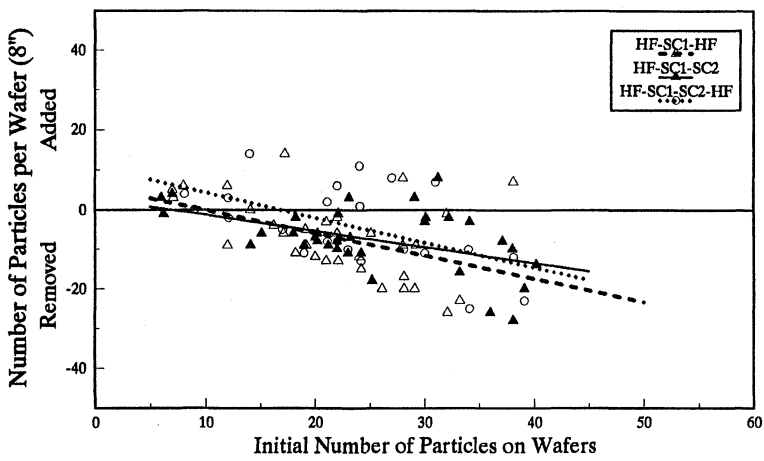


Fig. 5, Particle addition and removal as a function of the initial number of particles after cleaning using three different cleaning recipes.

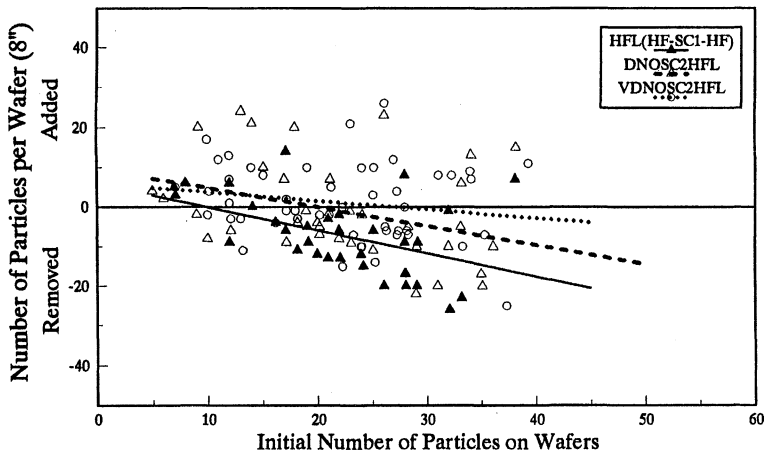
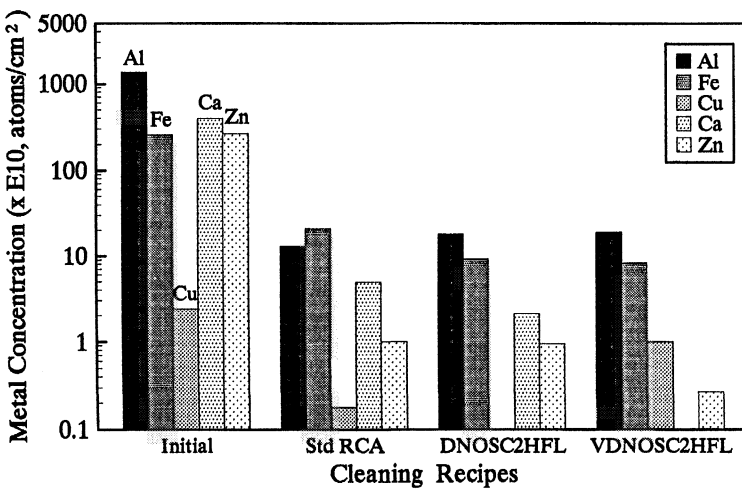
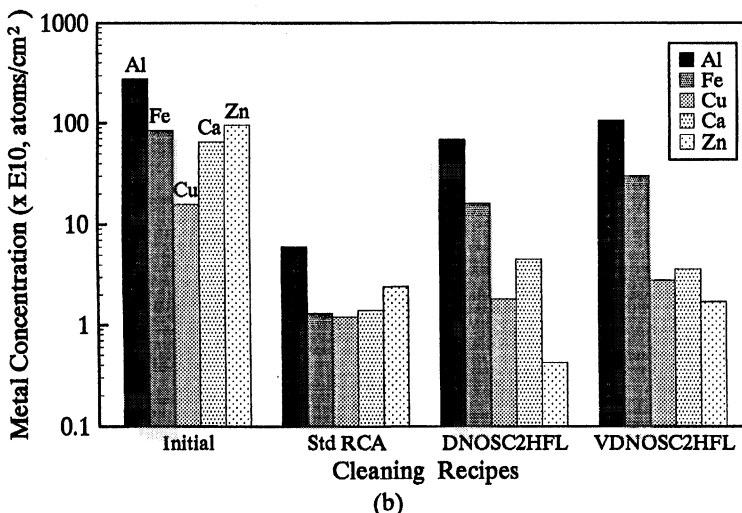


Fig. 6, Particle addition and removal as a function of the initial number of particles after cleaning using three different HF-last cleaning recipes.



(a)



(b)

Fig. 7, Metallic contamination levels before and after cleaning for wafers contaminated in (a) SC1 and (b) HF solutions containing metallic ions.

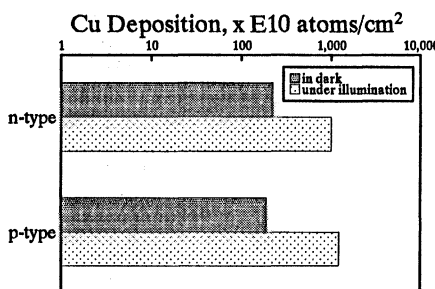


Fig. 8. Cu deposition on n-type and p-type Si wafers in the dark and under illumination in Cu containing dilute HF solutions.

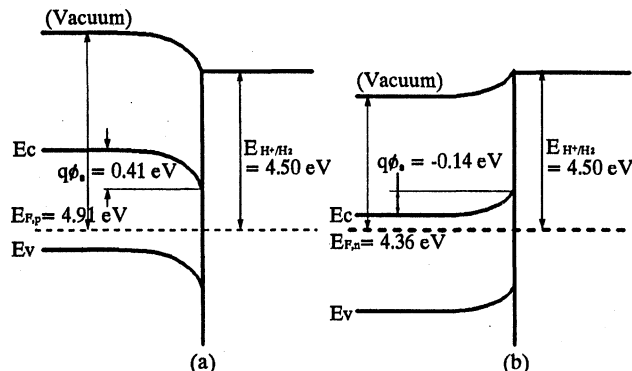


Fig. 9. Band diagrams of p-type and n-type Si wafers in a 50:1 dilute HF solutions.

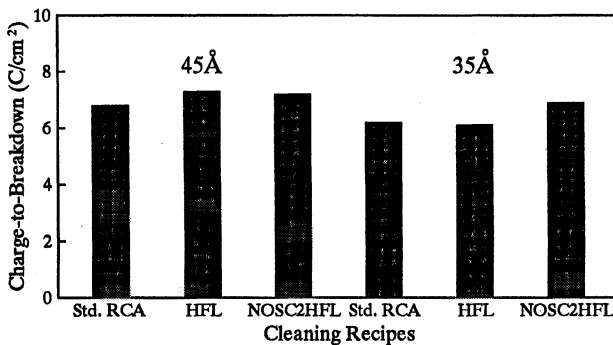


Fig. 10. Charge-to-breakdown of capacitors with 45 Å and 35 Å gate oxides.

## OPTIMISATION OF ETCHING UNIFORMITY AND REPEATABILITY IN DILUTED HF

E. Bellandi, M. Alessandri, A. Tonti, F. Pipia  
SGS-THOMSON Microelectronics, Via Olivetti 2, Agrate B<sup>za</sup> (MI), Italy

K. Wolke, M. Schenkl  
STEAG MicroTech, Carl-Benz Straße 10, Pliezhausen, Germany

M. Geomini, L.F.Tz. Kwakman  
PHILIPS Semiconductors, Gerstweg 2, Nijmegen, The Netherlands

### ABSTRACT

Diluted HF solution (DHF) from 0.1% to 1% is becoming more important as the most critical step in cost effective and manufacturable alternatives to the standard RCA cleaning, like the IMEC Twin-Clean™ and the LETI DDC cleaning concepts. For low etching times several factors must be considered to achieve an optimal etching uniformity and repeatability, such as dip-time itself, organic contamination, wafer pre-wetting.

In order to balance those factors a software algorithm applied to an inductive HF concentration monitor has been designed.

### INTRODUCTION

The actual SC1 process is performed at low temperatures or low ammonia concentration. In this condition a considerably low oxide etch rate is observed. Therefore when an etching chemistry, based on DHF, is adopted, major integration problems on real devices may appear, because of the presence of exposed and unprotected oxides on the same device, such as field oxides, ONO stacks and differential gate oxides (see figure 1). Because of these constraints, important changes to the process flow are necessary and, secondly, strict control of etch uniformity and repeatability of the HF chemistry is a key issue to achieve good and reproducible final oxide quality.

## EXPERIMENTAL

A STEAG MicroTech third generation automated wet bench, capable to process up to 50 six inch wafers per batch, has been used to evaluate and optimise etching uniformity and repeatability of diluted HF solutions. Target values were set at  $\pm 1\%$  in range for across wafer uniformity, across batch uniformity and batch to batch uniformity, with a maximum of 5.0 nm etched thermal oxide.

In all experiments, the etch rate has been evaluated on thermal oxide grown on three test wafers placed in the front, centre and rear of the batch. Silicon dummy wafers have been used to fill-up empty slots. The oxide thickness before and after etching has been accurately measured using a Tencor UV1250SE spectroscopic ellipsometer.

Immersion and extraction speed of the robotic handler was fixed to its highest value, and the transfer speed from the HF tank to the rinse tank set to a mechanically safe upper value.

Temperature has been set to  $21^\circ \pm 0.1^\circ$ .

Immersion and extraction time has been estimated in 1-2 seconds, while typical transfer time is 5-7".

## RESULTS AND DISCUSSION

To evaluate the relative impact of the transfer and immersion times, etch rate has been measured using different HF dip immersion times. Results are reported in figure 2 for a 0.36% HF (9 measurement points per wafer, 100 nm thick oxides) solution. In the same graph it is also reported the effect of different pre-wetting treatments prior to the HF dip (first step of the Twin-Clean process).

The apparent increase of the etch rate for short dip times is due to the ongoing etching during the extraction and transfer time, and the diffusion of the rinsing water into the HF carry-over layer. This phenomenon can be described by the following relation:

$$R_{\text{eff}} = \frac{\Delta t h}{t} = \frac{R \cdot t_{\text{eff}}}{t} \quad (1)$$

Where:  $\Delta t h$  is the amount of etched oxide, R and  $R_{\text{eff}}$  are the etch rate of the solution and the effective (measured) etch rate, respectively. t and  $t_{\text{eff}}$  are the dip time and the effective etching time, respectively.

$t_{\text{eff}}$  depends on the average introduction time ( $t_{\text{in}}$ ), the average extraction time ( $t_{\text{out}}$ ), the transfer time from the HF tank to the rinse tank ( $t_{\text{transf}}$ ) and the time needed to diffuse the rinsing water into the HF carry-over layer ( $t_{\text{diffH}_2\text{O}}$ ). The latter must be considered as

an average contribution, because the HF concentration on the wafer surface in the rinsing tank decays exponentially.

The effective etching time can be approximated as:

$$t_{\text{eff}} = t_{\text{in}} + t + t_{\text{out}} + t_{\text{transf}} + t_{\text{diffH}_2\text{O}} \quad (2)$$

In case of pre-wetting treatments prior to HF dip, the water carry-over layer must be taken into account. In this case the previous relation becomes:

$$t_{\text{eff}} = t - t_{\text{diffHF}} + t_{\text{out}} + t_{\text{transf}} + t_{\text{diffH}_2\text{O}} \quad (3)$$

In case of wet wafers,  $t_{\text{in}}$  is not taken into account because water carry-over prevents oxide etching during the immersion step.

The time required for HF to diffuse into the  $\text{H}_2\text{O}$  carry-over layer decreases the effective etching time and it is proportional to the carry-over thickness. In figure 3 the two cases ( $\text{H}_2\text{O}$  through HF in the rinse tank and HF through  $\text{H}_2\text{O}$  in the HF tank) are represented.

In case of very long dip times,  $t_{\text{eff}} \sim t$ , the etch rate becomes stable and independent from the pre-etch treatment.

The presence of organic contaminants on the top of the oxide, mainly generated by the clean room HEPA filters, impacts on the optical thickness measurement, and therefore on the correct etch rate measurement.

In fact the presence of an organic layer increases the measured optical thickness, and its thickness strongly depends on the exposure time to clean room air. After one day exposure this increasing can be as high as 5-7 Å.

Figure 4 shows a ToF SIMS analysis of a bare silicon wafer exposed to clean room air for several months.

In the same figure, it is clearly shown that a simple DIW rinse can however remove most of the contaminants. Therefore after an HF etching, no more contaminants are expected on the oxide surface, and the real amount of etched oxide ( $\Delta t_h$ ) is therefore:

$$\Delta t_h = \Delta t_{h_{\text{meas}}} - t_{\text{org}} \quad (4)$$

Where  $\Delta t_{h_{\text{meas}}}$  is the measured etched thickness and  $t_{\text{org}}$  is the oxide equivalent thickness of the organic layer.

Figure 5 shows the etch rate as a function of dip time for wafers exposed to clean room air and pre-cleaned ones. Measurement has been taken on 17 points per wafer, using 20 nm thick oxides. From the fit of that data, a 2.5 Å thick organic layer has been found.

To overcome this measurement problem oxide wafer should be cleaned before etch rate measurements and clean room air exposure must be avoided.

The across wafer etch uniformity for a 0.36% HF solution as a function of etch time and pre-HF treatment is given in figure 6. The uniformity is considerably worse for short dip times.

In case of dry wafers (without pre-wetting treatment), the non-uniformity is mainly due to the extraction time, while in case of wet wafers, non-uniformity is supposed to be related to the water carry-over non-homogeneity. Figure 7 shows typical thickness maps in case of dry (left) and wet (right) wafers. In case of dry wafers, there is a top-bottom gradient. This gradient fits with the hypothesis that the uniformity is dominated by the introduction and extraction times. In case of wet wafers, a more radial symmetry has been found. This etch pattern can be the result of the combined effects of insertion/extraction times and the presence of a non-uniform water carry-over layer.

The carry-over layer non-uniformity, due to the pre-etch step, seems to be a contributing factor also for the across batch uniformity. However, the original target value for this parameter has been achieved without major problems, since it is easily tuned by changing the HF flow distribution inside the tank (HF re-circulation speed).

To achieve a batch to batch uniformity below  $\pm 1\%$  for the equivalent etched oxide thickness and to increase, at the same time, the lifetime of the solution, it is necessary either to control accurately the HF concentration or to continuously change the etch time taking into account the etch rate evolution. To this extend, a real-time inductive sensor (Horiba) has been tested as a monitoring system for HF concentration. This sensor measures the conductivity of the HF solution in a wide concentration range, and supplies a direct read-out of the HF concentration with an accuracy of  $\pm 0.001\%$ .

To correlate the HF sensor readout with the etch rate measurements, etch rate has been measured during the HF bath life time. Over a five days period an increase of the bath etch rate has been observed (figure 8). This behaviour is probably due to the distillation effect caused by the non-negligible evaporation of the water whereby the HF bath concentration tends to increase.

In figure 9 it is shown the correlation between the concentration read out and the etch rate measurement. The trend, in this small concentration range, appears to be linear. Moreover the correlation between concentration monitor and HF concentration is not lost in the five days period, due to etch products dissolved in the liquid. (total amount of oxide etched  $\sim 0.03$  mol).

Within the experimental window explored, the linear fitting of the parameters allows to predict the etch rate from the HF sensor measurements with an absolute error (including measurement)  $< 1\%$ . An accurate real-time etch rate estimate is therefore possible using this concentration monitoring system, whose readout is used by a software package that automatically corrects the etch time to maintain the total amount of etched oxide constant, allowing also transfer/diffusion time corrections for wet and dry wafer cases.

The HF sensor has been also tested when spiking HCl and IPA into the HF bath. Conductivity is strongly affected by HCl spiking because of its high dissociation

degree, hence a concentration monitoring system can not be used in case of HF/HCl mixtures. IPA concentrations lower than 0.2% does not seem to affect concentration read out.

## CONCLUSIONS

Accurate oxide etching in diluted HF solutions has been demonstrated to be affected from several factors. For low HF concentrations and small amount of etched oxide, organics deposition on test wafers and transfer and diffusion time are a dominant factor, both for etch rate control and etching uniformity optimisation.

An inductive concentration monitor has been used to compensate the etch rate fluctuations through a linear correlation model, while a software algorithm has been developed to take into account transfer and diffusion times for dry and pre-wetted wafers.

This work has been supported by the Esprit SEA Project nr.20757 "Autowet"

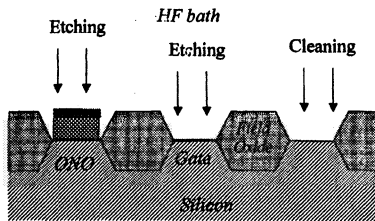


**Figure 1:** Etching of differential oxide

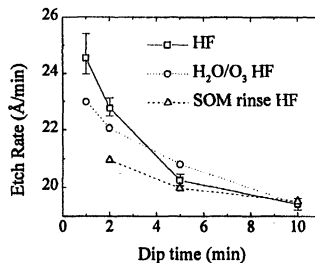


**Figure 2:** Etch rate as a function of dip time for wet and dry wafers

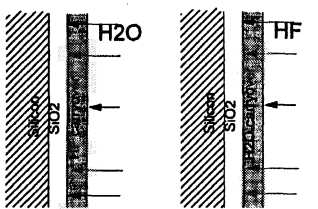


**Figure 3:** a) Water diffusion into HF carryover.  
b) HF diffusion in water carryover

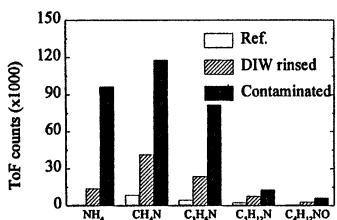


Figure 4: ToF SIMS analysis of a bare silicon wafer exposed to clean room air for several months.

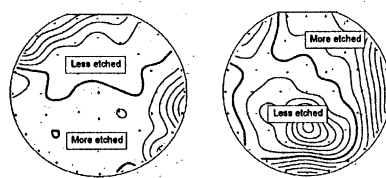


Figure 7: Etch rate maps for dry (left) and wet wafers (right).

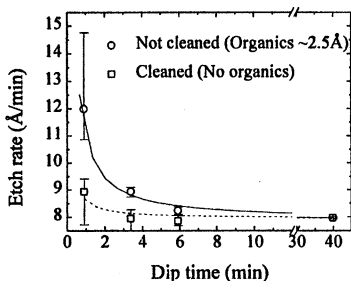


Figure 5: Etch rate as a function of dip time with and without pre-cleaning: influence of the organic contamination.

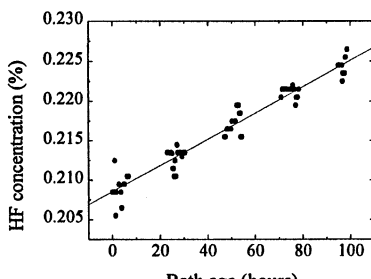


Figure 8: HF concentration as a function of bath age.

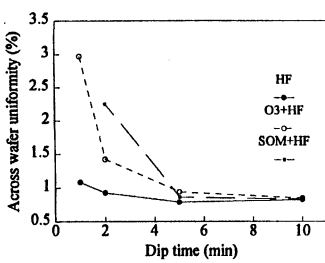


Figure 6: Across wafer uniformity as a function of dip time for wet and dry wafers.

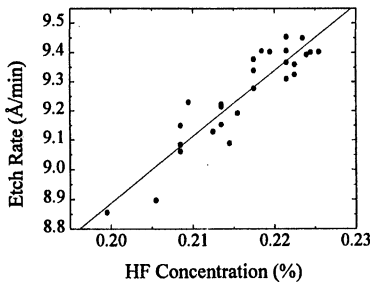


Figure 9: Correlation between Horiba concentration monitor and etch rate.

## H-TERMINATION ON Ge(100) AND Si(100) BY DILUTED HF DIPPING AND BY ANNEALING IN H<sub>2</sub>

Masao Sakuraba,\* Takashi Matsuura and Junichi Murota

Laboratory for Electronic Intelligent Systems  
Research Institute of Electrical Communication, Tohoku University  
2-1-1 Katahira, Aoba-Ku, Sendai 980-77, Japan.

H-termination on Ge(100) and Si(100) by diluted HF (DHF) solution dipping and by annealing in H<sub>2</sub> at 700°C was investigated. Coverage of Ge-hydride on the DHF dipped Ge(100) showed the maximum value around the HF concentration of 20%, while the Ge-hydride almost disappeared during the deionized water rinse for 5 minutes. In the DHF solution, H-termination is formed and maintained, which suggests that Ge-oxide removal process proceeds faster than Ge-oxide growth process. On the other hand, a sharp absorption peak was observed in the Fourier transform infrared spectroscopy from the ordered dimer structure formed by annealing in H<sub>2</sub>. H-termination of Ge(100), which was generated either by DHF dipping or by annealing in H<sub>2</sub>, decreased with surface oxidation much faster than the case of Si(100) during air exposure, although the characteristics of H-terminations of Ge(100) and Si(100) are qualitatively similar.

### INTRODUCTION

Si<sub>1-x</sub>Ge<sub>x</sub> (0 < x < 1) alloy films have been applied to various Si-based heterostructures (1-3), such as heterobipolar transistors and high electron/hole mobility transistors. Si-based atomically-controlled heterostructures are very attractive for the future high performance device. In atomically-controlled processes (4-6) using an ultraclean low temperature reaction environment of low pressure chemical vapor deposition (LPCVD), atomic-order ultrathin layer growth of Si on Ge(100) and Ge on Si(100) was greatly affected by H-termination on the initial surfaces (7,8). Although H-termination on the Si surface has been reported by many investigators (9,10) and H-termination on the Ge surface has been investigated mainly in an ultra-high vacuum environment (11), a successful H-termination on the Ge surface in the atmospheric pressure condition is scarcely reported.

In our previous work (12), it was suggested that the H-terminated Si dimer structure formed during ultraclean H<sub>2</sub>-cooling after CVD Si epitaxy on Si(100) revealed an excellent stability in air. In the present work, H-termination and its

\*Corresponding Author. FAX:+81-22-217-5565, e-mail:sakuraba@riec.tohoku.ac.jp

stability on Ge(100) as well as Si(100) were investigated in relation to the surface treatment condition.

## EXPERIMENTAL

The substrates used were the p-type Si(100) wafers of 2–20 ohm·cm with a mirror polished surface. As a Ge(100) substrate, the epitaxial Ge film (about 3000Å-thick) on Si(100) was grown by an ultraclean LPCVD system using  $\text{GeH}_4$  and  $\text{H}_2$  gases at 350°C (13). Wet chemical treatment of the substrates was examined by dipping into diluted HF (DHF) solutions with various HF concentration. For some of the chemically treated substrates, annealing and cooling in the  $\text{H}_2$  environment at 500Pa using the ultraclean LPCVD furnace (14) ( $\text{H}_2$ -annealing) was also examined. After the above treatments, coverages of Ge-hydrides and Si-hydrides were measured in  $\text{N}_2$  purged environment by the Fourier-transform infrared reflection absorption spectroscopy (FTIR/RAS) with multiple reflection. Evaluation of the native oxide growth on the substrates was performed by using the peak area ratio of the chemically-shifted peak to the core level emission peak of Ge 3d or Si 2p in x-ray photo-electron spectroscopy (XPS). The surface reconstructed structures were evaluated by reflection high-energy electron diffraction (RHEED). During the transport to each evaluation apparatus, the samples were exposed to cleanroom air (relative humidity (RH) of about 25% or 46%) for a few minutes.

## RESULTS AND DISCUSSION

Figure 1 shows the FTIR/RAS absorption spectra of the Ge(100) and Si(100) (a)(c)after DHF dipping for 2 minutes and (b)(d)after  $\text{H}_2$ -annealing at 700°C for 60 minutes and also cooling in  $\text{H}_2$  down to below 100°C. Here, HF concentration of DHF is 20% for Ge(100) and 0.5% for Si(100). After DHF dipping, broad absorption peaks were observed at  $\sim 2108\text{cm}^{-1}$  for Si(100) assigned as Si-dihydride (15) and  $\sim 2008\text{cm}^{-1}$  for Ge(100). The absorption wavenumbers are about  $100\text{cm}^{-1}$  different mainly due to differences of the binding force and the atomic weight between Si-H and Ge-H. After  $\text{H}_2$ -annealing, sharp absorption peaks are observed at  $\sim 2100\text{cm}^{-1}$  for Si(100) assigned as Si-monohydride in the dimer (16) (dimer monohydride), and at  $\sim 1992\text{cm}^{-1}$  for Ge(100). RHEED patterns of both the  $\text{H}_2$ -annealed Ge(100) and Si(100), taken just after air-exposure (25% RH) within 5 minutes, showed the sharp 2-fold streaks originated from the ordered dimer structure along the [011] azimuth due to the surface reconstruction. So, the sharp absorption peak at  $\sim 1992\text{cm}^{-1}$  can be also assigned as the dimer monohydride on Ge(100). For either Ge(100) or Si(100), the absorption peak position for the  $\text{H}_2$ -annealed surface is apparently shifted lower than that for the DHF dipped surface, that is, a wavenumber for the dimer monohydride is slightly lower than that for the dihydride. Thus, the characteristics of the spectra for Ge(100) and Si(100) are very similar, and similar H-termina-

ted structures are expected both on Si(100) and on Ge(100).

Figure 2 shows the HF concentration dependences of the FTIR absorbance of Ge-hydride and the time to DHF repelling just after picking up the sample from the DHF solution in air. After the DHF dipping for 2 minutes and the air exposure within a minute, the substrate was set into the N<sub>2</sub> purged FTIR/RAS apparatus. It is well known that the DHF dipped Si(100) has a hydrogen absorbed layer terminating the dangling bonds by using as low HF concentration as 1% (10), and easily shows a hydrophobicity. On the other hand, for the case of the DHF dipped Ge(100), higher HF concentration than 10% is more effective to obtain the hydrophobic H-terminated surface. However, too high HF concentration results in a decrease of H-termination. Takahagi et al. have reported that fluorine concentration on the DHF dipped Si(100) increases with the increase of HF concentration. In the same manner, the decrease of H-termination on Ge(100) in higher HF concentration region is considered to be due to termination not only by hydrogen atoms but also by fluorine atoms.

Figure 3 shows the deionized water (DIW) dipping time dependences of the FTIR absorbance of Ge-hydride and the XPS intensity of Ge-oxide on the 20%-DHF dipped Ge(100). The DIW was maintained pouring into the quartz beaker from upside in air and overflowing during the dipping. On the initial DHF dipped Ge(100), the Ge-oxide intensity is very low and the Ge-hydride is observed on the surface, which showed a hydrophobicity for the DHF solution as shown in Fig. 2. Within a few minutes, Ge-hydride rapidly decreases and Ge-oxide grows during DIW dipping. From these results, it is considered that the H-termination is formed and maintained in the DHF solution in which Ge-oxide removal process proceeds faster than Ge-oxide growth process. Ogawa et al. have shown the results that the dissolved oxygen (DO) in DHF solution plays an important role in H-termination on DHF dipped Si and explained that the Si etching rate on H-terminated Si surface would be related to the oxidation by DO (17). Therefore, it should be mentioned that the characteristics of H-termination as shown in Figs. 3 and 4 may depend on dissolved oxygen concentration (DOC) in DIW and/or DHF solution, because no special procedure to reduce the DOC was done in our present experiments for the Ge surface.

Figure 4 shows the air exposure time dependences of the FTIR absorbances of Ge-hydride and Si-hydride on the H<sub>2</sub>-annealed Ge(100) and Si(100). Under the annealing and cooling condition, dissociation of H<sub>2</sub> molecules results in H-termination of dangling bonds and highly stabilized reconstructed dimer monohydride on Si(100) can be obtained (12). In the case of Ge(100), the similar H-adsorption process is considered to proceed and to form the dimer monohydride from the results shown in Fig. 1. As shown in Fig. 4, the absorbance of each dimer monohydride decreases with the air exposure time. It is also clear that the decay time of the absorbance of the Ge(100) is much shorter than that of the Si(100). Correspondingly, the 2-fold streaks in RHEED pattern of Ge(100) almost disappeared after the air-exposure for 25 minutes, while that of Si(100) scarcely weakened after the air-exposure for 60

minutes. These results show that the Ge dimer monohydride possesses the stability in air for much shorter time than the Si dimer monohydride.

Figure 5 shows the air exposure time dependences of the XPS intensities of the oxides on Si(100) and Ge(100). RH of the air is 25% for Ge(100) and 46% for Si(100). Here, the DHF treatment was performed by dipping in 20%-DHF for 2 minutes for Ge(100), and in 2%-DHF for 30 seconds and DIW rinse for 3 minutes for Si(100). There is little difference between the DHF treatment and the H<sub>2</sub>-annealing, but there exists a large difference between the oxidation times of Si(100) and Ge(100). H-terminated Ge(100) is oxidized and  $I_{Ge-O}/I_{Ge}$  reaches around 0.2 for 30 minutes in air, corresponding to the disappearance of H-termination on Ge(100) as shown in Fig. 4. It is known by comparing Figs. 3 and 5 that the  $I_{Ge-O}/I_{Ge}$  value after DIW-dipping is smaller than that after air-exposure. This may be caused by the different oxidation processes in air and in DIW, that is, oxidation would depend on RH of the air and DOC of DIW.

In conclusion, H-termination of Ge(100) as well as Si(100) is formed either by DHF dipping or by annealing in H<sub>2</sub>. The characteristics of H-terminations of Ge(100) and Si(100) are qualitatively similar, although H-termination of Ge(100) has much weaker stability against oxidation in air or in DIW than the case of Si(100).

#### ACKNOWLEDGMENTS

This study was carried out in the Superclean Room of the Laboratory for Electronic Intelligent Systems, Research Institute of Electrical Communication, Tohoku University. This study was partially supported by a Grant-in-Aid for Scientific Research from the Ministry of Education, Science, Sports and Culture of Japan, the Research for the Future (No. JSPS-RFTF97P00202) from the Japan Society for Promotion of Science, and the Murata Science Foundation. Paper presentation was partially supported by the Telecommunications Advancement Foundation, Japan.

#### REFERENCES

1. S. S. Iyer, G. L. Patton, J. M. C. Stork, B. S. Meyerson and D. L. Harame, IEEE Trans. Electron Devices, **ED-36**, 2043 (1989).
2. J. C. Bean, Proc. IEEE, **80**, 571 (1992).
3. B. S. Meyerson, Proc. IEEE, **80**, 1592 (1992).
4. M. Sakuraba, J. Murota, N. Mikoshiba and S. Ono, J. Crystal Growth, **115**, 79 (1991).
5. J. Murota, M. Sakuraba and S. Ono, Appl. Phys. Lett., **62**, 2353 (1993).
6. J. Murota, M. Sakuraba, T. Watanabe, T. Matsuura and Y. Sawada, J. Phys. IV France, **5**, C5-1101 (1995).

7. T. Watanabe, M. Sakuraba, T. Matsuura and J. Murota, *Jpn. J. Appl. Phys.*, **36**, 4042 (1997).
8. S. Kobayashi, M. Sakuraba, T. Matsuura, J. Murota and N. Mikoshiba, *J. Crystal Growth*, **174** (in press).
9. Y. J. Chabal, *J. Vac. Sci. Technol. A*, **3**, 1448 (1985).
10. T. Takahagi, I. Nagai, A. Ishitani, H. Kuroda and Y. Nagasawa, *J. Appl. Phys.*, **64**, 3516 (1988).
11. L. Papagno, X. Y. Shen, J. Anderson, G. S. Spagnolo and G. J. Lapeyre, *Phys. Rev. B*, **34**, 7188 (1986).
12. M. Sakuraba, J. Murota and S. Ono, *J. Appl. Phys.*, **75**, 3701 (1994).
13. S. Kobayashi, M-L. Cheng, A. Kohlhase, T. Sato, J. Murota and N. Mikoshiba, *J. Crystal Growth*, **99**, 259 (1990).
14. J. Murota and S. Ono, *Jpn. J. Appl. Phys.*, **33** 2290 (1994).
15. B. W. Sheldon and J. S. Haggerty, *J. Am. Ceram. Soc.*, **74**, 1417 (1991).
16. O. Vatel, S. Verhaverbeke, H. Bender, M. Caymax, F. Chollet, B. Vermeire, P. Mertens, E. Andre and M. Heyns, *Jpn. J. Appl. Phys.*, **32**, L1489 (1993).
17. H. Ogawa, K. Ishikawa, M. T. Suzuki, Y. Hayami and S. Fujimura, *Jpn. J. Appl. Phys.*, **34**, 732 (1995).

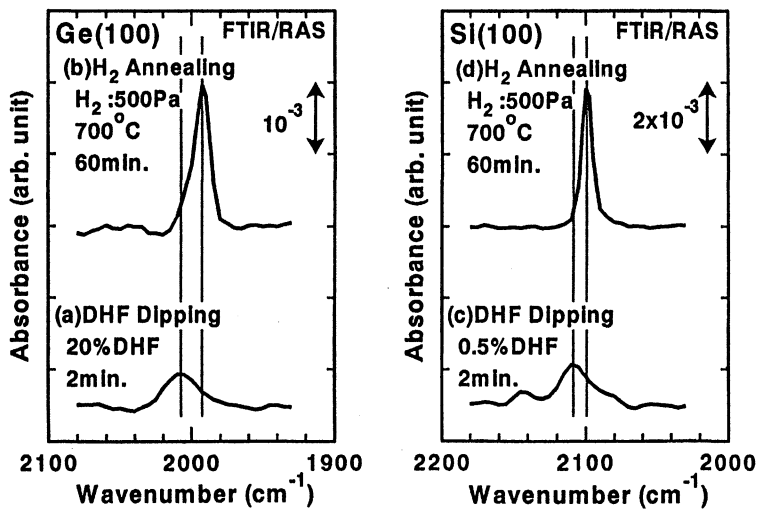


**Figure 1.** FTIR/RAS absorption spectra of the Ge(100) and Si(100) (a)(c)after DHF dipping for 2 minutes and (b)(d)after H<sub>2</sub>-annealing at 700 °C for 60 minutes and also cooling in H<sub>2</sub> down to below 100 °C.

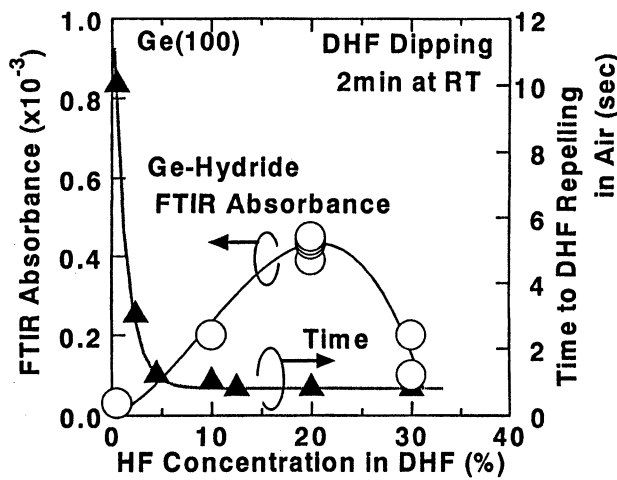


**Figure 2.** HF concentration dependences of the FTIR absorbance of Ge-hydride and the time to DHF repelling just after picking up the samples from the DHF solution in air.

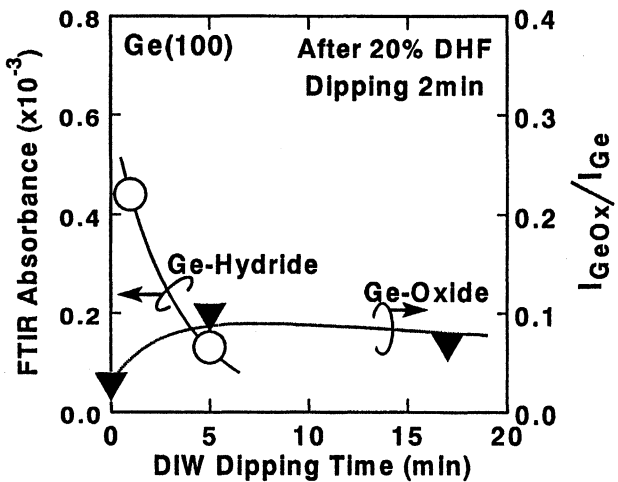


**Figure 3.** DIW dipping time dependences of the FTIR absorbance of Ge-hydride and the XPS intensity of Ge-oxide.

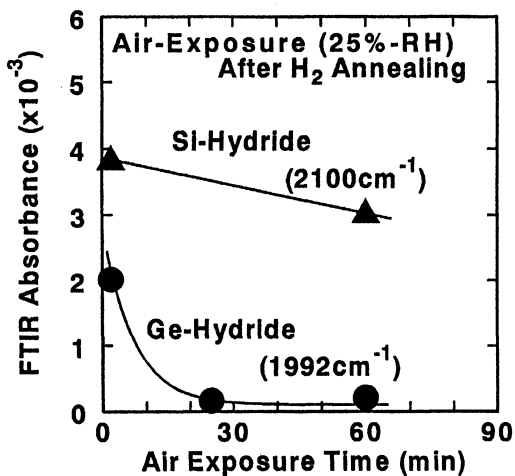


**Figure 4.** Air exposure time dependences of the FTIR absorbances of Ge-hydride and Si-hydride.

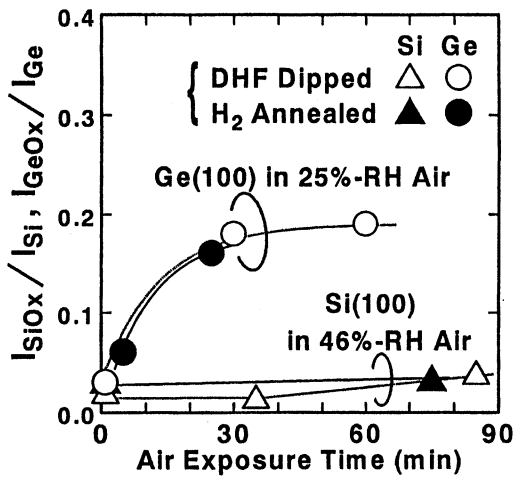


Figure 5. Air exposure time dependences of the XPS intensities of oxides on Ge(100) and Si(100).

# IN-LINE MONITORING OF HF-LAST CLEANING OF IMPLANTED AND NON-IMPLANTED SILICON SURFACES BY NON-CONTACT SURFACE CHARGE MEASUREMENTS

E. Kondoh, M.-A. Trauwaert, M. Heyns, and K. Maex

IMEC, Kapeldreef 75, 3001 Leuven, Belgium.

Silicon surfaces after HF-last cleaning were characterized by space charge measurements. A satisfactory good agreement was confirmed between space charge parameters and cleaning conditions. The growth of native oxide after HF-last cleaning was monitored comparatively with *in-situ* ellipsometry. The presence of top oxide layer on ion-implanted wafers were detected precisely. The most distinguished parameter was found to be minority carrier recombination lifetime.

## INTRODUCTION

Since wet etching by a dilute HF solution is the final procedure before silicon metallization thus is crucial for metal/silicon contact quality. Although the chemistry of Si surface during and after HF etching have been extensively studied, less attention has been paid to implanted surfaces. Low energy and high dose conditions for shallow junction formation, require more precise in-line approaches to characterize wafer surface conditions. Hydrophobicity, which appears during HF etching, is well-known as a good indicator of the completion of surface hydrogen-passivation. However, the hydrophilic-hydrophobic transition is not so clear on ion-implanted wafers as in the case of non-implanted wafers because of small water contact angle. This induces excess etching, leading to the damage of dielectric layers that define transistors and their performance. Non-destructive and non-contact surface charge measurements are attractive as a fab-level in-line monitor for surface characterization. This paper reports the use of surface charge measurement in monitoring HF-last cleaning of both implanted and non-implanted Si wafers. In the first instant, *in-situ* surface charge measurements are carried out on non-implanted Si wafers, in order to obtain reference data. *In-situ* ellipsometry is employed comparatively to support the surface charge data. Implanted wafers are then studied, and compared to the results on non-implanted wafers.

## SURFACE CHARGE MEASUREMENT

In this study, surface charge measurements were carried out by Space Charge Profiler (SCP) of QC solution, Inc. The principle of the SCP is the measurement of alternating-current surface photovoltage which corresponds to the change of surface barrier height (1). When light with a short wavelength is illuminated into the surface depletion layer, which originates from surface charge, photoexcited minority carriers pile up in the surface, while the majority carriers sweep to the bulk. This induces the dipolarization opposite to the surface electric field and reduces the surface barrier height. The recombination of the minority carriers proceeds while the light being not illuminated, so that the minority carrier lifetime can be measured from the response to the chopped light. The SCP tool determines

the following physical parameters under some assumptions which include the use of bulk Si and the homogenous distribution of the dopant.

- *Surface conductive type* is determined from the phase shift of ac-SPV.
- *Depletion layer width ( $W_d$ )* and *minority carrier lifetime ( $\tau$ )* are directly calculated from complex components of ac-SPV.
- *Surface charge ( $Q_s$ )* is calculated by  $Q_s = \pm qN_{sc}W_d$  where  $N_{sc}$  is bulk dopant concentration and  $q$  is the unit electric charge.
- *Surface dopant concentration* can be determined under a strong inversion condition.

## EXPERIMENTAL

Wafers used were Si(100), 6 inch in dia., lightly-doped with boron and with a resistivity of  $6.1\Omega\text{cm}$ . The wafers were cleaned by  $\text{H}_2\text{SO}_4/\text{H}_2\text{O}_2 + \text{DHF} + \text{NH}_4\text{OH}/\text{H}_2\text{O}_2/\text{H}_2\text{O} + \text{DHC}$  subsequently (so-called full clean, hereafter) in a FSI OC Mercury wafer cleaner. Then the wafers were implanted with  $\text{BF}_2^+$  or  $\text{As}^+$  at a dose of  $2\text{E}15 \text{ cm}^{-2}$  and at an acceleration voltage of 16 kV ( $\text{BF}_2^+$ ) or 30 kV ( $\text{As}^+$ ). Furnace and rapid-thermal annealing were carried out at  $850^\circ\text{C}$  for 30 min and  $1100^\circ\text{C}$  for 10 sec, respectively. The junction depth and the surface carrier concentration were estimated at about 150 nm and  $2 \times 20 \text{ cm}^{-3}$  for  $\text{BF}_2$ , and at about 150 nm and  $4 \times 20 \text{ cm}^{-3}$  for As, by using SUPREM-3™ simulator (Technology Modeling Associates, Inc.). For implanted wafers, their bulk properties were used as the wafer parameters for SCP measurements, since actual surface electrical properties are unknown. Therefore, quantitative discussion on those wafers are out of the scope of this study. All the experiments were conducted in a class 1 clean room at a pilot production line.

## RESULTS AND DISCUSSION

### Non-implanted surfaces

After the full clean, surface charge,  $Q_s$ , was  $6.45 \times 11 \text{ cm}^{-3}$  (positive) and minority carrier surface recombination lifetime,  $\tau$ , was  $8.7 \mu\text{s}$ . After HF dipping + water rinsing,  $Q_s$  decreased to  $\approx 1/5$  of the initial value. This decrease agrees with our different series of experiments by using SC1 + HF (2).

Figure 1 shows the change of  $Q_s$  with time of exposure to the clean room ambient. Time elapse was recorded just after drying. All the  $Q_s$  values have positive sign and increase with time, which is in good agreement with literature (3). When DI-water rinse was not carried out,  $Q_s$  remained unchanged during the first 20 min, then increased rapidly. The water-rinsed wafer shows a continuous and slow increase of  $Q_s$  compared to that of the non-rinsed wafer. The increase in  $Q_s$  can be attributed to the formation of Si dangling bonds caused by Si-H bond breaking (3), or more likely to the formation of native oxide layer which contains small valence Si. It has been reported that  $\tau$  measures surface conditions better than  $Q_s$  for HF-cleaned Si, since the strong positive charge, which originates from Si-H, would invert the surface (4). Figure 2 shows the change of  $\tau$  as a function of ambient-exposure time. Despite the downward change, the trend being observed is very similar to that seen in Fig. 1; i.e.,  $\tau$  changes monotonically in the case of water-rinsed wafer, while  $1/\tau$  is stationary for the first 20 min in the case of non-rinsed wafer.

The space charge data are compared to *in-situ* ellipsometric measurements ( $\lambda = 633$  nm). The change in ellipsometric thickness, determined by phase parameter,  $\Delta$ , with air-exposure time is plotted in Fig. 3. Note that phase parameter ( $\Delta$ ) increases with oxide thickness, and amplitude parameter ( $\Psi$ ) also increases but in a less extent. The ordinate shows the relative thickness change from the initial value measured 0.5 min after N<sub>2</sub> gun drying. The time trend of a rinsed sample is very similar to the SCP data. A peculiar change in the ellipsometric thickness and the subsequent abrupt increase are observed on a non-rinsed sample. The increase starts at around 20 min, which agrees the SCP data.

It is well established that Si surface just after HF dipping has residual F atoms and that water rinse removes them very efficiently (e.g. see reference 5). The non-rinsed surface is thus supposed to have more negative charge than the rinsed surface. The smaller initial  $Q_s$  and  $\tau$  obtained without rinsing agree with this background knowledge. It is also known that water rinsing oxidizes Si surface slightly (6). The increase in  $Q_s$  and  $\tau$  can be reasonably understood attributed due to surface oxidation.

Next significant difference between the rinsed and non-rinsed cases is the presence of a steady state in  $Q_s$  or in  $\tau$ , namely induction period. It has been pointed out that oxidation does not start readily on non-rinsed surface compared to rinsed surface due to the presence of residual fluorine atoms (5), which is fairly consistent with our data. Induction period can be seen also in ellipsometric data (Fig. 3); however, it is surprising that the decrease of ellipsometric thickness occurs during this period. To understand this phenomenon, raw ellipsometric parameters are plotted in Fig. 4. During the induction period, the non-rinsed wafer shows a profound change by 0.1° in  $\Psi$ , while the change in  $\Delta$  is relatively small. An explanation of this phenomenon is the compensation of surface states and the associated decrease in surface optical density (7). A simple model is the annihilation of lone dangling bonds, which could be present at the surface after HF etching. In this case, moisture in the atmosphere will react with the dangling bonds readily, resulting in formation of Si-OH bonds. However, this would accompany the change in surface charge, which is not clear in our data. Moreover, the adsorption of foreign species is supposed to change  $\Delta$  as well. Therefore, we can tentatively exclude this mechanism. Another possibility is the relaxation of surface atomic structure. After HF etching, H-terminated surface is disordered (8) and F atoms remains on surface probably in a physisorbed state. Such residual F atoms can migrate easily on the surface and would work catalitically, resulting in a compensated surface, presumably in a smooth surface. Moisture from the atmosphere would play a role in this tailoring effect. In this scheme, a significant change in the net surface charge is not necessary to take place, while surface dielectric parameters vary largely.

The non-rinsed surface showed a fast change both in surface charge and in ellipsometric parameters after the induction period. This may be caused by obeying a low-temperature oxidation mechanism where oxidation rate is inversely proposed to the oxide thickness. Layer-by-layer growth suggested in literature (5,6) could be seen as discontinuous changes in the curves of Figs. 1, 2, and 3, but is not clear.

Summarizing this section, the SCP data on HF-cleaned Si surfaces were studied comparatively with *in-situ* ellipsometric measurements. The surface charge of a Si wafer after chemical oxide growth decreased significantly by HF dipping. Surface charge and carrier recombination lifetime increased with ambient-exposure time. Without water rinsing,  $Q_s$  showed smaller values, indicative of residual surface F atoms. The induction period, where surface relaxation is likely to occur, are supposed to be caused by residual F atoms.

Table I. Summary of the effect of wafer processing on the SCP parameters

	BF <sub>2</sub> <sup>+</sup> dosed (p <sup>++</sup> )			As <sup>+</sup> dosed (n <sup>++</sup> )		
	Surface charge (q/cm <sup>-2</sup> )	Minority carrier lifetime (μs)	Conductive type	Surface charge (q/cm <sup>-2</sup> )	Minority carrier lifetime (μs)	Conductive type
As received	-1.5 × 10 <sup>10</sup>	18	n	-1.2 × 10 <sup>10</sup>	-20	n
After full clean*	-3.0 × 10 <sup>9</sup>	20	n	-3.8 × 10 <sup>9</sup>	-7	n
Short HF+DI (hydroxilation)	-2.7 × 10 <sup>9</sup>	-50	n	-3.4 × 10 <sup>9</sup>	25	n
HF dip	-3.6E × 10 <sup>9</sup>	29	n	-2.4 × 10 <sup>9</sup>	-15	n
HF dip +DI rinse	-3.0E × 10 <sup>9</sup>	33	n	-2.8 × 10 <sup>9</sup>	-13	n

\* H<sub>2</sub>SO<sub>4</sub>/H<sub>2</sub>O<sub>2</sub> + DHF + NH<sub>4</sub>OH/H<sub>2</sub>O<sub>2</sub>/H<sub>2</sub>O + DHC

#### Oxide removal on ion-implanted wafers

It is well known that water contact angle increases with HF dip time and the surface becomes highly hydrophobic owing to hydrogen termination (9). Therefore, water contact angle measurement is a semi-quantitative way to assess the hydrogen coverage of Si surface; and more practically, the completion of oxide etching is recognized as hydrophilic-hydrophobic transition. On the other hand, on heavily-doped silicon surfaces, since water contact angle is not so large as that on undoped or lightly-doped surfaces (10), the hydrophilic-hydrophobic transition is not so apparent. Till now, SCP measurements have been applied to characterize HF cleaning of lightly-doped Si wafers, and a fairly good correlation was found between SCP parameters and contact angle (4). In this section, the results of SCP measurements on heavily-doped, by ion-implantation, wafers are described.

After ion-implantation and the subsequent annealings, the wafers showed negative surface charge of around -1~2 × 10 q/cm<sup>2</sup>. The full clean decreased the negative charge, or added positive charge in appearance, as was seen in the case of non-implanted wafers. Either HF dipping for 90 sec or the subsequent water rinsing did not have a significant effect on surface charge as high as the full clean. Reciprocal recombination lifetime of a BF<sub>2</sub>-implanted wafer had positive sign except in the case of a short time HF dipping. Contrarily, As-implanted wafer showed negative values, while a short time HF dipping resulted in positive values. The results are summarized in Table I.

Figure 5 shows the effect of HF etch time on τ. Short times dipping up to 30 sec resulted in the opposite polarity in τ to the initial one, and further HF dipping re-established the initial polarity. The polarity change at 30-40 sec is consistent with the completion of surface oxide etching, as seen in contact angle measurements (Fig. 6). Note that the hydrophobic-hydrophilic transition cannot be recognized by eyes very easily, especially in the case of BF<sub>2</sub>-implanted wafers. This is because that the saturation contact angle is as small as that of the original (non-etched) surface (See Fig. 7). On the other hand, the change of Q<sub>s</sub> is not so clear as that of τ. Roughly, it seems that a short time HF dipping adds positive charge to the surface, and that a long time dipping adds more negative charge to BF<sub>2</sub>-implanted (p<sup>++</sup>) surface but contrarily adds positive charge to As-implanted (n<sup>++</sup>) surface.

Table II Process induced dependence of the minority carrier lifetime.

	$\text{BF}_2^+$ dosed ( $p^{++}$ )	$\text{As}^+$ dosed ( $n^{++}$ )
Add positive	Increase	Decrease
Add negative	Decrease (to negative)	Increase (to positive)

On the basis of the data of non-implanted wafers, it is safely said that the full clean adds positive charge, while HF dipping decreases it, or behaves to add negative charge in appearance. It is also clear that the subsequent water-rinsing removes F-originating negative charge. One more surface nature introduced from the HF-etching chemistry is that surface oxide is covered with OH groups at a very high density after HF-dipping + water-rinsing. The surface is highly hydrophilic thus should be negatively charged. This can be related to the polarity change of  $1/\tau$  that was seen after HF-dipping for short times. Hydrogen termination itself produces positively-charged surface (4,11). With supposing that similar chemistry works on implanted surfaces, the behavior of  $\tau$  can be summarized as in Table II. It is interesting to point out that  $p^{++}$  and  $n^{++}$  surfaces behave opposite except the surface conductive type (surface polarity). Clearly, the conductive type of implanted layer has a large influence on the SCP parameters especially on  $\tau$ . It is of a great concern which junction is detected by SCP. In our case,  $p^{++}/p$  and  $n^{++}/p$  junctions were formed by  $\text{BF}_2^+$ - and As-implantation, respectively. However, judging from the large dependence of the SCP parameters on process conditions and wafer conductive type, it can be said that SCP measures only the surface. From ellipsometric measurements, the penetration depth of the probe light that induces ac-photovoltage is roughly estimated at about 200 nm ( $\lambda = 633 \text{ nm}$ ) and is reasonably thought to be much smaller at the wavelength of the probe light ( $\lambda = 450 \text{ nm}$ ). This convinces us again that dominant ac-photocurrent is not generated at  $p^{++}/p$  or  $n^{++}/p$  junction beneath the surface.

However, it should be emphasized that, under the heavy doping conditions studied here, the principle of space charge measurement could be limitedly applied, because the principle assumes the use of uniformly and lightly doped bulk Si. Furthermore, the high dopant concentration could cause degeneration and bandgap narrowing, so that the surface electric structure is far away from that of bulk Si. Therefore, discussion on the origins of the observed SCP parameters is probably a too involved subject to be treated here in detail. It might be speculated that negative minority carrier lifetime suggests the accumulation of carrier at the surface, and that negative surface charge and n-type on  $p^{++}$  surface suggest surface inversion. Interpretation of the SCP parameters is confusing, and quantitative discussion is beyond the extent of this study. However, a clear correlation between the process conditions and the SCP results, especially in  $\tau$ , demonstrates that SCP can be used to characterize heavily-doped surfaces. In other words, the validity of the measurements can be verified only by such a comparison between the data and the wafer process conditions. However it must be noted the applicability is limited. We measured the change in  $Q_s$  and in  $\tau$  of  $\text{BF}_2^+$ -implanted wafers as a function of air-exposure time after HF-etching; however, the data did not show significant change, while *in-situ* ellipsometry showed a similar results as non-implanted wafers (Fig. 8).

## CONCLUSIONS

In the case of non-implanted wafers, HF-last cleaning decreases both surface charge ( $Q_s$ ) and minority carrier lifetime ( $\tau$ ) of chemically oxidized surfaces. Air exposure to a clean room ambient increases  $Q_s$  and  $\tau$ , which is speculated to be due to native oxide growth. Ellipsometric measurements showed very similar time trends. Skipping water rinsing over resulted in slightly small  $Q_s$  values and in the presence of the induction period for oxide growth. This phenomenon is discussed with respect to surface tailoring effect of residual fluorine atoms.

Another set of experiments was performed in order to monitor the oxide removal of implanted wafers. By comparing the space charge data with conventional contact angle measurements,  $\tau$  was found to be the best parameter to distinguish the presence of oxide, since the polarity of  $\tau$  changes when the oxide removal completes. Although the physical meanings of the measured data is somehow puzzling, our data clearly demonstrate that SCP detect the change of surface conditions. Since water contact angle on a heavily-doped wafer is too small to use the hydrophilic-hydrophobic transition as a clear identification of clean surface, surface charge measurement is though to be informative for blanket wafer cleaning characterization.

## REFERENCES

1. E. Kamieniecki and G. J. Foggiato, in *Handbook of Semiconductor Wafer Cleaning Technology*, W. Kern, Editor, p. 497, Noyes, Park Ridge, New Jersey (1993).
2. M.-A. Trauwaert, K. Kenis, M. Caymax, P. Mertens, and M. Heyns, these proceedings.
3. A. Philipossian, *J. Electrochem. Soc.*, **139**, 2956 (1992).
4. P. Roman, J. Staffa, M. Brubaker, S. Fakhouri, J. Ruzyllo and E. Kamieniecki, in *Proceedings of the Third International Symposium on Ultra Clean Processing of Silicon Surfaces*, M. Heyns, Editor, p. 145, Acco, Leuven, Belgium (1996).
5. T. Sunada, T. Yasaka, M. Takakura, T. Sugiyama, S. Miyazaki, and M. Hirose, *Jap. J. Appl. Phys.*, **29**, L2408 (1990).
6. M. Morita, T. Ohmi, E. Hasegawa, M. Kawakami, and K. Suma, *Appl. Phys. Lett.*, **55**, 562 (1989).
7. R.M.A. Azzam and N.M. Bashara, *Ellipsometry and Polarized Light*, North-Holland, Amsterdam (1987).
8. P. Dumas, Y.J. Chabal, P. Jakob, *Surf. Sci.*, **269/270**, 867 (1992).
9. S. Verhaeverbeke, PhD Thesis, Katholieke Universiteit Leuven, Belgium (1993).
10. Y Sato and M. Maeda, *Jap. J. Appl. Phys.*, **33**, 6508 (1994).
11. A.R. Plummer, *The Electrochemistry of Semiconductors*, P.J. Holmes, Editor, p. 61, Academic Press, London (1962).

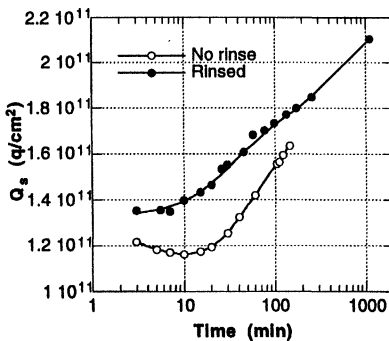


Figure 1 Change of space charge of non-implanted wafers with ambient-exposure time after HF cleaning.

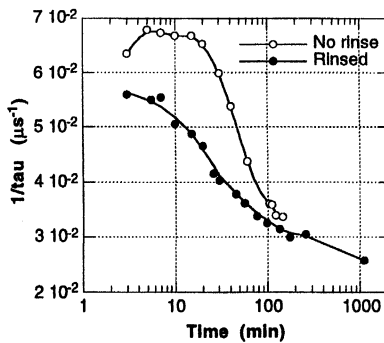


Figure 2 Change of reciprocal minority carrier lifetime of non-implanted wafers with ambient-exposure time after HF cleaning.

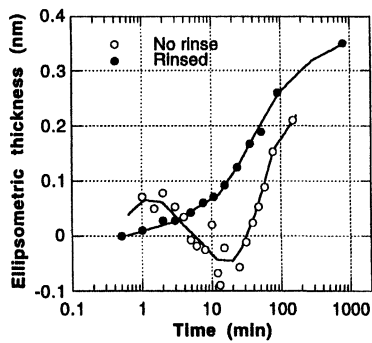


Figure 3 Change of ellipsometric oxide thickness on non-implanted wafers as a function of air-exposure time after HF cleaning.

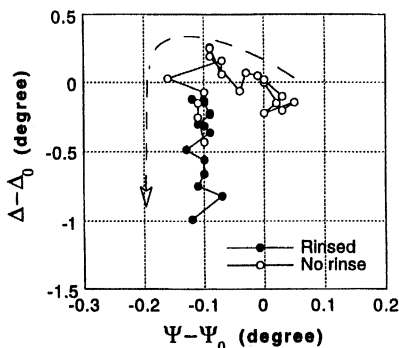


Figure 4 Time change of ellipsometric phase and amplitude parameters after HF cleaning. Reference is the first observation of the non-rinsed wafer (30 sec after HF treatment). The arrow indicate the direction of change.

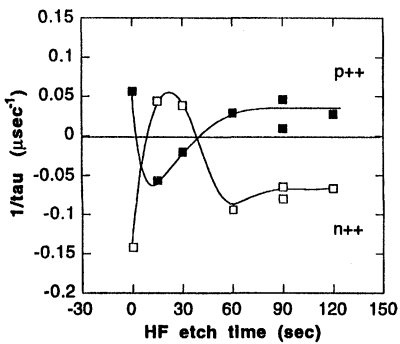


Figure 5 Change of reciprocal minority carrier lifetime of implanted wafers as a function of HF-dip time.

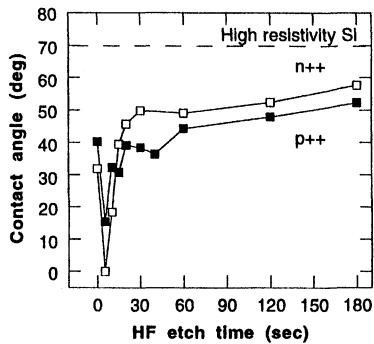


Figure 6 Contact angle measurements of implanted wafers as a function of HF-dip time.

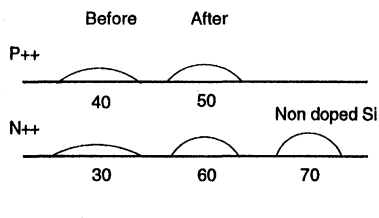


Figure 7 Schematic representation of the shapes of droplets before and after HF etching. Numbers show contact angles.

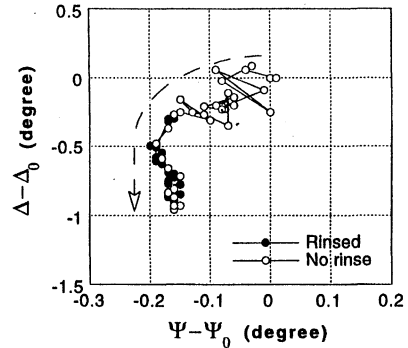


Figure 8 Time change of ellipsometric phase and amplitude parameters after HF cleaning. Reference is the first observation of the non-rinsed wafer (30 sec after HF treatment). The arrow indicate the direction of change.

## **WET CLEANING - Ozonated Water**



# THE BEHAVIOR OF OZONE IN WET CLEANING CHEMICALS

Jin-Goo Park and Jeoung-Hoon Han  
Department of Metallurgy and Materials Engineering  
Hanyang University, Ansan, 425-791, Korea

The purpose of this study was to investigate the behavior of ozone in semiconductor wet cleaning chemicals. The solubility and half life time of ozone in DI water, acidic and alkaline chemicals were measured as functions of input gas concentrations and time. The higher the pH of solutions, the lower solubility was measured. In addition, the solubility of ozone was a strong function of temperature. Lower temperatures resulted higher solubility. The half life time of ozone was dependent on the initial ozone concentration of the solutions. Ozone concentration above 2 ppm in DI water could passivate the silicon surface within 1 min into a state of complete hydrophilic. The ozone in the acidic solution also completely passivated bare wafers within 10 sec treatments.

## INTRODUCTION

Ozone was applied not only in the film deposition [1] but also in wet/dry cleanings in semiconductor processing [2,3]. Ozone in wet chemicals was used in place of H<sub>2</sub>O<sub>2</sub> for the removal of organics and surfactants. The application of ozone chemistry to wet cleaning has advantages in maintaining chemical purity, recycling and lowering the cost of ownership in the light of the environmental issues and size of wafers in the next generation wet cleaning processing.

The injection of ozone in DI water and H<sub>2</sub>SO<sub>4</sub> was used in semiconductor wet cleaning processes to replace the traditional sulfuric/peroxide process. Low temperature ozonated DI water showed its effectiveness in photo resist removal [4]. The passivation of HF etched surfaces with ozone is likely to form a different quality oxide from other peroxide based chemicals during wet cleaning processes [5,6]. The HF last process followed by ozonated DI water resulted in better breakdown voltage distribution than those without ozonated DI water [7]. Also the application of ozone in acidic chemicals such as HF and HCl was tried. The passivation of HF etched surfaces by ozone with 0.01% HCl provided good oxide integrity [8].

Even though there are active researches on the application of ozone in cleaning chemicals in terms of removing contaminants, the fundamental understanding on the behavior of ozone in various cleaning chemicals is nil. In this study the behavior of ozone --not only in acidic but also in alkaline chemicals -- was evaluated in terms of life time, solubility and reaction on silicon surfaces.

## EXPERIMENTAL

Ozone generated in an arc discharge type generator (Fischer 502) was supplied to a quartz reactor as shown in Figure 1. Aliquots of solutions were left in the reactor to observe the reaction with ozone. Teflon tubing was used for all experiments to minimize the possible reaction with ozone. A Teflon plate was placed in the reactor to reduce the interaction between the electrode of ozone analyzer and bubbles from incoming gas. A magnetic stirrer was used to obtain a rapid and uniform dissolution of ozone in solutions. Oxygen of 98% purity was used to generate ozone. Ultra high purity DI water and semiconductor grade wet cleaning chemicals were used for the experiment.

Wafers (p type, (100)) were precleaned in the mixture of  $H_2SO_4$  and  $H_2O_2$  and followed by 0.5 % HF etching. The concentrations of ozone as a gas phase and in liquid were measured by the titration method [8] and an electrolytic analyzer (Obisphere 3600), respectively. pH and redox potential of chemicals were measured by Orion Ag/AgCl electrodes with a Orion pH meter (Orion 520A). The wettability of surfaces was measured by a static contact angle analyzer (Krüss G10). The temperature of chemicals was controlled by a water bath.

## RESULTS AND DISCUSSION

### Generation of Ozone

A titration method was used in measurements of gaseous ozone concentrations. The generated ozone concentration was measured as a function of oxygen flow rates and applied current. The higher oxygen flow rates, the lower ozone concentration was measured. A flow rate of 50 l/hr was chosen to obtain a possible maximum concentration from the ozone generator. Figure 2 shows the measured ozone concentration as a function of input current. The generated ozone concentration was a linear function of the input power. The generated gaseous ozone concentrations ranged from 0.4 vol% to 4 vol% when the input power was changed from 0.65 A to 1.25 A. Considering the safety factor of the generator, a concentration of 4 vol% was used for the experiment unless otherwise stated.

### Ozone in DI Water

Figure 3 shows the solubility of ozone in DI water as a function of time at different input ozone concentrations. At a gas concentration of 4 vol%, a maximum soluble concentration of 15 ppm was measured. The higher the ozone concentrations, the higher the solubility in DI water. Since the dissolved ozone in DI water is a strong function of the initial input gas concentration, the desired ozone concentration in DI water could be easily controlled by the changes of input concentrations. It should be noted that around 15 minutes were required to reach a saturation of ozone in DI water independent of input ozone concentrations.

When the supply of ozone to DI water was cut-off, the half life time of ozone in DI water reduced as a function of initial concentrations as shown in Figure 4. The initial

ozone concentrations of 3.4 and 15.3 ppm resulted in the half life time of 88 and 33 min, respectively. The higher initial concentrations, the smaller value of half life time was observed.

The solubility of ozone was also a function of temperature in DI water as shown in Figure 5. When 4 vol% of ozone was injected into DI water at various temperatures the highest solubility of 25 ppm was measured at 15°C. At 50°C as low as 1 ppm was measured. The higher temperatures, the lower solubility was obtained. Also it was interesting to note that the saturation time of ozone in DI water was dependent on the maximum dissolved ozone concentrations. The higher the concentrations of ozone in DI water, the longer the time required to reach a saturation.

The half life time of ozone in DI water was also dependent on the temperature as shown in Figure 6. The largest values was measured at the lowest temperature used in the experiments. It indicates that the decomposition of ozone can be accelerated at higher temperatures. Table 1 shows the solubility and half life time of ozone at different temperatures.

Table 1. Half life time of ozone in DI water various initial ozone concentrations at different temperatures

Temperature, °C	Solubility of Ozone , C <sub>0</sub>	Half Life time (C/C <sub>0</sub> =1/2)
20	20.41 ppm	94 min
25	15.30 ppm	33 min
30	10.25 ppm	30 min
40	1.84 ppm	11 min
50	0.95 ppm	7 min

Figure 7 shows the change of pH and redox potentials as functions of time at different input ozone concentrations. Since ozone is acidic, the continuous supply of ozone resulted in the decrease of pH values. The degree of reduction of pH was a function of input ozone concentration. The redox potential increased to a constant value after 5 min and showed slight dependency on the input ozone concentrations.

The change of contact angles was measured as a function of treatment time in DI water of different ozone concentrations as shown in Figure 8. At above 2 ppm, the complete passivation of HF etched silicon surface was measured in 1 min. However the longer time was required to passivate the surface at lower concentrations than that. AFM and a spectroscopic ellipsometry analyses are going on to investigate the effect of ozone concentrations on silicon surfaces. All measurements in DI water were not done in the overflowing condition but in a reactor as a static condition. The experiments are on progress to observe the behavior of ozone in the overflowing situation.

### Ozone in Acidic Solutions

The solubility of ozone in H<sub>2</sub>SO<sub>4</sub> solutions was measured as a function of time at different H<sub>2</sub>SO<sub>4</sub> concentrations and temperatures as shown in Figure 9. As observed in the behavior of ozone in DI water, it also took around 15 min to reach a saturation point in acidic solutions. A slightly higher solubility of ozone in H<sub>2</sub>SO<sub>4</sub> was observed in higher concentration of H<sub>2</sub>SO<sub>4</sub> solutions due to a slightly lower pH.

At a higher temperature, a reduction of solubility was measured. Figure 10 shows the changes of solubilities of ozone as a function of time when the supply of ozone to H<sub>2</sub>SO<sub>4</sub> solutions was cut-off. The half life of H<sub>2</sub>SO<sub>4</sub> solutions was independent of solution concentrations. However the decrease of temperature to 48°C reduced it in half. When bare silicon wafers were treated in the ozone injected H<sub>2</sub>SO<sub>4</sub> solutions, the wafer was passivated completely even in 10 sec. The contact angles measured on silicon treated with ozone added H<sub>2</sub>SO<sub>4</sub> solutions were as low as these did in Piranha solutions (ca. 5°).

Dilute HCl (0.01 vol%, pH = 2.55) and HF (0.5 vol%, pH = 1.4) solutions were prepared and ozone was injected into them. Figure 11 shows the changes of solubility of ozone in dilute acidic solutions as a function of time. As discussed earlier, a slightly higher solubility was measured in HF solutions due to lower pH values in HF. The half life time of ozone in these solutions were very similar to each other. Table 2 shows the half life of acidic solutions.

Table 2. Half Life Time of Ozone in 0.5%HF and 0.01%HCl

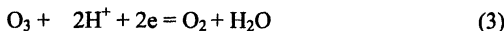
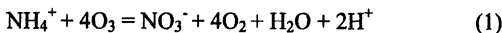
Solution	Temperature (°C)	Solubility of Ozone	Half Life time (C/C <sub>0</sub> =1/2)
0.5% HF	23	28 ppm	86 min
0.01% HCl	23	25 ppm	80 min

The contact angle measurement showed the complete hydrophilization (<5°) of silicon surfaces in ozone added HCl solutions. A contact angle of 20° was measured on surfaces in ozone added HF solutions. It indicates the competition between the etching reaction by HF and passivation reaction by ozone.

### Ozone in NH<sub>4</sub>OH Solutions

For the removal of particulate contamination from wafer surfaces, NH<sub>4</sub>OH and H<sub>2</sub>O<sub>2</sub> mixture solutions is indispensable in semiconductor wet cleaning processes. If H<sub>2</sub>O<sub>2</sub> could be replaced with O<sub>3</sub> in SC1 as we did in Piranha and SC2 solutions, the benefit out of it would be tremendous in economical and environmental aspects. However the solubility of ozone in high pH ranges has been known to be very low [10,11]. Figure 12 shows the pH and solubility changes at various concentrations of NH<sub>4</sub>OH solutions. The addition of ozone to NH<sub>4</sub>OH solutions decreased pH values rapidly when pH of

solutions reached below 9. In higher pH values than that, the decrease of pH (i.e. higher concentrations of NH<sub>4</sub>OH) was very small. In NH<sub>4</sub>OH solutions, possible reactions could be proposed [12] as shown below.



Even though much more complex reactions occur together in solutions, reaction (1) and (2) might be dominant above pH values of 9 and reaction (3) might be dominant in acidic solutions.

Also the solubility of ozone in NH<sub>4</sub>OH solutions above pH of 9 was virtually nil and started to increase below 9. When considered pH of SC1 ranged from 8.8 (0.01:1:5, NH<sub>4</sub>OH:H<sub>2</sub>O<sub>2</sub>: H<sub>2</sub>O) to 10.5 (1:1:5) at room temperature, if the pH of ozone in NH<sub>4</sub>OH solutions could be maintained between 9 and 10, it would be possible to replace H<sub>2</sub>O<sub>2</sub> with O<sub>3</sub> in SC1. Further research is in progress to optimize and maintain the solubility of ozone in NH<sub>4</sub>OH solutions with the characterization of ozone added SC1 solutions.

## SUMMARY AND CONCLUSIONS

The solubility of the ozone in wet cleaning chemicals is very dependent on the initial input ozone concentration, the temperature and the pH of the solutions. The higher input ozone concentrations, the higher ozone was dissolved in chemicals. The higher temperatures and pHs of solutions, the lower solubility of ozone in solutions was resulted. The half life time of chemicals was also very dependent on the dissolved ozone concentration, temperature and pH of solutions. The higher pH and temperature, the faster the decomposition of ozone occurred. The higher initial ozone concentration, the slower the decomposition of ozone was measured. The lower temperatures were applied to increase the amount of dissolved ozone in solutions. The dissolved ozone in water increased from 1 ppm to 25 ppm when the temperature decreased from 50 to 15°C. Above pH values of 9, the dissolution of ozone in alkaline solutions was almost nil. The lowering temperature of alkaline solutions to 10°C increased the solubility of ozone 4 to 5 times when compared to that at room temperature.

## ACKNOWLEDGMENTS

The authors express their thanks to Hanyang Technology for the financial support. Special thanks go to the Mr. J. W. Kim and J. K. Choi of Hanyang Technology for their guidance and support for this research.

## REFERENCES

1. K. Fujino, Y. Nishimoto, N. Tokumasu, and K. Maeda, *J. Electrochem. Soc.*, **137**(9), 2883 (1990)
2. J. R. Vig, in *Handbook of Semiconductor Wafer Cleaning Technology*, Ch. 6, W. Kern, Ed., Noyes Publications, 1993
3. T. Ohmi, T. Isagawa, M. Kogure, and T. Imaoka, *J. Electrochem. Soc.*, **140**(3), 804 (1993)
4. I. I. Kashkoush, B. Mathews and R. E. Novak, *The Abstract of MRS Spring Meeting*, San Francisco, 276 (1997)
5. C. Paillet, J. P. Joly, F. Tardif; K. Barla, P. Patrano and D. Levy, Proc. Fourth International Symposium on Cleaning Technology in Semiconductor Device Manufacturing, 95-20, pp. 366-370, J. Ruzyllo and R. E. Novak, Eds., The Electrochemical Society, Pennington, NJ (1996)
6. M. Meuris, H. Izunni, K. Kubo, S. Ojima, T. Ohmi and M. M. Heynes, Proc. Fourth International Symposium on Cleaning Technology in Semiconductor Device Manufacturing, 95-20, pp. 444-448, J. Ruzyllo and R. E. Novak, Eds., The Electrochemical Society, Pennington, NJ (1996)
7. J. G. Park, *Jpn. J. Appl. Physics*, **36**(9), 3701 (1997)
8. F. Tardif, T. Lardin, C. Paillet, J. P. Joly, A. Fleury, P. Patruno, D. Levy, and K. Barla, Proc. Fourth International Symposium on Cleaning Technology in Semiconductor Device Manufacturing, 95-20, pp. 49-59, J. Ruzyllo and R. E. Novak, Eds., The Electrochemical Society, Pennington, NJ (1996)
9. A. R. David and R. B. Deborah, *Ozone in Water Treatment*, Lewis Publishers, Michigan, 1991
10. H. Tomiyasu, H. Fukutomi, and G. Gordon, *Inorg. Chem.*, **24**, 2962 (1985)
11. S. Nakaresesoon, G. Gordon, *Ozone Sci. Engrg.*, **11**, 49 (1988)
12. R. G. Rice, *Handbook of Ozone Technology and Application*, Chapter 7, Butterworth Publishers, Boston, 1986

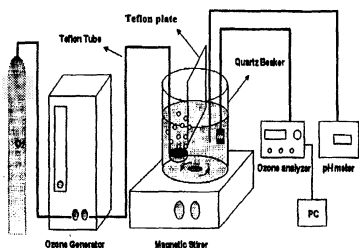


Figure 1. A schematic diagram of experimental set-up

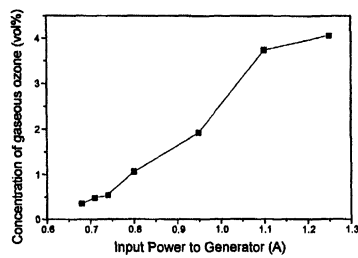


Figure 2. The ozone concentration as a function of input current

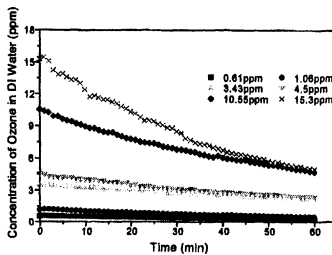


Figure 4. The change of ozone concentrations in D.I. Water as a function of time when stopped the supply of ozone to D.I. water

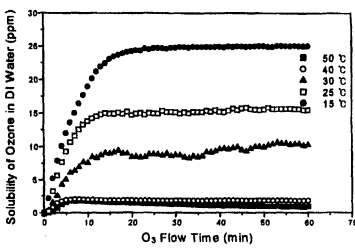


Figure 5. The change of ozone solubility in D.I. water as a function of time at different temperatures

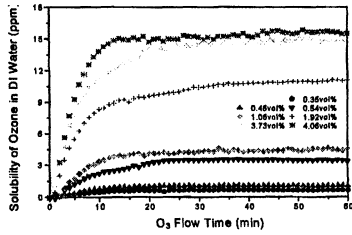


Figure 3. The change of ozone solubility in D.I. water as a function of time at room temperature

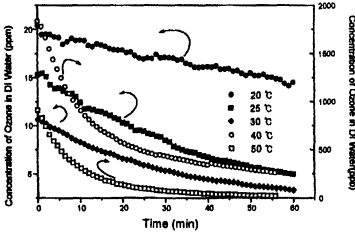


Figure 6. The change of ozone concentration in D.I. Water as a function of time when stopped the supply of ozone to D.I. water at different temperatures

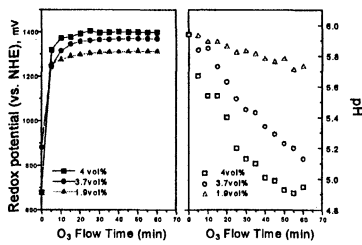


Figure 7. The change of pH and redox potentials as a function of time at different input ozone concentrations

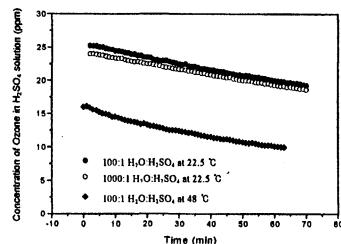


Figure 10. The change of ozone concentration as a function of time when stopped the supply of ozone to different  $\text{H}_2\text{SO}_4$  concentration and temperatures

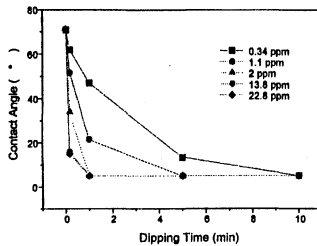


Figure 8. The change of contact angle as a function of treatment time with different ozone concentrations in D.I. water

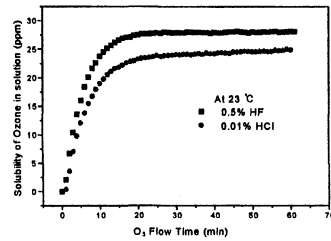


Figure 11. The change of ozone solubility in dilute acidic solutions as a function of time at room temperature

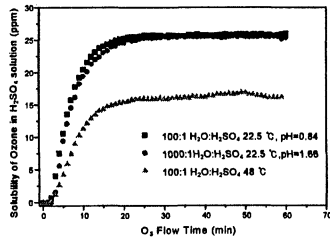


Figure 9. The change of ozone solubility as a function of time at different  $\text{H}_2\text{SO}_4$  concentrations and temperatures

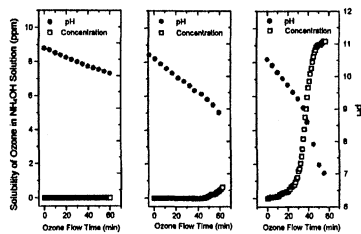


Figure 12. The pH and solubility changes at various concentrations of  $\text{NH}_4\text{OH}$  solutions

## **EFFICIENCY OF OZONE DISSOLUTION INTO AMBIENT TEMPERATURE RINSE BATHS**

K. Wolke\*, M. Schenkl\*, M. Alessandri\*\*, E. Bellandi\*\*

\* STEAG MicroTech GmbH, Carl-Benz-Str.10, 72124 Pliezhausen, Germany

\*\*SGS Thomson Microelectronics, Central R&D, Via Olivetti 2, 20041 Agrate Brianza,  
Italy

The use of ozone in ambient temperature rinse water gains importance in pre diffusion cleaning both for removal of organic contamination as well as for post treatment in HF last processing. In this work the efficiency of ozone dissolution into the rinse baths has been evaluated with respect to dissolved ozone concentration in the full range of rinse process parametrics. The influence of ozone bubbling in the rinse tank was evaluated for particle performance. Native oxide regrowth has been studied and compared to conventional SOM; SPM and SC1 cleaning. It has been shown that ozone concentrations in the Di H<sub>2</sub>O of up to 30 ppm are achievable without bubbles at good particle performance. No difference was found for the oxide regrowth performance to other oxidizing processes.

### **INTRODUCTION**

In today's S/C process technology the wafers are typically cleaned prior to diffusion processes using a sequence described by W. Kern in 1975 [1], which is commonly known as RCA cleaning. Although the process performance has been optimized permanently, f.e. with the use of megasonics or ultra clean diluted chemicals, the basic disadvantages of a very long sequence of up to ten steps and instable or quickly evaporating chemicals still drives the search for other cleaning concepts with at least the same performance but less chemical consumption and environmental impact. As part of this research HF last cleanings have been proposed using at least one ozonized water step (T. Ohmi [2], IMEC [3], DDC [4]). These concepts include ozonized water either as a first step to remove organic contamination and oxidize the wafer surface for optimal cleaning efficiency in the HF step or as an additive to the rinse after HF to exchange the hydrogen passivated surface by a hydrophilic one for better time stability. Typical process sequences with ozonized water are shown in table 1.

Lots of work has covered the performance of the HF step, however the optimization of the Di H<sub>2</sub>O step with ozone is still fairly unknown. The goal of this work to characterize the ozone rinse and the efficiency to ozonize deionized water at ambient temperature. Optimal process parameters should be ob-

tained to achieve best oxidation efficiency and particle performance in shortest time and with reasonable water consumption. Therefore the ozone concentration in the liquid for different Di H<sub>2</sub>O flows and pressures was studied. The ozone generator output and ingoing oxygen gas flow was varied to find the best working set point for the ozone supply. Using the results of this pre-evaluation the most efficient process was used to characterize the impact of ozone gas bubbles in the rinse tank. Although known to be accelerating the stripping of photo resist in water, for this application bubbles involve the risk of nonuniform re-oxidation or particulate contamination on the wafers. Finally the overall particle performance of the ozonized water step on hydrophilic and hydrophobic (HF treated) wafers was compared to conventional oxidation steps like SOM (sulphuric ozone mixture), SPM (sulphuric peroxide mixture) and APM (ammonia peroxide mixture).

#### EXPERIMENTAL PROCEDURE

Most of the experiments were performed in a STEAG MicroTech automated wet processor bench (AWP Gen. III) at SGS Thomson's R1 facility in Agrate-Brianza, Italy where flash memories are produced in 0.35 micron technology on 150 mm wafers. This equipment is configured as a hybrid tool capable for running the RCA clean as well as the IMEC HF last sequence with ozonized water. It is upgradable for 200 mm processing and uses standard 6 inch PFA cassettes in 8 inch compatible tanks. Wafer drying is done in a STEAG Marangoni Dryer. For additional cross check experiments the semi-automated wet bench in the STEAG production laboratory was used.

The rinse tank is made from quartz and is provided with a four sided overflow rim. The flow rate can be varied from 2 to 35 l / min. Optionally small amounts of HCl can be spiked using a metering pump connected to the deionized water line. The tank is equipped with a resistivity monitor rinsing control. To monitor the ozone concentration in the rinse tank inlet during the course of the experiments a BMT AQ963 liquid ozone monitor was installed just before the tank. DiH<sub>2</sub>O Recirculation is not possible in this tank.

The ozone was supplied by a SORBIOS SEMOZON 90.2 type generator directly at the module, running on 5.6 grade oxygen feed gas and designed to provide up to 90 g/h ozone. An ozone compatible gas filter implemented right at the output gas line of the generator was used to minimize any potential particle contamination in the process from the generator.

The dissolution of the ozone was done with a SORBIOS static mixer, which introduces the ozone gas into the liquid by permanent perturbation of the media in a special designed quartz tube. This method has been found to be the most effective one with respect to concentration, ozone distribution in tank and long term particle performance.

In order to separate the ozonized water and the non dissolved ozone/oxygen gas mixture one or two debubblers (degassifiers) were placed as close as possible to the process tank, in order to provide the largest volume possible for the gas to dissolve. A schematic diagram of the ozone generation and monitoring setup is shown in Fig. 1.

For the characterization of the surface passivation of HF treated wafers contact angle measurements as well as an SOPRA ES4G ellipsometer for oxide thickness measurement was used. Ellipsometry was used. As a silicon reference file for the ellipsometry the data from Jellison were used.

## RESULTS

### *Ozone concentration in the Di water*

In order to set up the right parametrics for the ozone generator SEMOZON E90.2 for optimal dissolution in the Di water the O<sub>3</sub> concentration in the liquid was measured for two different oxygen pressures and flows as a function of the ozone production rate, resp. the ozone generator power. The UPW pressure supplied to the system was 4 bar and remained constant during the course of the experiment. The results are summarized in Fig. 2. At low production rates the dissolved ozone in the Di water increased fairly linear with the generator power, but starts to saturate at about 60 g/h reaching its maximum at about 90 g/h. This dependency is independent of oxygen pressure and flow. However the absolute scale of ozone concentration in the water varied with the incoming oxygen pressure, reaching 26 ppm for the supplier recommended 2,5 bar, but close to 30 ppm for 3,3 bar.

In order to quantify the dependency of the ozone concentration in the UPW the O<sub>3</sub> gas flow was varied from 2 to 10 l / min for different H<sub>2</sub>O flows (4,8,10, 10 l/min). Nearly identical curves were obtained over the full range of rinse flow, showing a strong, but nonlinear dependency of the ozone concentration from the gas flow. A maximum was reached at approximately 8 l/min. At higher gas flows a slight, but significant decrease was observed. Since this behaviour might be caused by the specific properties of either the generator or the injection technology, these runs were repeated in the STEAG production lab in a set of cross check experiments using an ASTEX AX 8200 generator and a semi-permeable teflon membrane. At different absolute levels the same dependency was observed.

These results confirm that the dissolution efficiency at least for the range of parameters measured is not limited by the mixing technology of the ozone transfer into the liquid (fig. 3). The residence time of the ozone in the transfer area (which was kept approximately the same during the measurement) defines the maximum transfer rate and has to be optimized for best performance of ozonized water rinse.

#### *Oxide regrowth in ozonized Di water*

A key requirement for the use of ozonized ultra pure water in cleaning processes is the reproducibility and uniformity of the surface re-oxidation, especially on hydrophobic wafers. Qualitatively this can be characterized by measuring the contact angle of a small water droplet placed on the wafer after processing. After HF treatment of 3 min. in 0.5 % DHF a contact angle of approximately 75 deg. or more was observed, indicating complete hydrophobicity. The wafers were subsequently rinsed in ozonized Di water ( $O_3$  concentration 25 ppm, diH<sub>2</sub>O flow 5 l/min) for 30, 60 or 180 sec. and the contact angle was remeasured. Already after the 30 sec. rinse the angles were decreased to 25 to 35 degrees and after 180 sec. the contact angle was below 5 degrees and no reliable measurement was possible with the equipment used.

In order to further quantify the „hydrophilization“ with ozone the thickness of the grown oxide was measured by ellipsometry for high (25 ppm) and low concentration (5 ppm) ozone processes and compared to standard SOM or SC1 processes. As can be seen in Fig. 4 a stable oxide with a thickness of appr. 1,4 to 1,6 nm is formed in all three cleaning steps, however the time required to reach complete oxidation differs. Although having the longest process time of 10 minutes, the lowest thickness was found for the SC1 bath. While with SOM due to the higher process temperature and the additional oxidizing power of the sulphuric acid a stable hydrophilic surface is obtained already after 30 seconds, for the  $O_3$  rinse of high concentration one minute and with 5 ppm ozone in the water even 5 min. process time was needed. Thus for complete re-oxidation at short process times a maximized efficiency of the ozone dissolution into the UPW is a key factor. It has to be mentioned that a) the lowest thickness after re-oxidation was found for the 10 min. SC1 process and b) the absolute thickness numbers depend on the refractive index. For Fig. 4 data from Jellison were used for reference.

#### *Particle performance of ozonized Di Water rinse*

The final, but very important criterion for the use of ozonized water rinse in semiconductor cleaning processes is the particle performance. Especially in the case of HF last treatment the ozone rinse is the last step before drying, all re-contamination will reduce the cleaning efficiency of the chemical steps before. On the other hand it is known that at least when the ozone generators are switched on or off particles are released. Tests have been performed with a gas particle counter at the generator feed gas ( $O_2$ ) and ozone out line with and without particle filters (Pall SGL FPF6402VMM4). As

can be seen in table 2, the particle generation had been confirmed, but at least for the set up used in the experiments the filter had effectively reduced the contamination.

Particle recontamination of the rinse tank has been evaluated with and without ozone by running pre-measured particle wafers through a rinse and dry cycle. The list of different processes is shown below:

- Test 1: Marangoni dry only (no external rinse)
- Test 2: Rinse and dry without O<sub>3</sub> with hydrophobic wafers
- Test 3: Rinse and dry with O<sub>3</sub> with hydrophobic wafers
- Test 4: 5 min DHF, rinse and dry with hydrophilic wafers
- Test 5: 5 min DHF, ozone rinse and dry with hydrophilic wafers

The rinse processes were kept as close as possible to standard cascade rinses and consisted of a 2 min. high flow (25 l/min) step w/o ozone, followed by a 8 min low (5 l/min) flow in the non ozonized tests. In tests 3 and 5 the two minutes high flow is followed by 30 sec of low overflow, 7 minutes of low flow with ozone and finally 30 seconds of low overflow without ozone. During these tests degassifiers were used and no bubbles were observed in the tank. Each test consisted of three particle wafers with the rest of the batch filled with dummy wafers and was repeated at least five times. The contamination level of the test wafers before processing was less than 30 particles / wafer.

The mean delta count for each test is shown in Fig. 5. In all tests particle contamination was very low, but can be assigned to three groups. Good results were found for tests 1-3 hydrophobic wafers that were not HF dipped in the same process. Wafers in test 4 and 5 showed slightly higher particle count, however no difference can be seen with or without ozone in the rinse. This indicates that the particle level is not driven by the use of ozone, but by the impact of the DHF itself. Detailed data of experiment 5 (fig. 6) give typical distributions from wafer to wafer and run to run.

Another set of experiments was done to evaluate the influence of ozone gas bubbles in the tank during the process. Given the known fact that ozone generators might create particles it cannot be excluded that some portion of this contamination might pass the gas filters and adhere to the freshly hydrogen passivated silicon surface in the rinse. In fact this was observed when the debubblers were removed and bubbles could enter the tank with the wafers. Approximately 100 particles were added in a 'bubbling' ozone rinse and dry sequences comparable to a exp. 3 above. This difference is due to the fact that the particles in the gas phase (which usually have a positive zeta potential) will not dissolve into the liquid, but due to the negative zeta potential of Si surface will stick immediately when they get into contact with the wafer. This is even enhanced by the fact that bubbles tend to stick to solids because of less surface tension.

### *Discussion*

Above results have shown that rinsing with ozonized water can provide a uniformly oxidized, hydrophilic surface even on freshly hydrogen passivated wafers at typical cascade overflow rinses times. The transfer mechanism is depending on the residence time of the ozone gas in the UPW, just long transfer lengths are preferable. The experiments have shown that ozone concentrations of 20 ppm and more ensure a re-oxidation of the surface within 5 minutes, and even with lower concentration and increased process time no difference in oxide thickness was observed. However particle recontamination or even silicon pitting by ozone bubbles cannot be accepted in critical cleaning steps. Thus any addition of light point defects has to be minimized or even eliminated. Thus bubble free injection systems or at least highly efficient debubblers are needed for good particle performance. An optimized rinse process derived from the experiments is summarized in table 3 for a system that provides 20 ppm or more ozone concentration.

An HF last process run with this recipe did not contribute any contamination to the o/a process performance. By introduction of HCl in the first process step of the recipe metallic performance even might be improved. Finally even the cost of ownership of the process is kept reasonable, since water consumption is reduced significantly by introducing low flow steps wherever possible. Together with the advantages of HF last processing in general, the use of ozonized di water during rinsing gives a good alternative to conventional cleaning with the RCA sequence.

### *Acknowledgements*

The authors would like to thank Stefan Rümmelin for his contributions during the course of experiments.

This work is part of the ESPRIT project 20757 AUTOWET and was supported by the European Community.

### *References*

- [1] W. Kern, D. Poutinen, RCA rev. 31,187 (1970)
- [2] T. Ohmi , 'Proposal of advanced wet cleaning of Silicon surface', Proc. of 4th Int. Symp. of Cleaning Technology (1994)
- [3] M. Meuris, M. Heyns, 'The IMEC Clean concept', Proc. od 2nd Int. Symp. UCPSS, Brugges, Belgium (1994)
- [4] F. Tardif, et. al., 'Diluted Dynamic Clean: DDC', Proc. of 3rd Int. Symp. UCPSS, Antwerp, Belgium (1996)

Process sequence	Step 1	Step 2	Step 3	Step 4	Step 5
Ref. 1 (Ohmi)	Amb. Di H <sub>2</sub> O w/ O <sub>3</sub>	DHF w/H <sub>2</sub> O <sub>2</sub>	Amb. Di H <sub>2</sub> O w/O <sub>3</sub>	Di H <sub>2</sub> O (opt. DHF)	IPA dry
Ref. 2 (IMEC)	amb. Di H <sub>2</sub> O w/ O <sub>3</sub>	DHF w/ HCl	H <sub>2</sub> O w/ HCl	H <sub>2</sub> O (opt. w/ O <sub>3</sub> )	Marangoni Dry
Ref. 3 (DDC)	Di H <sub>2</sub> O w/ O <sub>3</sub>	DHF w/ HCl	H <sub>2</sub> O w/ O <sub>3</sub>	HF / HCl	HO / O <sub>3</sub> Rinse Dry

Table 1: Process sequences using ozonized water at ambient temperature

Particles (scfm)	In the feed gas line	Output line w/o filter	Output line w/ filter
Mean	10	1000	<10
Peak	30	3600	<10

Table 2: Particles in the ozone gas with and without gas filters.

Step	time (sec)	H <sub>2</sub> O flow (l/min)	ozone (Y/N)
1	120	30	n
2	30	5	n
3	420	5	y
4	30	5	n

Table 3: optimized rinse recipe for ozonized water rinse

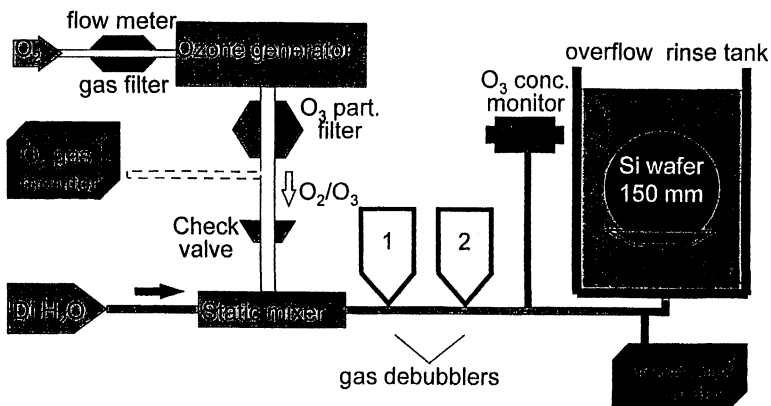


Fig. 1: Schematic setup of ozone dissolution and monitoring

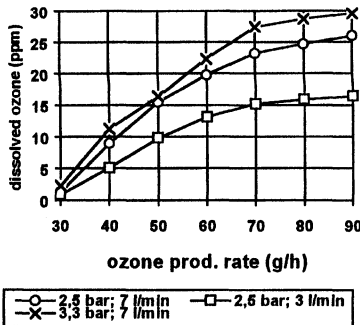


Fig. 2: Liquid ozone concentration as function of production rate in the ozone generator

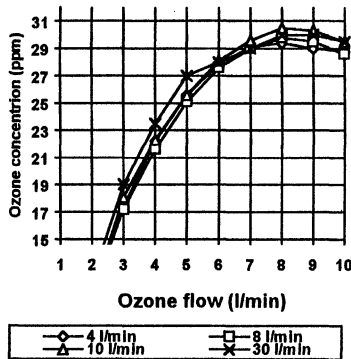


Fig. 3: Ozone concentration in DI water as a function of water flow and ozone gas flow.

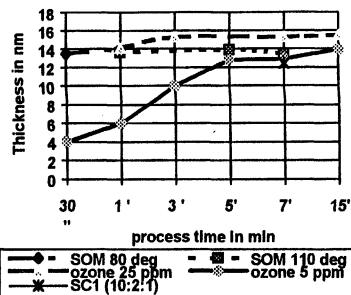


Fig. 4 Thickness of regrown oxide after HF treatment for different processes

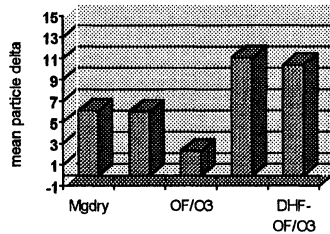


Fig. 5: Summary of particle data from different process sequences with and without ozone

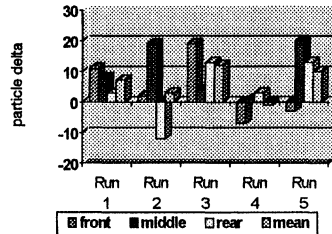


Fig. 6 Detailed results of particle measurements for the HF last - ozone sequence.

# EFFICIENCY OF OZONATED DI WATER IN REMOVING ORGANIC CONTAMINATION

C. Kenens, S. De Gendt, D.M. Knotter\*, L.M. Loewenstein\*\*, M. Meuris,  
W. Vandervorst and M.M Heyns

IMEC vzw, Kapeldreef 75, B-3001 Leuven, Belgium

\*Philips Research, Eindhoven, The Nederlands, industrial affiliate at IMEC

\*\*Texas Instruments, Dallas, TX, USA, industrial affiliate at IMEC

## ABSTRACT

Ozonated DI water has been applied for the removal of organic contamination on silicon surfaces. The impact of various parameters such as temperature, acidity, immersion time and the variation of the ozone production conditions (oxygen flow and generator yield) has been evaluated for removing a photoresist primer. The most important factors for removal of this contamination seemed to be (elevated) temperature combined with the ozone concentration. The acidity of the solution was of little influence. Increased immersion times resulted in improved removal efficiency.

## INTRODUCTION

In semiconductor technology the trend of scaling down the device-geometries without decreasing their performance, implies more stringent cleanliness of the wafer-surface. Most effort has been dedicated towards the removal of metals and particles. With shrinking device dimensions problems associated with organics become more critical (1).

The organic compound under investigation (HMDS, HexaMethylDiSilazane), is used in the IC-processing as a photoresist primer. After the necessary processsteps are completed, the residue of this compound should also be removed. Traditional cleaning sequences use SPM (Sulfuric Peroxide Mixture) to remove organic residues. However, since SPM utilises corrosive acids and requires a high temperature, it causes problems in terms of handling and chemical waste processing. Therefore an alternative cleaning procedure i.e. ozonated DI water, is evaluated in terms of removal efficiency. In fact,

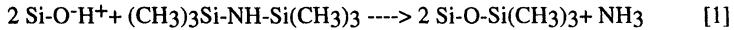
the purpose of this study is to define parameter conditions (e.g. temperature, pH, ozone concentration, immersion time) that have an impact on this removal efficiency.

Ozone has been used exhaustively in the field of waste treatment and drinking water sterilisation, because of its strong oxidising power. An additional benefit of ozone is its harmless residue after decomposition. In micro-electronics industry, ozone is looked upon as a potential replacer for H<sub>2</sub>O<sub>2</sub> (SPM vs. SOM(Sulfuric Ozonized Mixtures)), as both have high oxidation potentials (E<sub>0</sub> = 2.07 eV for O<sub>3</sub> in gasphase, E<sub>0</sub> = 1.78 eV for H<sub>2</sub>O<sub>2</sub>, and 1.24 eV for O<sub>3</sub> when dissolved in water). The strong oxidising (and thus cleaning) effect of ozonated water might be due to the decomposition products. When ozone is dissolved in water, its self-decomposition is accelerated. Although an exact mechanism is not known, it is believed that the decomposition of ozone leads to the generation of OH\* radicals. These radicals are believed to play an important role in decomposing organic material (2,3). A potential drawback of ozonated water is the relative low solubility of ozone in water (about 20 ppm at room temperature (4)).

The organic surface coverage has been monitored by TOF-SIMS. This analysis technique is especially suited for detection of trace amounts of complex organic materials on surfaces (5). Contact angle measurements gave an idea of the wettability and thus were an indication of the cleaning tendency : a better cleaning results in a smaller amount of organic contamination and thus a more hydrophylic surface.

## EXPERIMENTAL SETUP

For the experiments a set of p-type <100> Cz wafers was used. All received a standard FS1b (SPM-dilutedHF-SC1-SC2) clean. Afterwards, the wafers were primed with HMDS on a SVG track 8838VP, and post baked for 10 minutes at 100°C. HMDS reacts with the surface silanol groups according to the following reaction :



This reaction is highly selective and converts all silanol groups, leaving a monolayer coverage of TMS groups (TriMethylSiloxane). The surface becomes hydrophobic in nature (maximum contact angle ±70°).

The ozone was produced with a Sandor (Labor Ozonisator - Type 301.7; 30 g/m<sup>3</sup>) generator. The gas was bubbled through a static bath containing DI-water and placed in a thermostatic bath until stabilisation of the ozone concentration. Upon stabilisation (ozone saturation dependent on parameters under study), the ozone bubbling was stopped and the contaminated wafers were immersed in the solution.

Several variables were considered to have an impact on HMDS removal efficiency: i.e. temperature, pH, ozone concentration and immersion time. Ozone concentration was controlled by two parameters of the ozone generator : the yield of the generator and the O<sub>2</sub> flow-rate. Additionally, the immersion time in the ozonated DI water was evaluated. An overview of the parameter set is given in Table I. The complete experimental matrix is made by means of DOE (Design Of Experiments), quadratic model, to reduce the number of experiments but is not shown here because of its large extent (36 trials per immersion time, including reproducability-check).

Table I : Variables with their range of variation

Variables	Range
Temperature	20°C, 45°C, 70°C
Initial pH (adding HCl)	2, 4.5, 7
O <sub>2</sub> flow	2 l/min, 4.5 l/min, 7 l/min
Generator Yield	60 %, 80%, 100% (*)
Immersion time	10", 60" (**)

(\*) % of the current/voltage characteristics of the ozone generator

(\*\*) Use of short immersion times to see relative differences in parameter-dependency

As a reference for the ozonated DI clean efficiency, several other cleaning procedures were evaluated as well. An overview is presented in Table II.

Table II : Cleaning procedures as a reference

	Procedure	Temperature	Immersion Time
1	DI-water	20°C	1'
2	SPM (4:1)	90°C	1'
3	SPM (4:1)	90°C	10'
4	SOM	90°C	1'
5	SOM	90°C	10'

Immediately after cleaning, the contact angle of a 5 µl H<sub>2</sub>O droplet was determined at five different positions on the wafer. The TOF-SIMS analysis was performed on a TRIFT I spectrometer (Charles Evans & Ass., California, USA).

## RESULTS AND DISCUSSION

### Ozone

It might be useful to first evaluate the parameter dependence on the ozone behaviour itself before analysing the impact on HMDS removal. For each trial with a certain combination of experimental variables, the ozone concentration after stabilisation has been recorded. Statistical evaluation of the presented data based on the quadratic model (DOE), reveals that all parameters but pH (in the acid-range studied in these experiments) have an effect on the ozone concentration. The extent to which either parameter influences the measured ozone concentration can be derived from Figure 1. The ozone concentration is plotted as a function of the generator yield for varying temperature and oxygen flow.

As can be seen in Figure 1, it is obvious that increasing the generator yield leads to an increasing ozone concentration. Also, bath temperature and ozone concentration are inversely related, due to lower solubility of the ozone (6) and faster decay at elevated temperatures. Additionally, for our type of generator and bubbler (perforated PFA tube), an inverse relationship can be seen between ozone concentration and oxygen flow. In summary, to obtain maximal ozone concentrations in static solutions, one should operate at low temperature, with low O<sub>2</sub> flow and high generator yield.

### HMDS

The cleaning efficiency is evaluated based on the wettability (the contact angle) of the surfaces. A low contact angle corresponds to a more hydrophylic and thus to a cleaner surface. This contact angle is directly related to the surface coverage of TMS groups, namely the ratio of the TOF-SIMS intensity at mass 73 (representing the TMS in the positive spectra) versus the sum of intensities of this mass and the one of the Si<sup>+</sup> peak (mass 28) (see formula 2). This relationship has been proven earlier (7), the fitted model here is given by formula 3.

$$\text{ratio} = [(I_{73}^+)/(I_{73}^+ + I_{28}^+)] \quad [2]$$

$$[\cos(\text{Contact Angle}) = -10.5 \text{ (ratio)} + 0.965] \quad [3]$$

As the surface coverage is related to the chemical treatment of the surface, a quantitative assessment of the efficiency of the treatment by means of the contact angle is justified.

In order to study the removal efficiency of the ozonated DI water for HMDS contaminated wafers, first the reference cleaning procedures are looked at. An overview is presented in table III. The measured contact angles indicate that immersion in DI water does not affect the HMDS surface coating (the angle of an uncleaned wafer is  $70.4^\circ \pm 2.5$ ), while either SPM or SOM at both immersion times (1 min and 10 min) leads to full removal of the HMDS. This near complete HMDS removal is confirmed by TOF-SIMS, as can be seen in Figure 2 where the mass range between 30 and 90 amu for the positive spectrum of a HMDS coated wafer and a SPM cleaned wafer (1 min) is shown. The peaks at masses 43 and 73, characteristic for HMDS, are fully removed after the clean.

Table III : Contact angles after the reference cleaning procedures.

	<b>Procedure</b>	<b>Contact Angle (<math>^\circ</math>)</b>
<b>1</b>	DI-water	$67.7 \pm 1.34$
<b>2</b>	SPM (4:1)	<5
<b>3</b>	SPM (4:1)	<5
<b>4</b>	SOM	<5
<b>5</b>	SOM	<5

Statistical evaluation of the presented data based on the quadratic model reveals that temperature, ozone concentration (yield and flow) and pH influence the cleaning efficiency. Obvious observation is also that cleaning efficiency is dependent on wafer immersion time (similar trends observable for 10s and 60s immersion time, though more pronounced for 60s). The parameter dependence as described by the quadratic model is represented graphically in Figure 3, for temperature versus pH, temperature versus flow, and temperature versus yield dependence, respectively. The figures represent the (model based) contour lines indicating the contact angle, thus a low number represents a higher cleaning efficiency. These plots allow to immediately derive the parameter dependence of cleaning efficiency.

It can be seen from figure 3A, that the cleaning efficiency is strongly dependent on the bath temperature : increased temperatures result in smaller contact angles and thus in more efficient removal of the organic compound. The pH dependence seems to be of importance only at elevated temperatures where a higher initial acidity of the solution reduces the obtained cleaning efficiency. Figure 3B and C reveal the same temperature dependence, while the flow and yield dependence only play at elevated temperatures : an optimal cleaning at low flow and high yield values.

#### Combination : Ozone and HMDS

Looking now at the parameter-dependence of both the ozone-concentration and the cleaning efficiency of the ozonised/DI water procedure for HMDS removal, there is an equal trend concerning the yield and the oxygen flow : the highest ozone concentration and the most efficient clean at high yield and low flow. But for the temperature the dependence is contradictory : the highest ozone concentration is reached at low temperature but the removal of HMDS by O<sub>3</sub>/DI is more efficient at elevated temperature. This is confirmed in figure 4, where the (low) flow and (high) yield variability is combined by plotting the cleaning efficiency as a function of ozone concentration, temperature and pH. The calculation of the cleaning efficiency is based on formula [2] :

$$\text{Efficiency (\%)} = ((\text{ratio}_{\text{before}} - \text{ratio}_{\text{after}}) / \text{ratio}_{\text{before}}) * 100 \quad [4]$$

It can be concluded that temperature is the primary depending parameter for HMDS removal, but at any temperature, the ozone concentration correlates linearly with the cleaning efficiency. Also, a mild pH effect can be observed, at any temperature condition.

In an attempt to explain the removal of HMDS from silicon surfaces, one could assume that this is achieved according to a simple hydrolysis mechanism (Si-O-TMS + H<sub>2</sub>O  $\Rightarrow$  Si-OH + HO-TMS). It can be found in organic literature that TMS groups are frequently applied as protecting groups against oxidation of functional groups. Subsequent removal of these groups is achieved by hydrolysis in acidic environment. Nevertheless, a similar reaction pathway is unlikely in this case, as removal efficiency is inversely related with initial pH of the solution, also immersion of an HMDS coated wafer in DI water had little or no effect (see table III). Additionally, the above

hydrolysis mechanism would not be able to explain the dependence of removal efficiency with ozone concentration. Therefore, ozone and/or its reaction products indeed are responsible for removing TMS groups from the silicon-surfaces. Elevated temperatures can have a positive influence because then the ozone decomposition is activated and thus there are more reactive decomposition products present.

## CONCLUSIONS

The cleaning efficiency of ozonated DI water has been evaluated for HMDS contaminated wafers with reference to standard cleaning processes such as SPM or SOM. It was found that ozonated DI water is capable of removing surface TMS groups as demonstrated from contact angle and TOF-SIMS measurements. The experimental parameters that influence the removal efficiency are in decreasing order of importance: elevated temperature, ozone concentration ( $O_2$  flow and generator yield), and pH (and immersion time). The dependence on ozone concentration and the pH behaviour seem to exclude a simple hydrolysis mechanism. Also, no clear correlation between cleaning efficiency and ozone concentration is observed, as elevated temperatures favour removal efficiency, but disfavour ozone build-up in solution. The latter seems to indicate that some reactive ozone decomposition products are responsible for HMDS clean-up.

## REFERENCES

### Journals

1. K.J.Budde, W.J.Holzapfel, M.M.Beyer, J. Electrochem. Soc., **142**(3),888(1995)
2. G.Alder, R.Hill, J. Am. Chem. Soc., **72**, 1884(1950)
3. T.Isagawa, M.Kogure, T.Futatsuki, T.Ohmi, Annual Semicond. pure water conf.,**12**, 117(1993)
5. A.Benninghoven, Angew. Chem. Int. Ed. Engl., **33**, 1023(1994)
7. P.Van Velzeb, J.J.Ponjee, A.Benninghoven, Surf. Science, **37**, 147(1989)

### Society Proceedings Series

6. J.K.Tong, D.C.Grant, Proc. Electrochem. Soc., **18**, 92(1992)

### Book

4. Handbook of chemistry and physics, p.1703, The chemical rubber publishing co., Cleveland, OH (1962)

Figure 1 : Ozone concentration in DI water versus yield, flow (l/min) and temp. (°C)

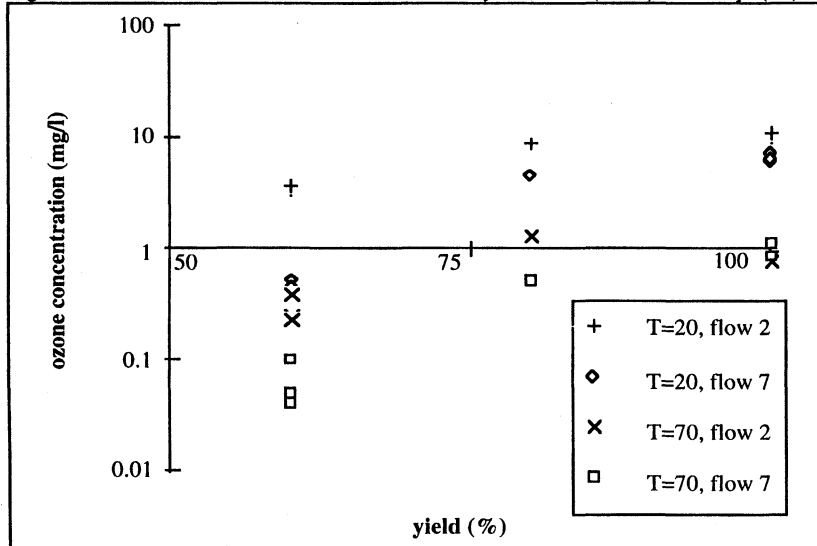


Figure 2 : Positive TOF-SIMS spectra of HMDS-primed and SPM-cleaned sample

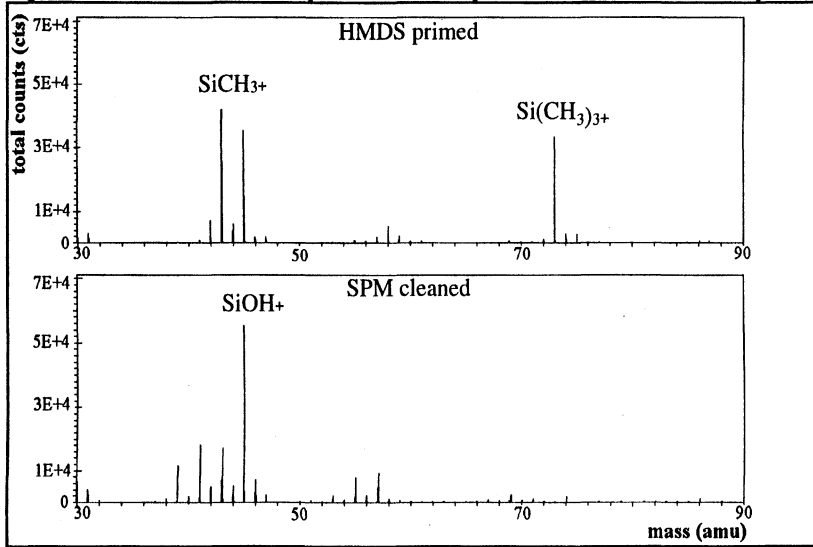


Figure 3 : Contour plots : contact angles for different experimental conditions (immersion time is 60 seconds)

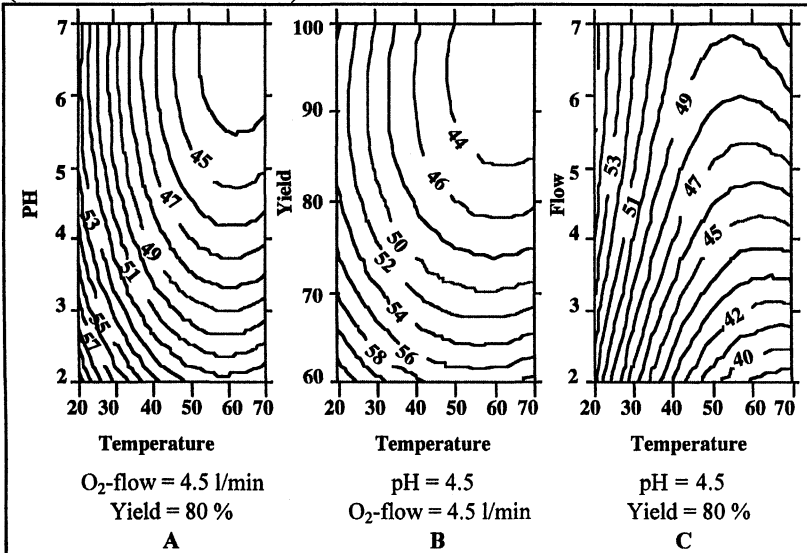
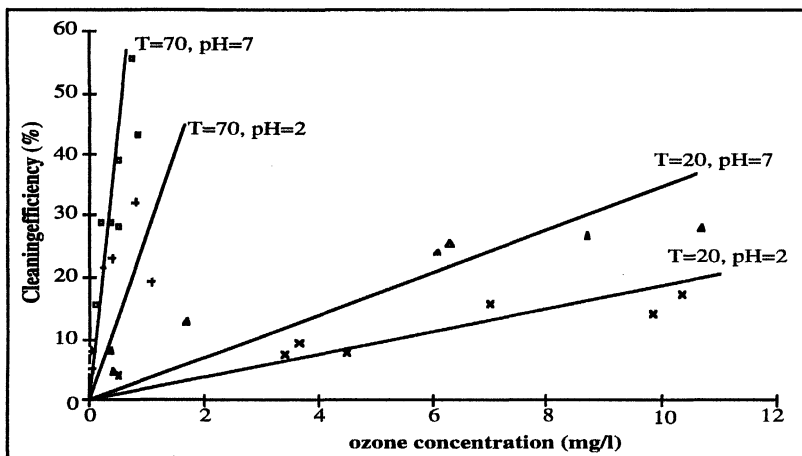


Figure 4 : Cleaning efficiency for HMDS contaminated wafers versus ozone concentration, temperature and pH (immersion time is 60 seconds)



# **Contamination Removal by Single-Wafer Spin Cleaning with Repetitive Use of Ozonized Water and dilute HF**

**Tsutomu Osaka, Akira Okamoto, Hitoshi Kuniyasu,  
and Takeshi Hattori**

ULSI R&D Laboratories, SONY Corporation, Atsugi 243, Japan

We have developed a new technique of single-wafer spin cleaning at room temperature while alternating the addition of ozonized water and dilute HF for 10 sec. each, then repeating the cycle until the surface cleanliness reaches the required level. The new spin cleaning sequence can efficiently remove both particulate and metallic contaminants as well as organic contaminants on the surface of silicon wafers in a short period without increasing the micro-roughness of the surface.

## **INTRODUCTION**

Wet chemical processing is the most repetitively applied processing step in any LSI fabrication sequence. Wafer-cleaning chemistry has remained essentially unchanged over the past 25 years, the most prevalent method in the semiconductor industry worldwide still being the hydrogen peroxide-based wet chemical process, most notably the RCA Standard Clean [1], in which wafers are sequentially immersed for minutes in chemicals such as a  $\text{NH}_4\text{OH}/\text{H}_2\text{O}_2/\text{H}_2\text{O}$  mixture or a  $\text{HCl}/\text{H}_2\text{O}_2/\text{H}_2\text{O}$  mixture at elevated temperatures as well as in dilute HF at room temperature. In some cases, a hot  $\text{H}_2\text{SO}_4/\text{H}_2\text{O}_2$  mixture is added at the beginning of the sequence.

In such immersion-type wet chemical cleaning, even if ultra-pure chemicals are introduced and then disposed of after each wafer-cleaning treatment, the contamination removal efficiency is dominated by the amount of impurities brought into the fresh solution by the to-be-cleaned wafers themselves [2][3]. In order to meet stricter wafer-cleanliness requirements in the future, new cleaning methods in which fresh chemicals are continuously supplied, such as single-wafer spin cleaning, will have to be employed. The spin-processing equipment has the advantage of a much smaller footprint than that of the conventional wet bench, but its throughput must be increased and its chemical consumption reduced [4]. To do so, a technique using alternative cost-effective chemicals rather than the conventional RCA Standard Clean, as well using a fewer number of chemicals, must be employed to shorten the cleaning period as well as to reduce chemical consumption.

In this paper, a new wafer-cleaning sequence using single-wafer spin cleaning is reported. The new technique is low cost, has high performance at room temperature, and requires a short time, using alternately only ozonized water and dilute HF (DHF), for removing contaminants, such as particles, metallics, and organics, on wafer surfaces.

## EXPERIMENTAL PROCEDURE

For this study, n-type, <100>-oriented, 200-mm diameter Czochralski-grown wafers were used. These wafers were intentionally contaminated with either particles, metals, or organic compounds.

For particle-removal evaluation, both polystyrene-latex-(PSL)-sphere-adhering and Al<sub>2</sub>O<sub>3</sub>-particle-adhering wafers were prepared. To deposit PSL spheres on the wafers, VLSI Standards' sphere deposition equipment was used. To deposit Al<sub>2</sub>O<sub>3</sub> particles on the wafers, the wafers were immersed in DHF and subsequently in DI water in which Al<sub>2</sub>O<sub>3</sub> particles were intentionally added, and finally rinsed in DI water.

For metal removal evaluation, Cu-, Fe-, and Al-contaminated wafers were used. To prepare Cu-contaminated wafers, test wafers were immersed in a DHF solution which was spiked with Cu to 10 ppm by adding the standard Cu-containing solution originally prepared for in atomic adsorption spectroscopic analysis. To prepare Fe or Al contaminated wafers, a contaminated SC-1 solution (NH<sub>4</sub>OH/H<sub>2</sub>O<sub>2</sub>/H<sub>2</sub>O) which was spiked with Fe or Al to 1 ppb by adding the standard Fe- or Al-containing solution. The contamination levels of Cu, Fe, and Al on the wafer surface were controlled on the order of 10<sup>12</sup>-10<sup>14</sup> atoms/cm<sup>2</sup> for each metal.

For evaluation of the organic-removal efficiency of repetitive single-wafer spin cleaning using ozonized water and DHF, after the silicon wafers were cleaned with ozonized water, they were intentionally contaminated by butylhydroxytoluene (BHT), one of the common antioxidants contained in plastic boxes, which causes organic contamination on the surface of silicon wafers stored in plastic boxes. For evaluating the surface roughness of silicon wafers, we prepared wafers on whose front surface As was implanted at the level of 3x10<sup>14</sup> atoms/cm<sup>2</sup>, then the wafers were annealed, because it is known [5] that micro-roughness occurs more readily on an impurity-doped (n<sup>+</sup>-type) surface than an n-type surface. The wafers were subjected to single-wafer spin cleaning, and the contamination (or micro-roughness) levels before and after the cleaning were compared.

The spin-cleaning sequence consists of pouring ozonized water onto the wafer surface, followed by pouring DHF. The pouring time was varied in order to determine the shortest time providing acceptable results, which was 10 sec. each for the ozonized water and the DHF, or a total of 20 sec. for one cycle. This sequence was repeated as many times as needed. After the last DHF treatment, DI water was poured on the wafer, and finally the wafer surface was dried by in-situ centrifugal spindrying. All the cleaning and drying were performed at room temperature in a nitrogen atmosphere to avoid water-spot formation.

The concentration of ozone in DI water was kept at 20 ppm throughout this study and was measured at the outlet of the ozone generator. The HF concentration in the DHF was kept at 1%. The temperature of the ozonized water and DHF solution was kept at 23°C (room temperature) throughout the experiment. The rotational speed of the wafer in the spin cleaner was kept at 1600 rpm. Fresh ozonized water and DHF were

supplied to the center area of the wafer surface continuously at a rate of 1.2 liters per min. and 1.5 liters per min., respectively. The ozonized water and DHF were disposed of after being poured on the wafer.

The metallic contaminants on the wafer before and after spin cleaning were measured using flameless atomic absorption spectrometry (FL-AAS) after liquid phase decomposition of the contaminants. The detection limits are  $1.5 \times 10^8$  atoms/cm<sup>2</sup> for Cu,  $4.0 \times 10^8$  atoms/cm<sup>2</sup> for Fe, and  $4.0 \times 10^8$  atoms/cm<sup>2</sup> for Al. Particulate contaminants on the wafer were measured using a laser-scanning inspection system using the light-scattering method. Organic contaminants on the wafer were analyzed using gas chromatography/mass spectrometry following thermodesorption (TD-GC/MS). Micro-roughness on the silicon surface before and after spin cleaning was measured using an atomic-force microscope (AFM).

## RESULTS AND DISCUSSION

### Particle Removal

Particulate contaminants on the wafer surface are removed very efficiently using this cleaning method.  $\text{Al}_2\text{O}_3$ -particle removal efficiency, or the ratio of  $\text{Al}_2\text{O}_3$  particles removed from the front surface of silicon wafers to the particles initially adhering, for various cycles of 20 sec. and 2 min. cleaning is shown in Fig.1. After one, two, and three cycles of cleaning, particles were removed by approximately 79%, 85%, and 87%, respectively, for both 20-sec. and 2-min. cycles. The reason there is virtually no difference in particle-removal efficiency between the 20-sec. cleaning cycle and 2-min. cleaning cycle may be as follows.

During the ozonized-water treatment, as can be seen in Fig.2, a chemical oxide film grows very rapidly on the wafer surface, and the growth of the oxide almost saturates at a thickness of approximately 0.7 nm at the end of the 10 sec. of ozonized-water pouring. The chemical oxide grows very slowly after 10 sec. This chemical oxide can be completely etched off from the wafer surface within 10 sec. by subsequently pouring DHF (1%). So, the minimum acceptable cleaning period is 10 sec. for the chemical concentrations used in this study. Pouring the chemicals for a longer time (>10 sec.) with the same or fewer number of cycles does not increase the particle-removal efficiency. Therefore, the 20-sec. cleaning cycle consisting of 10 sec. pouring of ozonized water and 10 sec. pouring of DHF(1%) is recommended to save time and chemical consumption. If 0.5% DHF is used, we recommend that DHF be poured for 15 sec., while keeping the pouring of ozonized water at 10 sec. Particles removed from the wafer surface flow away immediately during spin cleaning, so re-depositing of particles on the surface, usually observed in immersion wet chemical cleaning, is not observed.

PSL spheres were much more easily removed from the silicon surface than  $\text{Al}_2\text{O}_3$  particles. PSLs were removed by 98%, 99%, and 99.5%, respectively after one, two, and three cycles of the cleaning, as shown in Fig.3.

### Metal Removal

Metallic contaminants on the wafer surface, not only Fe and Al but also Cu, are effectively reduced by the alternative pouring of ozonized water and DHF. Cu contamination on a wafer surface intentionally contaminated as high as  $5 \times 10^{13}$  atoms/cm<sup>2</sup> was reduced to the  $5 \times 10^{11}$  atoms/cm<sup>2</sup> level after one cycle of the treatment, to  $2 \times 10^{10}$  atoms/cm<sup>2</sup> after three cycles, and to the  $10^9$  atoms/cm<sup>2</sup> level after 6 cycles, as is shown in Fig.4. On the other hand, Fe and Al contamination as high as  $10^{12}$ ~ $10^{13}$ atoms/cm<sup>2</sup> was reduced to the  $10^9$  atoms/cm<sup>2</sup> level or lower with only one cycle of the ozonized water-DHF treatment, as is shown in Fig.5 and 6.

The removal of metals is considered to be due to both dissolution of the metals by the ozonized water with very high redox potential and the lift-off of chemical oxide films from the silicon substrate by etching with HF. Most Fe and Al atoms on the wafer surface are ionized by the ozonized water, dissolve into the water and are removed from the wafer. Even if Fe and Al, which have higher oxide generation enthalpy than Si, remain in the chemical oxide grown during the ozonized-water treatment, these atoms in the chemical oxide are etched off with the chemical oxide on the wafer surface by DHF. Dissolved Fe and Al ions in the DHF are not re-deposited on the wafer surface because these metals have lower electronegativity than Si. Therefore, the removal efficiency of Fe and Al on the wafer surface is very high. On the other hand, even if some of the Cu atoms incorporated into the chemical oxide during the ozonized-water treatment are etched off with DHF, Cu atoms are apt to be re-deposited on the wafer surface from the DHF much more easily than Al and Fe, because Cu has a higher electronegativity than Si. Therefore, Cu removal efficiency is less than Fe and Al removal efficiency.

### Organic Contamination Removal

Organic contaminants are also removed from the wafer surfaces with this new cleaning technique. Trace organic contaminants on silicon wafers caused by out-gassing from the plastic box in which the wafers had been stored for a long time were removed by the first pouring of ozonized water, as is shown in Fig.7. Intentionally contaminated BHT on the wafer surface was removed by one cycle of the ozonized water-DHF cleaning, as is shown in Fig.8. The reason for this effectiveness is that ozonized water has a sufficiently high oxidation potential to oxidatively degrade organic contaminants, while DHF is capable of removing them by lifting off the native oxide film on which organic contaminants adsorb [6].

### Surface Roughness

Figure 9 shows typical AFM images of the surfaces of silicon wafers before and after spin cleaning with alternatively pouring ozonized water and DHF. The root-mean-square (RMS) roughness of the surface after as many as 12 cycles of cleaning was 0.28 nm. The RMS value of the surface before cleaning was 0.25 nm. Therefore, there is virtually no difference between the surface roughness before and after cleaning.

### Sequence Modification

When the native oxide films on the initial wafers are comparatively thick (>1nm) due to prolonged exposure of these wafers to the ambient air, it is recommended that 10 sec. or longer DHF pouring onto the initial wafers be employed before the cycle of the

ozonized water/DHF sequence starts, in order to remove the comparatively thick native oxide, uncovering noble metals adhering on the silicon surface, and enhancing the metal removal efficiency in the following cleaning sequence. Trace organic contaminants on the native oxide are also easily removed by DHF [6].

In the final step of cleaning, after the last DHF treatment, DI water is applied to the wafer if one wants to obtain a hydrophobic silicon surface, or ozonized water is applied to obtain a hydrophilic silicon surface.

## SUMMARY

Single-wafer spin cleaning at room temperature has been refined by using only ozonized water and DHF. The spin-cleaning sequence consists of pouring ozonized water onto a wafer surface for 10 sec., followed by pouring DHF for 10 sec. This short-time cleaning can efficiently remove metallic and particulate contaminants as well as organic contamination without increasing micro-roughness on the surface. This sequence can be repeated as many cycles as needed until the surface cleanliness reaches the required level.

In the final step of cleaning, after the last DHF treatment, DI water is applied to the wafer to obtain a hydrophobic silicon surface, or ozonized water to obtain a hydrophilic silicon surface. This low-cost, high-performance, room-temperature treatment in which fresh liquids are continuously supplied will meet future stricter wafer cleanliness and environmental requirements.

## REFERENCES

- [ 1 ] W. Kern and D. A. Puotineen, *RCA Review*, **31**, 187 (1970).
- [ 2 ] T. Osaka and T. Hattori, , in *Proceedings of the 5th International Symposium on Semiconductor Manufacturing (ISSM'96)*, Tokyo, pp.204-207 (1996). To be published in IEEE Trans. on Semiconductor Manufacturing (1998).
- [ 3 ] T. Hattori, in *Cleaning Technology in Semiconductor Device Manufacturing V*, J. Ruzzyllo and R. E. Novak, Editors, *The Electrochemical Society Proceedings Series, Pennington, NJ, to be published* (1998).
- [ 4 ] N. Yonekawa, S. Yashi, F. Kunimoto, T. Ohmi, and F. W. Kern, in *Cleaning Technology in Semiconductor Device Manufacturing III* , J. Ruzzyllo and R. E. Novak, Editors, PV94-7, pp.94-101, *The Electrochemical Society Proceedings Series, Pennington, NJ* (1994).
- [ 5 ] T. Ohmi, T. Imaoka, T. Kezuka, J. Takano, and M. Kogure, *J. Electrochem. Soc.*, **140**, 811 (1993).
- [ 6 ] K. Saga and T. Hattori, *J.Electrochem. Soc.*, **143**, 3279 (1996).

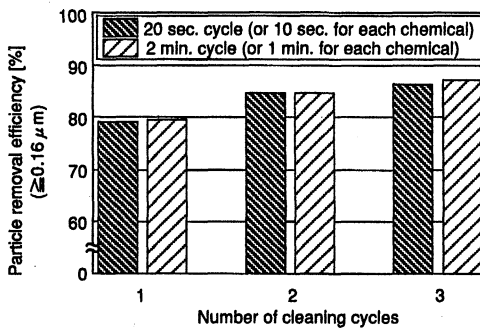


Fig. 1  $\text{Al}_2\text{O}_3$  particle removal efficiency as a function of the number of cleaning cycles.

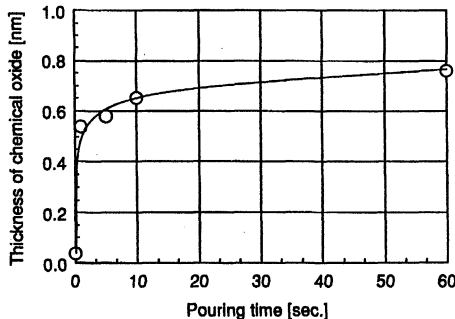


Fig. 2 Thickness of chemical oxide on a wafer surface measured with X-ray photoelectron spectrometry (XPS) as a function of ozonized-water pouring time.

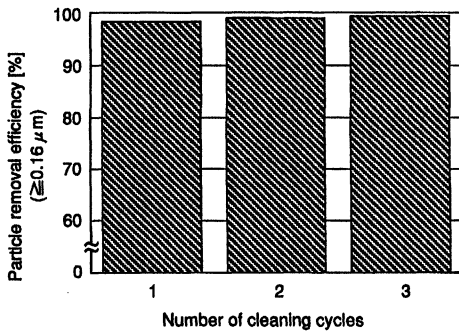


Fig. 3 PSL particle removal efficiency as a function of the number of cleaning cycles. One cycle consists of pouring of ozonized water and dilute HF for 10 sec. each.

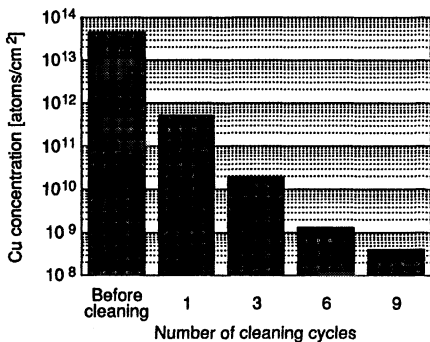


Fig. 4. Cu concentration on a wafer surface before and after cleaning as a function of the number of cleaning cycles.

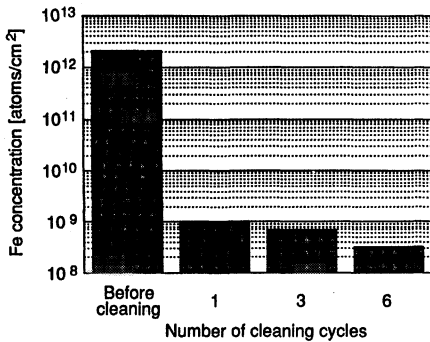


Fig. 5. Fe concentration on the wafer surface before and after cleaning as a function of the number of cleaning cycles.

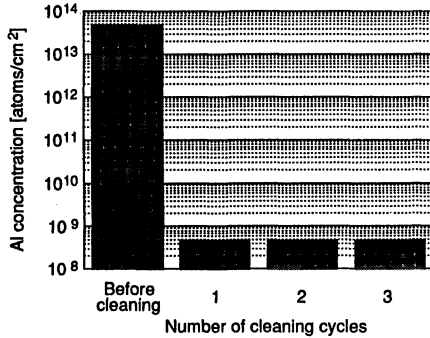


Fig. 6. Al concentration on a wafer surface before and after cleaning as a function of the number of cleaning cycles.

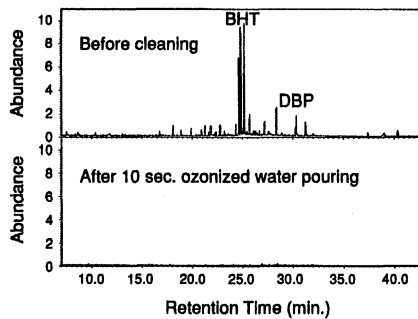


Fig.7 Gas chromatograms for organic contaminants absorbing on a silicon surface before and after 10 sec. ozonized-water cleaning.

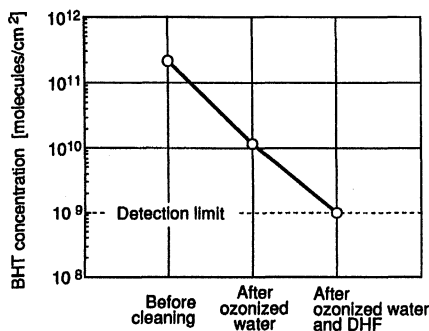


Fig.8. Organic (BHT) concentration on a wafer surface before and after cleaning.

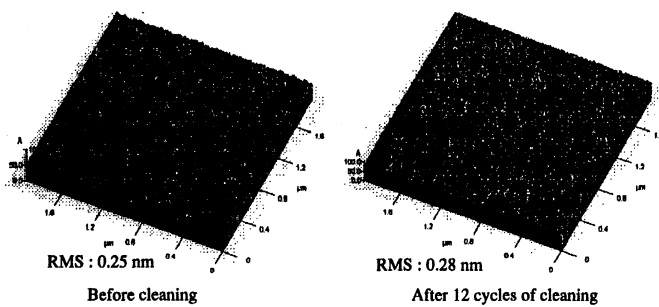


Fig. 9 Typical AFM images of the surface of an n<sup>+</sup> silicon wafer before and after 12 cycles of spin cleaning.

## **DIRECT REPLACEMENT CLEANING TECHNOLOGY BASED ON OZONATED WATER USING A SINGLE PROCESSING TANK**

**Yuji Fukazawa, Kunihiro Miyazaki, Yoshihiro Ogawa**

Toshiba corporation

Integrated Circuit Advanced Process Engineering Department.

Yokohama (AMC)

8,shinsugita-cho, isogo-ku, yokohama-city, 235 JAPAN

A new cleaning technology based on ozonated water(O<sub>3</sub> water) has been investigated. As is well known, O<sub>3</sub> water rinse alone shows the removal efficiency of some organic contaminants from silicon surfaces. Also hydrofluoric acid(HF) is well known as a chemical to remove the native oxide and some metallic contaminants except noble metal such as copper. A mixture of HF and O<sub>3</sub> water(HF/O<sub>3</sub>) can remove the native oxide and metallic contamination including copper. Another characteristic of this solution is the etching of silicon surface under the room temperature. The surface roughness by HF/O<sub>3</sub> is smaller than that of SC1. The etching rate of silicon by HF/O<sub>3</sub> depends on the concentration of HF and O<sub>3</sub> in this mixture. The etching of silicon surface is useful to remove the particles from the wafers. According to the zeta potential model, however, it is difficult to prevent the particle adhesion onto silicon surfaces in an acid solution. Application of a single processing tank which can replace the chemicals avoiding a contact to the air during cleaning can suppress the particle adhesion. A room temperature process, minimized chemical consumption and a simplified cleaning process can be established by this HF/O<sub>3</sub> cleaning technology using a single processing tank.

### **INTRODUCTION**

In semiconductor device manufacturing, the RCA clean which established in 1970 has been widely used for over 20 years.<sup>1</sup> The mixture of hydrogen peroxide(H<sub>2</sub>O<sub>2</sub>) with ammonium hydroxide(NH<sub>4</sub>OH) and hydrochloric acid(HCl), which is called as SC1 and SC2, is effective in removing the particles and the metallic contaminants respectively. Another mixture of H<sub>2</sub>O<sub>2</sub> and sulfuric acid(H<sub>2</sub>SO<sub>4</sub>) is also used to remove organic contamination from the silicon surfaces. Beside these H<sub>2</sub>O<sub>2</sub> based cleaning, diluted hydrofluoric acid(DHF) is effective in removing the native oxide and well used in conjunction with SC1,SC2 and H<sub>2</sub>O<sub>2</sub>/H<sub>2</sub>SO<sub>4</sub>. Each cleaning solution shows the removal efficiency of a certain contamination on the silicon surfaces, however, there is a side effect for each cleaning itself. For instance, the adhesion of metallic contaminant such

as Fe and the surface roughness by SC1 cleaning, or Cu adhesion in DHF became clear.<sup>2-4</sup> In recent years, some improvements such as a modification of chemical concentration and the addition of chelating agents into an alkaline solution have been suggested.<sup>5-8</sup> Another new cleaning technologies such as O<sub>3</sub> water,DHF/H<sub>2</sub>O<sub>2</sub>, electrolysis ionized water have also suggested as a new cleaning technology.<sup>9-11</sup> We suggested the mixture of HF and O<sub>3</sub> water(HF/O<sub>3</sub>) as a solution which can remove the Cu under the room temperature<sup>12</sup>. In this study, we examined the removal efficiency of metallic contaminants by this solution more detail. Another characteristic of this solution is the etching of silicon surface, therefore the etching rate of silicon and surface roughness was also examined in comparison with one by the SC1. Furthermore, we discuss the application of this cleaning solution to the other contamination such as organic and particles.

## EXPERIMENTAL

A single processing tank which can supply the O<sub>3</sub> water, HF and deionized(DI) water has been used in this study(Fig.1). Clean O<sub>3</sub> water was generated by dissolving pure ozone gas into the DI water through a membrane unit and that concentration can change from 2 to 10 ppm. The HF/O<sub>3</sub> solution was produced by the mixing of HF and O<sub>3</sub> water in the tank at a room temperature. All wafers were immersed into the HF/O<sub>3</sub> for a certain minutes and rinsed by the DI water which was directly injected into the processing tank, therefore wafers did not contact to the air till drying.

The metallic contamination removal efficiency was examined as a function of HF concentration. HF concentration also change from 0.05 to 0.5(weight%) under the O<sub>3</sub> concentration with 2ppm. The wafers intentionally contaminated by Cu, Fe and Ni at around  $1 \times 10^{12}$ atoms/cm<sup>2</sup> were prepared and immersed into the HF/O<sub>3</sub> solution for 3 minutes. The surface concentration of each metal before and after was determined by atomic absorption spectroscopy(AAS) combined with the vapor phase decomposition (VPD).

In order to measure the etching rate of silicon and oxide, P(100) patterned silicon wafers with the thermal oxide on the surface were used in this study. The etching rate of oxide was measured by ellipsometry on the oxide area before and after HF/O<sub>3</sub> etching. The step height of silicon surface after removing the patterned oxide was measured in order to calculate the etching rate of silicon. Wafers were immersed into the HF/O<sub>3</sub> solution for 3 min with the mixing range from 0.05/2 to 0.5/10(weight% / ppm) at the room temperature.

The mixing ratio of HF/O<sub>3</sub> with 0.25/2(weight%/ppm) was chosen for the inspection of the surface roughness. The surface roughness by the HF/O<sub>3</sub> was examined by atomic force microscopy(AFM) in comparison with that of SC1. The etching amount was measured by ellipsometry using polysilicon and was varied from 2.5nm to 20nm by the control of immersion time.

## RESULTS AND DISCUSSION

The HF/O<sub>3</sub> solution is effective in removing the metallic contamination including Cu which is difficult to remove by HF only.<sup>12</sup> It is considered that the control of redox potential and pH is effective in removing the metallic contamination. The redox potential and pH of HF/O<sub>3</sub> can be controlled by the O<sub>3</sub> and HF respectively, however, concentration is important to make the removal efficiency high. Figure 2 shows the removal efficiency of Cu, Fe and Ni by HF/O<sub>3</sub> as a function of HF concentration(O<sub>3</sub>=2ppm). The removal efficiency of Cu by HF/O<sub>3</sub> decreases when HF concentration is too high, while Fe and Ni do not show such a result. We consider that the deposition rate of Cu onto the silicon surface is faster than that of dissolution in HF/O<sub>3</sub> solution when HF concentration is too high. Adjustment of each concentration of HF and O<sub>3</sub> in the HF/O<sub>3</sub> solution is important to remove the metallic contaminants effectively.

Another characteristic of this solution is the etching of silicon surface. The silicon etching rate by the HF/O<sub>3</sub> solution can be controlled by the concentration of HF and O<sub>3</sub> as shown in Fig.3. The etching rate of thermal oxide is smaller than that of silicon when HF concentration is small. It is considered that the mechanism of silicon etching by the HF/O<sub>3</sub> solution is due to the reaction of oxidation by O<sub>3</sub> and then the dissolution of chemical oxide by HF. If the etching rate of chemical oxide by O<sub>3</sub> is faster than that of thermal oxide, the silicon etching do not occur because of the protection of silicon surface by the chemical oxide. This data shows that the etching rate of chemical oxide by O<sub>3</sub> is larger than that of thermal oxide.

The etching of silicon surfaces is useful for the removal of particles from the silicon surfaces, however, the surface roughness has become a critical issue for the device performances such as gate oxide integrity. The surface roughness by SC1 increase when the etching amount become large, on the other hand, that of HF/O<sub>3</sub> is not affected by the etching depth and it keeps the surface roughness smooth as same as HF only(Fig.4). This result is due to the difference of silicon etching mechanism between an acid solution and alkaline one. Figure 5 shows the comparison of AFM picture which etching depth is 20nm by HF/O<sub>3</sub> and SC1.

Beside above contamination, we have to consider the native oxide, organic contaminants and particles. Obviously, this solution can remove the native oxide by HF as shown in Fig.3. Another our experiment shows that the O<sub>3</sub> water rinse is effective in removing the organic contamination which adhered onto the silicon surfaces in the clean room. Figure 6 shows the removal efficiency of diethyl phthalate(DOP) on the wafers surface in comparison with H<sub>2</sub>O<sub>2</sub> and HF alone.

According to the zeta potential model, it is difficult to suppress the particle adhesion onto the silicon surface in an acid solution.<sup>13</sup> To avoid this problem, we used a single processing tank which can replace the chemical without contact to the air. Direct DI

water rinse injected into the HF/O<sub>3</sub> solution changes pH continuously from 2 to neutral(pH=7), and the zeta potential of the wafer surface and particles such as SiO<sub>2</sub> and SiN become same polarity at the pH nearly 5. Moreover, the silicon etching still occurs during the pH from 5 to 7 because of the diluted HF/O<sub>3</sub> solution but lower etching rate. Another technology such as a optimization of vessel design which easily overflow the particle from the vessel by DI water rinse or ultrasonic irradiation during the cleaning will enhance the particle removal efficiency.<sup>14</sup>

Following is the one of examples of simplified cleaning process using a single processing tank(Fig.7). So that the organic contamination tend to adhere onto the silicon surface in the clean room and to protect the other contamination such as a native oxide and metallic contamination, removing that organic contamination at first will enhance the cleaning efficiency. The O<sub>3</sub> water rinse alone will need to remove the organic contaminants without any damage of oxide and silicon surfaces, but not effective in removing the native oxide and metallic contamination. Sequentially injection of HF into O<sub>3</sub> water using a single processing tank and then the mixing of HF/O<sub>3</sub> solution in the tank can remove the native oxide and metallic contaminants. Furthermore, HF/O<sub>3</sub> solution can etch the silicon surface off and become easy to remove the particles from the silicon surfaces. The use of sonic energy such as megasonic will enhance the particle removal efficiency.

Beside these process performances, a room temperature cleaning process, low chemical consumption and a simplified cleaning technology is required in the future semiconductor manufacturing. The HF/O<sub>3</sub> cleaning consists of two chemicals(HF,O<sub>3</sub>) and the O<sub>3</sub> water can be produced at the point of use, and moreover, it is easy to decompose after cleaning. This cleaning technology eliminates DI water rinse between O<sub>3</sub> and HF/O<sub>3</sub> and reduces DI water consumption and makes the process time short.

## CONCLUSION

A room temperature cleaning process, minimized chemical consumption and a simplified cleaning technology can be established by the O<sub>3</sub> water based cleaning using a single processing tank. The HF/O<sub>3</sub> solution is made by a mixing of HF and O<sub>3</sub> water, therefore this solution shows the removal efficiency of the native oxide and organic contamination. Metallic contaminants including the Cu which is difficult to remove by HF only can be also removed by this solution. Another characteristic of this solution is the etching of the wafer surfaces under the room temperature. Each concentration of HF and O<sub>3</sub> in this solution can control the etching rate of oxide and silicon. The surface roughness by HF/O<sub>3</sub> cleaning is smaller than that of SC1 and that will enhance the device performances such as gate oxide integrity. Particle removal depends on the etching of silicon surface, however, it is difficult to suppress the particle adhesion in a acid solution according to the zeta potential model. The direct replacement of HF/O<sub>3</sub> by DI water using a single processing tank is useful to suppress the particle adhesion onto

the silicon surfaces. The optimization of vessel design which easily overflow the particle from the vessel or application of another technology such as a megasonic can enhance further the efficiency of the particle removal.

We discussed the cleaning of silicon surfaces using a single processing tank tool, however, this cleaning technology can apply to a spray tool or a single wafer processor.

## REFERENCES

1. W.Kern and D.A.poutinen, RCA Rev.,31,187(1970)
2. J.Atsumi, S.Ohtsuka, S.Munehira, and K.Kajiyama, Proceeding of the First International Symposium on Cleaning Technology in Semiconductor Device Manufacturing, in Semiconductor Cleaning Technology/1989, PV90-9,59 J.Ruzyllo and R.E.Novak, Editors, The Electrochemical Society Proceeding Series, Pennington, NJ(1989)
3. J.Ryuta, T.Yoshimi, H.Kondo, H.Okuda, and Y.Shimanuki, Jpn. J. Appl. Phys., 31, 2338(1992)
4. E.Hsu, H.G.Parks, R.Craigin, S.Tomooka, J.S.Ramberg, and R.K.Lowry, J. Electrochem. Soc.,39, 3659(1992)
5. T.Ohmi, M.Miyashita, M.Itano, T.Imaoka, and I.Kawanabe, IEEE Trans. Electron Devices, 39, 537(1992)Cu adhesion in HF
6. O.J.Anttila, M.V.Tilli, M.Schaekers, and C.L.Claeys, J. Electrochem. Soc., 139, 1180(1992)
7. S.Verhaverbeke, M.Meuris, P.W.Mertens, and M.M.Heyns, IEDM 91, 3.6.1(1991)
8. H.Muraoka, I.Hayashida, and T.Nozaki, 29<sup>th</sup> Annual Meeting on Radioisotope in Physical Science and Industries, June(1992)
9. T.Ohmi, T.Isagawa, M.Kogure, and T.Imaoka, J. Electrochem. Soc.,140, 804(1993)
10. T.Shimono and M.Tsuji, The Electrochemical Society Meeting Abstract Vol.91-1, Washington DC(1991)
11. Y.Shiramizu, K.Watanabe, M.Tanaka, H.Aoki, and H.Kitajima, J. Electrochem. Soc., Vol.143,May(1996)
12. Y.Fukazawa, K.Sanpei, T.Nakajima, K.Takase, K.Miyazaki, Proceeding of the Second International Symposium on Ultra Clean Processing of Silicon Surfaces, 267, M.Heins, Editor, acco(1994)
13. M.Itano, T.Kezuka, M.Ishii, T.Ueno, M.Kubo, and T.Ohmi, J. Electrochem. Soc., 142, 971(1995)
14. S.Schwartzman, A.Mayer, and W.Kern, RCA Review., 46, 81(1985)

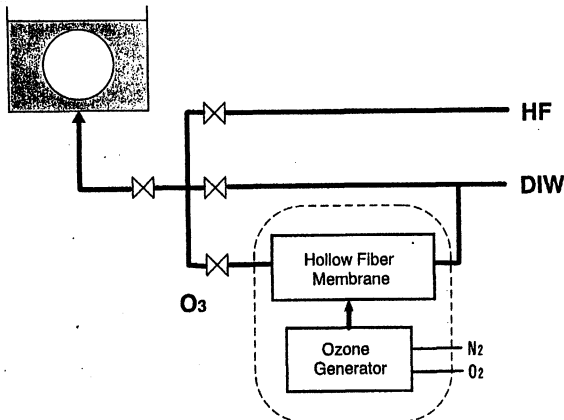


Fig.1 Experimental Diagram

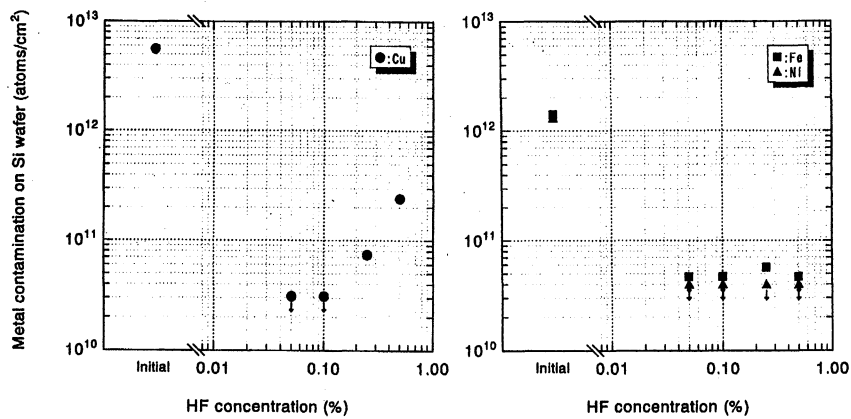


Fig.2 Metallic contamination removal efficiency by HF/O3 cleaning(3min)

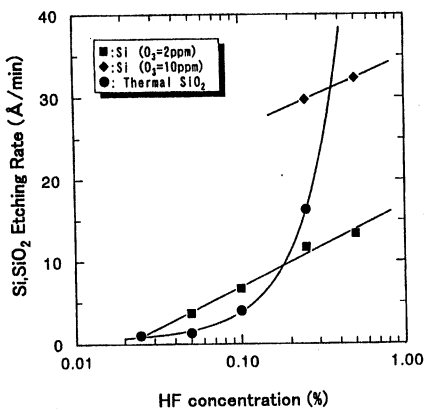


Fig.3 Si etching rate by HF/O<sub>3</sub>

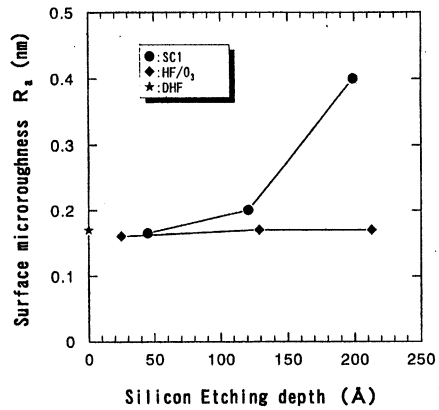


Fig.4 Surface roughness of silicon surface by SC1 and HF/O<sub>3</sub> etching

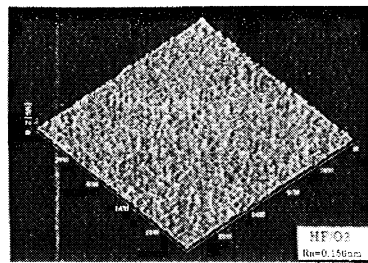
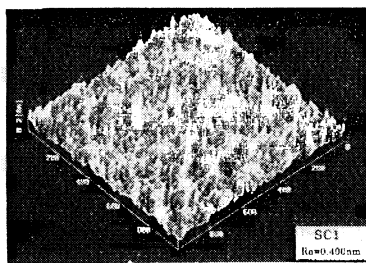


Fig. 5 AFM profiles of the silicon surface after 20nm etching by  
(a)SC1 and (b)HF/O<sub>3</sub>

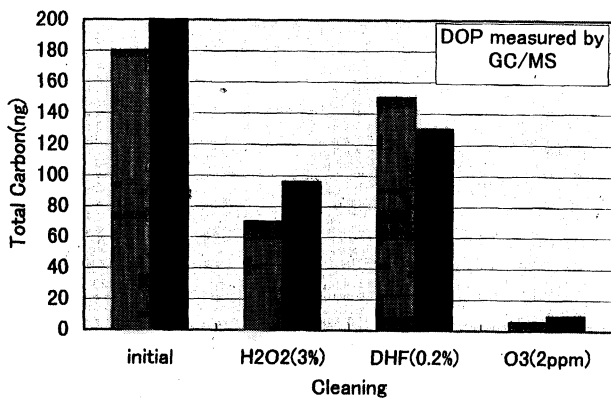


Fig. 6 Removal efficiency of DOP by O<sub>3</sub> water

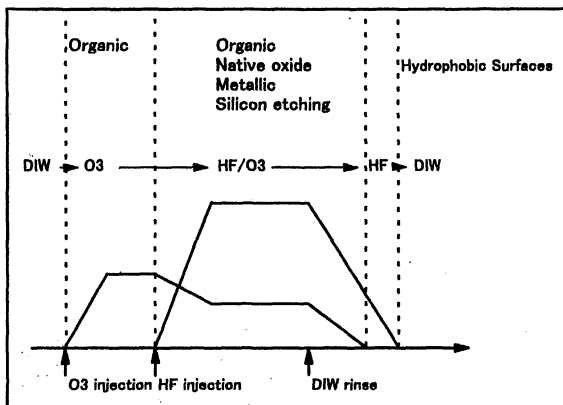


Fig. 7 Example of cleaning sequence of HF/O<sub>3</sub> using a single processing tank

## **OPTIMIZATION OF OZONIZED DI RINSE FOR HF LAST PRE-GATE CLEAN**

**L. Li, W. Lee, T. Gilton, and F. González**  
**Micron Technology Inc., M.S. 306, 8000 S. Federal Way, P.O. Box 6,**  
**Boise, ID 83707-0006**

### **ABSTRACT**

High volume manufacturing clean processes needed for pre-gate clean require efficient removal of metals and particulates. Although the HF last process has recently been seen as an attractive alternative to RCA cleans in the removal of metals, it has been demonstrated that particulate density is higher. The optimal surface condition for a HF last pre-gate clean was determined by applying an extended ozonized DI rinse step at different timed intervals to a regular 5 min DI rinse. The surface passivation was shown to be critical for efficient particle removal and for its impact on the electrical properties of the thin gate oxide films grown on such surface. The particle (LPD) data was correlated with the ozonized rinse time, contact angle, and XPS chemical bond composition. Metallic levels were detected on the VPD-TXRF technique and were shown to be at a low level. The HF last pre-gate clean process demonstrated that even a 4 ppm dissolved ozone level in the 120 s extended ozonated rinse time has a strong oxidizing effect and is adequate to almost completely passivate the silicon surface. In this work, the post HF ozone ( $O_3$ ) concentration in the extended rinse step was characterized to modify the surface passivation and thereby produce a manufacturing-friendly, HF last pre-gate clean process.

### **INTRODUCTION**

The motivation for replacing the current RCA pre-gate cleaning process lies in the lower manufacturing cost of the HF last process: it uses fewer chemicals and is simpler to use. As reported by Tardif et al., the diluted dynamic clean (DDC) was an effective way to substitute for the RCA-based processing (2). As part of the DDC process, the ozonizer was also added in the HF last type process to reduce particles. However, the diluted HF was combined with a dilute HCl solution in ozonized DI water. The challenge was to improve the effectiveness of the ozone levels in the DI water rinse for GOI improvement and particle reduction. In the gate oxide application, the use of ozone levels in the 3 ppm range was described in an overflow rinsing tank at room temperature. The silicon substrates were found to be highly reactive to the dissolved oxygen when treated in an ozonizer or in a partially degassified DI water. Consequently, ozone, which oxidizes well

even at room temperature, can potentially replace the hydrogen peroxide for chemical oxidation. During the first minutes of an over-etch, the oxidation reaction is highly active. Therefore, the ozonized DI water can be used in both the HF bath and rinsing bath.

As reported by Park and Pas, the ozone content in the DI water was not near the saturation limit for continuous ozone injection (3). Using extended ozone rinse times, high oxygen concentration levels have been demonstrated that do affect the GOI and the particle distributions. The impact of water marks, which contain residues and particles, on device yield has been significant as the device feature sizes decrease. A key parameter in the source of microcontamination is the hydrophobic or hydrophilic nature of the silicon surface and the drying process. It has been noted that the electrically defective devices can be attributed to thicker gate oxide within the particles or residue spots.

Nelson investigated the effects of the ozonizer on the ozone water last clean by studying the degree of oxygen passivation of the silicon surface as reflected by the chemical oxide thickness (4). He found that the chemical oxide thickness can be controlled by the ozonated water dispense time. He demonstrated that the completely passivated silicon surface is less susceptible to particle contamination.

The focus of this paper is on the addition of the DI ozone rinse immediately after the HF bath in a manufacturing environment. This study further investigates the optimal ozonizer times in the rinse module performed prior to the thin gate oxidation step. The data also reviews the particle removal with light point defect (LPD) data from a Tencor 6200 system; the metallic levels with the vapor phase decomposition, total x-ray reflective fluorescence (VPD-TXRF) data; the silicon-oxygen composition data using x-ray photoelectron spectroscopy (XPS); and the contact angle measurements. The surface chemistry and metal contamination for different O<sub>3</sub>-treated wafers were also optimized in the cleaning process in order to understand the electrical performance correlating to the cleanings.

## EXPERIMENT

The shortloop tests were conducted with [100] Cz, p-type, 17 Ω-cm, 8-inch wafers, using 1 ppb level grade chemicals. The thin gate oxide thickness was 9nm grown under wet conditions at 800°C with trichlorocarbonate (TLC). The wafer loading was performed under diluted oxygen. The test structures were MOS capacitors using a polysilicon top plate and clear backside of the wafer. The silicon defects in the wafers were measured and characterized before the clean experiment and were at a low defect density.

The wafers were run through the sulfuric peroxide mixture (SPM) + DI rinse + HF + DI rinse cleaning sequence. An automatic cleaning tool was used with separate tanks for SPM, HF, and rinse. The rinse tank was specially designed with an ozonizing unit. The final rinse was a 5 min pure DI water followed by different extended O<sub>3</sub> rinse by injecting the O<sub>3</sub> into the rinse tank. The extended O<sub>3</sub> rinse times were 30 s, 60 s, and

120 s, which were selected to optimize a manufacturing process. The drying cycle was performed in a Marangoni dryer.

The contact angle of water droplets was carried out with well-established angle measurement techniques. The x-ray photoelectron spectroscopy (XPS) was carried out on a Perkin-Elmer model PH5600 high vacuum system using a magnesium/zirconium source.

The VPD-TXRF tool was used in the vapor phase decomposition techniques for enhanced surface contamination resolution. The LPD particle measurements were accomplished with a Tencor 6200 system. The fluence measurements were taken with a Keithley automated system.

## RESULTS AND DISCUSSION

Figure 1 presents the surface passivation changing as a function of O<sub>3</sub> rinse time. We can see that the contact angle between a droplet of DI water and the wafer surface decreases almost linearly with the O<sub>3</sub> rinse time. The contact angle is sensitive to the surface conditioning such that a small value indicates a hydrophilic surface and a large value, a hydrophobic surface. Also, the oxygen passivation uniformity was determined across the wafer surface. The contact angle was an average value of five readings per wafer. By measuring the droplet contact angle, the oxygen passivation was characterized from its hydrophobic surface condition to its variation across the wafer. To minimize the interaction from the prior HF step, the 5 min rinse prior to the ozonizer will remove the cross-over chemicals such that a clean chemical oxide will form during the ozonizing cycle.

Figure 2 shows the graph of the average number of particles per wafer for the cleaning procedure with different ozone final rinses. Since the contact angle decreased with ozone rinse time, it is clearly seen that the silicon surface was shifting from a hydrophobic wafer surface to a hydrophilic wafer surface. Thus, the particle density decreased with the ozone rinse time indicating that the surface condition change was beneficial to the particle removal performance. The typical particle size was small, 0.11–0.22 μm, and we suspect that most of the particles were introduced during the rinse and/or the drying cycle. Although the particles were small, the particle reduction could explain the electrical improvement in the GOI fluence measurement and distribution.

Following the XPS surface analysis results in Table I, it is noted that the silicon-to-silicon percentage decreased with the increasing ozone rinse time, while the oxygen content in the surface increased. The XPS data focused at a 45° angle supports the premise that the higher ozonated water is oxidizing the highly reactive wafer surface and forms a clean, chemical oxide film.

The GOI experiment was carried out to correlate the influence of surface preparation to the electrical characteristics of the device. The Q<sub>bd</sub> data in figure 3 shows that the longer ozone rinse times provide better gate oxide integrity. The cumulative

probability plot of the fluence measurement shows the various extended ozone rinse distributions. Thus, a correlation is established that the longer ozone rinse times have the more complete oxygen passivated wafer surface.

Table II gives the VPD-TXRF surface analysis results of a wide range of contamination elements. The copper, zinc, iron, and sulfur levels were consistently level at about 2.5E09, 1.5E10, 2.7E10, and 1.4E11 atoms/cm<sup>2</sup>, respectively, on all samples. However, the nickel, titanium, and chlorine levels dropped with the rinse time. Overall, the ozone DI water rinse will not affect the metallic contamination level.

In figure 4, the contact angle changes with staging time in a clean room environment. To demonstrate further native oxidation after the HF last process with and without DI ozonated water rinse, the staging test time in hours indicates that the longer staging time lowers the droplet contact angle. The wafer surface is continually changing with staging time. The surface with ozone DI water rinse is slightly more stable than without the ozone rinse. The 120 s ozone rinse time has a surface that is virtually hydrophilic independent of staging time.

Table III shows that oxygen level is related to the amount of time in ozonator. The importance of the increasing level of dissolved oxygen is that the bath is more reactive with the longer rinse times. The 4 ppm of dissolved oxygen is significantly high enough to have strong oxidation properties. The higher fluence, lower contact angle, and low particle counts indicate that the oxidation was optimal for a manufacturing environment.

## CONCLUSION

The effect of a longer ozone DI water rinse time did dramatically reduce the particulate density. The GOI fluence data support the beneficial effect of lower particulate count in the extended ozone rinse. The dissolved ozone concentration in the DI water was most effective even at 4 ppm. The reduced particle count was associated with the formation of the clean, chemical oxide film. The optimization of the ozone DI water rinser lies in the short cycle time needed to almost completely passivate the silicon surface.

## ACKNOWLEDGMENTS

Special thanks to Mark Durcan and Trung Doan for their support in this work.

## REFERENCES

1. T. Roche, S. Adler, R. Cosway, S. Schauer, and L. Liu, in Cleaning Technology in Semiconductor Device Manufacturing/1995, J. Ruzyllo and R. E. Novak, Editors, Vol. 95-20, p. 300, The Electrochemical Society, Pennington, NJ (1996).
2. F. Tardif, C. Paillet, A. M. Papon, J. P. Joly, D. Levy, K. Barla, and P. Patruno, in Cleaning Technology in Semiconductor Device Manufacturing/1995, J. Ruzyllo and R. E. Novak, Editors, Vol. 95-20, pp. 575-580, The Electrochemical Society, Pennington, NJ (1996).
3. J.-G. Park and M. F. Pas, in Cleaning Technology in Semiconductor Device Manufacturing/1995, J. Ruzyllo and R. E. Novak, Editors, Vol. 95-20, p. 83, The Electrochemical Society, Pennington, NJ (1996).
4. S. Nelson, in Semiconductor Pure Water/1986, M. K. Balazs, Editor, pp. 230-242, Balazs Analytical Laboratories, Sunnyvale, CA (1986).

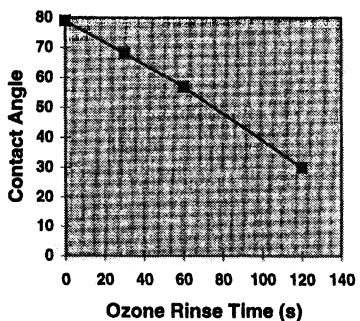


Figure 1. Contact angle changes as a function of ozone rinse time.

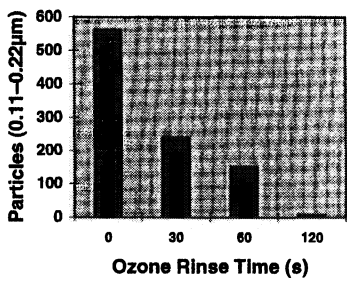
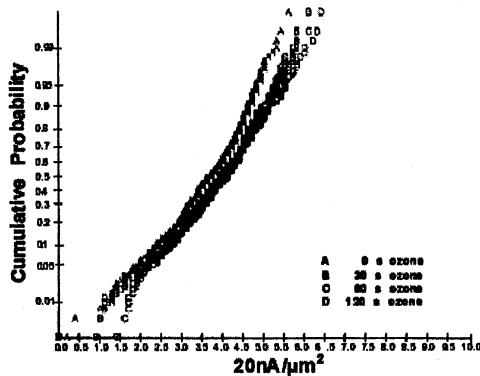
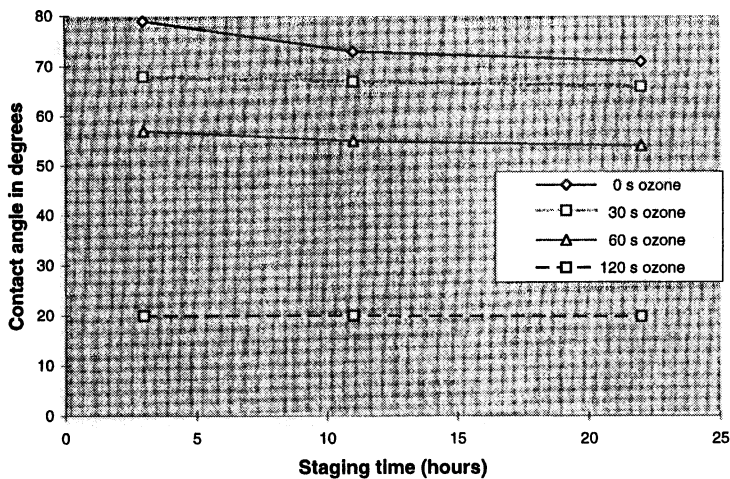


Figure 2. Particle counts after different HF last, ozone rinse process.



**Figure 3.** GOI data for characterizing the different HF last, ozone rinse processes.



**Figure 4.** Contact angle change with staging time was compared with DI rinse time. For the ozone group of 120 s rinse time, the contact angle falls below 20°.

**Table I.** The XPS results show the matrix of bare silicon wafers that were processed with different ozone DI rinse time versus the chemical bonds and composition

Group	Tilt	O	Si-O	Si-Si
HF, DI	45°	10.11	1.40	79.39
HF, DI 30 s O <sub>3</sub>	45°	11.06	0.80	78.63
HF, DI 60 s O <sub>3</sub>	45°	28.82	7.56	57.35
HF, DI 120 s O <sub>3</sub>	45°	34.63	9.13	38.01

**Table II.** The TXRF results show the concentration levels in atoms/cm<sup>2</sup> versus the ozone rinse time. LDL=the lower detection limit.

Group	Sulfur	Chlorine	Calcium	Titanium	Iron	Nickel	Copper	Zinc
No O <sub>3</sub>	1.4E11	3.6E10	5.4E10	8.0E09	2.5E10	3.5E10	2.6E09	1.5E10
30 s O <sub>3</sub>	1.3E11	2.7E10	8.0E09	4.4E09	LDL	2.2E10	2.5E09	1.3E10
60 s O <sub>3</sub>	1.4E11	1.0E11	8.7E09	4.3E09	LDL	1.7E10	2.3E09	1.2E10
120 s O <sub>3</sub>	5.5E11	4.0E11	LDL	2.1E09	3.0E10	LDL	2.5E09	2.0E10

**Table III.** The oxygen concentration level in ppma is shown as a function of rinse time with ozonizer.

Groups	No O <sub>3</sub>	30 s O <sub>3</sub>	60 s O <sub>3</sub>	120 s O <sub>3</sub>
[O <sub>3</sub> ] in ppm	0	0.5	2.3	4

# **COMPARISON OF CLEANING EFFICIENCIES OF NOBLE METALS ON Si SURFACE BETWEEN O<sub>3</sub>-UPW AND SPM**

**Jae-Dong Joo\*, Jong-Soo Kim, Hiroshi Morita\*\*, and Tadahiro Ohmi**

Department of Electronic Engineering, Graduate School of Engineering,  
Tohoku University, Sendai 980-77, Japan

\* PE Group, FAB Team II , Kiheung Plant, Semiconductor Manufacturing Business,  
Samsung Electronics Co., Ltd., San #24, Ningseo-Ri,  
Kiheung-Eup, Yongin-City, Kyungki-Do, 449-900, Korea

\*\* Research & Development Division, Corporate Research & Development Center,  
Kurita Water Industries Ltd. 7-1, Wakamiya, Morinosato,  
Atsugi-City, Kanagawa, 243-01, Japan

In this study, we investigated the cleaning efficiencies of various chemical solutions for noble metals such as Cu and Ag. Cu on Si surface could be removed fundamentally by typical dissolvable chemical solutions such as ozonized ultrapure water (O<sub>3</sub>-UPW) and SPM except Cu included in metal induced oxide (MIO) and chemical oxide. On the other hand, Ag could be removed below the detection limit by cleaning with both of O<sub>3</sub>-UPW and SPM solutions. The different cleaning efficiency of O<sub>3</sub>-UPW and SPM solutions for Cu and Ag could be explained by the fact that the standard heat of formation of silver-oxide(Ag<sub>2</sub>O) is relatively higher, -30.6kJ/mol, than that, -155.2 kJ/mol, of Cu. As the result, it was confirmed that the O<sub>3</sub>-UPW solution having an ozone concentration more than about 2ppm can remove very effectively both of Cu and Ag on Si surface. Consequently, we can have some advantages if we use O<sub>3</sub>-UPW process of room temperature instead of conventional SPM process of relatively high temperature.

## **INTRODUCTION**

With down scaling of ultra large scale integrated (ULSI) devices, metal contamination-free Si surface is essential to realize the high performance. It has been well known that the metallic contamination on the Si surface causes fatal effects on the device performance(1). Among them, noble metals such Cu, Ag and Au with high oxidation-reduction (redox) potential form chemical bond with Si substrate and are hardly removed from Si surface(2). Moreover, Cu is the easiest to be contaminated in device manufacturing processes, especially implantation, ashing and dry etch processes(3). Although sulfuric acid-hydrogen peroxide mixture (SPM) chemicals has been used widely

as a cleaning solution for metal and organic contamination, the process temperature is relatively high of around 120~150°C. In this study, we will evaluate the cleaning efficiencies of ozonized ultrapure water ( $O_3$ -UPW) which is conducted at room temperature and SPM for noble metals such as Cu and Ag on Si surface.

## EXPERIMENT

For this work, p-type (100) Cz Si wafers with a resistivity range of  $7\sim 15 \Omega \cdot cm$  were used. Each Si wafer was dipped in 0.5% diluted hydro-fluoric acid (DHF) solution for 1 minute for removing chemical oxide following a SPM cleaning for 10 minutes for removing hydrocarbon contaminant. The hydrophobic Si wafers were contaminated by dipping in UPW and DHF spiked with 1 ppm  $CuCl_2$  and 1 ppm  $Ag_2SO_4$  for 3 minutes followed by a post-UPW rinse for 10 minutes and dried by  $N_2$ -blowing.

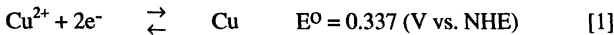
These four kinds of initially contaminated wafers were cleaned by a conventional SPM cleaning solution with the mixing ratio of 4:1 (sulfuric acid:hydrogen peroxide acid) at 90°C and  $O_3$ -UPW with different ozone concentrations, 0.3~10 ppm, and different cleaning time, 5 seconds~30 minutes, followed by post-UPW rinse for 10 minutes. These SPM and  $O_3$ -UPW solutions have a dissolution ability for Cu and no etching ability for both of Si and  $SiO_2$  substrates. In addition, we evaluated Cu cleaning efficiency of hydrofluoric acid-hydrogen peroxide mixture with non-ionic surfactant (FPMS) which has both of dissolution ability for Cu and etching ability for Si and  $SiO_2$  substrates. The FPMS solution used in this study is a mixture including 0.5% HF, 1.0%  $H_2O_2$  and 50 ppm non-ionic surfactant. And we think that this result may show a relationship between the effects of metal-induced-oxidation (MIO)(4) and chemical oxidation and Cu cleaning efficiency.

Cu and Ag cleaning efficiencies were evaluated by measuring the metal concentrations on Si surfaces before and after cleaning with total reflection x-ray fluorescence spectroscopy (TRXRF), Technos 610T, of which the detection limit is  $2 \times 10^9$  atoms/cm<sup>2</sup> for Cu and  $1 \times 10^{11}$  atoms/cm<sup>2</sup> for Ag on Si surface(5). The metal particle growing effect on Si surface is checked using Scanning Electron Microscope (SEM) with a minimum visible particle size of 100 Å. Finally, the nature of the particles deposited on Si surfaces is characterized by Scanning Auger Microprobe (SAM) with a minimum electron beam size of 150 Å.

## RESULTS AND DISCUSSION

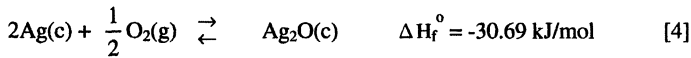
In the potential-pH diagrams of Fig.1 and Fig.2, we summarized the dissolution behaviors of Cu and Ag in previously mentioned typical dissolvable chemical solutions such as  $O_3$ -UPW, SPM and FPMS. Therefore, we can expect that the contaminated Cu and Ag on Si surface are fundamentally removed by cleaning with these dissolvable chemical solutions. As revealed in our previous research(2), metal particle is grown on Si surface in UPW and DHF contaminated with  $CuCl_2$  and  $Ag_2SO_4$  by redox reaction

between Cu<sup>2+</sup> and Ag<sup>+</sup> in solutions and hydrophobic Si surface and the redox reaction is expressed in the following reaction equation:



where E<sup>⊖</sup> is standard reduction potential (redox potential in standard state) and NHE is normal hydrogen electrode as a reference electrode. In these reactions, the metallic ions, Cu<sup>2+</sup> and Ag<sup>+</sup>, take electron from Si substrate and the electron is transferred from the Cu and Ag metallized to another metallic ions adsorbed on the metal Cu and Ag. And then, the metal particles are grown by this successive electron transfer process and MIO(4) of positively charged Si on the surface can be occurred in UPW which has no chemical oxidation effect. Fig.3 shows the metal Cu and Ag particles grown on Si surface in UPW spiked with 1ppm CuCl<sub>2</sub> for 3 minutes followed by a 10 minute-UPW rinse. In this SEM analysis, we also found that the metal particle growing effect on Si surfaces in DHF. From the SAM survey spectra for metal particles of Cu and Ag in Fig.4, it was confirmed that the metal particles grown on Si surface in UPW were composed absolutely of elementary Cu and Ag respectively and complied with the equations of [1] and [2]. As for the Si LVV peak shown in spectra of Fig.4, we think that it is the Si LVV peak produced from Si substrate beneath the metal Cu particle due to a matrix effect.

In this study, we used an O<sub>3</sub>-UPW solution with the ozone concentration of 0.3~10ppm at room temperature and a SPM solution with the mixing ratio of 4:1 (sulfuric acid:hydrogen peroxide acid) at 90°C. The cleaning efficiencies of O<sub>3</sub>-UPW for Cu and Ag are shown in the Fig.5. The initial concentration levels of Cu and Ag are drastically reduced by O<sub>3</sub>-UPW cleaning in a few minutes and saturated in about 10 minutes. As for Ag, the saturated concentration is below the detection limit of 1x10<sup>11</sup> atoms/cm<sup>2</sup> regardless of the species of contamination solution. However, the residual Cu concentration after O<sub>3</sub>-UPW cleaning is higher than the detection limit of 2x10<sup>9</sup> atoms/cm<sup>2</sup> with a dependence of O<sub>3</sub>-UPW cleaning efficiency on the species of contamination solution. In the same procedure to the case of O<sub>3</sub>-UPW cleaning, we evaluated SPM cleaning efficiency in Fig.6. With comparing the results of Fig.5 and Fig.6, the O<sub>3</sub>-UPW cleaning efficiency for noble metals such as Cu and Ag is very nearly same to that of SPM except the fact that the initial removal efficiency of SPM is a little higher than that of O<sub>3</sub>-UPW. Here, we should note that the results of Fig.5 and Fig.6 show a dependence of cleaning efficiency for only Cu on contamination solution as described above. The dependence of cleaning efficiency for Cu on contamination solution is explained by the fact that Cu can be included in MIO(4) grown during contamination in UPW not DHF although it can be also included in chemical oxide grown during cleaning process by both of O<sub>3</sub>-UPW and SPM solutions. The reason why the case of Ag can not be included in chemical oxide and MIO can be explained by the fact that the standard heat of formation of silver-oxide(Ag<sub>2</sub>O) is higher than that of copper-oxide(CuO) as shown in following equations of [3] and [4](6).



where  $\Delta H_f^{\circ}$  is the standard heat of formation of metal-oxide at 25°C and, c and g mean crystalline and gaseous respectively. In order to verify the idea above mentioned, we evaluated the dependence of Cu and Ag cleaning efficiencies on initial contamination level. As shown in Fig.7, the residual Cu concentration after cleaning by using O<sub>3</sub>-UPW and SPM solutions increases with initial Cu concentration as a function of dipping time in UPW spiked with 10ppb CuCl<sub>2</sub> showing a dependence of cleaning efficiency on initial Cu concentration, however, it can be removed below the detection limit of  $2 \times 10^9$  atoms/cm<sup>2</sup> by FPMS cleaning. This result can be explained by the fact Cu is included in MIO grown during contamination in UPW and chemical oxide grown during cleaning and it can not be removed by O<sub>3</sub>-UPW and SPM which have no etching ability for both of Si and SiO<sub>2</sub> substrates.

On the other hand, Cu contaminated in DHF spiked with 10ppb CuCl<sub>2</sub> was removed below the detection limit after cleaning by using O<sub>3</sub>-UPW and SPM solutions and the dependence of cleaning efficiency on initial Cu concentration was not shown in Fig.8. This means that Cu contaminated in DHF is not affected by MIO effect and easily removed by cleaning with O<sub>3</sub>-UPW and SPM solutions. In our previous research(4), Cu contaminated in DHF showed a dependence of Cu cleaning efficiency of O<sub>3</sub>-UPW and SPM solutions on initial Cu level. According to the results, the amount of Cu included in chemical oxide grown during O<sub>3</sub>-UPW and SPM cleaning increased with the initial Cu concentration on Si surface. This is the reason why Cu contaminated in DHF containing a relatively low, 10ppb, CuCl<sub>2</sub> concentration can be removed below the detection limit by O<sub>3</sub>-UPW and SPM cleaning.

On contrary to the case of Cu in Fig.7, in Fig.9, Ag contaminated in UPW spiked with 10ppb CuCl<sub>2</sub> was removed below the detection limit after cleaning and the dependence of cleaning efficiency on initial Ag concentration was not shown. From this result, therefore, we can estimate that Ag can not be affected by MIO and chemical oxidation effect since the standard heat of formation of silver-oxide(Ag<sub>2</sub>O) is relatively high as shown in equation [4].

Finally, in the Fig.10, we evaluated the metal cleaning efficiencies of O<sub>3</sub>-UPW varying the ozone concentration in O<sub>3</sub>-UPW with a fixed cleaning time of 10minutes. For initial Cu and Ag contamination, hydrophobic Si wafers were dipped in DHF spiked with 1ppm CuCl<sub>2</sub> and Ag<sub>2</sub>SO<sub>4</sub> respectively for 3minutes followed by a post-rinse for 10minutes. These contaminated Si wafers were cleaned by O<sub>3</sub>-UPW solution of which ozone concentration was varied in a range of 0.3ppm~10ppm. Both of Cu and Ag on Si

surface reduced to around  $1 \times 10^{11}$  atoms/cm<sup>2</sup> by cleaning with O<sub>3</sub>-UPW solution containing only 0.3ppm-ozone. When above 2ppm-ozone was used in O<sub>3</sub>-UPW solution, Ag was removed below the detection limit and most of Cu impurities were removed except the amount of Cu included in chemical oxide grown in O<sub>3</sub>-UPW solution. As the result, it was confirmed that the O<sub>3</sub>-UPW solution having an ozone concentration than about 2ppm can remove very effectively noble metals such as Cu and Ag on Si surface.

## CONCLUSION

In this study, we investigated the cleaning efficiencies of as O<sub>3</sub>-UPW ,SPM and FPMS solutions for noble metals such as Cu and Ag. Cu cleaning efficiency of these typical dissoluble chemical solutions such as O<sub>3</sub>-UPW and SPM showed a dependence of the contamination solution and initial level, however, not in the case of FPMS solution. This dependence of Cu cleaning efficiency could be interpreted by oxidation effect of Si surface due to MIO and chemical oxidation.

On the other hand, Ag could be removed below the detection limit by cleaning with both of O<sub>3</sub>-UPW and SPM solutions and showed no dependence of Ag cleaning efficiency. The different cleaning efficiency of O<sub>3</sub>-UPW and SPM solutions for Cu and Ag could be explained by the fact that the standard heat of formation of silver-oxide(Ag<sub>2</sub>O) is relatively higher, -30.6kJ/mol, than that, -155.2 kJ/mol, of Cu.

Through this research, the effective cleaning efficiency of O<sub>3</sub>-UPW solution for both of Cu and Ag on Si surface was achieved by using above 2ppm-ozone and 5minute-dipping time. As the result, in the point of cleaning efficiency for Cu and Ag, two kinds of cleaning solutions of O<sub>3</sub>-UPW and SPM are very nearly same. Consequently, we can have some many advantages such as reduction of a large volume of chemicals and UPW consumption and no chemical vapor generation if we use O<sub>3</sub>-UPW solution of room temperature process in stead of conventional SPM solution of relatively high temperature process as a cleaning solution for noble metals such as Cu and Ag.

## REFERENCE

1. T.Ohmi, T.Imaoka, I.Sugiyama, and T.Kenzuka, *J.Electrochem.Soc.*, 139, No.11, 3317, 1992.
2. H.Morinaga, M.Suyama, M.Nose, S.Verhaverbeke and T.Ohmi, *IEICE Trans. Electron.*, E79-C, 343,1996.
3. N.Anzai, Y.Kureishi, S.Shimizu, and T.Nitta, in *Proceedings of 1st Workshopon ULSI Ultra Clean Technology*, p.75, 1989.
4. J.S.Kim, H.Morita, J.D.Joo, and T.Ohmi, *J.Electrochem.Soc.*, 144, No.9, 3275, 1997.
5. Technos, *TREX 610T Technical Manual*, Technos, 1991
6. Robert C. Weast and Melvin J. Astle, *Handbook of Chemistry and Physics*, 62nd ed.(1981~1982), CRC press, Inc., 1982

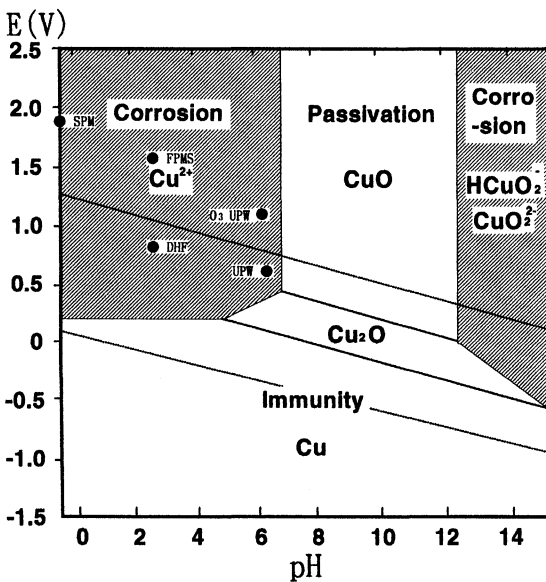


Fig.1 Domains of corrosion, immunity and passivation of Cu in Cu-water system based on the Potential-pH Diagram

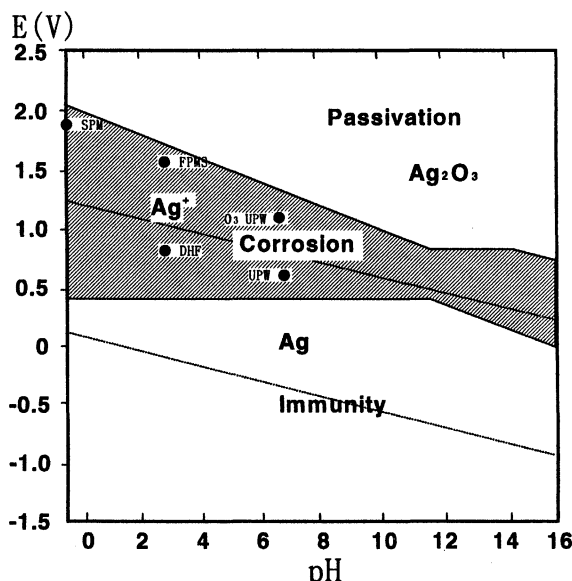


Fig.2 Domains of corrosion, immunity and passivation of Ag in Ag-water system based on the Potential-pH Diagram

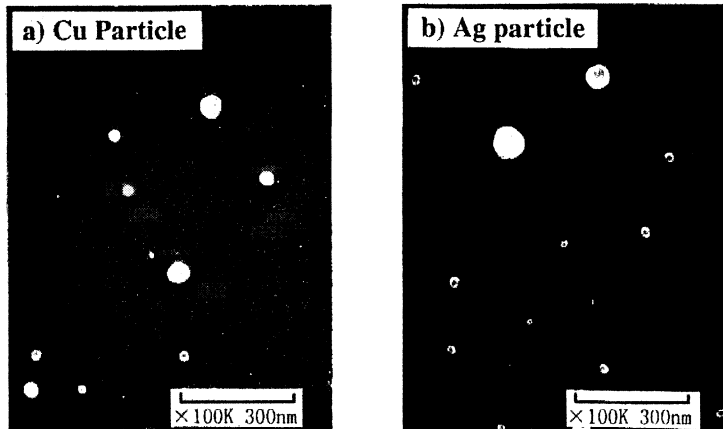


Fig.3 SEM photos of metal particle of a)Cu and b)Ag grown on Si surfaces contaminated in ultrapure water (UPW) spiked 1ppm CuCl<sub>2</sub> and Ag<sub>2</sub>SO<sub>4</sub> respectively for 3min.

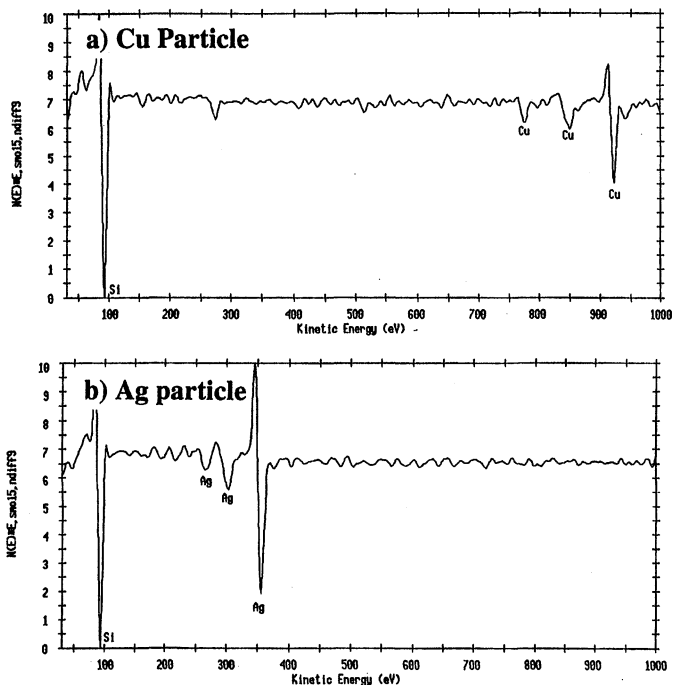


Fig.4 Auger spectra of metal particle of a)Cu and b)Ag grown on Si surfaces contaminated in ultrapure water (UPW) spiked 1ppm CuCl<sub>2</sub> and Ag<sub>2</sub>SO<sub>4</sub> respectively for 3min.

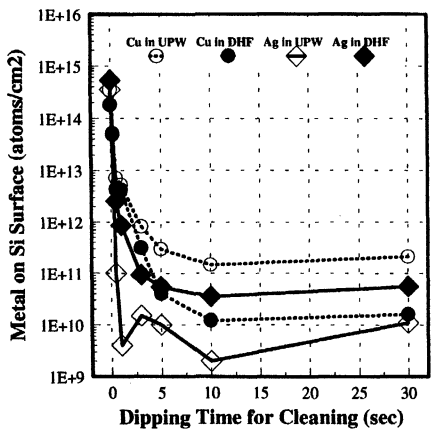


Fig.5 The cleaning efficiency of O<sub>3</sub>-UPW with 5ppm-ozone for Cu and Ag contaminated in UPW and DHF for 3min. as a function of dipping time

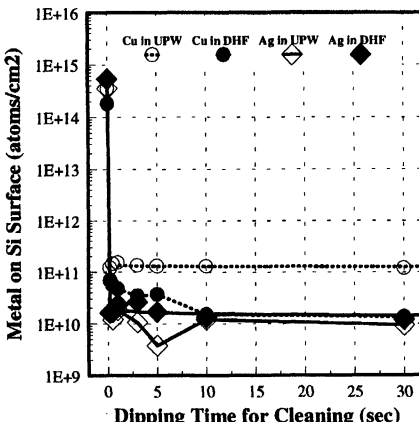


Fig.6 The cleaning efficiency of SPM for Cu and Ag contaminated in UPW and DHF for 3min. as a function of dipping time

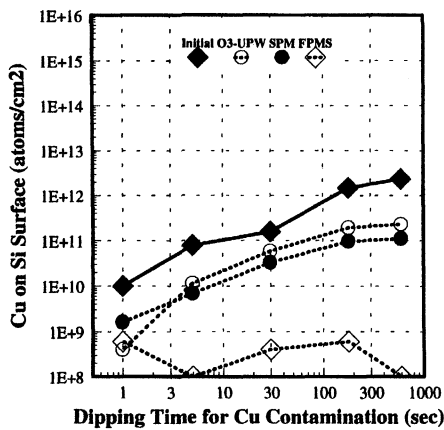


Fig.7 The cleaning efficiency of various chemical solutions for Cu on Si surface contaminated in UPW spiked with 10ppb CuCl<sub>2</sub> for different dipping time

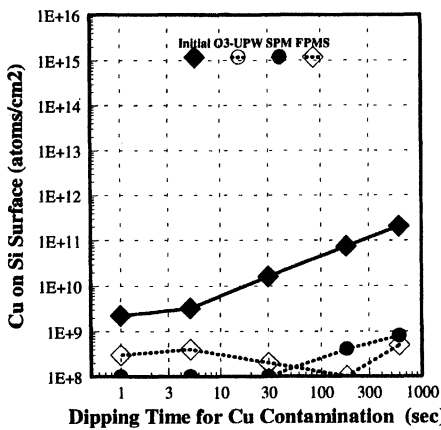


Fig.8 The cleaning efficiency of various chemical solutions for Cu on Si surface contaminated in DHF spiked with 10ppb CuCl<sub>2</sub> for different dipping time

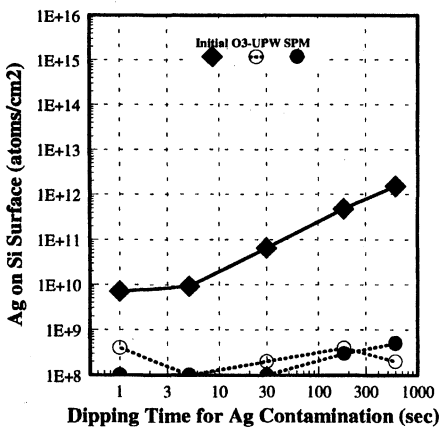


Fig.9 The cleaning efficiency of O<sub>3</sub>-UPW and SPM for Ag on Si surface contaminated in UPW spiked with 10ppb Ag<sub>2</sub>SO<sub>4</sub> for different dipping time

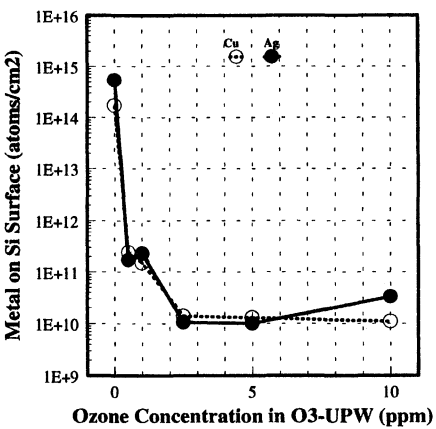


Fig.10 The dependence of Cu and Ag cleaning efficiency on ozone concentration in O<sub>3</sub>-UPW for a fixed dipping time of 10min.

## **GAS-PHASE CLEANING**



# **Fe REMOVAL EFFECTS OF SILICON CHLORIDES ( $\text{SiCl}_x$ ) DURING UV/ $\text{Cl}_2$ DRY CLEANING**

Rinji Sugino, Yoshiko Okui, Mayumi Shigeno, Satoshi Ohkubo, Kanetake Takasaki, and Takashi Ito

*Fujitsu Laboratories Ltd.  
10-1 Morinosato-Wakamiya, Atsugi 243-01, Japan*

While investigating the surface dependence of the dry cleaning technique that uses Cl-radicals generated by UV irradiation (UV/ $\text{Cl}_2$ ), we found that silicon chlorides ( $\text{SiCl}_x$  ( $x=1\text{-}4$ )), etching products created from the reaction between Si and Cl-radicals, can remove Fe contaminants.  $\text{SiCl}_4$  gas removes Fe contaminants existing on both Si and  $\text{SiO}_2$  surfaces without surface dependence. As a result of the direct reaction between the dry cleaning gas and a reagent of the Fe contaminants,  $\text{SiCl}_4$  apparently reacts with Fe contaminants to produce the  $\text{FeCl}_3$ , which has a high-vapor pressure. The results and a thermochemical consideration of the direct reaction substantiates the removal of Fe contamination on both Si and  $\text{SiO}_2$  surfaces during UV/ $\text{Cl}_2$  dry cleaning.

## **INTRODUCTION**

Dry cleaning technology that uses gases to remove metal contaminants on Si wafer surfaces is expected to solve problems associated with wet chemical cleaning.<sup>[1-4]</sup> Gases can be replaced faster and easier than wet chemicals in cleaning chambers, deep trenches, and contact holes. We have developed a dry cleaning technique that uses ultraviolet (UV) excited Cl-radicals named UV/ $\text{Cl}_2$ , and demonstrated the complete removal of surface metal contaminants such as Fe and Al.<sup>[2,5]</sup> The main problem of this dry cleaning technique from a practical point of view, however, is its surface dependence. UV/ $\text{Cl}_2$  can be used to remove Fe contaminants on Si surfaces, but is not completely effective on  $\text{SiO}_2$  surfaces. We began this study by investigating why UV/ $\text{Cl}_2$  cannot remove Fe contaminants from  $\text{SiO}_2$  surfaces. Consequently, we found that Fe contaminants do not react with Cl-radicals directly, but with silicon chlorides ( $\text{SiCl}_x$  ( $x=1\text{-}4$ )), the etching products created from the Si and Cl-radicals.<sup>[6]</sup>

In this paper, we first describe cleaning inhomogeneity by using UV/ $\text{Cl}_2$ . Then, we demonstrate the dry cleaning ability of  $\text{SiCl}_x$  as the cleaning source gas for removing Fe contaminants from Si and  $\text{SiO}_2$  surfaces. Details of the Fe removal effects of  $\text{Cl}_2$  and  $\text{SiCl}_4$  gas on both Si and  $\text{SiO}_2$  surfaces are shown. In addition, we describe the results of the direct reaction between  $\text{SiCl}_4$  or  $\text{Cl}_2$  as the dry cleaning gas and a reagent of the Fe contamination. Based on our observations and thermochemical analysis of the direct reaction, we discuss the reactivity of Fe contaminants with dry cleaning gas on wafer surfaces.

## SURFACE DEPENDENCE OF UV/Cl<sub>2</sub> AND EFFECTS OF SiCl<sub>x</sub> FOR Fe REMOVAL

Figure 1 shows the spectra of the Fe 2p<sub>3/2</sub> region and the surface Fe concentrations obtained from Si and SiO<sub>2</sub> surfaces both before and after UV/Cl<sub>2</sub> cleaning. The Si and SiO<sub>2</sub> surfaces were intentionally contaminated by immersing them in an ammonium and hydrogen-peroxide solution containing Fe. The Fe concentration on the surfaces was determined by flameless atomic absorption spectrophotometry (AAS), which measures the Fe concentration of the HF solution that recovered the surface Fe using an HF-scanning dissolution method. Dry cleaning was carried out using UV-excited dry cleaning equipment consisting of a quartz chamber, a halogen lamp for wafer heating, and a microwave-excited UV mercury lamp. High-purity Cl<sub>2</sub> (99.999%) was used as the cleaning gas and typically maintained at a pressure of 2.7 kPa during cleaning. A UV light source with a wavelength of 200 to 300 nm at 22 mW/cm<sup>2</sup> was irradiated on each dry cleaning process. Before cleaning, Fe contaminants on both surfaces were observed to similarly bond with three oxygen atoms (O-Fe=O<sub>2</sub>) at the peak of 711 eV.<sup>[7]</sup> This Fe peak disappeared on the Si surface after UV/Cl<sub>2</sub> dry cleaning. Also, the Fe concentration decreased to below the limit of detection. However, for an SiO<sub>2</sub> surface, the peak site, the shape of the peak in the Fe 2p<sub>3/2</sub> region, and the surface Fe concentration remained unchanged. The Fe concentration on an SiO<sub>2</sub> surface never diminished by UV/Cl<sub>2</sub> cleaning.

These results indicate that the Fe compounds before cleaning are the same composition as Fe<sub>2</sub>O<sub>3</sub> and/or Fe(OH)<sub>3</sub> for both Si and SiO<sub>2</sub> surfaces, although UV/Cl<sub>2</sub> dry cleaning was effective only on Si surfaces. Additionally, the Fe compounds can be assumed to leave both surfaces similarly because the Si surface was also covered with the native oxide layer. The difference between the case of Si and SiO<sub>2</sub> is that Si surfaces had been etched through the native oxide,<sup>[8]</sup> while SiO<sub>2</sub> surfaces had not been etched at all. Consequently, it can be expected that the etching products of Si such as SiCl<sub>x</sub> during UV/Cl<sub>2</sub> dry cleaning plays an important role in the removal of Fe contaminants. To investigate the effect of SiCl<sub>x</sub> on Fe removal, we conducted an experiment as follows. First, a Si wafer was intentionally cut in half, and one half was oxidized and contaminated with Fe. The half bare Si wafer was treated with HF solution before being inserted into the chamber to remove native oxide. Then, both halves were placed together in a dry cleaning chamber. Figure 2 shows the Fe concentration on the SiO<sub>2</sub> surface after UV/Cl<sub>2</sub> dry cleaning coexisting with Si. It was decreased for the first time on the SiO<sub>2</sub> surfaces by UV/Cl<sub>2</sub> dry cleaning with Si present. Fe concentration decreased with an increase in temperature when Si was present. On the other hand, it had no effect on the Fe concentration on exclusively SiO<sub>2</sub> surfaces at all experimental temperatures. Fe contaminants on SiO<sub>2</sub> surfaces do not react with Cl-radicals directly, but with the etching products of SiCl<sub>x</sub> created from the Si and Cl-radicals. These results indicate the removal of Fe by SiCl<sub>x</sub>, which is produced during UV/Cl<sub>2</sub> dry cleaning.

## ROLE OF $\text{SiCl}_4$ AND $\text{Cl}_2$ IN DRY CLEANING

For a stable supply of  $\text{SiCl}_x$ , we tried to use  $\text{SiCl}_4$  as the dry cleaning gas.  $\text{SiCl}_4$  gas that had a low vapor pressure was introduced to the chamber after evacuation. A UV light irradiated all dry cleaning processes. Figures 3 and 4 show the Fe concentration after each dry cleaning system according to the surface temperature of both Si and  $\text{SiO}_2$ . Comparisons of the removal effects were then made between  $\text{UV}/\text{Cl}_2$ ,  $\text{UV}/\text{SiCl}_4$ , and  $\text{UV}/\text{Cl}_2+\text{SiCl}_4$ . The  $\text{UV}/\text{Cl}_2+\text{SiCl}_4$  dry cleaning system employed a gas flow ratio of 5 and 195 ml/min  $\text{Cl}_2$  and  $\text{SiCl}_4$ , respectively. The  $\text{UV}/\text{SiCl}_4$  could remove Fe contaminants in both cases without surface dependence, while  $\text{UV}/\text{Cl}_2$  hardly removed them from  $\text{SiO}_2$  surfaces. When the  $\text{UV}/\text{SiCl}_4$  system was used however, the Fe concentration on both Si and  $\text{SiO}_2$  surfaces did not reach the limit of detection, while the Si surface was cleaned using  $\text{UV}/\text{Cl}_2$ . On the other hand,  $\text{UV}/\text{Cl}_2+\text{SiCl}_4$  on the Si surface reached the limit of detection at a cleaning temperature of 380°C. Dry cleaning by the  $\text{UV}/\text{Cl}_2+\text{SiCl}_4$  system was found to be very effective on Si surfaces. However, the same effectiveness of  $\text{UV}/\text{Cl}_2+\text{SiCl}_4$  could not be obtained on  $\text{SiO}_2$  surfaces, and there was no apparent difference between cleaning  $\text{SiO}_2$  surfaces with the  $\text{UV}/\text{Cl}_2+\text{SiCl}_4$  and with the  $\text{UV}/\text{SiCl}_4$ .

These results demonstrate that silicon chlorides react with Fe contaminants to produce Fe compounds which have a high-vapor pressure. Also, in the case of  $\text{UV}/\text{Cl}_2$  dry cleaning on Si surfaces, Fe contaminants do not react with Cl-radicals directly, but with the etching products of  $\text{SiCl}_x$  created from the Si and Cl-radicals. On the other hand, Cl-radicals cannot react and penetrate an  $\text{SiO}_2$  layer that was formed by thermal-oxidation. Therefore, when cleaning  $\text{SiO}_2$  surfaces it is essential to supply the  $\text{SiCl}_x$  externally.  $\text{SiCl}_4$  gas is very effective in the dry cleaning system, as it can remove Fe contaminants without surface dependence. The role of each UV cleaning system can best be seen by the cleaning models shown in Figure 5. The following are supplementary explanations of the cleaning model. Through Fe contamination, which results from immersing the wafers into an ammonium and hydrogen-peroxide solution, small amounts of Fe seem to exist inside the surface. The Fe contaminants exist as  $\text{FeO}_x$ . When using  $\text{UV}/\text{Cl}_2+\text{SiCl}_4$ ,  $\text{SiCl}_4$  reacts with only the  $\text{FeO}_x$  existing on the top surface. On the Si surface, Cl-radicals from the small addition of  $\text{Cl}_2$  in the gas mixture penetrate the native oxide and then produce  $\text{SiCl}_x$ . The  $\text{FeO}_x$  existing inside the native oxide reacts with the  $\text{SiCl}_x$ , and then vaporizes from the Si surface. On an  $\text{SiO}_2$  surface,  $\text{FeO}_x$  reacts with  $\text{SiCl}_4$  only.  $\text{Cl}_2$  also does not play any role in  $\text{SiO}_2$  surface cleaning because Cl-radicals cannot penetrate the  $\text{SiO}_2$  layer, or react directly with the  $\text{FeO}_x$  formed in this contamination process. When a  $\text{UV}/\text{SiCl}_4$  system is used for both Si and  $\text{SiO}_2$ ,  $\text{SiCl}_4$  reacts only with the top  $\text{FeO}_x$ . Therefore, the Fe concentration on both surfaces decreases only by one order of magnitude from the initial level, as shown in Figures 3 and 4. In the case of using  $\text{UV}/\text{Cl}_2$  on a Si surface,  $\text{FeO}_x$  does not react with Cl-radicals directly, but with the etching products of  $\text{SiCl}_x$  created from Si and Cl-radicals. Conversely, Cl-radicals cannot react and penetrate an  $\text{SiO}_2$  layer which was formed by thermal-oxidation.

## REACTIVITY OF SiCl<sub>4</sub> OR Cl<sub>2</sub> WITH Fe<sub>2</sub>O<sub>3</sub>

It is important to understand the dry cleaning mechanism on a wafer surface to clarify the reaction between SiCl<sub>4</sub> and FeO<sub>x</sub>. We investigated the reactivity and the products based on the direct reaction between SiCl<sub>4</sub> or Cl<sub>2</sub> dry cleaning gas and Fe<sub>2</sub>O<sub>3</sub> or Fe (metallic) as Fe sources. Figure 6 shows the experimental apparatus for studying the direct reaction. A commercial reagent of each Fe source was placed in the glass tube, and then the dry cleaning gas was introduced into the tube at a temperature of 500°C (nearly the temperature used in the dry cleaning for wafers). SiCl<sub>4</sub> and Cl<sub>2</sub> dry cleaning gases were introduced through a bubbler with Ar carrier gas and a regulator, respectively. The reaction was carried out at the atmospheric pressure for two hours. Observation continued during the reaction. After the reaction was finished, a product sticking to the trap and the tube was recovered.

The results of the direct reaction on each dry cleaning gas and Fe source are summarized in Table I and explained as follows: SiCl<sub>4</sub> reacted with Fe<sub>2</sub>O<sub>3</sub>, and a purple product was obtained. However, the reaction between Cl<sub>2</sub> and Fe<sub>2</sub>O<sub>3</sub> had not taken place. On the other hand, Fe did not react with SiCl<sub>4</sub>, but with Cl<sub>2</sub>. The resulting products from the reaction systems of both SiCl<sub>4</sub>/Fe<sub>2</sub>O<sub>3</sub> and Cl<sub>2</sub>/Fe are purplish crystal that change to yellow upon exposure to the atmosphere. Furthermore, the Cl ion and Fe ion concentrations of the products were determined with titration. As a result, the product could be considered to be FeCl<sub>3</sub>. This is also the most likely product as a compound having a high vapor pressure and containing Fe and Cl. Each reaction formula and the standard free energy of formation ( $\Delta G_f, 800$ ) are given in Table I. The reaction observations conformed to the thermochemical estimation.

These results from the direct reaction between a cleaning gas and an Fe source support the role of UV dry cleaning for wafer surfaces. The Fe contaminants have the same composition as Fe<sub>2</sub>O<sub>3</sub> for both Si and SiO<sub>2</sub> surfaces, as indicated in the XPS results of Figure 1. On wafer surfaces, SiCl<sub>4</sub> can be considered to first reduce Fe<sub>2</sub>O<sub>3</sub> and then produce FeCl<sub>3</sub>, because the standard free energy of formation on the reaction indicates  $\Delta G_f, 800 < 0$ . On the other hand, it is inconceivable that the reaction of Cl<sub>2</sub> with Fe<sub>2</sub>O<sub>3</sub>, which indicated that  $\Delta G_f, 800 > 0$ , could occur. Although the dry cleaning experiments were conducted under a low-pressure atmosphere and UV irradiation, the thermochemical data used was based on 1 atm and disregarded any UV effects. From the thermochemical perspective, we can confirm the cleaning ability of SiCl<sub>4</sub> on Fe contaminants.

During LSI manufacturing processes, the Fe contaminants introduced to wafer surfaces from the immersion into the ammonium solution are presumably not only Fe<sub>2</sub>O<sub>3</sub> but also Fe particles from equipment and/or the environment. Contamination such as particles cannot be classified as either Fe oxide or metallic compounds. In this study, we found that Cl<sub>2</sub> is highly effective in removing Fe-metallic. For LSI production, dry cleaning processes should use multiple gases for removing several Fe compounds.

On the other hand, Fe contaminants had been removed by only one order of

magnitude after UV/Cl<sub>2</sub>+SiCl<sub>4</sub> for an SiO<sub>2</sub> surface. To remove Fe existing inside, it will be essential to etch the surface slightly or to use other dry cleaning gases which easily penetrate the SiO<sub>2</sub> layer.

## CONCLUSION

Conventional UV/Cl<sub>2</sub> dry cleaning can be used to remove metal contaminants from Si surfaces, but does not completely work on SiO<sub>2</sub> surfaces. We found that metal contaminants react with the SiCl<sub>x</sub> etching products created from a reaction between Si and Cl-radicals. We could overcome the problem of surface selectivity in dry cleaning by using an SiCl<sub>4</sub> dry cleaning gas. SiCl<sub>4</sub> removes Fe contaminants from both Si and SiO<sub>2</sub> surfaces, whereas conventional UV/Cl<sub>2</sub> dry cleaning was hardly effective in removing Fe contaminants from SiO<sub>2</sub> surfaces. The use of a Cl<sub>2</sub>+SiCl<sub>4</sub> (5:195 ml/min) gas mixture can be mentioned specifically for dry cleaning. Dry cleaning technology improves significantly with the use of an SiCl<sub>4</sub> system instead of Cl<sub>2</sub> alone. The results from the direct reaction between the cleaning gas and the Fe source supports the role of UV dry cleaning for wafer surfaces. From a thermochemical examination, we could confirm the cleaning ability of SiCl<sub>4</sub> for Fe contaminants.

## ACKNOWLEDGEMENTS

The authors thank Y. Sato, M. Okuno, H. Mori, T. Nakanishi, S. Koguchi, R. Iida, and Y. Takamatsu for helpful suggestions.

## REFERENCES

- [1] R. M. Gluck, in *Proc. of the 2nd International Symposium on Cleaning Technology in Semiconductor Device Manufacturing*, ECS PV.92-12 pp.48-55.
- [2] R. Sugino et al., *ibid.* pp. 72-79.
- [3] J. C. Ivankovits et al., *ibid.* pp.105-109.
- [4] A. S. Lawing et al., in *Proc. of the 4th International Symposium on Cleaning Technology in Semiconductor Device Manufacturing*, ECS PV.95-20 pp.150-157.
- [5] R. Sugino et al., IEICE Trans. Electron. E75-C 829 (1992).
- [6] R. Sugino et al., in *Proceedings of International Symposium on Semiconductor Manufacturing*, pp.262-265, September 17-19, 1995 Austin, TX.
- [7] C. D. Wagner et al., in *Handbook of X-ray Photoelectron Spectroscopy* (Ed. G. E. Muilenberg), p76, Parkin-Elmer.
- [8] R. Sugino et al., *J. Appl. Phys.* 76 5498 (1994).
- [9] "JANAF Thermochemical Tables" 3rd Education, *J. Phys. Chem. Ref. Data*, 14 Supplement No. 1 (1985).

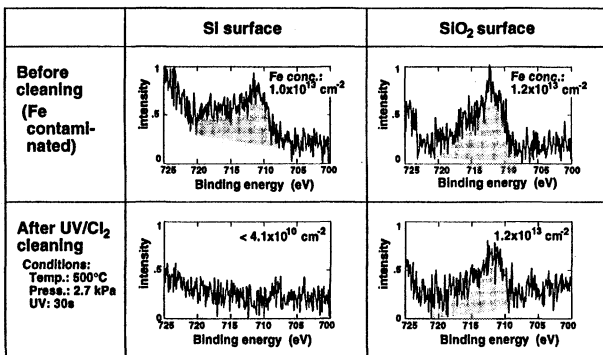


FIG. 1. XPS spectra of  $\text{Fe 2p}_{3/2}$  region on Si and  $\text{SiO}_2$  surfaces.

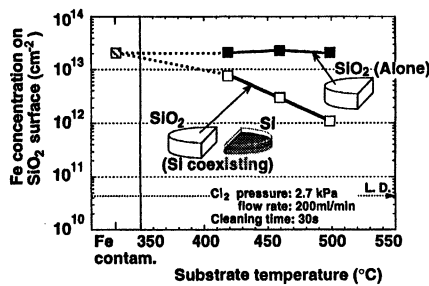


FIG. 2. Fe concentration on the  $\text{SiO}_2$  surface after UV/ $\text{Cl}_2$  dry cleaning coexisting Si.

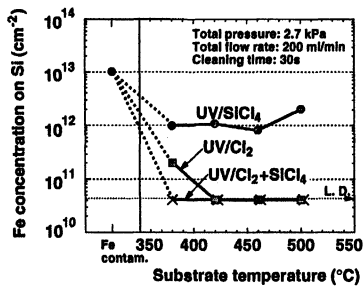


FIG. 3. Dry cleaning Si surface using various cleaning systems.

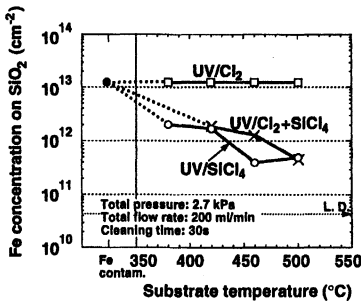


FIG. 4. Dry cleaning  $\text{SiO}_2$  surface using various cleaning systems.

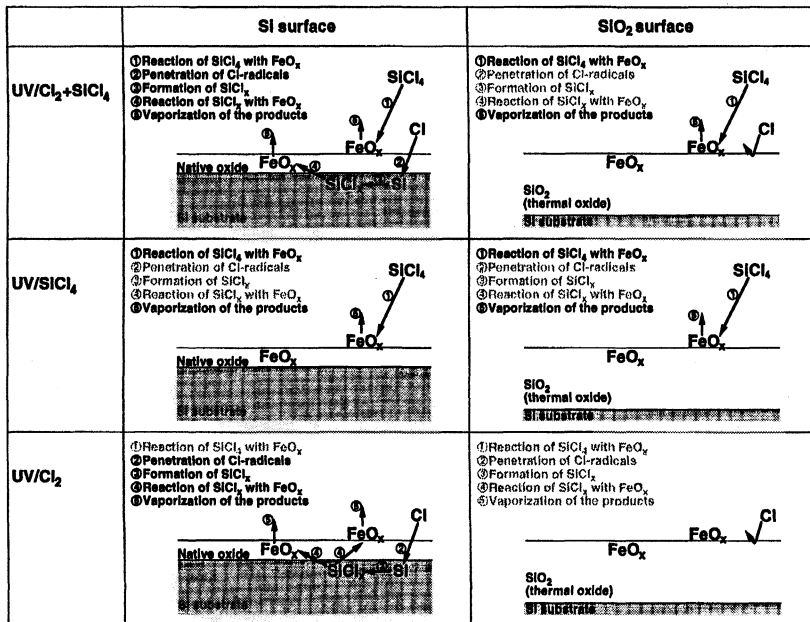


FIG. 5. Dry cleaning model for Si and  $\text{SiO}_2$  surfaces for various UV dry cleaning systems.

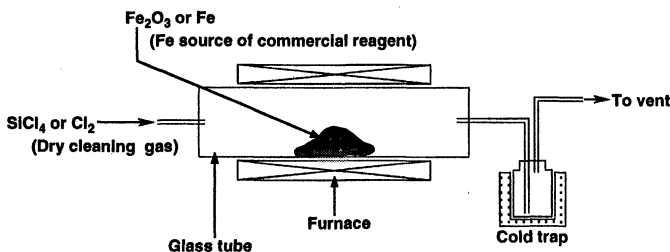


FIG. 6. Experimental apparatus for direct reaction between dry cleaning gas and Fe source.

Table I. Observation results of direct reaction and thermochemical discussion.

Results of direct reaction		Thermochemical discussion		
Dry cleaning gas / Fe source	Observation of reaction?	Reaction formula Reactant → Productant	ΔG <sub>f</sub> (kJ)	Estimate
SiCl <sub>4</sub> / Fe <sub>2</sub> O <sub>3</sub>	Yes	$\frac{3}{4}\text{SiCl}_4 + \frac{1}{2}\text{Fe}_2\text{O}_3 \rightarrow \text{FeCl}_3 + \frac{3}{4}\text{SiO}_2$	-81.9	Possible
Cl <sub>2</sub> / Fe <sub>2</sub> O <sub>3</sub>	No	$\frac{3}{2}\text{Cl}_2 + \frac{1}{2}\text{Fe}_2\text{O}_3 \rightarrow \text{FeCl}_3 + \frac{3}{4}\text{O}_2$	73.9	Impossible
SiCl <sub>4</sub> / Fe	No	$\frac{3}{4}\text{SiCl}_4 + \text{Fe} \rightarrow \text{FeCl}_3 + \frac{3}{4}\text{Si}$	185.7	Impossible
Cl <sub>2</sub> / Fe	Yes	$\frac{3}{2}\text{Cl}_2 + \text{Fe} \rightarrow \text{FeCl}_3$	-232.1	Possible

The standard free energy of formation ( $\Delta G_{f,800}$ ) is found as below.

The standard heat of formation ( $\Delta H_{800}$ ) and standard entropy ( $S_{800}$ ) for reactants and productants at 800K<sup>[9]</sup> are shown in Table II.

$$\Delta G_{f,800} = \Delta H_{f,800} - T\Delta S_{f,800} \quad (\text{T: } 800\text{K})$$

$$\Delta H_{f,800} = -\sum v \Delta H_{\text{reactant}} + \sum v \Delta H_{\text{productant}}$$

$$\Delta S_{f,800} = -\sum v S_{\text{reactant}} + \sum v S_{\text{productant}}$$

(v: stoichiometric coefficient)

Table II. Thermochemical data at 800K related to the direct reaction.

	Standard heat of formation ΔH (kJ mol⁻¹)	Standard entropy S (J K⁻¹ mol⁻¹)
SiCl <sub>4</sub> (g)	-660.9	428.8
Cl <sub>2</sub> (g)	0	258.5
Fe <sub>2</sub> O <sub>3</sub>	-812.9	216.3
Fe	0	56.8
FeCl <sub>3</sub>	-382.9	256.1
SiO <sub>2</sub>	-906.5	100.3
O <sub>2</sub>	0	235.9
Si	0	41.6

# The Mechanism of Copper Removal from a Bare Silicon Surface with Ultraviolet Excited Chlorine

A. Scott Lawing and Herbert H. Sawin  
Massachusetts Institute of Technology  
Department of Chemical Engineering  
Cambridge, MA 02139

Ty Fayfield  
FSI International  
Chaska, MN 55318

The surface mechanism which drives copper removal from a bare silicon surface in the UV/Cl<sub>2</sub> process has been established through a series of wavelength dependent experiments. Copper removal efficiency and the chemical state of copper reaction products on the wafer surface were determined with *in situ* X-Ray Photoelectron Spectroscopy (XPS). Copper removal involves the photon stimulated reduction and desorption of copper chlorides, and not silicon etching or Si<sub>x</sub>ClyM<sub>z</sub> complex formation as has been postulated in the literature. By balancing the effects of chlorination (pressure) and reduction (UV flux to the surface), efficient copper removal is achieved at lower pressure and temperature than has been reported previously.

## Introduction

Ultraviolet excited chlorine (UV/Cl<sub>2</sub>) has shown promise in removing transition metals, including copper(1,2,3,4). The mechanism by which UV/Cl<sub>2</sub> acts to remove transition metals from the wafer surface is poorly understood. The UV/Cl<sub>2</sub> process involves the simultaneous exposure of the wafer surface to chlorine gas and ultraviolet light. Molecular chlorine absorbs UV radiation in the wavelength range of 250-400 nm and dissociates to form atomic chlorine(5). It has been established that atomic chlorine will etch bulk silicon at conditions where molecular chlorine will not(6). The UV/Cl<sub>2</sub> process does not etch silicon dioxide at the conditions typically used for a metals removal process, although substrate etching through a native ("chemical") oxide has been observed(4,7). Sugino *et al.*(3,8) contend that gas phase chlorine radical generation and silicon etching are crucial to transition metal removal with UV/Cl<sub>2</sub>. Furthermore, it has been suggested that a "lift-off" mechanism(9,10), joint evaporation of metal chlorides with SiCl<sub>x</sub> species(11), or the formation of a metal-Si-Cl complex(10,11), are potential processes by which metals with low vapor pressure chlorides are removed from the surface in the UV/Cl<sub>2</sub> process. All of these mechanisms, whether explicitly or implicitly, invoke silicon etching. Conversely, we have observed similar removal efficiencies from

bare silicon and silicon dioxide surfaces with the UV/Cl<sub>2</sub> process suggesting that substrate etching is not required for metal removal, and have indirect evidence that the photochemical reduction of copper chlorides is important to the removal process(1).

The goal of this work was to separate the effects of gas phase (dissociation of molecular chlorine) and surface (photochemical reduction of surface chlorides) photolysis in order to elucidate the mechanism by which UV/Cl<sub>2</sub> acts to remove copper from wafer surfaces. To accomplish this we selected two wavelengths from our lamp output. The 367 nm wavelength is contained within the region in which chlorine absorbs strongly, so we would obtain significant gas phase dissociation of molecular chlorine in this region. The 245 nm wavelength is not contained within the chlorine absorption band and is the most energetic wavelength available, so we would expect to obtain the most efficient reduction of copper chlorides without causing significant gas phase dissociation. The pre- and post-process amount and chemical state of copper was monitored with *in situ* XPS.

### Experimental

The experimental apparatus in which these experiments were performed and the methods used have been described previously(1). The clustered system allows us to perform controlled trace metal contamination via sputtering, UV/Cl<sub>2</sub> processing, and XPS analysis while maintaining a base pressure of 10<sup>-7</sup> Torr. The UV/Cl<sub>2</sub> reactor is illustrated in Figure 1. In addition to the illumination system described previously, monochromators were used in this work. With this arrangement, ~1.5 mWatts/cm<sup>2</sup> and 3 mWatts/cm<sup>2</sup> were obtained for the 245 and 367 nm wavelengths, respectively, with an effective 8 nm full-width-at-half-maximum peak. The full spectrum output of the illumination system is illustrated in Figure 2.

Samples used in these experiments were 1 cm x 1 cm n-type Si <100> 1-5 Ω-cm with a 4000 Å thermal oxide. All samples were pre-cleaned (including an oxide strip) before processing. Samples subjected to the cleaning sequence exhibited strongly hydrophobic character, and XPS analysis indicated oxygen coverage on the order of 1/3 monolayer and a minimum amount of carbon contamination.

Figure 3 illustrates the 2p spectra of copper metal, copper dichloride and copper monochloride. The 2p<sub>3/2</sub> emission for metallic copper occurs at 931.9 eV. CuCl<sub>2</sub> is distinguished from Cu and CuCl by the presence of "shake-up" satellites, and a positive binding energy shift with respect to the metal. The main line for 2p<sub>3/2</sub> emission from CuCl<sub>2</sub> occurs at nominally 932.6 eV. It is difficult to distinguish CuCl from metallic copper on the basis of peak shape, since CuCl does not exhibit the satellite structure observed in CuCl<sub>2</sub>. We have observed a consistent negative shift in binding energy of the 2p<sub>3/2</sub> and 2p<sub>1/2</sub> emission which we attribute to formation of CuCl. The 2p<sub>3/2</sub> peak for CuCl occurs at nominally 931.2 eV, but has been observed as low as 930.4 eV. Other investigators(12,13) have reported a similar (though smaller in magnitude) binding energy shift for CuCl. In all of the figures presented here a reference line is superimposed, corresponding to the binding energy of metallic copper, to aid in visualizing chemical shifts. All spectra were normalized to the binding energy of Si at 99.75 eV.

## Results and Discussion

Figure 4 shows copper 2p spectra illustrating the effect of 245 nm UV on CuCl<sub>2</sub>. All of the peak intensities are directly comparable (as are all of the spectra within any of the figures presented here). In the as deposited state at a coverage of 0.05 ML, the copper is metallic. After 30 minutes of 245 nm UV exposure at 5 Torr chlorine and 55°C, all of the copper is present as CuCl<sub>2</sub>. The sample was re-introduced to the UV/Cl<sub>2</sub> chamber, and after 30 minutes of 245 nm UV exposure *under vacuum* at 41°C, all of the CuCl<sub>2</sub> has been removed from the surface. Note that CuCl<sub>2</sub> is removed from the surface with UV illumination at conditions where it is otherwise stable. This result implies a UV driven reduction process. It also implies that silicon etching is not required for copper removal since copper is removed from the surface in the absence of chlorine.

Figure 5 shows copper 2p photoelectron emission spectra illustrating the effect of a 60 minute exposure to UV illumination at 20 mTorr chlorine and 65 °C. All three samples were characterized by an initial metallic copper coverage of ~0.1 ML. Sample 1 was not exposed to UV and all of the copper on this sample is present as CuCl<sub>2</sub>. Sample 2 was exposed to 367 nm UV and the majority of the copper on this sample is present as CuCl<sub>2</sub>. Sample 3 was exposed to 245 nm UV and all of the copper on this sample is present as CuCl. Note that there is little difference between the sample held in the dark and the sample exposed to 367 nm UV. The sample exposed to 245 nm UV is in a reduced state and exhibits a lower copper coverage relative to the other two. A UV stimulated reduction process is operative at low chlorine pressure in the absence of gas phase chlorine radical production, i.e. 245 nm radiation, (note that the UV reduction process was not observed at 5 Torr as illustrated in Figure 4), maintaining the surface copper as CuCl. In the presence of UV which stimulates the production of chlorine radicals, i.e. 367 nm radiation, the chlorination reaction dominates and the surface is very similar to one exposed to no UV at all, where the surface copper is present mainly as CuCl<sub>2</sub>.

Figure 6 shows copper 2p spectra illustrating the effect of a 60 minute exposure to UV illumination on pre-chlorinated samples. Both samples were characterized by the initial level of metallic copper (~0.1 ML) as represented by the uppermost spectrum and the initial level of CuCl<sub>2</sub> represented by the second spectrum from the top. Sample 1 was exposed to 367 nm UV and the intensity of the photoemission is significantly decreased. Sample 2 was exposed to 245 nm UV and the copper has been removed almost to the detection limit. Under illumination by either wavelength under vacuum, CuCl<sub>2</sub> is completely reduced. In the absence of chlorine radicals the UV stimulated reduction process is active even at 367 nm, although it is more efficient at 245 nm. Comparison of figures 5 & 6 shows that copper removal is much more efficient in the absence of gas-phase chlorine. Even though CuCl<sub>2</sub> is not observed in significant quantity on the surface under the influence of 245 nm UV in a chlorine atmosphere (Figure 5) the interconversion of CuCl and CuCl<sub>2</sub> through chlorination and reduction processes is affecting the removal efficiency.

Figure 7 shows copper 2p spectra illustrating the effect of chlorine pressure on the removal process with 245 nm UV at 75°C. All three samples were characterized by the initial level of metallic copper as represented by the uppermost spectrum. All three samples were held at the pressure indicated for 60 minutes. As the pressure is increased, the post process level of copper on the surface increases as does the relative proportion of CuCl<sub>2</sub>. Note that the data represented in this figure were collected with a different quartz tube than the rest of the data presented here. The UV flux to the sample was attenuated relative to the other tube, accounting for the higher relative proportion of CuCl<sub>2</sub>.

Figure 8 shows copper 2p spectra illustrating the effect of temperature on the removal process with 245 nm UV in 20 mTorr chlorine. All three samples were characterized by the initial level of metallic copper as represented by the uppermost spectrum. All three samples were held at the temperature indicated for 60 minutes. Removal efficiency and relative concentration of CuCl on the surface increase with temperature between 25 and 105 C°.

The data presented in Figures 4-8 suggest that the volatile product in the UV/Cl<sub>2</sub> removal of copper is a form of CuCl, most likely the monomer. In all cases, efficient removal is coupled with CuCl present on the surface, while inefficient removal is coupled with a higher proportion of CuCl<sub>2</sub>. Our previous results suggest that (at least in the dark) formation of the trimer (CuCl)<sub>3</sub> is inhibited in the low coverage regime in which these experiments were performed(1). In support of our hypothesis, UV laser induced desorption from both CuCl and chlorinated copper surfaces has been studied(14,15,16,17). The product distributions from both surfaces contain significant quantities of the monomer CuCl, and in the case of desorption from solid CuCl, which we believe is most analogous to our system, the desorbed species is primarily CuCl. These results are significantly different than those obtained in thermal desorption experiments, where the desorbed products are almost exclusively due to the trimer (CuCl)<sub>3</sub>(18). In other discussions of the UV/Cl<sub>2</sub> process, including our own(1,9,10,11), the vapor pressure of the metal chloride species has been proposed as a metric for judging the potential to remove metals at a given temperature. Using vapor pressure as a metric implies thermodynamic equilibrium, whereas the flooding of the wafer surface with energetic photons can give rise to a fundamentally non-equilibrium process. Equilibrium considerations do not account for the observed removal rates since the equilibrium vapor pressure of the trimer is ~10<sup>-12</sup> Torr at 75 °C (19,20,21) and the concentration of the monomer is ~25 orders of magnitude less than that of the trimer in the gas phase(22). These values correspond to an equilibrium flux of ~10<sup>-6</sup> and 10<sup>-31</sup> ML/sec for the trimer and monomer respectively. We suspect that there is a photon stimulated process which causes CuCl to desorb from the surface at temperatures much lower, and in quantities much higher, than would be predicted from vapor equilibrium considerations or a purely thermal process.

Figures 9 and 10 illustrate improved copper removal processes based on the proposed copper removal mechanism. In both of these experiments the sample surface was subjected to the full lamp fluence, corresponding to broad band UV radiation (as illustrated in Figure 2) at a level of ~1 Watt/cm<sup>2</sup> in the wavelength range 235-400 nm.

Figure 9 shows copper 2p photoelectron emission spectra illustrating a "pulsed process". This sample was subjected to three cycles of chlorination in 5 Torr chlorine at 40 °C in the dark followed by evacuation of the chlorine in the chamber and full spectrum UV exposure under vacuum for 30 seconds at 40 °C. After three chlorination/UV exposure cycles the initial level of metallic copper (~0.1 ML) has been removed to nearly the detection limit. Note that after a UV exposure, copper is completely reduced to the metallic state. The much higher power of the full lamp fluence is capable of reducing CuCl<sub>2</sub> completely to metallic copper in less than 30 seconds. Of course, the added power corresponds to the introduction of additional wavelengths, but we have already shown that the reduction process is operative over a broad wavelength range. Figure 10 shows copper 2p photoelectron emission spectra illustrating a low pressure/low temperature process. An initial copper coverage of ~0.05 ML was exposed to full spectrum UV in 50 mTorr chlorine for 60 seconds at 75 °C. Copper is removed to nearly the detection limit after this process.

Figures 9 and 10 also support the contention of photon stimulated desorption of CuCl as the volatilization mechanism. Note that the full lamp fluence is capable of removing copper from the surface approximately two orders of magnitude faster than the lower power monochromated light. This power dependence of the removal process is good evidence for a non-thermal (i.e. photon stimulated) desorption process. Also note that the data in Figure 9, as well as that in Figure 6, represent copper removal under conditions where silicon should not be etched (and in fact, on none of the surfaces represented by Figures 4-9 did we observe significant roughening, which we have previously correlated with silicon etching(1)). This coupled with the fact that we are able to remove copper with equal efficiency from an oxide surface(1) rule out the possibility of a "lift-off" or complexing mechanism involving the interaction of copper chloride moieties with silicon etch products.

Lowering the temperature and pressure at which the process is performed allows us to operate in a much less aggressive and more controllable process regime in terms of; etching, chlorine incorporation, and roughening. Linear extrapolation of higher pressure results would lead us to expect a silicon etch rate of less than 10 Å/min at 50 mTorr and 75 °C(1,6,23,24). A UV/Cl<sub>2</sub> process performed at 5 Torr for 1 minute at 75 °C results in the formation of a SiCl<sub>x</sub> reaction layer ~ 8 Å thick, while a process performed at 50 mTorr for 1 minute at 75 °C results in a chlorine surface coverage of ~0.9 ML, as judged by XPS. A surface processed for 60 seconds at 75 °C and 50 mTorr exhibits surface roughness of 1.31 Å R<sub>A</sub> and 1.73 Å R<sub>MS</sub> while a surface processed for 60 seconds at 75 °C and 5 Torr exhibits roughness of 4.67 Å R<sub>A</sub> and 5.88 Å R<sub>MS</sub>. By way of comparison, a "virgin" silicon surface will exhibit surface roughness on the order of 1 Å R<sub>MS</sub>.

### Conclusions

The wavelength dependence of the removal of trace amounts of copper from bare silicon surfaces with UV/Cl<sub>2</sub> has been established. These results suggest that copper removal is driven by the photochemical reduction and photon enhanced desorption of

copper chlorides, and not silicon etching or complex formation. The copper removal mechanism is schematically illustrated in Figure 11. In practice, removal efficiency can be maximized by balancing the photon flux to the surface with the chlorine pressure such that a high surface concentration of CuCl is maintained.

### Acknowledgments

This work was funded by FSI International. We would like to acknowledge the support and input of Dr. Jeffery W. Butterbaugh at FSI.

### References

1. A.S. Lawing, A.J. Muscat, H.H. Sawin and J.W. Butterbaugh, *Proceedings of the Fourth International Symposium on Cleaning Technology in Semiconductor Device Manufacturing*, PV 95-20, J. Ruzyllo and R.E. Novak eds., p. 150, The Electrochemical Society, Pennington, N.J.(1996).
2. J. W. Butterbaugh, D. C. Gray, C. F. Hiatt, H. H. Sawin, and A.S. Lawing, *Proceedings of the Second International Symposium on Ultra Clean Processing of Silicon Surfaces*, M. Heyns, M. Meuris, and P. Mertens eds., p. 229, Acco, Leuven, Belgium (1994).
3. R. Sugino, Y. Okui, M. Okuno, M. Shigeno, Y. Sato, A. Ohsawa, and T. Ito, IEICE Trans. Electron., Vol. E75-C, No. 7, 829-833 (1992).
4. R. Sugino, Y. Nara, T. Yamakazi, S. Watanabe, and T. Ito, Extended Abstracts of the 19th Conference on Solid State Devices and Materials, August 25-27, 1987, Tokyo (Business Center of Academic Societies, Tokyo, 1987), pp. 207-210.
5. H. Okabe, *Photochemistry of Small Molecules*, Wiley Inter-Science, N.Y., p. 185 (1978).
6. E.A. Ogryzlo, D.E. Ibbotson, D.L. Flamm, and J.A. Mucha, *J. Appl. Phys.* 67 (6), 3115-3120 (1990).
7. R. Sugino, Y. Nara, H. Horie, T. Ito, *J. Appl. Phys.*, 76 (9), 5498-5502 (1994).
8. R. Sugino, in U.S. Patent #5,178,721 (Fujitsu Limited, Tokyo, Japan, 1993).
9. J. Ruzyllo, in *Handbook of Semiconductor Wafer Cleaning Technology: Science, Technology, and Applications*, W. Kern, ed., p. 208, Park Ridge N.J.: Noyes Publications (1993).
10. Y. Sato, R. Sugino, and T. Ito, Fujitsu Sci. Tech. J., 27 (4), 317-328 (1991).
11. B.E. Deal and C.R. Helms, in *Handbook of Semiconductor Wafer Cleaning Technology: Science, Technology, and Applications*, W. Kern, ed., p. 316, Park Ridge N.J.: Noyes Publications (1993).
12. S.W. Gaarenstroom and N. Winograd, *J. Chem. Phys.*, 67, 3500 (1977).
13. W. Sesselmann and T.J. Chuang, *Surface Science*, Vol 176, No. 1-2, 32-66 (1986).
14. W. Sesselmann, E.E. Marinero, and T.J. Chuang, *Surface Science*, Vol. 178, 787-797 (1986).
15. W. Sesselmann, E.E. Marinero, and T.J. Chuang, *Appl. Phys. A*, Vol. 41, 209-221 (1986).
16. G.N.A. van Veen, T. Baller, and A.E. DeVries, *J. Appl. Phys.*, 60 (10), 3746-3749 (1986).
17. G.N.A. van Veen, T.S. Baller, and J. Dieleman, *Appl. Phys. A*, Vol. 47, 183-192 (1988).
18. H.F. Winters, *J. Vac. Sci. Technol. A*, 3 (3), 786-790 (1985).
19. R. Colton and J.H. Canterford, *Halides of the First Row Transition Metals*, p. 490, Wiley-Interscience, New York (1969).
20. R.R. Hammer and N.W. Gregory, *J. Phys. Chem.*, Vol. 68, No. 11, 3229-3233 (1964).
21. R.A.J. Shelton, *Trans. Faraday Soc.*, Vol. 57, 2113, (1961).
22. E.G. King, A. D. Mah, and L.B. Pankratz, *Thermodynamic Properties of Copper and its Inorganic Compounds*, The International Copper Research Association and the U.S. Department of the Interior, Bureau of Mines, p. 172, (1973).
23. E. Ikawa, S. Sugito, and Y. Kurogi, *Surface Science*, Vol. 183, 276-288 (1987).
24. H. Okano, Y. Horiike, and M Sekine, *Jap. J. Appl. Phys.*, part 1, Vol. 24, No. 1, 68-74 (1985).

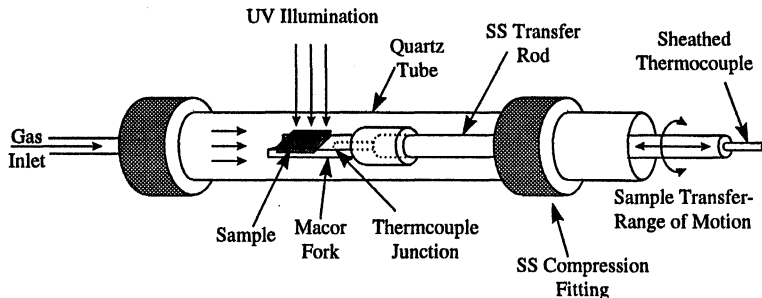


Figure 1 - Schematic Diagram of the UV/Cl<sub>2</sub> Reactor.

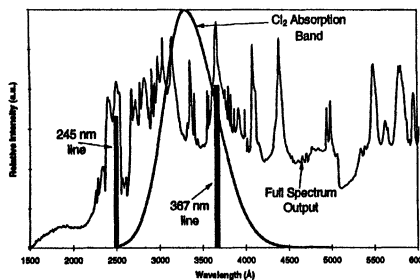


Figure 2 - Full Spectrum Output of the UV Illumination System, with the Cl<sub>2</sub> absorption band and the 245 and 367 nm lines superimposed.

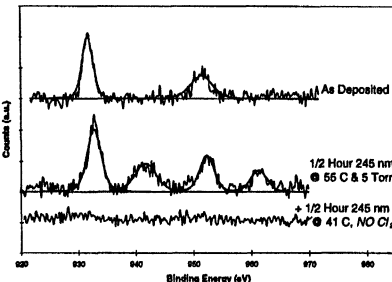


Figure 4 - Copper 2p photoelectron emission spectra illustrating the effect of 245 nm UV on CuCl<sub>2</sub>.

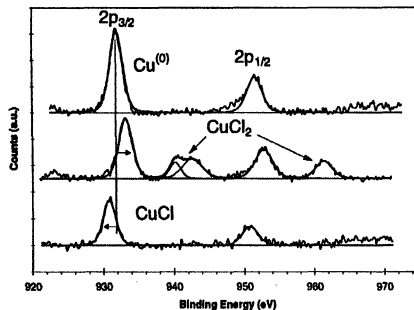


Figure 3 - Copper 2p photoelectron emission spectra illustrating the identifying features of copper metal(Cu<sup>(0)</sup>), CuCl and CuCl<sub>2</sub>.

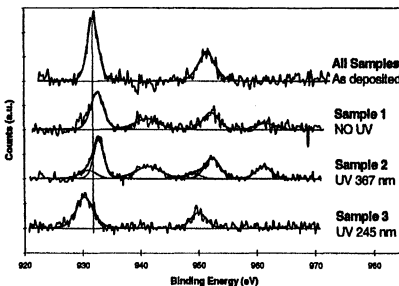


Figure 5 - Copper 2p photoelectron emission spectra illustrating the effect of UV illumination at 20 mTorr chlorine and 65 °C.

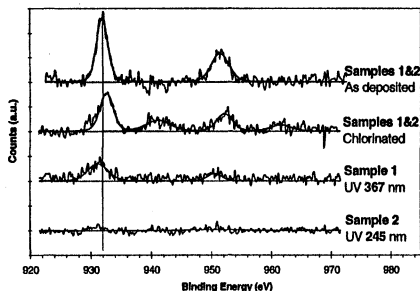


Figure 6 - Copper 2p photoelectron emission spectra illustrating the effect of UV illumination on pre-chlorinated samples.

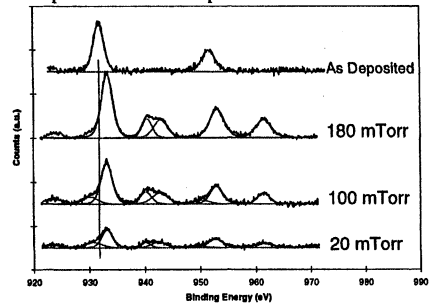


Figure 7 - Copper 2p photoelectron emission spectra illustrating the effect of chlorine pressure on removal with 245 nm UV at 75 °C.

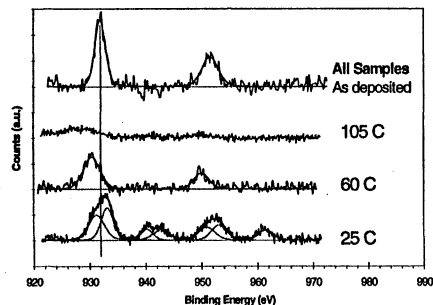


Figure 8 - Copper 2p photoelectron emission spectra illustrating the effect of temperature on removal with 245 nm UV in 20 mTorr chlorine.

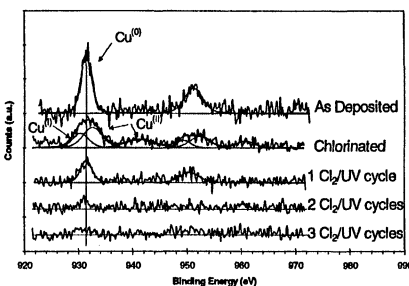


Figure 9 - Copper 2p photoelectron emission spectra illustrating a "pulsed process".

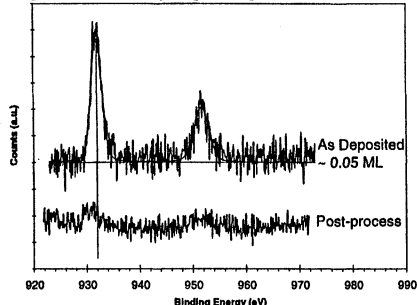


Figure 10 - Copper 2p photoelectron emission spectra illustrating a low pressure/low temperature process.

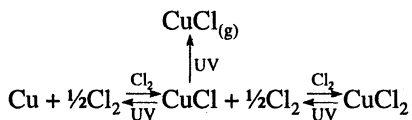


Figure 11 - Schematic representation of the UV/Cl<sub>2</sub> copper removal mechanism. Chlorine flux forces the equilibrium to the right. Gas phase chlorine radical generation accelerates the forward reaction. UV photons cause the reduction of copper chlorides. UV also stimulates the desorption of CuCl, the volatile product. Efficient copper removal is realized when the UV flux and the chlorine flux to the surface are balanced, resulting in a high surface concentration of CuCl.

# HYDROGEN PLASMA CLEANING OF OXIDE-PATTERNEDE SI WAFERS FOR LOW TEMPERATURE SI EPITAXY

Hwan-Kuk Yuh, Jin-Won Park, Ki-Hyun Hwang, Euijoon Yoon  
and Ki-Woong Whang\*

School of Materials Science and Engineering and Inter-University Semiconductor Research Center (ISRC), Seoul National University, Seoul 151-742, Korea

\*School of Electrical Engineering & ISRC, Seoul National University

Hydrogen plasma cleaning was used to clean the oxide patterned Si wafer *in situ* before low-temperature (510°C) Si homoepitaxy by ultrahigh vacuum electron cyclotron resonance chemical vapor deposition. After proper *in situ* hydrogen plasma cleaning of the patterned wafer, it was possible to obtain a defect-free undoped Si epitaxial layer. However, in case of boron doped Si epitaxial growth, Si epilayers had a defective zone away from the bird's beak along the window edges and a sound zone at the center of the window. Cross section transmission electron microscopy (XTEM) and energy dispersive spectroscopy (EDS) results suggested that the specific region with many defects was rich in oxygen concentration. The formation of oxynitrides during the oxide pattern formation or the redeposition of sputtered oxygen clusters could vary the oxygen concentration on the window. The excessive oxygen on the surface at a particular distance away from the bird's beak could result in amorphous boron oxide to impede the epitaxial growth of Si.

## INTRODUCTION

Gas-phase cleaning becomes more and more important for the development of ultra large scale integration (ULSI) technology [1]. It is also advantageous to the conventional wet cleaning technique in terms of process stability, the prevention of recontamination, reduction in environmentally hazardous waste. Especially, the process clustering can be easily achieved by gas-phase cleaning.

The gas-phase cleaning can be applicable to pre-cleaning for low temperature epitaxial growth [2,3], post-etch cleaning [4], pre-metal contact cleaning [5] and so on.

Low temperature Si epitaxial growth was reported by many researchers [2,3], and the *in situ* wafer cleaning is the important process for low temperature epitaxy [6]. The wafer cleaning needs *in situ* cleaning as well as wet cleaning for complete removal of native oxide. The general *in situ* cleaning, thermal cleaning, requires heating substrate over 800°C which cause oxide erosion and stress. Therefore, it is necessary to clean the wafer using plasma, photo and other energy sources for *in situ* cleaning of the oxide-patterned wafers at low temperature.

Conventional plasma cleaning techniques using Ar, H<sub>2</sub>, and NF<sub>3</sub> are reported to have some problems when they are applied to oxide-patterned wafers. The quality of epilayers grown after Ar plasma cleaning degraded due to the oxygen clusters at the interface between the substrate and the epilayer [7]. The oxygen cluster was believed to come from the redeposition of oxygen species sputtered from the oxide mask. Addition of hydrogen to Ar plasma cleaning could reduce the formation of the oxygen cluster [8]. Hydrogen plasma is better for low temperature cleaning due to high reactivity of the hydrogen species generated in the plasma. It is known that electron cyclotron resonance (ECR) plasma is of high density, and its average ion energy is low, compared to radio frequency (RF) plasma. In this study oxide-patterned Si wafers were *in situ* cleaned by ECR hydrogen plasma at 510°C and silicon epilayers were deposited by ultra-high vacuum electron cyclotron resonance chemical vapor deposition (UHV-ECRCVD) at the same temperature.

## EXPERIMENTAL

The UHV-ECRCVD reactor used in this study has been described in detail elsewhere [6]. Briefly, the reactor is composed of a ultrahigh vacuum main chamber, a loadlock and an ECR source. SiH<sub>4</sub> and B<sub>2</sub>H<sub>6</sub> were introduced to downstream hydrogen plasma through a gas dispersal ring [9]. Process parameters such as reactor pressure, microwave power, substrate DC bias, magnet current, etc., were optimize to obtain dislocation-free B-doped Si layers at 510°C.

Oxide-patterned wafers were made by a standard local oxidation of silicon

(LOCOS) process. The wafers were *ex situ* cleaned, loaded into the main chamber, and subsequently cleaned *in situ* by hydrogen plasma. The ion dose to the oxide-patterned wafer during plasma cleaning was adjusted by changing process parameters such as microwave power, substrate DC bias, magnet current and cleaning time [6].

Immediately after the *in situ* cleaning, undoped and boron-doped silicon epitayers were grown at a fixed condition: substrate temperature 510°C, microwave power 50 W, magnet current 40 A, H<sub>2</sub> flow rate 74 sccm, SiH<sub>4</sub> flow rate 2 sccm, dilute B<sub>2</sub>H<sub>6</sub> (200 ppm in hydrogen) flow rate 3 sccm and total pressure of 8 mTorr. Structural quality of the Si epitaxial layers was analyzed by *in situ* reflection high energy electron diffraction (RHEED), scanning electron microscopy (SEM), dilute Schimmel etching, cross section transmission electron microscopy (XTEM) and energy dispersive spectroscopy (EDS). A large-area window (5x5 mm<sup>2</sup>) was prepared at center of the wafer for RHEED analysis.

## RESULTS AND DISCUSSION

### Boron-doped Si epitaxial layers

The oxide-patterned wafers were cleaned by hydrogen plasma for 20min at high ion flux condition: microwave power 100 W, magnet current 50 A, DC bias +10 V, H<sub>2</sub> flow rate 74 sccm, substrate temperature 510°C and total pressure of 2 mTorr. Si epitaxial layers were grown at the same temperature. RHEED pattern was spotty, implying that the Si layers were very defective. It was likely that the excessive cleaning resulted in damaged surface regions or contaminate surface from the redeposition of oxygen clusters from the oxide mask. Accordingly, plasma condition was adjusted to a lower ion flux condition.

Cleaning was performed for 20 min at the low ion flux condition: microwave power 50 W, magnet current 40 A, dc bias +30 V. The RHEED pattern from the Si layer in this case had half-order streaks, indicating that the Si layer were structurally of high quality. The layer grown on the mask was a mixed layer of amorphous and polycrystalline Si, as determined by XTEM. Dilute Schimmel etching method was used to delineate structural defects in the Si layer. The low-magnification SEM image in Fig. 1(a) shows that Si layer grown on the window area had high density of defects.

Cleaning time was reduced from 20 min to 2 min, resulting in reduced ion dose. The Si epitaxial layer had 2x1 surface reconstruction, as confirmed by RHEED. The Si layer was also examined by dilute Schimmel etching method. Defect density of the epitaxial layer was much lower than previous layer, as shown in Fig. 1(b). Fig. 1(b) also shows marks of side-wall defects along the oxide/Si edges [10]. It is interesting to note, however, that another band of defective zone was observed along the side-wall defects within the epitaxial Si layer. The average distance between the side-wall defect and the new defective band was 0.2  $\mu\text{m}$  and independent of the size of the window. XTEM analysis of the epitaxial layers on Si 0.7  $\mu\text{m}$ -wide windows revealed defects at the center of window, as shown in Fig. 2 (a), as well as side-wall defects investigated by other researchers. The selective area diffraction pattern (SADP) in Fig. 2(b) from the defected center region indicated that the region consisted of single crystal with high density of twins and some polycrystals. XTEM of the larger window area (Fig. 3) showed clearly the defective bands at 0.2  $\mu\text{m}$  from the side-wall defect and the defect-free zone at the center of the window.

#### Undoped Si epitaxial layers

Undoped Si layers were grown at the same growth condition of Fig. 3. Defect-free Si epitaxial layers were obtained at the window area, as shown in Fig. 4. Side-wall defects and the transition from epilayer to amorphous/polysilicon at the bird's beak were clearly shown. This abrupt changes in structural quality of the Si epilayer at the window area resulted from the presence of boron during deposition. It is well known that boron reacts readily with oxygen to form an amorphous layer which possibly impede the growth of high-quality epilayers [11,12].

#### Origin of the defective band formation

The Si epitaxial layer grown at a larger window (1.6  $\mu\text{m}$ ) was investigated to study the distribution of defects by XTEM (Fig. 3). Fig. 3 shows the presence of two defected zone (0.2  $\mu\text{m}$ ) and a sound zone (0.8  $\mu\text{m}$ ) at the center. The impurity concentrations at the interfaces between epitaxial layer and substrate of each zone were analyzed with EDS. Concentration of oxygen at the defected zone was twice higher than that at a sound zone. It is presumed that the origin of defects is an amorphous phase formed by reaction between

boron and oxygen species at the defect band region  $0.2\mu\text{m}$  away from the side wall. The reasons for the local variation of the oxygen content are not certain at the moment, however, there are two possible explanations for the phenomenon.

First, oxynitride can be formed near the bird's beak during the LOCOS process [13]. Once it is formed, it is more resistant to hydrogen plasma than the native oxide. Thus, it is likely that some of the oxynitride is left on the surface and readily reacts with boron during epitaxial growth to form amorphous layers. The presence of amorphous layer will eventually result in defective layers. Second, oxygen clusters from the bird's beak can redeposit on the window area. The sputtered oxygen clusters will be scattered in the gas phase, however, some of them will be redeposited. Since the maximum distance that the scattered oxygen cluster can travel in the gas phase is on the order of mean free path, the concentration of oxygen cluster on the window surface will reach a maximum at a certain distance from the bird's beak. More oxygen clusters can be sputtered from the bird's beak compared to the field oxide. Ions can be easily deflected by local charging effect [14] and the incident ion can move toward field oxide [15]. Moreover, applied +30V dc bias makes electrical potential of oxide lower than that of Si window. High compressive stress at the bird's beak area [16] can enhance the sputtering yield.

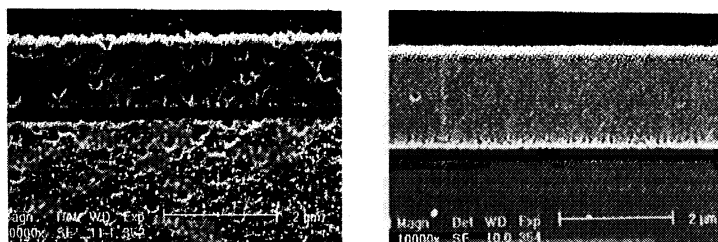
## CONCLUSION

Low-temperature Si epitaxial growth on LOCOS-patterned Si wafer was made by UHV-ECR-CVD. After proper *in situ* hydrogen plasma cleaning of the patterned wafer, it was possible to obtain high-quality undoped epitaxial layers. However, for the boron-doped Si, a new defective band besides side-wall defects was observed. XTEM and EDS results suggested that the region was high in oxygen concentration. The formation of oxynitrides during the oxide pattern formation or the redeposition of sputtered oxygen clusters could vary the oxygen concentration on the window. The excessive oxygen on the surface could resulted in amorphous boron oxide to impede the epitaxial growth of Si.

## REFERENCE

1. J. Ruzylo, Microcontamination 6, 39 (1988).

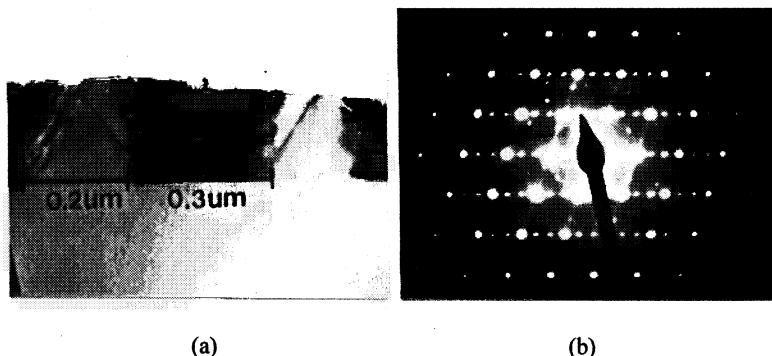
2. J. Murota, N. Nakamura, M. Kato and N. Mikoshida, *Appl. Phys. Lett.* **54**, 1007 (1989).
3. N. Kasai and N. Endo, *J. Electrochem. Soc.* **139**, 1982 (1992).
4. J. P. Simko, G. S. Oehrlein and T. M. Mayer, *J. Electrochem. Soc.* **138**, 277 (1991).
5. W. Tsai, M. Delfino, M. E. Day and J. A. Fair, *IEEE Trans. on Elec. Dev.* **41**, 1396 (1994).
6. H-S. Tae, S-J. Park, S-H. Hwang, K-H. Hwang, E. Yoon and K-W. Whang, *J. Vac. Sci. Technol. B* **13**, 908 (1995).
7. T.-R. Yew, R. Reif, *J. Appl. Phys.* **65**, 2500 (1989).
8. T.-R. Yew, R. Reif, *J. Appl. Phys.* **68**, 4681 (1990).
9. J-W. Park, K-H. Hwang, S-J. Joo, E. Yoon, S-H. Hwang and K-W. Whang, *J. Vac. Sci. Technol. A* **14**, 1072 (1996).
10. R. Bashir, G. W. Neudeck, Y. Haw, E. P. Kvam, J. P. Denton, *J. Vac. Sci. Technol. B* **13**, 923 (1995).
11. E. de Fesart, S. S. Rhee and K. L. Wang, *Appl. Phys. Lett.* **49**, 847 (1986).
12. G. Lippert, D. Kruger, H. P. Zeindl, J. Ramm, E. Bugiel and H. J. Osten, *Mat. Res. Soc. Symp. Proc.* **315**, 85 (1993).
13. E. Kooi, J. G. van Lierop, and J. A. Appels, *J. Electrochem. Soc.* **123**, 1117 (1976).
14. J. C. Arnold and H. H. Sawin, *J. Appl. Phys.* **70**, 5314 (1991).
15. M. Ardehali, *Appl. Phys. Lett.* **64**, 169 (1994).
16. K. Kobayashi, Y. Inoue, T. Nichimura, M. Hirayama, Y. Akasaka, and T. Kato, *J. Electrochem. Soc.* **137**, 1987 (1990).



(a)

(b)

Fig. 1. SEM micrographs of the Schimmel-etched B-doped Si epilayers after hydrogen plasma cleaning a) for 20 minutes at a low ion flux condition, b) for 2 minutes at the same condition. Center regions are window areas.



(a)

(b)

Fig. 2 (a) XTEM micrograph of the B-doped Si epilayer on Si window region,  
(b) SADP of the epilayer region.

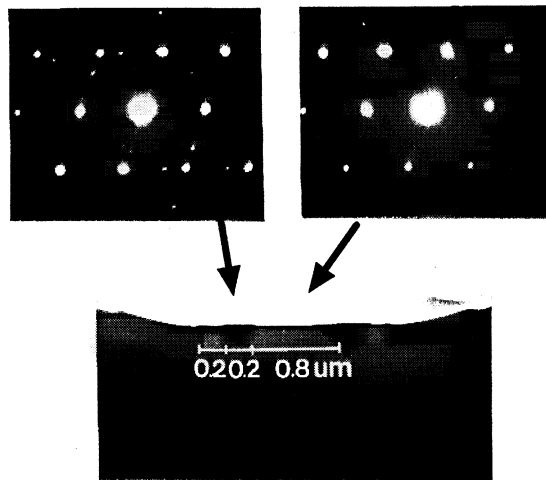


Fig. 3. XTEM micrograph of the B-doped Si epilayer grown on a larger window. SADP's from the defect-free and defective regions are shown above.

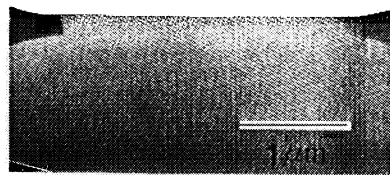


Fig. 4. XTEM micrograph of the defect-free undoped Si epilayer.

# **Effects Controlling Initiation and Termination of Gas-Phase Cleaning Reactions**

J. Staffa, S. Fakhouri, M. Brubaker, P. Roman, and J. Ruzyllo  
*Electronic Materials and Processing Laboratory*  
*Department of Electrical Engineering*  
*The Pennsylvania State University*  
*University Park, PA 16801*

In contrast to wet cleans, the cleaning reactions in the gas phase may be significantly affected by the surface condition of the incoming wafer. Additionally, effective termination of the cleaning reaction, which in wet cleans is accomplished through a deionized water rinse, is not as straightforward in the case of dry cleaning processes. In this experiment the UV/nitrogen exposure was found effective in controlling initiation of the etch reaction while UV exposure, pressure, temperature, and ambient composition were used to control termination of surface reactions.

## **INTRODUCTION**

The pre-existing condition of the surface prior to the process plays an important role in the outcome of the gas-phase process. Among the differences between anhydrous HF (AHF): methanol gas-phase etching and the dilute HF (dHF): water process is the scarcity of moisture available during the gas-phase process. During a wet etch, the effect of the surface hydration of the oxide is largely masked by the availability of water in solution. In contrast, the gas-phase oxide etch is largely limited by the availability of hydroxyl groups necessary to initiate the etch reaction [1]. In the course of the investigation of the AHF: methanol process, it was observed that thermal oxides, grown under the same process conditions, but having different histories between the thermal oxidation and the AHF: methanol etch, display greatly differing etch rates when etched under identical process conditions [2].

On the other hand, following each process it is important to leave the surface in a stable condition. Passivation of the silicon surface implies a surface which is controlled and not evolving after the process is complete. In liquid-phase processes, DI water rinses are used to remove reactants and reaction products. This terminates the reaction and provides a stable surface for the next step in the process sequence. Because the rinse is absent in gas-phase processing, other methods of terminating gas-phase reactions are necessary. The purpose of this experiment was to explore the effects determining initiation and termination of the gas-phase cleaning reactions and to study ways of controlling them.

## **EXPERIMENTAL**

P-type (100) silicon wafers were oxidized at 900 °C to an oxide thickness of 200 Å and set aside to age. The change in the AHF:methanol etch rate of thermal oxides

produced by the aging of the  $\text{SiO}_2$  surface was observed by etching different wafers in a commercial gas-phase cleaning tool [3] over a period of days under identical gas-phase etch conditions. The oxide thickness before and after the etch process was measured through ellipsometry. In our previous work [2] it was determined that an anneal applied prior to oxide etching can be used to control the oxide etch rate. In this study, UV/ $\text{N}_2$  pretreatments at 0.1 mtorr performed prior to the oxide etch process were studied as a low temperature alternative to thermal anneals. Their effect on surface moisture was determined through SIMS and their effect on the etch rate of the aged oxides was also studied.

The surface charge profiling (SCP) method [4] was used to study the evolution of the surface in air following the gas-phase cleaning sequences, and X-ray photoelectron spectroscopy (XPS) was used to determine the surface coverage of the major species. The surface charge profiling (SCP) method is non-contact surface photovoltaic (SPV) measurement which yields information on the charge present on the surface and the recombination lifetime of minority carriers at the surface. Because the probe does not contact the surface, it is well suited for studying time evolution of the surface without altering the state of the surface through the measurement itself. XPS and SCP measurements were performed on separate wafers after each step of the process sequence.

## RESULTS AND DISCUSSION

### Control of Initiation of Oxide Etching

As  $\text{SiO}_2$  was exposed to cleanroom air following a dry oxidation, the gas-phase etch rate of the oxides rose as the time of exposure to air increased as shown in Fig.1. It was presumed and then confirmed using SIMS measurements that the accumulation of moisture on the oxide surface was the reason for these variations. Surface hydration related to aging has manifested itself previously as an agent for roughening silicon oxides during thermal oxidation [5]. Chemisorbed hydroxyl groups on the surface hydrogen bond with water, and the condensation on the surface is not homogeneous across the wafer. The surface hydration may cause non-uniformities in wafer-to-wafer etch rate and etch uniformity across the wafer as well as  $\text{SiO}_2$  particle generation in areas of the wafer where excessive amounts of moisture are present.

The effect of surface hydration on the AHF:methanol process may be limited through a thermal anneal prior to the process at 250 °C [2]. It was observed that thermal anneals reduce the etch rate to pre-aging levels. That the change induced by the thermal treatments is in fact related to surface dehydration is indicated by the effect of methanol flow rate during the AHF: methanol process on annealed and unannealed wafers. At lower methanol partial pressures there is a significant difference in the etch rates of annealed and unannealed wafers. In the absence of methanol, the level of surface hydration becomes the determining factor in the initiation of the etch process. The initiation of the reaction by the moisture present on the surface independently of methanol flow adversely affects the control of the process. Therefore, it is necessary to curtail the amount of moisture present on the surface prior to the chemical gas-phase oxide etching process.

An elevated temperature process step immediately prior to the oxide etch is impractical because the temperature sensitive nature of the AHF:methanol etch process would necessitate an extended cooling period between the two process steps. An *in situ* UV irradiation step has been found in this study to produce the same effect without elevating the temperature above 60-70 °C. The etch rate of an aged oxide as a function of exposure time in UV is presented in Fig.2. It was observed that the etch rate stabilizes after thirty seconds and that this duration is sufficient to dehydrate the surface. SIMS was used to compare the hydration of the oxide aged for one week in the clean room with the hydration of the oxide aged for one week and exposed to the UV desorption process. The total silanol peak measured through SIMS is the sum of two components: moisture chemisorbed to the surface prior to the SIMS measurement and physisorbed moisture which becomes chemisorbed to the surface because of the measurement itself. It is possible to remove the component contributed by the physisorbed moisture through UV pretreatments. However, UV pretreatments did not remove chemisorbed water from the surface.

#### Termination of the Gas-Phase Surface Cleaning Reactions

In order to prevent uncontrolled variations of the surface chemistry after completion of the gas-phase surface treatments, a designated reaction quenching step is needed. Such a step would play the role the deionized (DI) water rinse does in liquid chemical processing. As the electric charge on the silicon surface reflects the electrochemical condition of the surface, its variation as a function of time can be used to monitor surface stability.

The surface charge evolution following the gas-phase and liquid-phase oxide etch processes of concern in this experiment is shown in Fig.3. As seen, the AHF:methanol process leaves a stable surface which shows little change in surface charge. The dHF process, on the other hand, shows increasing charge during the first twenty minutes of air exposure. It is expected that the level of physisorbed moisture on the surface is higher following the rinse than it is on the AHF:methanol surface, and requires some time to reach equilibrium with the clean room air. Initially, the physisorbed hydroxyl groups neutralize some of the charge on the surface, resulting in a lower initial induced depletion width. As the hydroxyl groups desorb, leaving hydrogen terminated bonds, the surface charge rises to match that of the AHF:methanol process. It should be noted that because of the more complete hydrogen termination of the surface, a surface following a dHF process displays better long-term surface stability than one following the AHF:methanol process [6].

This difference between the dHF and the AHF:methanol surfaces can have a significant effect on the outcome of a subsequent UV/Cl<sub>2</sub> process. The UV/Cl<sub>2</sub> process is typically used to remove metals from the surface as well as to remove the top ~30 Å of silicon, in order to remove any damage from previous processing. It has been observed through XPS that chlorine readily replaces fluorine on the silicon surface, at surface concentrations higher than those of the original fluorine coverage. Chlorine is known to be an unstable passivator in the presence of moisture on the surface, or in the ambient, forming volatile HCl and leaving behind hydroxyl groups in its place. The surface charge evolution following the UV/Cl<sub>2</sub> process is shown in Fig.4 and the surface recombination

lifetime evolution is shown in Fig.5. The surface charge following the UV/Cl<sub>2</sub> process subsequent to the AHF:methanol process drops to its stable value more quickly than it does after the UV/Cl<sub>2</sub> process that follows the dHF etch. This is an indication that the volatile reactants and products are desorbing from the surface more quickly after the gas-phase oxide etch probably because of the absence of an adsorbed layer of moisture. The recombination lifetime of the dHF + UV/Cl<sub>2</sub> surface also takes considerably longer to reach its maximum than the AHF:methanol + UV/Cl<sub>2</sub> surface. This initial increase is linked to changes in the depletion width across which carriers are swept and recombine. The change is induced by changes in the surface charge. After reaching its maximum, the recombination lifetime of the dHF + UV/Cl<sub>2</sub> surface is unstable and quickly begins to decay. A reduction in recombination lifetime has been found to be associated with reoxidation of the surface and may take over a day to begin in a fully hydrogen passivated surface. The excess moisture of the dHF + UV/Cl<sub>2</sub> surface is making the surface more unstable, as chlorine is readily replaced on the surface by hydroxyl groups originating from either the ambient or the surface of the wafer.

It is of interest to know what the stability of the surface is following the UV/O<sub>2</sub> process which has typically been used to passivate the surface after the UV/Cl<sub>2</sub> process. The surface charge measurement revealed that the effect of the UV/O<sub>2</sub> process is to accelerate the desorption of species from the surface. However, the surface charge was still evolving after the wafers were removed from the process chamber. Interestingly, the UV/O<sub>2</sub> process did not appear to affect the final stable charge of the surface. Differences in the condition in the condition of the surface originating during the oxide etch process persist even after both the UV/Cl<sub>2</sub> and UV/O<sub>2</sub> processes. The recombination lifetimes once again all exhibited the rising edge associated with the change in depletion width caused by reactant and product desorption. The AHF:methanol + UV/Cl<sub>2</sub> + UV/O<sub>2</sub> process sequence does not appear to lead to a fully passivated surface because the recombination lifetime slowly decreases to a stable level following the process. The surface following the dHF + UV/Cl<sub>2</sub> + UV/O<sub>2</sub> process exhibited a much faster transition to a final stable surface recombination lifetime because of the enhancement of the oxidation of the surface by the excess moisture. The oxide produced through this process will have a high silanol concentration, however.

The UV/O<sub>2</sub> process has been employed previously as a means of passivating a very reactive chlorinated/fluorinated silicon surface which would otherwise rapidly become contaminated between the surface preparation and gate oxidation steps. As shown in Fig.6, the UV/O<sub>2</sub> process does significantly increase the amount of oxygen present on the surface. However, it does not significantly reduce the concentration of either fluorine or chlorine on the surface. Because the liquid-phase rinse which would normally remove the halogens is not suitable for cluster tool applications, a gas-phase alternative, or "dry rinse" must be developed.

If, instead of the UV/O<sub>2</sub> process, methanol is flowed into the chamber at pressures and temperatures favorable to its adsorption on the surface of the wafer, the amount of chlorine remaining on the surface is significantly reduced, while the amount of fluorine remains as low as it was following the UV/Cl<sub>2</sub> process. Some increase in the amount of carbon is also observed, however. The Si=Si-Cl present on the surface is replaced by Si=Si-O-CH<sub>3</sub> + HCl (g). A subsequent UV/N<sub>2</sub> process is used to desorb reaction

products, such as HCl, from the surface. In order to further the passivation of the silicon surface and detach the methyl group left from the reaction of methanol with the surface chlorine, the UV/O<sub>2</sub> process follows. The XPS scan of the resulting surface, shown in Fig. 7, contains fairly modest amounts of the halogens and carbon and an amount of oxygen roughly comparable to that seen in native oxide.

Because halogens are known to be relatively unstable for passivating the silicon surface, reducing the surface halogen concentration was expected to result in a more stable surface. The UV/O<sub>2</sub> process alone did not successfully passivate the surface as it did not remove halogens from the surface. The post-UV/Cl<sub>2</sub> process methanol adsorption, on the other hand, did remove halogens from the surface and, as determined from surface charge measurements, did result in a stable surface when combined with a low partial pressure UV/O<sub>2</sub> process, which passivates the surface. Both the surface charge and surface recombination lifetime, which is shown in Fig. 8, are constant.

## CONCLUSIONS

The results of this study indicate that in the case of gas-phase surface preparation, the condition of the surface of the incoming wafer has to be carefully controlled because of possible effects of pre-existing moisture on etch uniformity and processes subsequent to the etch process. This study shows that this can be accomplished through a UV desorption pretreatment applied *in situ* before the oxide etch. Also, effective methods of quenching gas-phase cleaning reactions by removal of reactants and reaction products is necessary in order to obtain a surface which is stable prior to further processing. A methanol adsorption process followed by a reduced pressure UV/N<sub>2</sub> process for desorption of reactive species and a low partial pressure UV/O<sub>2</sub> process for removal of chemisorbed methyl groups and complete oxygen passivation of the surface were employed to reduce halogen concentration and produce stable oxygen terminated surfaces.

## ACKNOWLEDGMENTS

This study was supported by the Semiconductor Research Corporation project no. BJ-443. Also, support from SubMicron Systems Corporation and QC Solutions, Inc. is acknowledged.

## REFERENCES

1. K. Torek, J. Ruzylo, R. Grant, and R. Novak, *J. Electrochem. Soc.*, **142**, p.1322 (1995)
2. J. Staffa and J. Ruzylo, *Proceedings of the Third International Symposium on Ultra Clean Processing of Silicon Surfaces*, 261 (1996)
3. Primaxx Enterprises Ltd., Allentown, PA
4. SCP Model 110, QC Solutions, Inc. Billerica, MA
5. M. Grundner, P. O. Hahn, I. Lampert, *Proc. of the First Int. Symp. on Cleaning Tech. in Sem. Dev. Man.*, p.328 (1989)
6. K. Torek, A. Mieckowski, and J. Ruzylo, *Proc. of the Fourth Int. Symp. on Cleaning Tech. in Semi. Dev. Man.*, p.208 (1995)

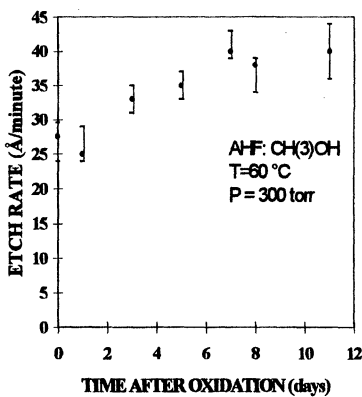


Figure 1 - Etch rate of the AHF:methanol process as a function of oxide exposure to clean room ambient following oxidation.

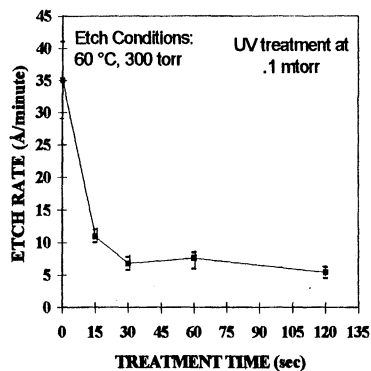


Figure 2 - The etch rate of an aged oxide during the AHF:methanol process as a function of time of exposure to UV irradiation before etching.

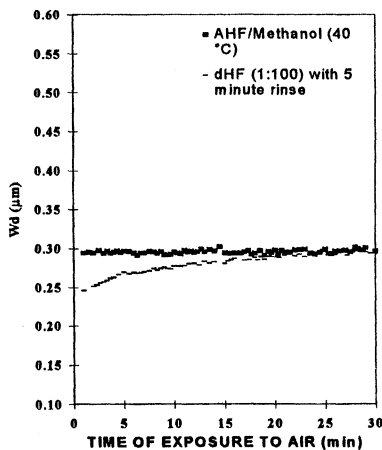


Figure 3 - Surface charge evolution in air following the AHF:methanol and dHF + DI rinse processes.

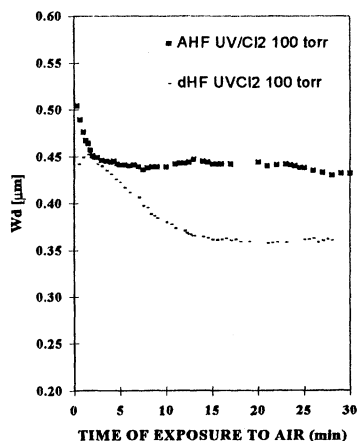


Figure 4 - Surface charge evolution in air following the UV/Cl<sub>2</sub> process subsequent to either the AHF:methanol or dHF + DI rinse process.

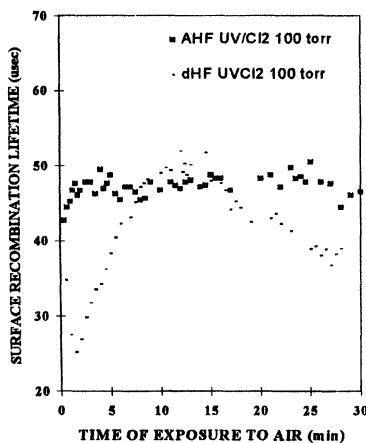


Figure 5 - Surface recombination lifetime evolution in air following the UV/Cl<sub>2</sub> process subsequent to either the AHF:methanol or dHF + DI rinse process.

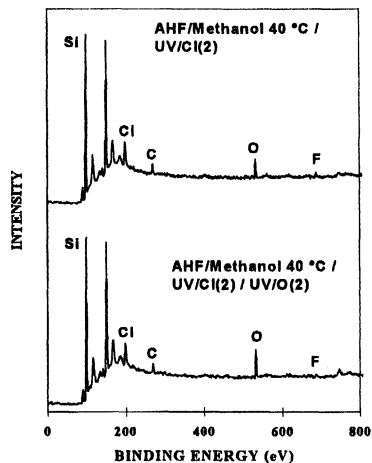


Figure 6 - XPS spectra of silicon surfaces following the AHF/methanol + UV/Cl<sub>2</sub> process sequence and the AHF/methanol + UV/Cl<sub>2</sub> + UV/O<sub>2</sub> process sequence.

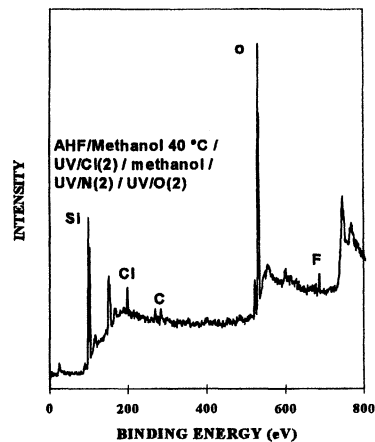


Figure 7 - XPS spectrum of a surface passivated with the UV/O<sub>2</sub> process with halogen levels reduced by methanol adsorption.

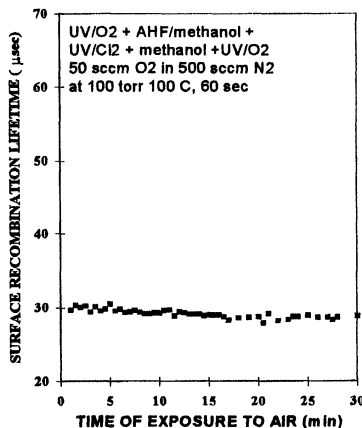


Figure 8 - Surface recombination lifetime evolution in air following the "dry rinse" process.

## **DRY CLEANING FOR DEEP SUBMICRON VIAS**

A. L. P. Rotondaro, D. B. Aldrich, P. B. Smith and C. Appel  
Texas Instruments Incorporated  
Semiconductor Process & Design Center  
13570 North Central Expressway, Dallas, TX 75243, USA

Submicron vias (down to 0.40  $\mu\text{m}$ ) were fabricated using an optimized dry cleaning process based on a chemistry consisting of oxygen ( $\text{O}_2$ ) and hexafluoroethane ( $\text{C}_2\text{F}_6$ ). Improved electrical characteristics were obtained for the dry cleaned samples compared with solvent cleaned control samples. The dry clean process represents a significant improvement over the solvent clean process from an environment standpoint with inherently lower cost of waste treatment and disposal.

### **INTRODUCTION**

Cleaning of vias is a critical step in the production of highly reliable submicron devices. This is becoming a non-trivial task to accomplish as the via diameter is reduced to meet sub-quarter-micron integration requirements. Polymer buildup in the vias during via etch is a problem that has drawn the attention of several research groups. A polymer free etch process has not been desirable, mainly because polymer sidewall deposition is used to assure high anisotropy for the via etch process [1]. High via resistance and low via yield result when the polymer remain at the bottom of the via [2,3].

Cleaning after via etch is commonly addressed using a combination of dry and wet processes. A typical process sequence consists of an oxygen plasma ash followed by a solvent clean [3]. The solvent clean is needed because the oxygen plasma ash process is ineffective in removing in-via polymer residues [2]. However, the cleaning efficiency of the solvent step is being severely challenged as the via diameter is being reduced and the via aspect ratio is being increased.

Dry cleaning appears as a robust solution for the cleaning of deep submicron vias. Compared to wet methods, dry cleaning is not susceptible to restrictions in removing contaminants from high aspect ratio structures. Moreover, a dry cleaning approach presents much lower environmental impact with lower cost in chemical disposal and treatment.

In this paper, a dry cleaning process is developed and optimized as a replacement for the solvent cleaning step in the fabrication of vias of 0.40 or 0.45  $\mu\text{m}$  diameter. The process was optimized for low via resistance and high via yield.

### **EXPERIMENTAL**

The dry cleaning process was developed in a Mattson ASPEN II asher. The system has an inductively coupled plasma (ICP) source that generates the excited species

remotely from the wafer surface. Two grounded metal grids prevent charged species from reaching the wafers, assuring an isotropic process without any charge damage [4]. Hexafluoroethane ( $C_2F_6$ ) was added to the oxygen ( $O_2$ ) plasma to accomplish the polymer removal. The  $O_2$  flow was fixed at 3000 sccm for all processes and the  $C_2F_6$  flow was varied between 0 and 30 sccm.

Figure 1 shows a schematic cross-section of the via structure used in our studies. The final thickness of the interlevel dielectric (ILD) material on top of the first interconnect level (M1) is approximately 950 nm resulting in vias with a 2.5:1 aspect ratio. Vias were etched using an Applied Materials HDP oxide etch reactor. The via etch stops in the TiN layer on top of the first interconnect level. The etch reactor has *in-situ* ash capability that was used to remove the photoresist pattern after the via etch. Following the via etch and *in-situ* ash, the wafers were cleaned and received a deionized (DI) water rinse and a spin-dry. The via cleaning was either performed using a dry cleaning process or using solvent. The solvent process consists of a 10 minutes immersion in Microstrip 2001, an N-methyl-pyrrolidinone (NMP) based solvent, with ultrasonic agitation. The via fabrication was completed with via fill and the deposition and definition of the second interconnect level (M2).

Residue removal was physically assessed using scanning electron microscopy (SEM) inspection. Via resistance was measured on Van Der Pauw structures and via chains. No via resistance filter was applied for the definition of via yield. This means that all structures that conducted electricity were considered as yielding.

## RESULTS AND DISCUSSION

The  $O_2$  plasma ash performed *in-situ* at the etch reactor was unable to remove the polymer films that formed inside the vias during via etch, as can be seen in Figure 2. This result was expected, as the polymer film inside the vias is believed to be composed of Si, O, C, H and the exposed metal. Fluorinated chemistries would remove such films, but they also could attack the ILD materials, causing an increase in via diameter or an undercut of the ILD layers. In order to investigate the effect of the  $C_2F_6$  plasma on the ILD materials, the change in via diameter was monitored as a function of the  $C_2F_6$  flow rate. A long process time of 120 seconds was used to amplify the effects and make the SEM measurements more reliable. The results show that a direct correlation exists between the  $C_2F_6$  flow and the increase of the via size (Figure 3). By limiting the maximum acceptable change in via diameter to 0.01  $\mu m$ , the parameter space for  $C_2F_6$  flow and process duration could be derived. The region under the curve in Figure 4 represents the selected parameter space. As expected, the higher the  $C_2F_6$  flow, the shorter the process duration is allowed.

Complete removal of the in-via polymer could be achieved even for processes with low  $C_2F_6$  flow and short duration (figure 5a). However, cross-section SEM analysis showed that the use of  $O_2 + C_2F_6$  plasma causes significant undercut of the TiN layer on top of M1 (Figure 5b) for non-optimized processes. The parameter space for minimizing the TiN undercut is much more restrictive than the one derived to keep the via diameter

change under 0.01  $\mu\text{m}$ . To achieve minimum TiN undercut and keep a good process window, low flow of  $\text{C}_2\text{F}_6$  (6 sccm) was selected.

The removal of the in-via polymer film and the TiN layer on top of M1 using the  $\text{O}_2 + \text{C}_2\text{F}_6$  process has a significant impact in reducing the via resistance compared to the solvent treated control samples (Figure 6). Moreover, tighter via resistance distributions are obtained with the dry cleaning processes as can be seen in Figure 6 from the values of via resistance at 10 and 90 % occurrence relative to the median value. These results indicate that the removal of the TiN layer eliminates a significant component of the via resistance value and deviation. The via resistance distribution can also be affected by the via size. The dispersion of the via resistance values is much more pronounced for solvent cleaned vias of 0.40  $\mu\text{m}$  compared to 0.45  $\mu\text{m}$  vias (Figure 6). On the other hand, the via resistance distribution for the dry cleaned samples is not affected by the via size (Figure 6). This indicates that the dry clean process could be easily extended for the processing of smaller diameter vias. The degree of TiN undercut has no significant impact on the via resistance value and distribution, as can be seen in Figure 6 when comparing the results for a process that undercuts the TiN layer (Dry-1) to the results for a process that has minimum TiN undercut (Dry-2).

On Van Der Pauw structures, the via yield for dry clean processes that undercut the TiN layer is comparable or even better than the one observed for the solvent cleaned samples (Figure 7). However, for long via chains, yield degradation correlates with the amount of TiN undercut resulting from the dry clean. Processes that severely undercut the TiN layer present significant reduction in yield whereas processes with minimum TiN undercut have yield comparable to or better than the Van Der Pauw structures (Figure 7). The yield reduction on long via chains for the processes that undercut the TiN layer might be related to the interaction of the void formed at the undercut region with the via fill process.

It is clear that, although desirable from the standpoint of improving the via resistance distribution (lower values and tighter distribution), the removal of the TiN layer has to be performed with minimal undercut to assure high yield values. Figure 8 shows typical 0.40  $\mu\text{m}$  vias fabricated with the dry process that was optimized for total removal of the TiN layer at the bottom of the vias with minimum undercut.

## CONCLUSIONS

A dry cleaning process based on  $\text{C}_2\text{F}_6$   $\text{O}_2$  plasma chemistry was developed and optimized for the fabrication of vias down to 0.40  $\mu\text{m}$  diameter. It can effectively be used as a substitute for the existing solvent process for via clean providing lower via resistance with a tighter distribution and high yield. It appears capable of being successful for cleaning smaller diameter ( $< 0.40 \mu\text{m}$ ) vias and higher aspect ratio structures. The dry cleaning process also has the inherent advantage of reducing waste treatment and disposal being much more environmentally friendly compared with the solvent process.

## REFERENCES

1. H. Shan et al., J. Electrochem. Soc., **141**, 2904 (1994).
2. J. K. Tong et al., in Cleaning Technology in Semiconductor Device Manufacturing IV, R. E. Novak and J. Ruzyllo Editors, PV **95-20**, p.235, The Electrochemical Society Proceedings Series, Pennington, NJ (1995).
3. S. Marks et al., in Cleaning Technology in Semiconductor Device Manufacturing IV, R. E. Novak and J. Ruzyllo Editors, PV **95-20**, p.214, The Electrochemical Society Proceedings Series, Pennington, NJ (1995).
4. L. M. Loewenstein et al., in Cleaning Technology in Semiconductor Device Manufacturing IV, R. E. Novak and J. Ruzyllo Editors, PV **95-20**, p.225, The Electrochemical Society Proceedings Series, Pennington, NJ (1995).

## FIGURES

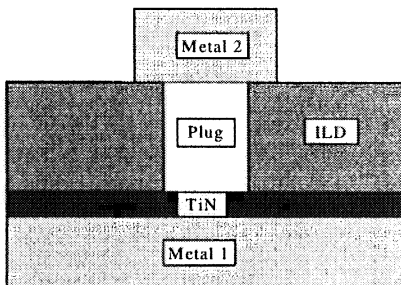


**Figure 1:** Schematic cross-section of the via structure used in these experiments.

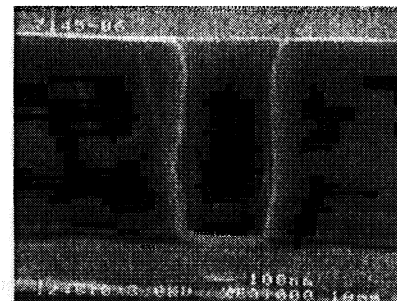


**Figure 2:** Typical SEM cross-section photograph of a  $0.40 \mu\text{m}$  via after etch and pure  $\text{O}_2$  ash.

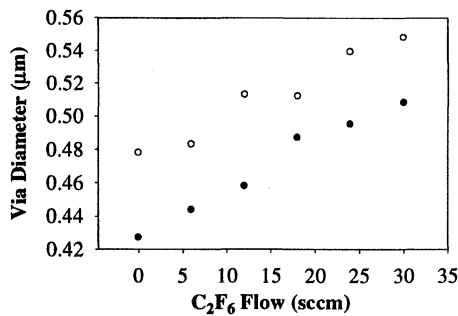


**Figure 3:** Via diameter as a function of the C<sub>2</sub>F<sub>6</sub> flow rate for dry cleaning processes with 120 seconds duration. The initial via size was 0.48 and 0.43 μm diameter.

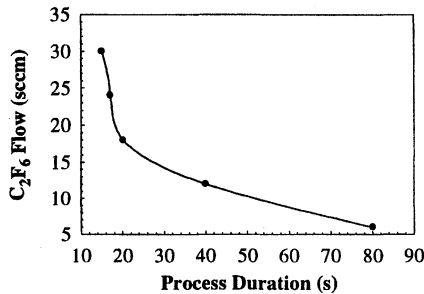


**Figure 4:** Upper boundary of the parameter space for C<sub>2</sub>F<sub>6</sub> flow and process duration that cause less than 0.01 μm change in via diameter.

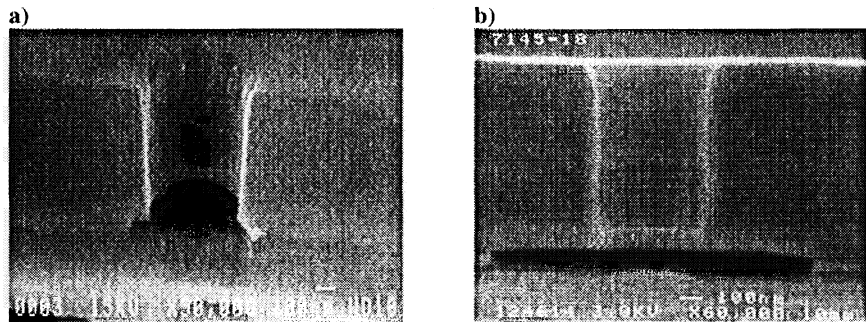


**Figure 5:** Typical SEM cross-section photographs of 0.40 μm diameter vias cleaned for 40 sec using O<sub>2</sub> C<sub>2</sub>F<sub>6</sub> processes: a) Low C<sub>2</sub>F<sub>6</sub> flow (6 sccm), b) High C<sub>2</sub>F<sub>6</sub> flow (30 sccm).

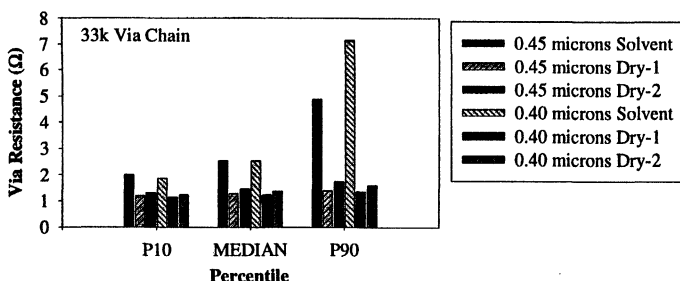


**Figure 6:** Via resistance distribution for  $33 \times 10^3$  via chains. Vias with  $0.45$  and  $0.40 \mu\text{m}$  diameter were probed. Dry-1 and Dry-2 indicate processes that remove the TiN layer with and without undercut, respectively.

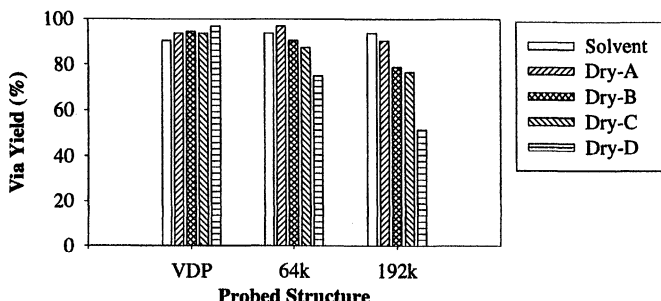


**Figure 7:** Via yield for via chains. Dry-A to Dry-D indicate dry clean processes with an increasing amount of TiN undercut.

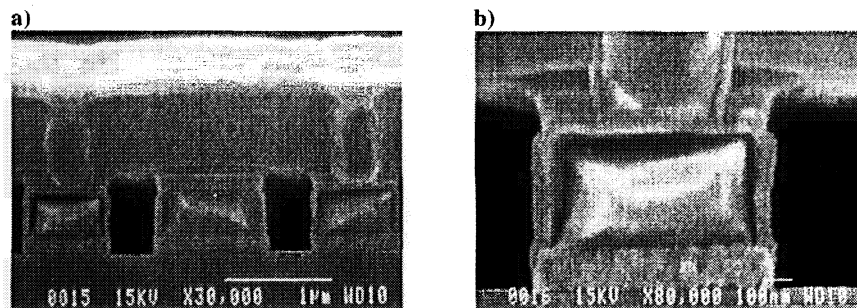


**Figure 8:** Typical SEM photographs of  $0.40 \mu\text{m}$  vias fabricated with the optimized dry cleaning process that removes the TiN layer without undercutting it.

## CLEANING OF SiO<sub>2</sub> BULK LAYERS WITH SUCCESSIVE PROCESSING OF POLY-SI CVD AND UV/Cl<sub>2</sub>

Rinji Sugino, Yoko Tada, and Takashi Ito

Fujitsu Laboratories Ltd.

10-1 Morinosato-Wakamiya, Atsugi 243-01, Japan

Yoshiko Okui and Jun Sakuma

Fujitsu Limited

4-4-1 Kamikodanaka Nakahara, Kawasaki 211-88, Japan

We have developed a method to remove Fe contaminants from SiO<sub>2</sub> bulk layers using a technique in which poly-Si is first deposited on a Si wafer surface and then etched off. The poly-Si layer was formed by chemical vapor deposition (CVD) on an SiO<sub>2</sub> surface intentionally contaminated with Fe. The poly-Si was etched with Cl radicals generated by ultraviolet irradiation, a process called UV/Cl<sub>2</sub>. Fe concentration in the SiO<sub>2</sub> that was exposed after etching decreased by two orders of magnitude from the original contamination level of 10<sup>12</sup> atoms/cm<sup>2</sup>. On the other hand, Fe concentration in the Si substrate remained unchanged after the poly-Si CVD and UV/Cl<sub>2</sub> processes. The Fe removal results are independent of the thickness of poly-Si when between 50 and 400 nm, and are also independent of either the presence or absence of phosphorous doping in the poly-Si.

### INTRODUCTION

Metal contaminants such as Fe, Cu, and Ni in Si substrates lower the yield and performance of LSIs.<sup>[1,2]</sup> Ordinarily, metal contaminants on Si substrate surfaces must be removed by processes prior to thermal processes during LSI manufacturing.<sup>[3,4]</sup> On the other hand, metal contaminants once introduced to the Si substrate through an ion or plasma process cannot be removed by any surface cleaning processes. Thus, gettering processes used to precipitate the metal contaminants in the Si substrate have been developed.<sup>[5-8]</sup> However, these processes have some problems in that the gettered metals in the Si substrate are sometimes diffused again during thermal-cycles in manufacturing processes.

Metal contaminants in the Si substrate should also be eliminated out. Our investigations have focused on the capabilities of poly-Si as a getter material. Using a technique that consists of poly-Si deposition and its subsequent etching on the front surface of a Si wafer, we tried to remove the metal contaminants existing in the bulk layers. That is, gettered metal contaminants in the poly-Si layer were removed by etching off the poly-Si. The poly-Si layer was formed by CVD and etching was done with

UV/Cl<sub>2</sub>. UV/Cl<sub>2</sub> removes metal contaminants on the Si surface with a slight etching.<sup>[9,10]</sup> Additionally, the SiO<sub>2</sub> layer grown by the thermal oxidation of Si is not etched with UV/Cl<sub>2</sub> at all, although the Si was etched rapidly.<sup>[11]</sup>

Using this new technique of poly-Si CVD succeeded by UV/Cl<sub>2</sub> (poly-Si CVD & UV/Cl<sub>2</sub>), we could remove Fe contaminants from an SiO<sub>2</sub> bulk layer. This paper describes such Fe removal effects. A pronounced decrease of Fe concentration in an intentionally contaminated SiO<sub>2</sub> layer will be shown. In addition, we will discuss the difference of Fe removal effects on SiO<sub>2</sub> and Si with this poly-Si CVD & UV/Cl<sub>2</sub> technique.

## EXPERIMENT

Figure 1 shows the process steps of the Fe contamination procedure. We used four-inch, boron doped p-type Si wafers with a resistivity between 9 and 11 Ωcm and having (100)-oriented surfaces. The Si wafers were first cleaned with a standard RCA solution such as NH<sub>4</sub>OH-H<sub>2</sub>O<sub>2</sub>-H<sub>2</sub>O (1:1.5:4) and deionized water. After this wet cleaning step, wafers were contaminated by the following process. First, the clean Si wafer was coated with photo-resist dissolving Fe-resinate (N. E. Chemcat Co. Ltd.). Fe-resinate is a metallo-organic which is usually used as a decorative source for ceramics, plastics, and glass. The chemical structure of Fe-resinate is an organic-complex which coordinate Fe atom. It was a useful Fe source for our experiment because it is soluble in the photo-resist. The Fe concentration in the photo-resist was 3 ppm. After the Fe-contaminated resist coating was applied to the Si wafer, the organic was removed by an O<sub>2</sub> plasma ashing process, which was done in a ballel-type plasma ashing. Fe contaminants remaining on the surface are considered slightly penetrate the Si substrate through the plasma ashing process.<sup>[12]</sup> Then the wafers were oxidized with dry O<sub>2</sub> in a thermal-oxidation furnace after being cleaned with an H<sub>2</sub>SO<sub>4</sub>-H<sub>2</sub>O solution, HNO<sub>3</sub>, and deionized water. The oxidation temperatures were 900°C while a 15 nm thick oxide layer was formed and 850°C while a 5 nm layer was formed. After oxidation, the SiO<sub>2</sub> and Si bulk layers could be quantitatively contaminated with Fe.

The process details of poly-Si CVD & UV/Cl<sub>2</sub> are as follows. Poly-Si was deposited on the contaminated SiO<sub>2</sub> surface at 620°C and in a 100% SiH<sub>4</sub> atmosphere in a low pressure CVD chamber. Phosphorous ions (phos.+<sup>+</sup>) were implanted into the poly-Si layer. The wafers were annealed in N<sub>2</sub> at 900°C in a furnace tube for 30 min. After removing the native oxide on the poly-Si using a diluted HF solution, the poly-Si layer was etched by UV/Cl<sub>2</sub> under the following conditions: high-purity (99.999%) Cl<sub>2</sub> gas was maintained at 4.0 kPa during etching in a temperature of 480°C under UV light with a wavelength of 200 to 300 nm at 22 mW/cm<sup>2</sup>. The single wafer system of UV/Cl<sub>2</sub> dry etching/cleaning equipment consisted of a quartz chamber, a halogen lamp to heat the wafer, and a microwave-excited UV mercury lamp. Each wafer was over-etched to 200% of the thickness of the poly-Si.

The Fe concentration in an  $\text{SiO}_2$  layer was determined by flameless atomic absorption spectrophotometry (AAS) which measured the Fe concentration of the HF solution that recovered the Fe by HF-scanning dissolution. The concentration was represented in terms of atoms/cm<sup>2</sup> which was converted from the total number of Fe atoms in the  $\text{SiO}_2$ . The Fe concentration in the Si bulk was determined by the surface photo-voltage (SPV) method. The quantification of Fe concentration in a Si substrate and the detection limits were given a detailed description from in a previous study of Jastrzebski, et al.<sup>[13]</sup> In this experiment, Si wafers that were treated with Intrinsic-Gettering were not used. Furthermore, oxygen precipitates in the Si substrate were not supposed to form under the thermal budget. Therefore, the Fe concentration detection region by SPV was estimated to be from  $10^9$  atoms/cm<sup>3</sup> to  $10^{14}$  atoms/cm<sup>3</sup>.

### Fe REMOVAL EFFECT ON $\text{SiO}_2$ AND Si

Figure 2 shows the Fe concentration of both the  $\text{SiO}_2$  layer and the Si substrate before and after poly-Si CVD & UV/ $\text{Cl}_2$ . As shown in cases of Fe contamination (indicated on the left side in Fig. 2), our method could produce contamination levels of  $10^{12}$  atoms/cm<sup>2</sup> in  $\text{SiO}_2$  and  $10^{13}$  atoms/cm<sup>3</sup> in the Si substrate. A reference sample, which was oxidized without the contaminated resist coating and plasma ashing exhibited concentrations of  $\leq 10^{10}$  atoms/cm<sup>2</sup> orders in  $\text{SiO}_2$  and  $10^{10}$  atoms/cm<sup>3</sup> orders in the Si substrate. Applying poly-Si CVD & UV/ $\text{Cl}_2$  to the Fe-contaminated wafer, Fe concentration in  $\text{SiO}_2$  decreased by two orders of magnitude from the Fe contamination level, which is below the detectable limit of AAS. On the other hand, Fe concentration in a Si substrate remained unchanged after poly-Si CVD & UV/ $\text{Cl}_2$ . This suggests that poly-Si CVD & UV/ $\text{Cl}_2$  removes Fe only in the  $\text{SiO}_2$  layer. At  $\text{SiO}_2$  thickness of 5 and 15 nm, the poly-Si CVD & UV/ $\text{Cl}_2$  could remove the Fe in  $\text{SiO}_2$  completely, although it does not act on the Si substrate.

We studied the dependence of the poly-Si thickness and phos.+ doping of the poly-Si on the Fe removal effects. From A to D in Figure 3 indicate each different condition of poly-Si formed on an  $\text{SiO}_2$  layer with a thickness of 5 nm, as follows: A and B have 400 nm thick poly-Si, C and D have 50 nm thick poly-Si, and B and D have no phos.+ implantation in the poly-Si. The conditions of phos.+ implantation were 70 keV and a  $4 \times 10^{15}$  dose/cm<sup>2</sup> for a 400 nm thick poly-Si, and 4 keV and a  $5 \times 10^{14}$  dose/cm<sup>2</sup> for a 50 nm thick poly-Si. The concentration and distribution of phosphorous on both thicknesses of poly-Si were estimated as being similar. In each condition, Fe concentration in  $\text{SiO}_2$  decreased by two orders of magnitude from the Fe contamination level, which is below the limit of detectable by AAS. On the other hand, Fe concentration in the Si substrate was unchanged by the poly-Si CVD & UV/ $\text{Cl}_2$  process. That is, there was no significant difference in poly-Si condition for Fe removal effects. These results suggest that poly-Si deposited on an  $\text{SiO}_2$  surface getter Fe existing in the  $\text{SiO}_2$  layer, although the Fe

gettering effect of poly-Si cannot extend to the Si substrate.

### Fe BEHAVIOR IN EACH BULK LAYER

We investigated the behavior of the Fe contaminants before and after poly-Si CVD & UV/Cl<sub>2</sub> by the use of secondary ion mass spectroscopy (SIMS). Figure 4 shows SIMS profiles of <sup>54</sup>Fe. O<sub>2</sub> ion was used as the primary ion. A sample, presence of Fe contamination, was subjected to a 400 nm-thick-poly-Si CVD after phos.+ implantation and annealing. The reference sample was not subjected to the Fe contamination process. The peak of the <sup>30</sup>Si profile is presumed to be the SiO<sub>2</sub> layer. Thus, the region between the top surface and the <sup>30</sup>Si peak point is considered as the poly-Si layer. A peak of <sup>54</sup>Fe is observable in the poly-Si region. Fe contaminants in the SiO<sub>2</sub> can be considered to have diffused into the poly-Si layer because little sign of <sup>54</sup>Fe was observed from the reference profile.

In the sample having 400 nm of poly-Si, inaccuracies in information from the area adjacent to the SiO<sub>2</sub> and Si substrate interface may be caused by a lowering of the depth-resolution during deep sputtering with primary ions. The right side of Figure 5 shows SIMS profiles of a sample after the poly-Si was etched off. The remarkable lowering of the Fe signal in the SiO<sub>2</sub> was observed by comparing a profile after poly-Si CVD & UV/Cl<sub>2</sub> with a profile of a sample having only Fe contamination. On the other hand, the <sup>54</sup>Fe peak observed in Si near the interface was not affected by poly-Si CVD & UV/Cl<sub>2</sub>. The above SIMS results are expected to support the results of AAS and SPV regarding Fe concentration in both SiO<sub>2</sub> and Si.

### Fe REMOVAL MECHANISM

The previous results can be explained by using the scheme in Figure 6 as follows. Poly-Si deposition on an SiO<sub>2</sub> can getter the Fe in the SiO<sub>2</sub>. It seems that the poly-Si absorbs the Fe from the SiO<sub>2</sub>. This effect is independent of the thickness of poly-Si when between 50 and 400 nm. The Fe gettering ability is also unaffected by the presence or absence of phosphorous in the poly-Si. The annealing affect for the Fe gettering of poly-Si cannot be considered in this study, since all samples were annealed at 900°C for 30 min. Clean SiO<sub>2</sub> can be obtained by etching off the Fe-gettered poly-Si by UV/Cl<sub>2</sub>. It can be thought that the Fe in poly-Si vaporizes to form Fe chloride of high-vapor pressure simultaneous with the Cl radical etching. Then, a surface of clean SiO<sub>2</sub> is exposed having the same thickness of SiO<sub>2</sub> before poly-Si CVD because Cl radicals do not etch the SiO<sub>2</sub> at all.

Using UV/Cl<sub>2</sub> without poly-Si CVD did not remove the Fe in the SiO<sub>2</sub>. We have confirmed that the Fe concentration in SiO<sub>2</sub> did not change before and after UV/Cl<sub>2</sub> only.

It can be assumed that the SiO<sub>2</sub> suppresses the penetration of Cl radicals so that they cannot reach the Fe atoms.

In this experiment, the effect of poly-Si CVD & UV/Cl<sub>2</sub> did not clean the Si layer. Generally, it is known that poly-Si deposited on the back side of a wafer to be used as getter material for Extrinsic Gettering (EG) precipitates metal contaminants such as Fe and Cu into the Si substrate.<sup>[7]</sup> However, the gettering effects of EG should be studied for a sample that has undergone the full LSI manufacturing process. Samples are subjected to a quite larger thermal budget during full processing than was the case with our samples. Under the conditions in our experiment, Fe atoms may be considered to exist more stably in the Si layer than the SiO<sub>2</sub> layer. In addition, poly-Si layers such as electrode materials and buffer layers for field oxidation, which are unintended gettering, are expected to clean neighboring SiO<sub>2</sub> layers during the LSI manufacturing process.

## CONCLUSIONS

Fe contaminants existing in SiO<sub>2</sub> bulk layers can be removed by poly-Si CVD succeeded by a UV/Cl<sub>2</sub> etching process. The Fe removal effects were confirmed by the use of wafers intentionally contaminated through oxidation and photo-resist methods. Poly-Si was deposited on the contaminated SiO<sub>2</sub> surface and then etched to a 200% over-etching condition. After the poly-Si CVD & UV/Cl<sub>2</sub> processes were carried out on the Fe-contaminated wafer, the Fe concentration in SiO<sub>2</sub> decreased by two orders of magnitude from the original level. On the other hand, Fe concentration in the Si substrate remained unchanged after poly-Si CVD & UV/Cl<sub>2</sub>. This tendency did not vary with the SiO<sub>2</sub> thickness or under several poly-Si conditions. The quantitative results of each were supported by SIMS analysis. A poly-Si layer such as electrode materials and buffer layers for field oxidation are expect to clean neighboring SiO<sub>2</sub> layers during LSI manufacturing processes.

## ACKNOWLEDGEMENTS

The authors thank Y. Sato, M. Okuno, H. Mori, T. Ogawa,, S. Fujimura, K. Yamazaki, K. Watanabe, and T. Ikehata for sample measuring and helpful suggestions.

## REFERENCES

- [1] A. Ohsawa et al., in Proc. of the 6th Silicon Materials Science and Technology Symp., 'Semiconductor Silicon/1990' in ECS Spring Meeting (The Electrochemical Society, Pennington, NJ) PV.90-7 pp.601-613 (1990).
- [2] W. B. Henly et al., 1993 IEEE/IRPS, pp.22-27.

- [3] W. Kern and D. A. Puotinen, RCA Review **31**, 187 (1970).
- [4] R. Takizawa et al., Jpn. J. Appl. Phys. **27** L2210 (1988).
- [5] J. S. Kang and D. K. Schroder, J Appl. Phys. **65** 2974 (1989).
- [6] M. Miyazaki et al., Jpn. J. Appl. Phys. **28** L519 (1989).
- [7] H. Yamanaka et al., *ibid.* **32** L738 (1993).
- [8] M. C. Chen and V. J. Silvestri, J. Electrochem. Soc. **129** 1294 (1982).
- [9] T. Ito et al., in Proc. of the 1st International Symp. on Cleaning Technology in Semiconductor Device Manufacturing (The Electrochemical Society, Pennington, NJ) **PV.90-9** pp.114-120 (1989).
- [10] R. Sugino et al., in Proc. of the 2nd International Symp. on Cleaning Technology in Semiconductor Device Manufacturing (The Electrochemical Society, Pennington, NJ) **PV.92-12** pp.72-79 (1991).
- [11] R. Sugino et al., J. Appl. Phys. **76** 5498 (1994).
- [12] S. Fujimura and H. Yano, J Electrochemical Soc. **135** 1195 (1988).
- [13] L. Jastrzebski et al., J Electrochemical Soc. **140** 1152 (1993).

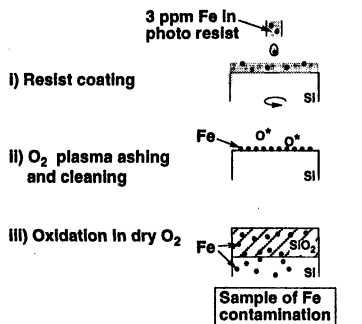


Fig. 1. Experimental procedure for Fe contamination.

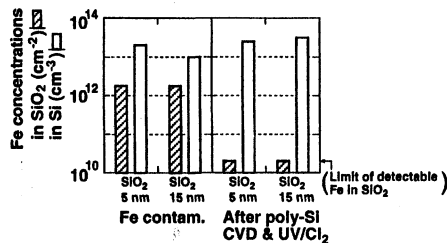


Fig. 2. Fe concentration in SiO<sub>2</sub> and Si before and after poly-Si CVD & UV/Cl<sub>2</sub>.  
Phosphorous ion was implanted into poly-Si.

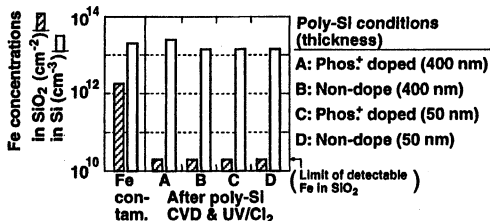


Fig. 3. Fe concentration in SiO<sub>2</sub> and Si before and after poly-Si CVD & UV/Cl<sub>2</sub>. SiO<sub>2</sub> thickness was 5 nm.

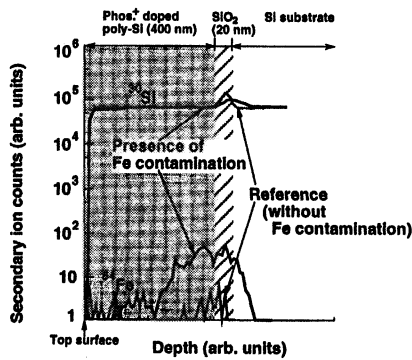


Fig. 4. SIMS profiles of  $^{54}\text{Fe}$  and  $^{30}\text{Si}$ .  
Sample was measured before etching off poly-Si layer.

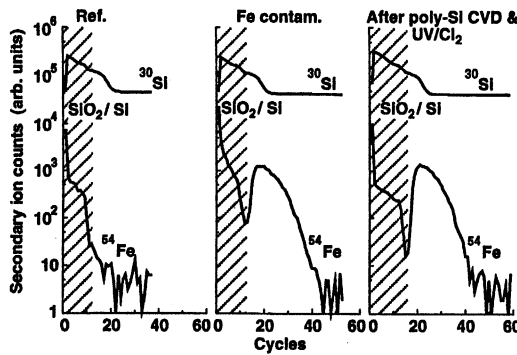


Fig. 5. SIMS profiles of  $^{54}\text{Fe}$  and  $^{30}\text{Si}$ . (Sample on left: after oxidation of clean Si, middle: Fe contamination, and right: after poly-Si CVD &  $\text{UV}/\text{Cl}_2$ .)

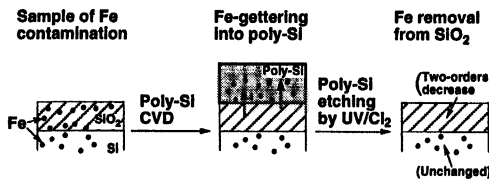


Fig. 6. Steps of Fe removal scheme using poly-Si CVD &  $\text{UV}/\text{Cl}_2$ .

# VAPOR PHASE CLEANING OF CU, FE, AND NA FROM WAFER SURFACES USING 1,1,1,5,5,5-HEXAFLUORO-2,4-PENTANEDIONE

S.E. Beck, E.A. Robertson III, M.A. George, D.A. Moniot, J.L. Waskiewicz,  
D.A. Bohling, K.M. Young, and A.A. Badowski  
Air Products and Chemicals, Inc.  
7201 Hamilton Blvd., Allentown, PA 18195, USA

Trace metal cleans with vapor phase 1,1,1,5,5,5-hexafluoro-2,4 pentanedione ( $H^+hfac$ ) are shown to remove Cu, Fe, and Na from silicon wafers to levels of  $5 \times 10^9$  Cu atoms/cm<sup>2</sup>,  $3 \times 10^{11}$  Fe atoms/cm<sup>2</sup>, and  $1 \times 10^{11}$  Na atoms/cm<sup>2</sup> for the conditions studied. The use of halogenated co-reactants, including HCl, SiCl<sub>4</sub>, Cl<sub>2</sub>, and HF, was explored. It was found that the chlorinated species hinder the removal of Fe, but accelerate the removal of Cu. We also demonstrate removal of Ca, K, Li, Ni, and Zn with this approach.

## INTRODUCTION

Elements such as the transition, alkali, and alkaline earth metals are deleterious to IC device performance and must be removed from silicon wafer surfaces during device processing. By far, the most common methods to remove these contaminants rely on liquid-based cleaning techniques [1]. The use of wet cleans becomes more challenging with decreasing minimum device dimension, with heightened emphasis on reducing waste streams, and with the switch to single wafer processing requiring vacuum-based cluster tools. As the number of process steps increases more wafer cleans are also required, thus intensifying these problems. Wet cleans have come under scrutiny because (1) they are not effective at cleaning high aspect ratio features, (2) they produce large amounts of slightly contaminated aqueous acid and base solutions, (3) the cleaning solutions are limited in their purity, and (4) they are not vacuum compatible. Gas/vapor phase cleans have been suggested as one way to address these problems.

One approach that has demonstrated the potential for vapor phase removal of some metals is the use of chelation compounds, where the vapor phase chelating ligand reacts with the metal species on the wafer surface, forming a volatile coordination compound. The compound desorbs from the wafer surface at low temperatures and the gas flow or vacuum removes it from the vicinity of the wafer. The chelation compound of interest in this study is 1,1,1,5,5,5-hexafluoro-2,4-pentanedione ( $H^+hfac$ ). Also discussed are the reactions of metals with  $H^+hfac$  and a co-reactant, such as HCl, SiCl<sub>4</sub>, Cl<sub>2</sub>, or HF.

## EXPERIMENTAL

The primary focus of this work was to study the reaction of H<sup>+</sup>hfac with sub-monolayers of Cu, Fe, and Na on silicon wafers. Submonolayer (< 10<sup>15</sup> atoms/cm<sup>2</sup>) samples of Cu and Fe were prepared via evaporation, producing CuO, Cu<sub>2</sub>O, FeOOH, and Fe<sub>2</sub>O<sub>3</sub>, as determined by XPS. Sodium was deposited on the wafer surface via a spin-on technique using a 0.0005% solution of NaOH in deionized water. The intentionally contaminated wafers, or 1 cm × 1 cm pieces thereof, were placed in a vertical quartz furnace capable of handling wafers up to 3 inches in diameter. A syringe pump (ATI Orion Sage Model M365) connected to the source end of the furnace by a 0.005" PEEK capillary was used to inject the H<sup>+</sup>hfac into the process chamber at a rate of 0.1 ml/min. All exposures were performed in a synthetic air (79% N<sub>2</sub> / 21% O<sub>2</sub>) ambient at a total pressure of 7.6 Torr. For the experiments involving HF, a gold coated six-way cross was used and the injection rate of H<sup>+</sup>hfac into the process chamber was increased to 0.2 ml/min so that the residence time of H<sup>+</sup>hfac in both reactors was held constant. After exposure to H<sup>+</sup>hfac, surface metal concentrations were determined by surface SIMS and TXRF.

## RESULTS

### H<sup>+</sup>hfac Exposures

Our initial studies focused on exposing surface contaminants to H<sup>+</sup>hfac. Cu and Fe were chosen for this study due to their prevalence as major contaminants in IC processing that produce deep levels in the Si bandgap. Figure 1 depicts the results of Cu and Fe contaminated surfaces exposed to H<sup>+</sup>hfac at 300°C for times ranging from 1.5 to 40 minutes. Exposures of Cu and Fe to H<sup>+</sup>hfac as a function of temperature revealed that Cu is removed in the temperature range of 20°C to 400°C and Fe is removed in the temperature range of 150°C to 400°C.

Alkali and alkaline earth metals were also chosen for study because they are highly mobile ionic contaminants; sodium is historically the most important contaminant in this group. Figure 2 shows the result of exposing samples contaminated with Na to H<sup>+</sup>hfac. Sodium is removed at 190°C and above, which is consistent with the sublimation temperature of 185°C for Na(hfac) [2]. Vapor phase removal of Na was confirmed via two methods. First, a Na contaminated sample heated to 300°C for 60 minutes in an air ambient did not exhibit any difference in SIMS depth profile compared to an untreated sample. This data point is shown on Fig. 2 as an open circle. Thus, the results depicted in Fig. 2 are not due to Na diffusion into the sample. Second, by cryo-trapping the reactor effluent and analyzing the trapped liquid by ICP-MS, we confirmed that Na was transported out of the reactor during H<sup>+</sup>hfac reactions with the Na contaminated samples.

Other alkali and alkaline earth metals contaminants were introduced to wafer surfaces by a spin-on technique as Li<sub>2</sub>O, KOH, and CaO<sub>2</sub>. Results of 60 min H<sup>+</sup>hfac exposures of these species at 300°C are shown in Table I. In all cases these contaminants reacted with H<sup>+</sup>hfac, producing a less contaminated surface.

To gain additional insight into the reaction of H<sup>+</sup>hfac with the surface contaminants, powders of the metal oxides were reacted with H<sup>+</sup>hfac in a closed reactor which was sampled by a mass spectrometer. Using this methodology we have shown that the reaction of H<sup>+</sup>hfac with iron oxides results in volatile species including Fe(hfac)<sub>3</sub>, Fe(tfa)<sub>x</sub>(hfac)<sub>3-x</sub>, and Fe(methylhfac)(hfac)<sub>2</sub> [3]. Table II shows the results of the reactions of copper oxides and NaOH with H<sup>+</sup>hfac. The reaction of H<sup>+</sup>hfac with these species forms Cu(hfac)<sub>2</sub> and Na(hfac), which are volatile at the temperatures of the cleaning process.

**TABLE I** Result of H<sup>+</sup>hfac exposure at 300°C, 7.6 Torr, for 60 minute.

Contaminant	Surface Concentration Before Exposure (atoms/cm <sup>2</sup> )	Surface Concentration After Exposure (atoms/cm <sup>2</sup> )
<b>Li</b>	$(1.15 \pm 0.07) \times 10^{14}$	$(4.5 \pm 1.3) \times 10^{11}$
<b>K</b>	$(2.6 \pm 0.5) \times 10^{14}$	$(1.3 \pm 0.3) \times 10^{13}$
<b>Ca</b>	$(7.4 \pm 0.7) \times 10^{14}$	$(3 \pm 0.2) \times 10^{14}$

**TABLE II** Species detected via solid probe mass spectrometry for reactions of H<sup>+</sup>hfac with copper oxides and NaOH. Note: hfac = C<sub>5</sub>HF<sub>6</sub>O<sub>2</sub>.

H <sup>+</sup> hfac Reacted With	Ion Detected (amu)	Identification
<b>CuO or Cu<sub>2</sub>O</b>	63	Cu
	69	CF <sub>3</sub>
	139	C <sub>4</sub> H <sub>2</sub> F <sub>3</sub> O <sub>2</sub>
	201	CuC <sub>4</sub> HF <sub>3</sub> O <sub>2</sub>
	208	H <sup>+</sup> hfac
	270	Cu(hfac)
	339	CuC <sub>6</sub> HF <sub>9</sub> O <sub>2</sub>
	408	CuC <sub>9</sub> H <sub>2</sub> F <sub>9</sub> O <sub>4</sub>
	477	Cu(hfac) <sub>2</sub>
<b>NaOH</b>	69	CF <sub>3</sub>
	139	C <sub>4</sub> H <sub>2</sub> F <sub>3</sub> O <sub>2</sub>
	208	H <sup>+</sup> hfac
	230	Na(hfac)

#### H<sup>+</sup>hfac with Co-Reactants

Under the conditions of this study, the final Fe concentration after a reaction with H<sup>+</sup>hfac is limited to approximately 10<sup>11</sup> atoms/cm<sup>2</sup>. Most likely, this limit arises due to a

surface related phenomenon. In an attempt to surpass the lower limit of  $10^{11}$  Fe atoms/cm<sup>2</sup>, we exposed Fe contaminated samples to H<sup>+</sup>hfac and halogen containing co-reactants. The strategy for this experiment was based on past work with metal chloride powders showing that the metal chlorides have higher etch rates in H<sup>+</sup>hfac than the corresponding metal oxides [4]. The co-reactants included HF, HCl, Cl<sub>2</sub>, and SiCl<sub>4</sub>.

Exposures in atmospheres containing chlorine-based reactants were done for 40 minutes at 300°C and a total pressure of 7.6 Torr. These exposures produced the surface concentrations shown in Table III. In all cases Cu is removed to acceptable levels for state-of the-art devices. However, the lowest Fe concentrations achieved with the co-reactants was still higher than the levels for H<sup>+</sup>hfac alone, indicating that the co-reactants hinder the removal process. The levels achieved for Ni and Zn exposed to H<sup>+</sup>hfac are also acceptable, though less Ni and Zn were removed with the mixtures than with H<sup>+</sup>hfac alone.

Figure 3 shows the results of exposing Fe contaminated samples to ambients containing H<sup>+</sup>hfac, HF, and HF plus H<sup>+</sup>hfac for times ranging from 3 to 40 minutes at a wafer temperature of 300°C. The samples used in this portion of the study were contaminated by dipping the wafers for 10 minutes in an SC1 bath at 70°C, which was intentionally contaminated with 50 ppb of Fe. A small amount of Fe was removed in the ambient containing HF only. On the other hand, no statistically significant difference is observed for removing Fe in an ambient containing both H<sup>+</sup>hfac and HF as compare to H<sup>+</sup>hfac alone. In both cases, a final Fe concentration of approximately  $3 \times 10^{11}$  atoms/cm<sup>2</sup> was achieved within the first few minutes of exposure, which is of practical importance for implementation into a production environment. The samples used in this study were also contaminated with Zn at a level of  $(1.9 \pm 0.15) \times 10^{13}$  Zn atoms/cm<sup>2</sup>. Exposure to HF did not change the Zn surface concentration. Conversely, exposure to H<sup>+</sup>hfac and H<sup>+</sup>hfac plus HF resulted in final surface concentrations of  $(4 \pm 2) \times 10^{11}$  Zn atoms/cm<sup>2</sup> and  $(3 \pm 1.3) \times 10^{11}$  Zn atoms/cm<sup>2</sup>, respectively.

**TABLE III** Surface concentrations after exposure to H<sup>+</sup>hfac and a halogenated species.

Sample	Cu (atoms/cm <sup>2</sup> )	Fe (atoms/cm <sup>2</sup> )	Ni (atoms/cm <sup>2</sup> )	Zn (atoms/cm <sup>2</sup> )
No Exposure	$(1.7 \pm 0.4) \times 10^{12}$	$(3.8 \pm 0.17) \times 10^{14}$	$(1.6 \pm 0.5) \times 10^{13}$	$(9 \pm 3) \times 10^{13}$
H <sup>+</sup> hfac	$(1.7 \pm 0.5) \times 10^{10}$	$(3 \pm 1) \times 10^{11}$	$(8 \pm 6) \times 10^9$	$(3 \pm 1.7) \times 10^{10}$
HCl/H <sup>+</sup> hfac	$(1.4 \pm 0.8) \times 10^{10}$	$(1.4 \pm 0.3) \times 10^{12}$	$(2.4 \pm 0.2) \times 10^{10}$	$(6.6 \pm 1.3) \times 10^{10}$
SiCl <sub>4</sub> /H <sup>+</sup> hfac	$(5 \pm 2) \times 10^9$	$(1.2 \pm 0.6) \times 10^{13}$	$(1.0 \pm 0.6) \times 10^{11}$	$(1.4 \pm 1) \times 10^{11}$
Cl <sub>2</sub> /H <sup>+</sup> hfac	$(9 \pm 1.7) \times 10^9$	$(2.4 \pm 0.9) \times 10^{12}$	$(1.3 \pm 0.3) \times 10^{10}$	$(5 \pm 2.5) \times 10^{10}$

## DISCUSSION

The reaction of H<sup>+</sup>hfac with the metals studied proceeds by a variety of mechanisms with the nucleophilic substitution reaction predominating. The reaction of H<sup>+</sup>hfac

with Cu was very rapid and occurred at all temperatures studied. Reactions of H<sup>+</sup>hfac with thin films of copper oxides have verified that the nucleophilic substitution reaction predominates[5]. The reaction of H<sup>+</sup>hfac with Fe is much more complex and results in a variety of reactions [6]. These reactions include the nucleophilic substitution reaction and the formation of mixed ligand systems such as Fe(tfa)<sub>x</sub>(hfac)<sub>3-x</sub> and Fe(methylhfac)(hfac)<sub>2</sub>. Reactions of H<sup>+</sup>hfac with iron oxide powders have confirmed these reactions [3]. Additionally, the reaction of H<sup>+</sup>hfac with surface Na is a nucleophilic substitution reaction producing Na(hfac) and H<sub>2</sub>O as the volatile species.

Although the near submonolayer concentrations of metals have been reduced by several orders of magnitude, some metal still resides on the wafer surface after H<sup>+</sup>hfac exposure. This is especially true for Fe. We speculate that the remaining metal may not be a metal oxide or hydroxide, but may be a metal silicate or silicide. If the surface metal exists as a silicate or silicide on the wafer surface, the reaction of the metal with H<sup>+</sup>hfac could be significantly affected.

In an attempt to overcome the presence of metal silicates and silicides, in particular those of Fe, intentionally contaminated wafers were exposed to halogen containing co-reactants and H<sup>+</sup>hfac. Using H<sup>+</sup>hfac and a chlorinated species produced final Fe, Ni, and Zn concentrations higher than H<sup>+</sup>hfac itself. These results suggest that the chlorine may actually hinder the removal of some species; this result is in distinct contradiction to our previous work with metal chloride powders [4] and may indicate a more complex surface reaction than achieved with the powders. On the other hand, consistent with the work with metal chloride powders, chlorine did assist in removing Cu. Additionally, chlorine-based co-reactants do not roughen the silicon surface at the temperatures where H<sup>+</sup>hfac forms volatile complexes. Silicon surfaces exposed to H<sup>+</sup>hfac plus Cl<sub>2</sub> showed no measurable change in the surface roughness by tapping mode AFM. Previously it was shown that H<sup>+</sup>hfac does not roughen silicon surfaces under normal processing conditions [7]. Thus, by using temperatures typical for H<sup>+</sup>hfac processing for the co-reactant processes it is possible to overcome the issue of surface roughening typically encountered with UV/Cl<sub>2</sub> treatments.

No difference in final Fe surface concentration was observed for Fe contaminated samples exposed to either HF with H<sup>+</sup>hfac or H<sup>+</sup>hfac alone. This may be due to entrapment of some of the metals in the chemical oxide produced by the SC1 bath used for doping these samples. Comparing the results for Zn from the SC1 contaminated samples ( $3 \times 10^{11}$  Zn atoms/cm<sup>2</sup>) and the evaporation contaminated samples ( $3 \times 10^{10}$  Zn atoms/cm<sup>2</sup>) we see that more Zn was removed from evaporated sample. Therefore, the two methods for contaminating the wafer surfaces produce different surfaces.

## SUMMARY

The results of this study show the potential for using H<sup>+</sup>hfac as a component in vapor phase cleans for future microelectronics applications. We have shown that a variety of contaminants; including Cu, Fe, Na, Ca, K, Li, Ni, and Zn are removed to varying

degrees with a H<sup>+</sup>hfac-based vapor phase chemistry. Most likely, the removal efficiency depends on process conditions. We have shown that Cu, Fe, and Na react with H<sup>+</sup>hfac by a nucleophilic substitution reaction, with the reaction with Fe also producing volatile mixed ligands. When a chlorine-containing co-reactant was used, less Fe, Ni, and Zn were removed. In distinct contrast, the chlorine-based co-reactant with H<sup>+</sup>hfac promoted the removal of Cu. When HF was the co-reactant, no difference was observed for Fe removal at the conditions studied.

#### ACKNOWLEDGMENTS

This work was supported by the ARPA-NCAICM program (contract no. N0014-94-C-0076) and by internal research funds from Air Products and Chemicals, Inc. Schumacher supplied the H<sup>+</sup>hfac used in this study. The authors would like to thank Andrew Lane of Texas Instruments for supplying the evaporated samples used in this work.

#### REFERENCES

1. W. Kern, ed., *Handbook of Semiconductor Wafer Cleaning Technology: Science, Technology, and Applications*, Noyes Publications, Park Ridge, NJ (1993).
2. R. Belcher, A.W.I. Dudeney, W.I. Stephen, *J. Inorg. Nucl. Chem.*, **31**, 625 (1969).
3. M.A. George, S.E. Beck, D.A. Moniot, K.M. Young, D.A. Bohling, G. Voloshin, and D.W. Hess, to appear in *Structure and Evolution of Surfaces*, R. Cammarata, E. Chasson, T. Einstein, and E. Williams, Editors, Materials Research Society Proceedings, Pittsburgh, PA (1997).
4. D.A. Roberts, G.O. Voloshin, J.A.T. Norman, D.A. Bohling, S.E. Beck, S.W. Rynders, and M.A. George, *Semicon Europa* (1994).
5. M.A. George, D.W. Hess, S.E. Beck, J.C. Ivankovits, D.A. Bohling, B.S. Felker, and A.P. Lane, *J. Electrochem. Soc.*, **142**, 961 (1995).
6. M.A. George, D.W. Hess, S.E. Beck, K. Young, G. Voloshin, D.A. Bohling, and A.P. Lane, *J. Electrochem. Soc.*, **143**, 3257 (1996).
7. S.E. Beck, A.G. Gilcinski, B.S. Felker, J.G. Langan, D.A. Bohling, M.A. George, J.C. Ivankovits, and R.M. Rynders, in *Interface Control of Electrical, Chemical, and Mechanical Properties*, S.P. Murarka, K. Rose, T. Ohmi, and T. Seidel, Editors, vol. 318, p. 263, Materials Research Society Proceedings, Pittsburgh, PA (1994).

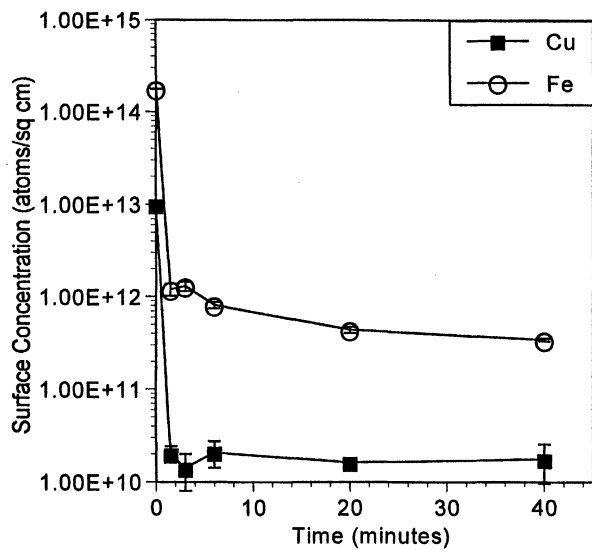


**Figure 1** Final Cu and Fe surface concentrations after exposure to  $\text{H}^+\text{hfac}$  at  $300^\circ\text{C}$ .

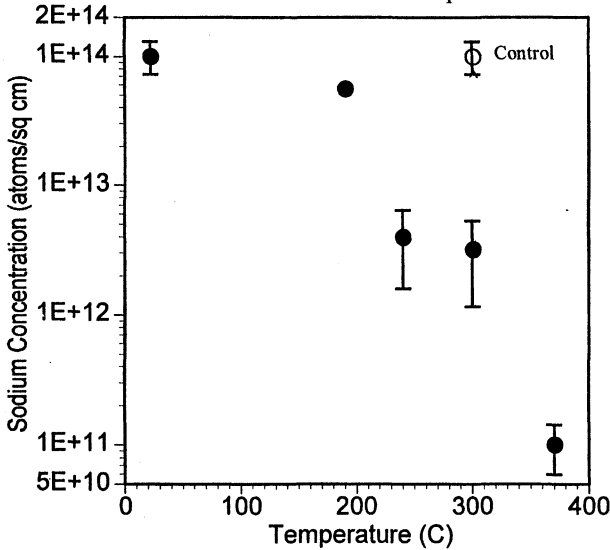


**Figure 2** Final Na surface concentration after 40 minute exposure to  $\text{H}^+\text{hfac}$ .

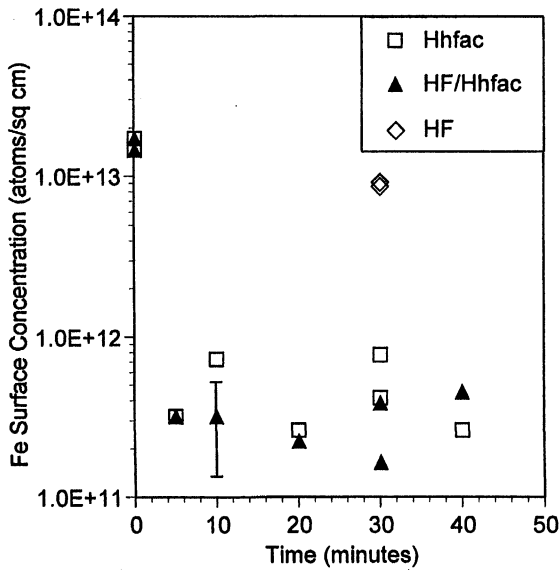


**Figure 3** Final Fe surface concentration after exposure to  $H^+hfac$ , HF, and  $H^+hfac$  plus HF at 300°C.

## DRY PROCESS FOR THE DEFINITION OF SUB-0.1 $\mu$ m W/TiN GATES

A. L. P. Rotondaro, H. Yang, J. C. Hu, R. Kraft, G. A. Brown and C. Appel  
Texas Instruments Incorporated  
Semiconductor Process & Design Center  
13570 North Central Expressway, Dallas, TX 75243, USA

Chemical downflow etch based on a chemistry consisting of oxygen ( $O_2$ ) and hexafluoroethane ( $C_2F_6$ ) was used to successfully fabricate sub-0.1  $\mu$ m W/TiN gate structures on ultra-thin (< 3 nm) silicon dioxide. The electrical characteristics of the devices indicate excellent process uniformity and no charge or corner damage effects.

### INTRODUCTION

The fabrication of advanced sub-0.1  $\mu$ m devices will require the substitution of the highly doped polysilicon gate electrode by new gate materials [1]. The gate electrode stack for advanced devices should:

- provide low sheet resistance to minimize interconnect delays [1],
- have a work function near to the silicon mid-gap to enable both n and p-type transistors to operate in surface channel mode [2],
- prevent gate electrode depletion effects to assure that the effective oxide thickness is equal to the physical oxide thickness [3].

TiN is a very promising candidate for gate electrode material, as it presents work function near Si mid-gap (4.65 eV) and eliminates gate depletion effects. However, TiN has a quite high resistivity (120 m $\Omega$ .cm) and needs to be used in conjunction with a material with higher conductivity for low interconnect delays to be achieved. For that purpose, W with a resistivity of 8 m $\Omega$ .cm has been used [2,4].

The definition of the gate electrode stack on ultra-thin (< 3 nm) gate oxides for sub-0.1  $\mu$ m transistors imposes a severe challenge to the etch process. Very high selectivity to  $SiO_2$  has to be achieved to avoid oxide punchthrough and subsequent damage to the silicon in the source and drain regions. Even when successful in stopping in the gate oxide, the gate etch process introduces corner damage to the gate structure that needs to be annealed to guarantee good gate oxide integrity (GOI) properties of the transistor. This brings us the issue of how to anneal the corner damage on metal gate structures as W and TiN readily oxidize in conventional oxidation processes. One solution to this problem is to slightly undercut the TiN layer moving the active gate region away from the damaged corners [4]. Wet etch has been used in this case but as the selectivity of the wet etch towards W is very low, the W sidewall needs to be protected with a spacer prior to the TiN undercut etch [4]. This adds significant complexity to the device fabrication flow and severely reduces the process window as the amount of undercut, and

consequently the effective gate length, depends on the spacer thickness. Another approach is to etch the TiN with a process that does not cause corner damage.

In this paper, a novel all dry process for defining sub-0.1  $\mu\text{m}$  W/TiN gates on ultra-thin ( $< 3$  nm) gate oxides is presented. The process was optimized to have high selectivity to gate oxide and W eliminating the need of capping the W during TiN etch. Also, it does not introduce charge or corner damage to the gate oxide making unnecessary the gate annealing (or "smiling oxidation") after etch.

## EXPERIMENTAL

The thickness of the different materials used in the metal gate stack was respectively: 50-150 nm of W, 10-30 nm of TiN and 3-5 nm gate oxide. The gate stack was anisotropically etched with a proprietary process to halfway into the TiN layer. This prevents damage to the gate oxide. Subsequently, isotropic chemical downflow etch (CDE) was used to remove the remaining TiN with high selectivity towards the gate oxide.

The CDE process was developed in a Mattson ASPEN II ashser. The system has an inductively coupled plasma (ICP) source that generates the excited species remote from the wafer surface. Two grounded metal grids prevent charged species from reaching the wafers assuring an isotropic process without any charge damage [5]. Oxygen ( $\text{O}_2$ ) and hexafluorethane ( $\text{C}_2\text{F}_6$ ) were selected as process gases. A flow ratio of  $\text{O}_2$  to  $\text{C}_2\text{F}_6$  higher than 100 to 1 was used. Two process temperatures were investigated, 250 °C with the wafers placed on a heated chuck or room temperature with the wafers raised on three pins.

The optimization of the gate profile was assessed with transmission electron microscopy (TEM) analysis. The TiN thickness for the etch rate studies was measured using a 4-point probe system. The photoresist and oxide thickness were measured with an Optiprobe Thermawave tool.

The ramp voltage breakdown characteristics of the thin gate oxides was measured using the American Society of Testing Materials (ASTM) test method F-1771. The measurements were performed on capacitors with an active area of 0.01  $\text{cm}^2$ . Two types of capacitors were probed:

- nested capacitors where the edges of the top electrode were located on thin gate oxide;
- overlap capacitors where the edges of the top electrode were located on thick field oxide.

Local oxidation of silicon (LOCOS) isolation was used for the capacitor fabrication. Three failure distributions were analysed:

- $V_{\text{crit}}$  determined by the voltage at a current threshold of  $10^{-3} \text{ A/cm}^2$ , which correlates with the onset of conduction;
- $V_{\text{sf}}$  determined by the voltage at a current threshold of  $0.1 \text{ A/cm}^2$ , which corresponds to the oxide soft failure component (an industry benchmark value);

- $V_{hf}$  determined by an abrupt increase in the current through the capacitor indicating permanent breakdown.

## RESULTS AND DISCUSSION

In Figure 1 the TiN removal is shown as a function of the exposure time to the  $O_2+C_2F_6$  process for blanket TiN layers processed at 250 °C (Hot) and at room temperature (Cold). It is possible to notice that the process temperature does not have a strong impact on the TiN removal process. TiN is normally etched using chlorine-based plasmas.  $TiO_2$  is extremely non-volatile (indeed refractory) and  $TiF_4$  is normally considered non-volatile as it sublimes at 284 °C at one atmosphere pressure. Thus, it is very surprising that the TiN removal can be adequately performed with an oxygen/fluorine ambient having a high O to F ratio, as the one used. A possible explanation to this is that the process under study is performed at low pressures (less than 2 torr) which could reduce the temperature at which  $TiF_4$  becomes volatile to below the process temperature, resulting in the etch of the TiN film.

In the case of the  $SiO_2$  etch rate, the process temperature has a strong impact on the etch speed, as can be seen by the  $SiO_2$  loss plotted as a function of the exposure to the  $O_2+C_2F_6$  process (Figure 2). The etch selectivity of TiN towards  $SiO_2$ , calculated using the results from Figures 1 and 2, is equal to 8 and 21 respectively for the case of 250 °C and room temperature processing. It is clear that room temperature (< 50 °C) processing has to be used to maximize the selectivity, minimizing the  $SiO_2$  loss.

The TiN removal process can be integrated with the photoresist ash step simplifying the fabrication process. The photoresist layer might get cross-linked during the anisotropic etch of the top layers and the addition of  $C_2F_6$  to the  $O_2$  plasma has proved to be very effective in stripping hardened photoresist without leaving polymer residues or "ears". Also, in the case where surface image photolithographic schemes are used, the removal of the silylated hard mask with fluorinated chemistries showed to be very efficient. The ash rate of photoresist in the  $O_2+C_2F_6$  environment strongly depends on the process temperature, as can be seen in Figure 3 for DUV positive photoresist. The removal of cross-linked and silylated photoresist follows the same trend, indicating that processing at 250 °C is desirable for fast photoresist stripping.

To accommodate the requirements of having fast TiN and photoresist removal keeping high selectivity to  $SiO_2$  and W, the CDE process was divided in three steps:

- First, an  $O_2$  with  $C_2F_6$  process of short duration at 250 °C is used to remove the cross-linked/silylated photoresist and partially etch the TiN.
- Second, a pure  $O_2$  ash at 250 °C is used to strip the bulk photoresist layer.
- Finally, an  $O_2$  with  $C_2F_6$  step at room temperature is used to completely remove the remaining TiN with high selectivity to  $SiO_2$ .

The duration of the various steps was optimized to minimize W and gate oxide loss as well as TiN undercut. This can be seen in Figure 4 for a metal gate with 0.18  $\mu m$  W length. The TiN undercut was reduced to a minimum and the gate oxide loss was

negligible. The CDE process was then tuned for the fabrication of sub-0.1  $\mu\text{m}$  metal gate devices on < 3 nm gate oxides. In Figure 5 the TEM picture of a metal gate with 0.06  $\mu\text{m}$  W length is shown to illustrate the capabilities of the developed CDE process.

In Figure 6, the GOI characteristics of nested and overlap capacitors fabricated with W/TiN top electrode on 2.8 nm gate oxide are presented. Very sharp Weibull distributions for  $V_{\text{crit}}$ ,  $V_{\text{sf}}$  and  $V_{\text{hf}}$  were obtained indicating excellent uniformity of the gate fabrication process. The nested devices have shown consistently better GOI values compared with the overlap ones (Figure 6). This proves that the CDE process does not cause any charge or corner damage to the gate oxide. It consequently eliminates the need of undercutting the TiN layer or performing a gate annealing for the fabrication of high performance sub-0.1  $\mu\text{m}$  metal gate devices.

## CONCLUSIONS

An advanced CDE process was developed and optimized for the definition of sub-0.1  $\mu\text{m}$  metal gate structures. The substrate temperature and the gases used were chosen for high selectivity towards W and  $\text{SiO}_2$  eliminating the need of capping the W sidewall and preventing charge or corner damage to the gate oxide. The process can be integrated with the resist removal step simplifying the fabrication flow. Devices with 0.06  $\mu\text{m}$  gate length were successfully fabricated on < 3 nm gate oxide presenting excellent electrical characteristics.

## REFERENCES

1. T. Ohmi, Jpn. J. Appl. Phys., **33**, 6747 (1994).
2. D. H. Lee et al., Symp. VLSI Technol., 119 (1995).
3. C. Hu, IEDM Tech. Dig., 319 (1996).
4. D. H. Lee et al., Symp. VLSI Technol., 208 (1996).
5. L. M. Loewenstein et al., in Cleaning Technology in Semiconductor Device Manufacturing IV, J. Ruzyllo and R.E. Novak Editors, **PV95-20**, p.225, The Electrochemical Society Proceedings Series, Pennington, NJ (1995).

## FIGURES

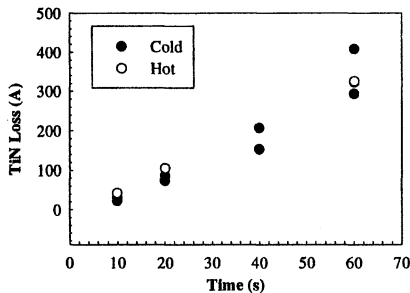


**Figure 1:** TiN loss as a function of the exposure time to the  $O_2+C_2F_6$  process. The wafers were processed at 250 °C (Hot - open circles) or at room temperature (Cold - full circles).

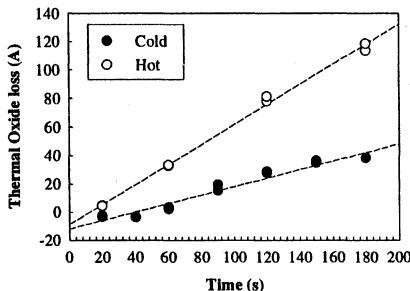


**Figure 2:**  $SiO_2$  loss as a function of the exposure time to the  $O_2+C_2F_6$  process. The wafers were processed at 250 °C (Hot - open circles) or at room temperature (Cold - full circles).

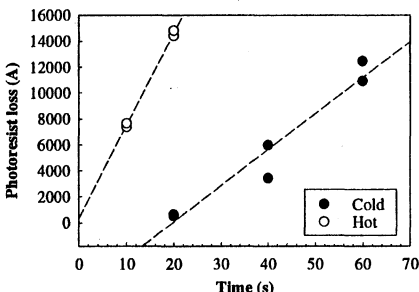


**Figure 3:** Photoresist loss as a function of the exposure time to the  $O_2+C_2F_6$  process. The wafers were processed at 250 °C (Hot - open circles) or at room temperature (Cold - full circles).

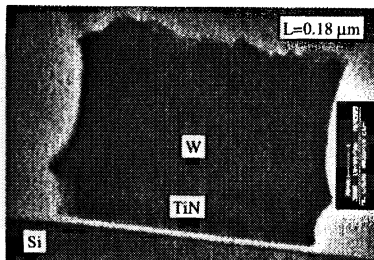


**Figure 4:** Typical TEM photograph of a metal gate structure with  $0.18 \mu\text{m}$  W length fabricated with the optimized CDE process on 3 nm gate oxide.

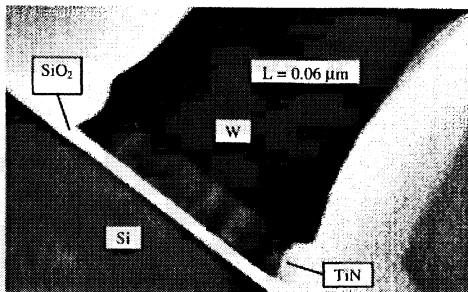


**Figure 5:** Typical TEM photograph of a metal gate structure with  $0.06 \mu\text{m}$  W length fabricated with the optimized CDE process on 3 nm gate oxide.

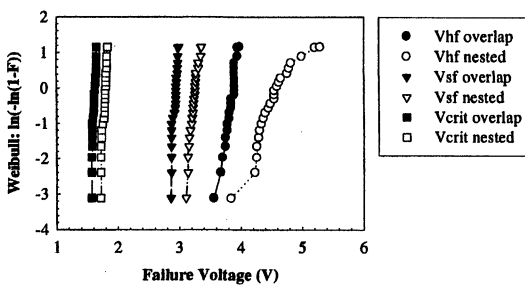


**Figure 6:** Ramp voltage breakdown characteristics of 2.8 nm gate oxide capacitors with W/TiN top electrode fabricated with the optimized CDE process. The capacitor area is  $0.01 \text{ cm}^2$ .  $V_{hf}$  (circles) indicate hard failure,  $V_{sf}$  (inv-triangles) indicate  $0.1 \text{ A/cm}^2$  current threshold, and  $V_{crit}$  (squares) indicate  $10^3 \text{ A/cm}^2$  current threshold. Open symbols represent nested capacitors and full symbols represent overlap capacitors.

# THERMOPHORESIS ASSISTED CRYOGENIC AEROSOL CLEANING OF WAFERS

Natraj Narayanswami

*FSI International Inc.*

*MS 4-8071, 322, Lake Hazeltine Drive, Chaska, MN 55318, USA*

## ABSTRACT

The role of thermophoresis in cryogenic aerosol cleaning of wafers is examined. Simple scaling analyses are presented for quantification of (a) the effect of thermophoretic forces on particle suspension from a wafer surface and (b) wafer temperatures required to prevent re-deposition of suspended particles. Additionally, some experimental results demonstrating the effectiveness of thermophoretic control of particle re-deposition are presented.

## INTRODUCTION

The phenomenon of thermophoresis (Fig. 1) plays a very important role in wafer cleaning. Temperature gradients established within the processing chamber can cause thermophoretic drift of suspended contaminant particles towards cold surfaces. Such drifts can result in undesirable particle re-deposition on clean wafers, reducing the overall cleaning efficiency. It is therefore critical that the thermophoretic drift be controlled, and, to the extent possible, directed in a positive manner that actually assists particle removal.

Particle motion due to thermophoresis has been studied in the past by several researchers [1-8] but literature on its application to practical problems in the semiconductor industry is scarce. The present study focuses on thermophoretic effects in wafer cleaning using a cryogenic aerosol (Fig. 2). Such a cleaning process typically causes severe temperature gradients within the processing chamber. The wafer temperature can potentially fall to levels significantly below that of the surrounding chamber walls. Since thermophoretic drift of particles is always towards the colder surface, the potential for particle redeposition of contaminant particles onto a cold wafer is significant.

The specific objectives of this study are therefore : (a) to quantify the effect of thermophoretic forces in suspending a dislodged particle during cryogenic cleaning, (b) to theoretically determine wafer temperatures required to prevent particle re-deposition, and (c) to experimentally demonstrate the effectiveness of thermophoretic control in wafer cleaning.

## THEORY

In a cryogenic aerosol cleaning process, in addition to flow of the cryogenic aerosol itself, a stream of non-cryogenic carrier gas flow typically helps maintain a positive flow towards

the chamber exhaust at all times. During a typical cleaning ‘pass’ the wafer is exposed in turn to the cryogenic flow (Fig. 2a) and to warmer gas flow (Fig. 2b). Flow across the wafer generates a velocity boundary layer over it. In addition, any temperature gradient between the wafer surface and flow stream produces a thermal boundary layer. Further, particle concentration gradients adjacent to the wafer may generate a concentration boundary layer as well. The motion of a particle in such a concentration layer is described by the equation:

$$u \frac{\partial \omega}{\partial x} + v \frac{\partial \omega}{\partial y} = D \frac{\partial^2 \omega}{\partial y^2} - \frac{\partial(v_{ty}\omega)}{\partial y} - v_g \frac{\partial \omega}{\partial y} \quad (1)$$

where  $x$  and  $y$  are coordinates parallel to and normal to the wafer, respectively and  $u$  and  $v$  are the corresponding fluid velocities,  $\omega$  is the dimensionless particle concentration,  $D$  is the particle diffusivity,  $v_{ty}$  is the component of the thermophoretic velocity normal to the wafer and  $v_g$  is the gravitational settling velocity. Diffusion and thermophoresis parallel to the wafer surface are neglected. The thermophoretic drift velocity is given by [2]:

$$v_{ty} = -K \frac{\nu}{T} (\nabla T) = -K \frac{\nu}{T} \left( \frac{\partial T}{\partial y} \right) \quad (2)$$

where  $\nu$  is the fluid kinematic viscosity,  $T$  is temperature and  $K$  is a function of the Knudsen number ( $Kn = 2 \lambda/d_p$ , where  $\lambda$  is the mean free path in the gas) and the ratio of thermal conductivities of the fluid and particle ( $k_g/k_p$ ). Using this, Eqn. 1 may be re-written as:

$$u \frac{\partial \omega}{\partial x} + v \frac{\partial \omega}{\partial y} = D \frac{\partial^2 \omega}{\partial y^2} + \frac{K\nu}{T} \frac{\partial T}{\partial y} \frac{\partial \omega}{\partial y} - v_g \frac{\partial \omega}{\partial y} \quad (3)$$

Within the concentration boundary layer of thickness  $\delta_c$ , the diffusion term scales as:

$$D \frac{\partial^2 \omega}{\partial y^2} \sim \frac{D}{\delta_c^2} \quad (4)$$

The thermophoresis term scales as:

$$\frac{K\nu}{T} \frac{\partial T}{\partial y} \frac{\partial \omega}{\partial y} \sim \frac{\nu |N_t|}{\delta_c \delta_T} \quad (5)$$

$$\text{where } |N_t| = K \frac{|T_w - T_\infty|}{T} \quad (6)$$

where  $\delta_T$  is the thermal boundary layer thickness, and the subscripts  $w$  and  $\infty$  refer to the wafer and its immediate surroundings (e.g. the flow itself), respectively. The gravitational term scales as:

$$v_g \frac{\partial \omega}{\partial y} \sim \frac{\rho_p d_p^2 g f(Kn)}{18 \mu \delta_c} \quad (7)$$

where  $\rho_p$  and  $d_p$  are the density and diameter of the particle, respectively,  $g$  is the gravitational acceleration and  $\mu$  is the fluid viscosity.

Further analysis of Eqn. 3 yields the following correlations based on the Prandtl number  $Pr = \nu/\alpha$ , the Schmidt number  $Sc = \nu/D$  and the Reynolds number  $Re_x = u_\infty x/\nu$ , where  $\alpha$  is the thermal diffusivity and  $u_\infty$  is the flow velocity:

If thermophoresis dominates over diffusion,

$$|N_t| \gg Sc^{-2/3} Pr^{-1/3} \quad (8)$$

If thermophoresis dominates over gravitational settling,

$$|N_t| \gg \frac{\rho_p g}{18\mu} d_p^2 f(Kn) \frac{\delta}{\nu \text{Pr}^{1/3}} \quad (9)$$

where  $\delta$  is the velocity boundary layer thickness.

## RESULTS

In the following discussion, the term 'NTD' denotes the normalized absolute temperature difference  $|T_w - T_\infty|/T_\infty$ . The cryogenic fluid and contaminant particles are assumed to be Nitrogen and Si, respectively.

### Suspension of dislodged particles

During the cleaning of the wafer with the aerosol, the wafer surface is initially much warmer than the aerosol stream flowing over it (Fig. 2a). For example, the wafer may be at a nominal temperature of 20° - 60°C., while the aerosol temperature is about -173 °C. This temperature gradient decreases with processing time as the wafer gets progressively colder. However, the wafer temperature never falls below that of the flow stream and hence a positive (useful) thermophoretic lift force on particles is maintained throughout the cleaning process. This thermophoretic force on a contaminant particle is given by [1]:

$$F_T = \frac{(-6\pi\mu\nu d_p C_s) \left( \frac{k_a}{k_p} + C_t Kn \right) \left( \frac{\nabla T}{T_\infty} \right)}{(1 + 3C_m Kn) \left( 1 + 2\frac{k_a}{k_p} + 2C_t Kn \right)} \quad (10)$$

where,  $\nabla T$  is the temperature gradient normal to the wafer and  $C_m$ ,  $C_s$  and  $C_t$  are constants.

For typical flow conditions, particles of size  $\leq 1 \mu\text{m}$  are small enough to lie entirely within the viscous sublayer of the velocity boundary layer, assuming that the boundary layer is turbulent. The turbulent lift force on such particles is given by [9]:

$$F_L = \rho\nu^2 (56.9 \pm 1.1) \left( \frac{d_p u_*}{2\nu_\infty} \right)^{1.87 \pm 0.04} \quad (11)$$

where  $u_* = \sqrt{\tau_w/\rho}$  is the friction velocity and  $\tau_w$  is the shear stress at the wafer surface. Figure 3b shows the thermophoretic, turbulent lift and gravitational forces as a function of particle size for  $T_w$  only 5 K warmer than the flow. Clearly, the turbulent lift force is dominant but even the thermophoresis force can by itself overcome gravity for particles of size  $\leq 1 \mu\text{m}$  and help suspend and remove particles from the wafer surface. It is thus beneficial to maintain as high a temperature gradient between the hot wafer and cold stream as possible by heating the wafer to the extent allowable.

### Prevention of particle re-deposition

During the intermediate stage of the cleaning (Fig. 2b) when a cold wafer may be exposed for a brief period to a warmer carrier gas flow within the chamber, thermophoresis can overcome settling by diffusion for all particles larger than 0.05  $\mu\text{m}$  even for an NTD as low as 0.01 (Fig. 3d). For particles of size 0.15  $\mu\text{m}$ , thermophoresis can overcome gravitational

settling for an NTD > 0.05. For larger particles, say, 0.5  $\mu\text{m}$  and 0.8  $\mu\text{m}$ , thermophoresis can overcome gravitational settling only for NTDs > 0.25 and 0.5, respectively (Fig. 2). The absolute temperature of the wafer surface that needs to be maintained to prevent redeposition clearly increases with particle size and has to be quite large for large particles (Fig. 3c).

### **Experiments on thermophoretic control**

The benefits of thermophoretic control in particle removal from the wafer processing chamber is demonstrated by the experimental results shown in Fig. 3d. The plot shows the number of > 0.15  $\mu\text{m}$  sized particles re-deposited onto the wafer at processing conditions involving a high and a low exhaust chamber wall temperature (60° C. and 20 °C., respectively), and two different pressures. The re-deposition is lower at the lower temperature for both pressures. Clearly, the advantage at the lower chamber exhaust temperature stems from the ability of the exhaust to attract more contaminants away from the main processing chamber and wafer by thermophoresis.

### **Conclusions**

The study yields the following conclusions regarding the effect of thermophoresis in wafer cleaning using cryogenic aerosols:

- (a) thermophoretic forces assist turbulent lift forces in the suspension and removal of contaminant particles from the wafer surface for particles of size  $\leq 1 \mu\text{m}$ , for wafer temperatures only 5 K above that of the flow stream. For larger particles, the suspension is due to turbulent lift alone.
- (b) positive thermophoretic forces induced by wafer heating can prevent re-deposition of suspended particles onto the cleaned wafer. The heating required is greater for larger particles. For 0.15  $\mu\text{m}$  particles, the wafer temperature needs to be at least 5% greater than that of the surrounding gas. For 0.8  $\mu\text{m}$  particles, the temperature has to be 50% greater.
- (c) experiments clearly confirm the positive effects of thermophoretic control by demonstrating that particle re-deposition counts can be lowered by lowering the temperature of the exhaust portion of the processing chamber.

### **ACKNOWLEDGMENTS**

The author would like to thank G. Thomas, J. F. Weygand and L. Zimmerman of FSI International Inc. for providing the experimental data presented in this paper.

### **REFERENCES**

1. L. Talbot et al., *J. Fluid Mech.*, **101**, Pt. 4, 737 (1980).
2. W. W. Nazaroff and G. R. Cass, *J. Aerosol Sci.*, **18**, No. 4, 445 (1987).
3. K. L. Walker et al., *J. Coll. Interf. Sci.*, **69**, No. 1, 138, Mar. (1979).
4. S. E. Pratsinis and K. Kim, *J. Aerosol Sci.*, **20**, No. 1, 101 (1989).
5. S. A. Gökoğlu and D. E. Rosner, *AIAA J.*, **24**, 172, Jan. (1986).
6. F. Schmidt et al., *J. Aerosol Sci.*, **25**, Suppl. 1, 581, (1994).
7. S. Jayaraj, *Heat Mass Trans.*, **30**, 167, (1995).
8. R. K. Ahluwalia and K. H. Im, *NASA TR DE85-010484* (1985).
9. A. M. Mollinger and F. T. M. Nieuwstadt, *J. Fluid Mech.*, **316**, 285 (1996).

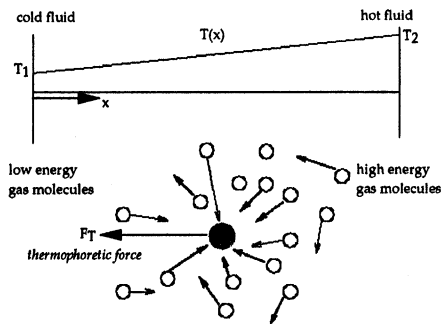
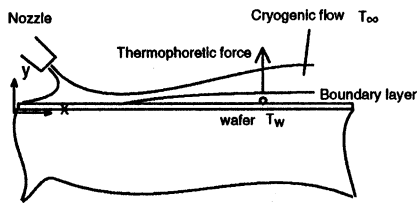
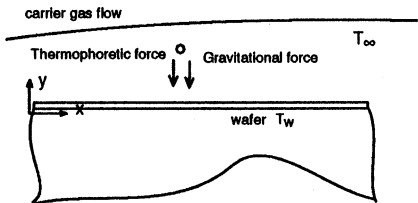


Figure 1: Schematic of the thermophoresis effect; the shaded circle denotes the contaminant particle and the hollow circles denote gas molecules. The particle experiences drift towards the colder region.



(a) Main cleaning step – particle suspension and removal is effected for wafer temperatures higher than that of the flow



(b) Intermediate step – particle re-deposition is of concern if the wafer is colder than the carrier gas

Figure 2: Schematic of the thermophoresis effect during (a) the main cleaning step when the wafer experiences cryogenic flow and (b) intermediate step when the wafer experiences a warmer carrier gas flow.

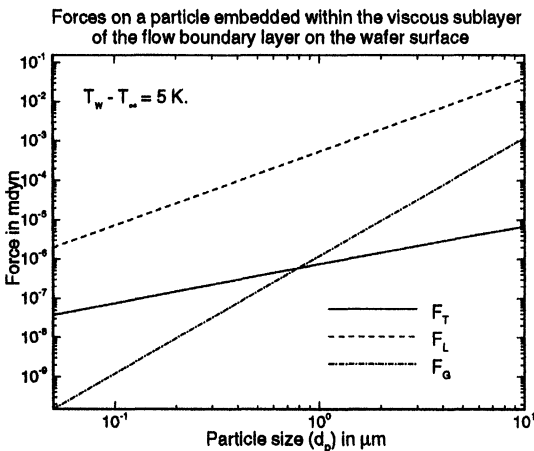


Figure 3a: Turbulent lift force ( $F_L$ ), thermophoretic force ( $F_T$ ) and gravitational force ( $F_G$ ) on a contaminant particle within the turbulent boundary layer of the flow stream over the wafer.

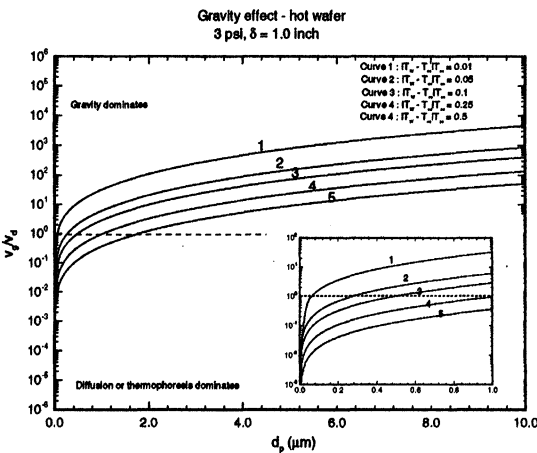


Figure 3b: Gravitational settling effect vs. particle size at a chamber pressure of 3 psi, for flow over a surface whose temperature is greater than the flow temperature, i.e.,  $T_w > T_\infty$

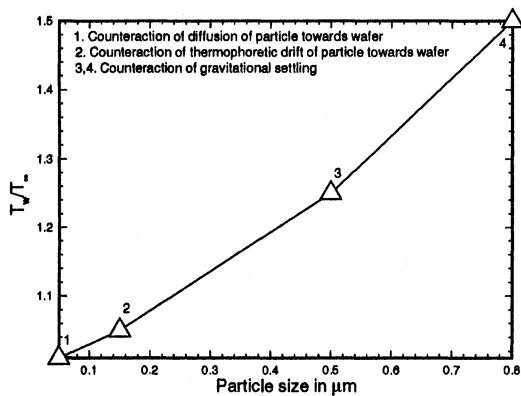


Figure 3c: Wafer temperature as a function of particle size for prevention of particle redeposition during the intermediate stage

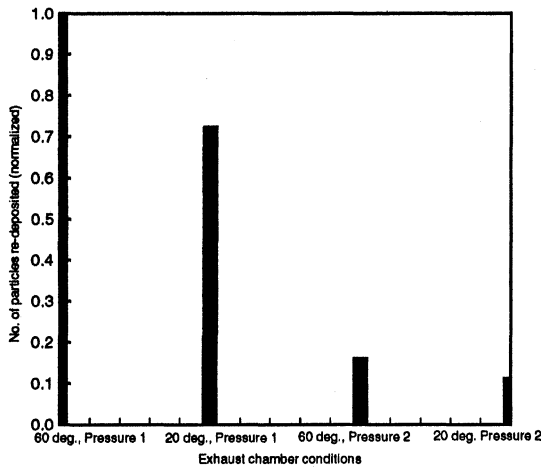


Figure 3d: Particle re-deposition levels as a function of temperature of exhaust portion of the processing chamber.

# ON THE GENERATION OF CRYOGENIC AEROSOLS FOR WAFER PROCESSING

Natraj Narayanswami

*FSI International Inc.*

MS 4-8071, 322, Lake Hazeltine Drive, Chaska, MN 55318, USA

## ABSTRACT

Experiments have shown that cryogenic aerosols successfully remove wafer surface contaminants through mechanical impact. Effective cleaning depends on the ability to control the aerosol. This requires a clear knowledge of aerosol formation mechanisms. This study examines the formation of cryogenic aerosol in a freely expanding Argon jet, using a theoretical model. Results for a pure gas jet indicate the formation of aerosol clusters of mean size  $\sim 1 \mu\text{m}$ . If the expanded fluid contains seed clusters, the growth of the clusters appears to be favored over nucleation and nuclei growth.

## INTRODUCTION

Cryogenic aerosols have been successfully used to clean wafer surfaces. Such aerosols can be generated by rapid expansion, in the form of a free jet, of a pressurized fluid such as Ar or N<sub>2</sub> or a mixture of the two [1,2]. The fluid may be initially in a purely gaseous or partially liquefied state. Contaminant particles adhering to the wafer surface are dislodged by impact of high kinetic energy aerosol clusters and are removed by a co-flowing gas stream (Fig. 1). The cleaning efficiency depends on aerosol composition and flow characteristics. It is therefore critical to have control over the aerosol formation. This demands a clear knowledge of aerosol formation mechanisms.

The present study examines the formation of a cryogenic Argon aerosol through expansion from a gaseous or partially liquefied state. The mean cluster size obtained under various expansion strengths is calculated using a model of homogeneous nucleation and cluster growth. The initial liquid phase, if any, is assumed to be dispersed in the gas phase as seed clusters. The model is derived from previous theoretical efforts [3-7] in aerosol dynamics and is described briefly in the following section.

## THEORETICAL MODEL

The aerosol cluster formation and growth equations are based on the work in Ref. 3 but are re-cast in the following dimensionless form for conditions of temporally steady flow:

$$\bar{M}_{vX} = -g_s \bar{J} - \bar{R}_{ch} - \bar{R}_{cs} \quad (1)$$

$$\bar{N}_{hX} = \bar{J} \quad (2)$$

$$\bar{M}_{hX} = g_s \bar{J} + \bar{R}_{ch} \quad (3)$$

$$\bar{N}_{sX} = 0 \quad (4)$$

$$\bar{M}_{sX} = \bar{R}_{cs} \quad (5)$$

where  $\bar{M}_v$ ,  $\bar{M}_h$  and  $\bar{M}_s$  denote mass concentrations of vapor, homogeneous nucleation ("HN") clusters and seed clusters, respectively,  $\bar{N}_h$  and  $\bar{N}_s$  denote number concentrations of HN and seed clusters, respectively,  $\bar{J}$  denotes the nucleation rate, and  $\bar{R}_{ch}$  and  $\bar{R}_{cs}$  denote growth rates of HN and seed clusters, respectively. The subscript  $X$  denotes differentiation with respect to distance  $X$  along the jet axis.

Equation (1) describes the variation in the total mass of condensable vapor with axial distance in the jet. Vapor molecules combine to form either new homogeneous nuclei ("H-nuclei") or condense over existing H-nuclei or over seed clusters. Equation (2) describes the rate of H-nuclei formation. Equation (3) describes the change in total mass of such H-nuclei. Equation (4) indicates that the number of seed clusters introduced remains constant. Equation (5) describes the change in total mass of the seed clusters.

The number of molecules that combine to form a H-nucleus is given by :

$$g_s = \frac{32\pi\sigma^3\nu_1^2}{3(kT\ln S)^3} \quad (6)$$

where  $\sigma$ ,  $\nu_1$ ,  $k$  and  $S$  refer to the liquid-vapor surface tension, molecular volume, Boltzmann constant and vapor saturation ratio, respectively, and  $T$  denotes temperature. The rate of formation of homogeneous nuclei is described by classical nucleation theory [4,5]:

$$J = 2S^2 N_{sat}^2 \nu_1 \sqrt{\frac{\sigma}{2\pi m_1}} \exp\left(\frac{-16\pi\sigma^3\nu_1^2}{3k^3 T^3 \ln^2 S}\right) \quad (7)$$

where  $N_{sat} = p_{sat}[T]/(kT)$  denotes the number of vapor molecules at saturation at temperature  $T$  and  $p$  denotes pressure. The rate of condensation on an existing H-nucleus or cluster depends on cluster diameter  $d_p$  and on the Knudsen number  $Kn$  and is given by:

$$R_c = \alpha \frac{\pi}{4} d_p^2 N_{sat} c_1 \left(S - e^{d_k/d_p}\right) f(Kn) \quad (8)$$

where,

$$f(Kn) = \frac{1.333Kn(1+Kn)}{1 + 1.71Kn + 1.333Kn^2}; \quad c_1 = \sqrt{\frac{8kT}{\pi m_1}}; \quad d_k = \frac{2\pi d_1^3 \sigma}{3kT}; \quad Kn = \frac{2\lambda}{d_p} \quad (9)$$

and  $\alpha$  is a constant,  $\lambda$  is the mean free path in the vapor and  $m_1$  is the molecular mass. The equation for  $R_c$  applies to both HN and seed clusters. The two are distinguished by the subscripts *ch* and *cs*, respectively.

In an expanding vapor stream, both pressure and temperature fall rapidly and influence condensation. Condensation, in turn, removes mass from the vapor but changes its pressure and temperature through heat addition. Thus, condensation dynamics and gas dynamics are coupled. The link between the two is the local mass fraction of condensate given by :

$$g(X) = (\bar{M}_h + \bar{M}_s) / \bar{M}_{vo} \quad (10)$$

where the subscript 0 denotes the nozzle location or  $X = 0$ . Following Ref. 4, the gas dynamics equations are written as differential relations for  $p$ ,  $T$ , density  $\rho$  and velocity  $u$ :

$$\frac{dp}{p} = \frac{\left[\frac{L}{C_{po}T} - \frac{1}{1-g}\right] dg - \frac{dA}{A}}{1 - \mathcal{R} \frac{1-g}{C_{po}} - \frac{1-g}{\gamma M^2}} \quad (11)$$

$$\frac{dT}{T} = \frac{\mathcal{R}(1-g)}{C_{po}} \frac{dp}{p} + \frac{L}{C_{po}T} dg \quad (12)$$

$$\frac{du}{u} = -\frac{1-g}{\gamma M^2} \frac{dp}{p} \quad (13)$$

$$\frac{d\rho}{\rho} = -\frac{dg}{1-g} - \frac{du}{u} \quad (14)$$

$$\rho = \frac{p}{RT} \quad (15)$$

where  $L$  is the latent heat of vaporization/sublimation,  $C_{po}$  is the specific heat at constant pressure,  $A$  is the local jet cross sectional area,  $M$  is the local Mach number,  $\gamma$  is the ratio of specific heats and  $\mathcal{R}$  is the gas constant.

The solution of the coupled cluster formation and gas dynamics system of equations is achieved by iterating from an initial guess profile (e.g. a condensation-free adiabatic expansion along the jet axis) until a converged solution is reached. At any location  $X$ , the HN cluster mean diameter ( $d_{ph}$ ) and the seed cluster mean diameter ( $d_{ps}$ ) are then computed from:

$$d_{ph} = \left( \frac{6\bar{M}_h m_1}{\pi \rho_c N_h} \right)^{1/3}; \quad d_{ps} = \left( \frac{6\bar{M}_s m_1}{\pi \rho_c N_s} \right)^{1/3} \quad (16)$$

In the following section, the validity of the coupled model is first established through comparison of calculations with available experimental data for water vapor condensation within an expansion nozzle. The model is then applied to the study of Argon aerosol formation in a free-jet expansion.

## RESULTS

### Validation of Theoretical Model

The theoretical model accurately predicts water vapor condensation. Figure 2 shows the close agreement between computed and experimental pressure profiles along the nozzle axis for condensing water vapor flow within an expansion nozzle. The pressure profiles show significant deviation from the adiabatic (no-condensation) curves, beginning at the location of onset of condensation. This pressure deviation behavior is typical for a condensing vapor in an expansion and is caused by heat transfer from condensing clusters back into the remaining vapor.

### Argon Aerosol Formation

A schematic of an expanding Argon aerosol jet is shown in Fig. 1. In a typical arrangement of this nature, the nozzle to chamber pressure ratio is usually large enough to generate supersonic flow. In the absence of condensation, the supersonic jet may be assumed to expand adiabatically with its dimensionless cross sectional area varying from  $A = 1.0$  at the nozzle to a local (larger) value at a chosen downstream location  $X$ . The local  $A$  is a function of the local flow Mach number  $M$  and is given by:

$$A = \frac{1}{M} \left[ \frac{2}{\gamma+1} \left( 1 + \frac{\gamma-1}{2} M^2 \right) \right]^\beta; \quad \beta = \frac{\gamma+1}{2(\gamma-1)} \quad (17)$$

As an example, for a nozzle pressure and temperature of 60 psi and 100 K, respectively, and a chamber (downstream location) pressure of 3 psi, the A at that downstream location is approximately 3.45. The A value can be taken as a measure of the expansion strength, i.e., larger the value at a given location, stronger the expansion.

Results for an expanding Argon jet initially in purely gaseous phase are shown in Figs. 3a-c. Pressure profiles along the jet axis are shown for various expansion strengths (A values). As was observed previously for the water vapor expansion, condensation results in pressures significantly higher than the adiabatic values. The A = 1.3 and A = 1.7 profiles show a smooth rise in pressure at the location of onset of condensation ("OC"). However, the A  $\geq$  1.85 profiles show a rather abrupt increase at the OC location. These abrupt changes are due to 'thermal choking' of the flow wherein the heat transfer back into the vapor from the condensing clusters reaches a maximum allowable limit.

Profiles of condensate mass fraction  $g$  and saturation ratio  $S$  for various expansion strengths are shown in Fig. 3b. As in the case of the pressure profiles, the  $g$  profiles show a significant increase beginning at the OC locations. The total amount of condensate formed is greater for stronger expansions. For example  $g = 4.8\%$ , 8%, and 10% at the same downstream distance ( $X = 30.0$ ) for A = 1.3, 1.85 and 3.45, respectively. The saturation ratio increases initially and reaches a maximum at the OC location. Following initiation of condensation, the saturation level in the vapor decreases. High saturation levels can be reached in the metastable vapor before condensation. For example, for all the expansion strengths, the peak saturation ratio is well above 3.0 at condensation onset.

Figure 3c shows profiles of mean cluster diameter  $d_{ph}$  computed up to a downstream distance of  $X = 30.0$ . The values are quite large, even for modest expansions, at the most downstream location. For example, for  $1.05 < A \leq 1.7$ ,  $d_{ph}$  is typically greater than 0.5  $\mu\text{m}$ . Additionally, as A increased from 1.1 to 1.7, the maximum mean diameter decreases. Since stronger expansions are known to result in greater overall condensation, the above trend suggests that stronger expansions tend to favor production of new nuclei over condensational growth of existing nuclei. For very strong expansions,  $d_{ph}$  initially increases, but drops abruptly at the OC location and remains fairly constant thereafter. For example, for A = 2.0 and 3.45,  $d_{ph}$  reaches a maximum of only about 0.06  $\mu\text{m}$  at  $X = 30.0$ . This may be attributed to the formation of a large number of new nuclei and negligible growth of existing clusters.

As mentioned earlier, liquid present in the initial total mass of the mixture within the nozzle is modeled as seed clusters suspended in vapor. The growth profiles of seed clusters display interesting behavior (Figs. 4a,b). For a modest expansion strength of A = 1.3 but negligible liquid mass fraction, seed clusters of initial size 0.01 - 0.1  $\mu\text{m}$  grow quickly to nearly 1  $\mu\text{m}$  (Fig. 4a), indicating that seed clusters tend to attract a significant portion of the vapor molecules. For the same expansion strength and a finite liquid mass fraction of 0.3, seed clusters of initial size 0.05 - 0.1  $\mu\text{m}$  tend to initially decrease in size (evaporate) but then recover to grow again to nearly 1.0  $\mu\text{m}$  (Fig. 4b). Thus, overall, seed cluster growth appears to be favored over nucleation and nuclei growth. This behavior is observed to be similar in stronger expansions as well.

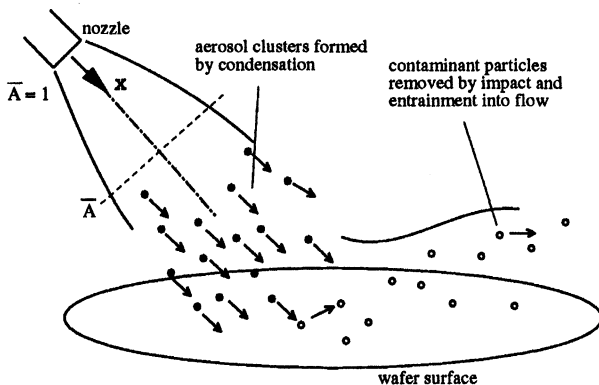


Figure 1: Schematic of contaminant particle removal from wafer surface by aerosol jet impingement

## CONCLUSIONS

The study yields the following conclusions regarding the formation of an Argon cryogenic aerosol by free expansion:

- (a) the total amount of condensate increases with expansion strength.
- (b) the production of new nuclei, rather than condensational growth of existing nuclei, is favored at high expansion strengths; consequently, the mean aerosol cluster diameter decreases with expansion strength at a given axial location.
- (c) moderate expansion strengths result in aerosol clusters of about 1  $\mu\text{m}$  mean size, while high expansion strengths result in sub-micron mean sizes.
- (d) seed clusters of initial size 0.01 - 0.1  $\mu\text{m}$  rapidly grow to about 1  $\mu\text{m}$  mean size, for moderate expansion strengths.
- (e) the growth of seed clusters is favored over nucleation and nuclei growth, in general.

## REFERENCES

1. W. T. McDermott et al., Microcontamination, Oct. (1991)
2. J. F. Weygand et al., MICRO, **47**, Apr. (1997)
3. D. R. Warren and J. H. Seinfeld, Aerosol Sci. and Tech., **3**, 135 (1984).
4. P. P. Wegener and B. J. C. Wu, in Adv. Coll. Interf. Sci., Elsevier Scientific Publishing Co., **7**, 325 (1977).
5. J. J. Wu, D. W. Cooper and R. J. Miller, J. Vac. Sci. Technol. A, **8**, No. 3, 1961 (1990).
6. P. G. Hill, J. Fluid Mech., **25**, Pt. 3, 593 (1966).
7. R. A. Zohoransky et al., J. Chem. Phys., No. 103, **20**, 9038 (1995).
8. J. D. Anderson, Jr., Modern Compressible Flow, McGraw Hill (1990).

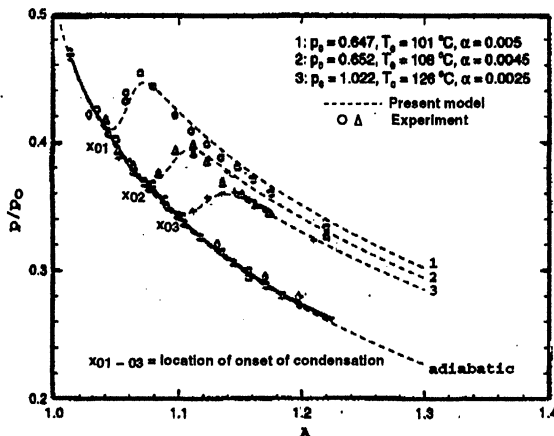


Figure 2: Comparison of pressure profile calculations using present model with experimental data of Ref 6 - water vapor condensation in a nozzle flow

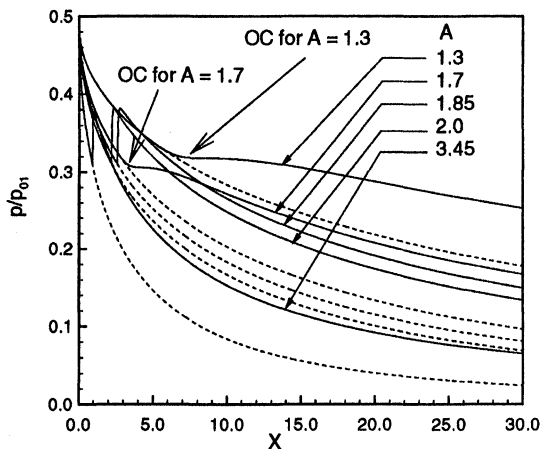


Figure 3a: Pressure profiles for free expansion of pure Argon vapor for different expansion strengths; - - - no condensation, —— with condensation

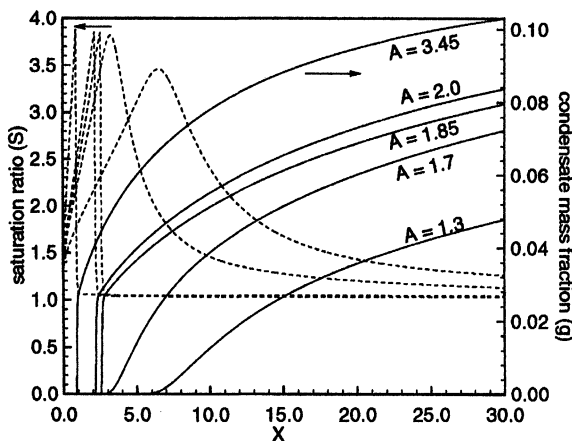


Figure 3b: Computed condensate mass fractions ( $g$ ) and saturation ratios ( $S$ ) for Argon gas jet free expansion in the absence of seed clusters; - - - ( $g$ ), —— ( $S$ )

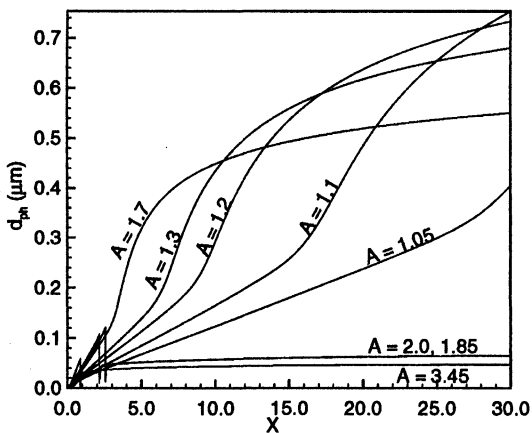


Figure 3c: Profile of mean cluster diameter  $d_{ph}$  for Argon gas jet free expansion in the absence of seed clusters

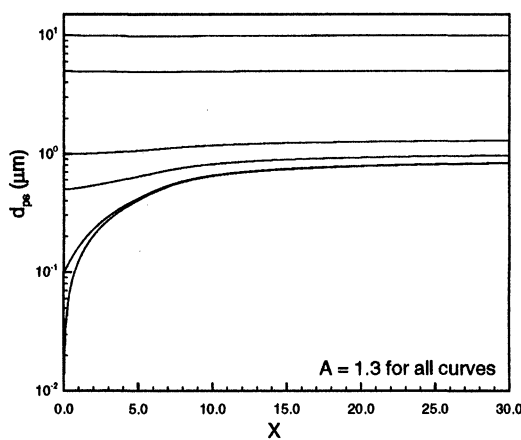


Figure 4a: Profile of seed cluster mean diameter  $d_{ps}$  for  $A = 1.3$  for Argon gas jet free expansion and negligible initial liquid mass fraction

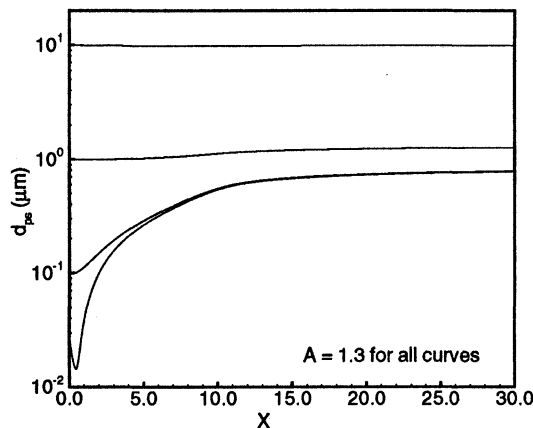


Figure 4b: Profile of seed cluster mean diameter  $d_{ps}$  for  $A = 1.3$  and initial liquid mass fraction of 0.3 for Argon free jet expansion

# **COMPARISON OF PROCESS EMISSIONS DURING C<sub>3</sub>F<sub>8</sub> AND C<sub>2</sub>F<sub>6</sub> PECVD CLEANING USING EXTRACTIVE FTIR**

L. Zazzera & W. Reagen  
3M Company, St. Paul, MN., 55144

A. Cheng  
Texas Instruments Incorporated, Dallas, TX., 75265

## **ABSTRACT**

In this work, Fourier Transform Infrared spectroscopy is used to monitor perfluorocompound process emissions during in situ cleaning of a plasma enhanced chemical vapor deposition chamber. Gas mixtures containing CF<sub>4</sub>, C<sub>2</sub>F<sub>6</sub>, C<sub>3</sub>F<sub>8</sub>, SiF<sub>4</sub> and COF<sub>2</sub> are identified and quantified simultaneously using fourier transform infrared spectroscopy. The results from this study show that the lower flow rate and higher utilization of etch gas during a C<sub>3</sub>F<sub>8</sub> chamber cleaning process can contribute to reductions in net perfluorocompound emissions relative to a C<sub>2</sub>F<sub>6</sub> cleaning process of similar duration. This work also demonstrates that FTIR spectroscopy can provide information which is necessary to support the development of alternative chamber cleaning chemistry. In this way, monitoring methods based on FTIR spectroscopy are valuable to the semiconductor industry's perfluorocompound emission reduction objectives.

## **INTRODUCTION**

Each new generation of silicon integrated circuits demonstrates dramatic increases in both the number of devices per chip and the circuit speed. The miniaturization of the semiconductor devices necessary for this density and speed has in large part been made possible by advances in contamination prevention. Contaminants introduced during the various steps in semiconductor manufacturing generally reduce yields and degrade electrical performance.(1)

In situ cleaning of plasma enhanced chemical vapor deposition (PECVD) chambers is a process designed to reduce the formation of particles which could deposit on the silicon wafers and reduce yields. In situ cleaning for PECVD uses perfluorocompounds (PFCs) to produce a fluorine-based plasma inside the PECVD reactor. The in situ cleans are advantageous, because unlike conventional cleaning they do not have the cost, time, environmental, safety and health issues associated with disassembling and manually cleaning the reactor.

Despite the advantages and wide spread use of PFCs in semiconductor manufacturing, PFC use is being scrutinized because of the potential contribution to global warming. The United States Environmental Protection Agency (USEPA) and the semiconductor industry have developed a voluntary program, memorandum of understanding (MOU), to reduce greenhouse gas emissions.(2) Several options are being

considered to help reach the emission reduction objectives of the industry. Feasibility testing and development of these options will require gas sampling and testing methods which provide information on the composition of various effluent streams.

In recent years, extractive fourier transform infrared (FTIR) spectroscopy has developed into an effective technology in field analysis.(3). Reports from the USEPA document the capability of extractive FTIR to generate highly accurate emissions data for a wide range of VOCs in difficult test matrices. (4-5) Additionally, the EPA has prepared a library of quantitative IR spectra which contains most of the hazardous air pollutant (HAP) listed compounds. FTIR spectroscopy has recently been used for the analysis of selected exhaust gases during Reactive Ion Etching (RIE) and PECVD. (6)

The purpose of this work was to demonstrate the use of FTIR spectroscopy for process emissions monitoring, and to compare the performance of the C<sub>3</sub>F<sub>8</sub> and C<sub>2</sub>F<sub>6</sub> chamber cleaning processes based on the amounts of gas required, the efficiencies of the gas utilization and the net emission of PFCs. The results from this study show that the lower flow rate and higher utilization of etch gas during the C<sub>3</sub>F<sub>8</sub> chamber cleaning process can contribute to significant reductions in net PFC emissions compared to a C<sub>2</sub>F<sub>6</sub> cleaning process of similar duration.

The PECVD chamber cleaning processes called for approximately 44 % less C<sub>3</sub>F<sub>8</sub> etch gas than C<sub>2</sub>F<sub>6</sub> by volume. Considering the molecular weights of each gas, then approximately 25 % less C<sub>3</sub>F<sub>8</sub> etch gas is required compared to C<sub>2</sub>F<sub>6</sub> chamber cleaning processes of equivalent duration. The C<sub>3</sub>F<sub>8</sub> etch gas had significantly higher utilization, i.e. a greater percent of C<sub>3</sub>F<sub>8</sub> was destroyed in the plasma, than C<sub>2</sub>F<sub>6</sub>. The range of etch gas utilizations were 31-34 % and 52-60 % for C<sub>2</sub>F<sub>6</sub> and C<sub>3</sub>F<sub>8</sub>, respectively. For both cleaning processes, CF<sub>4</sub> and unreacted C<sub>2</sub>F<sub>6</sub> or C<sub>3</sub>F<sub>8</sub> are the primary PFC emissions. Comparison of process emissions revealed that the C<sub>3</sub>F<sub>8</sub> clean resulted in net PFC emission reductions of 42-66 % based on the combined mass of all the PFCs emitted. The C<sub>3</sub>F<sub>8</sub> cleaning process resulted in net PFC emission reductions of 55-74 % based on the CO<sub>2</sub> equivalence of all the PFCs emitted, e.g. based on the mass and global warming potentials of unreacted etch gas and CF<sub>4</sub>.

## EXPERIMENTAL

PECVD chamber cleaning. - The cleaning was performed after depositing various dielectric films onto 150 mm wafers. The thickness of the deposited film varied by type of dielectric, but for each type of dielectric the thickness of deposited films were kept constant by controlling the time per deposition and the number of depositions between cleans. Comparisons between C<sub>3</sub>F<sub>8</sub> and C<sub>2</sub>F<sub>6</sub> cleaning processes were based on films of the same dielectric material and thickness.

The flow rates of the cleaning gases were defined by the PECVD tool manufacturers standard process recipe and controlled by mass flow controllers on the PECVD tool. The C<sub>3</sub>F<sub>8</sub> flow rate was 890 sccm and the O<sub>2</sub> flow rate was 1110 sccm for the C<sub>3</sub>F<sub>8</sub> chamber clean. The C<sub>2</sub>F<sub>6</sub> and O<sub>2</sub> flow rates were 1600 sccm for the C<sub>2</sub>F<sub>6</sub> chamber clean. The RF power was the same for the C<sub>3</sub>F<sub>8</sub> and C<sub>2</sub>F<sub>6</sub> chamber cleans.

**Emissions monitoring.** - Infrared spectra were collected using a MIDAC G-5000 FTIR spectrometer with a mercury cadmium telluride (MCT) detector and zinc selenide beam splitter. A Teflon™ sample line was used to extract process emissions from the exhaust of the process tool vacuum, Figure 1.

Theoretical minimum detection limits (MDLs) were reported using visual spectral addition (Lab Calc, Galactic Industries Corp.) of reference spectra to exhaust test data. The following MDLs are representative of instrument performance configured with a 1.1 cm gas cell, using 16 co-added scans at 0.5 cm<sup>-1</sup> resolution, triangular apodization: CF4 (7 ppmv, 1283 cm<sup>-1</sup>), C2F6 (50 ppmv, 1116 cm<sup>-1</sup>), C3F8 (80 ppmv, 1007 cm<sup>-1</sup>), COF2 (160 ppmv, 1944 cm<sup>-1</sup>), SiF4 (30ppmv, 1032 cm<sup>-1</sup>) and SF6 (9 ppmv, 948 cm<sup>-1</sup>).

The percent recovery (Eqn. 1) indicates the relative error between the concentration of the spike gas actually measured by FTIR ( $C_{\text{measured}}$ ) and the theoretical concentration ( $C_{\text{th}}$ ) of the spike gas in the exhaust. Table I. Lists the percent recovery for three separate matrix spike exercises, and indicates that the theoretical and measured concentrations of the spiked gas agreed within approximately 10 %.

$$\text{Recovery}(\%) = \left( \frac{C_{\text{measured}}}{C_{\text{th}}} \right) \times 100 \quad [1]$$

Table I. The theoretical and measured concentrations of the spiked gas.

Process	C <sub>Spike</sub> (ppmv)	C <sub>Theoretical</sub>	C <sub>Measured</sub>	% Recovery
C <sub>2</sub> F <sub>6</sub> RF Off	CF <sub>4</sub> (2525)	505 ppmv	563 ppmv	111 %
C <sub>3</sub> F <sub>8</sub> RF On	C <sub>2</sub> F <sub>6</sub> (4998)	1015 ppmv	1096 ppmv	108 %
C <sub>2</sub> F <sub>6</sub> RF On	C <sub>3</sub> F <sub>8</sub> (5077)	1000 ppmv	1095 ppmv	109 %

The theoretical concentration for a given gas ( $C_{\text{th}}$ ) in the sampled exhaust is defined below (Eqn. 2). In this work Flow<sub>spike</sub> and the total flow through the FTIR gas cell (Flow<sub>total</sub> were set using mass flow controllers at 0.2 slpm and 1.0 slpm, respectively. Flow<sub>exhaust</sub> was 0.8 slpm.

$$C_{\text{th}} = \left[ \left( C_{\text{spike}} \times \text{Flow}_{\text{spike}} \right) + \left( C_{\text{exhaust}} \times \text{Flow}_{\text{exhaust}} \right) \right] \left( \text{Flow}_{\text{total}} \right)^{-1} \quad [2]$$

Under these conditions, Equation 2 gives the flow-weighted average concentration of the spiked compound in the spiked sample stream and Equation 1 gives its accepted percent recovery. (7)

**Data Analysis.** - All PFCs were identified and quantified using a 3M quantitative library spectrum and a minimum 4 point calibration curve which was generated at 3M by following EPA guidelines for extractive FTIR. (8)

Throughout the study, selected samples were collected in polypropylene sample bottles and analyzed on-site using a gas chromatograph (GC) equipped with a mass spectrometer (MS) detector. Good agreement was observed between the GC-MS and FTIR results, Table II.

Table II. Comparison of FTIR results to GC-MS.

1600 sccm C <sub>2</sub> F <sub>6</sub> , RF Power - Off					
Analytical Method	CF <sub>4</sub> ppmv	C <sub>2</sub> F <sub>6</sub> ppmv	C <sub>3</sub> F <sub>8</sub> ppmv	SiF <sub>4</sub> ppmv	COF <sub>2</sub> ppmv
FTIR, Average, n=5	< 7	25000	< 80	< 30	< 160
FTIR, 1 sigma		100			
GC-MS, Average, n=3	< 10	23000	< 10	< 10	< 10
GC-MS, 1 sigma		350			

Another check of quantitative accuracy is provided by comparing the FTIR measured mass to the mass given by the PECVD tool's mass flow controller (MFC) for a given time interval, Table III. This check is performed under RF power off conditions during both C<sub>2</sub>F<sub>6</sub> and C<sub>3</sub>F<sub>8</sub> flow. The MFC defined mass of C<sub>2</sub>F<sub>6</sub> and C<sub>3</sub>F<sub>8</sub> which passes through the reactor over a 10 minute time interval is based on the process flow rates of 1600 sccm and 890 sccm for C<sub>2</sub>F<sub>6</sub> and C<sub>3</sub>F<sub>8</sub>, respectively. The results in Table III indicate that the FTIR measured mass and the mass given by the PECVD tool's MFC agree within 1 % .

Table III. Comparison of FTIR measured mass to MFC process flows.

TOOL PARAMETERS		Delta	
FEED GAS	MFC MASS (g)	FTIR MEASURED MASS (g)	%
C <sub>3</sub> F <sub>8</sub>	75	75	0
C <sub>2</sub> F <sub>6</sub>	99	98	-1.0

**Mass of process emissions.** - In this report, comparison of C<sub>2</sub>F<sub>6</sub> and C<sub>3</sub>F<sub>8</sub> process emissions are based on the mass of effluent. The mass of effluent accounts for the volume of each gas species produced by multiplying the measured concentration (ppmv) of each gas species by the measured exhaust flow rate over a given time interval. The mass flow meter on the pump indicated a N<sub>2</sub> ballast flow rate of 59.8 ± 0.2 slpm, and was in good

agreement with the flow rate ( $60.4 \pm 0.3$  slpm) calculated from the measured FTIR concentration ( $14,744 \pm 54$  ppmv) of  $C_3F_8$  in the absence of RF power, Table IV.

Table IV. Exhaust flow rate calculation using the measured FTIR concentration of  $C_3F_8$  in the exhaust with the RF power turned off.

890 sccm $C_3F_8$ , RF Power Off	
$C_3F_8$ MFC Flow (sccm)	890
O <sub>2</sub> MFC Flow (sccm)	1110
Total MFC Flow before N <sub>2</sub> ballast (sccm)	2000
$C_3F_8$ concentration (ppmv) before N <sub>2</sub> ballast	445000
$C_3F_8$ concentration (ppmv) measured by FTIR, after N <sub>2</sub> ballast	14744
Pump N <sub>2</sub> Dilution Factor	30.2
Calculated Flow Rate (slpm)	60.4
Flow Rate from Mass Flow Meter (slpm)	59.8

The total time of the cleaning process was determined by summing the time intervals which showed significant amounts of SiF<sub>4</sub>, i.e. 3 times the minimum detection limit or > 90 ppmv. The volume of each gas species, in each consecutive time interval, was then converted to mass (grams) by assuming ideal gas behavior and standard temperature and pressure. The total mass of a given species emitted during a cleaning cycle was calculated by summing the masses associated with the consecutive time intervals.

Mass balance - Mass balance verifies that the mass of reactants entering the plasma reactor can be accounted for by the mass of the various effluent species. In this work the mass balance is based on the mass of fluorine going into the reactor as C<sub>2</sub>F<sub>6</sub> or C<sub>3</sub>F<sub>8</sub> (F<sub>in</sub>) and the mass of fluorine exhausted as CF<sub>4</sub>, C<sub>2</sub>F<sub>6</sub>, C<sub>3</sub>F<sub>8</sub>, SiF<sub>4</sub> and COF<sub>2</sub> (F<sub>out</sub>), Table V.

Table V. Mass of fluorine flowing into the PECVD chamber as C<sub>2</sub>F<sub>6</sub>, and the mass of fluorine exhausted out of the chamber as CF<sub>4</sub>, C<sub>2</sub>F<sub>6</sub>, SiF<sub>4</sub> and COF<sub>2</sub>.

Fluorine Mass Flowing In	Fluorine Mass Flowing Out As...				Delta
Fluorine from C <sub>2</sub> F <sub>6</sub>	CF <sub>4</sub>	C <sub>2</sub> F <sub>6</sub>	SiF <sub>4</sub>	COF <sub>2</sub>	Sum
86.0	6.3	62.0	11.2	11.3	90.7 + 5 %

## RESULTS

The C<sub>3</sub>F<sub>8</sub> and C<sub>2</sub>F<sub>6</sub> chamber cleaning processes were compared based on the amounts of etch gas required, the percent etch gas utilization and net PFC emissions.

Amount of etch gas required. - Comparison of the etch gas flow rates, 1600 sccm C<sub>2</sub>F<sub>6</sub> during the standard clean and 890 sccm during the C<sub>3</sub>F<sub>8</sub> clean, reveals that the C<sub>3</sub>F<sub>8</sub> process requires 44.3 % less etch gas by volume than the standard C<sub>2</sub>F<sub>6</sub> process.

Considering the molecular weights of each gas, the C<sub>3</sub>F<sub>8</sub> process flows 24.3 % less mass of etch gas than the standard C<sub>2</sub>F<sub>6</sub> process.

**Etch gas utilization** - The utilization of the etch gas refers to the percentage of the etch gas which reacts in the plasma to form other products. The utilization was found by measuring the etch gas concentration with the RF power off and on, Eqn. 3. The utilization of C<sub>2</sub>F<sub>6</sub> vs. C<sub>3</sub>F<sub>8</sub> are listed in the Table VI for various films and process conditions. The etch gas utilization determined by the FTIR method in this study confirmed the improved utilization of C<sub>3</sub>F<sub>8</sub> compared to C<sub>2</sub>F<sub>6</sub>.(9)

$$\%Utilization = \left[ \left( (C_3F_8, RF_{OFF}) - (C_3F_8, RF_{ON}) \right) / (C_3F_8, RF_{OFF}) \right] \times 100 \quad [3]$$

Table VI. Utilization (percent of etch gas destroyed in plasma) for C<sub>2</sub>F<sub>6</sub> and C<sub>3</sub>F<sub>8</sub>.

Dielectric Film	C <sub>2</sub> F <sub>6</sub> Utilization (%)	C <sub>3</sub> F <sub>8</sub> Utilization (%)
TEOS Oxide	31	60
Silane Oxide	33	54
High Stress Oxide	33	52
Oxynitride	34	55
Silicon Nitride	34	52

**Net PFC emissions** - The primary PFC emissions for both the C<sub>2</sub>F<sub>6</sub> and C<sub>3</sub>F<sub>8</sub> cleaning processes are CF<sub>4</sub> and unreacted C<sub>2</sub>F<sub>6</sub> or C<sub>3</sub>F<sub>8</sub>. Other primary emissions found in the exhaust of both cleaning processes were SiF<sub>4</sub> and COF<sub>2</sub>. Figures 2 and 3 plot the process emissions during the cleaning of a silicon dioxide film using a C<sub>2</sub>F<sub>6</sub> and C<sub>3</sub>F<sub>8</sub> plasma, respectively.

Comparison of PFC emissions during the C<sub>2</sub>F<sub>6</sub> and C<sub>3</sub>F<sub>8</sub> cleaning processes can be made based on the mass of the PFCs emitted, and on the CO<sub>2</sub> equivalence (metric tons) of the PFC emissions. PFCs and CO<sub>2</sub> are both greenhouse gases, thus the CO<sub>2</sub> equivalence (mass of CO<sub>2</sub> causing the same cumulative warming) of the PFCs emitted can be calculated. This calculation considers the mass and global warming potential (GWP) of each PFC emitted. The GWP of a greenhouse gas is a number calculated by integrating radiative forcing - a measure of the ability of a greenhouse gas to trap infrared radiation - as the gas decays overtime. This integration is performed over a specific period of time (integrated time horizon) and then divided by an identical integral for an equivalent mass of a reference gas (generally CO<sub>2</sub>). The resulting ratio is the GWP.(10) The GWP of a given greenhouse gas is the equivalent mass of carbon dioxide (CO<sub>2</sub>) which has the same potential for raising the earth's average surface temperature. The GWP values used in this report: CF<sub>4</sub> = 6,500, C<sub>2</sub>F<sub>6</sub> = 9,200 and C<sub>3</sub>F<sub>8</sub> = 7,000; are for a 100 year time horizon.(11)

Table VII, lists the mass (grams) of all the PFCs emitted and the corresponding CO<sub>2</sub> equivalence emissions (metric tons) for a chamber clean following deposition of silicon dioxide from silane. Table VII, shows that net emissions (C<sub>3</sub>F<sub>8</sub> relative to C<sub>2</sub>F<sub>6</sub>) are reduced 51 % and 62 % based on the PFC mass and CO<sub>2</sub> equivalence, respectively. Table VIII, lists net PFC emissions reductions for chamber cleans following deposition of various dielectric films using the same procedures and calculations described above for the silicon dioxide deposited from silane.

Table VII. Mass (g) and CO<sub>2</sub> equivalent (metric tons) of PFC emissions during high-pressure C<sub>2</sub>F<sub>6</sub> and C<sub>3</sub>F<sub>8</sub> chamber cleans following the deposition of silicon dioxide.

PFC	Mass of PFCs from C <sub>2</sub> F <sub>6</sub> Clean		Mass of PFCs from C <sub>3</sub> F <sub>8</sub> Clean	
	Mass (g)	CO <sub>2</sub> Equivalent (metric tons)	Mass (g)	CO <sub>2</sub> Equivalent (metric tons)
CF <sub>4</sub> (g)	7.3	0.047	8.3	0.05
C <sub>2</sub> F <sub>6</sub> (g)	75	0.69	0	0
C <sub>3</sub> F <sub>8</sub> (g)	0	0	32	0.22
Total	82.3	0.74	40	0.27
Net Emission Reduction {[Total (C <sub>2</sub> F <sub>6</sub> ) - Total (C <sub>3</sub> F <sub>8</sub> )] / Total (C <sub>2</sub> F <sub>6</sub> )} × 100		- 51 %	- 62 %	

The net PFC emissions reduction values in Table VIII are based on emissions during one C<sub>2</sub>F<sub>6</sub> and one C<sub>3</sub>F<sub>8</sub> chamber clean following deposition of the same film type and thickness.. The results in Table VIII show that in general the chamber cleans using C<sub>3</sub>F<sub>8</sub> resulted in lower net PFC emissions. The lower flow rate and higher utilization of etch gas during the C<sub>3</sub>F<sub>8</sub> chamber cleaning process, relative to the C<sub>2</sub>F<sub>6</sub> cleaning process, accounts for the reduction in net PFC emissions.

Table VIII. Net PFC emission reductions based on the total mass of all PFCs emitted and on the CO<sub>2</sub> equivalence of all PFCs emitted.

PRODUCTION PROCESSES	% NET PFC REDUCTION C <sub>3</sub> F <sub>8</sub> vs. C <sub>2</sub> F <sub>6</sub>	
	Based on mass of all PFCs emitted	Based on CO <sub>2</sub> equivalent of all PFCs emitted
DIELECTRIC FILM		
Silicon dioxide (silane)	51 %	62 %
Silicon dioxide (TEOS)	42 %	55 %
Silicon Nitride	54%	64 %
High Stress Silicon dioxide (silane)	66 %	74 %
Oxynitride	48 %	60 %

## CONCLUSIONS

The results from this study show that the lower flow rate and higher utilization of etch gas during the C<sub>3</sub>F<sub>8</sub> chamber cleaning processes contributed to 55 % - 74 % reductions in net CO<sub>2</sub> equivalent emissions relative to C<sub>2</sub>F<sub>6</sub> cleaning processes of similar duration. The primary emissions from both cleaning processes were mixtures of CF<sub>4</sub>, SiF<sub>4</sub>, COF<sub>2</sub>, and unreacted C<sub>2</sub>F<sub>6</sub> or C<sub>3</sub>F<sub>8</sub>. This work also demonstrates that process emission monitoring methods based on extractive FTIR spectroscopy are valuable to the semiconductor industry's PFC emission reduction objectives.

## ACKNOWLEDGMENTS

The authors acknowledge the work of Paul Mahal, San Jose, CA, for the C<sub>3</sub>F<sub>8</sub>/O<sub>2</sub> chamber cleaning process studied in this work.

## REFERENCES

---

1. D. Burkman, C. Peterson, L. Zazzera, R. Kopp, *Microcontamination*, **6**, 1, 57 (1988).
- 2 . E.A. Dutrow, SEMI Technical Program - A Partnership for PFC Emissions Reduction, SEMICON Southwest, p. 137, SEMI, Mountain View, CA (1996).
3. P.L. Hanst, S.T. Hanst, in *Gas Measurement in the Fundamental Infrared Region*, Vol. 1, Infrared Analysis, Anaheim, CA.
4. G.M. Plummer, T.A. Dunder, T.J. Geyer, L.L. Kinner, Proceedings of the AWMA 87th Annual Meeting and Exhibition, 94-RP-129.05, Cincinnati, p. 1-20 (1994).
- 5 . Appendix A to part 63-test methods, *Method 318-Extractive FTIR Method for the Measurement of Emissions*, USEPA EMTIC Bulletin Board, (1996).
6. A.E. Gubner and U. Kohler, *J. Molecular Structure*, **348**, 209, (1995).
- 7 (Draft) *Method 321-Measurement of Gaseous Hydrogen Chloride Emissions with FTIR Spectrometry*, USEPA EMTIC Bulletin Board Section 9.2, (1997).
8. *Protocol For The Use of FTIR Spectrometry*, EPA Contract No. 68-D2-0165, Work Assignment 3-12, EMTIC Bulletin Board 919-541-5742, September, p. 1-50, (1996).
9. J. Langan, P. Maroulis, R. Ridgeway, Solid State Technology, **39**, 7, 115 (1996)
10. IPCC Climate Change, *The Supplementary Report to the IPCC Scientific Assessment 1991*, J. J. Houghton, B. A. Callander and S. K. Varney, Editors, p. 205, Cambridge University Press, UK., (1992).
11. IPCC (Intergovernmental Panel on Climate Change) Climate Change, *The Science of Climate Change 1995*, J.J. Houghton, L.G. Meiro Philo, B.A. Callander, N. Harris, A. Kattenberg and K. Maskell, Editors, p. 16, Cambridge University Press, UK., (1996).

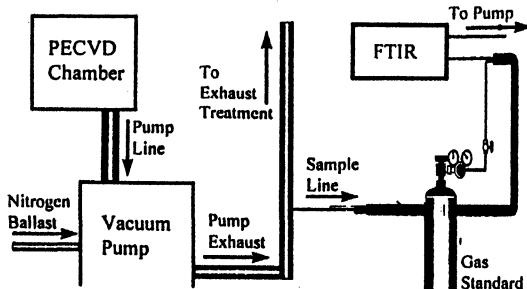


Figure 1. The FTIR sampling system extracted process emissions from the  $N_2$  ballast diluted exhaust exiting the process tool's vacuum pump. The pressure of the pump exhaust is typically close to atmospheric pressure, i.e. greater than 730 torr.

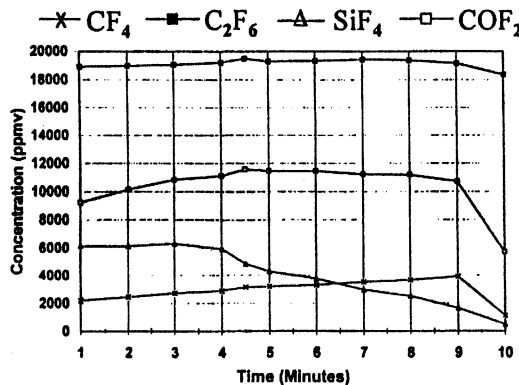


Figure 2. Process emissions in  $N_2$  ballast diluted exhaust during the in situ PECVD chamber cleaning of a silicon dioxide film from silane using a  $C_2F_6$  plasma.

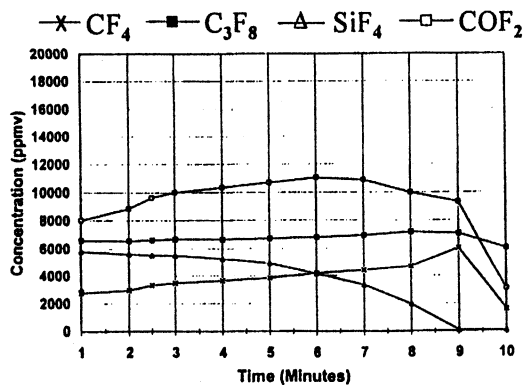


Figure 3. Process emissions in  $N_2$  ballast diluted exhaust during the in situ PECVD chamber cleaning of a silicon dioxide film from silane using a  $C_3F_8$  plasma.



**CHARACTERIZATION  
AND  
MONITORING**



# ELECTROCHEMICAL DETECTION OF IRON CONTAMINATION DURING SILICON WAFER CLEANING

Emil A. Kneer and Srinivas Raghavan  
Department of Materials Science & Engineering  
University of Arizona, Tucson, AZ 85721

Joong S. Jeon  
Advanced Micro Devices Inc., Sunnyvale, CA 94088-3453

Electrochemical direct current (DC) open circuit potential and alternating current (AC) impedance spectroscopy techniques were used to detect and characterize iron contamination onto n- and p-type silicon from iron spiked SC-1 solutions. It was found that the open circuit potential (OCP) of n- and p-type silicon became increasingly more positive as iron levels in SC-1 were increased in SC-1 from 0 to 100 ppb. The polarization resistance ( $R_p$ ) of n- and p-type silicon also increased by 10 to 20 kohms when silicon was exposed to SC-1 contaminated with 100 ppb added iron. Total Reflection X-ray Fluorescence (TXRF) and X-ray Photoelectron Spectroscopy (XPS) analyses were conducted to further characterize iron contamination/removal during immersion from SC-1 and SC-2 solutions.

## INTRODUCTION

The deposition and removal of iron and other metallic contaminants on silicon during RCA based cleaning procedures has been actively investigated (1-3). Some of these studies have looked at metallic contamination onto silicon from uncontaminated or intentionally contaminated process solutions (1,2). Other studies have used vacuum evaporated metals such as iron, copper, or nickel to contaminate SC-1 last or HF last exposed silicon, and characterized the effectiveness of RCA based cleaning sequences for the removal of the pre-deposited metallic contaminants (3).

During SC-1 exposure, a thin oxide, ~ 1 nm thick, forms on HF last treated silicon due to surface oxidation by hydrogen peroxide. This oxide is continually etched by the alkaline component ( $\text{NH}_4\text{OH}$ ) in the SC-1 solution. In a study by Tsuji et al. (4), who used HF-Vapor Phase Decomposition-Atomic Absorption Spectroscopy (HF-VPD-AAS) and XPS analyses, it was found that metallic impurities (Fe, Ni, Cu, Zn) were not deposited into the native oxide, but were adsorbed only at the surface of the oxide formed during SC-1 exposure. Recently, electrochemical DC open circuit potential measurement techniques have been used to detect iron contamination onto silicon from SC-1 solutions. Chyan et al. (5) showed that the open circuit potential of p-type silicon became more noble by hundreds of millivolts when exposed to 1:1:30 SC-1 intentionally spiked with 10 to 100 ppb levels of iron added as  $\text{Fe}(\text{NO}_3)_3$ .

The objective of this study was to further examine the use of silicon working electrodes for the detection of iron contamination during RCA based cleans. Electrochemical DC open circuit potential and AC polarization resistance measurements were conducted using both n- and p-type silicon as working electrodes, which were exposed to intentionally iron contaminated SC-1 solutions. DC open circuit potential measurements were also used to characterize the electrochemical behavior of iron contaminated silicon during cleaning in SC-2. TXRF and XPS analyses were also conducted to further characterize iron contamination and removal during SC-1 and SC-2 cleaning.

## EXPERIMENTAL

In this study, lightly doped [2 - 10  $\Omega\cdot\text{cm}$ ] and highly doped [0.005 - 0.02  $\Omega\cdot\text{cm}$ ] n- and p-type (100) silicon wafers were used. SC-1 solutions with a volume ratio of 1 NH<sub>4</sub>OH : 1 H<sub>2</sub>O<sub>2</sub> : 5 H<sub>2</sub>O, and SC-2 solutions with a volume ratio of 1 HCl : 1 H<sub>2</sub>O<sub>2</sub> : 5 H<sub>2</sub>O were prepared from electronic grade chemicals supplied by Olin Microelectronic Materials. Iron choline citrate (C<sub>33</sub>H<sub>57</sub>Fe<sub>2</sub>N<sub>3</sub>O<sub>24</sub>) of  $\geq 98\%$  purity purchased from Sigma® was used to control iron levels in SC-1 solutions.

Electrochemical testing was carried out on silicon wafer samples diced into 15 x 15 mm squares. DC open circuit potential (OCP) vs. time measurements were conducted using an EG&G PARC Model 273A potentiostat. AC impedance measurements were conducted using an EG&G PARC Model 6310 Electrochemical Impedance Analyzer. The AC polarization resistance values were calculated from Nyquist plots using a semicircle fit of the impedance data (6).

Prior to conducting the experiments, the silicon samples were first cleaned in a 1 H<sub>2</sub>O<sub>2</sub> : 4 H<sub>2</sub>SO<sub>4</sub> solution for 10 minutes ( $\sim 90^\circ\text{C}$ ) to remove organic contamination, and rinsed in DI water for 10 minutes. The samples were then etched for one minute in dilute (100:1) HF, rinsed in DI water for 10 minutes, and dried in blowing nitrogen. Pre-cleaned polypropylene and/or teflon® containers were used for measuring and handling the high purity solutions.

The electrochemical "dip" cell used for all tests is shown schematically in Figure 1. The cell consists of a teflon® block and bolt. The sealed bolt hole was machined to hold a Viton® o-ring which provided a compression seal to expose a  $\sim 1 \text{ cm}^2$  area of the silicon working electrode surface to the solution. Electrical contact was made from the silicon working electrode to the potentiostat using a conductive nickel print and a copper foil backside contact. Figure 2 shows the electrochemical test assembly. The dip cell was immersed in  $\sim 200 \text{ ml}$  solution contained in a thin walled polypropylene container. The container was fitted with a double junction, epoxy bodied Ag/AgCl reference electrode, and a high purity Pt foil counter electrode. Illumination conditions were maintained using a commercial 100 W bulb positioned above the cell.

The TXRF measurements were carried out using a Rigaku 3700 system with a minimum iron detection limit of  $2 \times 10^9 \text{ atoms/cm}^2$ . Angle resolved XPS analysis was conducted using a VG ESCALAB instrument.

## RESULTS

Figure 3 shows the DC open circuit potential (OCP) vs. time response for n-type [2 - 4  $\Omega\cdot\text{cm}$ ] silicon exposed to SC-1 solutions containing 0 to 100 ppb added iron. It may be seen from figure 3 that after 10 minutes exposure to the SC-1 solutions, there is an increase in OCP of about 50 mV and 180 mV when the iron level is increased from 0 ppb to 5 ppb and 100 ppb, respectively. Figure 4 shows the effect of iron addition to SC-1 solutions on the OCP of p-type [5 - 10  $\Omega\cdot\text{cm}$ ] silicon. After 10 minutes of exposure, the OCP of p-type silicon increased about 70 mV when the iron level was increased from 0 ppb to 5 ppb. The OCP exhibited a significant rise of about 380 mV when the iron level was increased to 100 ppb. It is apparent from figures 3 and 4 that as the level of iron contamination increased in the SC-1 solutions, the open circuit potential of n- and p-type silicon became increasingly more positive. It appears that the p-type silicon is more sensitive to iron contamination as compared to n-type silicon after 10 minutes exposure to SC-1. The OCP value for n<sup>+</sup>- and p<sup>+</sup>-type [0.005 - 0.02  $\Omega\cdot\text{cm}$ ] silicon was also evaluated in SC-1 solutions, and was found to increase by 250 to 300 mV when the iron level was increased from 0 to 100 ppb in SC-1.

An effort was made to determine from OCP measurements whether iron was incorporated into the oxide formed on silicon, or was adsorbed onto the oxide in the form of oxyhydroxides. For this experiment, n-type [2 - 4  $\Omega\cdot\text{cm}$ ] silicon was first exposed to SC-1 containing 0 ppb added iron, thus forming the native oxide. The SC-1 solution was then exchanged with an SC-1 solution containing 100 ppb added iron. The OCP vs. time data recorded during this step is shown in figure 5. Also shown in figure 5 is the OCP response of HF (last) treated silicon exposed to SC-1 containing 100 ppb added iron. It is evident from figure 5 that when the silicon pre-exposed to 0 ppb SC-1 is exposed to SC-1 containing 100 ppb iron, the OCP behavior is nearly identical to the behavior of a HF (last) sample initially exposed to 100 ppb SC-1. This result suggests that the increase in silicon OCP during exposure to iron contaminated SC-1 may be attributable to iron adsorption onto the native oxide surface, and not iron incorporation into the oxide, consistent with the findings of Tsuji et al. (4).

Electrochemical impedance analysis was conducted on n-, p-, n<sup>+</sup>, and p<sup>+</sup> type silicon samples exposed to SC-1 containing 0 to 100 ppb added iron. Figure 6 shows the Nyquist plots for p-type [5 - 10  $\Omega\cdot\text{cm}$ ] silicon exposed to SC-1 containing 0 or 100 ppb added iron measured after 60 minutes conditioning time at 50°C. The frequency range for the measurements was  $10^5$  to  $10^{-1}$  Hz. The polarization resistance ( $R_p$ ) values were calculated using a semicircle fit of the plotted data. The diameter of the semicircle (fit) is a good approximation of the polarization resistance [ohms], assuming that the silicon/solution interface can be represented by the equivalent circuit illustrated in figure 6.

Table I presents the polarization resistance values calculated for n- and p-type silicon from AC impedance measurements. The data in Table I indicates that the polarization resistance increased approximately 10 to 20 kohm for n- and p-type silicon when exposed to SC-1 solutions containing 100 ppb added iron at 50°C. The increase in polarization

resistance is consistent with the OCP results for SC-1 (100 ppb Fe) presented in figures 3 and 4, which indicate that the silicon surface becomes more noble upon exposure to iron contaminated SC-1. Heavily doped n<sup>+</sup> and p<sup>+</sup> silicon both exhibited an increase of about 20 kohms when exposed to SC-1 containing 100 ppb added iron.

From Table I, it may be seen that the polarization resistance values for n- and p-type silicon increased with decreasing temperature. For example, the polarization resistance of p-type silicon (SC-1, 0 ppb) was ~18 kohms at 50°C, and ~91 kohm at 25°C. It is likely that increasing SC-1 temperature enhances the dissolution of the oxide formed on silicon during SC-1 exposure, making it thinner and thus resulting in lower polarization resistance values. Table I also presents the polarization resistance values measured for p-type silicon showing the effect of increasing iron levels in SC-1 solution at 0, 20, 50, and 100 ppb at 50°C. In general, it was observed that the polarization resistance values for lightly or heavily doped n- or p-type silicon exhibited a detectable increase in polarization resistance up to iron levels of 50 ppb. Polarization resistance values for silicon typically plateaued out at added iron levels of 100 ppb in SC-1.

**Table I. Polarization resistance ( $R_p$ ) values measured for n- and p-silicon exposed to SC-1 containing different levels of added iron.**

p [5 – 10 Ω·cm]		Polarization Resistance ( $R_p$ , kΩ)*		
Temp (°C)	0 ppb	20 ppb	50 ppb	100 ppb
50	18 ± 3	25 ± 4	32 ± 4	34 ± 4
35	54 ± 16	-	-	150 ± 28
25	91 ± 8	-	-	266 ± 30

n [2 – 4 Ω·cm]		Polarization Resistance ( $R_p$ , kΩ)*		
Temp (°C)	0 ppb	20 ppb	50 ppb	100 ppb
50	12 ± 2	-	-	23 ± 3
25	27 ± 3	-	-	78 ± 5

\* 60 minute conditioning time

**Table II. Angle resolved XPS analysis of native oxide formed on p-type silicon after exposure to iron contaminated SC-1 solutions.**

Sample p-type (5 – 10 Ω·cm)	Fe 2p <sub>3/2</sub> Binding Energy (eV)	Relative Atomic % Composition through approximately 35 Å into the wafer surface*			
CLEAN** (60 min)		Fe	Si (oxide)	Si <sup>0</sup>	O
SC-1 (<1 ppb) 50°C	710.8	0.03	11.7	45.0	31.5
SC-1 (100 ppb) 50°C	711.0	0.27	12.3	34.0	34.0
1. SC-1 (100 ppb) 50°C	710.1	0.03	11.6	42.7	32.9
2. SC-2 (0 ppb) 50°C					

\* Cu, F, N, and C Atomic % not shown.

\*\* 10 minute DI rinse following intermediate and final cleans (25°C)

The results of XPS analysis conducted on p-type silicon exposed to different cleaning procedures are presented in Table II. The XPS analysis indicated no detectable Fe-Si bonding. All the Fe detected was in the form of  $\text{Fe}^{3+}$ , presumably in the form of  $\text{Fe}_2\text{O}_3$ .

Table III presents the results of a TXRF analysis of n- and p-type silicon samples. It may be seen that n-type silicon exposed to SC-1 exhibited an increase in surface iron contamination with increasing iron levels in SC-1. The iron contamination levels for n- and p-type silicon were similar after exposure to SC-1 containing 100 ppb added iron. Since the OCP response of silicon became more positive with increasing iron levels in SC-1, it may be concluded that increased levels of adsorbed iron rendered the oxide more noble. It is intriguing to note that although n- and p-type silicon had approximately the same amount of iron contamination levels after exposure to 100 ppb SC-1[15 minutes], the OCP response of p-type silicon was much more sensitive to iron levels. For samples pre-exposed to SC-1 [100 ppb] and treated in SC-2, iron levels were significantly reduced, indicating that iron was effectively removed by SC-2 exposure.

**Table III. Results of TXRF analyses conducted for n- and p-type silicon exposed to iron contaminated SC-1 solutions.**

CLEAN* (15 min)	Iron Contamination Level ( $\times 10^{12}$ atoms/cm $^2$ )	
	n-type	p-type
SC-1 (<1 ppb) 50°C	0.15 ± 0.05	-
SC-1 (20 ppb) 50°C	1.9 ± 0.5	-
SC-1 (100 ppb) 50°C	7.4 ± 0.6	4.9 ± 1.4
1. SC-1 (100 ppb) 50°C	0.12 ± 0.03	0.2 ± 0.1
2. SC-2 (<1 ppb) 50°C		

\*10 minute DI rinse following intermediate and final cleans (25°C)

The effect of SC-2 cleaning of n-type silicon samples pre-exposed to iron contaminated SC-1 was also evaluated using OCP vs. time measurements. Figure 7 shows the OCP vs. time response for silicon subjected to different pretreatments, and subsequently exposed to SC-2 at 50°C. In figure 7, it may be seen that that HF (last) treated silicon reaches an OCP of about -100 mV after 20 minutes of exposure to SC-2. In contrast, the sample A, pre-exposed to uncontaminated SC-1, exhibited an OCP of about 0 mV. This result indicates that the oxide formed on silicon in SC-1 has a more noble potential than the HF (last) silicon surface in SC-2.

The OCP response of the silicon sample B, pre-exposed to SC-1 containing 100 ppb added iron, is distinctly different from that of sample A. The OCP behavior of sample B exhibits a steady rise from about -50 mV up to +100 mV in the first 20 minutes of SC-2 exposure. Sample A exhibits an OCP response that stabilizes in about 5 minutes, and rises very gradually during the test period. The final potential of sample B is approximately 100 mV higher than sample A. According to the TXRF results presented in Table III, if SC-2

removes all the iron contamination that occurred on sample B, then the OCP of samples A and B should reach the same final value. The finding that the equilibrium value of OCP of sample B is higher than of sample A indicates that there is a difference in the nobility of the oxide on the samples. Leaching of iron from the surface of sample B somehow appears to leave a surface with a more noble OCP.

Air exposure (drying) of a sample following SC-1 treatment had an impact on its OCP response in SC-2. Figure 8 indicates that if a sample was tested in the dip cell by first exposing to SC-1 (100 ppb Fe), DI rinsed, and then exposed to SC-2, OCP values were 100 to 150 mV ( $t > 30$  minutes) with no air exposure between steps. When the sample was prepared in the cell but left to dry for 1 hour following SC-1 exposure and DI rinse, the OCP values in SC-2 increased up to about 200 mV. Samples exposed to SC-1 (100 ppb Fe) outside the cell, DI rinsed and dried for 1 hour, and placed in the cell for SC-2 exposure exhibited OCP values which were about 100 mV higher than samples pretreated inside the cell. It is evident that air exposure of SC-1 conditioned samples had an impact on electrochemical OCP results. The reasons for this are unclear at present.

## CONCLUSIONS

The detection of iron contamination onto silicon from SC-1 solutions was investigated using DC and AC electrochemical techniques. It was found that the open circuit potential of lightly or heavily doped n- or p-type silicon became increasingly more noble as iron levels in SC-1 increased from 0 to 100 ppb. The polarization resistance of silicon was found to increase 10 - 20 kohms when silicon was exposed to SC-1 containing 100 ppb added iron. The effect of doping did not significantly effect OCP vs. time or polarization resistance behavior. Electrochemical results for SC-1 exposures were consistent with TXRF results under the experimental conditions.

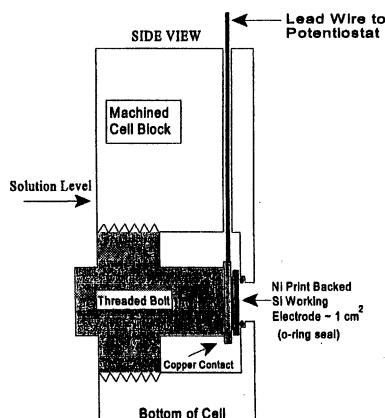
## ACKNOWLEDGEMENTS

The authors acknowledge financial support provided by Arizona SEMATECH Center of Excellence (AZ SCOE, # 95-BC-501) to carry out this work.

## REFERENCES

1. O. J. Anttila, M. V. Tilli, M. Schaekers, and C. L. Claeys, *J. Electrochem. Soc.*, **139**, 1180 (1992).
2. S. Dhanda, C. R. Helms, P. Gupta, B. B. Triplett, and M. Tran, *MRS Proc.*, **386**, 201 (1995).
3. C.R. Helms and H. Park, *MRS Proc.*, **315**, 287 (1993).
4. M. Tsuji, Y. Muramatsu, and N. Aoto, *Electrochem. Soc. Proc.*, **95-20**, 316 (1995).
5. O.M.R. Chyan, J. Chen, L. Chen, and F. Xu, *J. Electrochem. Soc.*, **144**, L17 (1997).
6. J.R. Macdonald, *Impedance Spectroscopy, Emphasizing Solid Materials and Systems*, John Wiley & Sons, Inc., (1987).

**Electrochemical Immersion Cell**



**ELECTROCHEMICAL TESTING SET-UP**

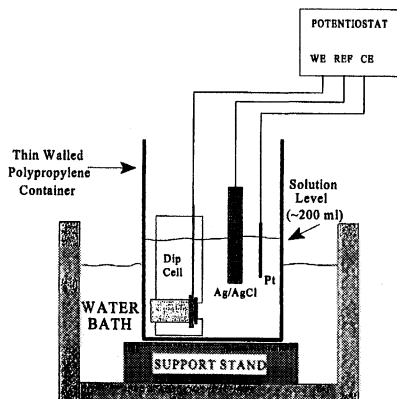


Fig 1. Schematic of electrochemical dip cell used for testing silicon in hot SC-1 and SC-2 solutions.

Fig 2. Schematic of electrochemical test set-up using the electrochemical dip cell.

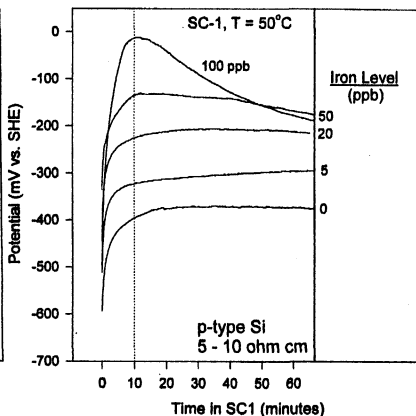
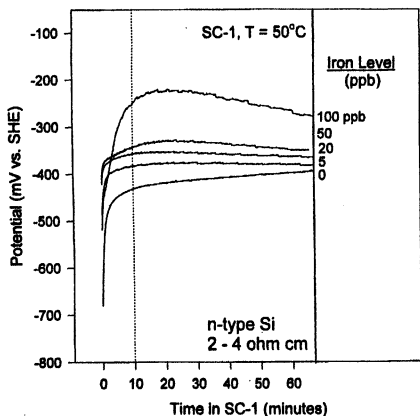


Fig 3. Open circuit potential vs. time curves for n-type silicon in SC-1 at 50°C containing ppb levels of added iron.

Fig 4. Open circuit potential vs. time curves for p-type silicon in SC-1 at 50°C containing ppb levels of added iron.

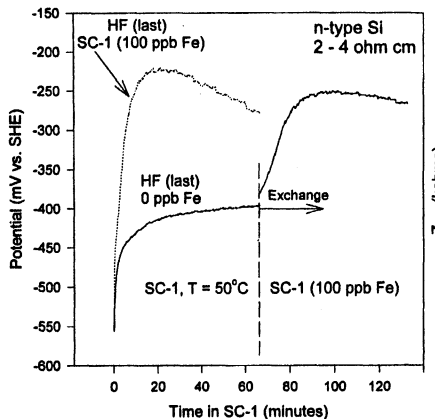


Fig. 5. Open circuit potential vs. time curves for n-type silicon exposed to SC-1 (0 ppb Fe). Solution then exchanged with SC-1 (100 ppb).

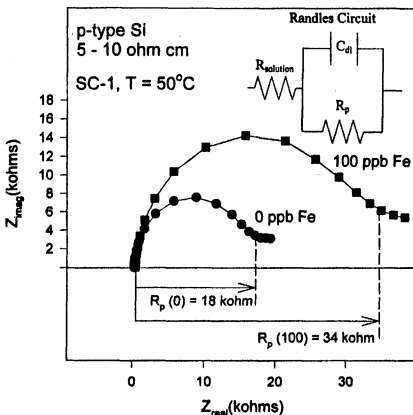


Fig. 6. AC impedance Nyquist plots measured for p-type silicon in SC-1 containing 0 or 100 ppb added iron.

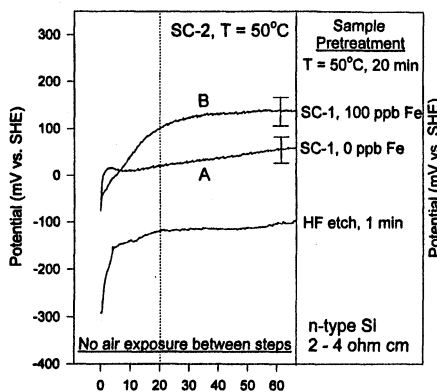


Fig. 7. Open circuit potential vs. time curves for n-type silicon pretreated as indicated and exposed to SC-2 at 50°C.

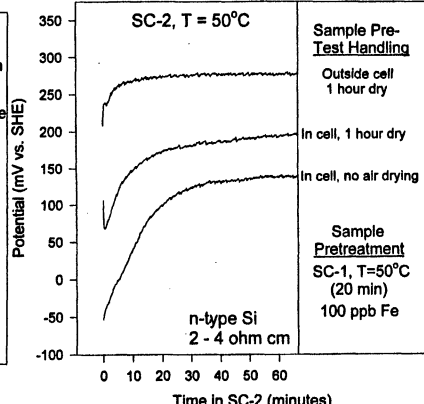


Fig. 8. Open circuit potential vs. time curves for n-type silicon in SC-2 at 50°C. Samples pretreated in SC-1 (100 ppb Fe).

# CHARACTERIZATION OF EVAPORATION IN A PURGED SYSTEM

Moshe Olim  
FSI International  
322 Lake Hazeltine Drive  
Chaska, MN 55318, USA

## ABSTRACT

The goal of the present investigation is development of a method to estimate the time interval required to evaporate a predetermined amount of liquid in a purged system. The physical parameters governing the evaporation process in a purged system are identified and collected in three nondimensional groups. The nondimensional equations are solved, and the time interval required to evaporate a given amount of liquid is presented as a function of the nondimensional groups.

## 1 Introduction

Some processes in the semiconductor industry include a step during which wafers are rinsed and dried by purging the processing chamber with dry gas. On one hand, it is imperative to the process performance that the wafers and the chamber be sufficiently dry thus suggesting long time intervals. On the other hand, it is desirable to minimize the process time. The desire to balance these contradicting requirements was the driving force behind the investigation presented herein.

## 2 Theory

In the present investigation it is assumed that: the gaseous phase is well mixed; the pressure in the chamber is constant; the volume of the liquid phase is negligible compared to that of the gaseous phase; the number of water droplets remains constant, and all droplets are of the same diameter at all times. With these assumptions it is possible to develop and solve the equations describing the process of evaporation of liquid in a purged system. Although the equations developed and solved below

apply to any combination of liquid and gas, the notation therein is simplified by the assumption that the liquid is water and that the gaseous phase consists of air and water vapor.

## 2.1 Mass Transfer

The first equation to be developed is that describing the evaporation rate. Assuming that the gaseous phase in the system is well-mixed and neglecting the solubility of the gas in the liquid, the process of evaporation is governed by the following differential equation which is a straight forward modification of equation (21.2-26) given in [1]:

$$\frac{dm_{H_2O,l}}{dt} = - \frac{dm_{H_2O,g}}{dt}|_{evaporation} = - M_{H_2O} k A \frac{P_{sat} - P_{H_2O}}{P_{tot} - P_{sat}} \quad (1)$$

where  $m_{H_2O}$  is the mass of water and the subscripts  $l, g$  indicate the liquid or gaseous phase,  $M_{H_2O}$  is the molecular weight of water,  $k$  is the mass transfer coefficient,  $A$  is the evaporation surface area,  $P_{H_2O}$  is the partial pressure of the vapor,  $P_{sat}$  is the saturation pressure, and  $P_{tot}$  is the total pressure. To estimate the time interval required to evaporate a given mass of liquid, equation (1) must be integrated until the liquid water mass is reduced to a sufficiently low level. This integration requires determination of the surface area across which the evaporation occurs, the partial vapor pressure in the system, and the mass transfer coefficient. The first of these three variables may be easily determined by assuming that during the evaporation process the number of droplets remains constant, thus leading to a simple relation between the area across which evaporation occurs, the droplet diameter  $D$ , and the mass of liquid water:  $A \approx 6 m_{H_2O,l}/D$ .

## 2.2 Vapor Pressure

In a well-mixed system the purge introduces dry gas at a given volumetric rate,  $Q$ , into the chamber whose volume is  $V$  while removing moist gas at the same rate  $Q$ . The effect of the purge on the amount of water in the gaseous phase may be described by the following differential equation:

$$\frac{dm_{H_2O,g}}{dt}|_{purge} = - Q M_{H_2O} C_{H_2O,g} = - Q M_{H_2O} \frac{P_{H_2O}}{R T} \quad (2)$$

where  $C_{H_2O,g}$  is the molar concentration of water in the gaseous phase,  $R$  is the universal gas constant, and  $T$  is the temperature.

The rate at which the vapor mass changes as a result of both purge and evaporation is the sum of the rates given in equations (1) and (2):

$$\frac{dm_{H_2O,g}}{dt} = \frac{dm_{H_2O,g}}{dt}|_{evaporation} + \frac{dm_{H_2O,g}}{dt}|_{purge}, \quad (3)$$

and the mass of the water in the gaseous phase is directly related to vapor pressure via the equation

$$m_{H_2O,g} = V M_{H_2O} C_{H_2O,g} = V M_{H_2O} \frac{P_{H_2O}}{R T} \quad (4)$$

which may be substituted into equation (3) yielding the following differential equation describing the rate of change of vapor pressure:

$$\frac{dP_{H_2O}}{dt} = \frac{k A R T}{V (P_{tot} - P_{sat})} P_{sat} - \left[ \frac{k A R T}{V (P_{tot} - P_{sat})} + \frac{Q}{V} \right] P_{H_2O}. \quad (5)$$

### 2.3 Mass Transfer Coefficient

In the present investigation it is assumed that the droplet diameter is significantly larger than the boundary layer. The appropriate evaporation model is therefore that which addresses evaporation of a droplet in a free stream. A correlation to evaluate the mass transfer coefficient,  $k$ , in a free stream is presented in [1] as equation (21.2-25):

$$k = \left[ 2 + 0.6 \left( \frac{D u_\infty}{\nu_g} \right)^{1/2} \left( \frac{\nu_g}{D'} \right)^{1/3} \right] \frac{C_g D'}{D} \quad (6)$$

where  $C_g$  is the molar concentration of the gas, and  $D'$  is the interfacial mass diffusivity.

Evaporation in a purged system may be fully described by solution of equations (1), (5), and (6) supplemented by relationships between the liquid water mass, droplet diameter, and area across which the evaporation takes place.

## 3 Nondimensionalization

The vapor pressure and time in equation (5) may be nondimensionalized with respect to  $P_{sat}$  and  $V/Q$ , respectively, to yield the following nondimensional variables:

$$\tilde{P} = \frac{P_{H_2O}}{P_{sat}} ; \quad \tilde{t} = \frac{Q t}{V} \quad (7)$$

substitution of which into equation (5) results in the following nondimensional equation:

$$\frac{d\tilde{P}}{d\tilde{t}} = \tilde{k} \alpha - (\tilde{k} \alpha + 1) \tilde{P}. \quad (8)$$

where

$$\tilde{k} = \frac{k A}{k_0 A_0} ; \quad \alpha = \frac{k_0 A_0 R T}{Q (P_{tot} - P_{sat})} \quad (9)$$

where  $k_0$  and  $A_0$  are the values of the mass transfer coefficient and the area based on the initial droplet diameter,  $D_0$ , and  $\alpha$  is constant.

A nondimensional liquid mass may be defined as  $\tilde{m} = m_{H_2O,i}/m_0$ , where  $m_0$  is the initial value of the liquid mass. Introduction of this nondimensionalization into equation (1) yields the following equation:

$$\frac{d\tilde{m}}{dt} = -\beta (1 - \tilde{P}) \tilde{k} \quad (10)$$

where

$$\beta = \frac{M_{H_2O} k_0 A_0 V P_{sat}}{m_0 Q (P_{tot} - P_{sat})} = \alpha \frac{M_{H_2O} V P_{sat}}{m_0 R T} . \quad (11)$$

An equation for  $\tilde{k}$  is obtained by multiplying the area  $A$  by equation (6), expressing the area in terms of liquid water mass, initial liquid water mass, and initial droplet diameter, and dividing the result by  $k_0 A_0$  which results in the following expression:

$$\tilde{k} = (2 + \gamma \tilde{m}^{1/6}) \frac{\tilde{m}^{1/3}}{2 + \gamma} \quad (12)$$

where the constant  $\gamma$  is defined as follows:

$$\gamma = 0.6 \left( \frac{D_0 u_\infty}{\nu_g} \right)^{1/2} \left( \frac{\nu_g}{D'} \right)^{1/3} . \quad (13)$$

The evaporation process is now fully described by equations (8), (10) and (12), which have three nondimensional variables:  $\tilde{P}$ ,  $\tilde{m}$ , and  $\tilde{k}$ , and three independent nondimensional parameters:  $\alpha$ ,  $\beta$ , and  $\gamma$ . To model the process the three equations must be solved until the nondimensional liquid mass,  $\tilde{m}$ , is reduced to a sufficiently low value.

## 4 Results

Equations (8), (10), and (12) constitute a system of three coupled equations for the variables  $\tilde{P}$ ,  $\tilde{k}$ , and  $\tilde{m}$ . These equations may be solved for any given combination of the parameters  $\alpha$ ,  $\beta$ , and  $\gamma$ . Their solution is depicted in Fig. 1 as a function of nondimensional time,  $\tilde{t}$ , for  $\alpha = \beta = \gamma = 1$ . In this simulation it was assumed that at the beginning of the process the gas was fully saturated with water, i.e.  $\tilde{P}_{(\tilde{t}=0)} = 1$ . The simulation was continued until the nondimensional mass,  $\tilde{m}$ , was reduced below  $10^{-2}$ , i.e. 99% of the liquid was evaporated.

The next step is to determine the time interval required to evaporate a given portion of the liquid water for various combinations of the three independent parameters,

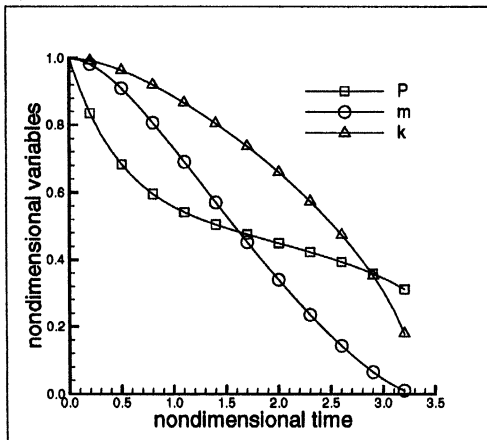


Figure 1: The three nondimensional variables,  $\tilde{P}$ ,  $\tilde{m}$ , and  $\tilde{k}$ , vs. nondimensional time for  $\alpha = \beta = \gamma = 1$ .

$\alpha$ ,  $\beta$ , and  $\gamma$ . A series of simulations were conducted for  $1 \leq \alpha \leq 10$ ,  $1 \leq \beta \leq 10$ , and  $1 \leq \gamma \leq 100$  using  $\tilde{P}_{(i=0)} = 1$ . The nondimensional time interval required to evaporate 95% of the initial liquid mass is shown in Fig. 2 for  $\gamma = 1$  and 100. The nondimensional time interval required to evaporate 99% of the initial liquid mass is shown in Fig. 3 for  $\gamma = 1$  and 100. The data shown in Figs. 2 and 3 indicate that the evaporation process is fairly insensitive to the value of the nondimensional variable  $\gamma$ .

#### 4.1 Example

To exemplify the method developed in the previous sections, consider a process chamber whose volume is 100 liter being purged with dry  $N_2$  at a flow rate of 10 liter/minute. The chamber is at atmospheric pressure and  $25^\circ C$ , and the initial humidity in the chamber is 100%. The initial water amount is 10g and the droplet diameter is 5mm. A mechanical stirring device creates a velocity of 2.5m/s in the vicinity of the droplets. Conversion of these data to SI units yields the following values:

$$V = 0.1 \text{ m}^3 ; Q = 167.e - 6 \text{ m}^3/\text{s} ; \quad (14)$$

$$T = 298 \text{ K} ; m_0 = 0.01 \text{ kg} ; u_\infty = 5 \text{ m/s} .$$

These data, in addition to the values of the kinematic viscosity of nitrogen,  $\nu_g = 1.5e - 5 \text{ m}^2/\text{s}$  (see [1]) and diffusion coefficient of water vapor in nitrogen,  $D' =$

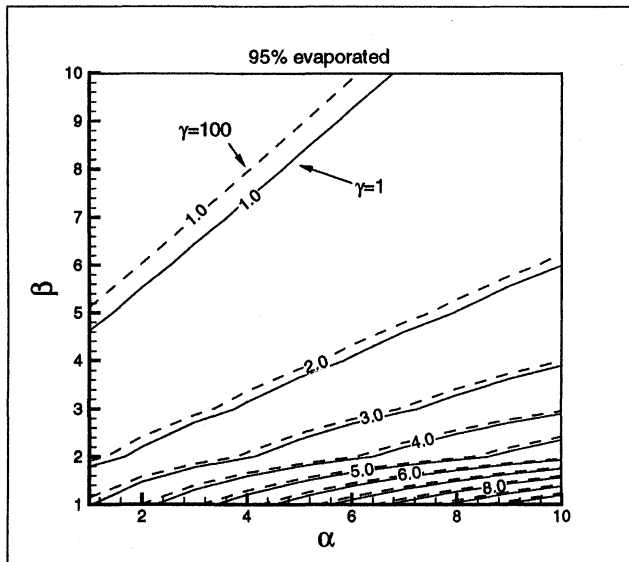


Figure 2: Nondimensional time required to evaporate 95% of the liquid mass for  $1 \leq \alpha \leq 10$ ,  $1 \leq \beta \leq 10$ ,  $\gamma = 1$  (solid lines), and  $\gamma = 100$  (dashed lines).

$3.6e - 5m^2/s$  (see [2]) yield the following nondimensional parameters:  $\alpha = 9.19$ ,  $\beta = 2.14$ ,  $\gamma = 12.9$  leading to  $\tilde{t} = 5.1$  from Figure 2. Thus, the time required to evaporate 95% of the water in the configuration described above is  $t = \tilde{t} \cdot V/Q = 5.1 \cdot 0.1/167.e - 6 = 3050$  s. The same values of  $\alpha$  and  $\beta$  lead to  $\tilde{t} = 5.5$  in Figure 3, i.e. the time required to evaporate 99% of the water is 3300 s. Increasing the temperature to  $35^\circ C$  yields  $\alpha = 9.72$ ,  $\beta = 3.72$  leading to  $\tilde{t} = 3.4$  in Figure 3. Thus, time interval required to evaporate 99% of the water is reduced to 2000 s.

## 5 Summary

A method to estimate the duration of the time interval required to evaporate a predetermined amount of liquid in a purged system has been developed. The equations describing the evaporation process have been developed and nondimensionalized thus collecting the governing physical parameters in three nondimensional groups. The equations were solved numerically, and the duration of the time interval required to evaporate a given amount of liquid in a purged system was presented as a function of the three nondimensional parameters.

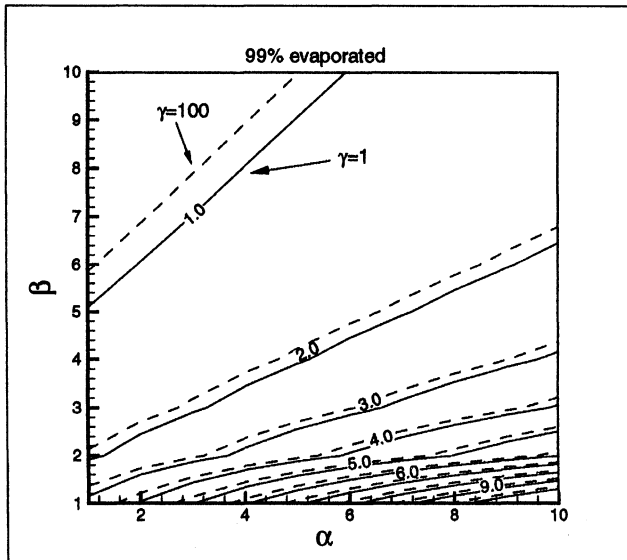


Figure 3: Nondimensional time required to evaporate 99% of the liquid mass for  $1 \leq \alpha \leq 10$ ,  $1 \leq \beta \leq 10$ ,  $\gamma = 1$  (solid lines), and  $\gamma = 100$  (dashed lines).

#### REFERENCES

1. R.B. Bird, W.E. Stewart, and E.N. Lightfoot, *Transport Phenomena*, John Wiley and Sons, NY, (1960).
2. A. Bejan, *Heat Transfer*, John Wiley and Sons, NY, (1993).

# APPLICATIONS OF NON-INVASIVE AC-SURFACE PHOTOVOLTAGE MONITORING IN INTEGRATED CIRCUIT CLEANING

**Kevin Torek, Whonchee Lee, David Palsulich, Larry Weston, Fernando González**  
**Micron Technology, Inc., 8000 S. Federal Way, M.S. 306,**  
**P.O. Box 6, Boise, ID 83707-0006**

## ABSTRACT

Efficient manufacturing of integrated circuits requires that wafer cleaning procedures consistently produce the desired state of the wafer surface. The ac-surface photovoltaic (ac-SPV) technique was used to characterize wafers subjected to different treatments and to monitor process tools. The responses of depletion width ( $W_d$ ) to variations in surface metallics, process variations, and mobile ions are reported. The results are compared with surface chemical analysis and Schottky diode leakage data. It is demonstrated that variations of  $W_d$  indicate metallic contamination, mobile ion contamination, and/or changes in process parameters. Schottky diode leakage and  $W_d$  profiles are found to be correlated. Responses that indicate out-of-control conditions with a high degree of certainty are identified.

## INTRODUCTION

There are many methods to monitor cleaning processes in integrated circuit manufacturing (1). Some very sensitive and powerful techniques are available but are typically off-line and destructive. However, surface potential and carrier lifetime measurements are relatively convenient, because they are non-contact and non-destructive. Surface photovoltaic, scanning Kelvin probe, and microwave reflectance are commercialized. In some cases, absolute data is obtained in the form of wafer maps. For example, Fe quantitation by SPV (2), metallic species identification by laser microwave photoconductive decay with injection level spectroscopy (3), and mobile ion determination by corona-oxide-semiconductor testing (4) yield absolute data.

The potential use of relative measurements for process monitoring is also widely applicable. Such measurements are possible with minimal invasion. However, baseline measurements are required to interpret relative measurements. Cleaning processes modify the Si depletion width and surface lifetime, leaving behind particular "fingerprints." The ac-surface photovoltaic (ac-SPV) technique detects the changing process conditions as changes in these fingerprints. Ideally, a catalog of responses to known variations would allow control limits to be established for virtually any process. In reality, reliable indication of yield-threatening conditions by ac-SPV is not always practical. Conditions that could be either inconsequential or threatening may result in the same ac-SPV

responses in some cases. In others, the ac-SPV may not be a reliable threat indicator. Therefore, reliable baseline measurements are required to understand the gage capabilities of ac-SPV.

This paper reviews the ac-SPV responses we have observed using a Surface Charge Profiler (SCP) (5) and compares them with other measurements. Responses to metallics and mobile ion contamination and to varying process conditions are discussed. For the electrical measurements, Schottky diode leakage was chosen as a measure of the condition of the Si surface. In fact, a leakage problem was associated with one of the tools in these experiments. Schottky diodes were used to investigate the leakage further.

## EXPERIMENT

The SCP uses a collimated, chopped, 2-mm diameter beam of 450 nm light (penetration depth 0.4  $\mu\text{m}$ ) to oscillate the surface barrier height. Typical ac-SPV wafer maps had readings for >1700 locations per wafer. Test wafers were p-type, <100>, 200 mm Cz and EPI. Several substrates were used for the experiments. Some were oxidized, some were native oxide wafers, and some were implanted wafers for the different experiments. Metallic contamination was added by dipping wafers in 10 ppb solutions of Cu, Mg, and Fe in deionized  $\text{H}_2\text{O}$  and adjusting the pH with HCl and NH<sub>4</sub>OH. Metallics were also added by running wafers through contaminated process tools. Surface photovoltage responses to changing the process procedures were also observed, including running dilute HF etches with and without degassification, and changing the wafer drying parameters. Mobile ions were added by human contamination. The ac-SPV measurements were correlated with total reflectance X-ray fluorescence (TXRF), inductively coupled plasma mass spectroscopy (ICPMS), and Schottky diode leakage. The ICPMS and TXRF measurements were performed using vapor phase decomposition and droplet surface etching.

## RESULTS AND DISCUSSION

Figures 1, 2, and 3 summarize the results of ac-SPV measurements on RCA-cleaned native oxide wafers dipped in separate 10 ppb solutions of Cu, Fe, and Mg and then rinsed and allowed to air dry. The concentration of metallics deposited from solution was controlled by adjusting the pH with HCl and NH<sub>4</sub>OH. Figure 1 shows the increase in depletion width ( $W_d$ ) with increasing Cu contamination. Cu diffuses quickly in Si and can de-activate B (6). The increase of  $W_d$  in figure 1 may be attributable to de-activated B. The response of  $W_d$  to Fe contamination is shown in figure 2.  $W_d$  does not respond clearly until the Fe contamination reaches  $>5 \times 10^{11} \text{ cm}^{-2}$ , above which it decreases to ~0.1x its original value. This response may be due to the state in which the deposited Fe is measured. Iron oxides are negatively charged (7), (8) and will decrease  $W_d$ . Mg contamination  $>1 \times 10^{11} \text{ cm}^{-2}$  also results in low  $W_d$ , as shown in figure 3.

The high sensitivity of this measurement (phase amplifier) allows detection of many different process and procedural changes. For example, figure 4 shows how different dryers result in different  $W_d$  patterns. These patterns are consistent from run to run. Dryer C in figure 4 shows very low  $W_d$ . This dryer is used to rinse metallized wafers. Figure 5 shows that, of 23 monitored tools, test wafers run in those used to treat metallized wafers always come out with low  $W_d$ . These systems are known to leave significant concentrations of Al, Fe, or both on the monitor wafers. In addition to metallics, changes in drying recipe parameters are also detected. Figure 6 shows how a drying recipe parameter change affected  $W_d$ .

One of the tools in figure 5 is associated with a device leakage problem. One of the differences between the problem tool and similar ones that do not have the problem is the use of point-of-use degassification. After performing a comprehensive set of other tests (bulk and surface chemical analyses, roughness measurements, and a legion of short-loop electrical tests), it was decided to investigate the degassifier.

In HF cleaning, reduction of dissolved O<sub>2</sub> to <50 ppb improves particle performance and surface smoothness (9). Table I illustrates particle performance and surface roughness measured with and without degassification (dissolved O<sub>2</sub> without degassification ~ 3ppm).

Table I. Degassifier Reductions of Particle Addition and Surface Roughening during HF Etching

Degassifier	Particle Delta (>0.16 μm)	rms Roughness (Å)	
		Center	Edge
ON	36	1.14	1.11
OFF	55	1.32	1.32

Ac-SPV measurements show that degassification also affects the Si surface electrical parameters. The features on the ac-SPV maps were reflected in the Schottky diode leakage data as well. Test wafers for this experiment were prepared by implantation through a screen oxide (BF<sub>2</sub>, 65 KeV, 1E13, 350Å), dopant activation, stripping the screen oxide, and RCA cleaning. Following the clean, the wafers were immersed for different times in dilute HF with the water either degassified or not. Figure 7 shows the depletion widths measured after soaking in 80:1 H<sub>2</sub>O:HF at 30°C. Soaking times in HF used were those that would etch either 1500 or 500Å of thermal SiO<sub>2</sub>. The ac-SPV was measured both before and after a rapid thermal anneal. The greatest effect of RTA on  $W_d$  was with degassification. With degassification, RTA drives  $W_d$  to lower values. Degassification increases  $W_d$  measured before RTA, but after RTA the same wafers have lower  $W_d$ . Longer soaking enhances the trends seen in figure 7. The trends were consistent on repeating the experiment.

Aluminum Schottky diodes were measured immediately following dot deposition. Figure 8 summarizes the leakage data (after RTP) by the circumferential average leakage at 2.5 V. The greatest distinction between degas/no degas in figure 8 is for the shorter

soaking time, with the degas showing higher overall leakage. This coincides with the lower post-RTP  $W_d$  (higher pre-RTP  $W_d$ ) for the degassified splits in figure 7. The leakage profile of the 1500Å soaking time was also changed by degassification. The changes are more dramatic for the longer soaking time. The trends in the leakage data were also consistent on repeating the experiment. The Schottky diode barrier is strongly affected by the cleanliness of the wafer surface and the porosity of any native oxide that reacts with the deposited Al. Thus, the surface condition due to degas/no degas and the soaking times treatments can be an indicator of its effects on the Si surface and the chemical oxide.

Besides the wafer-to-wafer correlation between  $W_d$  and diode leakage, the within-wafer data correlates as well. Radial variation of  $W_d$  coincides with that of the leakage. For example, figure 9 shows the radial variation of  $W_d$  for the 500Å, no degas split. The radial pattern is similar to the Schottky diode leakage in figure 8. This within-wafer pattern similarity between  $W_d$  and Schottky diode leakage holds across the four splits. The center-to-edge wafer uniformity indicates that the outer parts of the wafer show either a thinner and/or more porous chemical oxide from the clean operation.

While metallics such as Fe, Mg, and Al add negative charge, mobile ions add positive charge. Monitor wafers with thermal  $\text{SiO}_2$  were used to test the ac-SPV sensitivity to mobile ions. Figure 10 shows that there is hardly any response of  $W_d$  to mobile ion contamination of the oxide surface and that a rapid thermal drive-in shifts the charge centroid of the contamination such that  $W_d$  is increased.

## CONCLUSIONS

Ac-SPV senses process changes. Very low depletion widths ( $W_d$ ) indicate surface concentrations  $>1\times10^{11} \text{ cm}^{-2}$  of Fe, Mg, and/or Al contamination. Cu contamination of native oxide wafers increases  $W_d$ . Degassification during HF cleaning increases  $W_d$  and Schottky diode leakage. Mobile ions driven in from an oxide surface increase  $W_d$ . Fe contamination  $<1\times10^{11} \text{ cm}^{-2}$  on native oxide wafers inconsistently affects  $W_d$ . Finally,  $W_d$  is affected by many process changes, but very low  $W_d$  consistently indicates substantial surface concentrations of Fe, Mg, and/or Al.

## ACKNOWLEDGEMENTS

Special thanks to Mark Durcan and Trung Doan for the support in this work.

## REFERENCES

1. F. Tardif, J. P. Joly, and D. Walz, Proc. Conf. ALTECH 95, Den Haag, The Netherlands, Sept. 28-29, 1995.
2. W. B. Henley, Proc. SPIE, **2638**, 178 (1995).
3. Semilab Semiconductor Physics Laboratory RT., Foti ut 56, H-1047 Budapest, Hungary, WT-85 Lifetime Scanner Technical Note.
4. G. Horner and M. Peters, European Semiconductor, **17**, S3-S4 (1995).
5. E. Kamieniecki, P. Roman, D. Hwang, and J. Ruzylo, Proc. Second Intern. Symp. on Ultra-Clean Processing of Silicon Surfaces UCPSS'94, M. Heyns, ed., p. 189, Acco, Leuven (1994).
6. H. Prigge, P. Gerlach, P.O. Hahn, A. Schnegg, and H. Jacob, J. Electrochem. Soc., **138**, 1385 (1991).
7. J. Kato and Y. Maruo, J. Electrochem. Soc., **139**, 1756 (1992).
8. H. Shimizu and C. Munakata, Appl. Phys. Lett. **62**, 276 (1993).
9. G. N. DiBello, S. T. Bay, C. F. McConnell, J. W. Parker, and E. A. Cheney, Proc. Second Intern. Symp. on Ultra-Clean Processing of Silicon Surfaces UCPSS'94, M. Heyns, ed., p. 23, Acco, Leuven (1994).

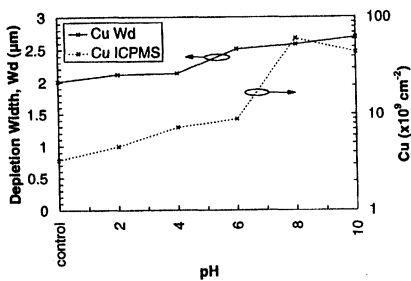


Figure 1. Increased depletion width due to Cu contamination.

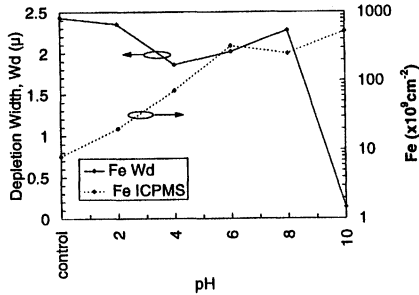


Figure 2. Fe surface contamination sensitivity.

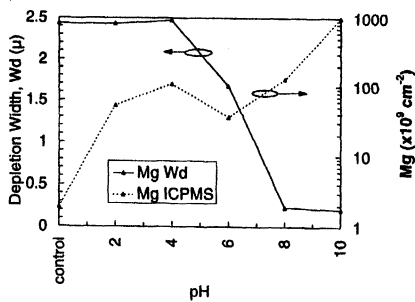


Figure 3. Mg surface contamination sensitivity.

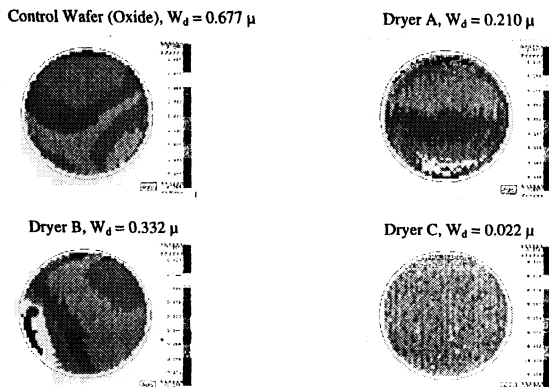


Figure 4. Depletion width maps showing characteristic "fingerprints" of different dryer types.

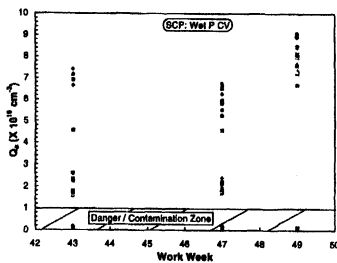


Figure 5. Low surface charge (depletion width) due to Fe and/or Al contamination.

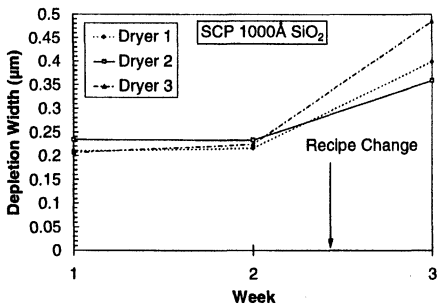


Figure 6. Depletion width alteration caused by a drying recipe change.

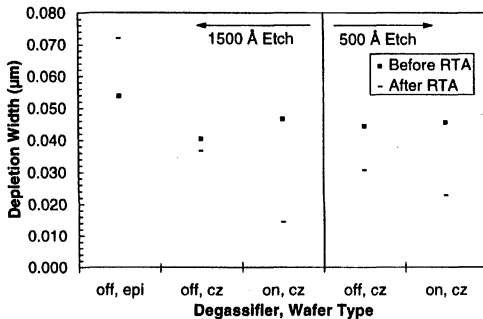


Figure 7. Effect of degassification during HF etching on depletion width.

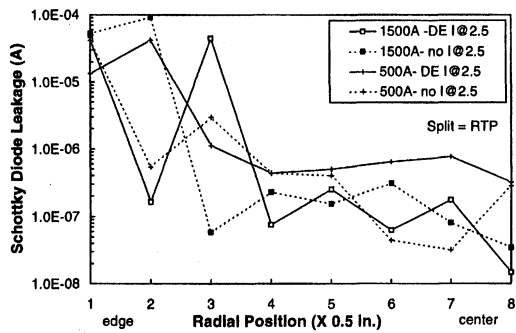


Figure 8. Al Schottky diode leakage radial distributions.

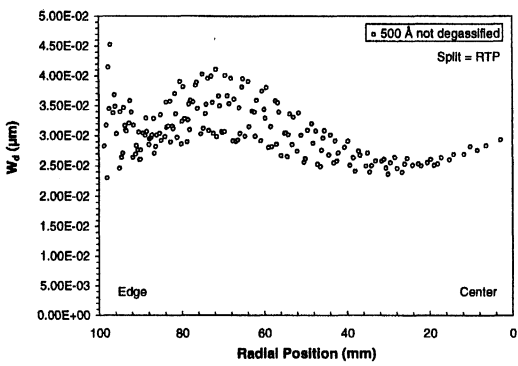


Figure 9. Depletion width radial distribution.

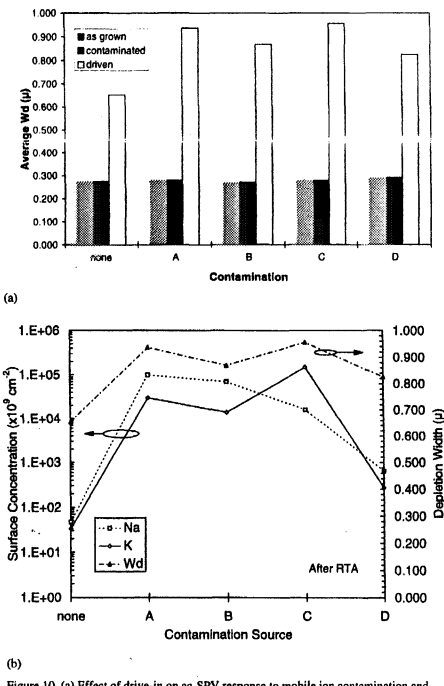


Figure 10. (a) Effect of drive-in on ac-SPV response to mobile ion contamination and (b) correlation between ac-SPV and mobile ion density.

# **MONITORING OF NOBLE METALS IN HF BASED CHEMISTRIES BY μ-PCD, SPV, SCI AND SCP**

A. Danel<sup>(1)</sup>, U. Straube<sup>(1)</sup>, G. Kamarinos<sup>(2)</sup>, E. Kamieniecki<sup>(3)</sup> and F. Tardif<sup>(1)</sup>

(1) Gressi-Leti-CEA/G, 17 rue des Martyrs , 38054 Grenoble Cedex 09, France

(2) ENSERG, LPCS, rue des Martyrs, BP 257, 38016 Grenoble Cedex 1, France

(3) QC Solutions, Inc., 150-U New Boston St., Woburn, MA 01801, USA

Traces of noble metals in HF based chemistries are studied using μ-PCD (microwave-Photo Conductivity Decay), SPV (Surface Photo Voltage), SCI (Surface Charge Imager) and SCP (Surface Charge Profiler) techniques. The increase of the surface recombination velocity of conventional Si wafers with the level of metallic contamination and associated roughness is used in μ-PCD and SPV. The SCP measures the surface lifetime and the surface depletion layer width simultaneously. Here, the change of the active doping concentration in the near surface region due to the noble metals is used to monitor very low levels of metal contamination. The very high illumination used by the SCI to measure the surface potential of the wafers restores the initial value of the doping and therefore contaminations can not be detected. Using the μ-PCD and the SCP, on-line monitoring allows low limit detection in 1% HF better than 1 ppb for silver and gold and 10 ppb for copper.

## **INTRODUCTION**

Monitoring of noble metals in HF is critical because of their detrimental effect on device yield and performance<sup>(1),(2)</sup>. The conventional spectroscopic methods such as ICPMS (Inductive Coupled Plasma Mass Spectrometry), AAS (Atomic Absorption Spectrometry) or TXRF (Total X-Ray Fluorescence) are sensitive to noble metals but slow and expensive. On the other hand the μ-PCD, SPV, SCI and SCP techniques are simple and non destructive tools which enable on-line characterization of wafer surface properties in the IC industry<sup>(3),(4),(5),(6)</sup>. Previously, the main work performed in this field focused on measurements of copper in the bulk<sup>(7),(8),(9)</sup> and subsurface region<sup>(10)</sup>. The degradation of surface recombination velocity as measured by μ-PCD was used to detect roughness<sup>(11)</sup> as well as noble metals<sup>(12)</sup>. This paper focuses on monitoring of these noble metals by measuring their effect on the silicon surface and near surface regions. The selective sensitivity of each method analyzed in this work is studied for its advantages in industrial applications.

## **GENERAL CONSIDERATIONS**

The tests described below were performed at LETI facilities on CZ (100), p-type 4" Si wafers with a bulk boron concentration of 6 to  $9.5 \cdot 10^{14}$  at/cm<sup>3</sup>. 1 ppb grade level chemicals were used. The wafers were cleaned in sulfuric peroxide mixture : CARO 3/1 140°C 10 min. rinsed and dried, immersed for 10 minutes in 1% or 20% HF spiked with Ag, Au, Cu or Pt and then measured by μ-PCD, SPV, SCI and SCP.

**μ-PCD** measures the decrease of the excess carrier density after short laser pulses<sup>(13)</sup>. This method is used widely on-line to characterize the bulk carrier lifetime of silicon substrate but can also be used to determine the surface recombination velocity (S). If the recombination is due mainly to the surface, Derhacobian's<sup>(14)</sup> equation can be used to calculate S from the surface lifetime  $\tau$  :

$$S = \sqrt{\frac{D}{\tau}} \cdot \tan\left(\frac{d}{2\sqrt{D\tau}}\right) \quad [1]$$

where d is the sample thickness and D is the effective carrier diffusion constant. A commercial system (WT-85 Lifetime Scanner) from SEMILAB was used to measure S under the condition of medium excitation (1.2 10<sup>14</sup> photons/cm<sup>2</sup>/s).

In the constant photon flux **SPV** method<sup>(15)</sup>, minority carrier diffusion length in the bulk L, and surface recombination velocity S are determined from the dependence of the surface photovoltage on the light penetration depth, under the condition of low excitation (10<sup>11</sup> to 10<sup>13</sup> photons/cm<sup>2</sup>/s). The same SPV apparatus is used under high excitation level<sup>(4)</sup> to measure the surface potential Vs. The **SCI** method uses 10<sup>19</sup> photons/cm<sup>2</sup>/s which lead to the flat bands condition. In this condition the SPV signal corresponds to Vs. Using Poisson's equation and Gauss's theorem, the surface charge (Qs) can be calculated from the active doping concentration in the surface space charge layer (Nsc) and the measured value of Vs<sup>(16)</sup>. A commercial system (SPV Station) from Semiconductor Diagnostics Inc. was used to measure S under condition of low excitation and Vs under condition of very high excitation.

The **SCP** is a non-contact and non-invasive method based on the surface photovoltage induced by a low intensity (10<sup>10</sup> to 10<sup>13</sup> photons/cm<sup>2</sup>/s) modulated light<sup>(17)</sup>. The penetration depth of the 450 nm blue light into Si is very shallow (< 0.4 μm) enhancing the sensitivity of this method to the surface and near surface properties : Qs, Nsc and the surface lifetime T. From the analysis of the real and imaginary components of the ac-SPV signal, the 1/T and the depletion layer width W are simultaneously determined. Under depletion conditions the charge density in the depletion layer is calculated as Qsc=-qNscW. As the surface of the semiconductor is electrically neutral, Qsc neutralizes the surface charge density Qs : Qsc=Qs. 1/T is given by equation [2] for a wafer in depletion state :

$$\frac{1}{T} = aSWN_{sc} \exp\left(\frac{-aW^2N_{sc}}{2}\right) \quad [2]$$

where  $a=q^2/(kT_p\epsilon)$  ,  $\epsilon$  is the silicon permittivity, q the elementary charge and  $kT_p/q=26$  mV at room temperature.

Under inversion conditions W is used to calculate Nsc : W reaches its maximum value Wmax, related to Nsc by equation [3]<sup>(16)</sup> :

$$W_{max} = \sqrt{\frac{4\epsilon kT_p \ln(N_{sc} / n_i)}{q^2 N_{sc}}} \quad [3]$$

where  $n_i$  is the intrinsic carrier concentration in the silicon. W and 1/T presented in this paper were measured with a commercial system (SCP Model 100) from QC Solutions.

## EFFECTS OF NOBLE METALS ON Si SURFACE PROPERTIES

Noble metals in HF based chemistries can oxidize the bare silicon since they have a higher electrochemical potential than  $\text{SiH}/\text{H}_2\text{SiF}_6$  <sup>(18),(19)</sup>. This effect leads to metal deposition under zero oxidation degree and to an anisotropic dissolution of the silicon. This causes a strong roughening of the surface. The possible electrical effects of this reaction are summarized below :

- Non-ionic deposition of metals : no change of  $Q_s$  is expected, increase of S reported earlier<sup>(4),(12)</sup>.
- Associated roughness : increase of S<sup>(11),(12)</sup>.
- Other effects directly or indirectly induced by noble metals (deep centers, pairing with boron, precipitation, ...) : possible modification of S,  $Q_s$  and  $N_{sc}$ . Some of these effects have been studied in HF by Lagowski et al. using the SPV and SCI<sup>(4)</sup> and during polishing by other authors<sup>(7),(8),(9),(10),(20)</sup>.

## DETECTION OF NOBLE METALS IN HF : TYPICAL RESULTS OBTAINED WITH $\mu$ -PCD, SPV, SCI AND SCP

In this approach, how the different methods can be used for this application, we intentionally limited the presented results to 1% HF spiked with Ag or Cu (figures 1 to 8). The same behaviour was observed for Au and Pt and for more concentrated HF. Of course the sensitivity depends on the noble metal and the dynamics are greater in diluted HF than in concentrated HF<sup>(6),(12)</sup>.

### $\mu$ -PCD

As demonstrated by Tardif et al.<sup>(12)</sup> both deposited noble metals and the associated roughness act as recombination centers. Roughness could behave like microstructures. In order to achieve the highest sensitivity and a good stability the HF dip has to be performed after a CARO<sup>(12)</sup>. Furthermore a high bulk lifetime is necessary to approximate the measured lifetime to the surface lifetime. This condition is reached for the conventional CZ wafers from the box used in this study for which lifetimes as high as 1600  $\mu$ s are currently measured with a proper surface passivation ( $I_2$ ). In figure 1 S calculated with equation [1] shows strong dependence on Ag and Cu contamination. This indicates that  $\mu$ -PCD used as described above enables HF bath purity to be monitored in industrial applications.

### SPV

In principle, the SPV is sensitive to the same effects as  $\mu$ -PCD. But as shown in figure 2 no changes of S are observed. This difference could be attributed to the low level of excitation used in SPV. Under the medium illumination level used in  $\mu$ -PCD, the surface is not in its equilibrium state and the recombination centers (noble metals and surface roughness) become active recombination centers. The surface states activation is affected by the different band bendings so that S measured by SPV and  $\mu$ -PCD are not the same. Since SPV and SCP measurements before and just after  $\mu$ -PCD are the same, modification of surface defects due to illumination during  $\mu$ -PCD measurements can be rejected.

## SCP

The SCP is expected to be sensitive to the degradation of S. However, and probably for the same reasons as SPV (very low excitation),  $1/T$  measured using SCP shows weak dependence on Cu contamination (Figure 3). On the other hand, a high sensitivity is reached for W (Figure 4). Since the surface of p-type wafers after a 10 min. 1% HF dip is in inversion<sup>(10),(21)</sup>, the increase of W can be attributed to a decrease in the active doping concentration in the near surface region (see equation [3]). The Nsc decay with the increase of metallic contamination can involve boron deactivation by pairing. Here pairs are labelled B-X, where X represents the defect(s) due to noble metals.

The temperature dependence of boron reactivation is studied for different contaminated wafers : wafers from the box where the boron deactivation is dominated by its interaction with hydrogen introduced during wafer polishing<sup>(10),(20)</sup>, and the wafers contaminated with Ag, Cu or Au where the boron deactivation could be due to unknown B-X pairs. Wafers were annealed on a hot plate in clean-room ambient air for 10 minutes at various temperatures. Nsc measurements using the SCP were performed after a 2 min. 1% HF dip in order to put surfaces in inversion. For all the noble metals the wafers behave the same way (Figure 5). The initial value of Nsc depends on the noble metal contamination. The final value after 200°C annealing is equal to the bulk doping concentration. This result suggests that the B-X defects might be the same whatever the noble metal. Since similar results are also obtained for untreated wafers from the box, X could be attributed to hydrogen. Arrhenius plot determined activation energy Ea of 1.19 eV was similar for out-of-the-box untreated wafers and noble metal contaminated wafers (Figure 6). In spite of the limited accuracy of measurements (due to the hot plate regulation  $\pm 3^\circ\text{C}$ ) Ea determined here is in good agreement with the previously reported experimental value for boron-hydrogen complex :  $Ea=1.28 \text{ eV}$ <sup>(10),(22)</sup>. Thus we can conclude that in the p-type wafers used in this study, observed boron deactivation is dominated by its interaction with hydrogen. This hydrogen is introduced during HF dip thanks to the noble metals deposited on the Si surface.

Figure 7 demonstrates the necessity of the CARO treatment before the HF dip. The SCP sensitivity increases if boron doping is first reactivated. The best industrial way to dissociate H-B pairs is a conventional CARO bath at 140°C for 10 min. Therefore this process also guarantees the necessary stability for industrial applications<sup>(12)</sup> (Figures 9 and 10).

## SCI and SCP

The SCI is sensitive to Qs and Nsc. But as can be seen in figure 8 at low frequency the SCI response is quite flat. As the measurements are made under a very high illumination level, the bulk value of doping concentration in the subsurface region is expected to be restored by the separation of B-X pairs. As noble metals deposit in HF with a zero oxidation degree both Qs and Nsc are constant, and hence Vs as well. For SCP and SCI a decrease in W and Vs is measured for high levels of contamination. It indicates a change of chemical state of the species involving the noble metals at the surface and/or in the near surface region. Furthermore this change corresponds to an increase of S as measured by SPV and decrease of T as measured by the SCP.

As shown in figure 8, a low contamination level can be detected by the SCI method by a frequency analysis of Vs measurements. Indeed, if the surface passivation after CARO plus HF is very good, then at a high frequency, carriers do not have enough time to recombine totally during one illumination cycle. Thus, Vs is underestimated and for a given frequency this systematic error decreases with the level of contamination. This result is consistent with the increase of S under high illumination as seen by  $\mu$ -PCD.

The sudden decrease of W (SCP) and Vs (SCI) for high contaminations with silver and copper is studied in figures 9 and 10. TXRF measurements allowed us to estimate this threshold at about  $10^{13}$  at/cm<sup>2</sup>. In this range, noble metals deposited first with zero oxidation degree are not stable. As can be seen in figures 9 and 10 it takes only a few minutes for silver to change and a few hours for copper.

### HF BATHS MONITORING WITH $\mu$ -PCD AND SCP

$\mu$ -PCD and SCP have been used with procedures described above to monitor HF baths cleanliness. Assuming that dispersion of measurements for the same level of contamination is Gaussian, the criterion of non-overlapping of the confidence intervals at 99% of probability is used to give the Low Limit Detections (LLD) in table 1.

Metal	detection limit in 1% HF		detection limit in 20% HF	
	SCP	$\mu$ -PCD	SCP	$\mu$ -PCD
Silver	< 1 ppb	< 1 ppb	< 1 ppb	< 1 ppb
Gold	< 1 ppb	< 1 ppb	< 1 ppb	< 10 ppb
Copper	1 ppb	< 10 ppb	< 100 ppb	< 100 ppb
Platinum	1 ppb	< 100 ppb	< 100 ppb	< 100 ppb

Table 1 : LLD of noble metals in 1% and 20% HF as measured by SCP and  $\mu$ -PCD.

Figures 11 and 12 demonstrate 1% HF bath monitoring done by SCP and  $\mu$ -PCD. It shows that 0.5 ppb of silver can be easily detected.

### CONCLUSION

Under medium ( $\mu$ -PCD) and high (SCI) levels of optical excitation, the surface recombination velocity increases with the noble metal concentration in HF.  $\mu$ -PCD using first a conventional CARO and then a 10 min. HF dip allows monitoring of HF bath purity via S. LLD with better than 1 ppb for silver and gold and 10 ppb for copper are obtained. Detection of noble metals in HF by SCI with sophisticated frequency analysis is possible but has not been studied in this work which mainly focuses on industrial applications.

The mechanism responsible for the change of the active doping concentration in the near surface region during HF dip spiked with noble metals was investigated. The first evaluation presented here suggests that noble metals deposited on Si surface are responsible for hydrogen contamination of the silicon. Then Nsc decrease is due to B-H pairing. Under low illumination (SPV and SCP) S is relatively constant and the SPV method is not sensitive enough to noble metals in HF for industrial monitoring. On the other hand H-B pairs are not dissociated during SCP measurements and traces of noble metals can be detected by a decrease of Nsc. The SCP and  $\mu$ -PCD methods give similar LLD's. The sensitivity of the SCP method is improved by a previous CARO treatment which reactivates boron doping.

LLD obtained with  $\mu$ -PCD is limited by the wafer to wafer dispersion. Reuse of the test wafers optimizes the monitoring cost and solves the problem of the initial dispersion of lifetime values for different new wafers. Whereas the initial lifetime values are lower, homogenization of uncontaminated wafers finally leads to the same detection limits. Using the SCP method makes monitoring free of wafer to wafer dispersion possible. Because noble metals in HF induce a change of the active doping concentration, and because the initial value of Nsc can be restored by simple thermal or optical treatment, a change of Nsc

between these two SCP measurements is related to the HF bath purity. The same test wafers can be used several times, and LLD better than the one presented here should be obtained.

### ACKNOWLEDGEMENTS

The authors thank K. Barla for measurements on SDI equipment, C. D'Assenza for TXRF measurements and U. Straube for his important work on  $\mu$ -PCD and SCI.

### REFERENCES

- [1] H. Wendt et al, J. Appl. Phys. 65, p. 2602, 1989.
- [2] A. Correia et al, J. Appl. Phys. 78, p. 6543, 1995.
- [3] T. S. Horanyi et al, J. Electrochem. Soc., Vol. 143, No. 1, January 1996.
- [4] J. Lagowski et al, J. Electrochem. Soc., Vol. 140, No. 4, April 1993.
- [5] J. Ruzyllo et al, SPIE's Microelectronic Manufacturing Symp., Austin, October 1996.
- [6] A. Danel et al, 192nd ECS meeting, Paris, August 1997.
- [7] P. Wagner et al, "Semiconductor Silicon-90", pp 675, 1995.
- [8] A. Mesli and T. Heiser, Physical Review B, Vol. 45, No. 20, May 1992.
- [9] A. A. Istratov et al, "Influence of interstitial copper in p-type silicon on diffusion length and lifetime of minority carriers" Submitted to Appl. Phys. Lett.
- [10] P. Roman et al, "Surface dopant concentration monitoring using non-contact Surface Charge Profiling (SCP)" Submitted to J. of Appl. Phys.
- [11] H. Daio and F. Shimura, Jpn. J. Appl. Phys., Vol. 32, p. 1792, December 1993.
- [12] F. Tardif et al, 192nd ECS meeting, Paris, August 1997.
- [13] A. Sanders and M. Kunst, Solid State Electr., Vol. 34, No. 9, p 1007, 1991.
- [14] N. Derhacobian et al., J. Appl. Phys., Vol. 76, No. 8, October 1994.
- [15] J. Lagowski et al., Semicond. Sci. Technol., Vol. 7, A185, 1992.
- [16] S. M. Sze, "Physics of Semiconductor Devices", John Wiley & Sons, New York, 1981, chapter 7.
- [17] E. Kamieniecki and G. Faggiato, "Handbook of Semiconductor Cleaning Technology", p. 497-536, Ed. W. Kern, Noyes Publ., 1993.
- [18] L. Mouché et al., J. Electrochem. Soc., Vol. 142, No. 7, July 1995.
- [19] H. Morinaga et al., IEICE Trans. Electron., Vol. E79-C, No. 3, March 1996.
- [20] H. Prigge et al., J. Electrochem. Soc., Vol. 138, No. 5, May 1991.
- [21] P. Roman et al., Proc. Ultraclean Semicon. Processing Technol. and Surface Chemical Cleaning and Passivation, Mat. Res. Soc., Vol. 386, p. 401, 1995.
- [22] T. Zundel and J. Weber, Phys. Rev. B, Vol. 39, p. 13549, 1989.

This work was carried out within the GRESSI consortium between CEA-LETI and France Télécom-CNET.

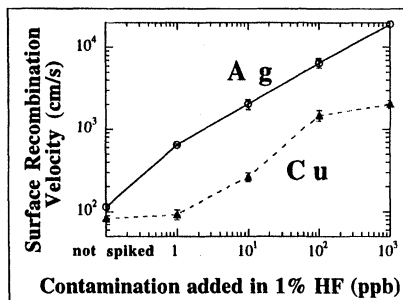


Figure 1 :  $\mu$ -PCD response for wafers dipped in CARO and then in HF bath spiked with Ag or Cu.

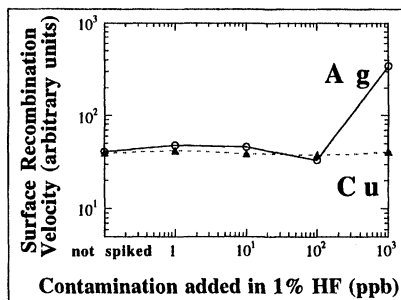


Figure 2 : SPV response for wafers dipped in CARO and then in HF bath spiked with Ag or Cu.

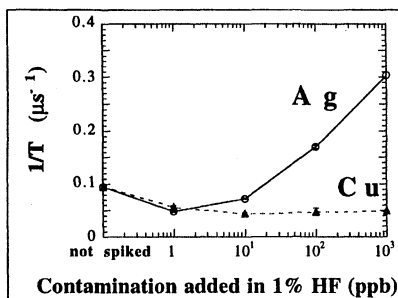


Figure 3 : SCP measured reciprocal of surface lifetime for wafers dipped in CARO and then 10 min. in 1% HF bath spiked with Ag or Cu.

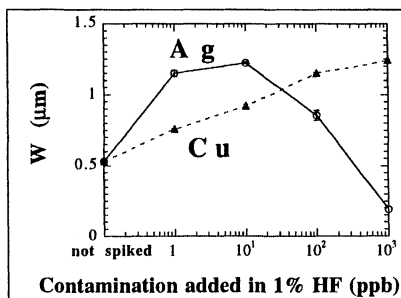


Figure 4 : SCP measured depletion layer width for wafers dipped in CARO and then 10 min. in 1% HF bath spiked with Ag or Cu.

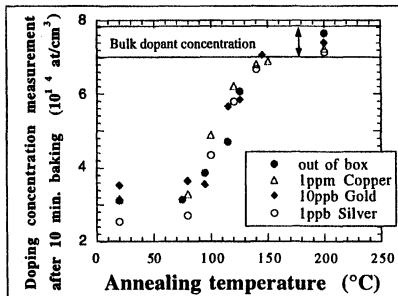


Figure 5 : Annealing of "B-H wafers" (from the box) and "B-X wafers" (CARO + 10 min. spiked 1% HF) Nsc measured by SCP after 2 min. 1% HF dip.

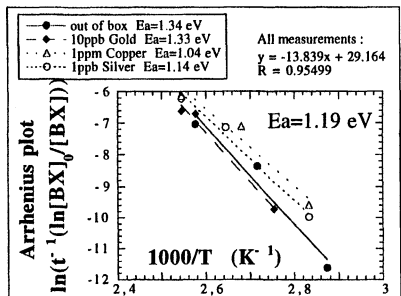


Figure 6 : Arrhenius plot for wafers of figure 5.  $[BX]_0 = N_{bulk} - N_{sc0}$  and  $[BX] = N_{bulk} - N_{sc}$   $N_{bulk}$  is  $N_{sc}$  after 200°C annealing.

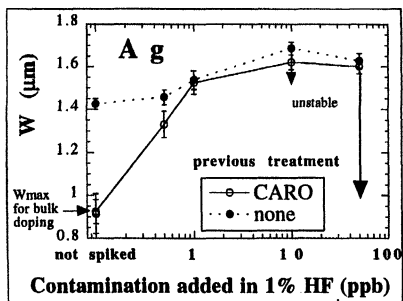


Figure 7 : Dependence of the SCP sensitivity on the previous treatment before HF dip.

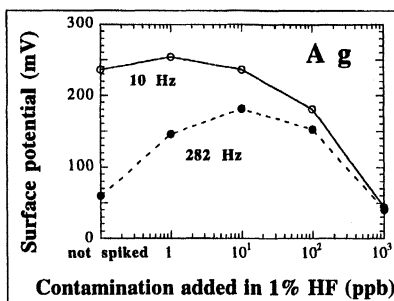


Figure 8 : Surface potential of wafers spiked with Ag measured by SCI at two frequencies.

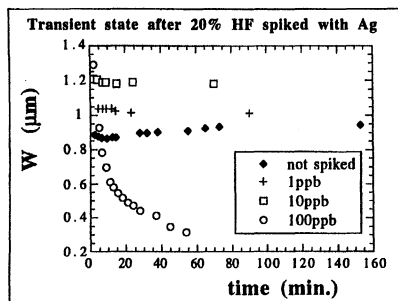


Figure 9 : Transient state after CARO + 10 min. 20% HF spiked with Ag. W measured by SCP, wafers stored in clean-room ambient air.

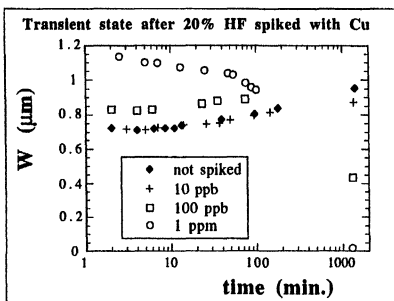


Figure 10 : Transient state after CARO + 10 min. 20% HF spiked with Cu. W measured by SCP, wafers stored in clean-room ambient air.

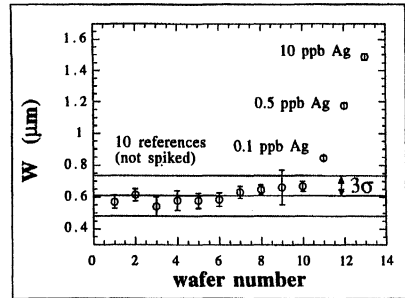


Figure 11 : 1% HF bath monitoring with SCP

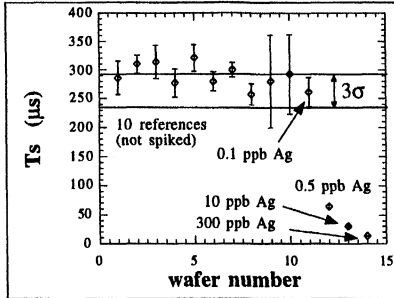


Figure 12 : 1% HF bath monitoring with  $\mu$ -PCD same wafers as in figure 11.

# **DETERMINATION OF NATIVE OXIDE REMOVAL IN A CLUSTER COMPATIBLE DRY CLEANING SYSTEM USING A SURFACE PHOTOVOLTAGE TECHNIQUE**

M. Brubaker, J. Staffa, P. Roman, S. Fakhouri, and J. Ruzyllo  
Electronic Materials and Processing Research Laboratory  
The Pennsylvania State University  
University Park, PA 16801

Surface Charge Profiling (SCP) was investigated as an in-line method of monitoring native/chemical oxide removal in dry cleaning processes. A correlation with wetting angle measurements indicate that the surface recombination lifetime measured by SCP is particularly sensitive to the presence of native/chemical oxide on the surface. A removal of the chemical oxide by the anhydrous HF(AHF)/methanol process was investigated. Various types of native/chemical oxide have been examined to determine the nature of the surface recombination centers. The results obtained indicate that these centers are associated with structural defects at the chemical oxide - silicon interface rather than surface metallic contaminants.

## **INTRODUCTION**

Gas-phase processing of silicon surfaces is expected to perform an increasingly important role in semiconductor device manufacturing operations. Dry cleaning systems used in conjunction with clustered technology allow for sensitive deposition processes to be performed on cleaned surfaces which are subject to virtually no recontamination or oxidation. Removal of the native/chemical oxide prior to subsequent processes is crucial in the formation of high quality silicon interfaces with metals as well as epitaxial layers. Hence, a technique for monitoring oxide removal inside the cluster tool is essential to insure that an oxide free surface has been achieved before any subsequent processes are performed.

The technique should be selectively sensitive to the properties of the surface and provide relevant information in real-time. In order to be suitable for in-line use the technique should not alter the wafer surface, or interfere with the motion of the wafer inside the cluster tool. Non-contact photoelectric methods are considered to be especially suitable for in-line use in clusters. The Surface Charge Profiling (SCP) method (1) is a non-contact SPV technique that was developed specifically to satisfy these criteria. The purpose of this research was to develop a methodology by which the SCP method can be used to monitor the condition of the silicon surface after gas-phase treatments.

Specifically, monitoring of native/chemical oxide removal was investigated from the point of view of potential future uses in contact metallization and/or epi deposition clusters.

## EXPERIMENTAL

P-type <100> silicon wafers were used for all experiments and unless otherwise indicated were subjected to a 15 min. hot plate anneal at 250°C to activate the boron dopants. This anneal of fresh wafers out of the box was needed to assure adequate accuracy and reproducibility of SCP measurements (2). Sample surfaces were prepared by immersion in a standard SC-1 wet clean (0.5:1:5) at 60°C for 7 minutes, which formed a chemical oxide with a thickness of about 1 nm, followed by a DI water rinse. All gas phase operations were implemented with a commercial dry cleaning module (3). Oxide etching was carried out using an anhydrous HF (AHF)/methanol process at 300 Torr. Other gas-phase treatments including UV/Cl<sub>2</sub> and UV/O<sub>2</sub> exposures were carried out using the same tool. Surfaces were mainly characterized with the stand alone SCP system which allows simultaneous, quick measurement of surface depletion width, surface recombination lifetime, and surface conductivity type. These parameters are sensitive to the physical and chemical state of the wafer surface, and hence, are useful in detecting process variance. The Si surface was studied using wetting angle measurements and XPS characterization. Additionally, TXRF measurements were carried out to identify selected metals on the surface.

## RESULTS AND DISCUSSION

The initial phase of the research provided a correlation between the presence of the native/chemical oxide and the surface recombination lifetime measured by SCP. The SC-1 oxide was subjected to the AHF process under varying conditions that produced no etching to complete etching (4,5). Wetting angle measurements were used as a diagnostic to determine whether the SC-1 oxide was present or not. Incomplete etching leaves a residual hydrophilic oxide layer resulting in a low wetting angle. Conversely, complete removal of the oxide produces a mostly hydrogen terminated bare silicon surface that is hydrophobic and exhibits a high contact angle. Figure 1 shows that surfaces which received complete etching feature an increased surface recombination lifetime while surfaces that received partial, or no etching maintained at a level closer to that of the initial SC-1 surface. The grouped nature of the data in Fig. 1 suggests that the surface recombination lifetime measured by SCP is particularly sensitive to features of the chemical oxide and its interface, increasing only upon complete etching of the SC-1 oxide. These initial results led us to the conclusion that the surface recombination lifetime measured by SCP has a potential to be an effective tool in monitoring the removal of the chemical oxide providing the exact nature of the effects involved will be understood.

It is reasonable to assume that the increase of the surface recombination lifetime upon complete oxide etching is due to the removal of recombination sites associated with

the SC-1 chemical oxide. The question is whether the origin of the chemical oxide affects the behavior of the surface recombination lifetime. Figure 2 shows the recombination lifetime of chemical oxides grown on bare silicon surfaces by SC-1 and SC-2 treatments with varying levels of NH<sub>4</sub>OH and HCl, respectively. These changes result in a solution where pH increases from left to right in Fig. 2. The chemical oxide produced in SC-1 solution results in a low lifetime at any concentration of NH<sub>4</sub>OH, while the SC-2 solution produces a chemical oxide with a lifetime similar to an etched surface. The water/peroxide solution alone produces a surface with a lifetime intermediate of the SC-1 and SC-2 chemical oxides. There are two mechanisms that can explain the above observations. The first is that the recombination sites are associated with metallic contaminants deposited on the surface during SC-1 treatment, while SC-2 effectively removes metallic contaminants. The second mechanism may involve structural defects in the chemical oxide such as trivalent silicon that could be a contributing factor to the low lifetime of SC-1 oxides, while the acidity of the SC-2 solution saturates trivalent silicon sites with hydrogen (6) and increases lifetime.

In order to resolve the above question the effects of metallic contamination of wafer surfaces on the surface recombination lifetime were investigated further. Iron and aluminum, both common contaminants in SC-1 solution are known to reduce recombination lifetime in the semiconductor bulk, however, metals deposited by cleaning solutions and not subjected to any subsequent drive-in step are located strictly at the surface. Oxidized surfaces were prepared in SC-1 solutions which were contaminated with iron or aluminum in 1 ppb to 1 ppm concentrations. The oxide was then removed by either dilute HF/water (1:100) or AHF/methanol process. The dilute HF/water etch will remove iron and aluminum from the surface (7,8) whereas AHF/methanol will etch the oxide while leaving metals on the surface (9). As shown in Fig. 3 the dilute HF/water etch increases the lifetime to the same level over the entire range of iron concentration investigated. However, the AHF etch shows a trend of decreasing lifetime with increasing iron concentration. This indicates that iron on an oxide free silicon surface does have an effect that reduces lifetime, but only at relatively high concentrations. TXRF measurements did confirm our initial observation that at low Fe surface concentration the change of the surface recombination lifetime is not related to the presence of Fe. These measurements showed that the Fe concentration after SC-1 treatment in this study was equal to  $2.3 \times 10^{11} \text{ cm}^{-2}$  and did not change after the AHF/methanol etch. The same process, however, resulted in a substantial increase of the surface recombination lifetime (Fig. 1) indicating that at low Fe concentrations the surface recombination lifetime is controlled by structural defects at the chemical oxide - Si interface. At higher concentrations, at which Fe outplated from SC-1 may conglomerate on the Si surface, the reduction of the surface recombination lifetime becomes a factor influencing the surface recombination lifetime. The response of the surface recombination lifetime to the presence of Al on the surface was different than for iron. As shown in Fig. 4 high concentrations of Al added to the surface from SC-1 solution has no influence on the surface recombination

lifetime. It is therefore unlikely that metals alone are responsible for the low lifetime of the SC-1 treated Si samples.

To determine the performance of SCP in monitoring dry cleans the effects of a complete dry cleaning sequence on the surface recombination lifetime measured by SCP were investigated. The dry cleaning sequence consisted of UV/O<sub>2</sub> organics removal, AHF/methanol oxide etch, and UV/Cl<sub>2</sub> metals removal. This clean was carried out on wafers which received an initial SC-1 pre-clean and on samples as received from the vendor. In order to test the effectiveness of the surface recombination lifetime in detecting the chemical oxide formed by SC-1 in the event of a failed oxide etching process, a dry cleaning sequence which omitted HF gas during the AHF/methanol step was performed. The surface recombination lifetime was measured after each process step in both dry cleaning sequences and is shown in Fig. 5 and Fig. 6. The surface recombination lifetimes of the samples treated in SC-1 and the samples out of the box are less than 5  $\mu$ s and maintain this level indefinitely in cleanroom ambient. The UV/O<sub>2</sub> exposure increases the lifetime to a value intermediate of the SC-1 and AHF levels, the extent of which depends on nature of the native/chemical oxide present. This increase is of a transitory nature and is due at least in part to the irradiation of the surface by the UV light. The mechanism by which UV light increases the surface recombination lifetime has been studied elsewhere (10-12). The AHF/methanol process with normal HF gas flow increases the lifetime to about 30  $\mu$ s due to the removal of the native/chemical oxide, in agreement with the wetting angle experiments. In the sequence where there is no HF gas flow the oxide is unetched and the lifetime remains at the level after UV/O<sub>2</sub>. This lifetime is statistically shown to be lower than the lifetime of the etched surfaces, and thus provides a means by which the presence or absence of the oxide can be determined for dry cleans with AHF/methanol as the last step. The UV/Cl<sub>2</sub> step in the no HF process increases the lifetime to the same level as an etched surface, however, XPS scans after UV/Cl<sub>2</sub> (shown in Fig. 7) indicate that the native/chemical oxide is still present. The UV/Cl<sub>2</sub> process has been shown to result in the diffusion of Cl radicals across the thin native/chemical oxide, through which metal complexation and silicon etching occur (13). As a result recombination sites associated with the native/chemical oxide are being passivated and/or removed by the UV/Cl<sub>2</sub> step and increasing the lifetime even though the oxide layer is still present. Fortunately, the lifetime after the UV/Cl<sub>2</sub> step for the normal HF process is increased to more than 40  $\mu$ s, still showing a distinction between normal and failed etching processes. It therefore appears that an increase of the surface recombination lifetime to at least 30  $\mu$ s is indicative of complete oxide removal in dry cleans that terminate with the AHF/methanol process, while an increase to at least 40  $\mu$ s is required in cleans that include the UV/Cl<sub>2</sub> process.

## CONCLUSION

A methodology has been investigated in which the surface recombination lifetime measured by the non-contact SCP method can be used to monitor the removal of native/chemical oxide in gas-phase surface conditioning. Oxidized surfaces with a low initial lifetime and with Fe contamination less than approximately  $10^{12} \text{ cm}^{-2}$  attain an increased lifetime upon complete removal of the oxide. Various factors that affect the lifetime were investigated in regards to their influence on monitoring the surface. This technique is compatible with integrated processes. Its most obvious application would be in surface preparation - blanket epi deposition clusters in which the SCP would be installed on the wafer handler to monitor wafers in between surface preparation and epi deposition steps.

## ACKNOWLEDGMENTS

This work was funded by the Semiconductor Research Corporation project no. BJ-443. SubMicron Systems Corp. and QC Solutions, Inc. are also acknowledged for their support. In addition, thanks are due to Karine Kenis for her assistance with TXRF measurements.

## REFERENCES

1. SCP Model 110, QC Solutions, Inc., Woburn, MA 01801.
2. P. Roman, J. Staffa, S. Fakhouri, M. Brubaker, J. Ruzyllo, K. Torek, and E. Kamieniecki, *J. Appl. Phys.* (in press).
3. Primaxx Dry Cleaning System, SubMicron Systems Corp., Allentown, PA 18106.
4. A. Izumi, T. Matsuka, T. Takeuchi, and A. Yamano, in *Cleaning Technology in Semiconductor Device Manufacturing*, J. Ruzyllo and R. E. Novak, Editors, PV 92-12, p. 260, The Electrochemistry Society Proceedings Series, Pennington, NJ (1992).
5. J. Ruzyllo, K. Torek, C. Daffron, R. Grant, and R. Novak, *J. Electrochem. Soc.*, 140, L64 (1993).
6. M. Grundner, P. O. Hahn, I. Lampert, A. Schnegg, and H. Jacob, in *Semiconductor Cleaning Technology/1989*, J. Ruzyllo and R. E. Novak, Editors, PV 90-9, p. 215, The Electrochemistry Society Proceedings Series, Pennington, NJ (1990).
7. K. Christenson, in *Cleaning Technology in Semiconductor Device Manufacturing*, J. Ruzyllo and R. E. Novak, Editors, PV 92-12, p. 286, The Electrochemistry Society Proceedings Series, Pennington, NJ (1992).
8. W. C. Krussel and D. I. Golland, in *Semiconductor Cleaning Technology/1989*, J. Ruzyllo and R. E. Novak, Editors, PV 90-9, p. 23, The Electrochemistry Society Proceedings Series, Pennington, NJ (1990).
9. K. Chang, J. Staffa, and J. Ruzyllo, unpublished results.
10. K. Katayama and F. Shimura, *Jpn. J. Appl. Phys.*, 31, L1001 (1992).

11. A. Buczkowski, G. A. Rozgonyi, and F. Shimura, Jpn. J. Appl. Phys., **32**, L218 (1993).
12. P. J. Caplan, E. H. Poindexter, and S. R. Morrison, J. Appl. Phys., **53**, 541 (1982).
13. R. Sugino, Y. Nara, H. Horie, and T. Ito, J. Appl. Phys., **76**, 5498 (1994).

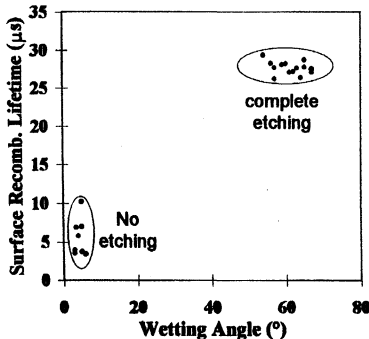


Figure 1. Surface Recombination Lifetime vs. Wetting Angle after AHF carried out at various etch times.

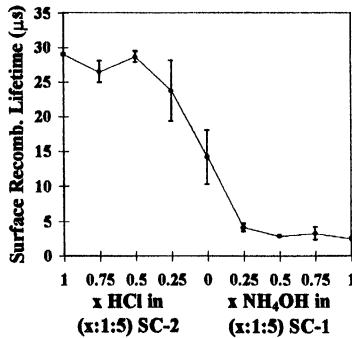


Figure 2. Surface recombination lifetime vs. concentration of HCl (SC-2) or NH<sub>4</sub>OH (SC-1) in H<sub>2</sub>O/H<sub>2</sub>O<sub>2</sub>.

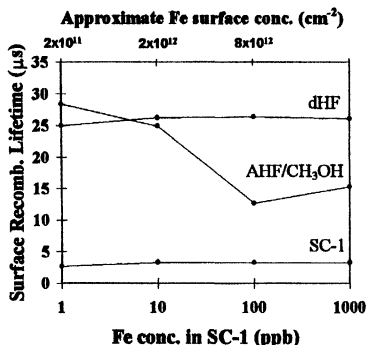


Figure 3. Surface recombination lifetime vs. Fe concentration in SC-1.

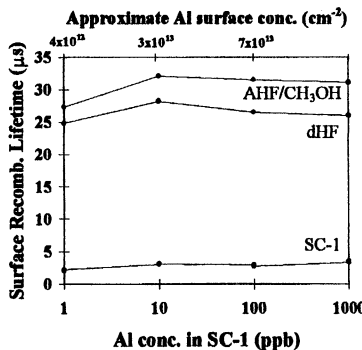


Figure 4. Surface recombination lifetime vs. Al concentration in SC-1.

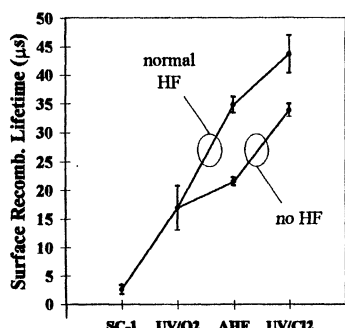


Figure 5. Surface recombination lifetime measured after each step in a dry cleaning sequence. Error bars represent one standard deviation.

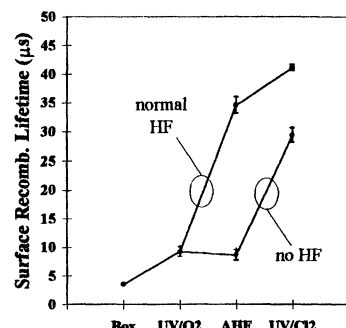


Figure 6. Surface recombination lifetime measured after each step in a dry cleaning sequence. Error bars represent one standard deviation.

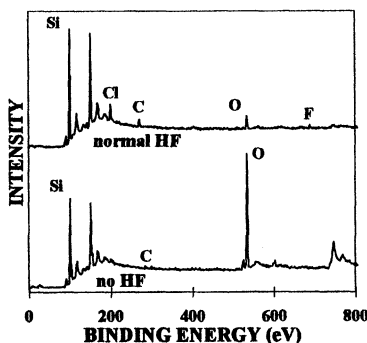


Figure 7. XPS survey scan comparison of surfaces after UV/Cl<sub>2</sub> with normal HF flow and with no HF flow sequences.

# IN-LINE X-RAY PHOTOELECTRON SPECTROSCOPY FOR ANHYDROUS HYDROGEN FLUORIDE CLEANING OPTIMIZATION

Barbara Froeschle\*, Frédérique Glowacki\*,

Anton J. Bauer\*\*, Igor Kasko\*\*, Richard Oechsner\*\*, and Claus Schneider\*\*

\* STEAG-AST elektronik GmbH, Daimlerstrasse 10, D-89160 Dornstadt, Germany

\*\* Fraunhofer-Institut fuer Integrierte Schaltungen, Bauelementetechnologie,  
Schottkystrasse 10, D-91058 Erlangen, Germany

## ABSTRACT

A novel in-line X-ray Photoelectron Spectroscopy module (XPS) was integrated into a state-of-the-art cluster tool also consisting of a STEAG AST Vapor Phase Cleaning module (VPC) and a STEAG AST Rapid Thermal Oxidation module (RTO). The in-line integration enabled fast measurements without exposing the wafers to atmosphere thus avoiding oxidation or contamination of the wafer surfaces during handling. A cleaning process using anhydrous HF (AHF)/methanol and ozone was carried out in the Vapor Phase Cleaning module. Surface concentration measurements by XPS of fluorine, carbon, and oxygen in the range from 0.01 to 1 monolayers on cleaned wafer surfaces and on regrown oxides (<0.5 nm) have been performed and used for rapid optimization of the cleaning procedure.

## INTRODUCTION

As film thickness decreases, Si/SiO<sub>2</sub> interface properties play a more significant role with respect to gate dielectric processing and integrity. Thus, pre-gate surface preparation becomes one of the most critical steps in future device technologies. The commonly used wet cleaning prior to gate oxide growth is not only expensive, but also environmentally detrimental, since large quantities of ultrapure liquids are manufactured and have to be treated properly after use. Wet cleaning is not compatible with multichamber process systems (cluster tools), which are increasingly considered as a key equipment in many future technological process sequences in advanced manufacturing e.g. gate oxidation (1, 2, 3).

The state-of-the art process monitoring in IC fabs relies on metrology tools physically separated from production equipment. This off-line concept suffers from major limitations, i.e., time consuming transportations and logistics, the need for monitor wafers, and a lack of direct feedback to equipment control. Recent R&D efforts aim at the integration of measurement tools into process equipment, cluster tools, or work cells (4). This integration, also anticipated by the published roadmaps (5), is mostly driven by the

need to enhance productivity, namely to save costly monitor wafers and to reduce the amount of batches misprocessed before the yield problem is detected. Therefore, solutions for direct in-line metrology, which can be integrated conveniently using well-standardized hardware and software interfaces are needed.

## EXPERIMENTAL

To investigate the properties of silicon surfaces after anhydrous HF cleaning, an in line X-ray Photoelectron Spectroscopy module was integrated into a gate oxide cluster consisting of a Vapor Phase Cleaning module and a Rapid Thermal Oxidation module (Fig.1).

### Vapor Phase Cleaning Module

The VPC process chamber (6) is made of Hastelloy<sup>TM</sup> to avoid contamination during the cleaning process. All parts of the reactor were kept at a temperature of 40°C. The VPC chamber wall was heated by an integrated, temperature controlled water circuit, whereas the quartz-window was heated by a hot air blower.

Anhydrous HF (AHF) of purity 99.9%, contained in a nickel cylinder at 40°C, was fed at cylinder pressure through a heated gas line into a temperature controlled mass flow controller. The methanol was supplied via a nitrogen bubbler kept at 20°C. All tubes in contact with either methanol or HF were heated to prevent condensation. Ozone at a concentration of about 5 % in oxygen was delivered from an ozone generator via a mass flow controller.

The wafer was heated through the quartz window with linear IR-Lamps. The temperature of the wafer was measured by an integrated thermocouple (PinTC<sup>TM</sup>). UV lamps, low pressure mercury vapor lamps with a total power of 120 Watt, are alternating with the IR lamps and can be independently controlled by the process recipe. Caused by using high silica glass as lamp envelope, the maximum in radiation is at the 254 nm wavelength.

### X-Ray Photoelectron Spectroscopy Module

The analytical module used here (Fig.2) was designed for integration into cluster equipment. The SEMI MESC/CTMC standards were used for footprint, for interfacing to a transport chamber, and for network communication with a cluster controller (6,7). The module consists of a vacuum chamber with a pumping system, a high-precision xy-mapping stage and an analytical instrument. For the attachment of the module to the cluster tool, a MESC port is used. As measurement instrument, an XPS was installed in

the module. Since the XPS analysis requires ultra-high vacuum, the vacuum chamber and the vacuum pump are designed accordingly. With an additional loadlock, the module can be used as a stand-alone system as well.

#### Etching of silicon dioxide

The silicon wafers were cleaned using standard Sulfuric Peroxide Mixture (SPM). Afterwards the remaining thin chemical oxide was etched in the VPC module at a temperature of 40°C and a AHF pressure of 50 mbar (12).

To improve the cleaning sequence oxygen or ozone/UV steps were performed in the same reactor by introducing ozone at a pressure of 700 mbar and a temperature of 200°C after the cleaning step. The ozone step was performed for 60 s at 700 mbar and at an ozone concentration of 5% in oxygen. During this ozone step the wafer was additionally illuminated with UV light. This cleaning procedures were compared to standard HF dipped wafers.

## RESULTS

#### Etch Rate of chemically grown oxide

AHF alone is insufficient to etch silicon oxide (8,9,10), but as seen in Eq.1, the presence of methanol will catalyze the reaction by providing hydroxyl groups.



In the process sequence used, the hydroxyl groups were delivered at the beginning of the process by the introduction of methanol. During AHF etching at 50 mbar no methanol was introduced. The hydroxyl groups were continuously delivered by the in-situ generation of water molecules, which catalyze the reaction by itself.

Contact angle measurements have been used to control the removal of the chemical oxide of about 4 to 6 monolayers (ML), which is formed during the SPM cleaning on the wafer surface. The measurements were performed directly after the etching by transferring the wafer to the measurement equipment. The dependence of contact angle of chemical oxide on the etching time is shown in Fig.3.

With increasing etching time the contact angle increases and reaches a plateau after about 40 s. The contact angle of 80° is reproducible for etching with AHF/methanol. In contrast, the contact angle for reference wafer with standard HF-dip is 82° due to the hydrogen passivated surface.

### General properties of the cleaned silicon surface

During the vapor phase etching no particles are generated on the wafer surface. Also no metallic contamination are found, as confirmed by Vapor Phase Decomposition-Atomic Absorption Spectroscopy (VPD-AAS).

Atomic Force Microscopy (AFM) of samples etched for 40 s under the above conditions shows a smooth silicon surface. The resulting Rms value is 0.16 nm which is comparable to the surface roughness of HF-dipped wafers.

### XPS-Characterization of the cleaned silicon surface

To investigate the properties of silicon surfaces after VPC cleaning, the samples were transferred directly after the cleaning to the in-line X-ray Photoelectron Spectroscopy module. This module allows for quick detection and quantification of relevant elements (i.e. O, F, C) on the wafer surface. The major advantage of this in-line measurement is that exposure of the wafer to atmosphere and therefore adsorption of i.e. hydrocarbons during the transport to the off-line measurement tool can be avoided. Furthermore, the results were available immediately after wafer processing and the process parameters could be optimized just for the next wafer.

The photoelectron analyzer is a newly developed double stage cylindrical electron analyzer, where the photoelectrons were excited with the Al K<sub>α1,2</sub> lines. The takeoff angle of the emitted photoelectrons is 60° with respect to the analyzer. The atomic concentration C(%) of each element was calculated by the dependence of the integrated peak area of F1s, O1s and C1s on the sensitiveness values (11).

The surface coverage in monolayers can be calculated under the assumption, that

- there is no influence of the analysis depth on the coverage
- the analysis depth  $\lambda_{Si}$  in silicon is 30.5 Å
- all elements are distributed uniformly
- the takeoff angle  $\theta$  is 60°

$$C \text{ (ML)} = \frac{C \text{ (%)} \cdot MD}{100\%} \quad [2]$$

where

$$MD = \lambda_{Si} \cdot \sqrt[3]{N_{Si}} \cdot \cos\theta \quad \text{is the measuring depth in monolayers, (5.6 ML).}$$

The results of the XPS control of the cleaning procedure are shown in Fig.4. The etching in AHF/methanol results in a higher fluorine content (0.23 ML) compared to HF-dipped wafers (0.02 ML). With additional ozone treatment at 40°C and 700 mbar the fluorine content rises to about 0.8 ML. In contrast, the carbon content decreases by the

treatment of AHF etched wafers in ozone. The effect is intensified by using UV light and, additionally, a higher temperature. The carbon content of a wafer cleaned in AHF/methanol with a subsequent ozone step at 200°C under UV irradiation is lower than 0.05 ML, compared to 0.8 ML for HF-dipped wafers. In-line measurements enable control of carbon content which is altered to wafer transport, by off-line measurement.

The oxygen content on ozone treated wafers increases in comparison to only AHF cleaned wafers due to the formation of a thin silicon dioxide layer on the surface of about one monolayer SiO<sub>2</sub> (0.3 nm). During the ozone step with additional UV light the oxygen content decreases lightly because of the decomposition of ozone with UV light, which leads to a lower oxidation rate. The oxygen content at higher temperatures, in contrast, increases because of the temperature dependent oxidation.

### Electrical characterization

Gate stacks using different cleaning sequences with a 4.0 nm thick gate oxide, which was grown directly after the cleaning process in the RTO module, are manufactured

As shown in Fig.5, samples treated with VPC show a higher Q<sub>BD</sub> value than the reference sample with standard HF-Dip. Especially the additional ozone step at 200°C under UV illumination has a positive effect on the Q<sub>BD</sub> value, which may be attributed to a more effective removal of hydrocarbon contamination (12).

## CONCLUSION

It can be demonstrated that the cleaning sequence using AHF/methanol with a subsequent ozone step at 200°C using UV light can reduce the carbon content of the silicon surface and leads to improved breakdown characteristics. The combination of pre-gate cleaning and rapid thermal oxidation in a cluster tool shows promising results for preparation of thin gate oxides in advanced manufacturing especially for hydrocarbon removal. The using of the in line XPS module for control of the cleaning process reduces the process optimization cycle in comparison of using off-line analytical tool.

## ACKNOWLEDGMENTS

The authors would like to thank Silke Paul, Rainer Schoenweis, and Matthias Beichele for assistance in preparing the samples and performing the contact angle measurements.

## REFERENCES

1. Cleaning and Contamination Monitoring Systems for the Semiconductor Industry, VLSI Research, Inc. San Jose, CA, April 1986.
2. J. Ruzyllo, "Microcontamination", Vol 6(3), 39 (1988).
3. P. Singer, Semiconductor International, Vol. 18, No. 8, 113, (1995).
4. G. G. Barna et al., *Solid State Technology*, Vol. 37, No. 4, pp.57-61, (1994).
5. The National Technology Roadmap for Semiconductors, SIA, p.123 (1994).
6. Barbara Froeschle, Frédérique Glowacki, Anton Bauer, Igor Kasko, Richard Oechsner, Claus Schneider, to be published in Volume 477 of the Materials Research Society Symposium Proceedings Series (1997).
7. L.Pfitzner in *Proc. of Fifth Int. Symp. on Semiconductor Manufacturing*, Tokyo, Japan, pp.54-7, (1996).
8. K. Torek, J. Ruzyllo, R. Grant, R. Novak, J. Electrochem. Soc., Vol 142, No 4, 1322 (1995).
9. C. S. Lee, J. T. Baek, H. J. Yoo, and S. I. Woo, J. Electrochem. Soc., Vol 143, No 3, 1099 (1996).
10. J. Ruzyllo, K. Torek, C. Daffron, R. Grant, and R. Novak, J. Electrochem. Soc., Vol 140, No 4, L64 (1993).
11. C. D. Wagner, W. M. Riggs, L. E. Davis, J. F. Moulder, G. E. Muilenberg, *Handbook of X-ray Photoelectron Spectroscopy*, Perker-Elmer Corporation (1979).
12. Barbara Froeschle, Lutz Deutschmann, Anton Bauer, Edmund Burte, to be published in Volume 470 of the Materials Research Society Symposium Proceedings Series (1997).

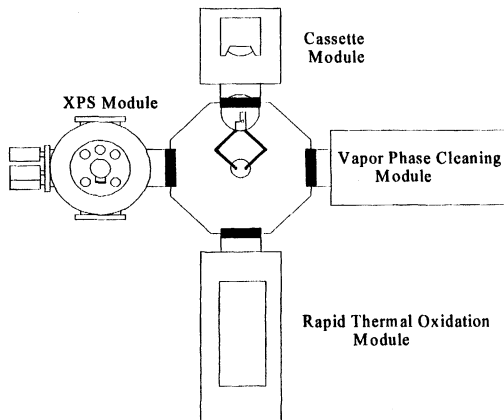


Fig.1: Foot print of the gate oxide cluster

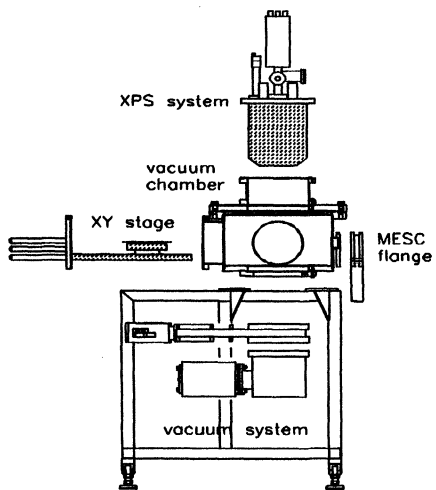


Fig.2: XPS Measurement Module

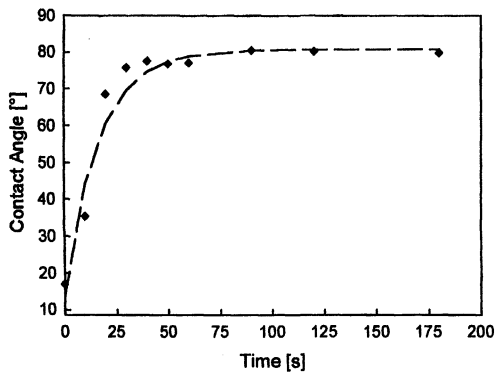
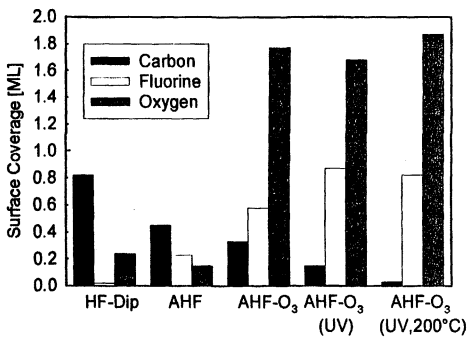
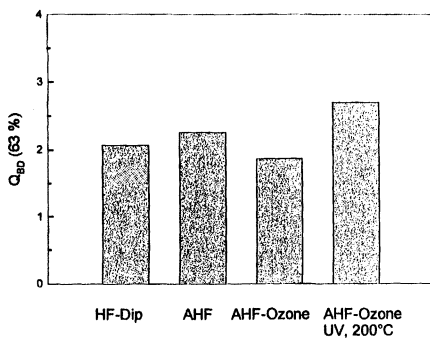


Fig.3: Dependence of contact angle on etching time



*Fig. 4: XPS measurements of differently cleaned wafer surfaces*



*Fig. 5: Charge to breakdown characteristics of oxides pre-oxidation cleaned with AHF using different process sequences.*

# Characterization of Silicon Oxide Etching in HF Vapor Process

Yong-Pil Han, A. Scott Lawing and Herbert H. Sawin

Department of Chemical Engineering  
Massachusetts Institute of Technology  
Cambridge, MA 02139

The oxide etching characteristics in the HF/H<sub>2</sub>O vapor process were studied. Oxide etching can be performed in two regimes (gas phase and condensed phase) depending on the process conditions. The boundary between the two regimes was mapped as a function of condition. Mass transport in the gas phase significantly affects the etching rate as well as other etching characteristics. We propose that low mass transfer resistance is essential in HF vapor etching or cleaning processes for good reproducibility and low contamination from the etching products.

## Introduction

Anhydrous HF vapor etching of oxide has been studied intensively to overcome some drawbacks of conventional wet chemical etching processes. Wet cleaning still prevails in industry in part because vapor phase (or gas phase) cleaning methods are very difficult to control due to a lack of understanding(1-3). Recently, distinctive advantages of HF vapor process have been reported: low recontamination of the wafer, the ability to penetrate narrow features, and vacuum compatibility. In conventional wet cleaning processes, wafers can be recontaminated by the cleaning solution, rinse water, or drying chamber. Such recontamination has not been observed in HF vapor processing. HF vapor processes avoid surface tension effects allowing the penetration of narrow trenches or contact holes without surfactant addition. One of the major advantages of HF vapor processing is its vacuum compatibility and suitability for clustered processing, which is predicted to become important in future manufacturing processes(4,5).

Numerous research groups have reported the etching mechanism of oxide in the HF vapor process. It is widely believed that the reaction occurs in a condensed layer on the surface from the vapor phase. Helms and Deal reported the mechanisms of HF/H<sub>2</sub>O etching of oxide involving a condensed regime and they claimed that the role of water is to provide a condensed layer on the surface(6). A gas phase etching mechanism has also been proposed for HF vapor etching by C. S. Lee *et al*(7).

In this paper, we report two different etching regimes of HF/H<sub>2</sub>O processing: gas phase and condensed phase etching of thermal oxide. Primarily, the etching rate has been characterized with respect to the wafer temperature, partial pressures of reactants, the flow rates, and the pressure. The purpose of this research is to provide background information for the design of new HF vapor etching or cleaning tools that can be integrated into a vacuum cluster machine.

## Experimental

In this study, the etching experiments were carried out in a stainless steel vacuum chamber connected to a vacuum wafer transfer system. Samples were introduced through a load lock chamber and transferred to the HF vapor reaction chamber. The base pressure of the system was maintained under  $10^{-7}$  Torr. The system can handle sample sizes between 1 cm square and 10 cm diameter silicon wafers. Fig. 1 shows a schematic of the HF reactor and gas handling system. The process gases were introduced through a specially designed gas handling system in which water vapor was supplied directly from the water tank via a mass flow controller without a carrier gas. Anhydrous HF and N<sub>2</sub> were supplied to the reactor through parallel mass flow controllers. All mass flow controllers were calibrated by measuring the speed of pressure rise of the reaction chamber. The entire gas handling system including mass flow controllers was maintained at 55 to 120 °C to prevent condensation within the system. The pressure of the reaction chamber was maintained by a throttle valve controlled by a capacitance manometer.

The etching rate of oxide was measured using *in situ* spectroscopic ellipsometry (J. J. Woollam M44) that monitored the oxide thickness in real time. Thermally grown oxide films on 10 cm wafers were used for the experiments. The samples for these experiments were 2.54 cm square samples or full 10 cm wafers. Each sample was subjected to a SC1 clean and followed by 100:1 diluted HF cleaning performed in a spin processor. Before each run, dry nitrogen was introduced into the reaction chamber to stabilize the pressure. Water vapor flow was begun 2 minutes before initiating the HF flow. This preconditioning with water was very important in obtaining reproducible results. The change in the film thickness as a function of time was measured by *in situ* ellipsometry at 40 different wavelengths.

HF and water partial pressures were selected to study both the gas phase and condensed phase etching regimes. The etching rate has also been measured at different total pressures and flow rates to investigate the effects of mass transport of reactant and product gases. The diameter of the gas showerhead was also varied to study the mass transport effects. Temperature of the sample was held constant during processing using a water cooled sample holder at a temperature lower than the chamber wall, thereby preventing condensation on the chamber walls.

## Results and Discussion

Ellipsometric measurements suggest that oxide etching can occur without a condensed layer on the surface under certain conditions. At lower temperatures and higher vapor pressures, a condensed layer was formed. Fig. 2 shows the regions in which condensation was observed during etching at 40 °C as a function of HF and H<sub>2</sub>O partial pressures in the feed gas. The data indicate that condensation occurred at lower partial pressures of reactant gases than predicted by the HF-H<sub>2</sub>O vapor equilibrium measurements of Munter (8,9). Ellipsometric observation of water condensation was also

carried out to confirm the temperature and pressure control of the reation chamber. The data generated in this experiment was in agreement with the steam tables. This depression of the condensation point indicates that the oxide etching product forms a ternary mixture of HF/SiF<sub>4</sub>/H<sub>2</sub>O thereby decreasing the vapor pressure and causing condensation. The reduction in vapor pressure by the ternary mixture HF/SiF<sub>4</sub>/H<sub>2</sub>O was measured by Munter *et al*(10). The etching rates of oxide in the condensed regime were very high (3,000-12,000 Å/min) as compared to those of a gas phase regime (0-300 Å/min). The region in which a condensed layer is formed is therefore a function of not only the partial pressures of HF and H<sub>2</sub>O in the feed gas, but also a function of the mass transport of the reactants to and the products from the sample.

We have categorized two different etching regimes: the gas phase regime and the condensed phase regime. In the gas phase etching regime, reactant molecules are adsorbed on the oxide surface in sub-monolayer, monolayer, or multilayer films. In the condensed phase regime, a condensed film is formed that is very non-uniform in thickness. The thickness and non-uniformity of the condensate film gives rise to measurable ellipsometric signals during oxide etching. The etching reaction in the condensate film is thought to occur in a manner that is very similar to that in wet HF etching. For both gas-phase and condensed phase etching, the products must desorb and diffuse from the surface. Since the surface kinetics are a function of both the partial pressure of the reactants and the transport to and from the surface, both surface kinetics and transport must be considered to correctly model the etching process.

#### Gas Phase Etching Regime

Without the formation of a condensed layer, the etching reaction must involve three steps: adsorption, reaction, and desorption(11). The etching rate in this regime is usually low (typically 0~400 Å/min) compared to that of the condensed regime. Fig. 3 shows the etching rate as a function of partial pressure of HF. The etching rate is generally proportional to the partial pressure of HF up to 35 Torr. A sudden increase in etching rate above 35 Torr is caused by the formation of a multilayer film on the surface. The etching rate of oxide is also linearly proportional to the partial pressure of H<sub>2</sub>O as is shown in Fig. 4. These results suggest that oxide etching proceed by adsorbed HF and H<sub>2</sub>O on the surface via a Langmuir-Hinshelwood mechanism. The Langmuir-Hinshelwood mechanism expresses the surface reaction rate in terms of a product of a rate coefficient and the surface coverages of the adsorbates.

The etching rate in the gas phase regime is proportional to HF and H<sub>2</sub>O partial pressures at very low partial pressure, but saturates under certain conditions determined by the mass transport to the sample. From Fig. 3 the etching rate for a total pressure of 250 Torr saturates at ~70 Å/min while the etching rate for 125 Torr shows a linear increase. If the oxide surface is saturated with product, the etching rate of oxide will be greatly affected by the mass transport rate of products to the bulk gas. The etching rate is proportional to the H<sub>2</sub>O partial pressure at low HF partial pressures, as is shown in Fig. 4 for a HF pressure of 7 Torr. This regime corresponds to the linear regime in HF partial pressure shown in the lower left corner of Fig. 3.

Although a detailed description of the reaction mechanism and transport is beyond the scope of this work, Fig. 5 shows that mass transport in the gas phase affects the oxide etching rate. The data given in this plot show that the observed etch rate varied with total process pressure even though the reaction temperature and partial pressure of the reactants was held constant. The data can be interpreted correctly when plotted versus  $(QD/Lp)^{1/2}$ , the scaling for a mass transfer controlled process. The mass transport rate is proportional to the concentration gradient and a mass transfer coefficient. The mass transfer coefficient in the gas phase is approximately the diffusivity divided by boundary layer thickness of gas phase. For laminar flow at low Reynolds numbers in a stagnation configuration, the mass boundary layer thickness is independent of the radial position. The mass transfer coefficient for laminar stagnation flow in the lubrication regime can be shown to be proportional to the square root of (the volumetric flow rate per showerhead area)(the diffusivity)/(the spacing between the showerhead and the sample). Since the volumetric flow rate and diffusivity are both inversely proportional to the pressure for an ideal gas, the transfer coefficient changes inversely with the process pressure. The transport coefficient (that can also be thought of as the reciprocal of resistance for mass transport) for a given showerhead scales in proportion to  $(QD/Lp)^{1/2}$  where Q is the feed gas molar flow rate, D is the diffusivity in the gas, L is the showerhead-sample spacing, and p is the process pressure. This implies that the HF vapor process should be operated at a high flow rate and low pressure to insure operation in the surface reaction limited regime. The surface reaction limited regime is probably more reproducible than the mass transfer limited regime unless careful reactor design has been made to assure uniform mass transport to the wafer.

Temperature dependencies of the etching rate were investigated by changing the sample temperature in the gas phase etching regime. Fig. 6 is an Arrhenius plot of the etching rate demonstrating that the rate decreases as temperature increases. Lower step coverages of the reactants on the surface may be partially responsible for the decreasing etching rate at higher temperatures. These results are consistent with previous observations(2,12). As shown in Fig.6, the etching reaction is complex and impossible to describe with one simple mechanism. The complexity of the plot may in part be explained by different adsorption regimes such as sub-monolayer, monolayer and multilayer adsorptions. The etching rate of thermal oxide is less than 25 Å/min at a temperature above 45 °C while BPSG is etched at a rate of more than 5,000 Å/min. These differences in etching rate can be used to selectively etch BPSG.

#### Condensed Phase Etching Regime

Etching rates of more than 3000 Å/min have been achieved in the condensed regime. We have identified condensation experimentally in this regime through the observation of an apparent increase in the oxide thickness (measured ellipsometrically) at the onset of etching. The presence of liquid phase condensation is confirmed indirectly by the increased pumping time needed to reach base pressure after the etching process. The reaction products dissolved in the condensed phase must desorb into the gas phase or be cleaned by a water rinse after the etching process otherwise the remaining reaction products produce "particulate" contamination on the wafer surface after etching. From

the observation that condensation is present at a lower pressure than predicted by the vapor-liquid equilibrium data from Munter *et al*, it is concluded that the product concentration in the condensed phase is high enough to reduce the vapor pressure of the liquid phase. High concentrations of the products in the condensed phase can lead to residues on the surface, which is one of the basic problems in the HF vapor etching process. To avoid this problem, HF vapor processing equipment must use a water rinse step after processing to remove particulates, or incorporate wafer heating while processing to desorb excess product more efficiently.

The etching rate increases as the partial pressure of HF increases as is shown in Fig. 7. The effect of HF partial pressure decreases under conditions which lead to poorer mass transport to the sample; i.e. higher pressure, lower flow rates, and larger showerhead. The smaller showerhead produces a higher etching rate than the larger showerhead at the same flow rate. In this regime the etching rate is not controlled by adsorption on the surface but is governed by the mass transfer rate of reactant from the gas phase to the condensed phase or the transfer of products built up in the condensed phase to the gas phase.

The temperature dependence of etching rate in the condensed regime is shown in an Arrhenius plot in Fig. 8 and exhibits a greatly reduced temperature dependence than was witnessed in Fig 6 for the same temperatures in the gas phase regime. The etching reaction in the condensed phase is thought to be similar to that of wet chemical etching in aqueous HF solution, where the etching rate increases with increasing temperature. Spierings(13) reported an activation energy for wet HF etching of 20~35 KJ/mol. Therefore, an increase of etching rate between 28~56 % would be expected with an increase in temperature from 30 to 40°C. At the higher etching rates in this regime, the mass transport of reactants to the surface may begin to affect the observed etching rate as well. To avoid these effects, HF vapor processing equipment should be designed to exhibit a high mass transfer rate through the use of high gas flow rates and/or reduced operating pressure.

## References

1. P. Singer, *Semiconductor International*, p. 88, (Oct. 1995).
2. M. Wong, M.M. Moslehi, and D.W. Reed, *J. Electrochem. Soc.*, **138**(6), 1799 (1991).
3. H. Watanabe, H. Kitajima, I. Honma, H. Ono, R. J. Wilhelm, and A. J. L. Sophie, *J. Electrochem. Soc.*, **142**(4), 1332 (1995).
4. C. Werkhoven, E. Granneman, M. Hendriks, R. de Blank, S. Verhaverbeke, P. Mertens, M. Meuris, W. Vandervorst, M. Heijns and A. Philipossian, *Proceedings of the International Electron Device Meeting*, 633 (1992).
5. V. Leeuwen, *Semiconductor International*, **13**(11), 86 (1990).
6. C. R. Helms and B. E. Deal, *J. Vac. Sci. Technol. A* **10**(4), 806 (1992).
7. C.S. Lee, J.T. Baek, H.J. Yoo, and S. I. Woo, *J. Electrochem. Soc.*, **143**(3), 10 (1996).
8. J. C. Brosheer, F. A. Lenfesty, and K. L. Elmore, *Ind. Eng. Chem.*, **39**, 423 (1947).
9. P. A. Munter, O. T. Aepli, and R. A. Kossatz, *Ind. Eng. Chem.*, **41**, 1504 (1947).
10. P. A. Munter, O. T. Aepli, and R. A. Kossatz, *Ind. Eng. Chem.*, **39**, 427 (1947).

11. W. J. C. Vermeulen, L. F. Tz. Kawakman, C. J. Werkhoven, E. H. A. Granneman, S. Verhaverbeke, and M. Heyns, *Proceedings of the Third International Symposium on Cleaning Technology in Semiconductor Device Manufacturing*, 241 (1994).
12. K. Torek, J. Ruzyllo, R. Grant, and R. Novak, *J. Electrochem. Soc.*, **142**(4), 1322 (1995).
13. G. A. C. M. Spierings, *Journal of Material Science*, **28**, 6261 (1993).

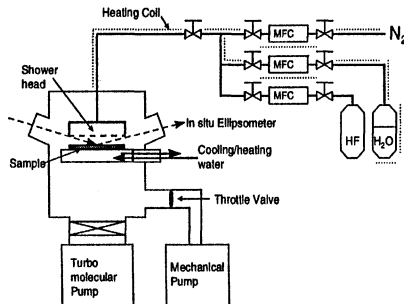


Fig. 1. Schematics of the HF vapor etching chamber and gas handling system. All gases are metered with mass flow controllers. The lines and mass flow controllers are heated so as to prevent condensation in the gas delivery system. The sample is mounted on a temperature-controlled surface that is cooler than the feed gas or chamber walls. Ellipsometry is used to monitor the etching rate and formation of films on the surface during etching.

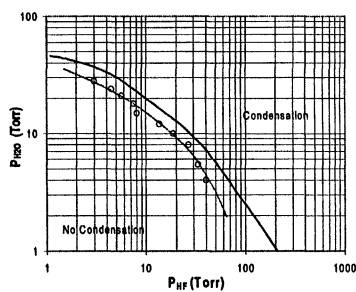


Fig. 2. Vapor-Liquid Equilibrium and Condensate Phase Diagram for HF-H<sub>2</sub>O at 40 °C. The solid line indicates HF-H<sub>2</sub>O phase equilibrium data from Munter *et al.* Formation of condensate films during oxide etching for these partial pressures are indicated for a total pressure of 250 Torr and total flow rate of 500 sccm.

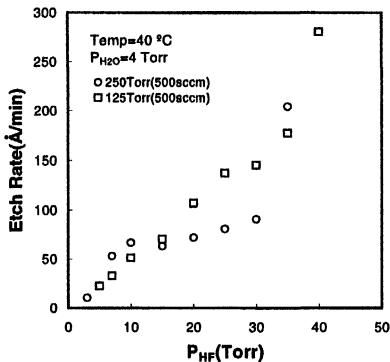


Fig. 3. Etching rate of thermal oxide as a function of P<sub>HF</sub>. Since the partial pressures of reactants in the feed gases of both data sets are the same, the deviations in the observed etching rates are attributed to mass transport limitations. Non monotonous trends with temperature indicate complex surface kinetics. Repeat experiments at 25 Torr indicate an experimental error of 10 Å/min. The difference between two curves is 5 times more than the experimental error.

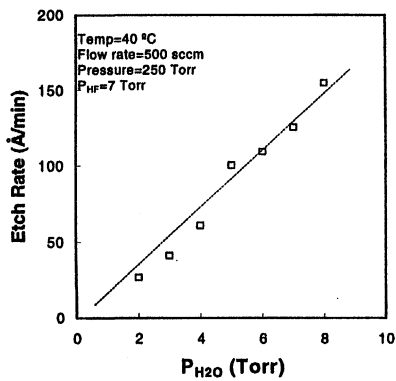


Fig.4. Etch rate of thermal oxide as a function of H<sub>2</sub>O partial pressure for low HF partial pressure, 7 Torr

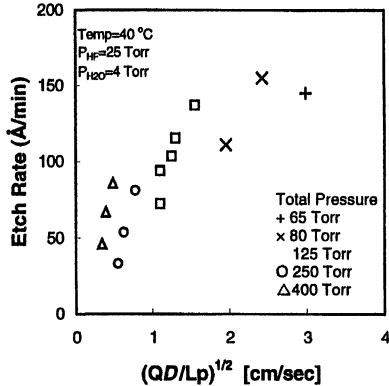


Fig.5. Etch rate as a function of (QD/Lp)<sup>1/2</sup>, the scaling for a mass transfer controlled etching process. The approximate linear response indicates that the mass transfer is dominant in that regime, however, the scattering in the data suggests a complex surface mechanism in which the products affect the etching kinetics. Spacings of 1.3, 2.0 and 2.6 cm were used.

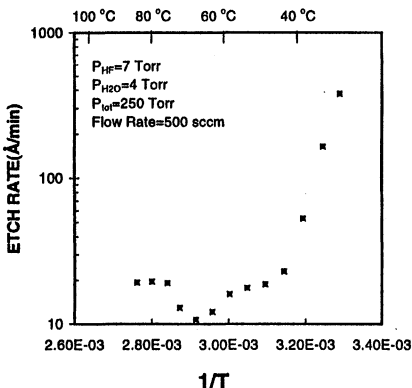


Fig. 6. Arrhenius plot showing etch rate as a function of Temperature for the gas phase etching regime. Under all conditions indicated in this plot, condensation was not observed by ellipsometry.

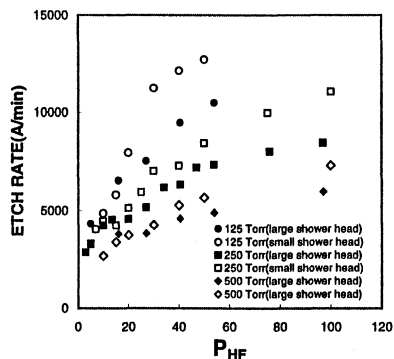


Fig. 7. Etch rate as a function of  $P_{\text{HF}}$  in the condensed regime.  $P_{\text{H}_2\text{O}}=27 \text{ Torr}$ ,  $T=40^\circ\text{C}$ , and Flow Rate = 500 sccm. The variation with pressure and showerhead size is consistent with mass transport effects reducing the etching rate.

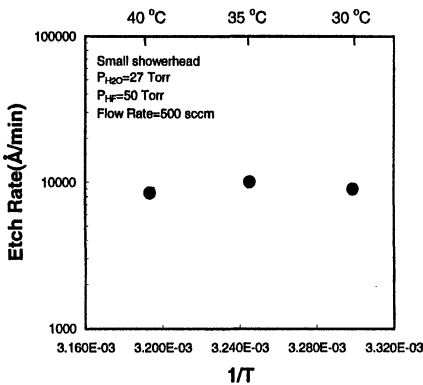


Fig. 8. Etch rate as a function of Temperature in the condensed regime. The lack of variation in the etching rate differs from that observed in the gas phase regime (Fig. 6) at the same temperatures. The temperature dependence in this regime is consistent with that of aqueous oxide etching in which a small increase in etching rate is observed with increasing temperature.

# **Surface Analysis of Clustered Dry Cleaning of Residue from an ICP Oxide Etch**

A. Scott Lawing, Yong-Pil Han and Herbert H. Sawin

Massachusetts Institute of Technology

Department of Chemical Engineering

Cambridge, MA 02139

A totally integrated: oxide etch in an Inductively Coupled Plasma (ICP) reactor, oxygen plasma Post Etch Treatment (PET), and dry cleaning sequence has been demonstrated on blanket and patterned 4" oxide wafers. The entire process sequence was performed in a clustered system in our laboratory. We support our cleaning results with *in-situ* X-ray Photoelectron Spectroscopy (XPS). Our results on blanket wafers indicate that in most cases, an *in situ* high density oxygen plasma PET is effective in removing fluorocarbon contamination. A vapor phase HF process removes the oxide film resulting in a fairly clean surface. On patterned oxide wafers, two distinct types of contamination have been observed.

## **Introduction**

In recent years, high density plasma etching has been investigated for semiconductor processing(1). In a high density plasma etcher the plasma is generated remotely from the wafer, and a separate power supply is used to control the energy with which ions bombard the wafer surface. In this configuration, somewhat separate control is maintained between the plasma density and the ion energy(2). This differentiates high density etchers from conventional parallel plate designs, where the plasma density and ion bombardment energy are intimately coupled.

Although the basic mechanism of the selective etching of SiO<sub>2</sub> over silicon is the same in high density etchers as in parallel plate reactors (i.e. the deposition of a passivating polymer film on the silicon surface), the specifics can be quite different. Because of the high plasma density, the passivating polymer films are generally much thicker in a high density reactor, not only because more polymer precursors are generated in the higher density plasma, but because the higher concentration of reactive fluorine demands that a thicker polymer film be deposited to prevent excessive silicon etching.

Here we apply our dry cleaning methodology, previously developed for the RIE/barrel ash system(3), to wafers etched in a high density plasma. The systems are different enough that clean-up remains a challenging problem. In addition to the high density oxide etching process, the ability to perform the entire process sequence under high vacuum conditions differentiates this work from the RIE/barrel ash system. The ability to avoid ambient contamination effects, and specifically the growth of native oxide films on the processed wafer surface, allows us to obtain a much more accurate

picture of the evolution of the wafer surface chemistry through the process sequence. In this work, blanket and patterned oxide films were etched in an Inductively Coupled Plasma (ICP) etcher in pure  $C_2F_6$  and mixtures of  $C_2F_6$  and  $CHF_3$ . An *in situ* oxygen plasma post-etch treatment (PET) was used to remove the bulk of the polymer contamination. A range of dry cleaning strategies were employed to attack the remainder of the contamination, and the processes used included combinations of vapor phase HF, UV/ $Cl_2$  and UV/ $O_2$ .

## Experimental

The experiments described here were performed in the Integrated Processing Apparatus in our laboratory, illustrated in Figure 1. This system consists of 13 chambers, most of which are configured to process 4" silicon wafers, connected to a central transfer tube. A sample transfer system, consisting of a cart running on rails down the length of the tube, allows samples to be moved along the length of the tube. In addition each chamber has a transfer rod associated with it, allowing wafers to be moved from the cart into/out of the individual chambers. This system allows for wafer transfer between any chamber connected to the apparatus while maintaining vacuum integrity. The base pressure of the transfer tube is in the low  $10^{-8}$ -mid  $10^{-9}$  Torr range. The chambers used in this work are; the UV/ $Cl_2$  chamber, the HF/Vapor chamber, the High Density (ICP) Etcher, and the Analytical Chamber. All of these chambers were designed in our laboratory.

In all of the experiments reported here the "top power" was supplied at 13.56 MHz. The wafer electrode, or "bottom power" was driven at either 10 Mhz or 11 Mhz. The oxygen plasma PET was performed in the high density etcher. All PET's were performed at 50 mTorr for 2 minutes.

In past vapor-phase HF processing experiments(3), and the blanket oxide experiments discussed in this chapter, we needn't be concerned with the etch rate regime in which the HF/Vapor process was performed. However, with patterned wafers, it is impossible to attack the native oxide aggressively. Because of the purely chemical and therefore isotropic nature of the vapor-phase HF etch, the side walls would be etched excessively. Therefore, we had to have an accurate understanding of the thickness of the native oxide on the wafer surface, and also be able to design an HF process which would only etch this thickness with minimal over etch. Figure 2 illustrates the two regimes of vapor phase HF etching at 40°C(4,5). By operating well into the non-condensing regime, a purely surface etching reaction takes place. This surface reaction is typified by etch rates on the order of 10's of Å/min, whereas the condensed etching regime is typified by etch rates on the order of 1000's of Å/min. We were therefore able to design a process to etch on the order of 100 Å of oxide, and maintain the integrity of the side walls while completely stripping the ~50 Å PET grown oxide.

The wafers used in this work were 5500 Å thermally grown oxide films on 4" p-type <100> silicon wafers. Both blanket oxide films and patterned wafers were used in these experiments. Two different masks were utilized for patterned wafers. The first

contained a 5 cm x 5 cm grating pattern of 2.5  $\mu\text{m}$  lines and 3.5  $\mu\text{m}$  spaces. This pattern was used for XPS analysis of the process sequence. The second pattern consisted of arrays of contact holes, ranging from 1.25 to 5  $\mu\text{m}$ . This contact mask also gave us valuable information about critical dimension control in a more realistic feature geometry.

## Results and Discussion

### Processing of Blanket Oxide Wafers

Figure 3 shows carbon 1s and silicon 2p photoelectron emission spectra at normal take-off illustrating the RIE/barrel ash cleaning sequence applied to a blanket oxide film etched at 300 W top/25 W bottom in pure  $\text{C}_2\text{F}_6$  at 45 mTorr and ashed in the high density reactor. The process sequence is represented by reading the spectra from top to bottom. The post-etch polymeric contamination is a ~50 Å thick film with an average F/C ratio of 1.35. The F/C ratio is quite a bit higher than what we observed in the RIE system, but not atypical of what is generally seen after a high density etch(6,7,8,9,10). The PET performed with 25 watts of bottom power removes the bulk of the fluorocarbon contamination and results in the growth of a >> 50 Å oxide. Note that the substrate peak is no longer resolved in the silicon spectrum, so the oxide thickness cannot be determined based on the XPS peak intensity. An initial UV/ $\text{Cl}_2$  process, performed at 5 Torr  $\text{Cl}_2$  for 1 minute, results in a reduction of the carbon intensity, but no apparent change in the chemical state of the carbon. The silicon spectrum shows a downward shift in the  $\text{SiO}_2$  bonding after the UV/ $\text{Cl}_2$  process, corresponding to the removal of oxide incorporated polymer residue, and analogous to the shift which was observed in the RIE system. A HF/vapor process results in the removal of the oxide film and reveals a large amount of mostly graphitic carbon. A second 5 Torr, 1 minute UV/ $\text{Cl}_2$  process reduces the carbon signal to near the background level.

In contrast to the RIE/barrel ash system, an organic clean prior to the HF/Vapor process is not required to achieve complete oxide removal in the high density system. Figure 4 shows carbon 1s and silicon 2p photoelectron emission spectra illustrating an HF only clean applied to a blanket oxide film etched at 300 W top/150 W bottom in 1:1  $\text{C}_2\text{F}_6:\text{CHF}_3$  at 10 mTorr. The post-etch polymer is ~90 Å thick with an F/C ratio of ~0.2. This PET was performed without the use of bottom power and the ~50 Å oxide grown in the PET is thinner than that represented in figure 3. Because of the efficiency of the oxygen plasma PET, we found it unnecessary to perform the UV/ $\text{Cl}_2$  polymer removal step prior to stripping the oxide with an HF/vapor process. In the RIE system, complete oxide removal was not observed unless the organic contamination was attacked before the oxide strip. The *in situ* PET is more efficient at polymer removal because of the higher density of reactive oxygen species as compared to a conventional barrel asher. Figure 5 shows survey spectra illustrating HF/Vapor only cleaning sequences on ICP etched and PET processed wafers compared to a UV/ $\text{Cl}_2$ -HF/Vapor cleaning sequence on an RIE etched barrel ashed wafer. Both of the post ICP etch polymers were ~ 5 Å thick with F/C ratios >1. The top/bottom power settings are given for the ICP etch and PET processes.

All of the surfaces appear similar chemically and are characterized by monolayer levels of fluorine, oxygen and carbon contamination.

#### Processing of Patterned Oxide Wafers

Figure 6 shows carbon 1s photoelectron emission spectra illustrating an integrated cleaning sequence applied to a patterned oxide wafer (line & space) etched at 300 W top/45 W bottom in 1:1 C<sub>2</sub>F<sub>6</sub>:CHF<sub>3</sub> at 5 mTorr. The process sequence is represented by reading the spectra from top to bottom. The post-etch polymer was ~25 Å thick with an F/C ratio of ~1.14. The PET resulted in the growth of a ~50 Å thick oxide. The UV/Cl<sub>2</sub> process conditions were 3 minutes at 2 Torr and 100°C. Qualitatively, the surface chemistry appears similar to what was observed on the blanket oxide samples. The most significant difference is the chemical state of the carbon contamination after the HF oxide strip, and especially after the UV/Cl<sub>2</sub> process. On patterned wafers, the residual carbon after the HF process is more highly fluorinated. And especially after the UV/Cl<sub>2</sub> process, where the carbon observed on the blanket wafers after a similar sequence was typically exclusively graphitic, a high degree of halogenation is observed.

Figure 7 illustrates the effect of UV/Cl<sub>2</sub> processing on the residual carbon contamination left on a patterned wafer surface after an ICP etch, PET and HF/Vapor process. Times indicated at right represent the cumulative UV/Cl<sub>2</sub> processing time. The initial level of contamination is reduced after 3 minutes of exposure, and is heavily halogenated, halogenation increasing with time from 0-3 minutes, with a chemical state distribution similar to what is shown in Figure 5. A further 3 minutes of processing has no effect on either the level of carbon or the chemical state.

The chemistry of carbon removal is obviously different on a patterned wafer surface. The most likely interpretation of these results is that the carbon which remains on the patterned wafers after UV/Cl<sub>2</sub> exposure is not associated with the exposed silicon surface but is incorporated in the oxide lines. We have already established that the UV/Cl<sub>2</sub> process is effective at removing polymer residue from an exposed silicon surface. Even incorporated carbon should be removed, since the etch rate of silicon in UV/Cl<sub>2</sub> is ~50 Å/min at 2 Torr and 100°C, because ~300 Å of substrate should have been removed in the process illustrated in Figure 7. This etching depth would be more than enough to remove any carbon which would have been incorporated into the substrate due to processing at the conditions used, especially if the ~50 Å of substrate consumed in the PET is considered. The efficacy of slight substrate etching (on the order of 100 Å) with UV/Cl<sub>2</sub> for the recovery of electrical properties after RIE has been established(11), and the degree of ion induced substrate damage and contamination incorporation is significantly less for the lower ion bombardment energies used in high density processing(12).

Figure 8 shows silicon 2p and oxygen 1s photoelectron emission spectra corresponding to the carbon spectra illustrated in Figure 6. The vertical lines corresponding to the binding energy of "clean" SiO<sub>2</sub> are included to aid in visualizing chemical shifts. Two distinct types of contamination are suggested by the spectra. The first ("type 1") is analogous to the polymer incorporated in the ash-grown oxide which

has been observed on blanket oxide films in both the high density and RIE systems(3). This contamination is typified by a positive shift in the SiO<sub>2</sub> binding energy in both the silicon 2p and oxygen 1s emission and is evident in the post etch and post HF/Vapor spectra illustrated in Figure 8. Note that the SiO<sub>2</sub> binding energy shifts back after the PET and UV/Cl<sub>2</sub> processes corresponding to the removal of the type 1 contamination (to the analysis depth of XPS) by these processes. The shift in binding energy most likely arises from the buildup of excess positive charge in the oxide due to the presence of incorporated carbon contamination. Baer *et al.*(13) have attributed a similar shift in a self-assembled monolayer SiO<sub>2</sub>/Si system to the generation of trapped charge at the SiO<sub>2</sub>/Si interface due to electron beam damage, while Kodama *et al.*(14) have noted that incorporated carbon causes positive charge build-up in a COB-DRAM device. The second type of incorporated contamination ("type 2") is not well understood. This contamination is typified by a peak at ~108.5 eV in the silicon 2p photoemission, and a peak at ~531.5 eV in the oxygen 1s photoemission (although the exact binding energies appear to be somewhat variable and tend to shift with the SiO<sub>2</sub> shift due to type 1 contamination), and we have assigned it the designation Si-O<sub>Polymer</sub>. Type 2 contamination is not removed by the UV/Cl<sub>2</sub> process.

Figure 9 shows AFM images and the corresponding line scans from contact mask samples which were etched in 1:1 C<sub>2</sub>F<sub>6</sub>:CHF<sub>3</sub> (5 mTorr) and 100% C<sub>2</sub>F<sub>6</sub> (15 mTorr) chemistries. It is interesting, and perhaps significant, that the samples etched at a condition that yields more type 2 contamination (i.e. 1:1 C<sub>2</sub>F<sub>6</sub>:CHF<sub>3</sub>) exhibit better critical dimension control. Note that the sidewalls are much more vertical on the features etched in the 1:1 chemistry. In the samples etched in pure C<sub>2</sub>F<sub>6</sub>, where type 2 contamination was not as pronounced, the sidewalls appear bowed, and the dimension at the top of the feature is larger than that at the bottom. Especially note the "arena" effect around the periphery of the contacts illustrated in Figure 9a. This raises the possibility that type 2 contamination is associated with effective pattern transfer. Other pieces of evidence support this. The type 2 contamination chemical state has thus far not been observed on blanket oxide wafers or a contact pattern wafer, even one etched at conditions which exhibit type 2 contamination on a line & space pattern. With the contact pattern, the analyzed surface is effectively blanket resist-over-oxide, since the areal density of contacts in the analyzed area is <0.01%. This would suggest that type 2 contamination is associated with features on the wafer, since it is not observed unless a detectable fraction of the surface is being etched. Also, notice that although resist "breakthrough" was observed over ~50% of the oxide surface on the sample represented by Figure 9a (note the alternating pattern of rough and smooth surface), there was always a "halo" of smooth oxide around the contacts. The same effect has been observed at the edges of oxide lines, even when the center of the line was roughened significantly. This would suggest that there is a passivation mechanism which depends on the presence of oxide etch products which is active in the region immediately adjacent to a feature being etched. Possibly, this passivation mechanism is coupled with the formation of type 2 contamination in the oxide adjacent to a feature being etched.

## Conclusions

Preliminary experiments on integrated processing have been performed with an eye towards developing a totally integrated ICP etch, oxygen plasma PET, and dry cleaning sequence. Both blanket and patterned oxide films have been studied. Our results indicate that in this system, an "HF only" cleaning sequence yields a surface with a low level of surface contamination. The reason for this is that the high density oxygen plasma PET is very efficient in removing surface polymeric contamination.

Two types of contamination were observed on patterned oxide wafers. Type 1 contamination is analogous to the incorporated polymer observed on blanket wafers in both the high density and RIE systems. Type 1 contamination is typified by a positive binding energy shift in both the silicon and oxygen SiO<sub>2</sub> photoemission and is removed by UV/Cl<sub>2</sub> processing. Type 2 contamination is due to chemically bonded contamination in the oxide layer. Type 2 contamination is identified by the emergence of additional peaks which exhibit a positive binding energy shift relative to SiO<sub>2</sub> in the silicon and a negative shift relative to SiO<sub>2</sub> in the oxygen photoemission. It is not significantly affected by UV/Cl<sub>2</sub> processing. The nature of type 2 contamination is in question, but it may be related to critical dimension control.

## References

1. P. Singer, Semiconductor International, Vol. 20, No. 6, 109-114 (1997).
2. M. Lieberman and R. Gottscho, "Design of High Density Plasma Sources for Materials Processing", Phys. of Thin Films: Advances in Res. and Dev., vol. 17, J. Vossen ed., Academic Press, Orlando, Florida (1993).
3. A.S. Lawing, A.J. Muscat, H.H. Sawin, submitted to J. Vac. Sci. Technol.
4. J.C. Brosheer, F.A. Lenfesty, and K.L. Elmore, Ind. & Eng. Chem., Vol. 39, No. 3, 423-431 (1947).
5. P.A. Munter, O.T. Aepli, and R.A. Kossatz, Ind. & Eng. Chem., Vol. 41, No. 7, 1504-1508 (1949).
6. G.S. Oehrlein, Y. Zhang, D. Vender, and M. Haverlag, J.Vac. Sci. Technol. A, vol. 12, no. 2, 323-332 (1994).
7. G.S. Oehrlein, Y. Zhang, D. Vender, and O. Joubert, J.Vac. Sci. Technol. A, vol. 12, no 2, 333-344 (1994).
8. Y. Miyakawa, K. Fujita, N. Hirashita, N. Ikegami, J. Hashimoto, T. Matsui, and J. Kanamori, Jpn. J. Appl. Phys., Vol. 33, No 12B, 7047-7052 (1994).
9. J.H. Park, S.W. Chung, J.J. Kim, and W.S. Kim, J. Vac. Sci. Technol. B, Vol. 14, No. 1, 478-482 (1996).
10. O. Joubert, P. Czuprynski, F.H. Bell, P. Berruyer, and R. Blanc, J. Vac. Sci. Technol. B, Vol. 15, No. 3, 629-639 (1997).
11. D.K. Hwang, K. Torek, and J. Ruzylo, Proceedings of the 1st International Symposium on Plasma Process Induced Damage, 137-140, AVS-IEEE/Electron Devices Society (1996).
12. G.S. Oehrlein, J. Vac. Sci. Technol. A, vol. 11, no 1, 34-46 (1993).
13. D.R. Baer, M.H. Engelhard, D.W. Schulte, D.E. Guenthier, Li-Qiong Wang, and P.C. Rieke, J. Vac. Sci. Technol. A, Vol. 12, No. 4, 2478-2490 (1994).
14. N. Kodama, H. Mori, S. Saito, and K. Koyama, Nuc. Inst. & Met. Phys. Res. B, Vol. 118, No. 1-4, 505-508 (1996).

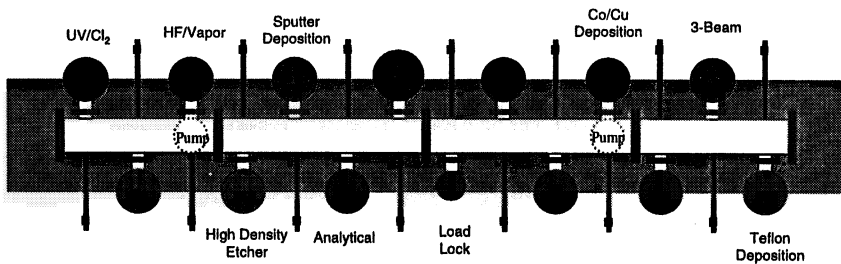


Figure 1 - Schematic diagram of the integrated processing apparatus.

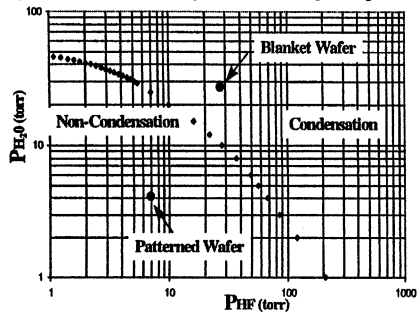


Figure 2 - Condensation and non-condensation regimes in vapor phase HF etching.

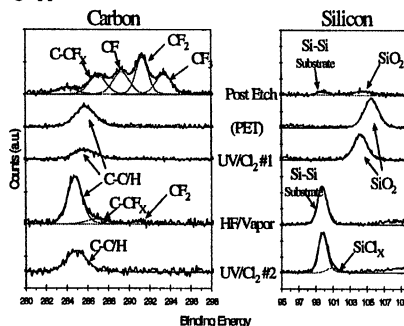


Figure 3 - Carbon 1s and silicon 2p spectra illustrating the RIE/barrel ash cleaning sequence applied to an ICP etched blanket oxide film.

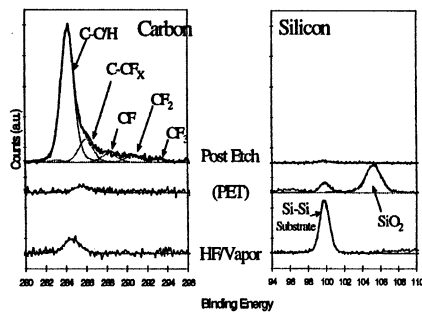


Figure 4 - Carbon 1s and silicon 2p spectra illustrating an HF only clean applied to a blanket oxide film.

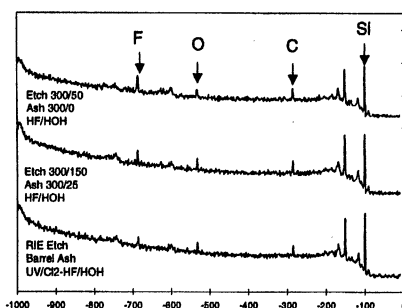


Figure 5 - Survey spectra illustrating HF/Vapor only cleaning sequences on ICP etched and PET processed wafers compared to a UV/Cl₂-HF/Vapor cleaning sequence on an RIE etched-barrel ashed wafer.

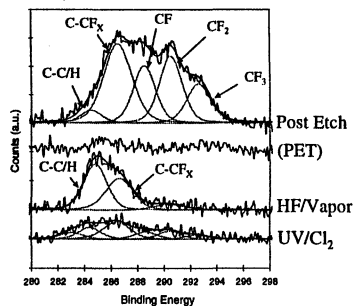


Figure 6 - Carbon 1s spectra illustrating an integrated cleaning sequence applied to a patterned oxide wafer.

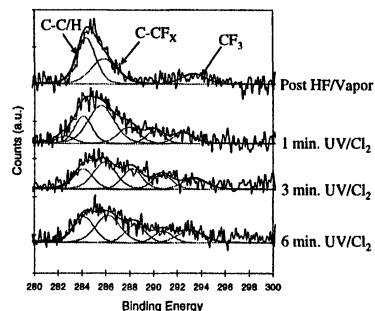


Figure 7 - Carbon 1s spectra illustrating the effect of UV/Cl₂ processing on a patterned oxide wafer.

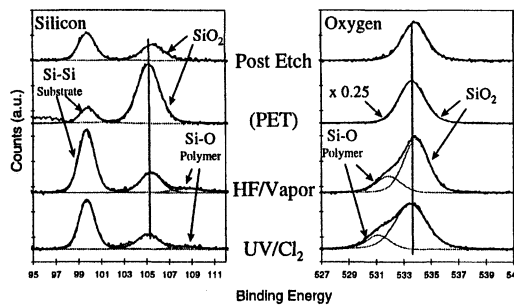


Figure 8 - Silicon 2p and oxygen 1s photoelectron emission spectra corresponding to the carbon spectra illustrated in Figure 6. The vertical lines corresponding to the binding energy of "clean" SiO<sub>2</sub> are included to aid in visualizing chemical shifts.

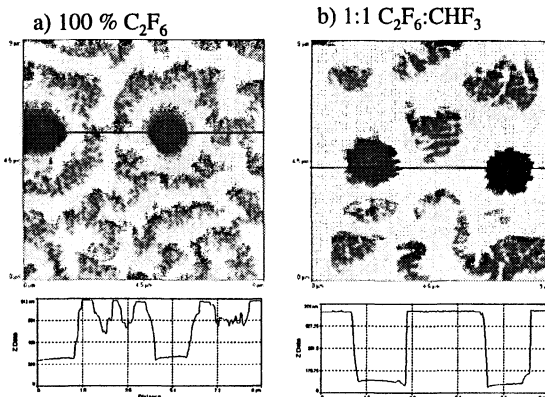


Figure 9 - AFM images and corresponding line scans from contact mask samples.

# **IN-SITU SURFACE ANALYSES OF SI(111) ELECTRODES IN FLUORIDE CONTAINING SOLUTIONS DURING CURRENT OSCILLATIONS**

S. Rauscher, O. Nast, H. Jungblut and H.J. Lewerenz

Hahn-Meitner-Institut Berlin GmbH Abteilung CG

Glienicker Str. 100, D-14109 Berlin

Electrochemically induced current oscillations of n- and p-type Si(111) in fluoride containing solutions and the corresponding chemical, electronical and morphological variations are investigated by different in-situ techniques: fast Fourier transform infrared spectroscopy, microwave reflectivity and atomic force microscopy. An oscillating behavior exhibiting the same frequency as the current is observed for the absorption due to Si-O bindings, the reflected microwave signal and the surface roughness. The results are discussed in terms of a competition between oxidation of silicon and oxide etching.

## **INTRODUCTION**

Oscillation phenomena are well known since long in the electrochemistry of metals (1). Corresponding research at semiconductor electrodes is less evolved. Most of the effort was directed towards investigations of silicon (2-10). Oscillations on Si samples in fluoride containing electrolytes can be observed at higher anodic potentials (above ca. 3 V vs. SCE), independently on crystal orientation and dopant type. This process is assumed to be caused by a competition between oxide formation (connected with current flow) and dissolution (currentless). The appearance of oscillations on n-Si requires illumination while the phenomenon on p-Si also takes place in the dark. Being of purely fundamental interest at first, it has turned out that photocurrent oscillations could successfully be used to produce high quality H-terminated Si(111) surfaces exhibiting interface state densities of about  $10^{10}$  cm $^{-2}$ eV $^{-1}$  (11, 12). In the present study the morphological changes, the amount of oxide and the integrated microwave signal during oscillations were investigated by different in-situ techniques: atomic force microscopy (AFM), Fourier transform infrared spectroscopy (FTIR) and microwave reflectivity (MR)(7) to gain some more insight into the processes accompanying the current oscillations.

## EXPERIMENTAL

An AFM electrochemistry cell made of plexiglas and a Nanoscope II were combined for the in-situ investigations of the silicon oxide/electrolyte interface. The experiments were performed under potentiostatic control using the standard three electrode potentiostatic arrangement with an EG&G (Model 362) potentiostat. Platinum wire (0.5 mm) served as counter electrode, a Luggin capillary connected with a saturated calomel electrode (SCE) as reference electrode. As working electrodes single crystals of p-type Si(111) doped with boron (specific resistivity of 13 Ωcm) were used. p-type silicon samples were utilized to prevent any interference between light-induced processes due to the laser detection system of the AFM and morphological changes caused by the oscillations. The misalignment was less than 0.1° from the <111> direction (X-ray diffraction measurements). A sealing ring made out of silicone was pressed onto the surface, forming a volume of 16 mm<sup>3</sup> and leaving 31 mm<sup>2</sup> of the Si surface free to the electrolyte. While investigating the surface the liquids in the cell could be changed without exposing the sample to air. Cantilevers with integrated tips consist of silicon nitride (Digital Instruments). To obtain reproducible initial conditions prior to in-situ AFM investigations the silicon substrates were prepared according to the following procedure:

- (1) cleaning with acetone in an ultrasonic bath (10 minutes),
- (2) cleaning with methanol in an ultrasonic bath (10 minutes),
- (3) forming a chemical oxide in H<sub>2</sub>SO<sub>4</sub>(96%):H<sub>2</sub>O<sub>2</sub>(30%):H<sub>2</sub>O (volume ratio 6:1:3) at 75°C for 10 minutes and finally,
- (4) etching in 40% NH<sub>4</sub>F (pH 8.0) for 15 minutes at 10 °C.

After step (1) and (2) the sample was dried with N<sub>2</sub>. Before and after step (3) the sample was extensively rinsed with ultrapure water (>18 MΩcm, Millipore-Q). After step (4) the specimen was shortly rinsed with water, dried in N<sub>2</sub> and mounted in the ECAFM within 30 seconds. We immediately investigated whether the preparation succeeded, i.e. a well defined surface was formed. Due to an anisotropic etching behavior of concentrated NH<sub>4</sub>F in Si(111)-1x1:H surfaces are obtained which exhibit large atomically flat terraces of ca. 200 nm in width separated by each other by steps of 3.1 Å in height. The in-situ AFM measurements during current oscillations were performed in 0.1 M NH<sub>4</sub>F, pH = 4.0 at a sample potential of + 5.2 V vs. SCE.

A commercially available Bruker infrared spectrometer was used for the FTIR measurements. Only 8 wavelength scans were made per spectrum (0.5 s per scan) in order to

follow the rapid changes during the current oscillations. As in the AFM experiments, a three electrode potentiostatic circuit (Pt counter electrode ring, saturated calomel reference electrode, HEKA potentiostat) was used. In contrast to the AFM experimental setup, n-Si(111) doped with phosphorus ( $50 \Omega\text{cm}$ ) was used as working electrode. Therefore, the sample had to be illuminated (white light,  $10 \text{ mWcm}^{-2}$ ) to provide the holes necessary for the oxidation process. It is, however, difficult to investigate the wavenumber region of the asymmetric Si-O stretching mode in the standard attenuated total reflection (ATR)-multiple internal reflection geometry using large crystals because of the high multiphonon absorption losses in Si. A thin ( $230 \mu\text{m}$ ) sample of seven mm length and therefore with a drastically reduced optical path length (11 mm) is used to become more sensitive in the spectral region between  $1000 \text{ cm}^{-1}$  and  $1300 \text{ cm}^{-1}$ . By means of a separate experiment it became possible to calibrate the Si-O signal integral with respect to oxygen coverage in monolayers (ML) assuming each Si atom to be fourfold oxidized (13).

The measured reflected microwave signal depends on the conductivity and thus on the concentration of free charge carriers  $n$  (electrons) and  $p$  (holes). Under illumination  $n$  and  $p$  is increased by the excess carrier concentration  $\Delta n$  and  $\Delta p$ , respectively, leading to an increase of the conductivity of

$$\Delta\sigma = \Delta n \mu_n + \Delta p \mu_p = \Delta n (\mu_n + \mu_p) = \Delta p (\mu_n + \mu_p) \quad [1]$$

( $\mu_n$ ,  $\mu_p$  electron and hole mobility, respectively). In our experiment the silicon surface was exposed to both, a stationary white light ( $30 \text{ mWcm}^{-2}$ ) and additionally to a chopped (853 Hz) light flux of a laser diode ( $\lambda = 780 \text{ nm}$ ,  $3.5 \text{ mWcm}^{-2}$ ). With lock-in amplification only the relative change of the microwave signal MW caused by the chopped light is detected which corresponds to

$$MW \sim \int_0^d \Delta p_{ch} dx \quad [2]$$

( $d$  sample thickness and  $\Delta p_{ch}$  the excess carrier concentration caused by the chopped light).

The simultaneous measurement of photocurrent and microwave reflectivity demands a specific electrochemical cell configuration: to avoid microwave transmission problems in solution, the microwave reflectivity and the excess reflectivity upon illumination are measured from the backside during illumination from the front (solution)

side. As working electrode low resistivity samples ( $50 \Omega\text{cm}$ ) were used. The three electrode potentiostatic circuit corresponds to the AFM and FTIR experiments.

Both, the FTIR as well as the MW experiments were performed in 0.1 M NaF, pH = 4.0, at a sample potential of + 6 V vs. SCE.

## RESULTS AND DISCUSSION

The roughness variation pursued in the AFM experiment will be discussed at first. For a quantitative determination of the roughness changes the following aspect has to be considered: there are two scan directions for obtaining a surface profile by AFM, the x and the y direction, respectively. For a  $2 \times 2 \mu\text{m}^2$  surface the x-axis scan is quickly obtained, i.e. the recording of one scan line needs only 50 ms. After obtaining this scan line the sample is moved by 10 nm into y-direction and a renewed sampling of the surface takes place into x-direction. Each image is composed of 200 scan lines. The overall time for the build up of one image therefore amounts to 10 s. If the morphological changes take place in a time range of seconds the x-direction of each micrograph then reflects (nearly) the instantaneous topography while the y-direction contains both, the spatial structure and its temporal change. For a quantitative analysis of the topographic changes this convolution should be avoided. This can be accomplished either by a higher scan rate or by sampling the surface only in x-direction (linescan). In this case the y-direction represents the temporal change of the linescan repeatedly obtained at the same place. This method was used for analyzing the morphological changes. Fig. 1(a) shows the temporal change of such a linescan, Fig. 1(b) the corresponding current transient together with roughness parameters obtained from Fig. 1(a). The roughness parameters were calculated by the software of the AFM and are defined by

$$R_a = \int_0^L |f(x)| dx \quad [3]$$

$f(x)$  is a cross sectional data profile which is drawn relative to a calculated averaged line. This line is defined such that the areas surrounded by the profile are equal above and below this line. Concerning the profile, however, one has to be conscious of the general problem that all structures being of comparable size as the tip (and smaller) cannot be satisfactorily resolved. So far the absolute accuracy of the  $R_a$  values is limited by the foremost tip apex and radius. Fig. 1(a) shows a roughening of the oxide/electrolyte interface at the increase

of the current while comparatively smooth surfaces are observed after the current maximum and in the time range around the current minimum. It can further be seen that the structures due to the roughening do not appear at the same places. This is also valid if many current peaks are pursued. The periodicity of the  $R_a$  values, however, is nearly maintained for two and more oscillations.

In Fig. 2 the charge  $Q - Q_m$  (b), the oxide coverage changes  $\Delta Si-O$  (c), the relative change of the microwave signal MW (d) and the roughness parameter (e) are plotted relative to the current oscillation (a). All data oscillate with the same frequency as the current, but exhibit different phase shifts. The charge  $Q - Q_m$  is calculated from the current density (Fig. 2(a)) by

$$Q - Q_m = \int_0^t (i(t) - i_m) dt \quad [4]$$

with  $i_m$  the average current density also plotted in Fig. 2(a). Under the assumption that  $i_m$  provides an average oxide coverage,  $i(t) > i_m$  means that oxide formation and  $i(t) < i_m$  that oxide dissolution predominates. If each silicon atom in silicon oxide is supposed to be fourfold oxidized a charge of  $0.5 \text{ mCcm}^{-2}$  is necessary for the oxidation of one monolayer (ML)  $Si(111)$ . Then a variation of the oxide coverage of  $\pm 5 \text{ ML}$  can be determined from Fig. 2(b). This agrees well with the  $\Delta Si-O$  change of  $\pm 20\%$  around an average corresponding to 24 ML obtained from the IR absorption experiment (Fig. 2(c)). From that we conclude that nearly all charge carriers contributing to the current are consumed for the oxide formation. The asymmetric shape of curve (b) and (c) indicates that oxide formation during the current peak (curve (a)) occurs faster than etching in the current valley. The minima of curve (b) and (c) coincide with  $i = i_m$  in the increasing and the corresponding maxima with  $i = i_m$  in the decaying part of the current oscillation (curve (a)). Because the current does never disappear during the oscillations a porous structure of the oxide has to be assumed rendering a more or less conductive contact between the silicon substrate and the electrolyte at all times.

Due to the applied potential the light induced charge carriers (holes) migrate to the surface. We assume that in case of large oxide coverage the charge carriers are predominantly dammed up at the surface and recombine with rates depending on the passivating property of the oxide coverage. For lower oxide coverages being more permeable for the electrolyte species the charge carriers will mainly pass the silicon/silicon oxide interface and contribute to the current leading to oxide formation. This behavior is reflected by the MW signal: during the steep current increase (Fig. 2(a)) the MW signal rapidly decreases

(Fig. 2(d)), indicating a strongly improved charge transfer rate. The subsequent increase of the MW signal is more gradual than the rapid decay of the current. In the time range around the current minimum, i.e. when the current changes only slightly, the MW signal rises continuously. This might indicate an increasing suppression of surface recombination. Consequently the surface recombination is lowest when the MW signal is maximal, i. e. when the oxide coverage is nearly minimal and the oxide formation tends to predominate the oxide dissolution again ( $i(t) \approx i_m$ ; Fig. 2(a, c, d)).

An increase of the current reflects a more effective oxide formation which is connected to a volume expansion at the silicon/silicon oxide interface. Therefore we assume that the roughening of the oxide surface commencing immediately after the current minimum (Fig. 2(e,a)) is caused by the increasing current. A larger roughness renders a more conductive contact between the electrolyte and the silicon substrate, the current (i.e. the charge transfer rate) increases and the MW signal decays again. The phase shift between the roughness and the current transient (roughness maximum before current maximum) might be explained by a local pH variation which is caused by the oxidation reaction and is possibly responsible for the maintenance of the oscillation (14 ).

#### ACKNOWLEDGEMENT

The Autors are indebted to F. Wünsch for his contribution to the microwave measurements.

#### REFERENCES

1. J. Wojtowicz, in *Modern Aspects of Electrochemistry*, J. O'M. Bockris and B. Conway, Editors, Vol. 8, Chap. 2, Plenum Press, New York (1972)
2. H. Gerischer and M. Lübke, *Ber. Bunsenges. Phys. Chem.*, **92**, 573 (1988)
3. F. Ozanam and J.-N. Chazalviel, A. Radi, and M. Etman, *Ber. Bunsenges. Phys. Chem.*, **95**, 98 (1991)
4. F. Ozanam and J.-N. Chazalviel, A. Radi, and M. Etman, *J. Electrochem. Soc.*, **139**, 2491 (1992)
5. J.-N. Chazalviel and F. Ozanam, *J. Electrochem. Soc.*, **139**, 2501 (1992)
6. H. Föll, *Appl. Phys.*, **A 53**, 8 (1991)
7. H. J. Lewerenz and G. Schlichthörl, *J. Electroanal. Chem.*, **327**, 85 (1992)

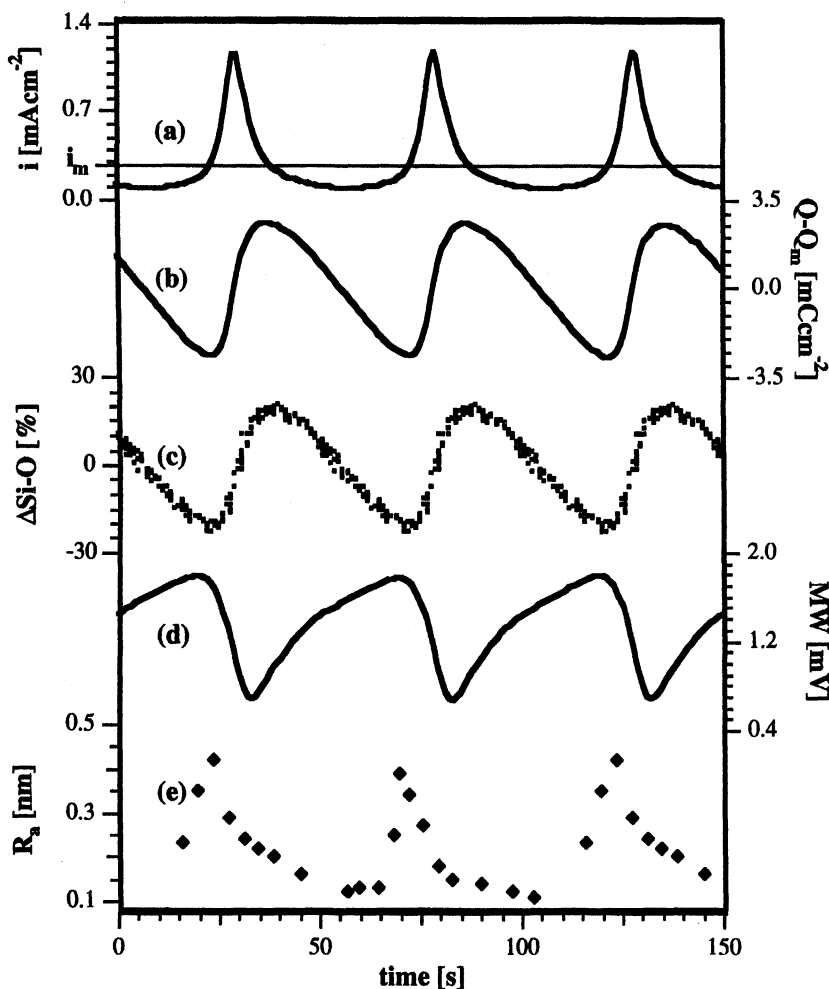


Fig. 2: Current density (a), change of the integrated IR absorption caused by Si-O bindings (b), accumulated charge minus average charge ((c), see text), microwave reflectivity (d) and roughness of the silicon oxide surface (e) during current oscillations.

8. H. J. Lewerenz, G. Schlichthörl, *J. Appl. Phys.*, **75**, 3544 (1994)
9. H. J. Lewerenz and M. Aggour, *J. Electroanal. Chem.*, **351**, 159 (1993)
10. M. Aggour, M. Giersig and H. J. Lewerenz, *J. Electroanal. Chem.*, **383**, 67 (1995)
11. J. Rappich, H. Jungblut, M. Aggour and H. J. Lewerenz, *J. Electrochem. Soc.*, **141**, L99 (1994)
12. S. Rauscher, Th. Dittrich, M. Aggour, J. Rappich, H. Flietner and H. J. Lewerenz, *Appl. Phys. Lett.*, **66**, 3018 (1995)
13. H.J. Lewerenz, accepted for publication in *J. Phys. Chem. (Special Issue)*
14. O. Nast, S. Rauscher, H. Jungblut and H.J. Lewerenz, submitted to *J. Electroanal. Chem.*

## FIGURES

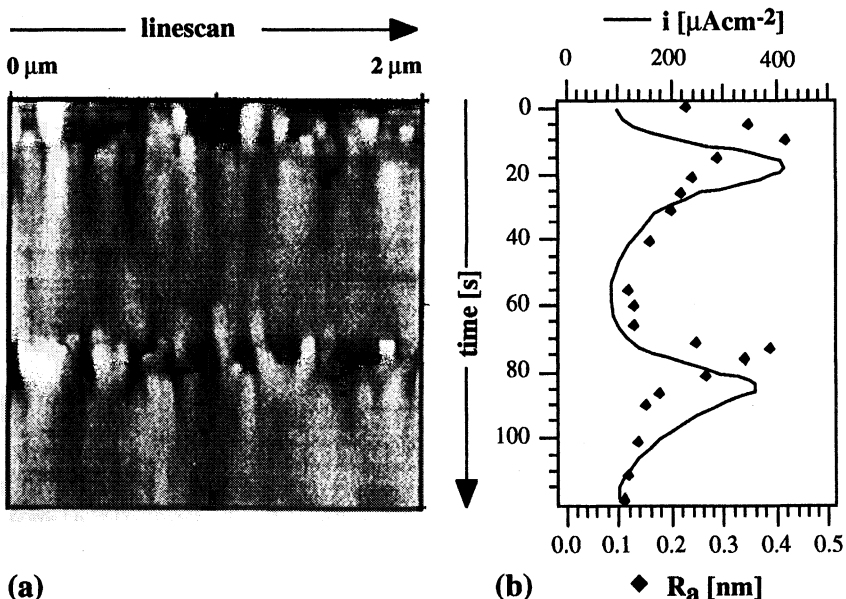


Fig. 1: In-situ AFM linescan of the silicon oxide/electrlyte interface during current oscillations (a). The corresponding current density and roughness are given in (b). Experimental parameters: 0.1 M NH<sub>4</sub>F, pH 4, U = 5.2 V vs. SCE.

# NATURAL HYDROCARBON DEPOSITION ON SILICON WAFERS AND REMOVAL AS MEASURED BY IMS

E. Ollier, S. Marthon, G. Quagliotti and F. Tardif  
Gressi-Leti-CEA/G, 17 rue des Martyrs , 38054 Grenoble Cedex 09, France

In this work, IMS (Ion Mobility Spectroscopy) is used to characterize the carbonated contamination deposited on wafers stored in the air flow of clean rooms and to evaluate the efficiency of conventional cleaning processes and ozonated DI water. Contamination by clean room air is fast and subject to variations of the sources. The ozonated DI water processes are efficient to remove hydrocarbon contaminants, especially by using high concentrations (20 ppm).

## INTRODUCTION

Volatile organic contaminants condensed on silicon wafers in clean rooms are suspected to induce severe defects in several steps of semiconductor manufacturing<sup>(1),(2)</sup> : decrease of gate oxide performance and reliability, modification of chemically amplified photoresists leading to degraded patterned dimensions<sup>(3),(4)</sup>, adhesion defects during wafer bonding... The contamination sources are numerous<sup>(5)</sup> : various equipment composed of polymers, wafer containers<sup>(6)</sup>, chemicals...

Among the analytical methods for organic contamination detection<sup>(5)</sup>, IMS (Ion Mobility Spectroscopy) presents many advantages, in particular a high sensitivity (low limits of detection maybe as low as 10-11 mol) and enables analyses to be performed at atmospheric pressure which provides information regarding light adsorbed molecules. In this work, IMS was used to measure the organic contamination of silicon wafers stored in clean rooms and to evaluate the efficiency of cleaning processes in terms of hydrocarbon removal.

## EXPERIMENTAL DETAILS

All the experiments were performed in LETI's facilities on CZ(100) p-type 14-22 Ω.cm 4" wafers.

### Organic contamination characterization by IMS

The experiments were carried out with a thermal desorption chamber coupled with an IMS equipment (MMS 160P from PCP Inc.-USA). The hydrocarbon molecules condensed on the wafer were outgassed by thermal ramping from 20°C to 250°C with a rate of 40°C/min and ionized by a radiative source. Ions were separated by their mobilities in the drift gas (air). Positive mode spectra were investigated.

The mobilities  $K_0$  reported in this paper are reduced mobilities calculated on the basis of drift times and corresponding to standard conditions (temperature : 273.15K and pressure : 760 Torr). The sample surface was 2 cm<sup>2</sup> (i.e. representing a desorption surface of about 4 cm<sup>2</sup>) and the detected intensities were corrected by subtracting the background signal level of the equipment (blank), which was defined by measuring the clean and stabilized

IMS equipment without any sample. As the IMS is outside the clean room in order to limit its contamination, the wafers were transported after contamination or cleanings in decontaminated boxes. Preparation of the 2 cm<sup>2</sup> samples was carried out just before they were placed in the desorption chamber.

#### **Deposition of hydrocarbon contamination in clean rooms**

Before exposure, the substrates were previously treated in a Sulfuric Peroxide Mixture (CARO 2/1 at 140°C) during 10 minutes followed by an ultraclean rinse in order to remove the last traces of hydrocarbons. The efficiency of this treatment was previously verified.

Then, the hydrocarbons were naturally deposited by storing the wafers in PFA carriers placed in open polypropylene boxes under clean air flow in three different types of clean rooms (classes 10, 100 and 1000) during 10 minutes to 3 months. The wafers stored 2 weeks and 3 months in a class 10 clean room were used to test the cleaning processes.

#### **Cleaning processes tested for organic contamination removal**

Conventional wet cleanings (SC1 and CARO) followed by an overflow rinsing tank and then spin drying were carried out on contaminated wafers. Furthermore, ozonated D.I. water followed by an IPA drying was investigated as well. The process parameters were :

- SC1 (NH<sub>4</sub>OH/H<sub>2</sub>O<sub>2</sub>/H<sub>2</sub>O : 0.25/1/5) : 50 and 70°C; 10 minutes
- CARO (H<sub>2</sub>SO<sub>4</sub>/H<sub>2</sub>O<sub>2</sub> : 3/1); 120°C; 10 minutes
- Ozonated ultraclean DI water with 2 ozone concentrations : 6 and 20 ppm.

## **RESULTS**

#### **Hydrocarbon deposition in clean rooms**

The organic contamination condensation was observed as a function of the time and in different clean room classes. Figure 1 illustrates the contamination occurring in a class 10 clean room for a storage time between 10 minutes and 3 months. In this figure, we chose to split two contributions : ammonia detected via NH<sub>4</sub><sup>+</sup> at K<sub>0</sub> = 3.15 cm<sup>2</sup>.V<sup>-1</sup>.s<sup>-1</sup> and all the hydrocarbon contaminants represented by the sum of their intensities. A very fast contamination of the wafers by ammonia occurs right from the first minutes of exposure and then reaches the saturation limit of the detector. The hydrocarbons deposit during the first hours of exposure. This contamination then increases drastically during the first week. Afterwards, from one week to three months, the experiments reveal appreciable fluctuations. These fluctuations can be attributed to the modifications of the airborne hydrocarbonated contamination in the clean room. These events may be due for example to the introduction of new equipment or polymer materials or to the variations of use of different processing chemicals.

In order to describe the hydrocarbon contamination accurately, table 1 shows the intensities measured on drift spectra for a few exposure times. Except for ammonia, table 1 shows two major contaminants detected at mobilities 2.01 and 1.82. Minor contaminant ions are detected with lower mobilities ranging from 1.65 to 1.17. They probably correspond to high molecular weight species. Some of them are not detected for long storage times. This suggests that contaminants are in equilibrium with the vapour phase and that some of them may leave the surface and be replaced by contaminants having a higher affinity with the wafer surface. This behaviour is very different from what occurs for the other types of contaminants : metallic and particles. Otherwise, the great difference of the intensity corresponding to the 2.01 mobility ion for a 56 day exposure with respect to the others can be noted. This difference may be explained by a variation of the contaminant sources in the clean room as this test was performed 5 months before the others.

Accurate identification of molecules is difficult but it can be noted that the 2.01 and 1.82 mobilities are consistent with two ions observed during thermal desorption of samples deliberately contaminated with diethyl-phthalate (DOP). This molecule was suspected by different authors to condense on wafers in clean rooms<sup>(7)</sup>. It is a widely used plasticizer for polymeric materials. According to mobility tables, the mobility 2.01 is also characteristic of N-Methyl Pyrrolidone, used in chemical processes such as photoresist stripping.

The contaminant detected at the reduced mobility  $K_0 = 1.82 \text{ cm}^2.\text{V}^{-1}.\text{s}^{-1}$  is always present in the clean room and the quantity condensed on wafers reaches a saturation level. It is characteristic of the clean room. As a consequence, it was used to compare its abundance in three classes of clean room. Figure 2 presents the evolution of the peak intensity from one week to one month for clean rooms of classes 1000, 100 and 10. It appears clearly that in spite of the lower particle concentration, class 10 and 100 clean rooms provide a higher organic contamination than class 1000. This result suggests that the problem of organic contamination becomes more important as the rooms become cleaner in terms of particles.

### Hydrocarbon removal from the wafers

The hydrocarbon removal efficiency of conventional cleanings (CARO and SC1) was investigated. These cleaning processes are well known for their hydrocarbon removal capabilities. Figure 3 shows the residual contamination observed at  $2.01 \text{ cm}^2.\text{V}^{-1}.\text{s}^{-1}$  after different cleaning treatments on wafers stored one week in a class 10 clean room. The SC1 efficiency increases with the temperature due to a kinetic effect. Nevertheless, the CARO process is the more efficient<sup>(8)</sup> as the residual signal is lower than the IMS low limit of detection in this used analysis configuration.

The oxidant properties of ozone were also tested. This process is very interesting because it consumes few chemicals. Figures 4 and 5 show the residual hydrocarbons left by 6 and 20 ppm of ozone in DI water. The exposure time in the class 10 clean room was about 3 months (82 days). In each figure, the spectrum of the cleaned sample is compared to the blank spectrum of the IMS equipment. The positions of the observed peaks are indicated with two items of information : the reduced mobility corresponding to the drift time and the intensity previously measured on the contaminated samples ( $I_0$ ). The peaks noted "r.i." correspond to the ions provided by the carrier gas which are usually called reactant ions. After cleaning, a high contamination by ammonia ( $K_0=3.15 \text{ cm}^2.\text{V}^{-1}.\text{s}^{-1}$ ) still remains. In fact, this contaminant probably condenses very quickly on wafers during the short time separating the end of the cleaning process and placing of the wafer in the clean transport boxes. This is consistent with the evolution observed in figure 1. Hydrocarbons are almost completely removed from the silicon wafer : the residual intensities are very low compared to the initial values. The residual signal corresponding to high molecular weight ions (mobilites higher than  $1.7 \text{ cm}^2.\text{V}^{-1}.\text{s}^{-1}$ ) are lower than the low limit of detection. The residual peaks are observed for mobilities : 2.10, 2.01 and  $1.82 \text{ cm}^2.\text{V}^{-1}.\text{s}^{-1}$ .

In order to evaluate the kinetics of hydrocarbon removal by ozonated DI water, the total hydrocarbon ions were measured for different cleaning times on wafers stored 3 months in a class 10 clean room. The results are presented in figure 6. The major part of organic contamination is removed within a short cleaning time. Comparison of the evolutions for the two ozone concentrations shows quite an important increase of the efficiency of the 20 ppm concentration bath over the 6 ppm one.

The contribution of the IPA drying following the ozonated ultraclean water treatment was also evaluated on wafers stored 2 weeks and 3 months in a class 10 clean room. The residual contamination is shown in figure 7. The intensities have to be compared to the

initial values given in table 1 for 18 and 82 days. It appears that the affinity between IPA molecules and organic contaminants is sufficient to remove a large part of them due to the solvent properties of IPA. Nevertheless, the best results were obtained by association of a 10 min ozonated water treatment and an IPA drying.

## CONCLUSION

Storage of silicon wafers in clean rooms leads to substrate contamination by ammonia even after very short times and by various hydrocarbons for longer times. Hydrocarbon contamination is particularly high in the more advanced clean room and can vary as a function of the organic sources present in the clean rooms. Furthermore, as the deposited hydrocarbons are in equilibrium with the contamination of the air, they can leave the surface. The hydrocarbon contamination can be removed by conventional cleaning processes (CARO and to a lesser extent by SC1). The ozonated DI water followed by an IPA drying, which enables few chemicals to be used, is also very efficient, particularly with a high ozone concentration. In the latter case, the process time can be reduced to less than 5 minutes.

## ACKNOWLEDGEMENTS

The authors would like to thank Bénédite Sandrier who performed most of the cleaning treatments.

## REFERENCES

- [1] S.R Kasi, M.Liehr, P.A.Thierry, H.Dallaporta and M.Offenberg, *Appl. Phys. Lett.*, 59, 108 (1991).
- [2] K.J.Budde, W.J. Holzapfel and M.M.Beyer, *J.Electrochem. Soc.*, 142, 888 (1995).
- [3] S.A. Mac Donald, N.J. Cleak, H.R. Wendt, C.G. Willson, C.D. Snyder, C.J. Knors, N.B. Deyoe, J.G. Maltabes, J.R. Morrow, A.E. Mc Guire, S.J. Holmes, *SPIE Vol. 1466 Advances in Resist Technology and Processing VIII* (1991).
- [4] Y. Kawai, A. Otaka, A. Tanaka, T. Matsuda, *Jpn. J. Appl. Phys.* Vol. 33, 7023 (1994).
- [5] A.J. Muller, L.A. Psota-Kelty, H.W. Krautter, J.D. Sinclair, *Solid State Technology* Vol. 37,9, 61 (1994).
- [6] K.J. Budde, *Proceedings of the Ultraclean Semiconductor Processing Technology and Surface Chemical Cleaning and Passivation Symposium*, San Francisco, CA , USA (1995)
- [7] A. Shimazaki, M. Tamaoki, Y. Sasaki, *Proceedings of the Fourth International Symposium on Cleaning Technology in Semiconductor Device Manufacturing*, Chicago, IL, USA (1995)
- [8]. F.Tardif, G.Quagliotti, T.Baffert, L.Secourgeon, *Proceedings of the Third International Symposium on UCPSS*, Antwerp (1996).

This work was carried out within the GRESSI consortium between CEA-LETI and France Télécom-CNET.

Ion Mobility cm <sup>2</sup> /(V.s)	Storage time (days)					
	8	11	18	21	56	82
3.15	>5100	>5100	>5100	>5100	>5100	>5100
2.01	1760	1665	1470	1480	145	3470
1.82	1550	1320	1330	1200	1890	1255
1.65	170	-	-	180	-	240
1.60	230	160	-	-	-	-
1.53	-	160	190	145	-	-
1.43	300	220	210	190	20	115
1.33	130	60	115	105	-	-
1.17	360	220	180	155	-	-

Table 1 : IMS detected intensities (a.u.) corresponding to different contaminants for several exposure times in a class 10 clean room.  
("-" indicates a signal lower than the low limit of detection)

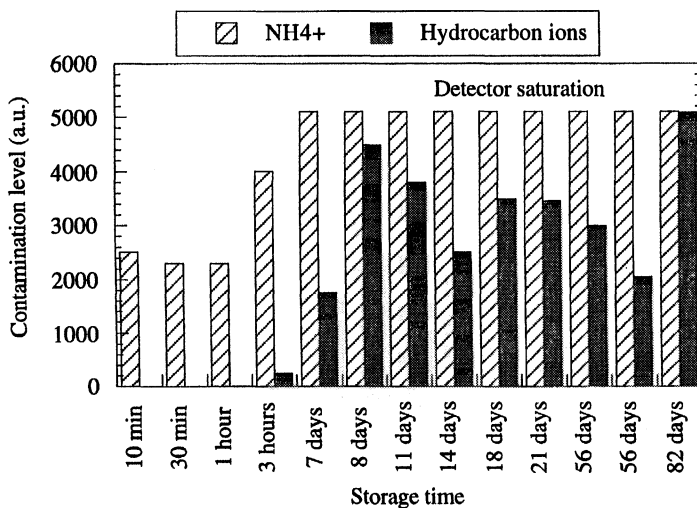


Figure 1 : Evolution of ammonia and hydrocarbon contaminations as a function of the storage time in a class 10 clean room.

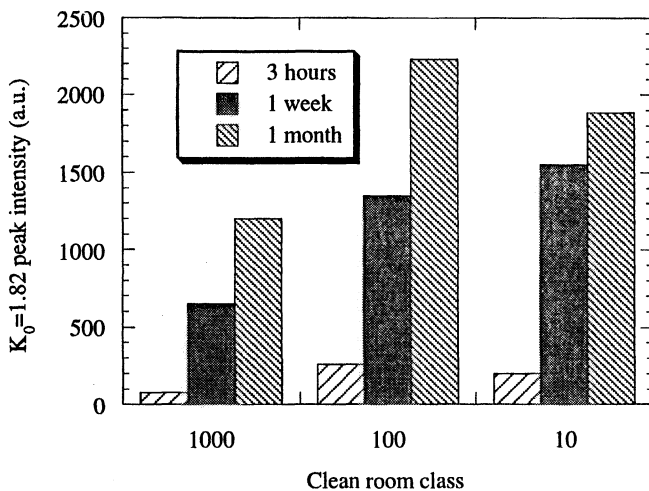


Figure 2 : Comparison of the hydrocarbon contamination in clean rooms of different classes.

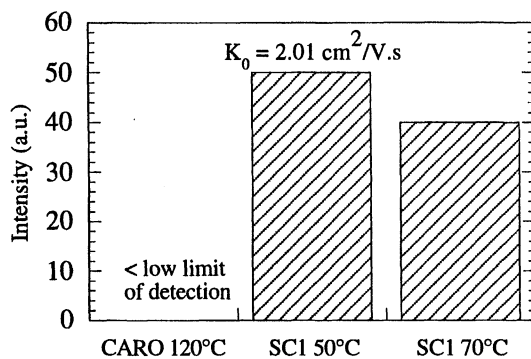


Figure 3 : Comparison of conventional cleanings in terms of hydrocarbon removal efficiency.

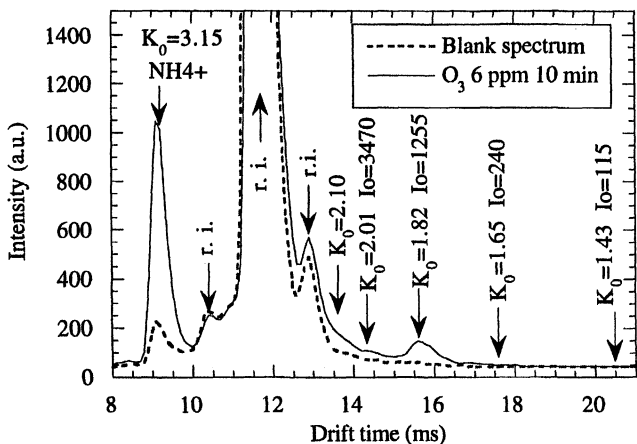


Figure 4 : IMS spectrum (positive mode) after a 10 min. 6 ppm  $O_3$  cleaning on a wafer stored in a class 10 clean room for 3 months, compared to the equipment background.  
 $I_0$  corresponds to the initial values obtained for the contaminated wafer.

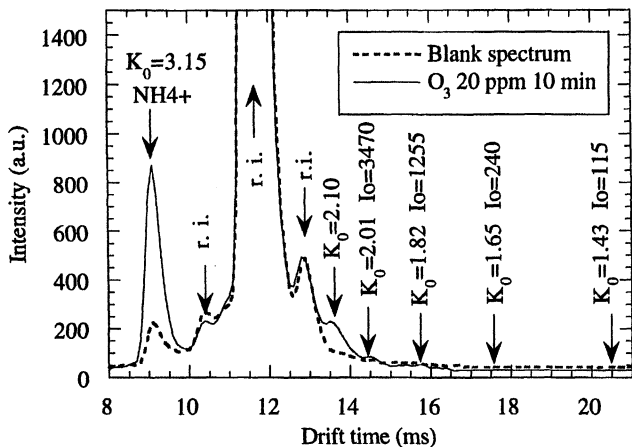


Figure 5 : IMS spectrum (positive mode) after a 10 min. 20 ppm  $O_3$  cleaning on a wafer stored in a class 10 clean room during 3 months.

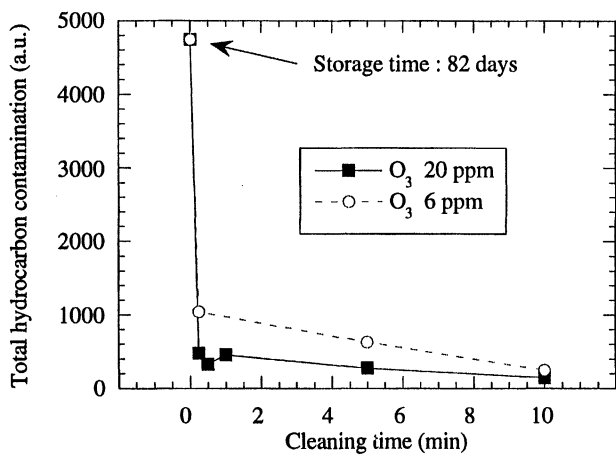


Figure 6 : Cleaning efficiency as a function of time of 6 and 20 ppm ozonated DI water treatments on hydrocarbons deposited during a 3 month storage in a class 10 clean room.

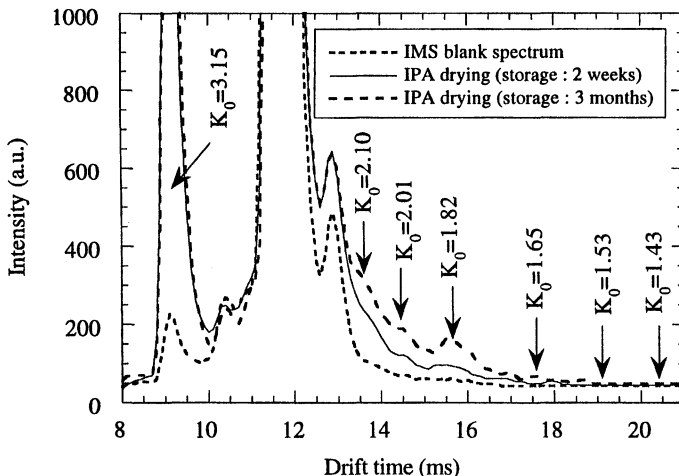


Figure 7 : Spectra (positive mode) corresponding to wafers exposed during 2 weeks and 3 months in a class 10 clean room and cleaned by an IPA drying.

## EVALUATION OF Si SURFACE CONDITIONS BY THE USE OF A SURFACE PHOTOVOLTAGE TECHNIQUE.

M.-A. Trauwaert, K. Kenis, M. Caymax, P.W. Mertens and M.M. Heyns  
IMEC, Kapeldreef 75, B-3001 Leuven, Belgium.

J. Vanhellemont, D. Gräf and P. Wagner  
Wacker Siltronic AG, P.O. Box 1140, D-84479 Burghausen, Germany.

Results are presented of the measurement of surface parameters as a tool for monitoring the condition of Si surfaces after various processes e.g. cleaning, impurity deposition and epi-layer growth. The surface charge and surface recombination lifetime are determined simultaneously, however, they may respond different to the varied conditions of the Si surface. The surface recombination lifetime is a reliable indicator for the oxide removal by HF-last treatments, while the surface charge will in well defined cases respond to the presence of Fe. The obtained values for the doping density of epi-layers are in agreement with independent measurements.

### INTRODUCTION

The Surface Charge Profiler (SCP) tool of QC Solutions, an automated non-contact system for in-line monitoring of electrical characteristics of surface and near-surface regions of silicon wafers has been used for the evaluation of Si surfaces. The physical and chemical condition of wafer surfaces strongly influence the surface charge and recombination lifetime, the main parameters obtained with SCP. After a brief overview of the operation principles possible applications in the cleaning area will be discussed e.g. SCP as monitor for the efficiency of HF last treatments and Fe and Ca deposition from SC-1 solution. A third application consists of the determination of the doping level of epi-layers, the growth of which results in well controlled surface conditions and very low contamination levels.

### EXPERIMENTAL DETAILS

#### Material

All measurements were performed on <100> 6 inch n- and p-type wafers with resistivities ranging between 8-16  $\Omega\text{cm}$  and 16-24  $\Omega\text{cm}$ , respectively. For the HF-last experiments wafers were dipped for 2 min. in a 2% HF:H<sub>2</sub>O solution at room temperature in a conventional wet bench, rinsed in DI water for 5 min. and blown dry with nitrogen.

To investigate the sensitivity of the SCP tool for metals, Fe and Ca were deposited on the Si surface from a SC-1 solution. The Si wafers were precleaned by a combination of a SPM (sulfuric peroxide mixture) standard clean and a diluted HF solution in an

attempt to remove particles and metallic impurities. To ensure identical initial conditions before the contamination all wafers were first immersed in a blank SC-1 solution (ammonium hydroxide/hydrogen peroxide/water solution) at 70°C and measured with SCP. The wafers were then immersed for a second time in the SC-1 solution, however, containing now different concentrations of Fe (0, 0.01, 0.1, 1 ppb) or Ca (0, 0.5, 5, 50 ppb). Immediately after the dip the wafers were rinsed in DI-water, dried and remeasured with SCP. Additional SCP measurements were performed after several days to monitor the time dependence of the surface condition. Finally, the metal concentration on the wafer surface was determined with Total X-ray Fluorescence (TXRF) in the Vapor Phase Decomposition - Droplet Surface Etching mode, with a detection limit of  $5 \times 10^8$  Fe/cm<sup>2</sup> and  $3 \times 10^9$  Ca/cm<sup>2</sup>, respectively.

Epi-layers of 5 μm were grown at a temperature of 1050°C using a SiHCl<sub>3</sub> source -in not optimized deposition conditions- on n-type and highly doped p-type substrates, with resistivities ranging between 10-15 Ωcm and 8-20 mΩcm, respectively. Doping of the layers to resistivities of 0.1, 0.3, 1, 10 and 30 Ωcm was performed by adding B<sub>2</sub>H<sub>6</sub> to the reaction gas. 4-points probe measurements on test wafers showed a non homogeneous doping distribution on the wafer surface. After epi-growth the wafers were kept in a N<sub>2</sub> ambient for several hours until the first SCP measurements.

### The SCP method

The Surface Charge Profiler (SCP) has been developed for the in-line monitoring of processes of microchip manufacturing by detecting deviations of the electrical parameters of surface and near-surface regions of silicon wafers (1,2). The main parameters are the surface charge, Q<sub>s</sub>, and the minority carrier surface recombination lifetime, τ, both depending strongly on the physical and chemical conditions of the wafer surface which are affected by wafer cleaning operations. The operation of the SCP is based on the surface photovoltage effect (SPV), the variation of the barrier height at the surface after illumination with a low intensity, chopped beam of short wavelength (450 nm), having a photon energy higher than the Si bandgap. The light penetration depth is very shallow (0.4 μm), which results in an outcome of the measurement dominated by characteristics of the surface and close sub-surface region, which is the active area in devices. The electrical characteristics of the surface, Q<sub>s</sub> and 1/τ, are determined from the analysis of the real and imaginary components of the ac-SPV signal (3).

The main advantage of the SCP method compared to other methods designed for in-line process monitoring on bare Si surfaces is that it is not altering the measured surface. No contact to surface, nor high voltage, nor high intensity illumination are required, each of which affects the height of the potential barrier of the measured surface. The light penetration depth in the case of SCP is also shallower than in other photoelectric methods used in semiconductor characterization. Moreover, SCP detects in short measurement time a global surface variation due to chemical contamination or terminations (4). The following measurements are performed with the SCP-110 tool of QC-Solutions.

## MONITORING CLEANING SEQUENCES

### Surface in equilibrium with ambient

The wafer surface always tends to reach an equilibrium with the surrounding ambient, e.g.  $Q_s$  and  $\tau$  will remain stable with time of exposure in the ambient (2). A preliminary experiment was therefore to successively measure the wafer kept in clean room environment in order to follow the evolution towards this equilibrium. This is demonstrated in Figure 1 for a p-type wafer, where the changes in  $Q_s$  between one equilibrium (in storage box) and another (class 1 ambient) are obvious. It appears that the clean room ambient adds negative charge on the surface of a p-type wafer. When placed in the storage box, the wafers are exposed to a new ambient resulting in new equilibrium conditions. For n-type wafers a similar decrease of  $Q_s$  and also of  $1/\tau$  is observed when exposed to clean room ambient. However, for p-type wafers no clear trend could be identified for  $1/\tau$ . P-type wafers with a thermally grown oxide on top are more stable as reflected by the constant value of  $Q_s$  in Figure 1. It should be noted that the observed transients are not induced by the measurement itself. The same trend is observed when measuring only the first and final value without performing intermediate measurements at several times.

This experiment demonstrates that the SCP outcome is influenced by the time at which the measurement is performed. Since most of the experiments will be based on the determination of deviations of the surface parameters, relevant results will only be obtained when a consistent time period for measurements is used (3).

### Monitoring of HF-last treatments

A first set of experiments was performed on wafers with HF-last treatments, a common step in silicon surface cleaning due to their high particle removal efficiency and low metallic contamination (5). The condition of the silicon surface following a diluted HF etch influences the outcome of the subsequent steps (epitaxy, contact formation, gate oxidation,...), and hence, the effect of the HF treatment should be carefully monitored.

$Q_s$  as well as  $1/\tau$  measurements were performed at several times after immersing bare wafers for 2 min. in 2% HF. The HF dip results in an increase of  $Q_s$  (e.g. positive charge was added), -which was more pronounced for n-type wafers- and again a time dependent effect was observed. In Figure 2 the results of successively measured surface parameters of p-type Si wafers (labeled 1, 2, and 3) are shown.  $Q_s$  increases smoothly with time towards a maximum, accompanied with, however, an abrupt change of  $1/\tau$ . The HF passivation remained stable during at least 5 days. A second HF dip after 40 hours did not add a significant amount of positive charge on wafer 1.

In a second experiment the HF dip followed a SC-1 clean. A p-type wafer was immersed entirely in SC-1 solution at 70°C for 10 min., followed by a partial dip in diluted HF (2%) for 1 min. Subsequently, the distribution of  $1/\tau$  along the diameter of the wafer was measured using SCP (Figure 3). The shape of the distribution curve distinguishes between the part of the wafer that was exposed to SC-1 only (higher value), and the part that following SC-1 was exposed to the HF treatment (lower value).

In both cases, bare Si wafers or SC-1 treated ones, an amorphous oxide layer is present on the Si surface. This layer induces surface states, which can act as traps for the mobile charge carriers, reducing their recombination lifetime. When immersing a silicon wafer in diluted HF, the amorphous surface oxide will be removed and moreover, replaced with a near perfect chemical termination of the silicon lattice (6-8). Since the electron negativity of H is less than O, both, however, higher than the electron negativity value of Si, the replacement of the Si-O groups by Si-H might explain the net increase of positive charge on n- as well as on p-type wafers. On the other hand, the Si-H bonds are so strong that the energy states which may interact with carriers near the band edge are located outside the silicon forbidden gap (7). This is in agreement with the observed drastic and reproducible increase of the surface recombination lifetime. As such  $1/\tau$  is a reliable indicator of the efficiency of the cleaning step in the removal of oxide layers.

### DETECTION OF Fe AND Ca

A SC-1 cleaning step not only results in the formation of a thin oxide layer but also adsorption of transition metals from the solution on Si surface can occur (9). Their detrimental effect on device performance is well-known and it is thus important to perform in-line detection. However, state-of-the-art IC processing requires reduction of metallic contaminants on the surface to the level of  $10^{10} \text{ cm}^{-2}$  and lower, and requiring therefor detection capabilities in the same range.

To determine the sensitivity level of the SCP tool the wafers were immersed in SC-1 solutions contaminated with Fe or Ca in a controlled way. Extrapolating the linear relationship between the surface concentration and the initial impurity concentration in the solution, respectively, as determined by Ryuta et al. surface concentrations between  $10^{10}$  and  $10^{12} \text{ cm}^{-2}$  are expected (10). Immediately after rinsing the wafers the SCP measurements were performed again in order to reduce the effect of storage time.

Figure 4 summarizes the most important results for n-type Si substrates. Both the SCP and TXRF values are averages over the wafer. Almost no difference is observed in the TXRF values on n- and p-type wafers, which have been immersed together in the same solution. The dotted line in figure 4 represents the average value of  $Q_s$  ( $-1.2 \times 10^{10} \text{ q/cm}^2$ ) over the eight wafers after the initial blank SC-1 dip. Fe, when present in a sufficient amount, will induce negative charge on the n-type surface as is clear from the decreasing trend with increasing Fe concentration. This can be explained by assuming that a  $\text{Fe}^{3+}$  ion replaces a  $\text{Si}^{4+}$  in the native oxide, resulting in a net negative charge in a similar way as has been reported earlier for Al(11,12). TXRF results show that a similar amount of Fe has been deposited out of the non-intentionally contaminated SC-1 solution as when spiked with 0.01 ppb Fe, however, differences in  $Q_s$  are observed. Only a slight positive (almost negligible) effect of the Ca content on the n-type wafers is observed. It appears that Ca does not add a sufficient amount of positive charge to be detected with the SCP tool or that its effect is overshadowed by the presence of some other species. The SCP sensitivity for Ca or in general for any other contaminant, might be increased by performing specific chemical pretreatments (4).

On p-type wafers neither Fe nor Ca affect  $Q_s$  in a way observable with SCP. A Fe concentration of  $2 \times 10^{12} \text{ at/cm}^2$  drives the p-type surface into accumulation, under which condition no SCP measurements can be performed, indicated by negative  $Q_s$  values.

Again a strong time dependence is observed reducing  $Q_s$  to a value apparently independent of the initial Fe concentration on the surface (Figure 4). This can be due to the interaction with the ambient during wafer storage in open boxes in the clean room (class 1) or changes in the oxidation state. This extra amount of negative charge has driven the wafers into inversion. Under these conditions the depletion layer width reaches its maximum value and will not follow the variations of the surface barrier anymore. Since  $Q_s$  depends on the depletion layer width, the listed value corresponds to this maximum, while the real  $Q_s$  could thus be much higher in absolute values and depending on the Fe concentration.

The surface recombination lifetime is not a good indicator, as it seems to be insensitive for the presence of Fe or Ca on the surface.

#### DETERMINATION OF THE DOPING DENSITY IN EPI-LAYERS

The lack of stability of the silicon surface after different treatments often leads to variations in  $Q_s$ , which are difficult to interpret. For that reason SCP measurements were performed on epi-layers grown on n- and p-type substrates, since epi-growth results in a very well controlled surface and a low contamination level. In that case the observed variations should only be due to differences in the doping concentration of the layers, which can easily be measured with SCP. By performing the measurements in mapping mode the doping distribution across the wafer can be determined.

The  $N_{sc}$  values averaged over the whole wafer are of the same order of magnitude as the nominal doping concentrations, while a difference between the epi-layers grown on the n-type and on p-type substrates is observed. Higher values were measured at the wafer edges compared to the center, in agreement with the 4 point probe measurements performed on test wafers. The SCP values are maintained during one week and increase afterwards. Since the resistivity of epi-layers is supposed to remain constant, the observed deviation is more probable due to a variation of  $Q_s$ . For reliable  $N_{sc}$  measurements inverted wafer surfaces are required e.g. a large positive charge on p-type surfaces. However, as was discussed already above  $Q_s$  does not remain stable when stored for prolonged times in a clean room environment and this does have an impact on the SCP measurement results and additional treatment may be necessary to re-establish the original inversion condition.

Finally, since the above mentioned nominal doping concentrations result from extrapolations, independent characterizations of the epi-layers have been performed. The doping concentration of the epi-layers was performed using Hg contact CV measurements. A large variation of the resistivity versus depth was observed for the two epi-layers on n-type substrate with the highest resistivity.

In Figure 5 the SCP results are compared with the doping density values as determined from the CV measurements. The line represents the 1-to-1 correspondence. Higher values are systematically obtained with SCP, however, a good agreement is obtained for the lower concentrations. The difference in doping of epi-layers on the n- and p-type substrates is also observed: higher values in the epi-layers grown on the p-type substrates, which is the opposite of the SCP results. Also the difference seems to be more important for the lower doping values, while for SCP this difference was more pronounced for the higher doping levels.

## SUMMARY

The obtained results show that in well defined cases SCP can be used as a reliable tool for fast monitoring of the surface conditions of bare and oxidized silicon surfaces. The removal of oxide layers by HF last treatments induces an immediate and unambiguous increase of  $1/\tau$ . The SCP tool detects an addition of negative charge after the deposition of Fe on the n-type wafer surface, while no clear correlation can be seen between the SCP signal and Fe on p-type or Ca on n- and p-type wafers, respectively, for surface concentrations between  $10^{10}$  and  $10^{12}$  metal atoms/cm<sup>2</sup>. The N<sub>sf</sub> determination in epi-layers when performed immediately after epi growth give good orders of magnitude of the doping concentration.

However, variations in values of the surface parameters are often observed, and identifying the cause of them is not straightforward. They might originate from external influences such as fluctuations of the ambient or chemical treatments which cannot always be quantified.

## ACKNOWLEDGMENTS

The authors would like to thank Dr. E. Kamieniecki and Prof. J. Ruzyllo for fruitful discussions and A. Paradis for its helpful assistance with the SCP measurements. M.-A. Trauwaert acknowledges the financial support from the Flemish institute for the promotion of scientific and technologic research in industry (IWT), Brussels, Belgium.

## REFERENCES

1. E. Kamieniecki, P. Roman, D. Hwang and J. Ruzyllo in proceedings of the "Second International Symposium on Ultra-Clean Processing of Silicon Surfaces" p. 189 (1994).
2. J. Ruzyllo, P. Roman, J. Staffa, I. Kaskoush and E. Kamieniecki, presented at "SPIE's Microelectronic Manufacturing 1996 Symposium", 16-17, October, 1996, Austin, Texas.
3. E. Kamieniecki and G.J. Foggiato, Handbook of Semiconductor Cleaning Technology, p. 497, ed. W. Kern, Noyes Publ. (1993).
4. F. Tardif, J.-P. Joly and D. Walz, Electrochem. Soc. Proc. **95-30**, 299 (1995).
5. M. Meuris, S. Verhaverbeke, P.W. Mertens, H.F. Schmidt, A. Rotondaro, M.M. Heyns, M. Depas, A. Philipossian and O. Vatet, in proceedings of the "23rd Symposium on ULSI Ultra Clean Technology" p. 235 (1994).
6. B.R. Weinberger, G.G. Peterson, T.C. Eschrich and H.A. Krasinski, J. Appl. Phys., **60**, 3232 (1986).
7. M. Morita, T. Ohmi, E. Hasegawa, M. Kawakami and M. Okwada, J. Appl. Phys., **68**, 1272 (1990).
8. D. Gräf, M. Grundner, R. Schulz and L. Mülhoff, J. Appl. Phys. **68**, 5155 (1990).
9. Y. Mori, K. Uemura and K. Shimanoe, J. Electrochem Soc., **142**, 3105 (1995).
10. J. Ryuta, T. Yoshimi, H. Kondo, H. Okuda, and Y. Shimanuki, Jpn. J. Appl. Phys. **31**, 2338 (1992).
11. H. Shimizu and C. Munakata, J. Appl. Phys. **73**, 8336 (1993).
12. H. Shimizu and C. Munakata, Appl. Phys. Lett. **64**, 3598 (1994).

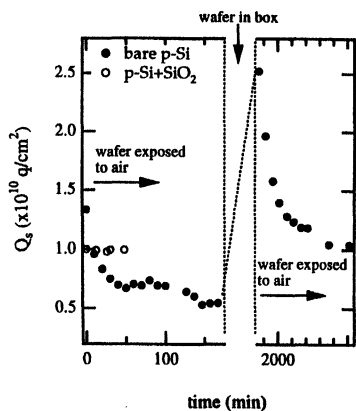


**Figure 1:** Variation of  $Q_s$  on a p-type wafer as a function of time, when removed from a storage box. For comparison the results of a similar experiment on a wafer with a thermally grown oxide of 2.5 nm is added.

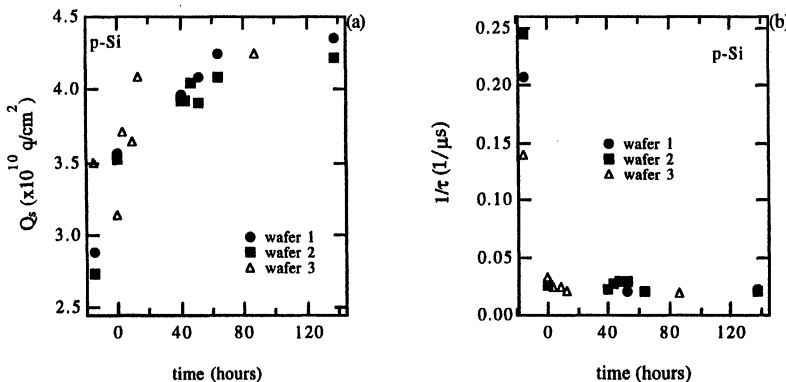


**Figure 2:**  $Q_s$  (a) and surface recombination lifetime (b) versus storage time on p-type wafers after a 2 min. immersion in 2% HF. Time 0 is immediately after the HF dip. After 40 h wafer 1 was dipped a second time.

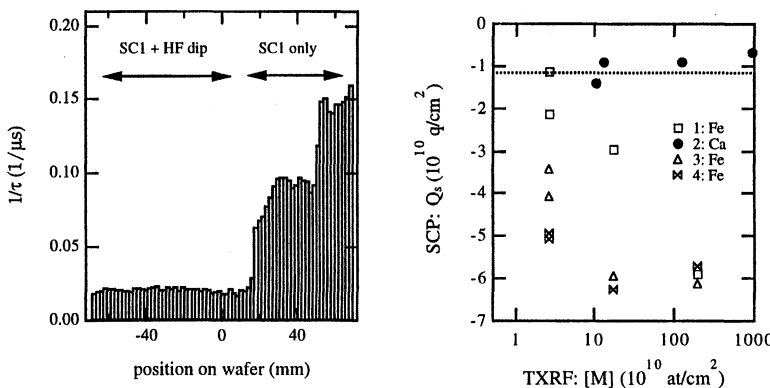


**Figure 3:** Distribution of  $Q_s$  along the diameter of a p-type wafer of which half was dipped in a diluted HF solution after immersion in SC-1. The measurement was performed immediately after the HF dip.

**Figure 4:**  $Q_s$  of n-type wafers measured under different conditions and at several times during the experiment: after immersion in Fe (1) and Ca (2) spiked SC-1, and after 3 (3) and 12 (4) days of storage in clean room (class 1) after immersion in Fe spiked SC-1.

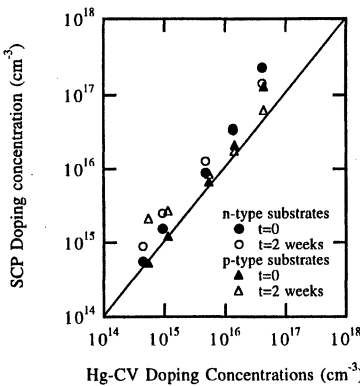


**Figure 5:** Doping concentration obtained with SCP versus the one obtained with Hg-CV measurements.

## CONTROL OF QUALITY OF SOLID SURFACE BY THE SELECTIVE WETTING METHOD

V.V. Bakovets  
Institute of Inorganic Chemistry SB RAS,  
Prospect Ak. Lavrent'eva 3, 630090, Russia

The results of cleaning and qualitative controlling silicon plate surface in planar technology are considered. The attention is devoted to the method of selective wetting and using this method for the qualitative analysis of silicon and its oxide.

### INTRODUCTION

The treatment of solid surface is an important stage of semiconductor device manufacturing. There are a lot of methods of solid surface treatment but reproducibility of these methods may be unsatisfactory. It is very important to know when the break takes place. It is evident that we could not control treatment quality of each sample by physical methods like the Auger spectroscopy, the Tunnel microscopy and others if we have to treat hundreds or thousands of samples.

It is necessary to use a simple, inexpensive and available method.

The attempt (1) of using *the wetting angle method* for checking solid surface state after washing samples in organic solvents is known. This method suits the case. However, attempts of using it in semiconductor device manufacturing were not successful. Bad reproducibility results were a reason of the failures.

### THEORY OF WETTING ANGLE STEADY STATE

Fig.1 shows the usual shape of liquid drop at steady state on the solid surface. Here,  $\sigma_i$  is the surface tension of i-th interface and  $\theta$  is the contact wetting angle. The steady state of this system is described by Young-Neumann equation:

$$\sigma_{sv} = \sigma_{ls} + \sigma_{lv} \cos \theta \quad [1]$$

The contact wetting angle is the parameter of solid surface state because  $\sigma_{sv}$  and  $\sigma_{lv}$  define this state. Each parameter  $\sigma_{sv}$ ,  $\sigma_{ls}$  and  $\sigma_{lv}$  is a function of vapour adsorption on the appropriate interface. These functions are Gibbs adsorption equations:

$$\sigma_i = \sigma_{i,0} - \sum_j \int_{A_j} \Gamma_j d\mu_j \quad , \quad [2]$$

where  $\sigma_{i,0}$  is the surface tension of i-th pure interface,  $\Gamma_j$  is the excess Gibbs adsorption and  $\mu_j$  is the chemical potential of j-th impurity. For the system: solid is silicon; liquid and vapour are water; - we have from equations [1] and [2]:

$$\Delta \cos \theta = [\int_{P_x} \Gamma_{H_2O} d\mu_{H_2O}] / \sigma_{H_2O} \quad , \quad [3]$$

where  $P_x$  is the partial pressure of water and  $\Delta \cos \theta$  is the changing  $\cos \theta$  parameter.

Fig. 2 shows calculation results of the changing  $\cos \theta$  parameter with filling

silicon surface by the water molecule monolayer. It means that the  $\cos\theta$  parameter can change from 0 to -0,3 when the water vapour pressure is changed from 1 torr to 5 torr, accordingly. Hence, the wetting angle method reproducibility depends strongly on purity of the air or other gases.

### SELECTIVE WETTING (SW) METHOD

The other situation arises when vapour is changed by liquid. In this case two insoluble or limitedly soluble liquids are used. There are a lot of liquids fitting the SW method but we consider here results obtained with distilled water and diethyl ether (medicine purity). Water is a surrounding and ether is a control drop. The purity of water is kept by slow pumping pure water.

Fig. 3 shows the chart of the selective wetting control equipment for uninterrupted control of silicon plates (3), one-by-one. Each plate is placed at the top of the wheel (2). The wheel is rotated and fixed when the low plate surface is located horizontal. The control liquid (ether) drop is formed by the capillary. Fig. 4 shows the optical system for drop form observation and the electronic system for measuring the wetting angle  $\theta$ . The electronic system measures  $x_2-x_1$  and  $y_2-y_1$  distances and calculates the wetting angle by equation:

$$\operatorname{tg}(\theta/2)=2(y_2-y_1)/(x_2-x_1). \quad [4]$$

### RESULTS

#### Reproducibility of the SW method

The results of the silicon plate examining are presented in Tab. I. All plates were polished on single polish-wheel. Then plates were exposed to standard treatment : acting by brush-washing; boiling in ammonium hydroxide / hydrogen peroxide solute; washing in bidistilled/deionized water; boiling in chlorine hydride / hydrogen peroxide solute; washing in bidistilled/deionized water.

Table I. The results of examining the silicon plates from single polish-wheel

N plate	1	2	3	4	5	6	7	...
$\theta$ , deg	159±3	156±1	159±2	156±3	156±2	157±1	156±3	...

It follows from Tab.I that the control angle  $\theta$  is 157±3 deg. In general, more than 200 samples were controlled.

Results for silicon plates from different polish-wheels but after the same standard treatment are presented in Tab. II.

Table II. The results of examining the silicon plates from different polish-wheels

N plate	1	2	3	4	5	6
$\theta$ , deg	156±2	156±2	158±2	159±2	156±2	156±2

It follows from Tab. II that the control angle  $\theta$  is  $157 \pm 3$  deg. Hence, the SW method is highly reproducible.

#### Break of standard treatment

The results for silicon plates exposed to the same treatment but without brush-washing are listed in Tab. III.

Table III. The results of examining the silicon plates without the brush-washing

N plate	1	2	3	4	5	6
$\theta$ , deg	$140 \pm 3$	$130-148$	$146 \pm 3$	$148 \pm 2$	$142 \pm 2$	$138 \pm 4$

It follows from Tab. III that the angle  $\theta$  reproducibility is very bad at breaking the standard treatment.

The results for silicon plates exposed to the standard treatment and kept in the nitrogen gas are presented in Tab. IV.

Table IV. The results of examining the silicon plates kept in the nitrogen gas

Keeping time, hour	0,3	0,5	1,0	24	24	24	24
$\theta$ , deg	$156 \pm 2$	$154 \pm 2$	$152 \pm 2$	$147 \pm 2$	$145 \pm 2$	$149 \pm 3$	$149 \pm 3$

It follows from Tab. IV that the wetting angle  $\theta$  decreases with keeping time. This angle  $\theta$  decreasing is a result of plate surface dehydration. Hence, the SW method is sensitive to the quality of surface treatment.

#### Silicon oxide removing

During the standard treatment the silicon plate surface is covered by silicon oxide. The oxide film thickness is close to 50-60 nm in such cases.

The influence of thermal oxide film thickness on selective wetting results is presented in Fig. 5. We can see that oxide removing decreases the angle  $\theta$  up to 40 deg. The angle change region is 3.0-4.0 nm.

It follows from Fig. 5 that the oxide films of less than 3.0 nm thickness consists of islands and a control liquid spreads among them.

#### Defectness of solid

It was also found that the SW method was sensitive to a defectness of solid (2). Fig. 6 shows the  $\theta$  angle change after layer by layer removal of silicon implanted by argon.  $\text{Ar}^+$  ion energy is 40 keV,  $D$  dose is  $10^{15} \text{ cm}^{-2}$ . The curve change of  $\theta$  is similar to the curve change of the defect content with  $d$  depth and to the curve change of  $k$  extinction coefficient. The  $k$  extinction coefficient was defined by ellipsometry.

The investigation of the silicon samples implanted by  $\text{Ar}^+$  ion of  $10^{12} \text{ cm}^{-2}$  dose shows that the SW method is sensitive to the surface concentration of defects as low as  $10^{11} \text{ cm}^{-2}$ .

Fig. 7 shows  $\cos\theta$  parameter dependence on  $D$  irradiation dose. The implantation conditions:  $\text{B}^+$  ion energy is 100 keV, temperature of silicon plates is 25°C.

It is clear that the wetting angle  $\theta$  increases with irradiation dose decrease. It means that surface concentration of monovacancies is decreases with the increase of the irradiation dose. Similar results were observed earlier (3).

## CONCLUSIONS

1. The reproducibility of the usual wetting angle method depends on the purity of air or other gases and is bad in device manufacture.
2. The selective wetting angle method is the simple, inexpensive and available method of the quality control of solid surface in semiconductor device manufacture.
3. The selective wetting method is highly reproducible if the treatment method is not changed.
4. The selective wetting method is highly sensitive to the break of technology treatment.

## REFERENCES

1. R.G. Flesser, J. Electrochem. Soc., **121**, 869 (1974).
2. L.F. Bakhturova, V.V. Bakovets, I.P. Dolgovesova and B.M. Ayupov, Semiconductirs, **27**, 327 (1993).
3. T.Lohner, G. Mezey, E. Katal, F.Paszti, A.Manuaba and J.Gyulai. Nuclear Instr. and Methods, **209/210**, 615 (1983).

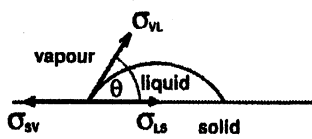


Fig. 1 Steady state of liquid drop on solid surface.

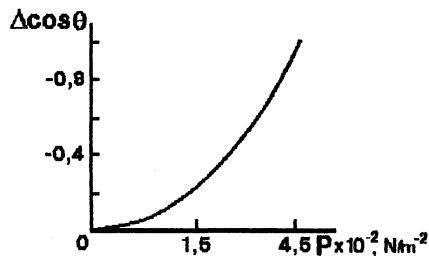


Fig. 2. Dependence of parameter  $\cos \theta$  on pressure of water vapour.

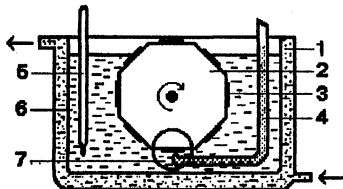


Fig. 3. The selective wetting control equipment for examining silicon plates. 1 - thermostatic water, 2 - wheel-holder, 3 - samples, 4 - capillary with ether, 5 - windows, 6 - water, 7 - thermometer.

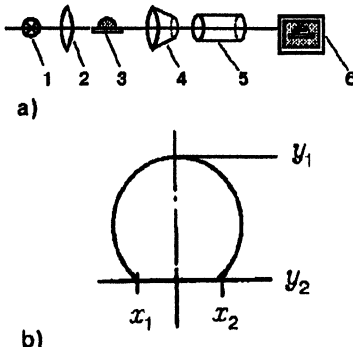


Fig. 4. Optical and electronic systems (a) for measuring drop form (b). 1 - lamp, 2 - lens, 3 - sample with drop, 4 - microscope, 5 - video-camera, 6 - computer.

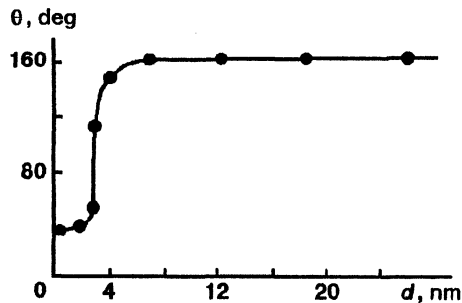


Fig. 5. The wetting angle dependence on thermal silicon oxide film of  $d$  thickness.

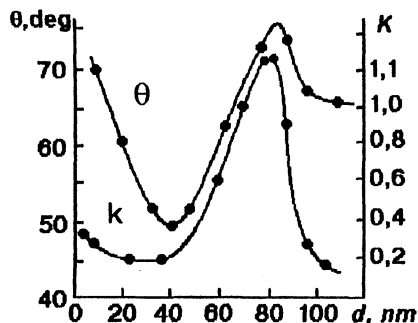


Fig. 6. The dependences of wetting angle  $\theta$  and differential extinction coefficient  $k$  on the thickness  $d$  of removed silicon layer.

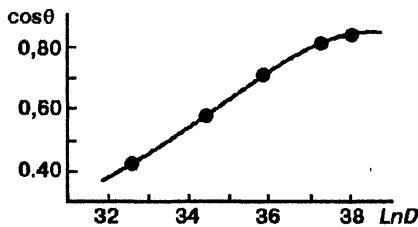


Fig. 7.  $\cos\theta$  parameter dependence on  $D$  irradiation dose.

## **RESIST STRIPPING**



# **PHOTORESIST STRIPPING USING OZONE/DEIONIZED WATER CHEMISTRY**

**Ismail I. Kashkoush, Robert Matthews, and Richard E. Novak**

SubMicron Systems Corporation, 6330 Hedgewood Dr. #150, Allentown, PA 18106

Sulfuric acid is combined with hydrogen peroxide to oxidize stripped photoresist material, though the use of sparged ozone in sulfuric solution is also used to remove resist residues on wafers following the ashing process. Although these mixtures have been used for many years, sulfuric acid processes also have proven to be costly. This is due to the need for frequent bath change-outs and the use of high temperature which impose safety and environmental concerns. As a result of these and other considerations, the use of mixtures of ozone and de-ionized water for photoresist stripping has been investigated. Results show that the technique effectively removes hard-baked resist (ashed and un-ashed) from bare silicon and patterned wafers and produces cleaner surfaces (i.e. particles and metals) when compared to outcomes from typical SPM processes.

## **INTRODUCTION**

Sulfuric acid and hydrogen peroxide mixture (SPM) has been used for photoresist stripping from silicon surfaces [1]. However, this chemistry is now playing a much diminished role in accomplishing this step [2]. Due to the severe hardening of exposed photoresist from high energy ion implantation, many IC manufacturers now use plasma ashing to remove up to 99% of the material. The remaining (unashed) material is typically removed in a wet stripping technique. The mixture is typically 3-10:1 (96%-98% H<sub>2</sub>SO<sub>4</sub> : 30% H<sub>2</sub>O<sub>2</sub>). As a result, SOM, which employs ozone instead of hydrogen peroxide to oxidize stripped photoresist material, has been steadily gaining adherents among the IC manufacturers.

While SPM and SOM solutions have contributed significantly to the IC manufacturing sequence, sulfuric acid-based steps have proven to be costly. Manufacturers must also use vast amounts of DI water to rinse off residual sulfuric acid and unoxidized particulate matter from wafer and carrier surfaces. DI water is another significant cost component. Other hidden costs are those for storing, distributing, and treating the sulfuric acid mixtures, as well as expenses incurred for replacing wet station components due to their shortened life-span from high bath temperatures and the corrosive properties of the acid [2].

The use of a novel process which uses de-ionized water and ozone mixtures to remove photoresist from bare silicon and patterned wafers [2-5] is demonstrated in this investigation.

The process does not use sulfuric acid or hydrogen peroxide; consequently, there is no need for de-ionized water rinsing steps. Unlike the SPM process, in which the resist is undercut and then oxidized by the hydrogen peroxide, the ozonated water process directly oxidizes the resist from the wafer surface; the resist is continually thinned during reaction and the solution remains "crystal clear" during the entire process time. Results show that the stripping rate increases with the dissolved ozone content in de-ionized water. An etch (stripping) rate of  $\geq 500$  Å/min is typically achieved on different resist types using this process. Compared to the proven traditional SPM process, this method provides for very low cost of ownership [2] and more environmentally sound wafer processing [3].

## EXPERIMENTAL SETUP

In the experimental setup, the liquid flows from the process vessel, to the pump, through a heat exchanger, to the filter through an ozonator, and back to the vessel. The ozone is generated from the ozone generator and fed to the ozonator where the ozone gas is mixed with de-ionized water. The gaseous ozone is also simultaneously fed to the bottom of the process vessel via a specially designed device that provides a uniform stream of gaseous ozone into the bath. Gaseous and dissolved ozone were monitored using inline ozone analyzers. A schematic diagram of the experimental setup is shown in figure 1.

Wafers were processed in a fully automated wet station in the Applications lab at SubMicron Systems Corp., Allentown, PA. Wafers coated with positive hard-baked resist were used for this study. Resist types used were: AZ1518 (A), HPR6512 (B), and Shipley SPR2 (C). Wafers also underwent different ashing and implantation processes prior to the DIO<sub>3</sub> step. The process sequence that was used for determining the stripping effectiveness was (DIW-O<sub>3</sub>) then dry. Surface inspection for complete resist removal was done visually using optical microscopy techniques. In addition, three different cleaning sequences were employed and particles (remaining on the surface and added to virgin test wafers) and ionic metals were monitored on the test wafers. These are: DIO<sub>3</sub><sup>TM</sup>/SC1/Rinse/Dry, DIO<sub>3</sub><sup>TM</sup>/Rinse/Dry, and DIO<sub>3</sub><sup>TM</sup>/Dry. The SC1 step was: 1:2:75 mix of NH<sub>4</sub>OH:H<sub>2</sub>O<sub>2</sub>:H<sub>2</sub>O at 70 C for 5 min with the aid of megasonic energy. After cleaning, the wafers were cascade rinsed for 5 min., then dried for 10 min. in a closed loop vacuum IPA (CLV) dryer.

## RESULTS AND DISCUSSION

The experimental setup was designed to fully characterize the removal of photoresist from bare silicon and patterned wafers using the ozone/water chemistry. Only results of stripping unashed and ashed wafers will be presented in this study. Variables studied in this study were: ozone (gaseous and aqueous) concentration, flow dynamics, and bath temperature. Figure 2 shows the dissolved ozone concentration versus the input gas concentration at different temperatures. As shown in figure 2, the concentration of dissolved ozone increases with the

increase in the concentration of the gaseous ozone. The bath temperature effect on the ozone solubility in de-ionized water can be also seen from either figure 2 or 3. As shown in either figure, the lower the temperature the higher the concentration of the dissolved ozone. More than 90 ppm of dissolved ozone can be achieved in de-ionized water at 5 °C and 300 ppm of gaseous ozone being injected.

Figure 4 shows the build up curves of ozone at various temperatures. A higher rate of ozone build up can be seen in the first 20 minutes after which the concentration approaches approximately saturation at that temperature. Approximately 25 ppm of dissolved ozone can be achieved after 25 min. of continuous ozone injection into the bath while a concentration of 35 ppm can be achieved at 15 °C at the same time. When the temperature was decreased to 5 °C, the ozone level achieved was about 90 ppm after 30 min. of ozone injection into the process bath.

The effect of ozone concentration on the stripping time was investigated under different conditions. The process time for complete resist removal was monitored. As shown in figure 5, the stripping rate increases with the increase in the dissolved ozone concentration in the process bath. A stripping rate of about 500 Å/min was achieved at ≥ 60 ppm while a rate of 200 Å/min was achieved at 10 ppm. Different resist types were used to study the effect of resist type on the stripping mechanism. As mentioned earlier, the resist types were: AZ1518 (A), HPR6512 (B), and Shipley SPR2 (C). As shown in figure 6, the stripping rate does not depend on the resist type. An average etch rate of 500 Å/min was obtained on 200 mm wafers for the three types of resist. Similar experiments were conducted on 150 mm wafers. A slightly higher stripping rate was obtained on 150 mm wafers. In addition, ashed wafers (remaining resist on tested wafers ranged from 500 Å to 1000 Å) were effectively stripped in about 5 minutes at a level of 70-80 ppm of dissolved ozone in the liquid. Similar stripping rates were obtained on patterned wafers. The excess ozone in the process bath is believed to compensate for the extra surface area of resist on patterned wafers.

#### Example: rough estimates:

To illustrate the concept, let's assume the following example:

Resist thickness (un-ashed)	= 10 000 Å
Resist thickness (ashed)	= 500 Å
Resist density	= 1.3 g/cm <sup>3</sup> (MW of CH <sub>2</sub> = 14 g/mole)
Number of 200-mm wafers	= 50 per lot
∴ Mass of un-ashed resist	= 2 g (0.14 moles)
∴ Mass of ashed resist	= 0.1 g (0.007 moles)
Typical O <sub>3</sub> production	= 100 g/hr (or 0.035 moles/min.)



[1]

As can be seen from equation (1), there will be 3 moles of O<sub>3</sub> required to oxidize 1 mole of photoresist. At 100% efficiency, the oxidation power will be: 0.035/3 = 0.0117 M/min. This equates to approximately 12 min. of processing time to fully oxidize the photoresist

(0.14/0.0117). If we assume 15% oxidation efficiency, the time required to oxidize these wafers can be calculated as follows:

Oxidation power	= 0.15 x 0.0117 = 0.00176 M/min.
Time required to oxidize un-ashed wafers	= 0.14 / 0.00176 $\cong$ 80 min.
Time required to oxidize ashed wafers	= 0.007 / 0.00176 $\cong$ 4 min.

However, the above calculated process times can be drastically reduced if an ozone-DIW system is designed to achieve high oxidizing power. In the experimental setup, 85-100 ppm of dissolved ozone was achieved in less than 25 min. If we assume that oxidation efficiency is 50% for that system (due to the high level of dissolved ozone that was achieved), the above results can be reduced as follows:

Oxidation power	= 0.5 x 0.0117 = 0.006 M/min.
Time required to oxidize un-ashed wafers	= 0.14 / 0.006 $\cong$ 24 min.
Time required to oxidize ashed wafers	= 0.007 / 0.006 $\cong$ 1.2 min.

These estimates are in very good agreement with results obtained for both un-ashed and ashed wafers (see figures 5 and 6). A resist thickness of 1.3  $\mu\text{m}$  was completely removed in 25 min. at a dissolved ozone level of  $\geq$  60 ppm as shown in both figures 5 and 6. Similarly, a layer of 2.2  $\mu\text{m}$  resist will require, theoretically, 51 min. to be completely oxidized. As shown in figure 5, the process time for that sample was 45 min. Obviously, the efficiency of both the ozonation system and process bath play an important role in raising the oxidizing power and consequently reducing the process time [5].

Unlike the SPM processes (in which the resist is undercut and floats away, then is oxidized by the hydrogen peroxide), the ozonated water process is a direct oxidation of the resist on the wafer surface [5]. The resist is continually thinned during reaction and the solution remains "crystal clear" during the entire process time. Wafers were observed in the early stages of the reaction (process). The difference in the remaining resist thickness is shown by the difference in the fringe pattern on the wafer surface as shown in figure 7 (A, B). It can be concluded from these observations that this process can be approximated as an etch process. The oxidizing agent ( $\text{O}_3$  in water) attacks the resist on the wafer surface. As the ozone is consumed in the reaction, fresh ozone is supplied. Some of this fresh  $\text{O}_3$  is absorbed in the liquid, some is consumed immediately by the reaction, and the excess is exhausted. This dynamic process continues until the resist is totally removed.

Experiments were conducted to investigate the particle addition and/or buildup during the  $\text{DIO}_3^{\text{TM}}$  process. Table 1 shows the particle addition (shown in ( )) on bare silicon wafers processed in the  $\text{DIO}_3^{\text{TM}}$  bath during 10 runs conducted separately from the stripping tests. As shown in Table 1, the particle addition on bare silicon wafers was less than 20 particles at 0.16  $\mu\text{m}$ . After 4 hours in cleanroom storage, the particle addition to the ashed wafers from the  $\text{DIO}_3^{\text{TM}}$  was very low (an average of 50 particles added at 0.16  $\mu\text{m}$  to a 200 mm wafer) [3]. By eliminating the sulfuric acid process, there is no buildup of sulfate residues on the wafers (time-dependent haze).

Experiments were also conducted to investigate the effectiveness of the DIO<sub>3</sub> process without the SC1 step. As shown in Table I, the final particle counts on the wafer surface in the DIO<sub>3</sub>/SC1/Rinse/Dry sequence is less than that obtained in both DIO<sub>3</sub>/Rinse/Dry and DIO<sub>3</sub>/Dry sequences. However, the final counts were improved (decreased) only by about 27% when the SC1 step was used while the those counts were increased by almost 50% when no SC1/Rinse steps were used before the dryer. There was no significant difference in particle addition to virgin wafers (with initial particle counts of  $\leq 20$  @ 0.16  $\mu\text{m}$ ) during the three cleaning processes, as shown in Table I.

In addition, the ionic metallic contamination was investigated for the same cleaning sequences and the TXRF results are shown in Table II. As expected from an SC1-last clean, the Fe and Zn surface concentrations were higher than those obtained when the SC1 step was not implemented (as shown in table 2 for both ashed and unashed wafers). No other elements (e.g. Mn, Ni, Cu) were detected. It is known that ionic impurities in the SC1 solution deposit on the wafer surface. Typically, an SC2 step is required to remove any metallic contamination that is deposited from the SC1 step. In fact, HCl injection to the DIO<sub>3</sub> process or to the rinse after DIO<sub>3</sub> will effectively remove any trace metals from the wafer surface, saving an SC2 step and lowering the cost of equipment ownership.

Nevertheless, the quality of the wafer surface is improved, especially concerning the oxide layer which is exceptionally clean and stable over time [3,6].

Since the DIO<sub>3</sub>™ process requires very little DIW, there is a saving of 99.5% of the water consumed compared to the sulfuric chemistries. Cost of ownership analysis between the SPM and DIO<sub>3</sub>™ processes for a typical process that produces 4 lots (50x200 mm wafers) per hour showed that a minimum cost reduction of about 60% can be obtained by using the ozone/deionized water techniques [2]. This performance is superior to the traditional sulfuric/peroxide mix processes in terms of contamination and water usage reduction, making the process more cost effective.

## CONCLUSIONS

Results showed clearly that a process which uses ozonated water is a viable substitute for those which employ sulfuric acid solutions for removing post-ash photoresist material from wafers, particularly following ashing steps. DIO<sub>3</sub> methodologies result in low metals contamination and low particles added. They exhibit processing speeds which meet or exceed those derived from processes which rely on sulfuric acid mixtures. Based on ozone and DI water, the process is inherently safe for operators and the environment. It also reduces operating expenses, because fewer chemicals must be purchased, managed and disposed. While the DIO<sub>3</sub> process has proven to be an ideal substitute for post-ash resist stripping, promising results have

been garnered from research into prospects for using super-ozonated water to remove non-ashed photoresist layers, thus eliminating the need in some cases for plasma stripping tools.

## REFERENCES

1. W. Kern, Handbook of Semiconductor Cleaning Technology, Kern, W. (Editor), Noyes, 1993.
2. I. Kashkoush, R. Novak, R. Matthews, and M. Lamarra, An Alternative to Conventional Post-Ash Resist Stripping, Future Fab International, Summer 1997.
3. I. Kashkoush, R. Matthews, R. Novak, E. Brause, F. Carrillo, and B. Rajaram, Proc. of the MRS '97 Spring Meeting, San Francisco, CA, 1997.
4. R. Matthews, US Patent # 5,464,480, November 7, 1995.
5. I. Kashkoush, R. Matthews, F. Carrillo, SMS Technical Reports, Aug. 96 and Jan./Feb. 1997 (not published).
6. L. Li, E. Grieger, K. Griffiths, S. Byrne, R. Hawthorne, Electrochem. Soc. Proc. Vol. 95-20, R. Novak and J. Ruzylo (Editors), 1996, pp. 449-454.

RUN #	DIO3/SC1/R/D	DIO3/R/D	DIO3/D
1	90 (11)	65 (8)	162 (15)
2	70 (12)	111 (22)	152 (16)
3	75 (15)	127 (21)	139 (19)
4	71 (14)	101 (18)	142 (29)
5	79 (17)	107 (16)	121 (7)
6	73 (11)	102 (23)	113 (4)
7	62 (9)	107 (11)	121 (12)
8	79(12)	109 (16)	143 (19)
9	87 (15)	87 (18)	165 (20)
10	73 (19)	99 (16)	132 (17)
Ave.	73 (14)	102 (17)	141 (16)

Table I. Final particle counts at  $\geq 0.16 \mu\text{m}$  on unashed wafers surface from different DIO3™ processes. Average particle add on is indicated in ( ).

#### Ashed wafers

DIO3/R/DRY		DIO3/SC1/R/DRY	
Fe	Zn	Fe	Zn
BDL	BDL	32	121
BDL	BDL	28	107

#### Unashed wafers

Fe	Zn	Fe	Zn
BDL	BDL	29	82
BDL	BDL	26	97

BDL: Below Detection Limit ( $\approx 1.5 \times 10^{10}$  atoms/cm $^2$ ).

Table II. Ionic metals on the wafer surface from different DIO3™ processes (units:  $10^{10}$  atoms/cm $^2$ ).

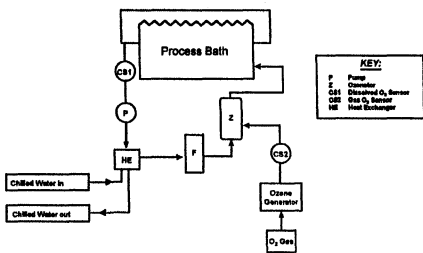


Figure 1. Experimental Setup.

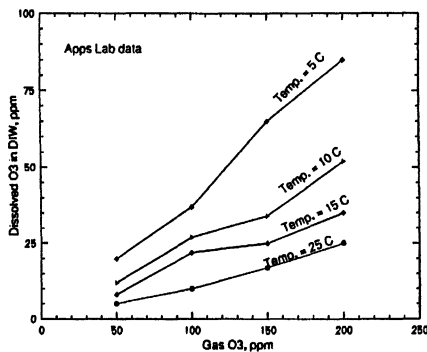
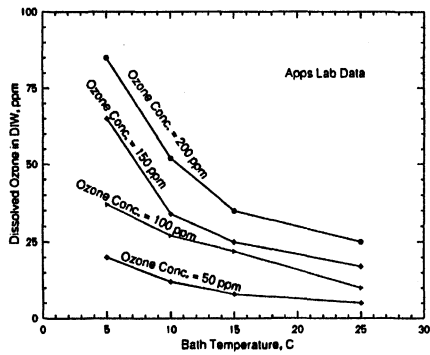
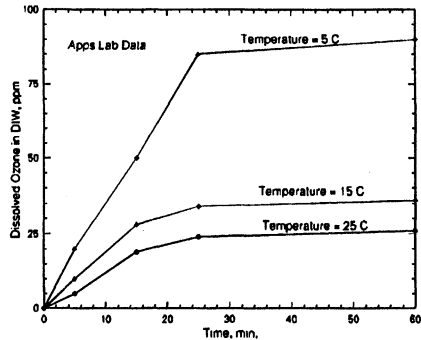


Figure 2. Dissolved O<sub>3</sub> as a Function of Gaseous O<sub>3</sub> at Various Temperatures.



**Figure 3. Dissolved O<sub>3</sub> as a Function of Bath Temperature.**



**Figure 4. Dissolved O<sub>3</sub> Buildup vs. Time.**

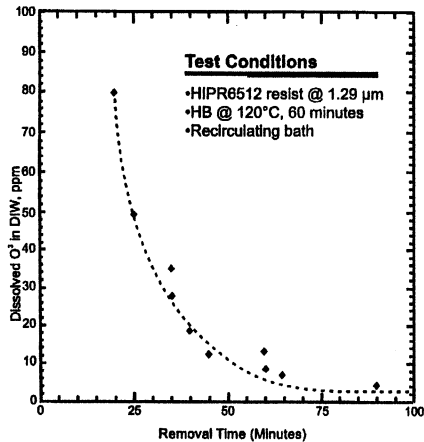


Figure 5. Stripping Time vs. Dissolved O<sub>3</sub>.

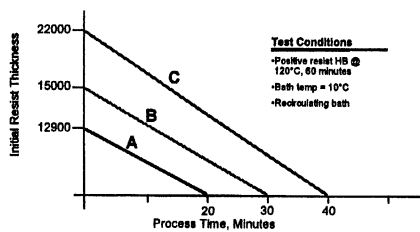
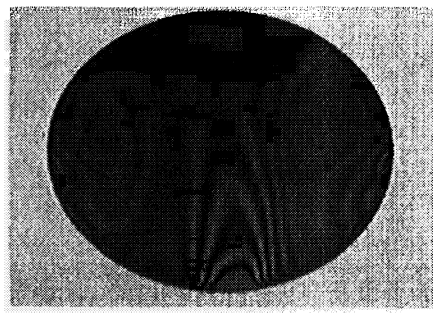
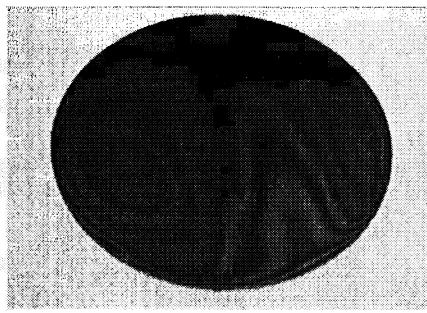


Figure 6. Etch Rates for Different Resist Types.



(A)



(B)

Figure 7. Mechanism of Resist Removal in the DIO3™ Process.

## MASS TRANSFER IN DI:O<sub>3</sub> RESIST STRIPPING

K. Christenson, S. Nelson, M. Olim, and G. Nelson  
FSI International,  
322 Lake Hazeltine Dr., Chaska, MN 55318

For those bulk photoresists that can be etched with ozonated DI water, the primary impediment to high removal rates is the quantity of organic matter to be oxidized. Etch rates are limited by the ozone generator capacity, the amount of O<sub>3</sub> that is dissolved into the water, the mass transfer of O<sub>3</sub> to the wafer surface and the reaction rate. This paper explores the necessary capacity of the ozone generator, the mass transfer of O<sub>3</sub> to the wafer surface and the effect of partially oxidized fragments of resist that dissolve into the water and are oxidized remotely.

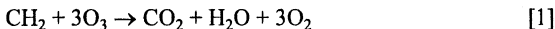
### INTRODUCTION

Interest in the removal of photo-resist with ozonated DI water (DIO) is building rapidly due to its potential low cost of ownership and environmental benefits. For those bulk photoresists that can be etched with ozonated DI water, the primary impediment to high removal rates is the quantity of organic matter to be oxidized. Etch rates are limited by the ozone generator capacity, the efficiency of the contactor system that introduces O<sub>3</sub> into the water, the mass transfer of O<sub>3</sub> to the wafer surface and the reaction rate. The mass transfer considerations in oxidation with O<sub>3</sub> are very different from those of other cleaning chemistries. The solubility and, hence, concentration of O<sub>3</sub> is very low, 50 ppm compared to 80,000 ppm for H<sub>2</sub>O<sub>2</sub> in SPM. However, O<sub>3</sub> is far more reactive than H<sub>2</sub>O<sub>2</sub>. This paper explores the necessary capacity of the ozone generator, the mass transfer of O<sub>3</sub> to the wafer surface and the effect of partially oxidized fragments of resist that dissolve into the water and are oxidized remotely.

### BACKGROUND CALCULATIONS

#### Generator Capacity

Photoresist (PR) is a polymer that consists of long, repeating chains of a monomer. This monomer is composed primarily of carbon and hydrogen with small amounts of oxygen, nitrogen and other elements. The quantity of ozone necessary to oxidize the PR can be estimated by assuming that it is composed entirely of CH<sub>2</sub> that is oxidized in the following reaction:



It takes 3 moles of O<sub>3</sub> to oxidize each "mole" of CH<sub>2</sub>. This equates to 10.3 grams (g) of O<sub>3</sub> for each gram of PR or 12.3 grams of O<sub>3</sub> per cubic centimeter of PR ( $\rho = 1.2$ ).

A 50-wafer load of 200 mm wafers coated with 1.2 microns of PR has a total of 1.8 cm<sup>3</sup> of PR and would require 22.1 g of O<sub>3</sub> to be completely oxidized. A typical semi-

conductor grade O<sub>3</sub> generator has a capacity of 90 g/hr and has the potential to oxidize all of this PR in 15 minutes. Process times of 30 to 35 minutes are claimed in the literature, implying a system efficiency of nearly 50% (1).

#### Ozone Available in Overflow System

Ozonated DI water (DIO) is typically used for PR stripping in an immersion system similar to an overflow rinser. In such a system, water flows upwards between the wafers at an average velocity of 1 cm/sec. Two boats of wafers are usually interleaved (or half-spaced) leaving a gap of approximately 0.3 cm between the wafer surfaces. The total volume in a 1-cm wide strip across a 200-mm wafer with 1.2-micron thick PR is  $2.4 \times 10^{-3} \text{ cm}^3$ . This volume of PR would require 30 mg of O<sub>3</sub> to completely oxidize. In one hour, 1,080 cm<sup>3</sup> of DIO would flow between the wafers across this 1-cm wide strip. With an O<sub>3</sub> concentration of 30 ppm, this 1,080 cc of DIO would contain 30 mg O<sub>3</sub>. This is barely enough to oxidize the resist, even at 100% efficiency.

#### Indiffusion Rate in Stagnant Bath

The total quantity of O<sub>3</sub> available in the flowing DIO is at best marginally able to account for the published etch rates. But the transport of this O<sub>3</sub> to the surface of the wafer relies on the slow process of diffusion. Not all of the O<sub>3</sub> in the flow contacts the surface of the wafer. Figure 1 shows the O<sub>3</sub> concentration profile in the DIO as a function of time in a stagnant bath, assuming a diffusion coefficient D of  $1 \times 10^{-5} \text{ cm}^2/\text{sec}$  and that all O<sub>3</sub> reaching the surface reacts immediately (2, 3). The concentration profile is defined by the "error function"

$$C = C_0 \operatorname{erf}(x/2\sqrt{Dt}) \quad [2]$$

The influx of O<sub>3</sub> F is given by Fick's First law as:

$$F = -D \frac{\partial C}{\partial x} \quad [3]$$

where C is the concentration (4). On a time scale of a few minutes, the concentration gradient of O<sub>3</sub>, and therefore the influx of O<sub>3</sub> at the surface, becomes small.

#### Indiffusion Rate in an Overflow Bath

The flow between the wafers in an overflow bath has a parabolic velocity distribution with zero fluid velocity at the wafer surfaces and 1.5 times the average velocity at the midpoint between the wafers (5, 6). This flow acts to refresh the O<sub>3</sub> near the surface of the wafer. At a distance of 0.018 cm the fluid velocity is 0.33 cm/sec, sufficient to cross a 200-mm wafer in one minute. The flux of O<sub>3</sub> to the wafer surface can be estimated, assuming that this flow supplies a constant concentration source of O<sub>3</sub> at a distance of 0.018 cm from the wafer. The influx of O<sub>3</sub> can be estimated by substituting  $\Delta C/\Delta x$  for  $\partial C/\partial x$  in Equation 3, where  $\Delta C = C - C_{\text{surface}} = C$  and  $\Delta x = 0.018 \text{ cm}$ . Using  $D = 1 \times 10^{-5} \text{ cm}^2/\text{sec}$ , the calculated influx is  $10^{-6} \text{ g/cm}^2 \cdot \text{min}$ . This equates to an etch rate of approximately 0.8 nm/min - 50 times below observed etch rates.

## ACCELERATION MECHANISMS

### Megasonic Streaming

It may be possible to increase substantially the mass transfer in an overflow system with the use of ultrasonics or Megasonics. Megasonic energy causes bulk fluid motion or streaming over a number of length scales (7, 8). Eckart streaming is characterized by flows larger than the acoustic wavelength ( $\lambda=0.18$  cm) and acts to mix the bath (9). Rayleigh streaming has a scale equal to the acoustic wavelength and would act to mix and hence distribute the  $O_3$  across the millimeter scale dimensions of the gap between the wafers (10). Schlichting streaming has dimensions much smaller than the wavelength and would act to bring  $O_3$  very close to the surface of the wafer (11). While difficult to calculate, a one to two order of magnitude increase in the  $O_3$  flux to the wafer surface with the use of megasonic energy cannot be ruled out.

### Dissolution of Short Chains

One possible acceleration mechanism is the dissolution of short chains of PR. As deposited, molecules of PR have between 100 and 10,000 carbon atoms and are hydrophobic. But as these long chains are oxidized, they break up into short fragments with some hydrophilic groups. At some point, the chains become short enough and have enough hydrophilic character to dissolve into the DIO. These fragments can then be transported away from the wafer surface and oxidized remotely.

Figure 2 shows the diameter, diffusion coefficient and typical range of diffusion in one second for these fragments as a function of length (12). The dissolution of fragments consisting of less than twenty  $CH_2$  units could account for the observed 50x excess in etch rate. In a few minutes, these fragments could diffuse away from the surface and be swept away. Schlichting streaming could move these fragments out into the flow stream much more rapidly.

The dissolution mechanism would also explain the increase in etch rate shown by the COLDSTRIP™ process, in which the  $O_3$  concentration in the DIO is increased by cooling the liquid (13). One would normally expect the reduction in reaction rate with cooling to more than offset any increase in the dissolved  $O_3$  concentration. But with dissolution, the reaction rate is less of an issue because there would be adequate time for the oxidation to occur away from the wafers in the fluid handling system. The overall increase in the absolute quantity of dissolved  $O_3$  would still be beneficial.

## SINGLE WAFER CONFIGURATION

If the PR is removed from the wafer in partially oxidized fragments, it should be possible to improve the overall efficiency by flushing these fragments out of the system. This is possible using a single-wafer spinner with DIO dispensed at the center as shown in Figure 3. In this experiment, the DIO was dispensed at ambient temperature from a 0.25 in. (I.D.) tube fixed normal to the center of the wafer at a distance of approximately 2 cm.

Away from the center of the wafer, the flow takes the form shown in Figure 4, with zero velocity at the surface of the wafer and the maximum velocity at the upper surface of the liquid. The fluid flows of this model can be calculated analytically (assuming laminar flow). The depth of the liquid as it sheets across the wafer scales with radius as  $r^{-2/3}$  and the average velocity as  $r^{1/3}$  (14). Figure 5 shows the fluid velocity at a height of 10 microns above the wafer, which increases with radius as  $r^{1/3}$  and with flow as  $Q^{1/3}$ . For instance, with rotation rate of 1,000 RPM and a flow of 1,200 cc/min, the fluid velocity 10 microns above the wafer surface at a radius of 4 cm is greater than 30 cm/sec. As shown in Figure 4, the fluid velocity is a parabolic function of the distance normal from the surface. The fluid layer 20 microns from the surface would have a velocity greater than 30 cm/sec. At velocities greater than 30 cm/sec, all of the fluid farther than 10  $\mu\text{m}$  away from the surface will be thrown from the wafer in less than 0.1 seconds.

The typical diffusion distance in time  $t$  is given by  $x = (Dt)^{1/2}$ . With a diffusion coefficient of  $1 \times 10^{-5} \text{ cm}^2/\text{sec}$  and a time of 0.1 seconds,  $\text{O}_3$  can diffuse a distance of 10 microns. Since the liquid closer than 10 microns from the surface takes longer than 0.1 seconds to cross the wafer, we would expect the  $\text{O}_3$  in this region to become depleted, much as in Figure 1. Very little  $\text{O}_3$  would have time to diffuse in from distances greater than 10 microns before being thrown from the wafer.

An upper boundary on the  $\text{O}_3$  available for etching can be estimated by calculating the volume of DIO that passes within 10 microns of the wafer surface. For the conditions above (1,200 cc/min, 1,000 RPM and a radius of 4 cm) and an  $\text{O}_3$  concentration of  $3 \times 10^{-5} \text{ g/cc}$ , at most  $3 \times 10^{-5} \text{ g/cm}^2 \cdot \text{sec}$  would be available for etching. This would correspond to an etch rate of 22 nm/min. Due to depletion of the  $\text{O}_3$ , the actual etch would be far lower.

Figure 6 shows experimentally obtained etch rates for the conditions of a 1,200 cc/min DIO flow, a radius of 4 cm and various rotation speeds. The data was taken as a line of points crossing the center of a 150-mm wafer. The etch rates in Figure 6 and Figure 7 have been normalized to an  $\text{O}_3$  concentration of 30 ppm. (Other work has shown that the etch rate scales linearly with  $\text{O}_3$  concentration in this system.) It is not clear whether the drop in etch rate from the center to the edges of the wafer is due to the evaporation of  $\text{O}_3$  from the thin sheet of fluid or the depletion of  $\text{O}_3$  near the wafer surface due to oxidation of the PR.

It is also possible that turbulence in the incoming fluid increase the mass transfer locally at the center of the wafer. Further work is necessary to determine whether the turbulence persist to the edge of the wafer. Such turbulence could account for the high etch rate in the single wafer system. But not in the thoroughly laminar overflow system.

The data in Figure 7 was obtained after an etch with a flow of 1,200 cc/min and a speed of 1,000 RPM. The PR was mechanically removed from the center of the wafer before the experiment to eliminate  $\text{O}_3$  depletion in this region. As the DIO traveled outward, it first encountered PR at a radius of 2 cm. At 2 cm, the undepleted DIO had

an etch rate of 280 nm/min, twelve times the etch rate possible if all of the resist were to be oxidized at the surface of the wafer. The resist molecules must be less than 8% oxidized when they dissolve and are swept away from the wafer. The etch rate in the depleted region is 150 nm/min, four times that of cooled immersion systems with a similar O<sub>3</sub> concentration (1). Flowing the resist fragments to drain allows for faster stripping.

## CONCLUSION

If applied efficiently, modern O<sub>3</sub> gas generators have sufficient capacity to fully oxidize over one micron of photoresist from fifty 200 mm wafers in 30 minutes. The primary limitation to efficient use of ozonated DI water is mass transport of the O<sub>3</sub> to the surface of the wafer. Megasonic energy can increase the supply of O<sub>3</sub> to the surface through streaming. Work with a single-wafer spinner showed that only a small fraction of the photoresist is oxidized at the surface of the wafer. Over 90% of the resist dissolves as small chains which are oxidized remotely in a bath system. Flushing these fragments to drain in the spinning system allows the spinning system to strip 4x faster than the immersion system at the same dissolved O<sub>3</sub> concentration.

## ACKNOWLEDGMENTS

The authors would like to thank Drs. L. Carter, D. Deal, R. Fayfield, S. Khandan and N. Narayanswami of FSI International for insightful discussions on these matters.

## REFERENCES

1. M. Dax, "Acid-Free Process Removes Photoresist," *Semiconductor International*, Oct., 1996, p. 74.
2. J. S. Kirkaldy and D. J. Young, *Diffusion in the Condensed State*, The Institute of Metals, London, **322**, 1987, p. 95.
3. J. Crank, *The Mathematics of Diffusion*, 2nd ed., Clarendon, Oxford, 1975, p. 20.
4. A. Fick, *Annln Phys*, **1855**, **170**, 59.
5. F. White, *Fluid Mechanics*, 2nd ed., McGraw-Hill, New York, 1986, p. 323.
6. K. Christenson, "Rinsing: A Critical Process in Contamination Removal," *Semiconductor Fabtech*, ICG, London, 1997, **6**, 333.
7. D. Zhang, D. Kittelson and B. Liu, "An Investigation of Large Scale Acoustic Streaming in Megasonic Cleaning," Proc. 1994 Microcontamination Conf., Cannon Communications, Santa Monica, CA, 1994, p. 215.
8. I. Kashkoush and A. Busnaina, "Numerical Simulation of Ultrasonic and Megasonic Cleaning Processes," Proc. 38th Ann. Tech. Meeting, Institute of Environmental Sciences, Mount Prospect, IL, 1992, p. 19.
9. C. Eckart, "Vortices and Streams Caused by Sound," *Phys. Rev.*, **73**(1), p. 68.
10. L. Rosenberg, *High Intensity Ultrasonic Fields*, Plenum Press, New York, 1971.
11. H. Schlichting, *Boundary Layer Theory*, Mc Graw Hill, New York, 1979.
12. J. Kirkaldy and D. Young, *Diffusion in the Condensed State*, The Institute of Metals, London, **322**, 1987, p. 96.

13. COLDSTRIP™ Legacy Systems Inc., Fremont, CA. US Patent 5,464,480.
14. S. Middleman and A. Hochberg, *Process Engineering Analysis in Semiconductor Device Fabrication*, McGraw-Hill, New York, 1993, p. 184.

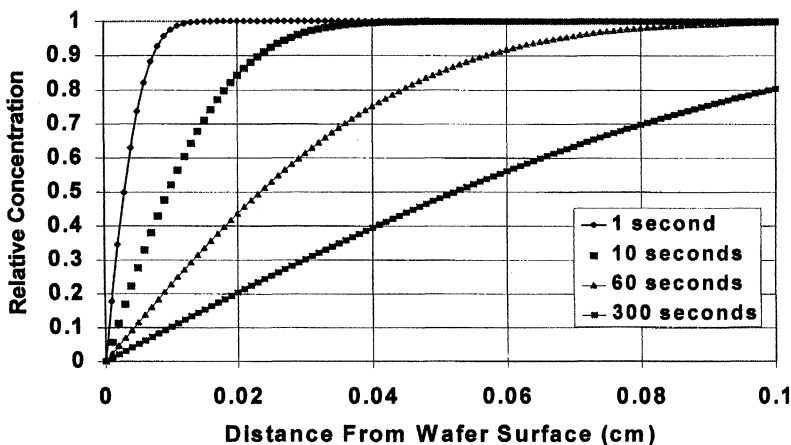


Figure 1: Concentration Near a Resist-coated Wafer

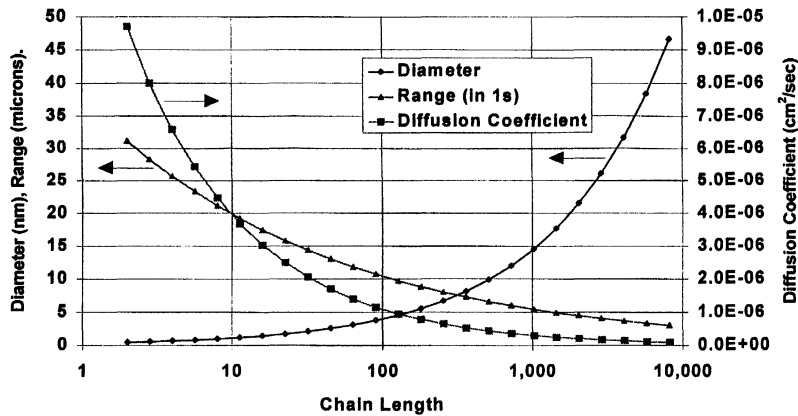
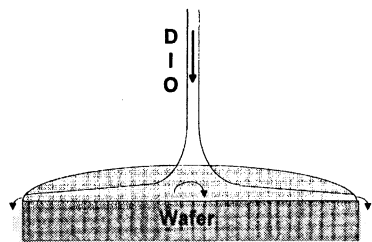
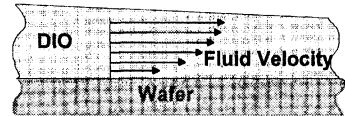


Figure 2: Diffusion vs. Polymer Chain Length



**Figure 3:** Single Wafer Etch Configuration



**Figure 4:** Fluid Velocity Profile

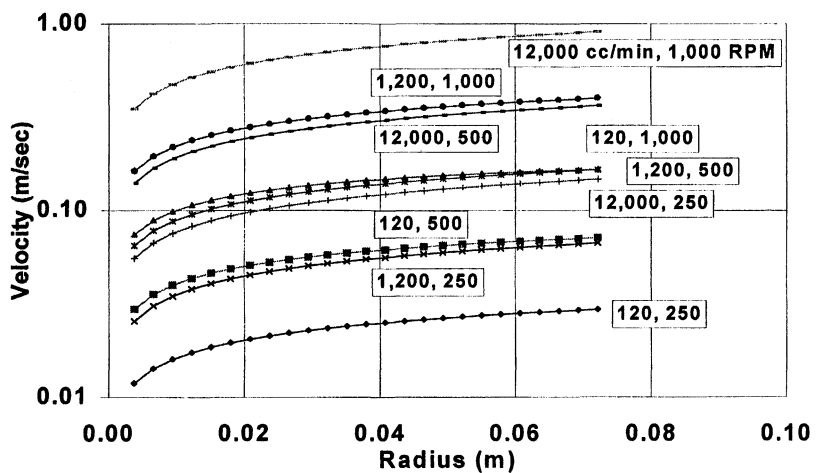


**Figure 5:** Sheet Velocity 10  $\mu\text{m}$  above the surface vs. Flow Rate and RPM

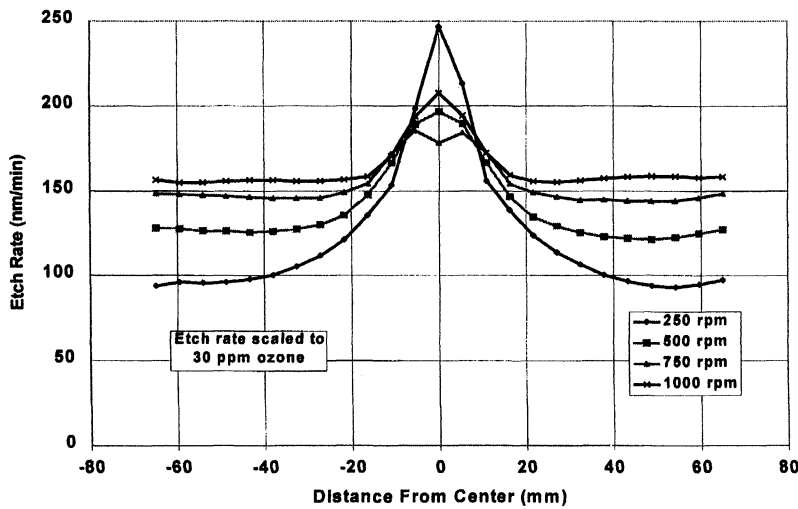


Figure 6: Etch Rate vs. RPM

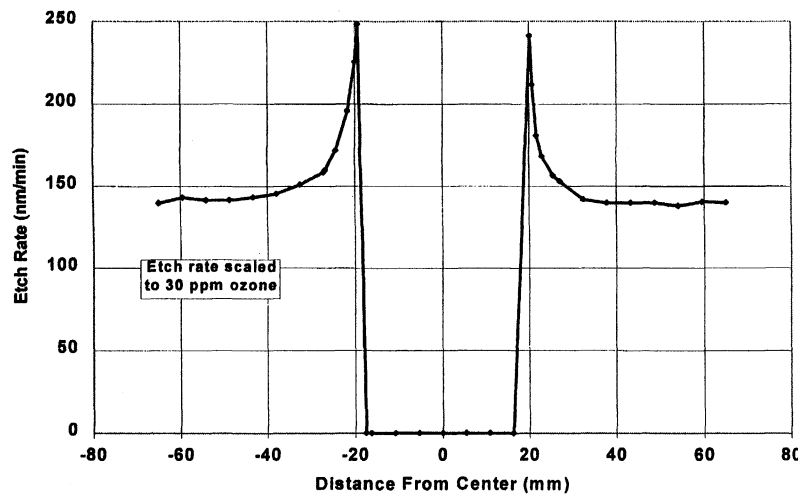


Figure 7: Effects of O<sub>3</sub> Depletion

# ROOM TEMPERATURE PHOTORESIST RESIDUE REMOVAL PROCESS BY USING KF/H<sub>2</sub>O<sub>2</sub>/H<sub>2</sub>O

Shunkichi Omae, Takayuki Jizaimaru, Senri Ojima\* and Tadahiro Ohmi

Department of Electronic Engineering, Graduate School of Engineering, Tohoku  
University, Aza-Aoba, Aramaki, Aoba-ku, Sendai 980-77, Japan

\*Development DIV. Nomura Micro Science Co., Ltd., 2-2-19, Okada, Atsugi 243, Japan

We have studied resist residual removal process by using the mixture of potassium fluoride(KF) and hydrogen peroxide(H<sub>2</sub>O<sub>2</sub>) in ultrapure water(UPW) at room temperature. We have evaluated cleaning efficiency of this process using Si wafers after reactive ion etching(RIE) and ion implantation. These substrates were treated with O<sub>2</sub> plasma ashing, and KF/H<sub>2</sub>O<sub>2</sub>/UPW or sulfuric acid/hydrogen peroxide mixture (SPM) in order to remove resist residual. Although SPM has been widely used as a solution in resist removal process, resist residual still remain on substrate surface after SPM cleaning. On the other hand, KF/H<sub>2</sub>O<sub>2</sub>/UPW can remove resist residual perfectly from substrate surface. Micro-roughness of substrate surface does not increase after KF/H<sub>2</sub>O<sub>2</sub>/UPW treatment. There are three key points in the new resist residue removal process. At first, this solution can etch both SiO<sub>2</sub> and Si, which are underlying of resist residue. Thus, this solution can lift off the resist residue from SiO<sub>2</sub> and Si surface. Finally, this solution can prevent from increasing of micro-roughness of Si by oxidation of Si. Since this newly developed cleaning technology does not generate chemical vapor, it is possible to make cost down.

## INTRODUCTION

Present resist stripping process usually consists of both dry and wet processes. O<sub>2</sub> plasma ashing, dry process, is usually used and is able to remove the most of the resist. SPM (H<sub>2</sub>SO<sub>4</sub>:H<sub>2</sub>O<sub>2</sub> = 4:1), wet process, is conventionally used after O<sub>2</sub> plasma ashing to remove resist residue. Recently, high energy ion irradiation process such as reactive ion etching (RIE) and high dose ion implantation are widely used in semiconductor manufacturing. Because these processes make resist hard, resist residue after O<sub>2</sub> plasma ashing is difficult to remove even with SPM treatment [1]. Therefore new cleaning technology for complete resist removal is required.

SPM cleaning is typically carried out at high temperature of 100-150 °C. This cleaning recipe, however, consumes a large volume of chemicals and produces a volume of exhausting chemical vapor due to high temperature process. This can result in drastic

increase in the production cost. So it is necessary to lower the cost of the resist residue removal process by reducing chemical consumption and vapor generation.

In this study, we have developed new resist residue removal recipe based on the above concepts. We propose new cleaning technology using KF/H<sub>2</sub>O<sub>2</sub>/UPW at room temperature. This newly developed resist residue removal technology is fundamentally different from the conventional technology in the point of removal mechanism. KF/H<sub>2</sub>O<sub>2</sub>/UPW solution lifts off resist residue by etching underlying of resist residue at room temperature without increasing a microroughness of Si surface.

In this paper we discuss the result and the mechanism of new resist residue removal by the mixture of KF and H<sub>2</sub>O<sub>2</sub> solution at room temperature in detail.

## Experimental

Figure 1 shows the experimental procedure of sample preparation. Two types of high-energy ion irradiated Cz p-type(100) Si wafers such as RIE and ion implanted wafers were prepared as samples. In the case of RIE, 650nm thick boron-doped phospho-silicate glass(BPSG) was deposited on a Si wafer, followed by coating with positive type photoresist of 100nm thickness. After i-line UV exposure and development, reactive ion etching was performed to make contact hole pattern. Argon and carbon fluoride gasses such as CHF<sub>3</sub> and CF<sub>4</sub> were used in the reactive ion etching processes. In the case of ion implanted sample, a Si wafer was coated with positive type photoresist of 100nm thickness. After exposure and development, phosphorus ions were implanted into the sample. The acceleration voltage was 95keV and the implant dose was  $5 \times 10^{15}$  atom/cm<sup>2</sup>. After RIE and ion implantation, resists were removed by O<sub>2</sub> plasma ashing, followed by wet cleaning. Wet cleaning solution were SPM or KF/H<sub>2</sub>O<sub>2</sub>/UPW. Figure 2 shows the experimental procedure of wet cleaning. Cleaning solution was put into inner bath and deaerated UPW was introduced outer bath. Both bathes are made by quarts. The outer bath is used for indirect megasonic irradiation and cooling inner bath since the chemical in inner bath was heated by megasonic irradiation. We used deaerated UPW with dissolved O<sub>2</sub> of 5ppb in order to enhance the power transmission of megasonic irradiation [2]. Megasonic irradiation generator was set under the outer bath. The applied frequency was 1 MHz and electric power density was 4.5 W/cm<sup>2</sup>. After wet cleaning, samples were rinsed by UPW with overflowing for 10 minutes.

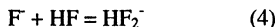
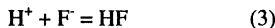
The resist residue removal efficiency was evaluated using scanning electron microscope (SEM). Atomic force microscope (AFM) was used to measure of surface microroughness after resist residue removal.

## RESULT AND DISCUSSION

Figure 3 shows SEM image of surfaces of the RIE sample after O<sub>2</sub> plasma ashing for 0, 5 and 7 minutes. Sample before O<sub>2</sub> plasma ashing have resist layer, but after O<sub>2</sub> plasma ashing, the resist layer is almost removed. However, circular resist residues are observed around contact hole after O<sub>2</sub> plasma ashing. No differences are found in those samples of any O<sub>2</sub> plasma ashing time of 5-7 minutes. In the case of RIE samples, the

most of resist can be removed by O<sub>2</sub> plasma ashing, but resist residue still slightly remains on the BPSG surface. These resist residues are estimated as CF polymer, because carbon fluoride gases that have deposition characteristics on sample surface were used in the RIE process [3].

Figure 4 shows SEM image of RIE sample surfaces. Figure 4(a) shows a sample surface right after O<sub>2</sub> plasma ashing for 5 minutes. Figure 4(b) shows a sample surface after O<sub>2</sub> plasma ashing for 5 minutes and SPM cleaning for 10 minutes. Figure 4(c) shows a sample surface after O<sub>2</sub> plasma ashing for 5 minutes and KF/H<sub>2</sub>O<sub>2</sub>/UPW cleaning for 1 minute. It is confirmed that the resist residue still remained around contact holes after SPM treatment. However KF/H<sub>2</sub>O<sub>2</sub>/UPW cleaning can remove the residue completely. Removal mechanism of organic material such as resist by SPM cleaning is decomposition of organic by oxidation [1]. CF polymer is very stable and have high chemical resistance so that it can not be decomposed and be removed by SPM cleaning. On the other hand, resist residue can be removed by KF/H<sub>2</sub>O<sub>2</sub>/UPW cleaning for only 1 minute. KF solution has etching characteristic of SiO<sub>2</sub> and thus the resist residue can be lifted off by etching SiO<sub>2</sub> substrate. HF solution can etch SiO<sub>2</sub> because this solution generate HF<sub>2</sub><sup>-</sup> ion [4]. KF solution also generates HF<sub>2</sub><sup>-</sup> ion that has etching characteristic of SiO<sub>2</sub> as follow equations.



KF molecules are completely dissociated in solution with equation (1). In KF solution, HF<sub>2</sub><sup>-</sup> ion is generated by combining H<sup>+</sup> with F<sup>-</sup>. So resist residue which is CF polymer is removed with SiO<sub>2</sub> in KF/H<sub>2</sub>O<sub>2</sub>/UPW cleaning by etching SiO<sub>2</sub> layer.

In ion implantation process, the surface at the wafers are conventionally covered by oxide in order to protect contamination from implantation into silicon substrate. However it is reported that oxygen knock-on from the oxide into silicon degrades device characteristics, especially if the semiconductor device is fabricated at low temperature [5]. Therefore ion implantation onto the bare silicon surface is preferable in the future low-temperature manufacturing. Thus we have investigated resist removal efficiency using silicon wafers which were implanted without surface oxides. Figure 5 shows SEM images of ion implanted sample surfaces. Figure 5(a) shows a sample surface after O<sub>2</sub> plasma ashing for 5 minutes. Figure 5(b) shows a sample surface after O<sub>2</sub> plasma ashing for 5 minutes and SPM cleaning for 10 minutes. Figure 5(c) show samples surface after O<sub>2</sub> plasma ashing for 5 minutes and KF/H<sub>2</sub>O<sub>2</sub>/UPW cleaning for 1 minute. It was again confirmed that the resist residue still remains after SPM treatment. However, after KF/H<sub>2</sub>O<sub>2</sub>/UPW cleaning, the residue was removed perfectly. As the surface of the resist becomes hard by ion implantation, SPM cleaning could not remove the residual [6].

However, KF/H<sub>2</sub>O<sub>2</sub>/UPW treatment can remove resist residue because of slight etching of Si surface. It is known that Si is etched by alkaline solution such as aqueous ammonia(NH<sub>4</sub>OH), potassium hydroxide(KOH) and sodium hydroxide (NaOH) [7]. KF is basic salt and pH of KF solution indicates weakly alkaline. For KF concentration is 5, 10 and 20wt%, pH is 7.1, 7.4 and 7.5, respectively.

KF solution is possible to etch both Si and SiO<sub>2</sub> because alkaline solution can etch Si and HF<sub>2</sub> ion can etch SiO<sub>2</sub>. In addition, this resist residue removal is promoted by megasonic irradiation.

Table 1 shows the micro-roughness of Si surface after KF/H<sub>2</sub>O<sub>2</sub>/UPW cleaning for 10 minutes measured by AFM and the etching rate of Si by KF/H<sub>2</sub>O<sub>2</sub>/UPW solution. Concentration of hydrogen peroxide(H<sub>2</sub>O<sub>2</sub>) in this experiment is 0, 0.5 and 1.0 wt%. Micro-roughness of initial Silicon is 0.11nm. After KF/UPW cleaning that does not contain H<sub>2</sub>O<sub>2</sub>, micro-roughness of Si surface is 6nm. On the other hand, in the case of H<sub>2</sub>O<sub>2</sub> concentration is 0.5 and 1.0 wt%, micro-roughness after KF/H<sub>2</sub>O<sub>2</sub>/UPW cleaning decrease 0.14nm and 0.13nm, respectively. Si surface is etched by KF solution, but it can increase surface micro-roughness. By adding H<sub>2</sub>O<sub>2</sub>, however, in solution, etching rate of Si decrease from 0.4nm/min to 0.1nm/min. This is because silicon surface is oxidized by H<sub>2</sub>O<sub>2</sub> and protected from excessive etching. Therefore KF/H<sub>2</sub>O<sub>2</sub>/UPW solution can remove resist residue without increasing micro-roughness of Si.

## CONCLUSION

We have found that KF/H<sub>2</sub>O<sub>2</sub>/UPW with 1MHz-megasonic irradiation can remove resist residual perfectly at room temperature. In semiconductor manufacturing, high energy ion irradiated process such as reactive ion etching and high dose ion implantation are widely used. As a result, resist surface becomes hard and it is difficult to remove resist residue after O<sub>2</sub> plasma ashing by conventional SPM cleaning. The resist residue can be removed by new wet solution, such as KF/H<sub>2</sub>O<sub>2</sub>/UPW. There is a fundamental difference in removal mechanism between SPM and KF/H<sub>2</sub>O<sub>2</sub>/UPW. Removal mechanism of resist by SPM cleaning is decomposition of organic by oxidation at high temperature about 100-150 °C. However the resist irradiated by high energy ions can not be decomposed by SPM. On the other hand, KF is aqueous fluoride and basic salt so that KF solution can etch both Si and SiO<sub>2</sub>. Thus KF/H<sub>2</sub>O<sub>2</sub>/UPW solution removes the resist residue by etching the underlying layer such as SiO<sub>2</sub> and Si. Megasonic irradiation enhances removal efficiency of resist residue. Moreover, increase in micro-roughness of Si surface can be prevented by adding H<sub>2</sub>O<sub>2</sub> about 1wt% in KF/UPW solution. Therefore, KF/H<sub>2</sub>O<sub>2</sub>/UPW solution can remove resist residue without increasing micro-roughness of Si surface. This solution consist of low concentration chemicals such as 10wt% of KF and 1wt% of H<sub>2</sub>O<sub>2</sub>. Consequently, this solution does not generate chemical vapor at room temperature, which reduces the running cost of clean room. Furthermore, minimization of resist removal equipment is enhanced by this cleaning method.

## REFERENCES

- [1]. J. Wei, G. Smolinsky, S. Verhaverbeke, and J. Parker, in Semiconductor Pure Water and Chemicals Conference/1997, **2**, p.81.
- [2]. K. Kawada, S. Okano, T. Kujime, H. Morita, T. Nitta, and T. Ohmi, 28th Symposium on ULSI Ultra Clean Technology Proceedings, p.105 (1996).
- [3]. J. Martsching, J. Amthor, and K. Mautz, No. 326, p. 536, 184th Electrochemical Society Meeting, New Orleans (1993).
- [4]. H. kikuyama, M. Waki, M. Miyashita, T. Yabune, N. Miki, J. Takano, and T. Ohmi, J.Electrochem. Soc., **141**, No.2, Feb., 1994.
- [5]. K. Kotani, T. Ohmi, S. Shimonishi, T. Migita, H. Komori, and T. Shibata, IEICE, E76-C, No4, April. 1993
- [6]. K. Hirose, H. Shimada, S. Shimomura, M. Onodera, and T. Ohmi, J.Electrochem. Soc., **141**, No.1, Jan. 1994.
- [7]. P. M. M. C. Bressers, J. J. Kelly, J. G. E. Gardeniers, and M. Elwenspoek, J.Electrochem. Soc., **143**, No. 5, May, 1996.

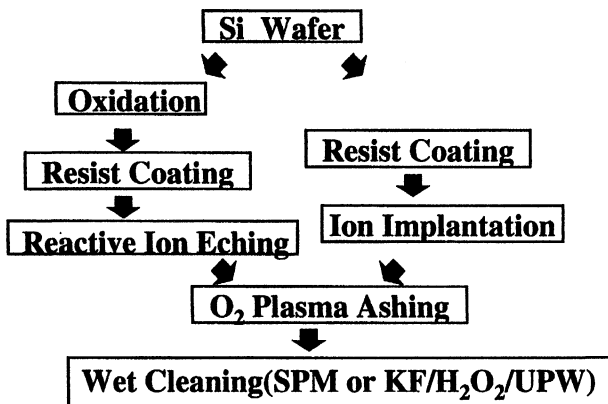


**Fig. 1 Procedure of sample preparation**

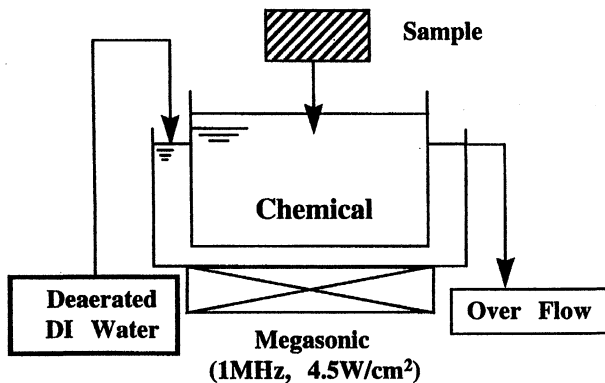


**Fig. 2 Experimental diagram of resist residue removal**

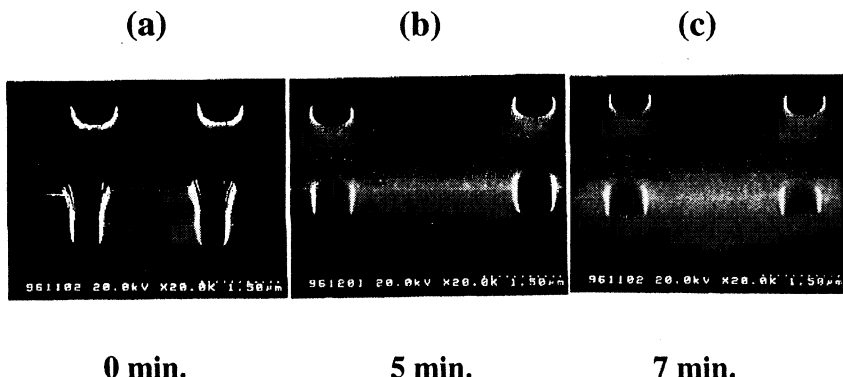


**Fig. 3 SEM images of RIE sample surfaces after O<sub>2</sub> plasma ashing process (ashing time: (a) 0 min, (b) 5min, (c) 7min).**

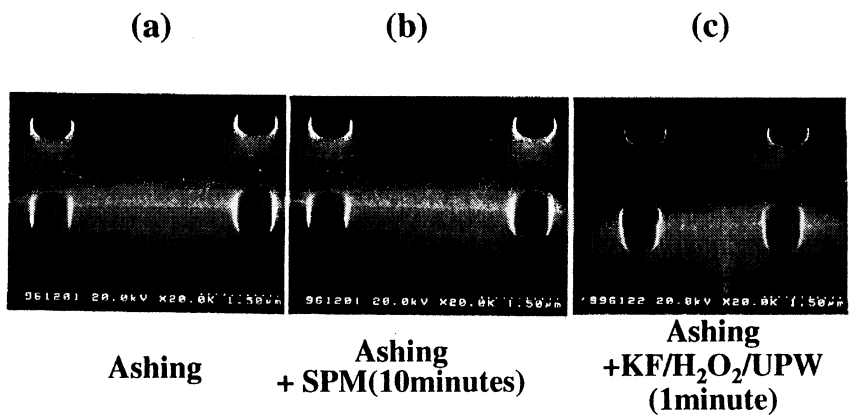
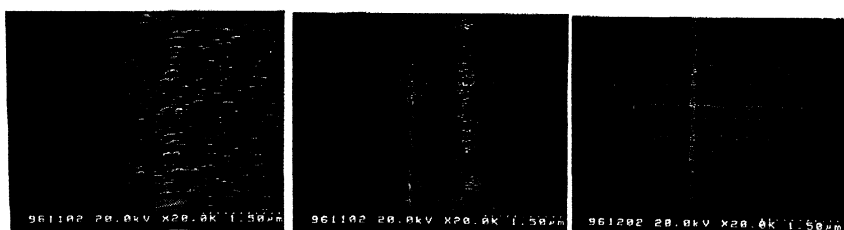


**Fig. 4 SEM images of RIE sample surfaces after O<sub>2</sub> plasma ashing (5min) and SPM or KF/H<sub>2</sub>O<sub>2</sub>/UPW(10/1/89wt %) cleaning.**



Ashing	Ashing + SPM(10minutes)	Ashing + KF/H <sub>2</sub> O <sub>2</sub> /UPW (1minute)
--------	-------------------------	----------------------------------------------------------

**Fig. 5 SEM images of ion implanted sample surfaces after O<sub>2</sub> plasma ashing (5min) and SPM or KF/H<sub>2</sub>O<sub>2</sub>/UPW (10/1/89wt%) cleaning.**

**Table 1.** Etching rate and micro-roughness of Si surface after KF/H<sub>2</sub>O<sub>2</sub>/UPW treatment at various H<sub>2</sub>O<sub>2</sub> concentration

	Si Etch Rate (nm/min)	Micro-Roughness : Ra (nm)
KF/UPW =10/90wt%	1.4	6.0
H <sub>2</sub> O <sub>2</sub> /KF/UPW =0.5/10/89.5wt%	0.4	0.14
H <sub>2</sub> O <sub>2</sub> /KF/UPW =1.0/10/89wt%	0.1	0.13
Initial silicon surface	—	0.11

## **Megasonic Frequency=1MHz**

**Treatment Time (Etching rate measurement) = 24hr**

**Treatment Time (Micro-roughness measurement) = 10min**

# ALTERNATIVE METHODS FOR RESIST STRIPPING

Jane Wei

National Semiconductor, 2900 Semiconductor Drive, Santa Clara, CA 95052 USA  
and

Steven Verhaverbeke

CFM Technologies, 1336 Enterprise Drive, West Chester, PA 19380, USA

Sulfuric processing for resist stripping can use either hydrogen peroxide or ozone as an oxidizing agent. Traditionally, hydrogen peroxide has been used, but is expensive and requires high temperature processing (125 °C or greater) and frequent bath change-outs (every 8 hours). Sulfuric/Ozone Mixtures (SOM) are compared both theoretically and experimentally. SOM mixtures are shown to last for at least 4 days of continuously processing lots of 50 ashed wafers. SOM followed with a full RCA clean is shown to be capable of removing hardened resist with heavy implant dose at high equipment throughput rates.

## INTRODUCTION

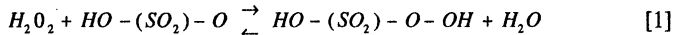
In the past, front-end resist stripping was performed with inorganic oxidizing mixtures. Inorganic acids such as sulfuric acid ( $H_2SO_4$ ), nitric acid ( $HNO_3$ ), chromic acid ( $H_2CrO_4$ ), phosphoric acid ( $H_3PO_4$ ) and hydrogen peroxide ( $H_2O_2$ ) were used since the early days of semiconductor manufacturing to strip resist layers (1). Even today, all of these chemicals can be found in use for resist stripping. Mixtures of sulfuric and chromic acids or sulfuric and nitric acids are typically used at 100 °C. In contrast, fuming nitric (> 95%  $HNO_3$ ) typically is used at room temperature. Some of these inorganic oxidizing mixtures also can be used in the back-end of line of wafer processing since many of the concentrated acids are not corrosive to metals at low water concentrations.

Today, the bulk of the resist usually is removed by ashing the photoresist and in practice wet stripping is limited mainly to post-ash stripping. Bulk photoresist stripping, however, is still a concern when the photoresist is not heavily processed. In this paper we will consider both post-ash and bulk photoresist stripping.

Since 1980, "Piranha" wet baths, mixtures of sulfuric acid and hydrogen peroxide, have become the most common method of post-ash resist stripping. When hydrogen peroxide and sulfuric acid are mixed, "Caro's acid" (i.e. monopersulfuric acid and  $H_2SO_5$ ) is formed. Caro's acid is the active etchant in Piranha baths.

## THEORETICAL CHEMICAL EVALUATION

The resist stripping solution, originally developed for Piranha baths, consists of a mixture of concentrated sulfuric acid (>95 wt.%) with highly concentrated (85-90 wt.%) hydrogen peroxide. Mixing these two chemicals results in the production of Caro's acid:



Concentrated sulfuric acid is an excellent solvent for Caro's acid, whereas the acid decomposes in water. As shown in reaction 1, water is produced in the reaction between hydrogen peroxide and sulfuric acid. The presence of water (i.e., as a result of using more dilute reactants) in the

mixture actually shifts the equilibrium of the reaction towards the reactants, minimizing the production of Caro's acid. Consequently, the production of Caro's acid in Piranha baths is optimized by using highly concentrated hydrogen peroxide (85-90 wt.%).

Caro's acid has 2 significant advantages as a photoresist stripper:

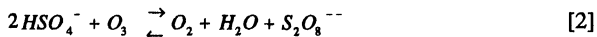
1. It is effective at room temperature, and
2. It is non-corrosive towards metals at room temperature in the absence of water.

However, highly concentrated hydrogen peroxide (85-90 wt.%) is extremely dangerous; it is a serious fire hazard, it is potentially detonable in the presence of small amounts of organic compounds, and it can cause severe chemical burns. As a result of safety issues associated with concentrated H<sub>2</sub>O<sub>2</sub>, the semiconductor industry has generally adopted the use of "laboratory concentrated" H<sub>2</sub>O<sub>2</sub> (approximately 31 wt.%) for all wet processing, including "Piranha" stripping.

In standard Piranha baths solution concentrations are generally about 4:1 H<sub>2</sub>SO<sub>4</sub> (>95 wt.%) to H<sub>2</sub>O<sub>2</sub> (31 wt.%). The excess water found in 31 wt.% H<sub>2</sub>O<sub>2</sub> shifts the equilibrium in reaction [1] away from the production of H<sub>2</sub>SO<sub>5</sub>. Additionally, the use of dilute H<sub>2</sub>O<sub>2</sub> leads to significant heating of the piranha solution when the reactants are mixed as a result of the heat of dilution of sulfuric acid. Caro's acid, which is quite heat sensitive, subsequently breaks down, resulting in low equilibrium concentrations of this oxidizing acid. As a result, the mixture of H<sub>2</sub>SO<sub>4</sub> and laboratory concentrated H<sub>2</sub>O<sub>2</sub> requires very high temperatures (i.e., up to 120 °C) in order to be effective in resist stripping. The resulting bath is quite unstable and hydrogen peroxide has to be added periodically. Every time dilute H<sub>2</sub>O<sub>2</sub> is added, more water is added and the solution becomes even more unstable. Consequently, Piranha baths typically must be changed every 8 - 12 hours.

## OZONE IN SULFURIC ACID

Recently, ozone has been introduced as an alternative to hydrogen peroxide in Piranha baths. Replacing H<sub>2</sub>O<sub>2</sub> by O<sub>3</sub> is very attractive from a cost of consumables point of view; H<sub>2</sub>O<sub>2</sub> is one of the most expensive chemicals, whereas O<sub>3</sub> can be generated in-situ from oxygen gas or even from air. Although the solubility of ozone in DI-water is known to be very low, ozone solubility in sulfuric acid is not a limiting factor for wet stripping, since the ozone quickly reacts with the sulfuric acid. When ozone is sparged into sulfuric acid, dipersulfuric acid (i.e., peroxydisulfuric acid or H<sub>2</sub>S<sub>2</sub>O<sub>8</sub>) is formed (2):



Note that the reaction [2] is written with sulfuric acid singly dissociated and H<sub>2</sub>S<sub>2</sub>O<sub>8</sub> completely dissociated. These are the dominant forms of both species in acid solutions. Dipersulfuric acid is very soluble in sulfuric acid.

## EXPERIMENTAL EVALUATION

The theoretical comparison of traditional Piranha processing with SOM clearly suggests that there are some distinct advantages of using ozone as an oxidizer instead of hydrogen peroxide. Experimental validation of SOM is necessary prior to using the process for manufacturing. In this paper, we present the results from a comprehensive set of experiments that were completed to compare standard Piranha processing with advanced SOM stripping.

## EXPERIMENTAL PROCEDURE

A number of experiments were performed to evaluate the effectiveness of sulfuric/ozone processing. The experimental design presented in this paper evaluated the use of SOM processing as compared with conventional 4:1 sulfuric acid/H<sub>2</sub>O<sub>2</sub> processing. A series of splits were performed on 96 virgin wafers. The wafers were coated with resist and half of the resist coated wafers were implanted. The implant consisted of an N<sup>+</sup> implant of As, at 100 Kev and with a dose of 1.4E16. In the second split, half of the wafers were ashed and half were not. Only minimal ashing was done (60 seconds compared with a POR of 90 seconds) to assure that some metallic residues were left on the wafer after ashing; TXRF validated the presence of post-ash metallic residues. Finally, the four sets of splits were stripped and cleaned in six different processes. This DOE resulted in 24 different experimental lots. The complete wafer preparation process is detailed in Figure 2.

In the cleaning split, a variety of different stripping and cleaning processes were tested. Traditional Piranha processing (SP: sulfuric/hydrogen peroxide) was run in a traditional wet bench at 125 °C for 10 minutes. SOM processing was completed in a CFM Full-Flow™ processing system at 120 °C for 12. In some cases the initial strip was the only cleaning process completed. In other splits the initial strip was followed by a second strip (of the same or different stripping technology) or a full RCA clean (HF/SC1/SC2) in the CFM Full-Flow™ tool. The resulting wafers were evaluated for haze and particles. Additionally, the residual photoresist and pattern were evaluated with light-field and dark-field microscopy and with AFM. Haze and particles were measured on a Tencor 6200. Light-field and dark-field pattern detection was performed with a standard optical microscope.

AFM analyses was performed using the Digital Instruments Nanoscope III with a Dimension 5000 large-sample-stage upgrade for tapping-mode atomic-force microscopy. Each wafer was analyzed near its center: on the implant area (i.e., the pad), in the field, and across the interface of pad/field. Small area scans (1 x 1 μm) were performed on and off the pad to determine micro-roughness, and large area scans (20 x 20 μm) were performed across the interface to determine step height.

A second DOE was performed to evaluate the time/temperature sensitivity of SOM processing. One lot of 24 implanted and ashed waters were tested. Table 2 shows the matrix of input variables studied.

The resulting wafers were evaluated with the same measurement techniques as used in the initial DOE: haze, particles, light-field and dark-field microscopy, and AFM microscopy.

## RESULTS

### SOM versus Piranha Processing

Haze measurements showed significant differences in the wafers. Differences were found between wafers depending on whether or not they were implanted or ashed. Similarly, haze values depended on how wafers were stripped and cleaned. For all cleaning processes, haze levels were found to be the highest for wafers that were implanted and not ashed. After implantation, the haze levels are always very high and indicate the implantation damage more than the cleaning process. Ashing dramatically reduced the haze. In general, stripping and cleaning sequences that begin with SOM processing have lower haze than those sequences that start with standard Piranha processing.

Once the wafers have been implanted, the haze measurements are dominated by the change in the surface structure resulting from implanting the wafers. The results of the light-field and dark-field studies showed that only the implanted wafers (ashed or non-ashed) exhibit patterns in the light-field.

The AFM photomicrographs provide clear pictures of the wafer surface after cleaning. The AFM photomicrographs are shown in Figures 3 and 4. Figure 3 is an AFM photograph of a pattern edge on a wafer that was processed in sulfuric/peroxide at 125 °C, two times for 10 minutes; residues are clearly visible. Figure 4 shows similar results on a pattern edge from a wafer processed in sulfuric/ozone at 120 °C for 12 minutes followed by an RCA clean; no residues remain. In both of these figures, the challenged resist was implanted. Table 3 gives the results of the AFM scans to measure microroughness and step height. These results show that SOM followed by RCA cleaning produces the lowest microroughness (i.e. the two height measurements are relatively consistent), both on and off of "the pad." The "off pad" microroughness is of particular importance since gates are generally built in this area. The pad represents the area on the wafer where implantation occurred. A significant step height exists between the implanted pad and the off pad area after processing with a full RCA clean. This step height is probably a result of different SC1 etch rates between the two areas which have different silicon structures. Since the implantation area was not annealed following implantation, the resulting pad is amorphous (in contrast to the crystalline structure surrounding the pad). The delineation between the implanted region and the un-doped crystalline silicon can be clearly seen in the photomicrographs. SOM followed with RCA cleaning is the most effective method for minimizing microroughness and resist residue. Additionally, residue was seen only with implanted wafers that were not ashed.

### **SOM Temperature/Time DOE**

Further experiments were run to see the temperature and/time effect on SOM process yield. The results from the haze and light-field and dark-field studies indicate that when the wafers were processed at 90° C some residue remained. This remaining resist residue was removed by RCA processing. The haze studies also showed that only RCA cleaning had a significant effect in reducing haze. Figure 5 is an AFM photomicrograph of the wafer pattern after processing at 90° C. Table 4 gives the microroughness and step heights from the AFM measurements. The results suggest that there is no significant difference between the two different temperatures.

### **Experimental Summary**

The experimental results clearly show that the sulfuric/ozone process run at low temperatures is capable of removing even the toughest resist layers, and, therefore, extremely high temperature processing is not necessary for good stripping. Implanted resist was found to be the only real challenge for resist stripping. Ashing of implanted resist is necessary for complete removal of this hardened resist. In contrast, resist that is not implanted is readily removed with all of the wet stripping solutions evaluated. A combination of ashing and sulfuric/ozone was found to readily remove the toughest resist layers. Wafers in which the SOM stripping was followed by an RCA clean were completely clean and exhibited extremely sharp pattern definition and low microroughness.

## THROUGHPUT

The results of the experimental study indicate that SOM followed by a full RCA cleaning provides the best removal of resist. These two processes can be completed sequentially in the same equipment (i.e., the CFM Full-Flow™ system) allowing for an improvement in throughput.

The CFM Full-Flow™ system is a fully-enclosed sequential wet-processing system configured with either one or two processing vessels. Each vessel can be a 50, 100 or 150 wafer unit, depending on the model. Since this system uses sequential processing in the same process vessel, the throughput for a CFM Full-Flow™ system is given by :

$$\text{Throughput} = \frac{\# \text{ of wafers}}{\text{recipe time}}$$

where :      Throughput = wafers processed/ hour  
                # of wafers = number of wafers which the system can process at the same time  
                recipe time (hours) = time of a full recipe

For photoresist stripping applications, the most efficient configuration is a dual system with each vessel containing 150 eight-inch wafers.

For ashed wafers, a sulfuric/ozone-only process presently requires 32 minutes; sulfuric/ozone followed by a full RCA clean, requires 65 minutes. For non-implanted photoresist, SOM-only processes are sufficient for stripping. For implanted photoresist, a sulfuric/ozone + RCA process is necessary. The throughput currently available on a dual 150-wafer vessel Full-Flow™ system is 563 and 277 wafers/hour, respectively.

## SUMMARY

The feasibility of replacing traditional Piranha processing with Sulfuric/Ozone processing was examined by an analysis of their respective chemistries. The theoretical predictions were tested experimentally. Theoretically, SOM produces a stronger oxidizing agent (i.e., dipersulfuric acid) but at a lower concentration than the oxidizer produced in Piranha baths (i.e. Caro's acid or monopersulfuric acid). Caro's acid is, however, much less stable than dipersulfuric acid. Calculations based on the oxidation efficiency of dipersulfuric acid indicate that there is sufficient oxidation capacity available to oxidize batches of 50 to 100 ashed wafers and that the SOM will efficiently oxidize such batches of wafers for up to a week before the bath becomes too diluted by water produced during the oxidation reaction. Data from actual equipment use of SOM indicate that there is little or no drop-off in performance with time over a large number of runs. In contrast, the initial concentration of the oxidizer produced in a Piranha bath is theoretically quite high, enough to readily oxidize an entire batch of 50 *un-ashed* wafers. Caro's acid, however, quickly decomposes in the presence of heat and water, and so the actual oxidizer concentration decreases rapidly and the lifetime of Piranha baths is relatively short (eight hours). The results of a DOE performed to evaluate the effectiveness of various stripping and cleaning procedures on implanted wafers (both ashed and un-ashed) show that SOM followed by RCA cleaning is capable of removing even hardened resist better than traditional Piranha processing. Finally, the ability to complete SOM processing and RCA cleaning is a single piece of equipment provides for increased throughput after wafers have been implanted.

## REFERENCES

1. L. H. Haplan and B.K. Bergin, "Residues from Wet Processing of Positive Resists," *J. Electrochem. Soc.*, 127, 386, 1980.
2. G. Valensi, J. Van Muylder and M. Pourbaix, *Atlas of Electrochemical Equilibria in Aqueous Solutions (NACE, Houston, TX, 1974)*, p. 545.

## TABLES AND FIGURES

**Table 1: Organic reactions with oxidizers**

Oxidizer	Generic Reaction With Organic Compounds
H <sub>2</sub> O <sub>2</sub>	-CH <sub>2</sub> - + 3 H <sub>2</sub> O <sub>2</sub> -> 4H <sub>2</sub> O + CO <sub>2</sub>
H <sub>2</sub> SO <sub>5</sub>	-CH <sub>2</sub> - + 3H <sub>2</sub> SO <sub>5</sub> -> 3H <sub>2</sub> SO <sub>4</sub> + CO <sub>2</sub> + H <sub>2</sub> O
O <sub>3</sub>	-CH <sub>2</sub> - + 3 O <sub>3</sub> -> 3O <sub>2</sub> + CO <sub>2</sub> + H <sub>2</sub> O
S <sub>2</sub> O <sub>8</sub> <sup>2-</sup>	-CH <sub>2</sub> - + 3 S <sub>2</sub> O <sub>8</sub> <sup>2-</sup> + 2H <sub>2</sub> O -> 6HSO <sub>4</sub> <sup>-</sup> + CO <sub>2</sub>

**Table 2: Input Variables for Time/Temperature DOE for SOM Processing.**

	Low Value	High Value
Time (minutes)	12	20
Temperature (°C)	90	120
Clean	No	Full RCA Clean

**Table 3: AFM Results of Microroughness and Step Height Measurements.**

Process	Microroughness				Step Height (nm)
	On Pad (A)		Off Pad (A)		
	R <sub>a</sub>	RMS	R <sub>a</sub>	RMS	
SO-FF	1.44	1.82	0.60	0.77	3.14
SO-FF	1.55	1.95	0.75	0.95	3.03
SP-SP	1.76	2.55	1.68	2.11	0.04
SP-SP	1.67	2.09	2.05	3.30	1.15
SO-NO	1.42	1.79	2.16	4.35	0.53
SO-NO	1.27	1.59	3.96	6.36	1.08

where,

SO = SOM in a CFM Full-Flow™ at 120° C for 12 minutes.

SP = sulfuric/hydrogen peroxide in a wet benches at 125° C for 10 min.

NO = No Clean

FF = Full RCA clean (HF-SC1-SC2) in CFM Full-Flow™ Tool

**Table 4: AFM Results of Microroughness and Step Height Measurements from Temperature/Time DOE.**

Process	Microroughness				Step Height (nm)
	On Pad (A)		Off Pad (A)		
	R <sub>a</sub>	RMS	R <sub>a</sub>	RMS	
SO-FF at 120° C	1.44	1.82	0.60	0.77	3.14
SO-FF at 120° C	1.55	1.95	0.75	0.95	3.03
SO-FF at 90° C	1.46	1.85	0.64	0.84	2.82
SO-FF at 90° C	1.57	1.97	0.68	0.86	3.90

SO, SP, NO and FF = same definition as in table 3

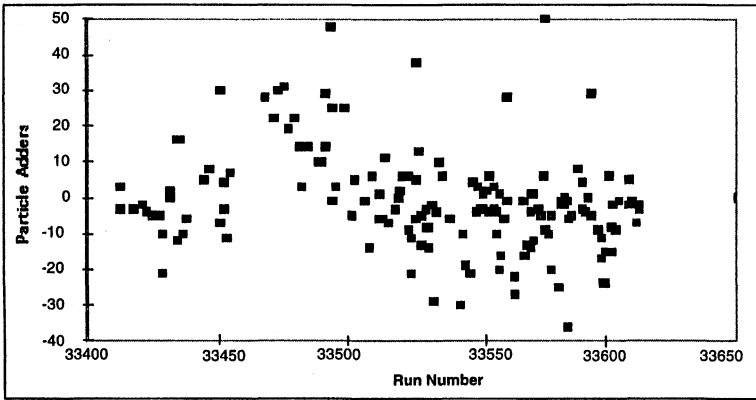


**Figure 1: Particle Adders >0.2 $\mu\text{m}$  from Sulfuric/Ozone Processing.**

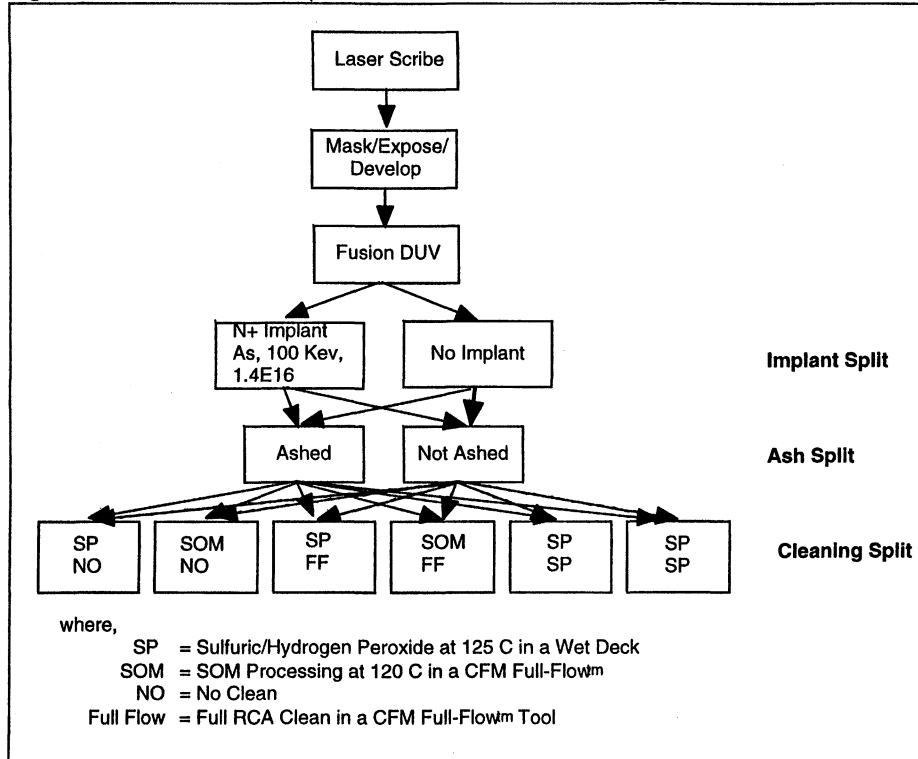
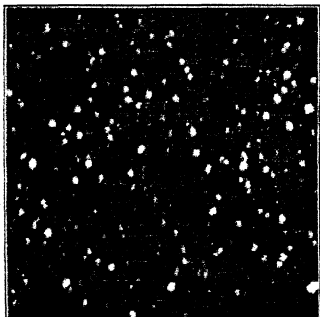


**Figure 2: Schematic Illustrating DOE Split-lot Preparation.**

**95463b23.001**



**95463b23.002**

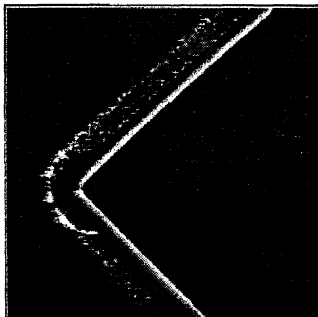
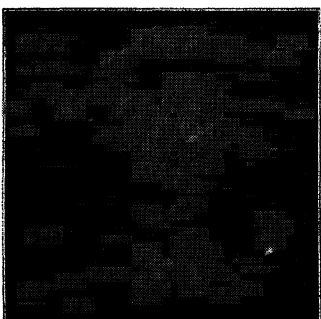


**Figure 3:** AFM photomicrographs of a wafer processed two times in a Piranha bath at 125 °C for 10 minutes. The picture on the left is the field; the picture on the right is the field/pad interface.

**95463a5.001**



**95463a5.002**

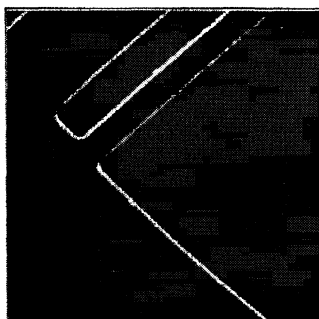
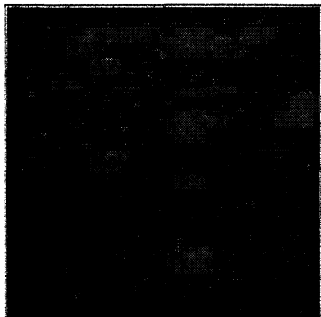


**Figure 4:** AFM photomicrographs of a wafer processed two times in SOM at 120° C for 12 minutes. The picture on the left is the field; the picture on the right is the field/pad interface.

**95463r20.001**



**95463r20.002**

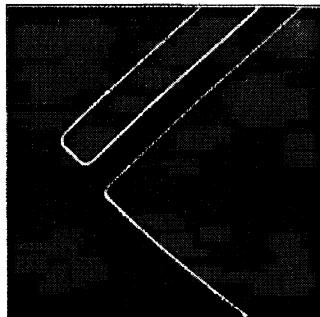


**Figure 5:** AFM photomicrographs of wafer processed two times in SOM at 90° C for 20 minutes. The picture on the left is the field; the picture on the right is the field/pad interface.

# **EVALUATION OF POST-ASHED PHOTORESIST CLEANING USING OXIDIZING CHEMISTRIES\***

**P.J. Resnick and C.A. Matlock\***

**Sandia National Laboratories  
Albuquerque, NM 87185**

## **ABSTRACT**

The use of sulfuric acid based chemistries for the removal of photoresist ashing residue was investigated. Samples were prepared by ion-implanting patterned, UV-hardened photoresist. The efficacy of post-ash cleaning was determined by measuring organic, metallic, and particulate surface concentrations. Sulfuric-nitric mixtures and sulfuric-hydrogen peroxide mixtures were highly effective for the removal of metallic contaminants. Neither chemistry was very effective for particulate and organic residue. Highly effective overall cleaning was observed when a sulfuric acid based clean was followed with an RCA-type process sequence. Redundant cleans provided no additional benefit. Post-ash cleaning may be simplified by either reducing the number of sulfuric acid based cleans, or for certain post-ash applications, by replacing them with RCA-type processes.

## **INTRODUCTION**

Oxidizing chemistries have been used for many years to strip photoresist and as a post-photoresist ashing clean. These oxidizing chemistries are typically based on sulfuric acid, combined with a strong oxidizer such as hydrogen peroxide or nitric acid. Although numerous studies have been performed to assess the efficacy of these sulfuric acid based chemistries for the removal of photoresist, relatively little information exists in the open literature regarding the use of these chemistries for post-ash cleaning. Much of the previous work on photoresist stripping has focused on optimizing the mixing ratio of the sulfuric chemistry to achieve a maximum adiabatic temperature (1,2). Such an

\*Present address: FSI International, Surface Conditioning Division, Chaska, MN 55318

This work was supported by the U.S. Department of Energy under contract no. DE-AC04-94AL85000. Sandia is a multiprogram laboratory operated by Sandia corporation, a Lockheed Martin Company, for the United States Department of Energy. This work was funded through a cooperative research and development agreement with SEMATECH.

optimization technique may be appropriate for the removal of bulk photoresist, but it is likely to have little value for the study of post-ash cleaning. Typically, oxygen plasma ashing is used to remove photoresist in front-end-of-line operations, rather than wet chemical stripping. However, these oxidizing wet chemistries are commonly used following front-end-of-line ashing steps as an additional safeguard against residual organic contamination, as well as a means to remove post-ash metallic contamination. Often these cleaning chemistries will be used at the end of a photolithography, implant, or etch process route, as well as at the beginning of a subsequent diffusion or CVD route. This type of process flow results in redundant cleaning steps. Although there is no reason to believe that such redundancy would have a deleterious effect on device fabrication or performance, there may be little or no value added by performing redundant cleans. Finally, the sulfuric acid based cleans are often used in combination with other cleaning chemistries such as SC-1 ( $\text{NH}_4\text{OH}:\text{H}_2\text{O}_2:\text{H}_2\text{O}$ ) and SC-2 ( $\text{HCl}:\text{H}_2\text{O}_2:\text{H}_2\text{O}$ ). The combination of these cleaning steps must be considered during an optimization of a post photoresist ashing clean sequence.

The objective of this study was to evaluate the efficacy of post-ash cleaning. The primary focus was on sulfuric acid based cleans. The efficacy of both sulfuric acid-hydrogen peroxide mixtures (SPM) and sulfuric acid-nitric acid mixtures (SNM) was evaluated. The value added by performing multiple cleans was investigated, as was the overall cleaning efficacy of process sequences that included RCA-type cleans. Process simplifications are proposed.

## EXPERIMENTAL

### Sample Preparation

Many factors are either known to affect or are believed to affect the efficacy of photoresist ashing (3). These factors include implant species and dose, photoresist thickness and track bake conditions, UV stabilization parameters, and perhaps most of all, the tool and process parameters that are used to perform the photoresist ash. All of the wafers that were prepared for this study were 150 mm monitor grade silicon, on which a 10 nm screen oxide had been grown. Following oxidation, photoresist was spun on, exposed on an I-line stepper using either a resolution test structure mask or a CMOS process layer mask, and track developed. Finally, the wafers were cured in a UV stabilizer, implanted with either  $^{75}\text{As}^+$  or  $^{31}\text{P}^+$  at various doses and energies, and ashed in a downstream oxygen plasma asher.

Two sets of samples were prepared. The first sample set was prepared for a screening experiment to examine metrology techniques and the effect of implant dose. A non-optimized ashing recipe was used following an  $^{75}\text{As}^+$  implant (1.4E14 @ 160 keV) to create a "worst case" contamination challenge. The second sample set was used to

evaluate the post-ash clean following an n-well implant ( $^{31}\text{P}^+$ , 1.7E13 @ 900 keV) used in CMOS device fabrication. These samples were processed through an optimized ash, and possess contamination levels that are representative of typical post-ash processes.

### Metrology

Multiple metrology techniques were employed to assess the effectiveness of the post-ash cleaning sequence. Because the wafers were photopatterned, a semi-quantitative laser light scattering technique could be employed to detect residual photoresist following the cleaning steps (4). This type of measurement, which allows for the detection of periodic defects that are easily identified as residual photoresist, as well as random defects, was performed on both a Tencor Surfscan 7700 and a Surfscan 6200. Residual metallic contamination was quantified by either total x-ray fluorescence (TXRF) spectroscopy or heavy ion backscattering (HIBS) spectroscopy. HIBS is most effective for detecting high-Z elements, and as a result was used sparingly during this study. Finally, residual organic contamination was quantified by using time-of-flight secondary ion mass spectrometry (TOF-SIMS). To quantify the TOF-SIMS data, organic species peak heights were normalized to the abundant and constant  $^{28}\text{Si}$  peak. TOF-SIMS and TXRF were performed on one wafer per experimental split. TXRF was performed on a single spot, and TOF-SIMS was performed on three spots per wafer.

### Cleaning Experiments

Wafers were measured on a Tencor Surfscan 7700 immediately after the plasma ashing step. Where defect levels were sufficiently low, high sensitivity measurements (light point defects  $> 0.15 \mu\text{m}$ , latex sphere equivalent) were also made on a Surfscan 6200. Following the initial measurement, samples were processed through various post-ash cleaning chemistries. Table I provides details on the individual cleaning chemistries and process conditions that were used throughout this study. Post-clean light scattering defect measurements were performed prior to off-line analytical work for measuring organic and metallic contamination.

The cleaning splits were chosen to evaluate the efficacy of individual sulfuric acid based chemistries, as well as the overall efficacy of cleaning sequences that include both sulfuric acid chemistries and RCA processes. These splits were conducted in three separate cleaning experiments, using a minimum of three wafers per split.

**Table I.** Parameters for individual process steps

Chemistry	Mixing Ratio	Temperature (°C)	Process Time (min.)
H <sub>2</sub> SO <sub>4</sub> :H <sub>2</sub> O <sub>2</sub> (SPM)	5:1	95	5
H <sub>2</sub> SO <sub>4</sub> :HNO <sub>3</sub> (SNM)	10:1	150	10
NH <sub>4</sub> OH:H <sub>2</sub> O <sub>2</sub> :H <sub>2</sub> O (SC-1)	1:4:64	45	10
HCl:H <sub>2</sub> O <sub>2</sub> :H <sub>2</sub> O (SC-2)	1:1:6	45	5
HF:H <sub>2</sub> O (HF)	1:15	24	0.5

## RESULTS AND DISCUSSION

In the initial screening experiment, wafers were photopatterned with a reticle test structure mask, implanted with arsenic at various doses, and stripped using an non-optimized ashing recipe. Following the ash, wafers were processed through a 5:1 SPM chemistry. This resulted in no substantial change in light scattering event count, as measured on a Tencor Surfscan 7700. Following the SPM clean, a dilute SC-1 megasonic clean was also performed. This produced a substantially cleaner surface, although numerous defects associated with certain mask structures still remained. Representative wafer maps are shown in Figure 1. Scanning probe microscopy analysis of the wafers following the ash revealed that the defects that remain were indeed artifacts of the original patterned photoresist. The morphology of these defects was similar to that which has been reported in the literature previously for ashed photoresist samples. (4). Carbonization of photoresist (e.g., a C/O ratio greater than 10) has been reported to render SPM chemistries ineffective (3). Post-ash photoresist presumably possesses a high C/O ratio, and therefore may be inert to oxidizing chemistries. The physical action of megasonics was significantly more effective than the purely chemical action of the SPM for the removal of bulk ash residue.

The remaining experiments were performed on a short loop product that was processed through n-well photolithography and implant, followed by an optimized ashing step. This short loop structure was used to evaluate post-ash cleaning on samples that possessed a realistic contamination challenge.

First, the post-ash cleaning efficacy of 5:1 SPM was compared to that of 10:1 SNM. These cleans were found to be equally efficacious. Both cleans performed very well with respect to metallic contamination removal; neither chemistry performed well with respect to particulate or organic contamination removal. Other researchers have also found that SPM, as a stand-alone process for post-ash cleaning, does not perform well with respect to particle contamination (5). Results for residual metallic contamination levels are shown in Figure 2. It is interesting to note that metallic contamination levels on the control group (wafers that received no subsequent clean following the ash) are relatively

low. By comparison, surface concentrations in the mid  $10^{11}$  atom/cm<sup>2</sup> range for transition metals such as iron are not uncommon following an SC-1 clean (6).

Next, experiments were performed to determine if redundant cleaning operations following the photoresist ash step provide any benefit. The cleaning sequence that is currently used for post n-well implant and photoresist ashing of a 0.5  $\mu\text{m}$  CMOS technology at Sandia Laboratories was used as a benchmark for these studies. This sequence, which includes numerous sulfuric acid based cleans, RCA cleans, and an HF dip, was adopted from a product flow used by a major U.S. chipmaker. Figure 3 shows Surfscan light point defect (LPD) data for redundant cleaning steps. The first two sulfuric acid based cleans are fairly ineffective. The LPD count is significantly reduced when RCA and HF cleans are included in the process sequence. The TOF-SIMS data, shown in Figure 4, show a similar behavior -- the sulfuric acid based cleans appear to be ineffective for removal of organic material ( $m/z$  41-74), but the addition of RCA/HF steps significantly reduces the amount of organic contamination detected on the surface. TXRF analysis of redundant cleaning steps was somewhat ambiguous, presumably due to an environmental contamination source. This analysis was repeated during the study of simplified process flows, discussed below.

Finally, it was of interest to determine if a simplified process flow has any measurably deleterious effects. Based on the results from the previous experiments, simplified process flows were created and compared to the benchmark cleaning sequence. LPD data for simplified product flows are shown in Figure 5. Although the benchmark cleaning sequence exhibited the lowest LPD count, there was no substantial difference between the splits (excluding Split #0, which received no post-ash clean), and all of the cleaning splits reduced the LPD levels to the original levels following oxide growth, or lower. The metallic contamination data, shown in Figure 6, showed that the most simplified split (Split #1b in Figure 6) possessed a slightly higher zinc level than the other splits. Calcium contamination levels (not shown in Figure 6) were also slightly elevated in the most simplified cleaning split. Iron contamination levels were below the practical lower detection limit in all of the cleaning splits. The other transition metals were all near or below the detection limit for each of the cleaning splits. Finally, TOF-SIMS data, shown in Figure 7, indicate that all of the cleaning splits performed equally well for the removal of organic contamination. Aluminum, not shown with these data, was slightly elevated in the most simplified cleaning split (Split #1b in Figure 7).

## CONCLUSIONS

The considerations involved in optimizing post-ash cleaning are substantially different than those used to optimize photoresist stripping. For post-ash cleaning, it is the removal of trace metallic contamination, particulates, and molecular organics that is desired, rather than the removal of bulk heavy organic material. Sulfuric acid based

chemistries are often used following photoresist ashing, and in fact, are often performed repetitively and with other cleaning chemistries. Because these cleans are effective for removing metallic contamination, they provide benefit for post-ash cleaning. However, such benefit may also be derived by using mineral acid cleaning chemistries such as HF, HCl or SC-2 for metallic contamination removal. Redundant cleans however, do not appear to have any added value. Simplified process flows that either reduce the number of sulfuric acid based cleans, or eliminate them entirely, appear to be viable alternatives for cleaning wafers after ashing hardened photoresist.

## REFERENCES

1. F. Pintchovski, J. B. Price, P. J. Tobin, J. Peavey, and K. Kobold, *J. Electrochem. Soc.*, **126**, 1426 (1979).
2. V. T. Nguyen, in *Cleaning Technology in Semiconductor Device Manufacturing (2<sup>nd</sup> International Symposium)*, J. Ruzyllo and R. Novak, Editors, PV **92-12**, p.483, The Electrochemical Society Proceedings Series, Pennington, NJ (1992).
3. K. Hirose, H. Shimado, S. Shimomura, M. Onodera, and T. Ohmi, *J. Electrochem. Soc.*, **141**, 192 (1994).
4. A.L.P. Rotondaro, M. Meuris, H. F. Schmidt, M. M. Heyns, C. Claeys, L. Hellemans, and J. Snauwaert, *ibid*, **142**, 211 (1995).
5. S. D. Hossain and M. F. Pas, in *Cleaning Technology in Semiconductor Device Manufacturing (3<sup>rd</sup> International Symposium)*, J. Ruzyllo and R. Novak, Editors, PV **94-7**, p.111, The Electrochemical Society Proceedings Series, Pennington, NJ (1992).
6. S. Dhanda, C. R. Helms, P. Gupta, B. B. Triplett, and M. Tran, in *Ultraclean Semiconductor Processing Technology and Surface Chemical Cleaning and Passivation*, M. Liehr, M. Heyns, M. Hirose, and H. Parks, Editors, p. 201, Materials Research Society Symposium Proceedings Vol. 386, Pittsburgh, PA (1995).

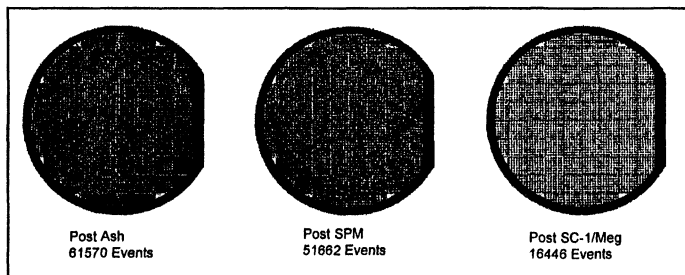
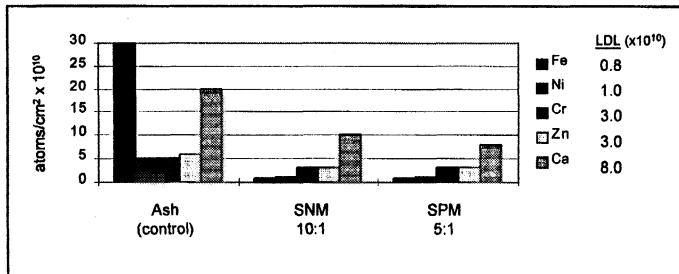
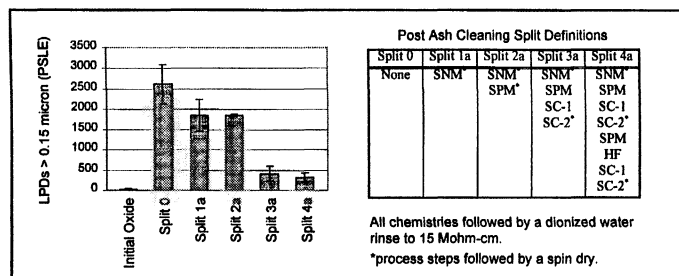


Figure 1. Tencor Surfscan 7700 event maps following photoresist ash (non-optimized), SPM processing, and dilute SC-1 with megasonics.



**Figure 2.** Metallic contamination following photoresist ash, sulfuric-nitric mixture, and sulfuric peroxide mixture processes (LDL = Lower Detection Limit).



**Figure 3.** Effect of redundant cleaning on LPD count.

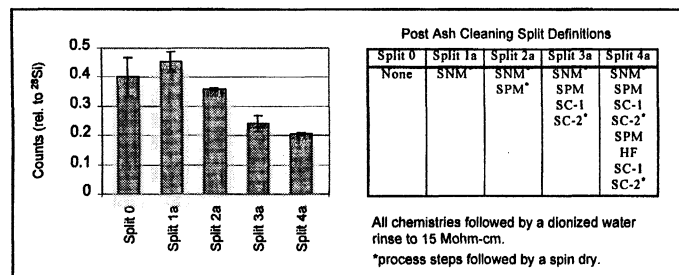


**Figure 4.** Effect of redundant cleans on organic contamination levels.

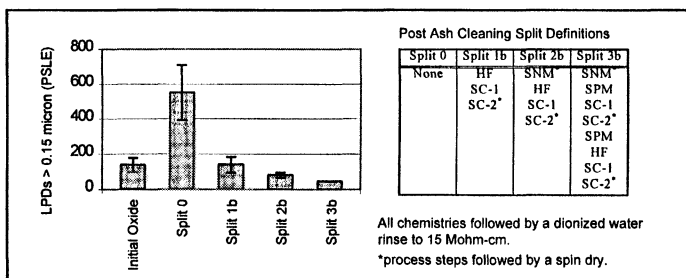


**Figure 5. LPD counts after simplified clean sequences (splits 1b and 2b).**

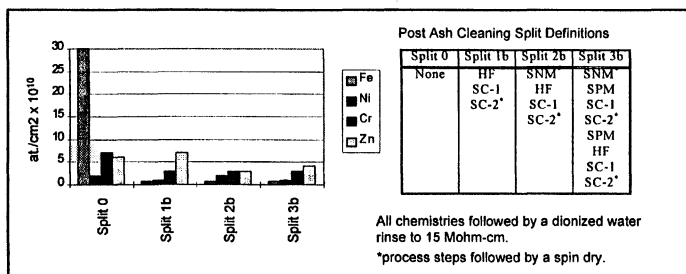


**Figure 6. Metallic contamination levels after simplified clean sequences (splits 1b and 2b).**

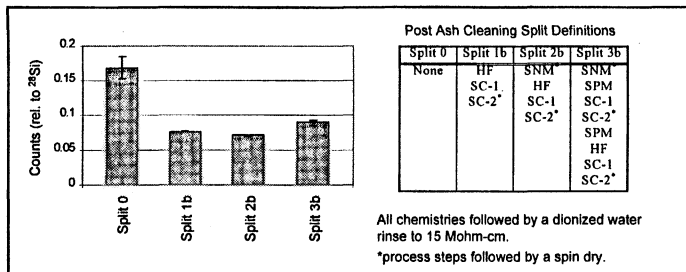


**Figure 7. Organic contamination levels after simplified clean sequences (Splits 1b and 2b).**

## **ORGANIC CONTAMINATION ON SILICON WAFER SURFACES IN PROCESSING ENVIRONMENTS**

Motoko Tanishima and Naomichi Abe

Technology Development Div.

FUJITSU LIMITED

4-1-1 Kamikodanaka, Nakahara-ku, Kawasaki 211-88, Japan

Recently, the airborne molecular contamination of semiconductor manufacturing process yields has been given much attention. Accordingly, we investigated the organic contamination of silicon wafer surfaces that occurs in processing equipment. Research has shown that wafer surfaces are contaminated at the fan filter unit (FFU) of processing equipment and that typical contaminants are organosilicones and additives such as DOP which originate from the materials and supply gas of FFUs. We also investigated the process effects caused by these contaminants. Consequently, it was found that cyclosiloxanes produce a haze on SiN and that trimethylsilanol causes bursts in exposed resist film.

### **INTRODUCTION**

As device fabrication has advanced, it has been found that the organic contamination of wafer surfaces in processing environments such as cleanroom ambients or processing equipment affects device yield, performance, and reliability [1, 2]. Our research of airborne organic contamination control through the selection of cleanroom construction material has shown that the organic contamination of wafer surfaces in cleanroom ambients also originates from processing chemicals such as HMDS and the components of processing equipment [3-5].

We then researched the organic contamination of wafer surfaces by processing equipment. Current processing equipment needs an FFU in its cassette I/O port to keep wafer surfaces free from particles. However, the FFU typically does not remove organic vapors and, in fact, may introduce organic contaminants onto wafer surfaces via outgassing. Therefore, wafer surface contamination from the FFU should be researched with respect to the influence of organics in the supply gas and the outgassing.

In this paper, we report on the organic contamination of wafer surfaces by the FFU through quantitative analyses and discuss the origins of these contaminants and the process effects related to them.

## EXPERIMENTAL

### Test unit for evaluating the FFU

Figure 1 shows a test unit constructed for evaluating the organic contamination from the FFU. The supporting module of the unit was made completely of stainless steel and the FFU to be evaluated was installed on it. The flow rate of the supply gas under the FFU was 0.35 m/s, the same as that in the cleanroom where a test unit was placed.

### Experimental details of the test unit

In general, an FFU is composed of a fan and a ULPA or HEPA filter connected by sealants or adhesives (Fig. 1). It has been pointed out that these materials, especially sealants, outgas organics. For this reason, it is important to select them carefully [6]. Two types of FFUs were tested. One was the general type employing materials whose outgassings are not controlled. The other was a low-outgas type of FFU using materials whose outgassings are controlled.

Cleanroom air, chemically filtered cleanroom air, and N<sub>2</sub> gas were supplied separately to the two types of FFU to determine the influence of the supply gas. The cleanroom in which the test unit was placed was constructed using low outgassing materials. The amount of airborne organics has been kept to several tens of  $\mu\text{g}/\text{m}^3$  and organics that are adsorbed by silicon wafer surfaces, such as siloxanes and di-2-ethylhexyl phthalate (DOP), have been reduced. The chemical filter for removing organics in the cleanroom air was made of activated carbon. The concentration of cleanroom air passing through it was several  $\mu\text{g}/\text{m}^3$ . The concentration of N<sub>2</sub> gas was 99.999%, which included organics in the amount of several  $\mu\text{g}/\text{m}^3$ .

### Method of analyzing wafer surface

Bare silicon wafers used in the experiment were first treated with an RCA cleaning method. Then they were exposed in the test unit and cleanroom for 48-hour periods (Fig. 1). These samples were analyzed by thermal desorption-gas chromatography/mass spectrometry (TD-GC/MS). The amount of individual organics detected is thus expressed by the equivalent n-hexadecane value in pg/cm<sup>2</sup>.

## RESULTS AND DISCUSSION

### Wafer surface organic contamination in the test unit and the cleanroom

Figure 2 shows the total ion-chromatogram (TIC) of adsorbates on silicon wafers in the test unit equipped with a general type of FFU employing various types of supply gas, and in the cleanroom. Each wafer surface has few differences in contamination in spite of using different supply gases (a-c). The wafer surfaces in the test unit were contaminated much more than those in the cleanroom. In this case, siloxanes, phosphate esters and phthalate esters etc. as the adsorbates in the test unit are easily recognized.

Figure 3 shows the total ion-chromatogram (TIC) of adsorbates on silicon wafers in the test unit equipped with a low-outgas type of FFU employing various types of supply gas, and in the cleanroom. Contaminants such as tributyl phosphate (TBP), dibutyl phthalate (DBP), and DOP were observed when the supply gas was cleanroom air. These contaminants are the same as those observed in the cleanroom, but, especially with DOP, in smaller amounts because these organics are adsorbed by the ULPA filter. When the supply gas is N<sub>2</sub> or is chemically filtered, the amount of these contaminants becomes negligible.

The main contaminants thus analyzed are summarized in Table 1. For the general type of FFU, the wafer surface is contaminated by numerous organics, independent of the supply gas. With the low-out gas type of FFU, some contaminants, which are those found in the cleanroom, are observed only in the test unit supplied with cleanroom air. These analytical results show that the contaminants originate in the materials and the supply gas of the FFU.

As for the contaminants from FFU materials, organosilicones are typical of outgassing from silicon and polyurethane sealants. DOP originates from the filters. In particular, the contamination increases when DOP is used to test the performance of a filter. Phosphate esters, phthalate esters, adipate esters, and N-butylbenzenesulfoneamide come from additives in the filters, the sealants, the adhesives, and the gaskets. These high molecular weight compounds exist even in the ambients of cleanrooms constructed with materials having low additives. Hence, wafer surfaces are contaminated by these chemicals even when the supply gas is cleanroom air. Trimethylsilanol is also in cleanroom air because although also originating in the silicon sealant, it is a decomposition product of HMDS, which is used in resist processes to promote adhesion.

#### Relation of wafer surface organic contamination to the process effects

We have found that haze on SiN and bursts in exposed resist film are caused by organically contaminated wafers, and that the typical contaminants are trimethylsilanol, cyclosiloxanes, and DOP. The relation of these contaminants to the process effects was identified through quantitative analyses.

SiN was deposited on various contaminated wafers by LP-CVD. Figure 4 shows haze on SiN observed by a surface particle counter. This shows that it is typical of haze to be detected as particles 0.2  $\mu$ m in diameter. Table 2 shows the relationship between the haze and the surface concentration of the organic contaminants. The relationship shows that the haze is observable when the surface concentration of low molecular weight cyclosiloxanes (D3 to D6) is more than 100 pg/cm<sup>2</sup> and that of high molecular weight cyclosiloxanes (D7 to D13) is more than 800 pg/cm<sup>2</sup>. The haze is also shown to be independent of the surface concentration of trimethylsilanol and DOP. It has been proven that the haze is caused by cyclosiloxanes, especially low molecular weight cyclosiloxanes (D3 to D6).

Resist film was spin-coated on various contaminated wafers and then exposed. We observed bursts in i-line resist film with an SEM (Fig. 5). Table 3 shows the relationship between bursts and the surface concentration of the organic contaminants. The results indicate that the number of bursts corresponds closely to the surface concentration of trimethylsilanol, but is not influenced by the surface concentration of cyclosiloxanes or DOP. This suggests that the bursts in exposed resist film are caused by the surface concentration of trimethylsilanol.

These results show that it is critical to prevent the wafer surface from being contaminated by cyclosiloxanes and trimethylsilanol, and that it is unnecessary to be concerned about contamination by DOP.

## SUMMARY

Typical contaminants adsorbed in process equipment include trimethylsilanol, cyclosiloxanes, and additives such as DOP. These contaminants originate in the materials and the supply gas of the FFU. In the FFU, this comes from sealants or from filters as their materials outgas cyclosiloxanes or additives. In regard to the supply gas, the quality of the cleanroom air influences the affect of contaminants, and especially that of trimethylsilanol.

Cyclosiloxanes cause a haze to form on SiN. Trimethylsilanol, which is a decomposition product of HMDS, causes bursts in exposed resist film . Therefore, the most attention should be given to organosilicones in all the contaminants.

## REFERENCES

- [1] A. Shimazaki, M. Tamaoki, and Y. Sasaki, Ext. Abst. 188th Meeting of The Electrochemical Society, October 1995, 476.
- [2] Devon Kinkead, Michael Joffe, John Higley, and Oleg Kishkovich, Technology Transfer #95052812A-TR SEMATECH, May 1995.
- [3] S. Kobayashi and Y. Wakayama, Proc. 5th International Symposium on Semiconductor Manufacturing, 313-316, 1996.
- [4] M. Tanishima, Y. Okui, and N. Abe, Ext. Abst. 57th Autumn Meeting of the Japan Society of Applied Physics, 1996, 10a-L-6. (in Japanese).
- [5] M. Tanishima, Realize Inc., Chemical Contamination in Semiconductor Manufacturing, 1997, to be published. (in Japanese).
- [6] Erik J. Mori, John D. Dowdy, and Larry W. Shive, Microcontamination, 35-37, November 1992.

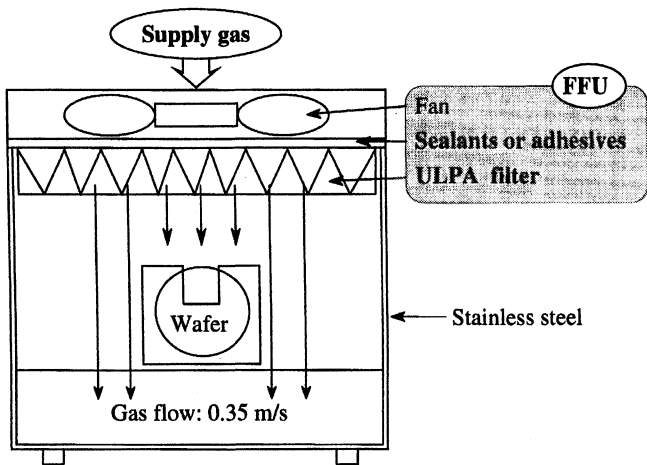


Fig. 1. Evaluation test unit for FFU.

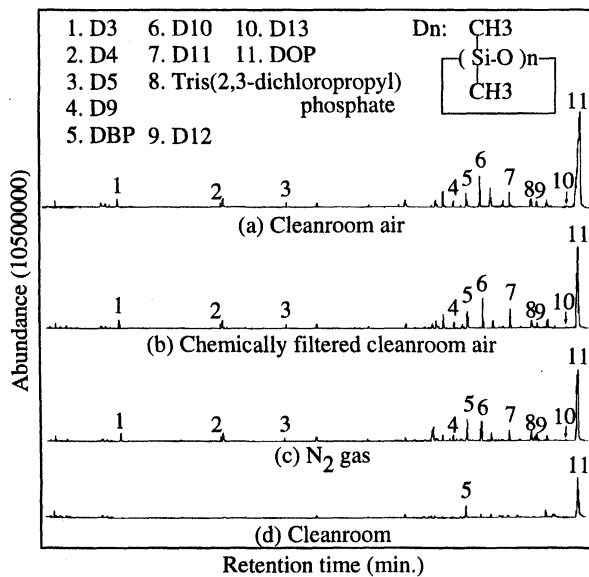


Fig. 2. TIC of adsorbates on silicon wafers in test unit with general type FFU and supply gas (a-c), and in cleanroom (d).

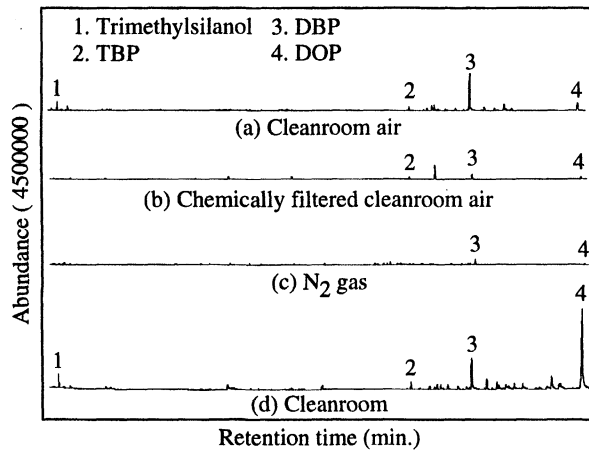


Fig. 3. TIC of adsorbates on silicon wafers in test unit with low-outgas type FFU and supply gas (a-c), and in cleanroom (d).

Table 1. Wafer surface contaminants in test unit and cleanroom.

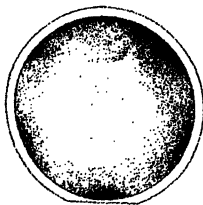
Contaminants	General types			FFU Low-outgas types			Cleanroom class 10
	CR	CF	N <sub>2</sub>	CR	CF	N <sub>2</sub>	
Cyclosiloxanes (to D13)	○	○	○	—	—	—	—
Trimethylsilanol	○	—	—	○	—	—	○
DOP	○	○	○	○	—	—	○
DBP	○	○	○	○	—	—	○
Butylbenzyl phthalate	○	○	○	—	—	—	—
TBP	○	○	○	○	—	—	○
Diethyl adipate	○	○	○	○	—	—	○
Dibutyl adipate	○	○	○	—	—	—	—
N-butylbenzenesulfone -amide	○	○	○	—	—	—	—
Tris (2,3-dichloropropyl) phosphate	○	○	○	—	—	—	—
Tris (2-chloroethyl) phosphate	○	○	○	—	—	—	—
Butyl palmitate	○	○	○	—	—	—	—
etc.							

Supply gas: CR: Cleanroom air

CF: Chemically filtered cleanroom air

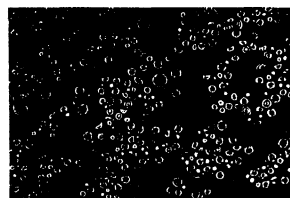
○: A notable amount

—: A negligible amount



Particle size ( $\mu\text{m}$ )	0.2	0.5	1.0
Number	8350	5	0

Fig. 4. Haze on SiN seen by a particle counter.



Burst size: 1  $\mu\text{m}$  to 100  $\mu\text{m}$

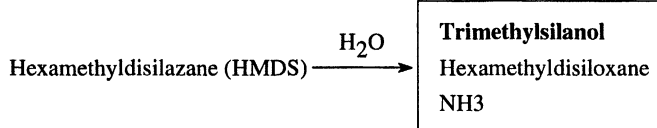
Fig. 5. SEM image of bursts in exposed i-line resist film.

Table 2. Relationship between haze and surface concentration of organosilicones and DOP.

Haze	Surface concentration (pg/cm <sup>2</sup> as hexadecane)			
	Trimethylsilanol	D3 to D6	D7 to D13	DOP
Yes	68	204	159	3516
Yes	57	113	142	1184
Yes	< 6	11	1609	4136
Yes	< 6	< 6	827	3473
No	< 6	< 6	238	1450
No	< 6	< 6	198	289
No	38	10	18	5784

Table 3. Relationship between exposed resist film bursts and surface concentration of organosilicones and DOP.

Number of bursts	Surface concentration (pg/cm <sup>2</sup> as hexadecane)			
	Trimethylsilanol	D3 to D6	D7 to D13	DOP
0	< 6	< 6	121	8108
0	28	< 6	91	7592
3	67	< 6	65	7031
31	85	< 6	41	6125
411	113	< 6	< 6	3938



## **PARTICLES**



# PARTICLE REMOVAL EFFICIENCY OF DILUTED HF SOLUTIONS

M. Alessandri, E. Bellandi, F. Pipia, B. Crivelli  
SGS-THOMSON Microelectronics, Via Olivetti 2, Agrate B<sup>za</sup> (MI), Italy

K. Wolke, M. Schenkl  
STEAG MicroTech, Carl-Benz Straße 10, Pliezhausen, Germany

## ABSTRACT

Particle removal efficiency of diluted HF solutions has been evaluated and compared to SC1 chemistry, in the frame of the study of possible effective and low cost alternatives to the standard RCA cycle for pre-diffusion cleaning. Particle removal efficiency has been measured using different particle types, such as SiO<sub>2</sub>, Si<sub>3</sub>N<sub>4</sub>, PSL and Al<sub>2</sub>O<sub>3</sub> as a function of HF dip time. Spiking of HCl and IPA in the HF tank has been tested too. The results confirm a good removal efficiency of the HF based chemistries, however still lower than the one obtained by megasonic SC1.

## INTRODUCTION

SC1 is well known to be very effective for particle removal efficiency. However, when a low ammonia concentration, a low temperature or a short dip time is used, particles are removed mainly by the megasonics energy (figure 1).

In the IMEC Twin-Clean™ and in the LETI DDC cleaning processes, oxide is grown by a separate oxidising step (SOM, SPM or water/O<sub>3</sub>) and then removed by an HF dip. Final treatment is generally a DIW rinse or a DIW/O<sub>3</sub> step.

HF concentrations lower than 0.5% and oxide etching as low as 50Å have to be used to avoid surface roughening and to reduce field oxide bird's beak over-etch.

Megasonics cannot be used during or after HF step because of their roughening action, that can be produced on hydrophobic surfaces, although it is reported that this effect is avoided by some surfactants<sup>2</sup>.

Another advantage of SC1 is the high pH value, that allows removed particles to remain in the bath without re-deposition on the wafer surface. Figure 2 shows the Zeta potential versus bath pH for nitride, oxide, alumina and silicon<sup>1</sup>.

SC1's pH is typically in area B of figure 2, where Z-potential for all the considered particles has the same sign of the silicon surface. A similar behaviour is present at low pH values (area A in figure 2), but to obtain a suitable pH it is necessary either to add HCl to HF bath or to use a high HF concentration.

pH of HF solution<sup>3</sup> as a function of its concentration is reported in figure 3.

For 0.2-0.3% HF, pH value is about 2 and only the silicon dioxide Z-potential has the same sign of silicon, hence alumina and silicon nitride particles tend to be deposited onto silicon surface.

However high HF concentration is not recommended for critical cleaning purposes, because of the high etch rate and the consequent poor etch uniformity for short dip times. HCl spiking is used in the DDC cleaning sequence<sup>2</sup>, but it prevents the use of conductive HF concentration monitoring systems.

## EXPERIMENTAL

A STEAG MicroTech third generation automated wet bench, with a Marangoni dryer, able to process 50 six inch wafers per batch, and providing both SC1 and HF positions, has been used for the experiments. 6" flat wafers have been intentionally contaminated, by shaking them in particle-added water, with different types of particles (oxide, nitride, alumina, PSL) and evaluated by a Tencor Surfscan 6200 before and after the cleaning step. The starting particle level was around 1000 p/wafer. Particles were supplied by NIST ( $\text{Si}_3\text{N}_4$ ), Duke Sci. ( $\text{Al}_2\text{O}_3$ ) and Bangs Lab (PSL and  $\text{SiO}_2$ ).

The particle removal efficiency has been evaluated on prime test wafers. Dummy wafers have been used to fill-up empty slots.

Reference SC1 was a 0.5:1:5 ( $\text{NH}_4\text{OH}:\text{H}_2\text{O}_2:\text{H}_2\text{O}$ ), at 65°C, 5' dip with Verteq Sunburst megasonics system.

Twin-Clean tests were performed using 0.2% HF at 21°C, with an etch rate of about 8 Å/min). A 7' DIW/ $\text{O}_3$  rinse step (~20ppm of  $\text{O}_3$ ) has been used before the HF dip.

## RESULTS AND DISCUSSION

Particle removal efficiency of  $\text{SiO}_2$  particles as a function of HF dip time is reported in figure 4. SC1 with megasonics removes these particles very effectively. Very good performances were obtained also by Twin-Clean even for very short dip times. However for dip times lower than 2' particles are not removed at all. It is therefore necessary to remove at least the thin chemical oxide grown in the first step of the cleaning sequence. In figure 5 it is reported the particle removal efficiency for silicon nitride

particles. SC1 megasonics is clearly very effective, while HF has relatively poor performance for smaller particles. This is supposed to be related to big particle agglomerates breakage and consequent re-deposition on the hydrophobic wafer surface.

HCl has been spiked on the HF bath, with concentration of 0.02% and 0.1%. The use IPA alcohol was proposed in some IMEC papers<sup>3</sup>. The tests were performed using 0.1% of IPA in the bath.

Figures 6 and 7 report respectively oxide and nitride particle removal efficiency for different spiking additive. HF dip time was fixed to 5'. No meaningful difference in particle removal efficiency has been observed among the different trials.

Figure 8 shows the particle removal efficiency for different particles type. PSL spheres are very easily removed both from Twin-Clean and SC1. Both Twin-Clean and SC1 megasonics can effectively remove Al<sub>2</sub>O<sub>3</sub> particles, that are supposed to be very challenging, because of their high Z potential.

## CONCLUSIONS

Particle removal efficiency of diluted HF, in the Twin-Clean sequence, has been proved to be very high, regardless of the particle type, even for very short dip times. However, SC1 megasonics demonstrates to have an higher removal efficiency, especially for silicon nitride particles, although the removal efficiency is strictly related to megasonics power. No impact of additives such as HCl and IPA has been found.

This work has been supported by the Esprit SEA Project nr.20757 "Autowet"

## REFERENCES

1. F.Tardif, T.Lardin, P.Boelen, R.Novak, I.Kashkoush, in Proc. of 3<sup>rd</sup> Int. Symp UCPSS, Antwerp, Belgium (1996).
2. T.Kujime, Y.Nishiyama, S.Okan, T.Ohmi, in Proc. of 3<sup>rd</sup> Int. Symp UCPSS, Antwerp, Belgium (1996).
3. S.Verhaverbeke, Dielectric Breakdown in Thermally Grown oxide Layers, p. 135, Thesis, IMEC

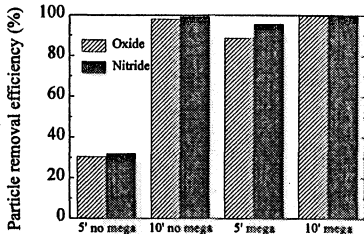


**Figure 1:** SC1 oxide and nitride particle removal efficiency.

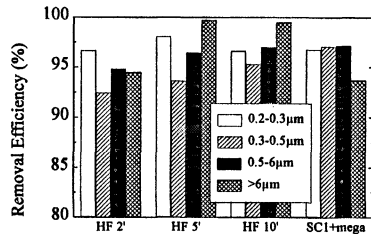


**Figure 4:** Oxide removal efficiency as a function of 0.2% HF dip time and of particle size.

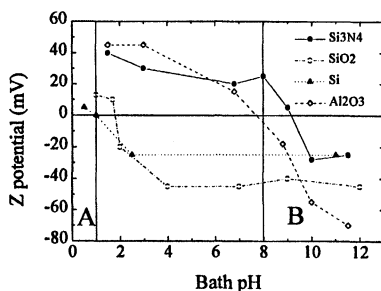


**Figure 2:** Z potential as a function of bath pH.

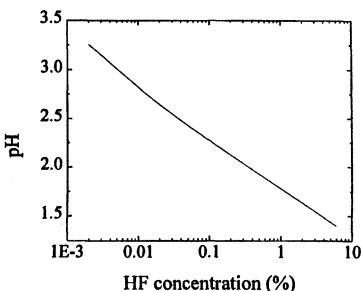


**Figure 3:** pH as a function of HF concentration

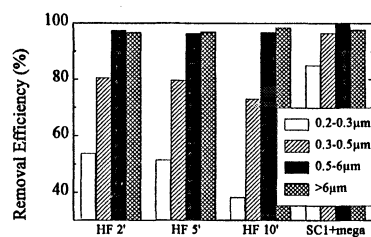


**Figure 5:** Nitride removal efficiency as a function of 0.2% HF dip time and of particle size.

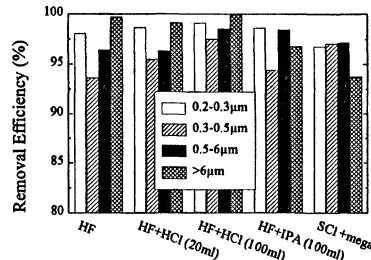


**Figure 6:** Oxide removal efficiency as a function of HF additives.

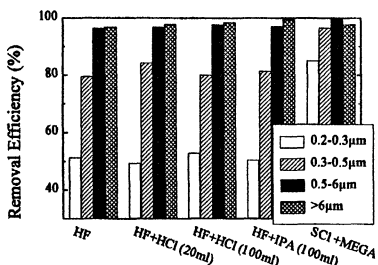


**Figure 7:** Nitride removal efficiency as a function of HF additives.

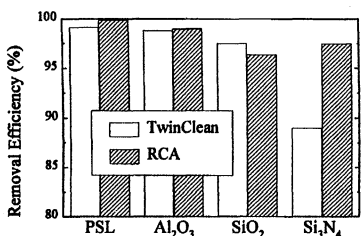


**Figure 8:** Particle removal efficiency for different particles.

# PARTICLES AND METALLIC IMPURITIES REMOVAL BY USING NEW SPIN CLEANER BASED ON UCT CLEANING CONCEPT

Kazuhiko Kawada, Mitsunori Nakamori, Hiroshi Morita,

Shoichi Okano, Takahisa Nitta\* and Tadahiro Ohmi

Department of Electronic Engineering,

Graduate School of Engineering, Tohoku University,

Sendai 980-77, Japan

\*Ultraclean Technology Research Institute,

4-1-7 Hongou, Bunkyou-ku, Tokyo 113, Japan

## ABSTRACT

An advanced spin cleaner based on UCT cleaning concept, which means total room temperature wet cleaning with no chemical vapor generation, for 200mm(8inch) wafer has been developing. Cleaning efficiencies of this spin cleaner for particles and metallic impurity were evaluated by impurity challenge tests. Removal test of  $\alpha$ -alumina ( $\text{Al}_2\text{O}_3$ ) particle and polystyrene latex (PSL) particle on Si wafer was carried out by using FPMS (hydrofluoric acid, hydrogen peroxide and surfactant mixture) solution and ultrapure water in a combination system of spin cleaning and megasonic irradiation. Cu impurity, which is hardly removed from Si surface, was chosen and efficiency of Cu removal was evaluated by FPMS solution. It was also found that we could perform the complete UCT cleaning and drying process of single wafer within a very short time.

## INTRODUCTION

Total room temperature wet cleaning technology (UCT cleaning) consisting of five steps has been developed for Si wafer surface cleaning without chemical vapor generation and consumption of a large volume of chemicals and ultrapure water (UPW)[1]. A new type spin cleaner based on UCT cleaning for 200mm (8 inch) wafer has been developing. The sequence of cleaning and drying process for this spin cleaner is described in Figure 1. It consists of 6 steps including a spin drying step. Almost all impurities are removed in ozonized UPW( $\text{O}_3$ -UPW) cleaning of the first step and FPMS cleaning with megasonic irradiation, which is ultrasonic of 1.6MHz

frequency, of the second step.

The features of developing equipment are as follows:

- Cleaner for 200mm (8inch) wafer
- Smaller size (400mm x 450mm footprint size)
- Single chamber and single wafer processing
- Quick cleaning and drying
- Three spouting megasonic irradiators
- Cleaning available both front and back sides
- Cleaning and drying in controlled ambient (N<sub>2</sub> Purge)

This spin cleaner is designed for cleaning over 200mm wafer with higher precision and clustering process equipment and the cleaner.

Removal of particle and metallic impurities by using this spin cleaner is evaluated in this study.

#### **Megasonic Irradiators**

Megasonic means ultrasonic over 1MHz frequency. Megasonic irradiation is an important technology for Si surface cleaning at room temperature, because of its least damage without cavitation and uniformity on surface cleaning[2]. There are two ways of megasonic irradiations for wet cleaning process. One is nozzle type irradiation which is applied for single wafer cleaning process, and the other one is bath type irradiation which is useful for batch type cleaning process. Three nozzle type irradiators are installed in the spin cleaner.

Two styles of megasonic irradiators were introduced in the cleaner. One is "Jet style" spouting nozzle, which spouts UPW or chemicals at a point on the wafer. The other is "Squall style" spouting nozzle, which blows solution like a liquid curtain from a slit. The megasonic frequency for both of jet style and squall style nozzles is 1.6MHz. Megasonic is propagated by the flow of UPW or chemicals from both type irradiators. In principle, squall style spouting nozzle is faster to remove particles and metallic impurities than jet type nozzle because squall style spouting nozzle can feed UPW or chemicals on the wide area of Si surface at the same time.

### **REMOVAL OF PARTICLES AND METALLIC IMPURITIES**

#### **Wafer Preparation for Cleaning Tests**

Particle and metallic impurity removal efficiencies of the spin cleaner were evaluated by impurity challenge tests. Cz(100) Si wafer were used in the tests. First, clean wafer surface with no contamination was prepared by precleaning in order to minimize fluctuation of tests. In case of particle removal test, PSL and Al<sub>2</sub>O<sub>3</sub> particles were prepared and thousands of each particle put uniformly on the surface of wafer by dipping in particle suspension. In case of metallic impurity removal tests, Cu was adsorbed on the Si surface by dipping in 1ppm CuCl<sub>2</sub> aqueous solution.

### Particle Removal

Particle removal efficiency by using squall style spouting nozzle was evaluated and the cleaning procedure is indicated in Figure 2. Si wafer was set to rotate on the turn table. Squall style spouting nozzle was installed on an arm and moved alternatively from outside of Si wafer toward the center of the wafer during operation. With continuous moving, the nozzle spouts cleaning solutions such as FPMS and UPW to the wafer with megasonic irradiation. UPW rinsing was carried out for 16 seconds after FPMS treatment. Finally, Si wafer was dried by 3000rpm rotation for 15 seconds.

UPW was used as a cleaning solution with megasonic irradiation in case of PSL removal test[3]. UPW flow rate was 7 l/min by using squall style nozzle and rotation speed was 1500rpm. In this cleaning test, the number of particles over 0.19 $\mu$ m diameter was reduced from about 5,000 to below 100 particles per 200mm wafer in only 8 seconds as shown in Figure 3. PSL particle was lifted off by lifting off vibration of megasonic irradiation and remove from Si surface.

On the other hand, it is much more difficult to remove Al<sub>2</sub>O<sub>3</sub> particle from Si surface than that in case of PSL particle. Al<sub>2</sub>O<sub>3</sub> particle removal was carried out by FPMS solution(0.5% HF, 0.5% H<sub>2</sub>O<sub>2</sub> and 50 ppm surfactant aqueous solution) with megasonic irradiation because Al<sub>2</sub>O<sub>3</sub> particle on Si surface cannot be remove by only UPW with megasonic irradiation. Flow rate of FPMS solution was 7 l/min by using squall style nozzle and rotation speed was 1500rpm. Figure 4 shows that PSL particle can be easily removed by using FPMS with megasonic. It is shown in Figure 5 that the number of Al<sub>2</sub>O<sub>3</sub> particle was reduced from about 7,000 to below 100 particles per wafer within 12 seconds.

When Al<sub>2</sub>O<sub>3</sub> particle was removed by using jet style nozzle, it was reduced to below 100 same as squall style nozzle. Cleaning time was, however, extended because the area irradiated by megasonic of jet style nozzle is smaller than that of squall style nozzle.

### Metallic Impurity Removal

The influence of cleaning time on Cu impurity removal tests by using either squall style or jet style megasonic irradiator were evaluated.

First, Si wafer was set to rotate on the turn table. Either squall style spouting nozzle or jet type spouting nozzle was installed on an arm and moved alternatively from outside of Si wafer toward the center of the wafer when in operation. And, the nozzle spouts FPMS cleaning solution to the wafer with megasonic irradiation. Flow rates of squall style nozzle and jet style nozzle were 7l/min and 0.8l/min, respectively and rotation speed of cleaning was 1500rpm for both of squall style nozzle and jet style nozzle. UPW rinsing was carried out for 16 seconds after FPMS with megasonic treatment. Finally, Si wafer was dried by 3000rpm rotation for 15 seconds. Residual

Cu on the surface was measured by Total Reflection X-ray Fluorescence Spectroscopy(TRXRF)before and after cleaning.

Initially contaminated wafer with Cu more than  $2 \times 10^{14}$  atom/cm<sup>2</sup> were cleaned by FPMS solution with and without megasonic irradiation. Megasonic irradiation showed no effect on Cu impurity removal. It was found that the optimal rotation speed was around 1,500rpm for both of squall and jet style spouting nozzle[4]. Figure 5 shows that Cu impurities were reduced below the detection limit of TRXRF after 16 seconds from the beginning of spouting by using both squall style nozzle and jet style nozzle though the residual Cu on the surface after cleaning by using squall style nozzle was ten times lower than that in the case of jet style nozzle. The uniformity of Cu removal on the wafer surface was investigated and after FPMS cleaning by using jet style nozzle, distribution as a function of distance from center of wafer was shown in Figure 7. In addition in case of squall style nozzle, Cu was also removed uniformly on the wafer surface.

## CONCLUSION

An advanced spin cleaner based on UCT cleaning concept, which is total room temperature wet cleaning, for 200mm wafer has been developing. PSL particle was removed by both of UPW and FPMS with megasonic irradiation after 8 seconds cleaning. Though Al<sub>2</sub>O<sub>3</sub> particle could not be removed by UPW with megasonic irradiation, it was removed by cleaning with FPMS solution with megasonic irradiation for 12 seconds. It was also confirmed that Cu impurity, which is hardly removed from Si surface, was reduced below  $2 \times 10^9$ atom/cm<sup>2</sup>, the detection limit of TRXRF and that the residual Cu distribution on the wafer after cleaning was quite uniform by using FPMS solution with and without megasonic irradiation after 16 seconds cleaning. Consequently, through this study, we confirmed that the performance of the newly developed advanced spin cleaner was excellent in the point of cleaning efficiency of metallic and particulate contaminants on Si wafer with a size above 200mm.

## REFERENCES

- [1] T. Ohmi, *J. Electrochem. Soc.*, **143**, 2957 (1996)
- [2] A. Fujie, *Kaijo Technical Report*, **2**, 3 (1996)
- [3] K. Kawada et al., *Proceedings of 29th Symposium on ULSI Ultra Clean Technology*, 67, Tokyo (1996)
- [4] H. Morita et al., *Proceedings of ISSM '96*, 337, Tokyo (1996)

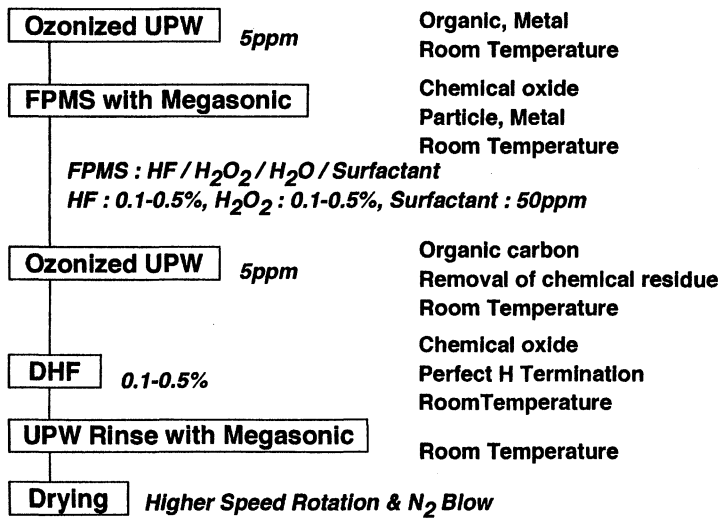


**Figure 1 Procedure of UCT Cleaning in Spin and Spout Cleaning**

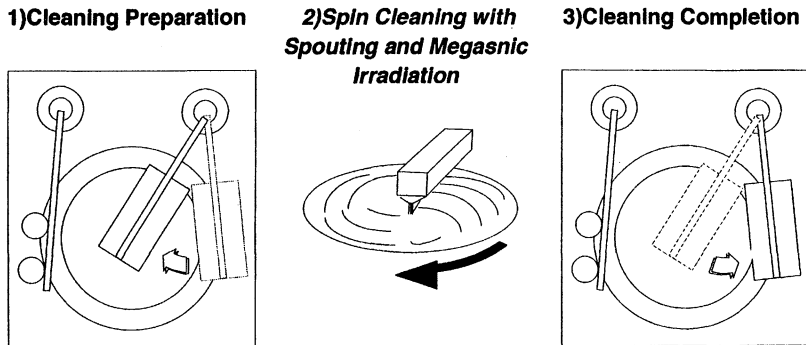


**Figure 2 Procedure for Wafer Cleaning Using Squall Type Nozzle**

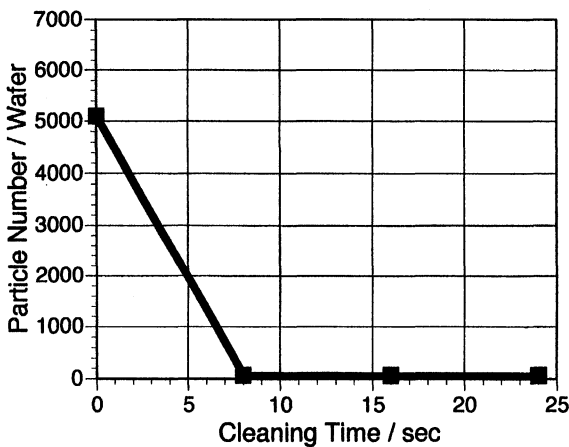


Figure 3 PSL Particle Removal  
(UPW with 1.6MHz Megasonic)

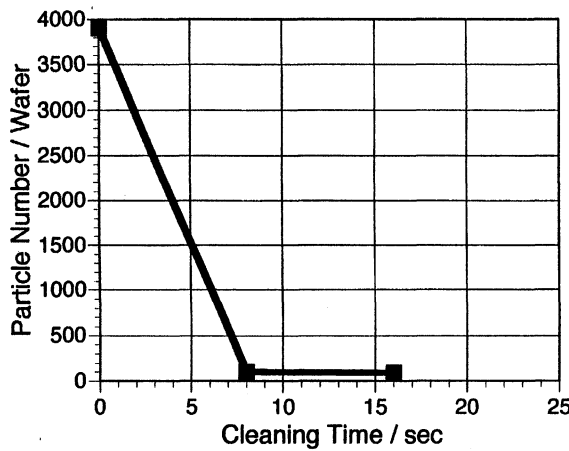


Figure 4 PSL Particle Removal  
(FPMS with 1.6MHz Megasonic)

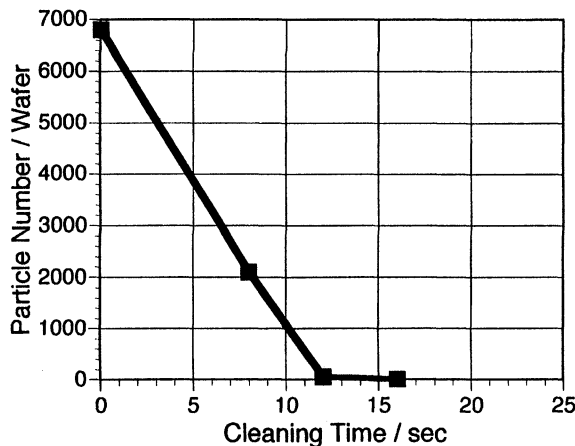


Figure 5 Al<sub>2</sub>O<sub>3</sub> Particle Removal  
(FPMS with 1.6MHz Megasonic)

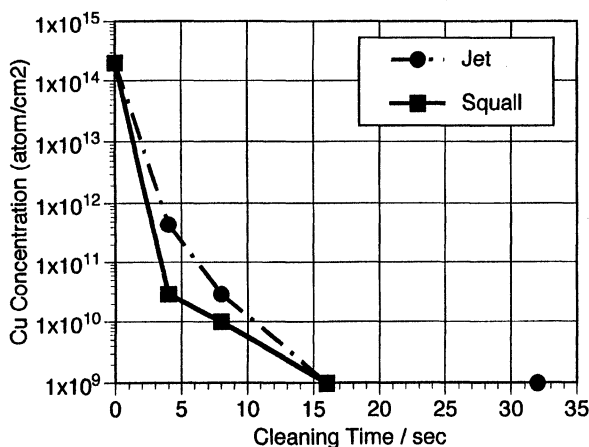


Figure 6 Time Dependence of Cu Removal  
Effect by FPMS Solution

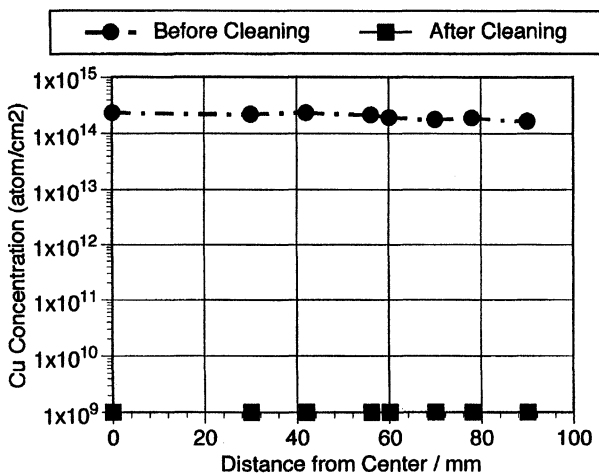


Figure 7 Cu Removal Uniformity of Spin Cleaning  
on 8 inch Wafer Surface by FPMS Solution

# **ANALYSIS FOR ADSORPTION BEHAVIOR OF PSL PARTICLE BY USING ATOMIC FORCE MICROSCOPY**

Akira KAWAI, Hiroshi HORIGUCHI

Department of Electrical Engineering, Nagaoka University of Technology,  
1603-1 Nagaoka, Niigata, Japan 940-21  
(E-mail: kawai@vos.nagaokaut.ac.jp)

Yoshihito TATEHABA, Kiyoshi SHIMADA, Eiichi ANDOH

Research and Development Department, SPC Electronics Corporation,  
2-1-3 Shibasaki, Chofu, Tokyo, Japan 182

Adsorption and cohesion properties among micro particles have strong contribution to the cleaning process in micro device manufacturing. These properties are analyzed by both force detection and direct removal techniques with an AFM micro tip. The slight difference from DMT theory for tip-particle adsorption can be observed, and deformation of particle is affected to the interaction. Experimental results for removing one of PSL particles directly are demonstrated by means of scratching, indentation and manipulation with the AFM tip.

## **1. INTRODUCTION**

In recent years, the adsorption of micro particle onto various substrates has been focused as one of the important problems in the LSI manufacturing. High density semiconductor device such as 256Mb-DRAM has a minimum design rule less than 0.3 micro meter. Therefore, there is no doubt that the adsorption of particle in micro size brings about circuit failure of micro devices. As decreasing diameter of adsorbed particle, the study for adsorption and removal mechanisms has become more important and difficult. The reason for this is that the nature of micro condensed cluster is different from that of bulk material.(1) In these days, moreover, the detection of particle less than 100nm on a substrate is extremely difficult for so-called particle counter. Usually, the adsorption (adhesion) mechanism between two solid surfaces has been analyzed theoretically by using the surface energy model based on van der Waal's (vdW) interaction.(2) Authors have also studied for the adhesion behavior between two materials based on surface energy model.(3,4) Particularly, the adhesion behavior of micro resist pattern on LSI substrates in both dry and wet conditions has been analyzed.

However, since the development of atomic force microscopy (AFM) (5), many researchers have studied for the surface chemistry in nano-meter size, for example, adsorption mechanism, atomic manipulation, nano-lithography and so on.(6-8) In these days, therefore, the AFM would be regarded as one of the appropriate tools for analyzing the adsorption phenomena of micro particle and cleaning processes.

In this paper, we analyze the adsorption and cohesion behavior among polystyrene-latex (PSL) particles by using an AFM system. Concretely, the vdW force of PSL particle can be analyzed with high sensitivity ordered nano-newton by measuring the adsorption force of micron tip. Moreover, removal of one of PSL particles from Si substrate can be performed.

## 2. EXPERIMENT

The PSL particles, which diameter were ranged from 40nm to 1 $\mu$ m, were dispersed on the Si(100) substrate in each diameter by the spin method. Actually, the liquid drop containing the particles were dropped onto the substrate rotating at 1000 rpm. As an AFM system, SPA300 made by Seiko Instruments Inc. were used. The cantilever tips covered with gold thin film were used, whose radius of curvature was approximately 40nm. The spring constant of the cantilevers was about 0.1 N/m (OMCL-TR400B, Olympus). In order to measure the adsorption force in both normal(45%RH) and dry(4%RH) ambient conditions, the force curve measurements were conducted for each sized particles using a dry chamber. The removal of PSL particle was also conducted by using cantilever tip of 7.2N/m spring constant, (OMCL-AC-240PS, Olympus) in dry condition.

For analyzing the inner stress distribution at the interface between the PSL particle and the Si substrate, two dimensional finite element method (FEM) was applied. The calculation was conducted based on plane strain model. Young modulus and poisson ratio of PSL particle were 2.7GPa and 0.34, respectively. Surface energy measurements of the polystyrene (PS) sheet and tip material were also carried out by the contact angle (CA) method. The two components (dispersion  $\gamma^d$  and polar  $\gamma^p$ ) model was used to calculate the surface free energy  $\gamma$  of each surface.(9,10)

$$\gamma = \gamma^d + \gamma^p \quad [1]$$

The detail of surface energy measurement is described in our previous reports.(4) Surface energy datas for each surface are summarized in Table I. The PSL particles condensed in an electrolyte solution were also observed by using transmission electron microscopy (TEM), H-500 (Hitachi).

## 3. RESULTS AND DISCUSSION

The PSL particles condensed on the Si substrate are characterized mainly used by the AFM micro tip. In order to analyze for the adsorption property, the force curve which indicates interaction acting between tip and particles is used. Moreover, deformation of PSL particle by contacting with AFM tip is simulated by FEM. Finally, by using AFM tip, we attempt to remove one of PSL particles condensed on the Si substrate.

### OBSERVATION OF CONDENSED PARTICLES

Figures 1 shows the photograph of PSL particle (136nm in diameter) observed by the TEM. It is clear that each particle is partly deformed by contacting with one another. This

deformation of particle takes place on the bases of vdW force inter particles. According to the JKR theory (11), surface energy  $\gamma$  of the PSL particles can be estimated with the amount of its deformation value 'a', as follows.

$$a^3 = 6w_A\pi R^2 / K = 12 \gamma \pi R^2 / K \quad [2]$$

where,  $w_A$  is the thermodynamic work of adhesion,  $R$  is radius of particle and  $K$  is modulus in volume. The  $\gamma$  value of each surface are also summarized in Table I. It is clear that the surface energy derived by the JKR model is larger than that obtained by contact angle method. As the reason of this deviation, accuracy of the modulus  $K$  of the PSL particle should be considered.

Figure 2(a) shows the AFM image of the PSL particles condensed on the Si substrate. It is clearly observed that these particles condense into a closed-pack structure. It can be also considered that some condensed layers would underlay of surface layer in same structure. The amount of deformation for each PSL particle can be estimated from the cross-sectional profile as shown in Fig.2(b). The deformation value of PSL particle is mostly same as that of the TEM image in Fig.1. Therefore, by using the AFM, the particle condensation behavior can be analyzed under the practical condition.

#### FORCE CURVE MEASUREMENT AND DMT THEORY

The force curve, which is defined as a force-distance correlation, is one of the meaningful datas measured by the AFM.(6,12) Figure 3 shows the typical force curve for PSL particles measured by using the gold cantilever tip. A maximum attractive force  $F$ , when the tip apart from the PSL particles after making a contact, is defined as the adsorption force of tip to the PSL particles. In our previous study (12), the amount of adsorption force  $F$  is directly proportional to the surface free energy  $\gamma$ , particularly to  $\gamma p$ , of the substrate.

Figure 4 shows the dependency of adsorption force  $F$  of AFM tip on radius of PSL particle. The adsorption force in normal (45%RH) condition extremely varies, and no dependency on the particle radius is observed. In this case, the Laplace force caused by water layer adsorbed on the surface would affect to the force curve measurement. On the other hand, the adsorption force  $F$  of AFM tip in dry (4%RH) condition decreases with the radius of particle. Therefore, in this study, the all experiments were conducted in the dry condition. It can be considered that the removal of one of the PSL particles would be able to performed easily, since the adsorption force decreases with particle sizes. In Fig.4, moreover, the calculated value of geometric mean based on the DMT model was also plotted. Hence, force acting inter particles based on the DMT theory can be expressed as following formula.(13)

$$F = (A/6D_0^2) * (R_1 * R_2)/(R_1 + R_2) \quad [3]$$

where symbol  $A$  represents Hamaker constant of particle,  $D_0$  is interactive distance between two spheres. The symbols  $R_1$  and  $R_2$  denote curvature of radius of each particle. In Fig.4, the measurement data obtained by force curve is deviated gradually from the geometric mean plot less than 1000nm in particle radius. As the reason of this, we assume

that the deformation of particle would occur by contacting with the AFM tip. Therefore, we attempt to estimate the particle deformation by FEM.

### **FEM ANALYSIS FOR PARTICLE DEFORMATION**

Figure 5 shows the deformed profile of PSL particle by contacting with the AFM tip. By deforming the particle, the effective distance of vdW interaction between two spherical surface becomes short. Hence, we defined the increment of curvature of radius as 30% of initial value and plotted the revised geometric mean value as shown in Fig.6. It is clear that the curve shifts toward smaller radius of PSL particle. Consequently, by taking into account the deformation effect, the revised geometric mean profile is similar to that of measurement value in Fig.4.

### **REMOVAL OF PSL PARTICLE BY AFM TIP**

By using the AFM tip, we attempt to analyze the removal property of one of PSL particles. Figure 7 shows the inner stress distribution in a PSL particle induced by direct removal process analyzed by FEM. By applying a certain deformation (10nm) by AFM tip, both tensile and compressive stresses concentrate at the two edges 'A' and 'C', respectively. As shown in Fig.8, it is clear that the stress concentration is enhanced as the diameter of PSL particle decreases, particularly less than 100nm in diameter.

Figures 9(a) to 9(c) show the AFM images of removal results by scratching, indentation and manipulating, respectively. The diameter of PSL particle for removal is 100nm. As shown in Fig.9(a), the PSL particles are deformed and the straight short line is drawn by the scratching. As the reason of this, it is considered that the adsorption energy among particles would be larger than cohesive energy of themselves. By indenting the tip into the closed-packing PSL particle arrays, a certain hole is formed as seen in Fig.9(b). It is clear that the some particles are piled up on the surface. As seen in Fig.9(c), the PSL particle positioning at the edge of terrace can be easily manipulated.

In order to remove the PSL particle directly by using the AFM tip, the adsorption force among them would act more effectively. Figures 10(a) to 10(c) show the AFM images of PSL particles after scratching by the AFM tip. As shown in Fig.10(a), in this case of PSL particle of 100nm in diameter, the scratched line is formed similarly to that in Fig.9(a). Figures 10(b) and 10(c) show the scratching results for PSL particles of 73 and 42nm in diameter, respectively. In spite of same scratching process as that in Fig.10(a), the each surface is considerably deformed and digged deeply. As the reason of this, it can be considered that the two factors, (i) decrease of adsorption force (in Fig.4) and (ii) stress concentration in a particle (in Fig.8) as decreasing of particle diameter, act to decrease cohesion among particles.

### **4. CONCLUSION**

By using the AFM micro tip, the adhesion and cohesion properties among PSL particles on the substrate can be analyzed. Dependency of adsorption force of AFM tip on radius of PSL particle is obtained by force curve measurement. Moreover, inner stress distribution of PSL particle is obtained by FEM analysis, and indentation and removal process are analyzed. The removal of a particles from condensed layer is also concretely

demonstrated. The cohesion among particle contributes strongly to removal the particle.

#### ACKNOWLEDGMENTS

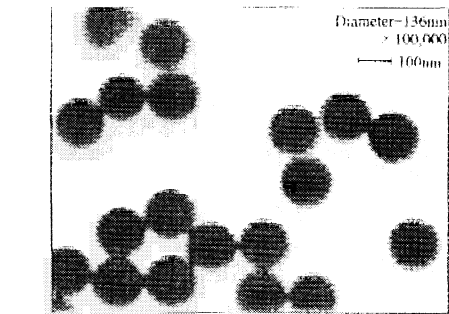
A part of this work was performed under the management of ASET in the MITI's R&D Program supported by NEDO. A part of this work was also performed under THE MURATA SCIENCE FOUNDATION, KAWASAKI STEEL 21st Century Foundation and SECOM SCIENCE AND TECHNOLOGY FOUNDATION.

#### REFERENCES

1. R. Kubo, J. Phys. Soc. Jpn., **17**, 740 (1962).
2. D. H. Kaelble, J. Appl. Polym. Sci., **18**, 1869 (1974).
3. H. Nagata, A. Kawai, Jpn. J. Appl. Phys., **28**, 2137 (1989).
4. A. Kawai, H. Nagata and M. Takata, Jpn. J. Appl. Phys., **31**, 3725 (1992).
5. G. Binnig, C. F. Quate and Ch. Gerber, Phys. Rev. Lett., **56**, 930 (1986).
6. N. A. Burnham, R. J. Colton and H. M. Pollock, Phys. Rev. Lett., **69**, 144 (1992).
7. R. S. Becker, J. A. Golovechenko and B. S. Swarzentruber, Nature, **325**, 419 (1987).
8. D. M. Eigler and E. K. Schweizer, Nature, **344**, 524 (1990).
9. F. M. Fowkes, Ind. Eng. Chem. Sci., **56**, 40 (1964).
10. T. Hata, Y. Kitazaki and T. Saito, J. Adhesion, **21**, 177 (1987).
11. K. L. Johnson, K. Kendall and A. D. Roberts, Proc. Roy. Soc. London, **A324**, 301 (1971).
12. A. Kawai, H. Nagata and M. Takata, Jpn. J. Appl. Phys., **31**, L977 (1992).
13. B. V. Derjaguin, V. M. Muller and Yu. P. Toporov, J. Colloid Interface Sci., **53**, 314 (1975).

Table I Surface free energies of each surface.

Sample	Dispersion $\gamma^d$	Polarity $\gamma^p$	surface energy $\gamma$	
PS sheet	38.0	1.58	39.6	CA method
Au film	42.3	0.12	42.4	CA method
Si(100) wafer	32.2	5.66	37.9	CA method
PSL particle (136nm in diameter)	-----	-----	163	JKR model



(a)

(b)

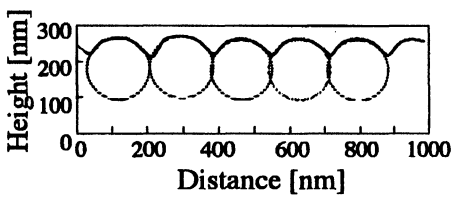
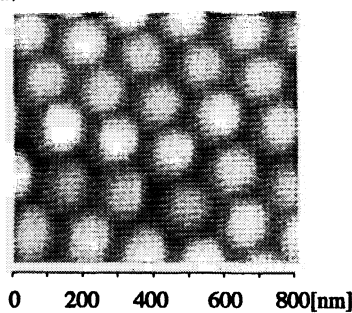


Fig.2 AFM image of PSL particles. (a):Particles condensed on Si substrate. (b): The cross sectional profile of PSL array. The dashed circles show particle predicted by surface profile.

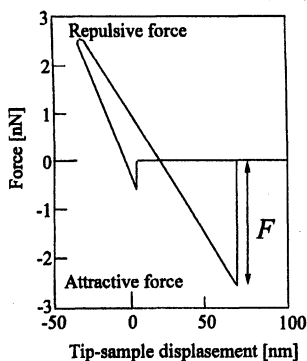


Fig.3 Typical force curve between AFM tip and condensed PSL particles. Attractive force  $F$  is defined as adsorption force.

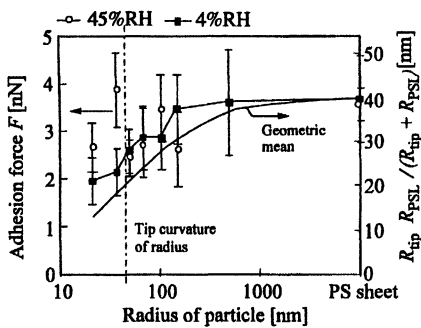


Fig.4 Dependency of adsorption force of AFM tip on radius of PSL particles. The measurements were carried out in twenty times in the same substrate. The error bar indicates each standard deviation.

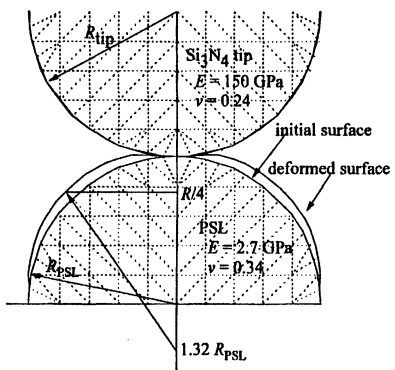


Fig.5 Deformation of PSL particle by contacting with the AFM tip estimated by FEM.

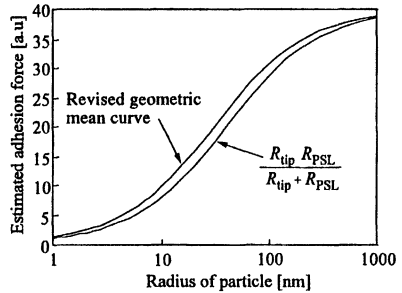


Fig.6 The shift of geometric mean curve by deformation effect.

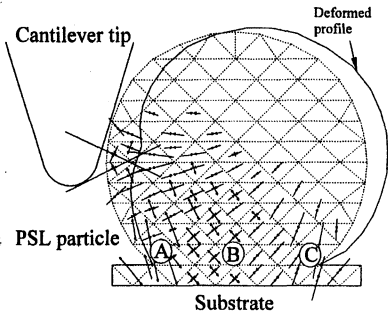


Fig.7 Inner stress distribution in PSL particle by direct removal using AFM tip. Two arrow heads face each other represent compressive stress, and those direct in opposite represent tensile stress.

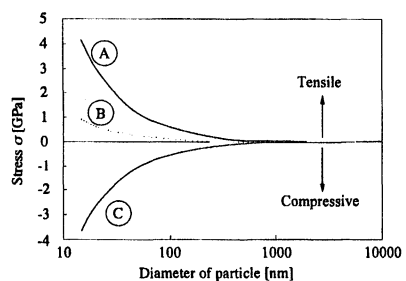


Fig.8 Stress concentration at the PSL-substrate interface as a function of PSL diameter. On the simulation, same deformation applied to each sized particle.

(a) Scratching

(b) Indentation

(c) manipulation.

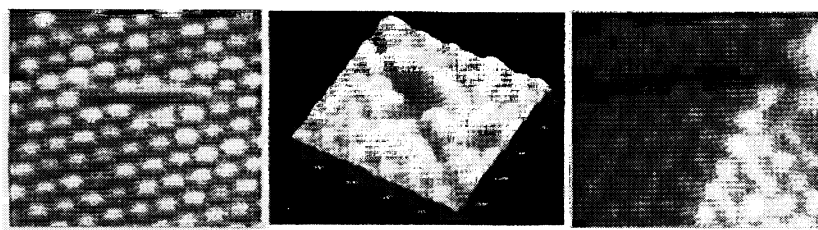
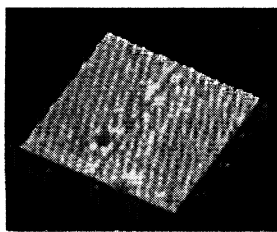
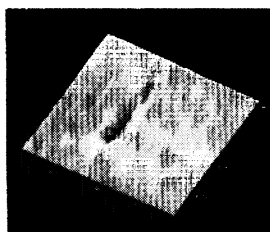


Fig.9 Removal of one of PSL particles condensed on Si substrate. The diameter of all particles is 100nm. Scan area is 1 $\mu\text{m}$  square.

(a) 100nm in diameter



(c) 42nm



(b) 73nm

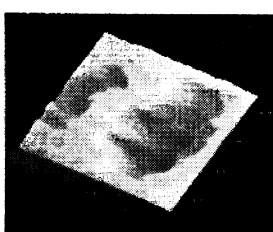


Fig.10 AFM images of PSL particles after scratching by the AFM tip. Scan area is 2 $\mu\text{m}$  in square.

## AGGRESSIVE SC-1 PARTICLE REMOVAL TECHNIQUES IN A SPRAY PROCESSOR AND THEIR EFFECTS ON OTHER METRICS

Shelley M. Smith and Kurt K. Christenson  
FSI International, 322 Lake Hazeltine Dr., MS4-8045, Chaska, MN 55318

By making use of plumbing unique to a centrifugal spray processor, we were able to significantly increase the flow rate of hot water in the APM (SC-1) step, and achieve over 99% removal of  $\text{Si}_3\text{N}_4$  particles  $>0.15 \mu\text{m}$  with a 4-minute dispense of APM. This three-fold reduction in dispense time is largely due to a  $20^\circ \text{C}$  rise in the on-wafer temperature. These results were incorporated into two particle-cleaning recipes, and the particle removal efficiencies of the new recipes over time are presented. In order to understand how recipes that are optimized for particle removal affect other metrics, surface roughness was measured using AFM, and metals-added data was measured using TXRF. The surface roughness results were insignificant,  $< 0.15 \text{ \AA}$  added to each wafer. Metals added were negligible. Ca and Ni were slightly above the detection limits of  $8 \times 10^{10}$  and  $0.8 \times 10^{10}$  atoms/cm<sup>2</sup> respectively, and Cu, Cr, Zn, Mn, Ti, and K were below the detection limits.

### INTRODUCTION

The effects of chemical sequence, dilution and temperature on particle-removal efficiencies for a variety of particle challenges have been extensively studied using an acid spray processor (1-3). By making use of plumbing unique to the spray processor, we were able to significantly increase the flow rate of hot water in the APM step, and achieve over 99% removal of  $\text{Si}_3\text{N}_4$  particles  $>0.15 \mu\text{m}$  with a 4-minute dispense of APM. This three-fold reduction in dispense time is largely due to a  $20^\circ \text{C}$  rise in the on-wafer temperature. These results were incorporated into two particle-cleaning recipes, and the particle-removal efficiencies of the new recipes over time are presented. Finally, in order to understand how recipes that are optimized for particle removal affect other metrics, surface roughness was measured using Atomic Force Microscopy (AFM), and metals-added data was measured using Total Reflection X-Ray Fluorescence (TXRF).

### EXPERIMENT

For these experiments, our standard APM chemistry ( $\text{NH}_4\text{OH}:\text{H}_2\text{O}_2:\text{H}_2\text{O}$ ) was modified by activating the hot wafer rinse (HWR) function during the chemical step. The HWR function dispenses approximately 7 liters/min of water heated to  $95^\circ \text{C}$ , and raises the on-wafer temperature of the combined solution by approximately  $20^\circ \text{C}$ . We

expected that the increase in temperature and total flow would increase the particle-removal rate and allow better particle-removal results for shorter dispense times.

P type, <100>, 200-mm CZ wafers were initially pre-cleaned to near background levels in an FSI MERCURY® MP spray processor with a B Clean chemistry sequence (SPM, DHF, APM, HPM). The “background” particle count was measured at >0.15 $\mu$ m on a Tencor Surfscan 6200 using a 3-mm edge exclusion. The background particle count averaged 70 counts.

The challenge wafers were prepared by immersing cleaned wafers for 1 minute in DI water containing finely ground Si<sub>3</sub>N<sub>4</sub> powder that had been initially heated and dispersed by agitation in an ultrasonic bath (4). The wafers were then rinsed and dried in a MERCURY OC spray processor. “Pre” counts (after contamination, before cleaning) of these highly contaminated wafers were estimated by the use of a large edge exclusion to prevent overloading the particle counter (5). The pre count averaged 34,400 particles at >0.15 $\mu$ m.

Three Si<sub>3</sub>N<sub>4</sub> challenge wafers were processed per run, in slots 1, 13, and 25. The dispense time of the APM solution was varied between 3 and 10 minutes. When combined with the HWR function, the original 1:1:16 APM ratio was diluted to approximately 1:1:65. Finally, to determine the effects of temperature, the in-line infrared chemical heater was either turned off (ambient temperature) or set to 95° C (6). The DI water heater was set to 95° C.

Once processed, the wafers were “post” counted. The % Particles Remaining (%PR) was calculated using the formula below:

$$\%PR = 100 * (C_{post} - C_b) / (C_{pre} - C_b)$$

Where C<sub>b</sub> is the particle background count before contamination, C<sub>pre</sub> is the count after contamination and C<sub>post</sub> is the count after the clean.

Based on the success of the first set of results, we wanted to determine how recipes that were optimized for particle removal affect other metrics, specifically surface roughness and metals added. We choose a range of recipes: IR heater versus no IR heater, APM only versus multiple chemical steps, and shorter versus longer APM times. These were compared to our standard B Clean recipe. The list of recipes and chemical times is given in Table I below. The flow rates of the SPM are 600 and 150 cc/min for H<sub>2</sub>SO<sub>4</sub> and H<sub>2</sub>O<sub>2</sub>, respectively. HF calls 2000 cc/min of 100:1 DHF. Finally, APM and HPM (HCl:H<sub>2</sub>O<sub>2</sub>:H<sub>2</sub>O) had identical flow rate ratios of 125:125:2000 cc/min. All chemicals are cleanroom-grade quality.

Table I. Cleaning Treatments

Recipe Name	Chemical Exposure Times (sec.)				
	SPM	APM	DHF	APM	HPM
5HAIR	--	300*	--	--	--
6HA	--	360†	--	--	--
20HAIR	--	1200*	--	--	--
SUPER5HAIR	--	300*	120	180	110
SUPER6HA	--	360†	120	180	110
BCLEAN	90	--	90	180	110

†APM step uses HWR

\*APM step uses HWR and is heated to 95°C with the IR heater

In order to test surface roughness and metals added, P type, <100>, 200-mm CZ wafers were initially pre-cleaned using a B Clean chemistry sequence. The surface roughness wafers were premeasured using AFM on a NanoScope III Dimension 5000. One area of 2 µm x 2 µm was imaged near the center of each wafer. One wafer of each metric type was processed in each recipe and then post measured for surface roughness and metals added. Two runs of each recipe were performed. Metals analysis by TXRF was made with a Technos TREX 610-T instrument. Each wafer was analyzed at three points located on a line, with one point at the center and the other two points roughly equidistant from the center to the edge. The area analyzed at each location was 1 cm in diameter. Surface roughness is reported as the difference between the pre and post values, and metals added is reported for each element as the average of the three points.

Based on some initial passive data collection (PDC) of the SUPER5HAIR and SUPER6HA recipes, it was decided to increase the first APM step of both recipes by 1 minute. This was to insure that the run-to-run variability of the recipes would be minimized, and the particle removal performance could be guaranteed. The final recipes were labeled SUPER6HAIR and SUPER7HA, one with and one without the IR heater during the first APM step. A breakdown of the recipe sequences is given below:

- 6 minutes APM + HWR + IR Heater, OR 7 minutes APM + HWR (no IR heater) (main particle-removal step)
- 2 minutes of 100:1 DHF (secondary particle-removal step)
- 3 minutes of hot 1:1:16 APM (grows native oxide)
- 2 minutes of 1:1:16 HPM (removes trace metals)
- Final rinse and dry.

A full boat of wafers were processed in each run, with Si<sub>3</sub>N<sub>4</sub> challenge wafers in slots 1, 5, 10, 15, 20 and 25. The particle removal efficiencies of both recipes were taken over a one-month time period.

## RESULTS AND DISCUSSION

The results of the first set of experiments are shown in Figure 1. After 4 minutes of dispense time with the IR heater, and after 5 minutes without, the %PR is at 0.1%; that is, 99.9% removal. Previous work showed that, without using HWR, a 12-minute dispense time was necessary to achieve >99% removal (3). By including the HWR function, the chemical dispense time was significantly reduced. Comparing the results with and without the IR heater showed that, by using the IR heater, the chemical dispense time can be decreased by at least a minute.

The improved particle-removal results are consistent with two hypotheses. First, it is known that both APM and HF solutions clean by etching the oxide on the wafer surface, undercutting whatever contaminants are on the oxide (7). By increasing the dispense time and/or temperature, the total amount of oxide etched increases, and thus the particle removal increases. In the HWR case, the chemicals are diluted, which would normally decrease the etch rate slightly. However, the significant increase in temperature more than compensates for the loss in concentration. The higher flow rates may also improve particle-removal performance due to the increased shear forces.

The surface roughness results are given in Table II. With the exception of the 20HAIR recipe, all the results are similar within the error of instrument ( $0.14 \text{ \AA}$ ), ranging between  $-0.15$  to  $0.15 \text{ \AA}$ . The trend in the data is that the longer the APM step, the more roughness measured. For an extreme case, we ran a process with 20 minutes of APM and HWR, 20HAIR, and even that recipe only added  $0.5 \text{ \AA}$  of roughness. These results meet the SIA specification of  $<1 \text{ \AA}$  for  $0.13 \mu\text{m}$  devices. Clearly, aggressive particle removal recipes can be used with minimal roughness occurring.

The metals-added results are given in Table III. All results are given in units of  $10^{10}$  atoms/cm<sup>2</sup>. For all cases, the metals Cu, Cr, Mn, Ti, and K are below the detection limits ( $<1$ ,  $<3$ ,  $<1$ ,  $<5$ , and  $<20$  respectively). Ca was at or slightly above the detection limit, ranging from  $<8$ -19. The one "high" result of 19 was not shown on the companion wafer and could have been due to handling. Ni was slightly above the detection limit of  $<1$ , ranging from 2-9. In the APM-only recipes, (5HAIR, 6HA, and 20HAIR), there were high levels of Zn, 70-170, and very small levels of Fe, 1.5-5. For the recipes that included HPM, both Zn and Fe were below the detection limits of  $<3$  and  $<0.8$ , respectively. The high levels of Zn in the APM-only recipes are easily explained by the fact that these experiments were done using "Cleanroom Grade" chemicals. These chemicals are not as clean as "Megabit" or "Terabit" chemicals which have metal limits in the ppt range. Therefore the high levels of Zn (and low levels of Fe) are a reflection of the metal contamination in the chemical. The results of the other recipes show that by terminating in an HPM step, the metals are easily removed.

**Table II. Change in Surface Roughness**

Run #	Recipe Name	AFM RMS Surface Roughness (Å)			
		Pre	Post	Delta	Average
1	5HAIR	2.1	2.0	-0.1	
9	5HAIR	1.8	1.8	0.0	-0.05 ± 0.14
4	6HA	2.0	2.0	0.0	
7	6HA	1.9	2.0	0.1	0.05 ± 0.14
5	20HAIR	2.1	2.5	0.4	
10	20HAIR	1.9	2.5	0.6	0.50 ± 0.14
2	BCLEAN	2.1	1.8	-0.3	
12	BCLEAN	1.7	1.7	0.0	-0.15 ± 0.14
3	SUPER5HAIR	2.0	1.8	-0.2	
8	SUPER5HAIR	1.9	2.0	0.1	-0.05 ± 0.14
6	SUPER6HA	2.0	2.1	0.1	
11	SUPER6HA	1.7	1.9	0.2	0.15 ± 0.14
<b>CONTROL</b>		1.6	1.7	0.1	0.10 ± 0.14

**Table III. Metals Added By TXRF (Average of 3 Spots)**

Run #	Recipe Name	Metal ( $10^{10}$ atoms/cm $^2$ )								
		Ca	Fe	Ni	Zn	Cu	Cr	Mn	Ti	K
1	5HAIR	9	2	4	120	<1	<3	<1	<5	<20
9	5HAIR	<8	2	3	80	<1	<3	<1	<5	<20
4	6HA	9	1.5	3	70	<1	<3	<1	<5	<20
7	6HA	10	2	3	100	<1	<3	<1	<5	<20
5	20HAIR	<8	2	9	130	<1	<3	<1	<5	<20
10	20HAIR	9	5	7	170	<1	<3	<1	<5	<20
2	BCLEAN	<8	<0.8	2	<3	<1	<3	<1	<5	<20
12	BCLEAN	<8	<0.8	7	<3	<1	<3	<1	<5	<20
3	SUPER5HAIR	9	<0.8	4	<3	<1	<3	<1	<5	<20
8	SUPER5HAIR	<8	<0.8	3	<3	<1	<3	<1	<5	<20
6	SUPER6HA	19	<0.8	3	<3	<1	<3	<1	<5	<20
11	SUPER6HA	<8	<0.8	2	<3	<1	<3	<1	<5	<20
<b>CONTROL</b>		<8	<0.8	3	<3	<1	<3	<1	<5	<20
Detect. Limit		<8	<0.8	<1	<3	<1	<3	<1	<5	<20

For the PDC results, see Figure 2 for the results with the IR heater (SUPER6HAIR) and Figure 3 for the results without the IR heater (SUPER7HA). All the results are reported as % Particles Remaining. Each run shows the average of the six wafers for that run, and the error bars at one sigma. Each graph also shows the average of all the runs and the upper and lower control limits at one standard deviation for all the data. The results are very good, with the SUPER6HAIR recipe having a run-to-run mean of 0.15%, or 99.85% particles removed, and the SUPER7HA recipe having a mean of 0.13%, or 99.87% removal. Both recipes have a sigma value of 0.17%. In fact, the data shows an improving trend over time, which could be an indication of our improving procedures and techniques.

## CONCLUSION

Our initial results demonstrated that by adding the HWR function to an APM step, we were able to drastically improve our particle-removal efficiencies to >99% removal at  $>0.15\text{ }\mu\text{m}$  particle size, and cut our chemical dispense time by two- or three-fold. The chemical consumption is further decreased, due to the fact that the chemical flow rates for  $\text{NH}_4\text{OH}$ ,  $\text{HCl}$ , and  $\text{H}_2\text{O}_2$  have been reduced to 125 cc/min from 250 cc/min. The surface roughness were very low,  $\leq 0.15\text{ \AA}$ , and showed that these aggressive particle-removal recipes can be used with minimal surface roughness occurring. Most of the metals added data was at or near the detection limits. The only exceptions were the APM-only recipes, which showed high amounts of Zn,  $70\text{--}170 \times 10^{10}\text{ atoms/cm}^2$ . The high levels of Zn were due to the quality of the incoming chemicals. By including an HPM step as the terminating step, the metals were removed to the detection limit. Finally, the PDC data showed excellent results, with a run-to-run mean of 0.15% Particles Remaining for the recipe with an IR heater, SUPER6HAIR, and a mean of 0.13% for the recipe without an IR heater, SUPER7HA. The run-to-run variability was low, being 0.17% for both recipes.

## ACKNOWLEDGMENTS

Thanks to MaryAnn Ruehling and Brent Carlson for their invaluable assistance in running the PDC experiments and graphing the data.

## REFERENCES

1. S. Smith and K. Christenson, "Effects of SC-1 Dilution and Temperature on Various Particle Removal Challenges," *Proceedings of the Fourth International Symposium on Cleaning Technology in Semiconductor Device Manufacturing*, ECS, Pennington, NJ, pp. 21-25 (1995).

2. K. Christenson, et. al., "Effects of Sequential Chemistries on Particle Removal," *Proceedings of the Fourth Annual Symposium on Cleaning Technology in Semiconductor Device Manufacturing*, ECS, Pennington, NJ, pp. 567-574 (1995).
3. S. Smith and K. Christenson, "Particle Removal For Different Particle Challenges and Cleaning Chemistries," *Proceedings of the IES Spring 1997 Meeting*, IES, Mount Prospect, IL, pp. 157-161 (1997).
4. K. Christenson, C. Bode and K. Johnson, "Preparation of Si<sub>3</sub>N<sub>4</sub> Particle Challenge Wafers" *Proceedings of the IES Spring 1996 Meeting*, IES, Mount Prospect, IL, pp. 112-119 (1996).
5. K. Christenson, C. Bode and K. Johnson, "Particle Counting Techniques for Accurate Measurement of High Particle Removal Efficiencies" *Proceedings of the IES Spring 1996 Meeting*, IES, Mount Prospect, IL, pp. 297-303 (1996).
6. K. Christenson, "The Effects of Increased Chemical Temperatures in a Centrifugal Spray Processor" *Proceedings of the Third Annual Symposium on Cleaning Technology in Semiconductor Device Manufacturing*, ECS, Pennington, NJ, pp. 474-483 (1994).
7. K. Christenson, "Particle Removal in Solutions of Dilute HF" *Proceedings of the 1996 Semiconductor Pure Water and Chemicals Conference*, Balazs Analytical Lab, Sunnyvale, CA, pp. 289-300 (1996).

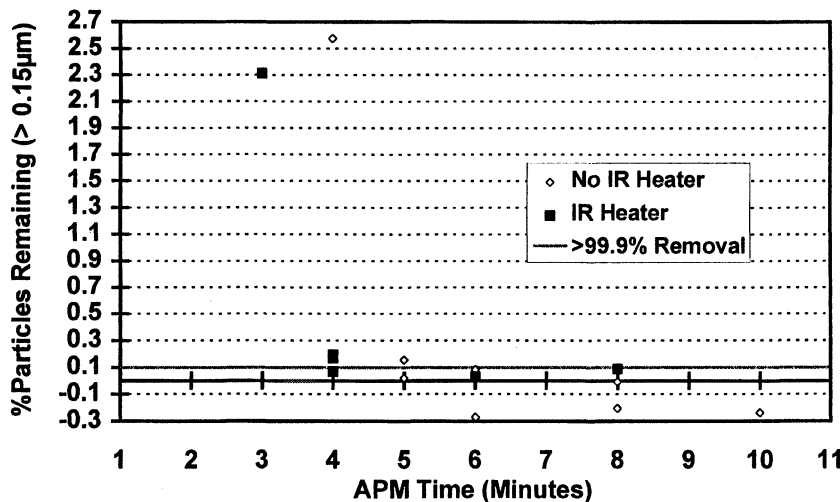


Figure 1. Particle Removal from Si<sub>3</sub>N<sub>4</sub> Challenge Wafers in APM+HWR Solutions

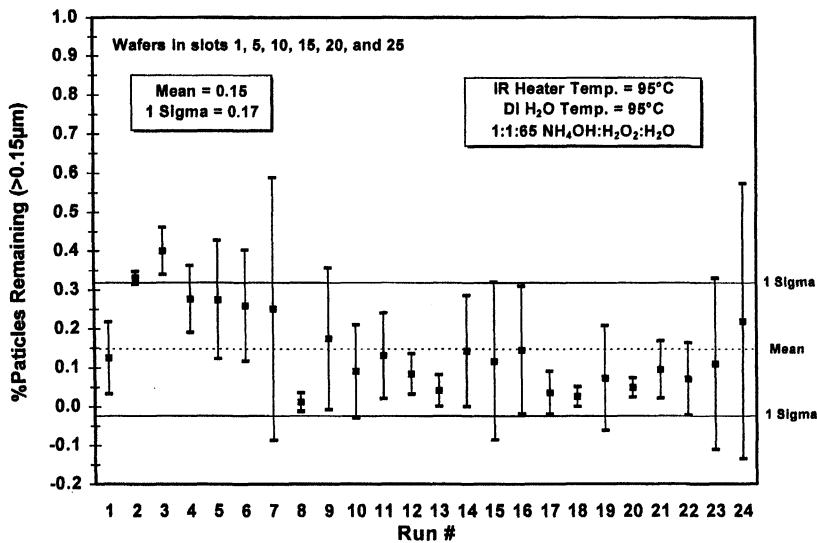


Figure 2. Particle Removal by SUPER6HAIR from 200 mm  $\text{Si}_3\text{N}_4$  Challenge Wafers

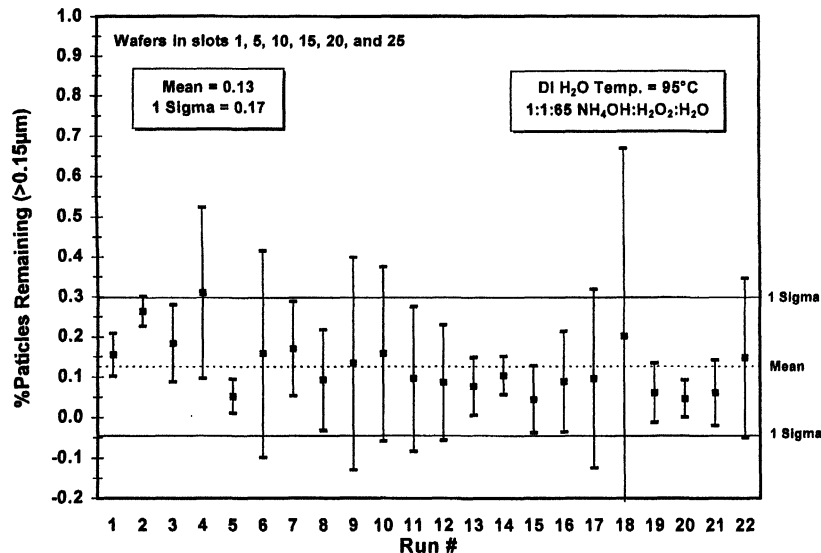


Figure 3. Particle Removal by SUPER7HA from 200 mm  $\text{Si}_3\text{N}_4$  Challenge Wafers

# EFFECTS OF SC1 ON Si<sub>3</sub>N<sub>4</sub> PARTICLE REMOVAL EFFICIENCY

J.Q. Liu\*, C. Lee\*\*, J.M. Rosamilia\*\*\*, T. Boone\*\*\*, G.S. Higashi\*

\*Bell Laboratories - Lucent Technologies  
9333 South John Young Parkway  
Orlando, FL 32819  
U.S.A.

\*\* Rice University  
Houston, TX  
U.S.A.

\*\*\*Bell Laboratories-Lucent Technologies  
600 Mountain Avenue  
Murray Hill, NJ 07974  
U.S.A.

Controlling particle contamination in wafer cleaning is crucial to reduce defect density and improve device performance and yield. Our previous design of experiment (DOE) investigated the impact of SC1/megasonic cleaning on modified RCA cleaning's Si<sub>3</sub>N<sub>4</sub> particle removal efficiency<sup>1</sup>. Interaction of SC1 conditions, bath temperature, megasonic power, and solution chemistry, on the modified RCA were evaluated. Megasonic power was found to be the dominate factor of improving particle efficiency among the three factors. In this study, SC1-only-cleaning is emphasized. Megasonic power, processing time, and bath temperatures are studied. The effects of particle sizes, megasonic rinse, and wafer load positions in the bath are also explored. The results show that megasonic power still plays a major role of the particle removal efficiency. Processing time, process temperature, megasonic rinse, and wafer positions in SC1 baths are all important factors for Si<sub>3</sub>N<sub>4</sub> particle removal efficiencies.

## INTRODUCTION

RCA clean has been the dominated method to remove wafer surface contamination by semiconductor industries for over twenty years<sup>2,3,4</sup>. The first step of RCA clean, Standard Clean 1 or SC1 (NH<sub>4</sub>OH/H<sub>2</sub>O<sub>2</sub>/H<sub>2</sub>O), effectively cleans surfaces through chemical oxide regeneration and surface etching. In SC1 solution, the surface etching and the repulsive electric force between surfaces and particles benefit particle removal<sup>5</sup>. Previous work has proven that SC1 itself is not sufficient to remove particle contamination without megasonics<sup>6</sup>. The mechanism of megasonics removing particles

were extensively studied. Cavitation and acoustic streaming are considered to be the main mechanism of particle removing<sup>7,8,9</sup>.

Previously we studied  $\text{Si}_3\text{N}_4$  particle removal efficiencies of complete cleaning sequences<sup>1</sup>. Table I shows the summary from a screening experiment. The screening experiment was used to compare  $\text{Si}_3\text{N}_4$  particle removal efficiencies among modified RCA clean on a spray tool, bench rinse with and without megasonics (800W), bench SC1 only with megasonics (800W), bench RCA clean, and bench modified RCA clean. It shows that modified RCA clean on the spray tool, bench RCA clean, and bench modified RCA clean have very similar particle removal efficiencies (around 99%). The average particle removal efficiency of the bench SC1/megasonic clean is around 85%. The particle removal efficiency of the bench Rinse/Dry with megasonic is much higher (around 58%) than that of Rinse/Dry without megasonic (around 0%). Our previous design of experiment (DOE) also investigated the impact of SC1 conditions on modified RCA cleaning's  $\text{Si}_3\text{N}_4$  particle removal efficiency<sup>1</sup>. Bath temperature, megasonic power, and solution chemistry of SC1 bath were evaluated. Megasonic power was found to be the dominate factor of improving particle efficiency among the three factors. Even though we are able to see effects of all factors in this DOE, the  $\text{Si}_3\text{N}_4$  particle removal efficiencies of this modified RCA clean are very high for all cells. In order to look into the effect of SC1 condition more closely, we followed the SC1-clean-only study.

## EXPERIMENTAL AND RESULTS

The standard challenge for particle removal from silicon wafers has been specified by the Semiconductor Industry of America (SIA) to be ">1,000 nitride" particles<sup>10,11</sup>.  $\text{Si}_3\text{N}_4$  particles are difficult to remove because they have least negative zeta potential in water and SC1 solution. A particle with a less negative zeta potential will have a less repulsive interaction (electrostatic double layer repulsion) with the wafer<sup>2</sup>. In this experiment, we use bath immersion method for  $\text{Si}_3\text{N}_4$  particle deposition, developed by Verteq, refined by IBM<sup>6</sup>, further refined by Lucent technologies. Silicon wafers were dipped in DI water containing a dispersion of  $\text{Si}_3\text{N}_4$  particles. The method produces wafers with a uniform spatial distribution of particles. Figure 1 shows a typical map of particle distribution on wafers, measured on a Tencor Surfscan 6200. The distribution is highly uniform across wafers. Total particle counts are in 3000 range and particle sizes distribution centered @ 0.3 micron.

In this study, we focus on the interaction of SC1 conditions on SC1-only-cleaning. The experiment was performed with a commercial available bench. Particles were measured on a Tencor Surfscan 6200. The concentration of SC1 is (1:1:10). Megasonic power (0W, 200W, 400W, and 800W), SC1 processing time (3min, 7min, and 15min), and bath temperatures (24°C, 40°C, 60°C, and 80°C) of SC1 are studied. The effect of megasonic rinse following SC1 bath was also investigated. Figure 2, 3, and 4 show the effect of SC1 process temperature, process time, and megasonic power when 800W megasonic power is used in the rinse bath. Figure 2 shows the temperature effect

when 7 min process time and 800W megasonic power in SC1 bath were used. Process temperatures at 24°C and 40°C give the optimized process temperatures. Figure 3 shows the process time effect when process temperature 60°C and 600W megasonic power were chosen for SC1 bath. We found that the most optimized process time in SC1 is 10 min. Figure 4 shows the megasonic power effect with 7 min. process time and 60°C for SC1 bath. It is found that megasonic power has the most significant impact on  $\text{Si}_3\text{N}_4$  particle removal efficiencies. Figure 4 shows that megasonic power is a dominant factor. High megasonic power is needed to remove these  $\text{Si}_3\text{N}_4$  particles.

The effect of megasonic rinse following SC1 bath in Figure 5 shows that megasonic rinse does improve  $\text{Si}_3\text{N}_4$  particle removal efficiencies. Figure 4 also shows that smaller particles are more difficult to remove. This result is similar to the previous results in DI water for PSL particles<sup>7,8,9</sup>. As shown in Figure 6, another interesting observation is that  $\text{Si}_3\text{N}_4$  particle removal efficiencies are higher for wafers located at two end of the bath than the wafers located at center of the bath. This may be related to the design of megasonics.

## DISCUSSIONS AND CONCLUSIONS

Megasonic power is found to be a dominant factor in SC1 clean. This result agrees with previously published results<sup>13</sup> (megasonic powers ranging from 0-300W were used). This may be due to the higher streaming velocity resulting from the increasing power since streaming velocity is proportional to power transmitted to the cleaning medium<sup>7,8</sup>. Particle removal efficiencies decrease with decreasing particle size since the ratio of removing force to adhesion force decrease as the particle size decrease. Processing time, process temperature, megasonic rinse, and wafer positions in SC1 baths are all important factors for  $\text{Si}_3\text{N}_4$  particle removal efficiencies.

## REFERENCES

1. J.Q. Liu, C. Lee, J.M. Rosamilia, T. Boone, V. Czitrom, and G.S. Higashi, Mat. Res. Soc. Symp. Accepted, (1997).
2. W. Kern, *Handbook of Semiconductor Wafer Cleaning Technology*, Noyes Publication, 1993.
3. W. Kern, J. Electrochem. Soc. **137**, 1887(1990).
4. W. Kern and D. Puotinen, RCA Rev. **31**, 187(1970).
5. T. Ohmi, Electrochemical Society Proceeding, **95-20**, 1(1996).
6. S.L. Cohen, D. Rath, G. Lee, B. Furman, K.P. Pope, R. Tsai, W. Syverson, C. Gow, and M. Liehr, Mat. Res. Soc. Symp. **386**, 13(1995).
7. A.A. Busnaina and F. Dai, Semiconductor International, page85, August 1997.
8. A. Busnaina and I. Kashkoush, Chem. Eng. Comm, **125**, 47(1993).

9. A. Busnaina and I. Kashkoush, and G.W. Gale, J. Electrochem. Soc., 142, 2812(1995).
10. K. Christenson, C. Bode, and K. Johnson, Proceedings of the Institute of Environmental Sciences, 112(1996).
11. The National Technology Roadmap for Semiconductors, Semiconductor Industry Association, San Jose, CA. 116(1994).
12. T. Boone, J.M. Rosamilia, J.Q. Liu, TM in preparation.
13. P.J. Resnick, C.L.J. Adkins, P.J. Clews, E.V. Thomas, S.T. Cannada, *Cleaning Technology in Semiconductor Device Manufacturing*, PV94-7, The Electrochemical Society, Inc., Pennington, NJ, 450(1994).

**Table I. Si<sub>3</sub>N<sub>4</sub> Particle Removal Efficiency for the Screening Experiment**

Particle Size(um)	Spray Clean	Bench RCA(%)	Bench Modified RCA(%)	Bench SC1/Meg(%)	Bench R/D w/o Meg(%)	Bebch R/D w Meg (%)
0.2	98.4	99.9	99.1	91.5	0.76	29.8
0.25	98.7	99.6	99.2	89.9	-2.61	35.7
0.3	99.4	99.8	99.6	72.9	-1.74	52.3
0.5	99.8	99.7	99.7	72.5	0.25	63.9
1	99.8	99.8	99.8	88.1	0.72	73.8
2	100	99.9	99.7	97.0	11.3	89.5

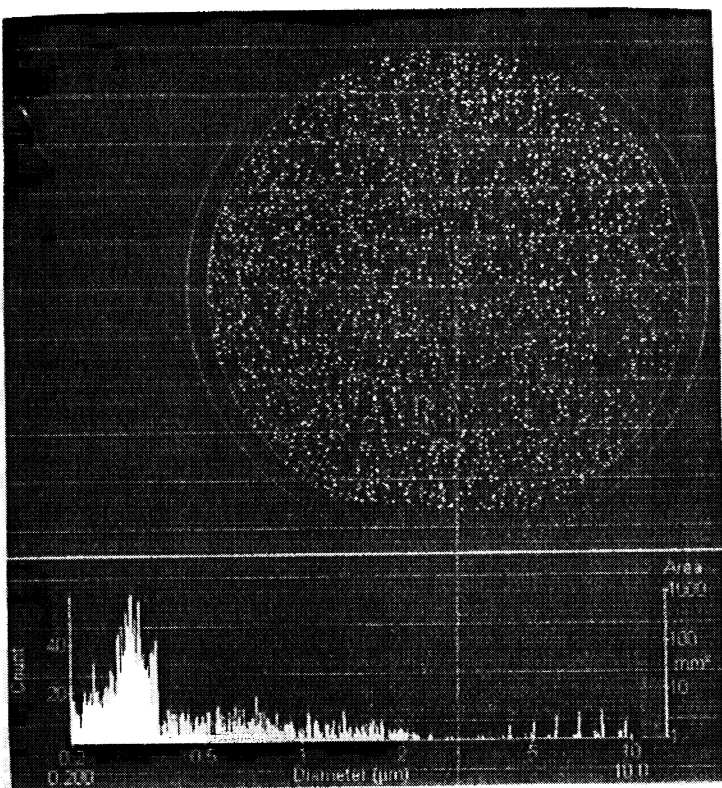


Figure 1. Map of silicon nitride particle distribution on wafers

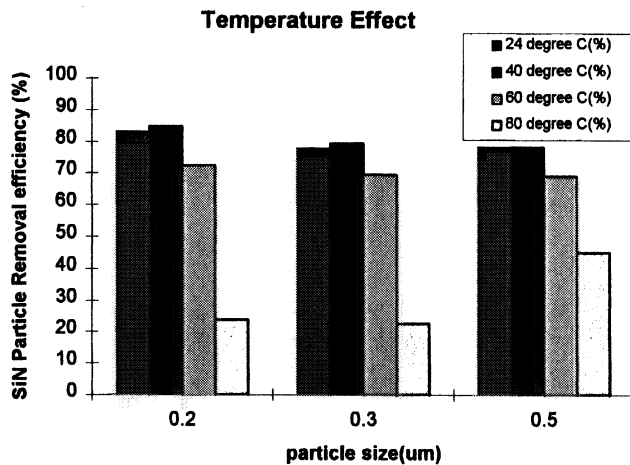


Figure 2. The effect of SC1 temperature on particle removal efficiency for SC1 clean.

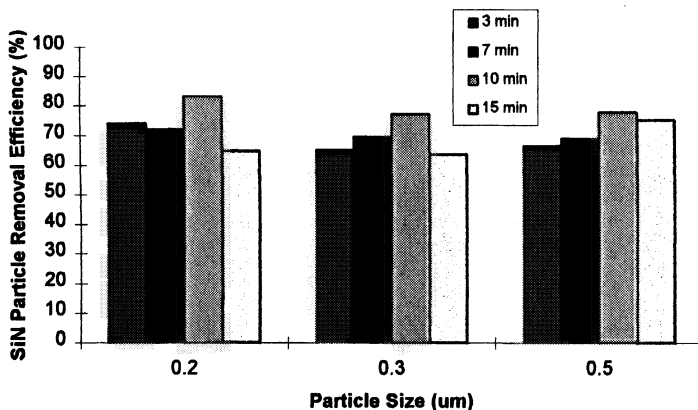


Figure 3. The effect of SC1 process time on particle removal efficiency for SC1 clean.

**SC1 cleaning @60 degree C with (1:1:10) ratio and  
800W rinse**

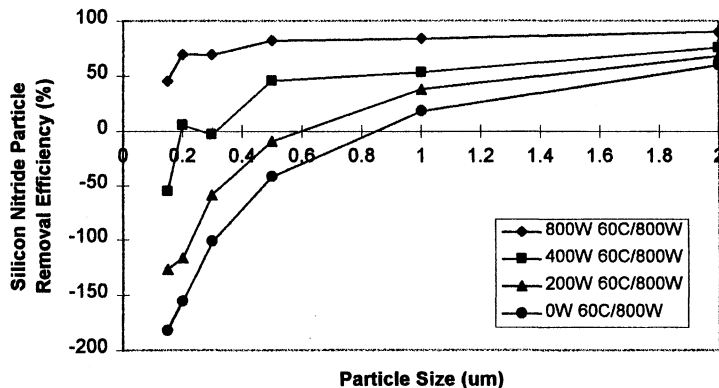


Figure 4. The effect of megasonic power in SC1 on particle removal efficiency for SC1 clean.

**SC1 Clean with and without Megasonic rinse @60 Degree C and (1:1:10) Ratio**

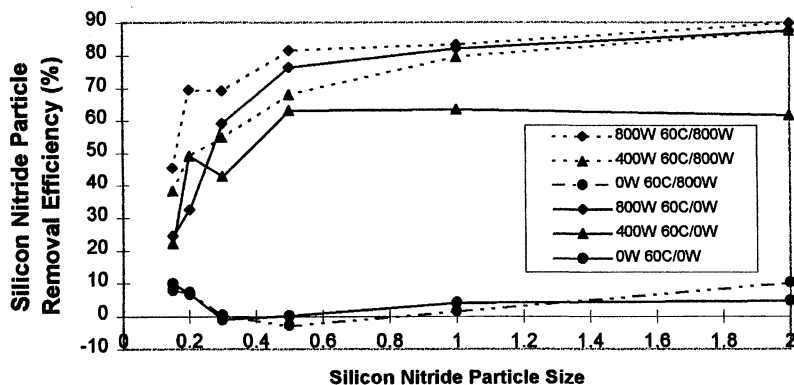


Figure 5. The effect of megasonic rinse on particle removal efficiency for SC1 clean.

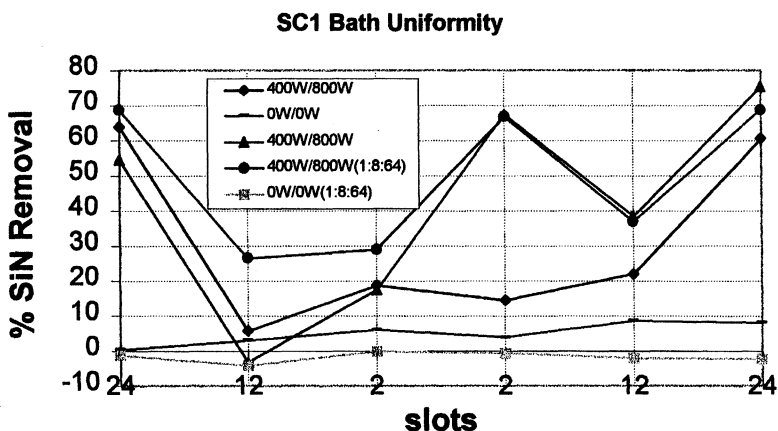


Figure 6. The effect of wafer positions in SC1 bath on particle removal efficiency for SC1 clean.

# ADHESION ENERGY OF POLYSTYRENE AND SUBSTRATE IN FUNCTION WATER

Yoshihito Tatehaba , Kiyoshi Shimada , Eiichi Ando

Research and Development Dept., SPC Electronics Corp.,  
2-1-3 Sibasaki, Chohu, Tokyo, Japan 182 (e-mail:sanki@tokyo.spc.co.jp)

Akira Kawai

Department of Electrical Engineering, Nagaoka University of Technology,  
1603-1 Kamitomioka, Nagaoka, Niigata, Japan 940-21  
(e-mail:kawai@vos.nagaokaut.ac.jp)

Adhesion of particle less than  $0.1\mu\text{m}$  onto substrate is a factor of yield declining at the following generation in semiconductor process. We throw light on the mechanisms of adhesion and removal for particle, which hastens the developments about removal of particle and re-adhering prevention in a liquid medicine with low concentration.

Removal of the polystyrene latex (PSL) particle on the substrate in the function water as liquid medicine with low concentration can be explained by using the adhesion theory based on thermodynamics. The cleaning results show the validity of this theory.

## 1.INTRODUCTION

In the LSI manufacturing, the cleaning process of micro particle adsorbed on the substrate is important to influence on yield. Because, the writing pattern size of 256Mb-DRAM is less than  $0.3\mu\text{m}$ . The micro particles of some  $10\mu\text{m}$  in diameter, which corresponds to the amount ranging from  $1/10$  to  $1/5$  of pattern width, would affect strongly to decline of the yield. Since the wafer diameter has extended from 8 to 12 inches, amount of the chemical cleaning liquids have significantly increased. Therefore, We throw light on the mechanisms of adhesion and removal for particle, which hastens the developments about removal of particle and re-adhering prevention in a chemical cleaning liquids with low concentration.

The mechanisms of adhesion and removal for a particle in a solution have been analyzed using the model combined with van der Waals Force (vdWF) of surface free energy and electrostatic force of electric double layer model based on the DLVO theory.(1) Therefore, the study for cleaning process has been analyzed with both the electrostatic force of particle as the zeta potential and the vdWF of particle on the substrate. Moreover, the liquids for chemical cleaning with low concentration and function water (electrolysis ionized water, ozone water) are of considerable practical concern.

In this study, The removal of the polystyrene latex (PSL) particle on the substrate in function water is analyzed using the adhesion theory based on thermodynamics.(2-3) We predict the removal of PSL on the substrate by the factors of vdWF which is expressed as surface free energy  $\gamma$  and it's component of dispersion  $\gamma^d$  and polar  $\gamma^p$  for liquids ( function water, various chemical liquids ), substrate and polystyrene, as follows.

$$\gamma = \gamma^d + \gamma^p \quad [1]$$

Finally the results of cleaning test are compared with that by prediction using this model.

## 2.EXPERIMENTAL

The removal study were performed with substrates, PSL and chemical liquids. Figure.1 shows the schematic model for balance of surface energy. For the experiment, silicon wafer (bare, hydrofluoric acid processing) and glass were used as the substrate. Polystyrene(PS) sheet was used for surface energy measurement instead of PSL. Chemical liquids and electrolysis ionized water (anode water;pH3 and cathode water;pH10) and ozone water (pH6) were used. Electrolysis ionized water were added hydrochloric acid 1.1mMol/L, ammonia water 0.6mMol/L. Ozone water of 5ppm in concentration was used.

The method used for measuring surface free energy  $\gamma_L$  and its components dispersion  $\gamma_L^d$  and polar  $\gamma_L^p$  of the chemical liquids were determined with the liquid's surface tension and contact angle of the paraffin. Each component is expressed as the following equations.(4)

$$\gamma_L^d = \frac{\{\gamma_L(1 + \cos \theta)\}^2}{4\gamma_S^d} \quad [2]$$

$$\gamma_L^p = \gamma - \gamma_L^d \quad [3]$$

$\gamma_L$  : Surface energy of liquid.(Surface tension)

$\gamma_L^d$  : dispersion component of surface free energy  $\gamma_L$  of liquid.

$\gamma_L^p$  : polar component of surface free energy  $\gamma_L$  of liquid.

$\gamma_S^d$  : dispersion component of praffin. (25.5mJ/m<sup>2</sup>)

$\theta$  : contact angle of liquid.

In order to measure the surface free energy  $\gamma_s$  and its components dispersion  $\gamma_s^d$  and polar  $\gamma_s^p$  of each substrates and PS sheet, the contact angle method which was used pure water, ethylene glycol, diido methane as standard liquid was applied.(5-6) These two components can be obtained by using Young-Duple equation, as follows.

$$\gamma_L(1 + \cos \theta) = 2(\gamma_S^d \cdot \gamma_L^d)^{1/2} + 2(\gamma_S^p \cdot \gamma_L^p)^{1/2} \quad [4]$$

$\gamma_S^p$  : polar component of surface free energy  $\gamma_S$  of solid.

$\gamma_S^d$  : dispersion component of surface free energy  $\gamma_S$  of solid.

The adhesion energy(Wa) was obtained by substituting the dispersion and polar components of these liquids, substrate and PS sheet, as shown in Eq.[5]. These adhesion energies would predict the adsorption behavior of PSL particle on the substrates in each liquid.

$$-Wa = \gamma_{12} - (\gamma_{13} - \gamma_{23}) \\ = (\sqrt{\gamma_1^d} - \sqrt{\gamma_2^d})^2 + (\sqrt{\gamma_1^p} - \sqrt{\gamma_2^p})^2 - \left\{ (\sqrt{\gamma_1^d} - \sqrt{\gamma_3^d})^2 + (\sqrt{\gamma_1^p} - \sqrt{\gamma_3^p})^2 + (\sqrt{\gamma_2^d} - \sqrt{\gamma_3^d})^2 + (\sqrt{\gamma_2^p} - \sqrt{\gamma_3^p})^2 \right\} \quad [5]$$

$\gamma_1^d$ : dispersion component of surface free energy of Si wafer and glass substrate.

$\gamma_1^p$ : polar component of surface free energy of Si wafer and glass substrate.

$\gamma_2^d$ : dispersion component of surface free energy of PSL.

$\gamma_2^p$ : polar component of surface free energy of PSL.

$\gamma_3^d$ : dispersion component of surface free energy of Function water and chemical liquids.

$\gamma_3^p$ : polar component of surface free energy of Function water and chemical liquids.

For the cleaning evaluation, the PSL particles adhered to a bare Si wafer (Si) of 6inch treated with hydrofluoric acid process (HF-Si) and to a glass substrate of 5 inch square by means of spraying. They exposed to atmosphere of the clean room about 12 hours. These samples dipped into the function water for 10 minutes. The similar processes were performed in hydrochloric acid and ammonia water of the amount of pH, which is same as that of the function water. The number of PSL particles before and after dipping was measured by using the laser particle counter. The removal efficiency was calculated with the results mentioned above. The PSL particle of  $0.13\mu\text{m}$  in diameter was used for the experiment for Si, HF-Si and the particle of  $1\mu\text{m}$  was used for glass substrate, because of the resolution of the detection system.

### 3.RESULTS AND DISCUSSION

Figure.2 shows the component map of surface free energy of each test liquid and substrate. The polar values of the liquids, Si and glass substrates are relatively high value. On the other hand, the polar values of the HF-Si, the PS sheet show relatively low value. Particularly, it can be observed that the surface free energy of Si substrate varies by HF surface treatment. In these results, dispersion and polar component reflect strongly the difference of surface chemistry of solid.

Figure.3 shows the adhesion energies ( $W_a$ ) between polystyrene latex and substrate in the various solutions. Hence, Eq.[5] can be transformed as the following equation.

$$\begin{aligned} -\frac{W_a}{2} &= \left( \sqrt{\gamma_3^d} - H \right)^2 + \left( \sqrt{\gamma_3^p} - K \right)^2 - R^2 \\ H &= \frac{\sqrt{\gamma_1^d} + \sqrt{\gamma_2^d}}{2} \\ K &= \frac{\sqrt{\gamma_1^p} - \sqrt{\gamma_2^p}}{2} \\ R^2 &= \frac{1}{4} \left\{ \left( \sqrt{\gamma_1^d} - \sqrt{\gamma_2^d} \right)^2 + \left( \sqrt{\gamma_1^p} - \sqrt{\gamma_2^p} \right)^2 \right\} \end{aligned} \quad [6]$$

Therefore, the data in Fig.3 can be expressed as shown in Fig.4.

Especially, Fig.4 is used for prediction whether PSL is removed by liquid penetration between the substrate and PSL. If the point of the surface energy ( $\gamma_s$ ) of liquid is plotted in the circle for the substrate, we can predict that the PSL particle is removed from the substrate in thermodynamics. Therefore, The particle on the glass substrate would be easily removed. Moreover, we can predict that the PSL would adhere weakly to the Si substrate. On the other hand, the removal of PSL on HF-Si is less likely occur.

Figure.5 shows the result of the cleaning test with various test liquids. As the samples, PSL adhered to Si, HF-Si and the glass substrate were used.

As seen in Fig.5(a), the removal efficiency decreases in order of glass substrate > Si > HF-Si. It can be distinctly observed that the cleaning results reflect strongly the dependency of substrate material. However, There is a difference of about  $40\text{-}50\text{ mJ/m}^2$  at the threshold level in Fig.5(a) for the removal prediction against to the cleaning results. This discrepancy would due to the practical adhesion force between substrate and PSL which is affected by the other factors. Moreover, in the Fig.5(b), As increasing the diameter of PSL, PSL particles can be easily removed from the substrate.

#### 4.CONCLUSION

The removal prediction of PSL particle adhered on the substrate by the surface free energy model can be explain the practical cleaning results. However, the cleaning result tends to remove the particle over the threshold level in the removal prediction, practical adhesion energy between substrate and PSL is smaller. As the reason for this is that the repulsion of between the substrate and PSL would be interpreted by the electrostatic force among them. Moreover, the particle diameter size has strongly affect to the adhesion phenomena. The removal of particle from the substrate extremely occurs above 1 $\mu\text{m}$  in diameter. Finally, it is important to define the factor of the difference between the threshold level of the removal estimate and the cleaning result, such as dependence of PSL size, the electrostatic force (zeta potential), the deformation of PSL particle by adhering to the substrate.

#### ACKNOWLEDGEMENTS

A part of This work performed under the management's of Association of Super-Advanced Electronics Technologies (ASET) in the Ministry of International Trade and Industry (MITI) Program of Super-Advanced Electronic Technologies supported by New Energy and Industrial Technology Development Organization(NEDO).

#### REFERENCES

- (1) A.Kitahara,K.Furusawa,M.Ozaki and H.Ohshima:Zeta Potential,102,Scientist Co.,Tokyo(1995)
- (2) Y.Tatehaba and A.Kawai:Extended Abstracts(The 44<sup>th</sup> Spring Meeting, 1997);The Japan Society of Applied Physics and Related Societies, No2, 777(1997)
- (3) Y.Tatehaba,K.Shimada,E.Ando and A.Kawai: Extended Abstracts(The 35<sup>th</sup> Symposium on Adhesion);The Adhesion Society of Japan,75(1997)
- (4) D.H.Kaelble:J.Appl.Polym. Sci, **18** 1869 (1974)
- (5) A.Kawai,H.Nagata and M.Takata:Jpn.J.Appl.phys.,**31**,3725(1992)
- (6) A.Kawai:Journal of the Adhesion Society of Japan,**33**,39(1996)

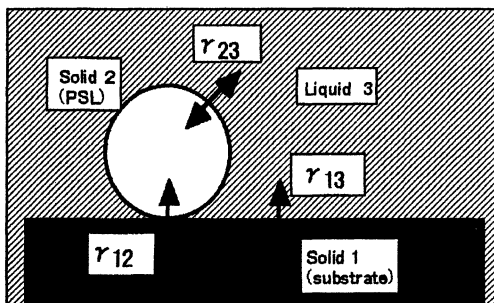


Fig.1.  
The balance among interface energies.

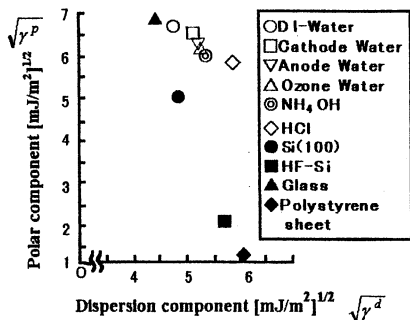


Fig.2.  
Component map of surface energy  
for test liquids, substrate and  
polystyrene.

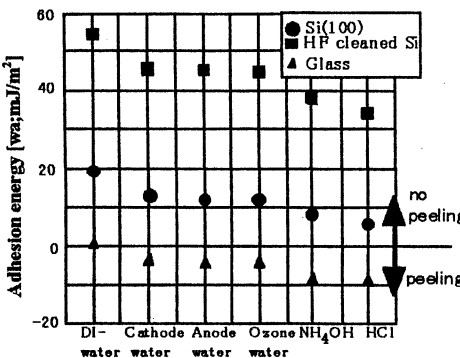


Fig.3.  
Adhesion energies between  
polystyrene and substrate in  
various liquids.

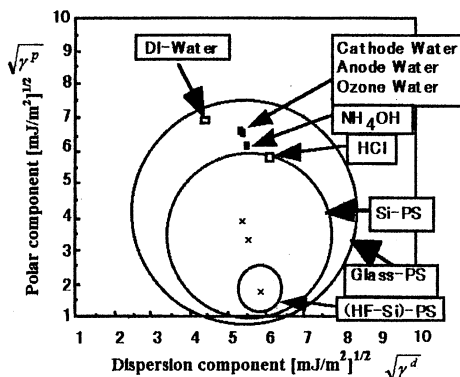


Fig.4.  
Prediction of adhesion for  
polystyrene latex on various  
substrates.

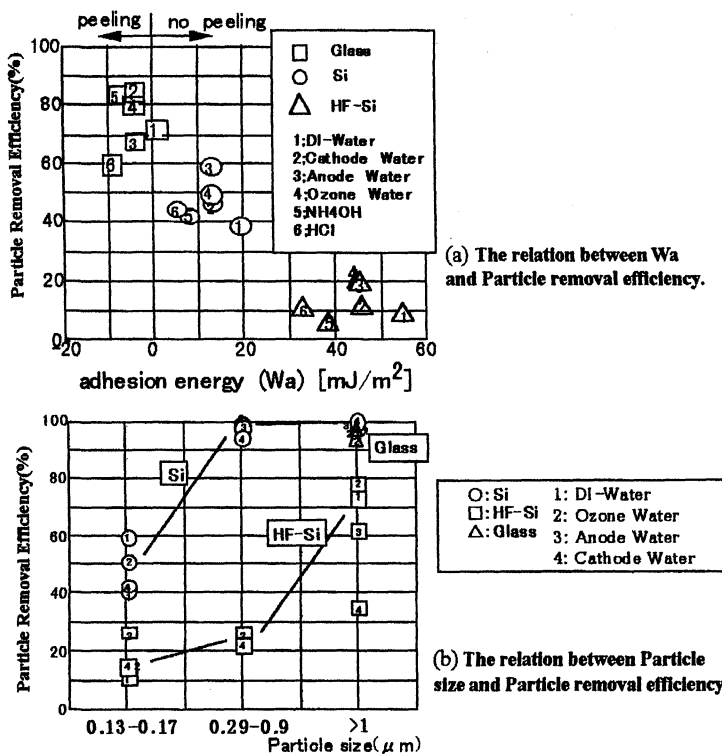


Fig.5. The experimental result for the removal of PSL particles from substrate in the cleaning liquids.



**BACK-END-OF-LINE  
CLEANING**



## CORROSION OF ALUMINUM ALLOYS DURING DRYING OF METALLIZED WAFERS

Rita Vos, Marc Meuris, Paul Mertens, Marc Heyns and Zach Hatcher<sup>1</sup>

IMEC, Kapeldreef 57, B-3001 Heverlee, BELGIUM

<sup>1</sup>Ashland Chemical, P.O. Box 2219, Columbus OH 43216, USA

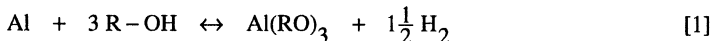
The corrosion of aluminum during isopropylalcohol (IPA)-vapor drying and during Marangoni drying is investigated and specifications for the cleanliness of the IPA used during both drying processes are determined. Therefore, a controlled contamination with some important contaminants which can be present in the IPA (i.e. water, n-propanol and the corrosive anions Cl<sup>-</sup>, F<sup>-</sup>, SO<sub>4</sub><sup>2-</sup> and PO<sub>4</sub><sup>3-</sup>) is performed. The amount of corrosion is determined electrically by measuring the resistance of thin aluminum lines.

When ultra-pure IPA is used, both an IPA-vapor dry and a Marangoni dry step are found to have no effect. When water is added to the IPA, no corrosion is detected even when water concentrations as high as 13% are spiked to the IPA. As far as the corrosive anions that were evaluated are concerned, only chloride is found to be corrosive. Corrosion during IPA-vapor drying is observed at lower Cl<sup>-</sup> concentrations compared to Marangoni drying. Moreover, water is found to inhibit the corrosion caused by exposure of aluminum lines to chloride containing IPA-vapors.

### INTRODUCTION

During the wafer cleaning cycle, drying after rinsing is an indispensable step and must be accomplished without recontamination or deterioration of the wafer surface. When metallized wafers are dried, corrosion reactions have to be minimized since they degrade the quality of the surface. The most commonly used technique for drying metallized wafers is spin rinse drying, whereby the water is physically removed from the wafer surface by centrifugal forces during spinning of the wafers. However, there is a general trend to use drying techniques with better performance concerning particle recontamination and drying spot formation on patterned wafers with topography (1,2). This is accomplished e.g. in solvent vapor dryers where the carry-over layer is replaced by condensed IPA during immersion of wet wafers in vapors of an organic solvent, mostly isopropylalcohol or IPA. Alternatively, other drying techniques have been developed in order to improve cycle time and to reduce IPA consumption. For instance, in Marangoni™ dryers (Steag Microtech) the wafers are dried by the so-called Marangoni effect (3,4) which arises from the introduction of an IPA/N<sub>2</sub> atmosphere at the top of an aqueous rinse bath while slowly withdrawing the wafers out of the vessel.

In many cases, aluminum alloys are used for metallization in integrated circuits. Under normal circumstances, this metal is considered to be rather inert and exhibits a passive behaviour because of its passivating surface oxide film. In alcoholic media, however, a very localized corrosion can be observed at cracks or dislocations in the passivating layer and the aluminum will corrode according to (5)



Moreover, the passivating layer can be further attacked by the interaction with certain anions which can considerably speed up the corrosion process (6). In addition, the corrosion rate of aluminum is significantly influenced by the presence or absence of water since (i) water can both provide a medium for the mobilization of dissolved aluminum cations or complexes with anions and alternatively (ii) water can be incorporated in the passive film hereby increasing its protectiveness. Therefore, very stringent specifications concerning the cleanliness of the IPA used during IPA-based drying processes are demanded by most IC-manufacturers.

In this study, the significance of the above corrosion reactions during an IPA-vapor drying step and during Marangoni drying is investigated. The effect of H<sub>2</sub>O and n-propanol, which are present as natural contaminants in IPA and are often claimed to corrode aluminum layers, is evaluated by performing a controlled contamination with these contaminants. In addition, also the effect of the corrosive anions Cl<sup>-</sup>, F<sup>-</sup>, SO<sub>4</sub><sup>2-</sup> and PO<sub>4</sub><sup>3-</sup> when present in the IPA is determined. Finally, meaningful requirements for the impurity levels in IPA are summarized.

Table I: Specifications for the most important contaminants in GigaBit™ IPA (Ashland Chemical).

Parameter	Specification
Assay (CH <sub>3</sub> CHOCH <sub>3</sub> )	> 99.8 %
Water	< 200 ppm
n-propanol	NA
Anions	
- Chloride	< 50 ppb
- Phosphate	< 50 ppb
- Sulfate, Fluoride	NA
Metals	< 1 ppb

## EXPERIMENTAL DETAILS

The IPA-vapor dryer used in this study is an K&S CVC-2000-2D. The temperature of the heating elements is set to 180 °C. The pre-dry time, i.e. the time the wafers are immersed in the IPA-vapors and the wafer/water interface is replaced by a wafer/IPA interface, is always 5 minutes unless mentioned otherwise. The dry time, i.e. the time for evaporating the condensed IPA on the wafer surface, is always 2 minutes. As a Marangoni dryer, a home-build experimental set-up is used, operated at room temperature.

All experiments are performed with ultra-pure IPA (GigaBit<sup>TM</sup> grade, Ashland Chemical). Specifications for the most important contaminants in IPA are listed in Table I. An overview of the additives used for spiking the IPA and the corresponding concentration range is given in Table II. If necessary, dilutions of the spiking solutions are made with IPA except for KCl which is added from a 5 M aqueous stock solution to the IPA.

Table II: Overview of the different additives used for spiking the IPA.

Additive	Spiking solution	Vendor	Grade	Concentration range spiked to the IPA
Water	DI-water	NA	NA	0-13%
n-propanol	n-propanol	Baker	Analytical grade	0-1000 ppm
Chloride	HCl (37 %)	Ashland	MegaBit <sup>TM</sup>	0-1000 ppm
	KCl	Fluka	BioChemika <sup>TM</sup>	0-100 ppm
Phosphate	H <sub>3</sub> PO <sub>4</sub> (85 %)	Ashland	GigaBit <sup>TM</sup>	0-10 ppm
Sulfate	H <sub>2</sub> SO <sub>4</sub> (96 %)	Ashland	GigaBit <sup>TM</sup>	0-10 ppm
Fluoride	HF (49 %)	Ashland	GigaBit <sup>TM</sup>	0-10 ppm

As test structures for the evaluation of the corrosion during drying, both bare aluminum meander lines and stacked Ti/TiN/Al/Ti/TiN meander structures are constructed: after deposition of the appropriate metal layers (700 nm Al/1% Si/0.5% Cu for the bare aluminum structures or 80 nm Ti, 30 nm TiN, 700 nm Al/1% Si/0.5% Cu, 80 nm Ti and 20 nm TiN for the stacked structures) and lithographic steps, wafers are etched (LAM TCP 9600) and stripped using standard procedure (H<sub>2</sub>O/CF<sub>4</sub>-plasma followed by wet solvent strip).

The corrosion of the lines is evaluated electrically by measuring the resistance after the wafers are rinsed for 5 minutes with DI-water and subsequently dried using different drying conditions. The obtained values are compared with the resistance of meanders on wafers which did not receive a rinse and dry treatment. In general, a change in the resistance R is correlated to changes in the cross-section of the metal lines according to

$$R = \frac{L \rho}{w t} \quad [2]$$

where L is the length,  $\rho$  the resistivity ( $3 \times 10^{-8} \Omega m$ ), w the width and t the thickness (0.7  $\mu m$ ) of the meander lines. For the IPA-vapor drying experiments, meander structures with a length of 4.63 m and a width of 0.8  $\mu m$  are used. For the Marangoni drying tests, another mask with meanders with a length of 6.137 m and a width of 0.7  $\mu m$  is used. This corresponds to theoretical resistances of 248 kOhm and 375 kOhm respectively for both test structures. From the measured resistances at different positions on the wafer, the yield was calculated according to

$$\text{Yield (\%)} = \frac{\text{Number of meanders with resistance } R_{\text{good}}}{\text{Total number of meanders measured}} \times 100 \quad [3]$$

As a criterion for counting the meander structures with resistance  $R_{\text{good}}$ , we took a  $1\sigma$ -criterion:

$$R_{\text{reference}} - \sigma_{\text{reference}} \leq R_{\text{good}} \leq R_{\text{reference}} + \sigma_{\text{reference}}$$

with  $R_{\text{reference}}$  the resistance of the same type of meander structure on a reference wafer which was not rinsed or dried in the IPA-vapor dryer, and  $\sigma_{\text{reference}}$  the corresponding standard deviation.

## RESULTS AND DISCUSSION

Since it is known that the corrosion rate of aluminum in 'pure' liquid alkanol solutions with a water content lower than 0.05% can be rather high (7), the influence of exposure to IPA-vapors upon the corrosion of aluminum is evaluated. Therefore, the electrical properties of bare and stacked aluminum lines are measured after drying using the ultra-pure GigaBit™ IPA. Table IIIa and Table IIIb show the results of the measured resistances respectively after IPA-vapor dry and after Marangoni dry. These data indicate that no corrosion due to IPA-vapor exposure occurs during the time scale of an IPA-vapor dry step; even when the wafers are put for two hours in the IPA-vapors no change in the electrical characteristics is observed. Also after a standard Marangoni dry, no effect on the resistance is measured. In addition, no change in the electrical yield as calculated using equation [3] is observed (data not shown).

Table IIIa: Average resistance of bare and stacked aluminum meanders after IPA-vapor dry with different pre-dry times .

Pre-dry	Resistance (kΩ)	
Condition	Bare	Stacked
Ref.	287 ± 11	260 ± 9
IPA-vapor 5 min	285 ± 9	258 ± 8
IPA-vapor 2 hours	282 ± 15	262 ± 9

Table IIIb: Average resistance of bare and stacked Al meanders after Marangoni dry .

Mg.dry	Resistance (kΩ)		
Cond.	time	Bare	Stacked
Ref.	-	394 ± 22	391 ± 18
MgDry	5 min.	393 ± 18	403 ± 15

In a second experiment, the IPA used during IPA-vapor drying is spiked with controlled amounts of water. No change in the resistance (see Table IV) nor the electrical yield is observed when the moisture concentration in the IPA increases. Even when 13% H<sub>2</sub>O (i.e. the azeotropic mixture) is added to the IPA, no significant change can be observed.

Since n-propanol is a stronger acid than IPA - pKa amounts to 15.9 for n-propanol vs. a pKa of 20 for IPA - IPA which contains traces of n-propanol is said to be more corrosive towards metals compared to pure IPA. In order to verify this, wafers with aluminum lines are dried using IPA spiked with various amounts of n-propanol. The measured resistances after IPA-vapor dry are summarized in Table V. These data show no significant change in the electrical properties when n-propanol is spiked to the IPA.

Table IV: Resistance of bare and stacked aluminum meander structures after IPA vapor dry with IPA spiked with different amounts of water.

Spiking of IPA	Pre-dry time	Resistance (kΩ)	
		Bare	Stacked
Reference - no dry	-	287 ± 11	260 ± 9
50 ppm H <sub>2</sub> O	5 min.	NA	266 ± 10
200 ppm H <sub>2</sub> O	5 min.	NA	260 ± 9
500 ppm H <sub>2</sub> O	5 min.	282 ± 12	259 ± 9
1% H <sub>2</sub> O	5 min.	278 ± 14	269 ± 11
13% H <sub>2</sub> O	5 min.	283 ± 12	261 ± 8
13% H <sub>2</sub> O	2 hours	278 ± 12	262 ± 10

Table V: Resistance of bare and stacked aluminum meander structures after IPA vapor dry with IPA spiked with different amounts of n-propanol.

Spiking of IPA	Pre-dry time	Resistance (kΩ)	
		Bare	Stacked
Reference	-	287 ± 11	260 ± 9
100 ppm n-propanol	5 min.	277 ± 14	261 ± 10
500 ppm n-propanol	5 min.	275 ± 10	264 ± 14
1000 ppm n-propanol	5 min.	282 ± 17	260 ± 11

Spiking of the IPA used during drying with HCl results in very severe changes of the electrical properties of metal lines. Especially the bare aluminum meanders are very sensitive to the presence of Cl<sup>-</sup>: for IPA-vapor dried wafers, the resistance starts to increase (see Table VIa) with a corresponding decrease in the yield when the concentration HCl is higher than 300 ppb (see Figure 1). For the stacked lines, the corrosion occurs only at a HCl concentration higher than 10 ppm. After Marangoni dry, the observed corrosion is less pronounced and is only visible at relatively high spiking levels of 100 ppm both for the bare and stacked lines as follows from the measured resistances (see Table VIb) and the electrical yield (see Figure 2). Most probably, temperature plays an important role and enhances the corrosion rate. As expected, also an increase in the exposure time in chloride containing IPA-vapors, results in an enhanced corrosion. With

SEM, however, no line degradation could be spotted even for the wafers who displayed the most severe corrosion. This can probably be attributed to the fact that the observed corrosion phenomenon is mainly a pitting-type corrosion (8) which is localized in space. With SEM, one typically looks at distances of 10 µm while the total length of the meander lines amounts to more than 4 m !

Water is found to have an corrosion inhibiting effect. Indeed, when water is added to IPA spiked with 100 ppm HCl, no corrosion at all is measured after drying with this spiked IPA. The same phenomenon has been reported previously in literature for the corrosion of the aluminum in liquid alcohols: it is thought that water favors the formation of a passive film and suppresses the corrosive behaviour of metals in chloride containing alkanols (9). The data presented here show that also in IPA-vapors, the corrosion caused by the chloride ion is suppressed by the addition of water.

Table VIa: Resistance of bare and stacked aluminum meander structures after IPA vapor dry with IPA spiked with different levels of chloride and water.

Spiking of IPA	Pre-dry time	Resistance (kΩ)	
		Bare	Stacked
Reference	-	287 ± 11	260 ± 9
50 ppb HCl	5 min	288 ± 11	273 ± 15
300 ppb HCl	5 min	277 ± 15	262 ± 11
750 ppb HCl	5 min	292 ± 11	273 ± 13
10 ppm HCl	5 min	<4 E5	277 ± 14
100 ppm HCl	5 min	< 3E5	266 ± 16
1000 ppm HCl	5 min	< 8E5	267 ± 15
1000 ppm HCl	2 hours	< 3E5	<3E3
100 ppm HCl + 13% H <sub>2</sub> O	5 min	293 ± 11	264 ± 11
100 ppm KCl	5 min	< 3E4	264 ± 9
100 ppm KCl	2 hours	< 2E5	244 ± 20

The corrosion observed when HCl is added to the IPA has to be, at least partially, attributed to the presence of the chloride ion since corrosion occurs also when the IPA is spiked with KCl. It is reported that the enhanced corrosion in the presence of chloride is due to a high solubility of aluminum chlorides in alcoholic solutions which approaches the solubility in aqueous media (10). However, the observed corrosion with KCl is not as severe as compared to the HCl spiked IPA. This can be explained by the fact that the KCl

was added from an aqueous solution to the IPA. On the other hand, it is also not unlikely that the presence of the hydrogen ion can affect the corrosion rate since  $H^+/H_2$  reduction is the cathodic reaction during the oxidation of Al.

Table VIIb: Resistance of bare and stacked aluminum meander structures after Marangoni dry with IPA spiked with different levels of chloride and water.

Spiking of IPA	Mg.dry time	Resistance (kΩ)	
		Bare	Stacked
Reference	-	394 ± 22	391 ± 18
750 ppb HCl	5 min	384 ± 18	404 ± 13
10 ppm HCl	5 min	386 ± 21	403 ± 13
100 ppm HCl	5 min	<1E7	<9E3
1000 ppm HCl	5 min.	<1E7	<3E5
100 ppm HCl	2 hours	<2E7	<3E6
100 ppm HCl + 13% H <sub>2</sub> O	5 min	393 ± 19	393 ± 19
100 ppm HCl + 13% H <sub>2</sub> O	2 hours	<1E5	387 ± 23

The corrosion by fluoride, sulfate and phosphate anions during IPA-vapor dry is examined by spiking the IPA respectively with HF, H<sub>2</sub>SO<sub>4</sub> and H<sub>3</sub>PO<sub>4</sub>. The resistance of aluminum lines after vapor dry is summarized in Tables VII, VIII and IX respectively for fluoride, sulfate and phosphate.

Table VII: Resistance of bare and stacked aluminum meander structures after IPA vapor dry with IPA spiked with fluoride.

Spiking of IPA	Pre-dry time	Resistance (kΩ)	
		Bare	Stacked
Reference	-	271 ± 14	267 ± 25
100 ppb HF	5 min.	277 ± 14	260 ± 40
1 ppm HF	5 min.	284 ± 8	269 ± 22
10 ppm HF	5 min.	282 ± 8	261 ± 40

These data show that  $F^-$ ,  $SO_4^{2-}$  and  $PO_4^{3-}$  are not as aggressive as  $Cl^-$  since the metal lines have not corroded and this when concentrations as high as 10 ppm are used for spiking the IPA. Also the electrical yield does not decrease when these anions are present in the IPA used during an IPA-vapor drying step (data not shown).

Table VIII: Resistance of bare and stacked aluminum meander structures after IPA vapor dry with IPA spiked with sulfate.

Spiking of IPA	Pre-dry time	Resistance (kΩ)	
		Bare	Stacked
Reference	-	$287 \pm 11$	$260 \pm 9$
50 ppb $H_2SO_4$	5 min.	$283 \pm 16$	$265 \pm 10$
1 ppm $H_2SO_4$	5 min.	$282 \pm 14$	$262 \pm 9$
10 ppm $H_2SO_4$	5 min.	$283 \pm 16$	$264 \pm 10$

Table IX: Resistance of bare and stacked aluminum meander structures after IPA vapor dry with IPA spiked with phosphate.

Spiking of IPA	Pre-dry time	Resistance (kΩ)	
		Bare	Stacked
Reference	-	$287 \pm 11$	$260 \pm 9$
50 ppb $H_3PO_4$	5 min.	$293 \pm 11$	$264 \pm 11$
10 ppm $H_3PO_4$	5 min.	$294 \pm 11$	$265 \pm 11$

## CONCLUSION

An IPA-vapor dry step nor a Marangoni dry step cause aluminum lines to corrode when ultra-pure IPA is used. Moisture concentration in IPA is found to be not critical for the drying of metallized wafers: even when wafers are dried with IPA containing 13 % of  $H_2O$ , no corrosion can be measured. Also when traces of n-propanol are present in the IPA, no corrosion is observed. Chloride in IPA is a possible serious cause of corrosion for aluminum during IPA-based drying processes. For the experimental conditions used in this study, however, after IPA-vapor dry a significant corrosion is observed when the chloride level exceeds above 300 ppb. A Marangoni drying process is found to be less sensitive to chloride contamination: corrosion occurs only at chloride levels of 100 ppm. Water acts as a corrosion inhibitor when chloride is present in the IPA. All the other

anions tested (i.e. F<sup>-</sup>, SO<sub>4</sub><sup>2-</sup>, PO<sub>4</sub><sup>3-</sup>) have no effect on the electrical properties of aluminum lines as was verified for IPA-vapor drying up to a concentration of 10 ppm.

#### ACKNOWLEDGEMENTS

Sophia Arnauts, Marcel Lux and Geert Doumen are gratefully acknowledged for their technical assistance.

#### REFERENCES

1. K. Skidmore, Semicond. Intern., **7**, 80 (1989).
2. S. Mackinnon, Microcontamination Conference Proc., **94**, 174 (1994).
3. J. Marra and J.A.M. Huethorst, Langmuir, **7**, 2748(1991).
4. A.F.M. Leenaars, J.A.M. Huethorst and J.J. Van Oekel, Langmuir, **6**, 1701 (1990).
5. P. Neufeld and A.K. Chakrabarty, Corr. Sci., **12**, 517 (1972).
6. T.E. Graedel, J. Electrochem. Soc., **136**, 204C (1989).
7. D. Behrens, in Corrosion Handbook: Corrosive agents and their interaction with materials. Behrens, Editor, Volume 6, p. 177, VCH Publishers, New York (1990).
8. W. Hubler and G. Wranglen, Proc. 4th Scand. Corros. Cong., 60 (1964).
9. J.T. Demo Jr., Chem. Eng. World VII **5**, 115 (1972).
10. P. Hronsky, Corrosion **37**, 161 (1981).

## FIGURES

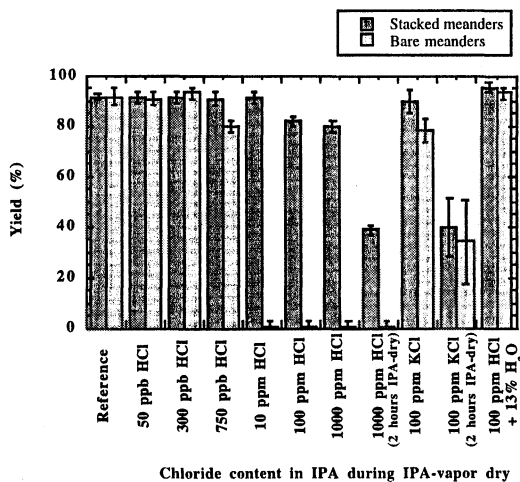


Figure 1: Electrical yield of bare and stacked aluminum lines after IPA-vapor dry when chloride is present in the IPA.

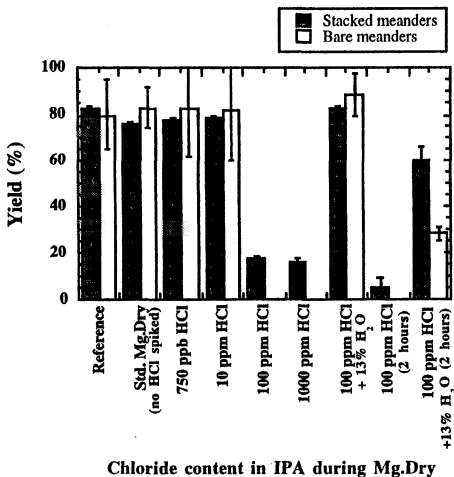


Figure 2: Electrical yield of bare and stacked aluminum lines after Marangoni dry when chloride is present in the IPA.

# NOVEL WET ETCHESES FOR SALICIDE STRIP PROCESSING

Sean O'Brien  
PO Box 650311 MS 3701  
Texas Instruments, Dallas TX 75265  
[sobrien@spdc.ti.com](mailto:sobrien@spdc.ti.com)

A superior method of post-silicide formation wet strip has been developed. This is a dual chemistry sequence involving removal of the unreacted metal followed by a 2<sup>nd</sup> process which is a slight etch of silicide for filament removal. Use of this dual-strip for both TiSi<sub>2</sub> and CoSi<sub>2</sub> technology should result in superior sheet resistance while maintaining excellent isolation leakage performance. The wet metal strip is targeted for an acidic peroxide solution, while the silicide filament etch solution is SC1 for TiSi<sub>2</sub>, or HF for CoSi<sub>2</sub>.

## INTRODUCTION

The traditional form of self-aligned silicide (salicide) processing involves a single wet chemical process which removes unreacted metal from the isolation and sidewall spacers, removes silicide filaments, but leaves the moat/gate silicide mostly untouched (1). In previous work the Ti process has evolved from a totally uncharacterized SC1 process, to a carefully controlled process with adjustable TiN/TiSi<sub>2</sub> etch selectivity.(2)

All of these processes are based on the theory of salicide strip, and a key element of this is the fact that during the etching process the desired silicide species on the gates and moats is being etched during the removal of unreacted metal covering the filaments. It is only after the metal is totally gone that filament removal begins. Loss of desired silicide is thus not minimized, and it can be much higher than the actual filament thickness.

A fully optimized process would remove absolutely zero silicide while the unreacted metal was being stripped, but then begin etching filaments after the metal had cleared. While this cannot be achieved with any single wet chemistry, it is trivial to accomplish using a dual-strip sequence. The 1<sup>st</sup> step is an etch of metal with nearly infinite selectivity to silicide, and the 2<sup>nd</sup> step is a well controlled silicide etch step. Assuming the stoichiometry of the filaments is exactly that of the desired silicide, then loss of silicide is minimized. In some cases it appears that the filament residue actually etches faster than the silicide.

None of the above discussion is specific to the actual metal. Titanium and cobalt salicide technology show virtually identical behavior in the analysis of the strip process sequence. In both technology flows a high selectivity strip of metal followed by a silicide etch result in superb performance. Of course the specific chemistry of both the high and low selectivity wet metal etches differ between the 2.

In titanium technology a peroxide solution is required for the removal of the TiN remaining after  $\text{TiSi}_2$  formation. By lowering the pH of this solution from 10.4 (1:1:5 SC1) to 6.5 ( $\text{H}_2\text{O}_2$ ) to 1.0 (1:1:5 SC2) the  $\text{TiSi}_2$  etch rate drops to zero. Choice of the exact strip chemistry must be based on cost-of-ownership since there is no evidence it impacts device performance and/or yield.

For cobalt there is typically a TiN capping layer which requires the use of peroxide etchants, this actually implies a 3-step strip sequence (TiN then Co then  $\text{CoSi}_2$ ). However, the use of acidic SC2 allows the Co strip to be nearly simultaneous with TiN removal. The underlying Co is essentially gone as soon as the TiN clears because the Co etch rate is so much higher than TiN. Cobalt atoms act as catalysts for decomposition of  $\text{H}_2\text{O}_2$ , and thus care must be taken to ensure low chemical usage. In the SC2 solutions there is no evidence of accelerated decomposition of the  $\text{H}_2\text{O}_2$ , probably due to the formation of chloro-cobalt coordination complexes which interfere with the catalytic decomposition cycle.

The removal of the silicide filaments is again metal-specific, SC1 will easily etch  $\text{TiSi}_2$  while it will not even remove 1 Å of  $\text{CoSi}_2$ . Fortunately IMEC researchers have found that the use of HF allows well controlled  $\text{CoSi}_2$  etching.(3) While the intentional removal of silicide may appear to be politically incorrect, this is exactly what determines the required overetch in the single-step SC1 titanium salicide strip processes. However in those outdated processes the silicide etch is poorly controlled, and usually not even measured. 30-70 Å of silicide must be removed in order to meet the stringent requirements for device isolation. Measurement, control, and understanding of this silicide removal can only improve the device functionality.

SC2 is a 1:1:5 mixture ( $\text{HCl}:\text{H}_2\text{O}_2:\text{H}_2\text{O}$ ) at 50 °C. DSC2 is a 1:10:75 ratio at 50 °C. SC1 is a 1:1:5 room temperature mixture of  $\text{NH}_4\text{OH}:\text{H}_2\text{O}_2:\text{H}_2\text{O}$ .  $\text{H}_2\text{O}_2$  means an undiluted mixture of 30% peroxide at 55 °C. These 150mm wafers were generated with sputtered TiN on a thick  $\text{SiO}_2$  film. For Co wafers 200 Å of TiN was sputtered onto 100 Å of Co on Si followed by RTP formation. 9-point sheet resistance was measured using the Prometrix RS-55. TiN thickness was calculated using 160  $\mu\text{ohm}\cdot\text{cm}$  resistivity.

## TiSi<sub>2</sub> TECHNOLOGY

### TiN Etching

The unreacted metal on the isolation SiO<sub>2</sub> is a TiN layer formed by reaction of Ti with N<sub>2</sub>. While this film is not pure TiN it is reasonably close. Removal of this TiN layer requires a peroxide type solution, the requirement of zero TiSi<sub>2</sub> etch rate drives the pH to lower levels, thus an SC2 solution is the obvious answer. As seen in Figure 1 and 2 the etch rate of sputtered TiN varies in a clear manner with temperature and concentration.

Since the TiN on a real device wafer is actually reacted Ti on oxide those are the type of pilots which should be used for final process window determination. Figure 3 shows the etch of this film. It is important to clear the TiN although a slight underetch may not be relevant since the TiSi<sub>2</sub> etch process will quickly remove any remaining TiN in seconds. As long as the time required to clear remaining TiN is a small fraction of the total TiSi<sub>2</sub> etch time no TiN overetch will be needed in step 1.

Optimization of the SC2 concentration must be based on throughput of the tool. As the concentration drops the etch time increases. As the temperature increases the etch rate increases, but the rate of bath aging is much higher. The bath lifetime of cooler and more dilute SC2 solutions is drastically longer than that of the outdated 1:1:5 80 °C solution thus there is a tradeoff between etch rate and chemical usage.(4) It is quite possible that H<sub>2</sub>O<sub>2</sub> decomposition will be irrelevant in determining the bath lifetime which instead would be based on buildup of particles and other contamination in the tank.

Another alternative is the use of sulfuric acid instead of HCl. Shown in Figure 4 is the etch of TiN in a spray piranha system. There appear to be no significant differences in the use of spray piranha for removal of the metal. Use of O<sub>3</sub>/H<sub>2</sub>SO<sub>4</sub> in a wet bench has not been studied, but it should be give similar results. The temperature of this solution can be raised to 150 °C thus the etch rate would be much higher.

### TiSi<sub>2</sub> Etching

Optimization of the filament removal process must be based on real devices. The most challenging, and therefore the defining structures, are those with shallow-trench isolation (STI) moats. Moat-moat isolation leakage across a 0.15 μm trench is a critical measurement for determining the minimum filament etch required. Narrow gate sheet resistance (0.12 μm lines) will determine the maximum etch which can be tolerated (since the filament etch will remove desired TiSi<sub>2</sub>).

TiSi<sub>2</sub> etching in SC1 has been presented previously.<sup>2</sup> Optimization of the SC1 concentration and temperature again should be based on maximum throughput of the tool. As the concentration drops the etch time increases. It is quite possible that an acceptable process would be a 10-15 minute etch in a 1:1:100 room temperature SC1. The bath

lifetime of such dilute SC1 solutions is quite possibly irrelevant in determining the change frequency and total chemical usage. In a multi-batch wet bench, the SC1 concentration can be dropped until the etch time matches the metal strip time without any impact to throughput.

## CoSi<sub>2</sub> TECHNOLOGY

### TiN & Co Etching

The TiN capping layer on the Co interferes with choosing an optimum process. In any solution with acidic pH the Co metal etches in a pure electrochemical process. The oxidation of the metal proceeds virtually independent of the exact identity of the chemical present. Thus it should be trivial to find a Co etch solution, extremely dilute HCl solutions are known to work easily. The etch rate of cobalt metal in a 1:200 50°C HCl solution is about 20 Å/min. However, the TiN layer drives the process towards that used in the preceding section, some type of dilute SC2.

As seen in Figure 5 the underlying CoSi<sub>2</sub> layer has only minor impact on the removal of the TiN cap. Removal of 200 Å of TiN in 10 minutes is very comparable to the DSC2 data in Figure 1.

### CoSi<sub>2</sub> Etching

Removal of CoSi filaments using HF should be easily achieved. Some extremely interesting chemistry is occurring because CoSi has a very high etch rate in 1000:1 HF as shown in Figure 6 (CoSi was used because there are probably no CoSi<sub>2</sub> filaments).

## PROCESS OPTIMIZATION

Optimizing this process should be based on cost of ownership since no device impact has been found within a reasonable process window. The total throughput of a processing tool varies widely depending on whether it is a single batch tool (full-flow or spray) or a multiple batch tool (wet bench). Chemical usage can be reduced which leads to longer etch times which leads to lower throughput. However, lower chemical concentration should result in much shorter rinse times thus saving water consumption and increasing throughput. It is not at all obvious whether a dilute chemistry process with long etch and short rinse times is superior to a concentrated process with shorter etch and longer rinse times. Total tool throughput and chemical/water usage must be calculated/measured for a very wide range of parameters in order to determine the truly optimized process.

A critical factor is bath aging, the tool cannot be used during replacement of the chemical bath. The stability of a wet etch solution depends on many factors. The heated

SC1 solution is one of the few in the semiconductor industry where the etch rate and selectivity change drastically with bath usage and aging. Evaporation of NH<sub>3</sub> and decomposition of H<sub>2</sub>O<sub>2</sub> lead to poor process control.

The dual-strip process almost totally eliminates this concern. The high selectivity of the metal etch step is not compromised with bath lifetime. Even though H<sub>2</sub>O<sub>2</sub> decomposes in SC2 solutions, an overetch does not impact the device wafers. Thus the metal strip can be configured so that wafers running in a fresh solution get a long overetch and wafers running in very old solution will just barely receive a sufficient etch.

The silicide etch process must be controlled but since this is done with a concentrated SC1 solution at room temperature there is much less change in etch rate over the age of the bath.

## CONCLUSIONS

A superior salicide strip process has been developed called the dual-strip sequence where the unreacted metal is removed with high selectivity to the silicide followed by a slight silicide etch for filament removal. This technique is useful for both Ti and Co silicide technology, and should apply for Ni also. The advantage of this sequence is that desired silicide on the gates and moats is not etched during the removal of the unreacted metal, thus resulting in lower device sheet resistance. In addition, the process stability of the etch solutions is easier to achieve if metal to silicide etch selectivity is no longer relevant.

## ACKNOWLEDGMENTS

I would like to thank Jorge Kittl, Qi Zhong Hong, and Terrence Breedijk for contributing pilot wafer flows, special processing, and important conversations. Thanks also go to Doug Prinslow as a co-inventor of the dual-strip salicide process. Jackie Kemp deserves all the credit for SEM inspection and getting the wafers ready for processing.

## REFERENCES

1. M.E. Alperin *et al*, IEEE Trans. on Elect. Devices, ED - 32(2), p. 141 (1985).
2. S.C. O'Brien and D. Prinslow, UCPSS, Antwerp (1996).
3. M.R. Baklanov, *et al*, J. Electrochem. Soc. 143(10) p. 3245 (1996).
4. T.Q. Hurd, *et al*, 40th Institute for Environmental Science, Annual Technical Meeting 1994 Proceedings Vol. 1, p. 218 (1994).

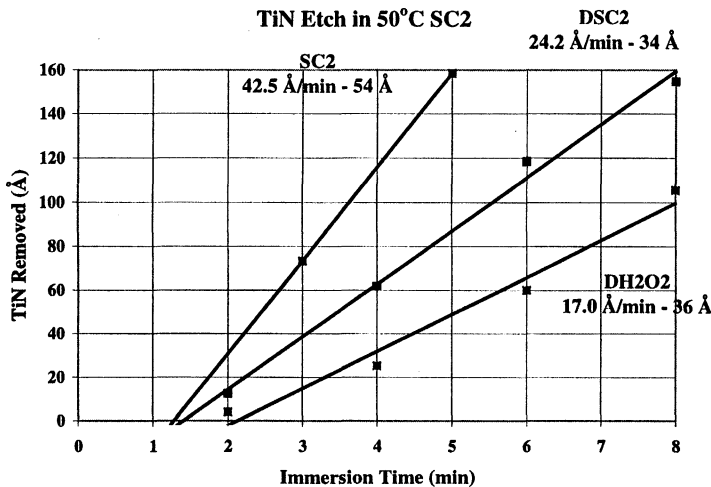


Figure 1 Sputtered TiN etch rate in H<sub>2</sub>O<sub>2</sub> solutions of various pH levels. DH<sub>2</sub>O<sub>2</sub> (6:1 dilution) has a pH of 7, DSC2 has a pH near 2, and SC2 is closer to 1. An initiation period of about 1 minute is seen on all sputtered TiN wafers.

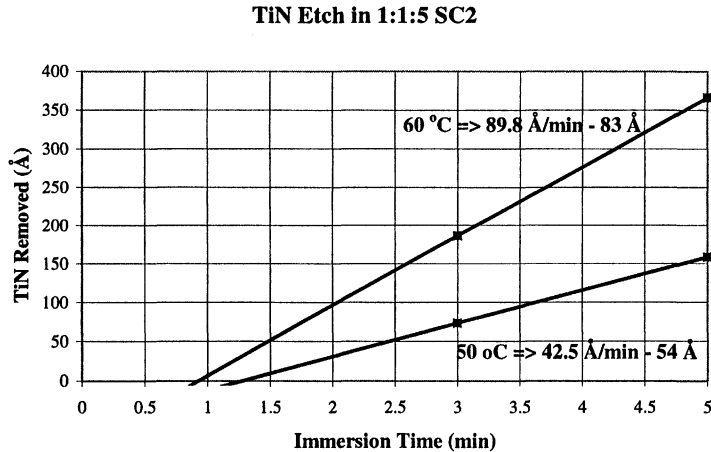


Figure 2 Temperature dependence of TiN etch rate in SC2. An activation energy of 0.693 eV is calculated from this data.

### Formed Ti etch in DSC2

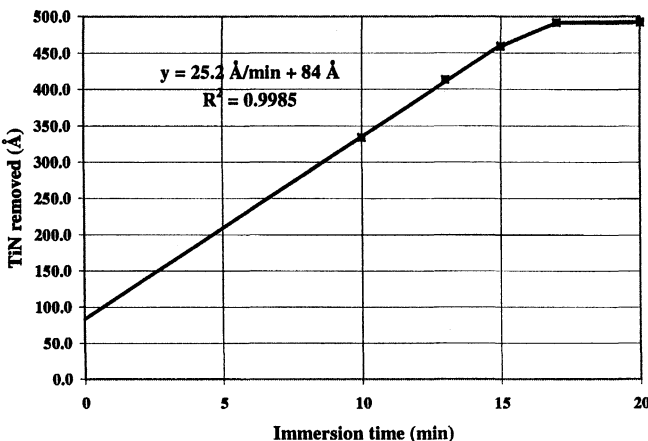


Figure 3 Etch rate of formed TiN in SC2. The y-intercept is a result of incompletely reacted and fast etching Ti on top of the TiN. The optimum process time is 17 minutes.

### TiN Etch in Spray Piranha 95 °C

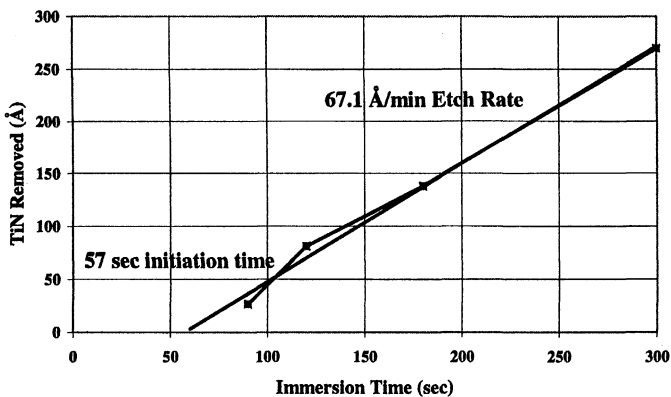


Figure 4 Etch rate of sputtered TiN in 95 °C spray piranha.

### TiN/CoSi Etch in DSC2

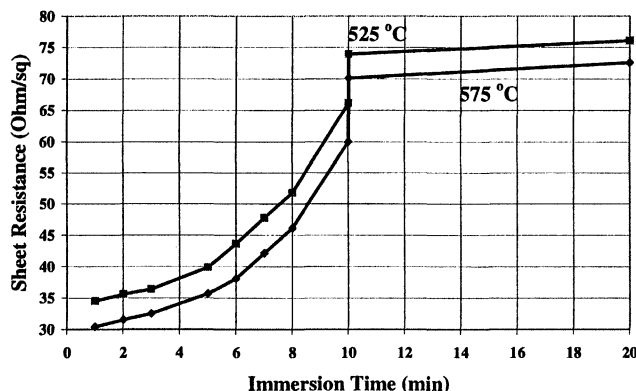


Figure 5      Etch of sputtered TiN on CoSi in DSC2 for 2 different CoSi formation temperatures.

### CoSi ER in 1000:1 HF

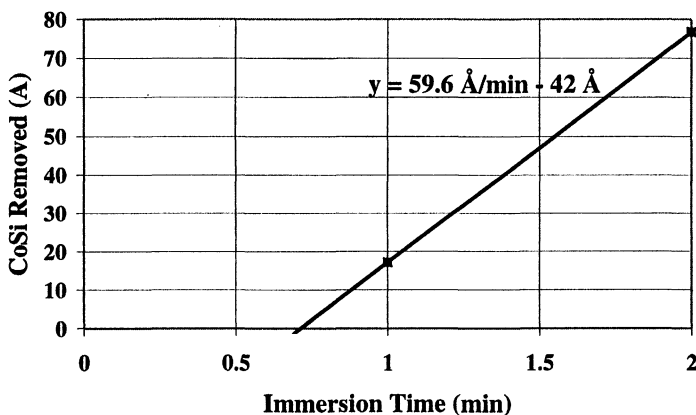


Figure 6      Etch rate of CoSi in 0.049% HF.

# **POST METAL ETCH POLYMER REMOVAL PROCESS**

## **THE ELIMINATION OF AN INTERMEDIATE RINSE STEP**

Sandra W. Graham  
SEMITOOL, Inc.  
655 W. Reserve Drive  
Kalispell, MT 59901 USA

### **ABSTRACT**

To achieve the necessary device performance, complete removal of residual polymer created during the plasma etch and photoresist strip process is critical. In addition, it is essential that the residue removal process not compromise the integrity of the metal lines. This work evaluates the impact of various post metal etch polymer removal processes on corrosion and/or attack of Al-Cu-Si metal lines. Two of the five process sequences evaluated resulted in no attack or corrosion of the metal lines.

### **INTRODUCTION**

In the design and manufacture of semiconductor devices, the geometry of the interconnect metal lines and the resulting resistance of these lines has a major impact on the speed and performance that the device can achieve. Residues that form during the plasma etch and photoresist strip processes can contribute to an increase in the resistance of the metal lines and a reduction in the device performance. The removal of these residues, a process commonly referred to as polymer removal, is necessary prior to subsequent processing of the device.

Elemental analysis of the polymer residue reveals that it consists of the same components as the metal lines themselves (1). It follows then that the chemicals used to remove the post etch residue are also capable of attacking the metal lines. This attack is often initiated by the introduction of deionized (DI) water onto the surface of the wafer while chemical is still present (2). The use of an intermediate rinse chemistry between the application of the chemical and the DI water rinse eliminates metal attack (2), but it also increases the chemical consumption and decreases the throughput of the process.

The objective of this study was to develop a polymer removal process for post metal etch that eliminates the attack and/or corrosion of the metal lines without the use of an intermediate rinse chemical. Process performance will be based on visual inspection of the wafers using an optical microscope and a SEM.

## BACKGROUND

Fluorine containing chemical solutions such as Ethylene Glycol/NH<sub>4</sub>F and Ethylene Glycol/HF/NH<sub>4</sub>F have been widely used in the semiconductor industry for the removal of post etch residue from metal lines. The use of an intermediate rinse chemical such as Ethylene Glycol has been necessary when using these types of chemicals in order to inhibit corrosion of the metal lines.

Scully, et. al., studied the corrosion characteristics of Al-0.5% Cu thin film in the presence of dilute ( $10^{-3}$ M) aqueous HF solutions (3). They found that attack of the metal film could be inhibited by sparging the dilute HF solution with CO<sub>2</sub> (4). Scully, et. al., postulate that the CO<sub>2</sub> passivates the metal, producing a more homogeneous, defect-free oxide film.

Mayumi, et. al., studied the impact of corrosion on contact failures (5). Al-0.9%Si-0.4%Cu films were exposed to various concentrations of fuming HNO<sub>3</sub>. The density of pits in the metal lines (corrosion) increased and then decreased as the concentration of fuming HNO<sub>3</sub> increased. For high concentrations of fuming HNO<sub>3</sub>, there were no pits or corrosion. Mayumi, et. al., attribute this result to the oxidizing power of the fuming HNO<sub>3</sub> solution. As the oxidizing power increases, the passivating film that forms on the Al alloy surface becomes more robust.

## EXPERIMENTAL

The wafers used in this experiment were 200 mm shortloop wafers. The films on the silicon wafers consisted of a hard mask on top of Al-Cu-Si over a TiN barrier layer on a blanket layer of P-TEOS. The metal etch process used BCl<sub>3</sub> and Cl<sub>2</sub> gases and was performed in an ECR etcher. The metal etch was followed by an H<sub>2</sub>O/O<sub>2</sub>/CF<sub>4</sub> ash and a hot DI water rinse. Wafers were then placed in a spray solvent system (SST) for post metal etch polymer removal using a NH<sub>4</sub>F-containing aqueous chemical (ELM-C30).

**Table I**

Test	Concentration of NH <sub>4</sub> F	Polymer Removal Sequence
Control Process	1.02 M (wafer #1)	Chemical followed by a DI water rinse and a heated N <sub>2</sub> dry.
Test condition 1	1.02 M (wafer #10)	Chemical followed by an IPA intermediate rinse, a DI water rinse and a heated N <sub>2</sub> dry.
Test condition 2	1.7 * 10 <sup>-1</sup> M (wafer #15)	Chemical followed by a rinse in CO <sub>2</sub> saturated DI water and a heated N <sub>2</sub> dry.
Test condition 3	2.0 * 10 <sup>-1</sup> M (wafer #13)	Chemical with CO <sub>2</sub> bubbled into it prior to delivery to the wafers, followed by a rinse in CO <sub>2</sub> saturated DI water and a heated N <sub>2</sub> dry.
Test condition 4	1.02 M (wafer #20)	Chemical followed by an ozonated DI water rinse and a heated N <sub>2</sub> dry.

The shortloop wafers were processed in the spray solvent system under a variety of conditions as summarized in Table I. The concentration of NH<sub>4</sub>F in the chemical is also listed in Table I for each test. Wafers were visually inspected for attack and thinning of the Al-Cu-Si metal lines using an optical microscope and a SEM.

## RESULTS AND DISCUSSION

A summary of the results are included in Table II. Visual inspection of the control wafer with an optical microscope revealed a discoloration of the metal lines, indicating a thinning of the lines. This observation was confirmed with SEM inspection.

Scully, et. al., (3) concluded from their study that aluminum alloy films exhibit localized breakdown of the passivating film and subsequent micropitting of the aluminum alloy when exposed to dilute fluoride solutions. This appears to be the mechanism that is responsible for attack of the metal lines on the control wafer.

The addition of an intermediate rinse to the process (i.e., test 1) eliminated the metal attack, but increased the process time and the chemical consumption. Tests 2 through 4 were performed in an effort to determine if an acceptable process could be developed that did not include an additional rinse step.

Test 2, which included the use of CO<sub>2</sub> saturated DI rinse water, was not successful at eliminating the metal attack. The use of CO<sub>2</sub> saturated DI rinse water was tried for several different concentrations of NH<sub>4</sub>F. The severity of the metal attack was proportional to the amount of NH<sub>4</sub>F, i.e., the higher the NH<sub>4</sub>F concentration, the more

severe the metal attack. However, the lower the  $\text{NH}_4\text{F}$  concentration, the less effective the chemical was at removing the post etch residue. These results were also observed for Test Condition 3.

**Table II**

Test	Process Description	Optical Inspection Results	SEM Inspection Results
Control process	No intermediate rinse between the chemical and the DI water rinse.	Attack and thinning of the metal lines.	Thinning of the metal lines.
Test Condition 1	IPA rinse in between the chemical and the DI rinse process.	No attack or thinning of the metal lines.	No thinning or attack of the metal lines. See Figure 1.
Test Condition 2	$\text{CO}_2$ injected into the DI rinse water (no intermediate rinse).	Evidence of thinning and attack of the metal lines.	Thinning of the metal lines. See Figure 2.
Test Condition 3	$\text{CO}_2$ bubbled into the chemical, followed by a $\text{CO}_2$ saturated DI water (no intermediate rinse).	Some of the wafers exhibited no metal attack, whereas other wafers did show signs of metal attack.	Thinning of the metal lines. See Figure 3.
Test Condition 4	$\text{O}_3$ injected into the DI rinse water (no intermediate rinse).	No thinning or attack of the metal lines	No thinning or attack of the metal lines. See Figure 4.

The use of an ozonated DI water rinse (i.e., test 4) was successful at eliminating the metal attack and corrosion while effectively removing the post etch residue from the surface of the wafer. It is postulated that the ozonated DI water passivates the metal lines faster than the fluoride solution can breakdown the passivating film. Ozonated DI water has a higher redox potential than  $\text{HNO}_3$  (6). It follows that if fuming  $\text{HNO}_3$  can form a strong passivating film (5) then a stronger oxidizer, such as ozonated DI water, would also be capable of forming a passivating film that would be robust enough to withstand breakdown caused by dilute fluoride solutions.

## CONCLUSIONS

Results of these experiments indicate that the use of O<sub>3</sub> can eliminate the need for an intermediate rinse chemical in a post metal etch residue removal process. The use of O<sub>3</sub> inhibits the metal attack and corrosion that can occur when DI water is introduced onto the surface of a wafer where a fluorine containing solution is present.

*This paper was presented at The 1997 Joint International Meeting of the Electrochemical Society and the International Society of Electrochemistry held in Paris, France August 31 - September 5, 1997. This paper will be published in the Symposium Proceedings: Cleaning Technology in Semiconductor Device Manufacturing V, to be published 1/98.*

## REFERENCES

1. Y. Wang, S.W. Graham, L. Chan, S.T. Loong, J. Electrochem. Soc., **144**, 1523 (1997).
2. P.L. Pai, C.H. Ting, W.M. Lee, R. Kuroda, (Metal Corrosion in Wet Resist-Stripping Process) Interface '89, KTI Microelectronics Seminar (1989).
3. J.R. Scully, R.P. Frankenthal, K.J. Hanson, D.J. Siconolfi, and J.D. Sinclair, J. Electrochem. Soc., **137**, 1365 (1990).
4. J.R. Scully, R.P. Frankenthal, K.J. Hanson, D.J. Siconolfi, and J.D. Sinclair, J. Electrochem. Soc., **137**, 1373 (1990).
5. S. Mayumi, I. Murozono, H. Nanatsue, and S. Ueda, J. Electrochem. Soc., **137**, 1861 (1990).
6. T. Ohmi, in Cleaning Technology in Semiconductor Device Manufacturing, R.E. Novak and J. Ruzyllo, Editors, PV **95-20**, p.1, The Electrochemical Society Proceedings Series, Pennington, NJ (1996).

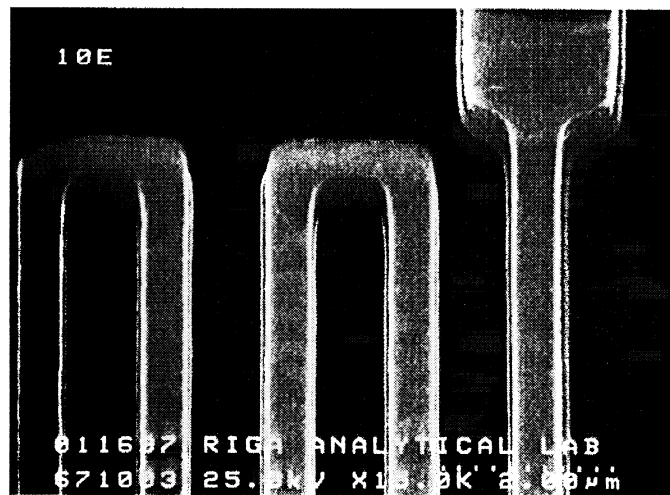


Figure 1. SEM photograph of wafer processed using Test Condition 1: IPA rinse in between the chemical and the DI rinse process.

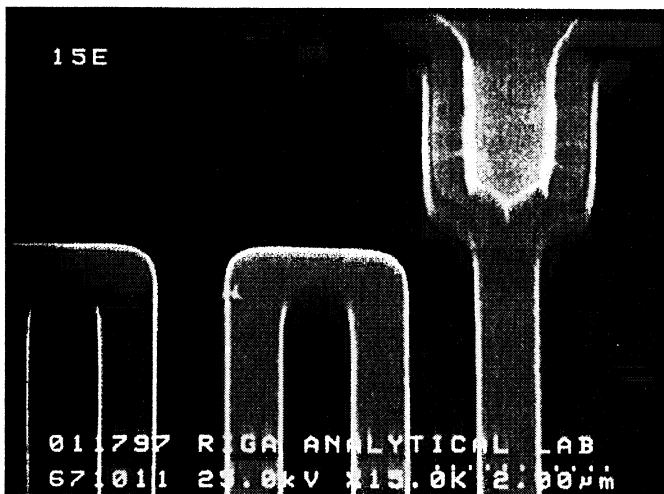


Figure 2. SEM photograph of wafer processed using Test Condition 2: CO<sub>2</sub> injected into the DI rinse water and no intermediate rinse.

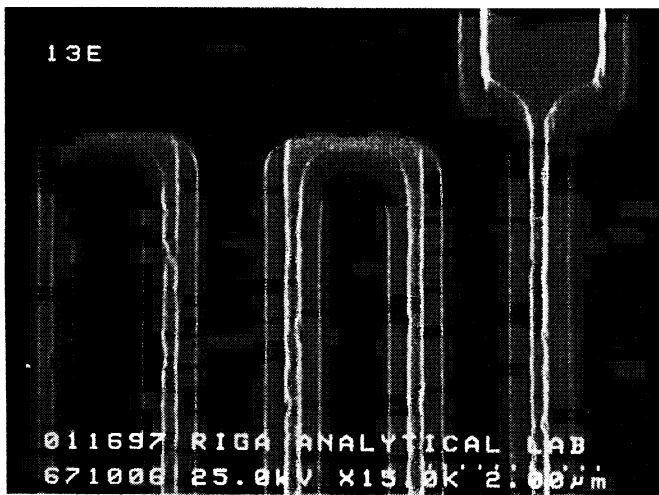


Figure 3. SEM photograph of wafer processed using Test Condition 3: CO<sub>2</sub> bubbled into the chemical, followed by a CO<sub>2</sub> saturated DI water and no intermediate rinse.

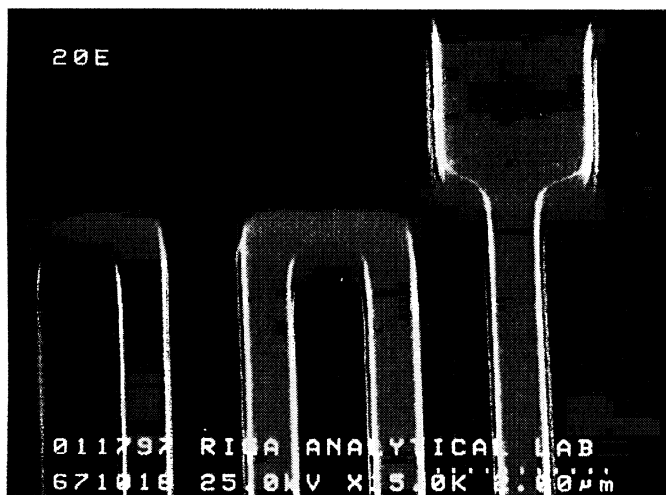


Figure 4. SEM photograph of wafer processed using Test Condition 4: O<sub>3</sub> injected into the DI rinse water and no intermediate rinse.

# **MOBILE ION CONTAMINATION AND DEFECT REDUCTION ON A POST-METAL ETCH CLEAN PROCESS**

K. E. Mautz, Ph.D.  
Motorola, Inc., Semiconductor Products Sector  
505 Barton Springs Rd., Suite 1050  
Austin, Texas 78704

Mobile and alkali ion contamination was monitored by Secondary Ion Mass Spectrometry techniques on sample wafers pulled after specific manufacturing steps. Equipment and process steps contributing to the ionic contamination were identified and modified to reduce the effect. Mobile and alkali ion contamination in dielectric oxides was reduced by the utilization of a clean process that removes the damaged oxide surface after plasma etch processing steps. Characterization of the clean process parameters that contributes to ionic contamination removal was done, as well as particle and defectivity reduction by process and equipment optimization.

## **INTRODUCTION**

The movement of alkali contamination in dielectric oxides has been a critical issue during the evolution of integrated circuit devices. Research on this topic has revealed the negative effects of this contamination (typically sodium, potassium and lithium ions) on electronic device performance due to its migration into transistor structures.

Ionic contamination reduction techniques were investigated following an analysis of mobile and alkali ion concentration and location on, or within the dielectric oxide films is discussed. Identification and monitoring of ionic contamination is typically done with Secondary Ion Mass Spectrometry (SIMS). Improvement in the sampling procedure and analysis of the SIMS data was accomplished during this study. Metallic contamination consisting of alkali metals and other mobile ions in dielectric oxides can be efficiently measured by generating SIMS-acquired depth profiles of the film [1, 2]. The identification of tools, processes, or materials that cause the ionic contamination and the resultant corrective actions to effectively lower the contamination in the circuit are discussed. An improvement of over 3 orders of magnitude was accomplished during this study [1-4].

## **EXPERIMENTAL**

Alkali ion contamination data in dielectric oxides were obtained using SIMS depth profiles with a spectrometer tool. The primary ion beam was 3.5 microamps of 15 KeV oxygen ions that impact the sample surface with a kinetic energy of 11.5 KeV, and the 4.5 KeV sample biasing provides the secondary ion acceleration. The primary ion beam was focused to a 65 $\mu$  spot size and rastered in a 250 $\mu$  square. The secondary contaminant ions from the collimated 62 $\mu$  circular collection area in the center of the sputter crater are counted

as a function of sputtering time. Typical mass resolutions are greater than 2000, especially for sodium.

Experimentation on the post-metal batch clean process equipment factors was done to determine the effects on dielectric film removal non-uniformity using film thickness metrology, and the reduction on overall integrated circuit alkali contamination was monitored by SIMS. Automated oxide film measurements were made using 9 data point locations per sample wafer. The plasma metal etch process that exposes the dielectric oxide to alkali contamination, was a RIE hexode tool set with a chlorine-based plasma chemistry. The oxide planarization process used a RIE hexode reactor with a fluorine-based chemistry. The ash was done using a stand-alone, heated chuck-downstream tool. Defects were measured using light scattering metrology and defects were imaged with SEM.

## RESULTS AND DISCUSSION

The monitoring technique uses SIMS to produce concentration depth profiles at the interface or within the dielectric oxide film. Alkali ions are initially present on the surface of the oxide film due to post-deposition processing, and within the oxide from process chamber contamination on control wafers. Ions on the surface can diffuse into, and migrate through the oxide due to thermal processing and mobility factors [1, 2]. The SIMS depth profile charts plot the mobile ion log count rate over the sputter time of the sample. The profile of a completed integrated circuit would contain the following characteristics: 1) an initial rise in silicon from the oxide passivation film, 2) a subsequent rise in aluminum ultimately rising above the silicon curve (indicating the metallization level) and slowly falling until crossing below the silicon curve (indicating the dielectric oxide layer interface), and 3) during the aluminum rise, alkali and other mobile ions begin to increase significantly and generally reach maximum near the metal-dielectric interface and either decay slowly or significantly thereafter, depending on the type and cleanliness (ionic contaminating potential) of the manufacturing processes used. Integration of the area below each ionic curve (using the aluminum-silicon crossover points as a layer markers) determines the concentration of the particular ion. Figure 1 displays a SIMS depth profile spectra after metal etching and a solvent clean with these characteristics.

Some assumptions are made in using this SIMS analytical approach. These include: 1) no homogeneous matrix, 2) the ionization cross-section for alkali metals in the silicon-oxygen-aluminum substrates with oxygen ion excitation is close to unity, and 3) subsequent integrated circuit manufacturing steps can affect the alkali metal ion distribution within the oxide film. To minimize this latter case, numerous samples are taken at various stages within the manufacturing process, and on a standardized test structure for each critical process tool.

To determine the alkali ion contribution from manufacturing processing blocks (multiple film and lithography steps), modules (individual layers), and operation steps (individual tool processes), samples are taken from each of these categories. For this sampling, test structures consisting of the module's basic film structures, or dielectric oxides (for non-deposition processes) can be used to reduce testing on valued device wafers. These samples are processed through the various steps (usually run in sequential operation steps) using 2-3 wafers per step along with control wafers, and all wafers are SIMS analyzed as a group. Using this sampling technique, it was determined that the

addition of alkali and mobile ions within integrated circuits are from several distinct processing steps, and the reduction of ionic contamination within each step was accomplished by experimentally determining the source of the contamination [1, 2].

The largest contributors to alkali and mobile ion contamination were the following: 1) plasma oxide etches, 2) plasma metal etches, 3) the plasma planarization etch of the dielectric oxide, 4) solvent cleaning of the dielectric oxide and patterned metal films, 5) metallization film deposition, and 6) dielectric oxide film deposition. The oxide and planarization plasma etches used materials (both process chamber parts and masking films) that were high in alkalis, and these were being driven into the oxide by the high dc bias conditions. The plasma metal etch and oxide planarization processes remove a significant amount of photoresist (which can contain significant amounts of alkali and other metallic ions) and this results in alkali contamination residue on the dielectric oxide. Solvent clean solutions used to remove post-etch or ash artifacts were found to contain moderate levels of alkali contamination initially, and the alkali concentration was decreasing as wafers were processed through the clean. The solvent solution added alkali contamination to wafers with exposed dielectric oxides and patterned metallization. The type of dielectric oxide was significant also, with PSG more strongly affected than BPSG, TEOS or thermal oxide films [2]. The metallization and dielectric oxide deposition equipment were found to contain high levels of alkalis due to the chamber clean materials and procedures used. All of these listed conditions were subsequently corrected and the reduction in alkalis on test structures and integrated circuits were verified by SIMS testing over time.

Significant alkali and mobile ion contamination was found to be added to the dielectric oxide films from the plasma metal etch process. This process utilizes high dc bias potentials on the wafer and low process pressures to produce anisotropic (directional) plasmas that result in metal lithography with vertical sidewalls. These process conditions also accelerate positively charged alkali and mobile ions in the plasma toward the wafer surface (ion bombardment). When the metal layer has cleared exposing the dielectric oxide underlayer, the ions can be implanted into the oxide. The depth that the ions are implanted into the oxide film is a function of the metal etch process conditions (such as dc bias and process pressures), ionic contaminant factors (such as mass/charge ratio and ionic size), and oxide film features such as density and physical surface conditions (mobility factors). Roughened oxide film surfaces (due to the ion bombardment sputtering and chemical etching of the surface) may allow the ions to penetrate into the film structure. Plasma oxide planarization etch processes show a similar effect especially from the photoresist layer clearing on the oxide film topography features.

The alkali and mobile ions then will migrate deeper into the oxide film during subsequent high temperature (greater than 300C) processes where they can affect electrical device performance (causing premature failure and reliability issues). Processes within the metal etch module are typically below 300C (for metal etch and ashing steps). Significant ionic contamination can also occur on the oxide film surface as a result of these plasma steps. This can be easily removed during wet processing steps (which are usually done following ashing or as a preclean to the next deposition step) such as DI water rinsing (immersion or spray processes) or solvent cleans (using alkali-amine solutions followed by intermediate solvent and DI water rinsing). Removal of the implanted alkali and mobile ion contamination is more difficult and cannot be removed by surface rinsing. The distribution of the contamination in the oxide film after the plasma metal etch reaches a maximum at a shallow depth (10-100Å) and rapidly decreases with depth of 200-350Å, where 90% of the plasma metal etch process induced contamination is contained.

The distribution of all contaminant ions in the oxide film differs due to the previously mentioned mobility factors. Subsequent processing steps involving long thermal cycles drive the ionic contaminants deeper into the oxide film. To prevent this effect, removal of the plasma damaged and contaminated oxide surface (skin) can be done following the plasma metal or oxide etch and ash process. Cleaning with dilute buffered hydrofluoric acid (BOE) chemistries can remove the oxide film uniformly to a controllable depth. The ionic contamination remaining would be inherent to the oxide film during deposition (due to processing, chemical purity, chamber conditions, vacuum integrity, etc.). This clean process was used to replace the solvent clean process that was adding alkali contamination to wafers. Figure 2 shows the SIMS depth profile after removal of the contaminated oxide surface using the BOE etchant clean solution process.

The alkali contaminated surface of the dielectric films from the post-etch processes was removed using the dilute BOE acid clean process in a batch spray chamber. Critical process parameters were identified and characterized to optimize the clean process. This process was optimized to gain additional reduction of the overall ionic contamination level. In addition, defectivity from a batch clean step following a metal etch and ash process was also characterized and analyzed using SIMS. The defects studied were particulate and veil polymer residue and were causing inspection failures and yield issues. Wet chemical spray batch processes are efficient in removing both defects with high throughput. Prior to introducing this tool into processing, characterizations were done to understand the mechanisms and process sensitivities to particle addition or removal, and veil polymer removal. These characterization results were used to create a process recipe to be used in volume processing of wafers. Metal etch processes use polymer-producing steps for corrosion control and maintaining sidewall integrity. These processes also produce particles due to chamber polymer deposit flaking (organic), or can trap other particles generated by mechanical movement (metallic). Veil polymers form on the surfaces of the metal lines and cannot be removed by DI water rinsing. The batch spray tool clean process is then relied on to remove these defects prior to the next deposition step [5].

The equipment used for removing the metallic ion-contaminated oxide surface was a dual-chamber, batch spray tool that combined: 1) a preclean rinse wetting step, 2) a clean step, 3) an intermediate rinse, 4) a deionized (DI) water rinse, and 5) various spin dry cycles. The clean chemistry was a dilute solution of buffered oxide etchant (HF-based) mixed with ethylene glycol, with or without a surfactant. The intermediate rinse was ethylene glycol at an elevated temperature. The clean process steps were also characterized and modified to remove particles created during or remaining after the metal etch process and ash step, and to remove the post-etch artifacts (veil polymer) that decorate the top surfaces or sidewalls of the metal lithography. Figure 3 shows an example of post-metal etch veil polymers. These polymers are produced by an interaction of the metal etch plasma chemistry acting on the photoresist skin and from back-sputtered aluminum and underlying oxide films. Spectral analysis of the veil polymer revealed these to be an inorganic mixture of aluminum and silicon oxides with metallic and organic contaminants. The primary constituent has been identified as  $\text{Al}_2\text{SiO}_5$  [6]. Various methodologies of wet chemical and vapor phase clean processes have been used to remove veil polymers and particles [6-8]. The clean step process was originally designed to remove the veil polymers without significantly damaging the underlying oxide surface and reduce the overall particle levels on the wafers (as compared to a DI water rinse only) [5].

Screening and characterization experiments were done on the clean process step using three oxide types: 1) TEOS (PECVD), 2) BPSG, and 3) a thermal oxide (Fox). The primary outputs for this characterization were the oxide film removal and non-uniformities. Four clean solution compositions were tested: 1) 4:1 (EG:BOE) without a surfactant, 2) 4:1 (EG:BOE) with a surfactant, 3) 3:1 (EG:BOE) without a surfactant, and 4) 3:1 (EG:BOE) with a surfactant. Three cassette wafer positions were used in this test, located at the forward (near door), middle, and rear of the cassette with bare silicon wafers occupying the other slots. All samples of oxide wafers was measured for oxide removal and non-uniformity to produce an average run value. The clean process step parameters varied were: 1) etchant solution temperature, 2) etchant solution clean time, 3) etchant flow, and 4) wafer cassette rotation speed [5].

The results of the clean process step parameter experimentation were as follows. The effectiveness of the clean process for oxide removal and non-uniformity was strongly affected by the: 1) temperature of the clean solution and intermediate rinse, 2) process step time of the clean solution, intermediate rinse and DI water rinse (in decreasing significance), 3) solution flow of the clean solution and intermediate rinse, and 4) spin speed of the clean, intermediate, and DI water rinse, with numerical groupings listed in decreasing significance. Temperature strongly affects both the oxide film thickness removed and non-uniformity of all oxide types. The 4:1 clean solution showed a stronger temperature effect than the 3:1 clean solution. As the temperature increased on both clean solutions, the non-uniformity improved (lower values) [5]. Longer clean solution step times resulted in higher effective oxide film removal and lower non-uniformities as expected. Higher clean solution flow pressures had a mixed effect on oxide removal and non-uniformities. For the 4:1 clean solution, TEOS and BPSG oxide films showed no effect on oxide removal and a slight decrease in the non-uniformity. On the Fox film there was a slight increase in the oxide removal and no effect on the non-uniformity. For the 3:1 clean solution, all oxide films increased slightly in oxide removal values, and non-uniformity values increased on TEOS, decreased on BPSG, and remained practically the same on the Fox film. Faster spin speeds caused a significant decrease for the 4:1 clean solution oxide removal and a slight decrease in all oxide type non-uniformities. Faster spin speeds on the 3:1 clean solution resulted in lower oxide removal, with the BPSG and Fox film non-uniformities increasing and the TEOS decreasing with higher spin speeds [5].

On spray clean tools the effects of an optimized rotation speed and cleaning time for removal of organics and metallic contamination has been described [9]. Overall, the oxide thickness removed was higher (as expected) on the 3:1 clean solution and the non-uniformities were lower. For the entire experiment, the spread of the data values for the BPSG and Fox non-uniformities were larger than expected. The clean step process parameters were chosen to minimize oxide loss (to targeted values) and non-uniformity values using slower spin speeds with medium flows for short step times. Surfactant addition to the clean solutions improved the non-uniformity values slightly (by 5-10%).

The other clean process recipe steps were investigated in terms of defectivity removal and particle additions. Optimum drying step times without particulate additions were found to range from 115-145% of the time required for water droplet clearing from the wafer edges during the spin dry cycle. Decreasing the dry spin speed (by 50%) during the last half of the step reduced particle levels by approximately 5%. The maximum temperature of the drying gas ( $N_2$ ) had a higher significance than the spin speed on the overall drying efficiency. Temperature effects in spray clean tools have been found to increase the

effectiveness of particle removal from surfaces [10]. The intermediate rinse step time was required to be greater than 1 minute with medium spin speeds and high flow to remove the clean solution and particles rapidly from the wafer surface. An elevated solution temperature (greater than 40C) was used to quickly and efficiently remove the clean solution from the wafers and prevent streaking. The DI water rinse time required greater than 3 minutes, with slow spin speeds at medium flows for effective rinsing. The preclean rinse was found to possess a wide process window. A short step time (less than 45 seconds) was needed to adequately wet all wafers in the cassette. The addition of the preclean step improved the clean step oxide removal non-uniformity value by 15-20% [5].

Characterization of the veil polymer removal times was done on test wafers with heavy veil formation. SEM analysis was used to determine the results after various clean solution exposure times, using the standard rinse and dry process. Veil formation was significantly reduced after 15 seconds of chemical exposure on all chemistries (using the baseline process parameters for all other process factors). After 25 seconds all but the heaviest veils were removed. The 35 second process time resulted in complete removal of all veil material. Surfactant addition had no measurable impact on the veil removal times. There was no apparent difference between the 4:1 and 3:1 (EG:BOE) clean solutions. Other process factor data indicated that damage to metal lithography was seen when using hot DI water rinses as opposed to cold (ambient) temperatures. There appeared to be a seasoning issue with the state of the spray process chamber. The process outputs were more consistent when running metal lithography tests on a chamber that was periodically rinsed during long periods of idle time as opposed to a chamber that was left dry for extended periods [5].

Wafer streaking defects can be caused by non-optimized batch clean processes. Two types of process-related wafer streaking were observed during this characterization. These were: 1) radial-caused by etched striations in the underlying oxide, and 2) irregular-crystalline defects occurring in random lines or areas. Radial wafer streaking occurred when the intermediate rinse was delayed or if the spin speed was increased prior to the intermediate rinse (done to promote removal of the clean solution). Radial streaking could also occur if the chemical manifold was purged of clean solution (with the cassette still spinning) prior to the intermediate rinse, producing etched striations in the underlying oxide. The streaking defects were prevented by modifying the overall clean process recipe, which included eliminating the offending steps [5].

The irregular crystalline defects were not due to the spray process recipe or tool factors. These were produced from an interaction of a hot wafer surface and clean solution exposure. Following the ash step, wafers are exited at a temperature in excess of 200C in a teflon cassette. If these wafers/cassette are placed into the batch spray processor without an adequate cool-down period (between 5-10 minutes) the last wafers that were ashed would be at a temperature high enough to rapidly evaporate the carrier solvent leaving wedge-shaped crystalline defects (primarily consisting of ammonium fluoride). This would serve as a mask on the underlying oxide during clean solution exposure that would replicate the wedge-shaped defects into the oxide prior to the ammonium fluoride re-dissolving into the solution. Veil removal on the metal surface was not affected due to the ability of the clean solution to re-dissolve the crystal. The lifetime of the crystalline mask on the wafer surface was determined to be less than 10 seconds. Analysis of the defects after completion of the process showed only the oxide background remaining. The linear pattern of the defects was due to the spray pattern from the manifold. The insertion of the preclean rinse step to reduce the wafer temperature and provide better wetting prevented these defects from

occurring, regardless of wafer temperature. Thermal stress defects (cracking, chipping, or breaking) typically found on wafers from a rapid cool-down during the preclean step were not seen. Figure 4 displays a SEM micrograph of the crystalline defects [5].

## CONCLUSION

Alkali and mobile ion contamination was monitored by improved sampling and SIMS data analysis techniques. Procedures were established for the identification, systematic reduction, and statistical process control of alkali and mobile ion levels in the dielectric oxide films. A clean process was created to remove the ionic contaminants on the film surface and within the plasma etch-damaged oxide skin. Characterization of various clean solution concentrations with and without a surfactant was done to minimize oxide film removal beyond the targeted value and non-uniformity. Other defects including particles (inorganic and organic) and post-etch artifacts (such as veil polymers) were removed by optimizing each of the clean process steps. Veil polymer was efficiently removed by all clean chemistries. Clean process recipes were modified to eliminate wafer streaking by the addition of a preclean rinse to prevent crystalline defects and deletion of purge steps to prevent radial striations in the underlying oxide film. This SIMS-based monitoring approach has produced a consistent downward reduction of mobile ions in integrated circuit devices.

## ACKNOWLEDGMENTS

The author wishes to thank Linda Hernandez, Tin Tran, Jeff Cadenhead, Tom Allen, H. Stevens, and Carrie Lundquist for their assistance in data collection and analysis.

## REFERENCES

1. Cadenhead et. al., *Ext. Abstr. 179th ECS Meet.*, **91-2**, 105 (1991).
2. Cadenhead et. al., *Intercon., Contact Metal., Multilevel Metal.*, **93-25**, 423 (1993).
3. Chonko et. al., *Intercon., Contact Metal., Multilevel Metal.*, **93-25**, 436 (1993).
4. M. Berry et. al., *Ext. Abstr. 182th ECS Meet.*, **92-2**, 581 (1992).
5. K. Mautz, *Proc. of 4th Intl. Symp. Cleaning Technol. Semi. Device Manufact.*, **95-20**, 401 (1995).
6. B. Bohannon and B. Poarch, *Proc. Symp. Contam. Control Defect Red. Semi. Manufact. II*, **94-3**, 26 (1994).
7. S. O'Brien, et. al., *Proc. 3rd Intl. Symp. Cleaning Technol. Semi. Device Manufact.*, **94-7**, 233 (1994).
8. C. Draper, et. al., *Proc. 3rd Intl. Symp. Cleaning Technol. Semi. Device Manufact.*, **94-7**, 392 (1994).
9. N. Yonekawa, et. al., *Proc. 3rd Intl. Symp. Cleaning Technol. Semi. Device Manufact.*, **94-7**, 94 (1994).
10. K. Christenson, *Proc. 3rd Intl. Symp. Cleaning Technol. Semi. Device Manufact.*, **94-7**, 474 (1994).

## FIGURES

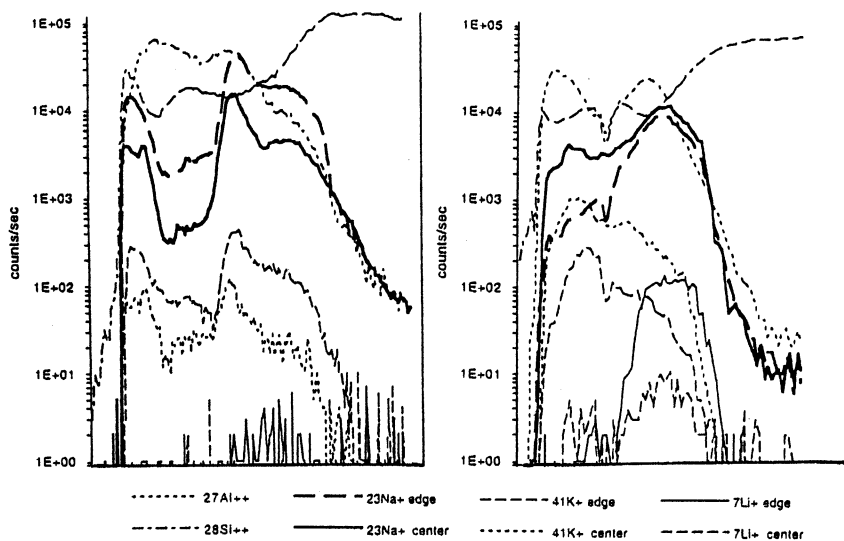


Fig. 1. SIMS depth profile after metal etching using the solvent clean.

Fig. 2. SIMS depth profile after metal etching using the BOE clean process.



Fig. 3. Veil polymer defects from the plasma metal etch process.

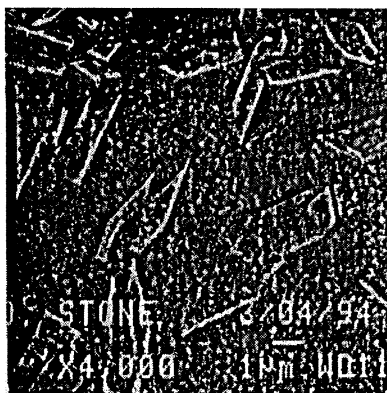


Fig. 4. Crystalline defects from the clean solution interaction with hot wafers.

## APPLICABILITY OF HF SOLUTIONS FOR CONTACT HOLE CLEANING ON TOP OF TiSi<sub>2</sub>

M. R. Baklanov\*, E. Kondoh, S. Vanhaelemersch and K. Maex  
IMEC, Kapeldreef 75, B-3001 Leuven, Belgium

Issues of contact hole cleaning after dry etching are discussed. Dry etch residue, which consists of a teflon-like polymer and metal fluorides, is removed by oxidising agents; however, a thin SiO<sub>2</sub> film forms on top of TiSi<sub>2</sub> during these treatments. Therefore, the contact holes must be cleaned furthermore prior to metal-plug formation. Two different SiO<sub>2</sub> removal procedures are investigated. Cleaning by HF solutions is shown to have problems related to the interaction of HF with TiSi<sub>2</sub> and to mass transport in narrow hydrophilic contact holes. Contrarily, *in-situ* low energy ion etching is shown not to have such drawbacks, therefore, is thought to be an appropriate alternative.

### INTRODUCTION

Metal silicide etching in a carbon-fluoride plasma leads to the formation of a complex protective film containing both metal fluorides and CF<sub>x</sub> polymer (namely teflon-like polymer) [1-3]. This film is crucial in contact hole etching on metal silicide, because it determines the etch selectivity of inter-layer dielectric (ILD) towards silicide, and because it affects dry etching performance such as etch uniformity. The composition, thickness, and properties of the protective film depend on etching conditions such as plasma composition [2]. The protective film must be removed after contact hole etching to decrease contact resistance between metal plug and silicide. Cleaning of blanked Ti and Co silicide wafers after dry etching in a CF<sub>4</sub>/CHF<sub>3</sub> plasma were studied previously [2,3]. Residual films were found to be removed by the combination of oxygen-plasma afterglow treatment and the subsequent sulphuric acid/hydrogen peroxide mixture (SPM) solution treatment. In this case, oxygen plasma ashes the teflon-like polymer, and SPM dissolves metal fluorides. These procedures were confirmed to be satisfactory for the cleaning of patterned device wafers.

However, after the oxygen plasma and SPM treatments, silicide surface is covered with a film which consists of SiO<sub>2</sub> (3 - 4 nm) and surface compounds like F-Ti-O [3]. This film effects the contact resistance. Therefore, an advanced cleaning procedure needs an additional *final* cleaning before metal-plug formation. The use of a HF-based solution is straightforward because of its strong SiO<sub>2</sub> etch ability; however, caution must be paid not to attack metal silicides or ILD sidewall (usually SiO<sub>2</sub>) [4,5].

The goal of this work is to characterise the final cleaning procedure of TiSi<sub>2</sub> surface. We discuss mainly the application of HF solutions to contact/via hole cleaning. Low energy ion sputtering cleaning is comparatively studied.

### EFFECT OF CLEANING CONDITIONS ON CONTACT RESISTANCE

Figure 1 shows typical kinetic curves of TiSi<sub>2</sub> etching in HF solutions. The etch rate depends on HF concentration. There appears an induction period at the beginning

of etching. This induction period increases with decreasing the HF concentration. The etch rate of  $\text{SiO}_2$  in a HF solution has been found to be time-independent and to increase proportionally with the HF concentration. Naturally, this induction period is thought to correspond to the removal of surface  $\text{SiO}_2$ ; moreover, it is suggested that the surface  $\text{SiO}_2$  film can be removed selectively from the silicide surface.

Figure 2 supports this explanation. Here, the ellipsometric angle and sheet resistance of  $\text{TiSi}_2$  films were measured as a function of etching time. For times shorter than 30 sec, only the ellipsometric phase parameter  $\Delta$  is changed, indicative of the etching of the surface  $\text{SiO}_2$  film. Therefore, the optimal etch time is defined as a time when the sheet resistance of  $\text{TiSi}_2$  starts to increase. According to XPS analyses, the combination of oxygen plasma, SPM, and HF-dipping results in clean silicide surface without metal fluorides or polymers. However, in spite of the chemical cleanliness, a longer cleaning of  $\text{TiSi}_2$  in a diluted HF solution leads to a nontrivial increase of the contact resistance.

Kelvin-type structures were used to analyse the effect of HF etching on contact resistance. After contact hole opening, wafers were cleaned by an oxygen plasma ( $240^\circ\text{C}$ ,  $P = 1$  Torr, and  $t = 40$  s) and by a SPM solution ( $90^\circ\text{C}$ , 10 min). Scanning electron microscope (SEM) inspections have shown that there is no significant residual photoresist or RIE-related residue inside holes. The wafer was then dipped in a HF solution just before the deposition of a Ti/TiN stack layer (30/80 nm). In the second series of experiments, wafers were *in situ* etched by low-energy ions (SSE: soft sputtering etching) prior to the Ti/TiN deposition. Finally, the contact holes were filled by W chemical vapour deposition (CVD), and the contact resistance was measured.

Figure 3 shows the dependence of the contact resistance on etch time for HF etching and for SSE. One can see a clear difference in the behaviour of the contact resistance. In the case of HF cleaning (0.2%), the optimal time ( $t_{\text{opt}}$ ) appears at around 40 sec, at which the etching of surface  $\text{SiO}_2$  completes as seen in the above-mentioned ellipsometric data. For  $t < t_{\text{opt}}$ ,  $\text{SiO}_2$  still remains at the interface between silicide and Ti/TiN, which leads to high contact resistance. On the other hand, for  $t > t_{\text{opt}}$ , the silicide surface is supposed to be clean (i.e., no  $\text{SiO}_2$  layer). The increase of contact resistance cannot be attributed to the sheet resistance increase shown in Fig. 2, since the interfacial resistance is most dominant. We suppose that the resistance increase for  $t > t_{\text{opt}}$  is due to an irreversible change of silicide surface [6].

The final cleaning by *in situ* soft-sputtering etching shows excellent contact resistance values for etch times from 10 to 50 sec. That is, even 10 s of SSE seems to be sufficient long to remove surface  $\text{SiO}_2$ .

Figure 4 shows the dependence of the contact resistance on contact hole size. The cleaning by HF solutions results in good resistance only for the holes larger than  $0.45 \mu\text{m}$ . Since all the contact holes were overetched (i.e., silicide was engraved) during RIE, it is clear that this behaviour is not due to micro loading effect. Therefore, this phenomenon is related to the removal of the silicide surface oxide. SSE data does not show a significant increase in the contact resistance down to  $0.35 \mu\text{m}$ . Moreover, our recent results show that SSE is applicable down to  $0.25 \mu\text{m}$ . These facts allow us to conjecture that problems in HF-based silicide surface cleaning is specified by chemical processes inside the contact holes. These problems can be divided into three aspects: (1) HF etching chemistry of  $\text{TiSi}_2$  and (2) of  $\text{SiO}_2$ , and (3) mass transport of reagents in contact holes.

HF etching chemistry of  $\text{TiSi}_2$  and the correlation with the contact resistance have been analysed previously [6]. It was shown that the difference in chemical

activities of C49 and C54 phases of TiSi<sub>2</sub> leads to the preferential removal of C49 phase. The C49 phase remains with a significant amount at the boundaries and triple points of C54 grains even in an optimised C49-C54 transformation technology. The relative amount of C49 phase increases with decreasing line width [5]. TiSi<sub>2</sub> film surface becomes porous or rougher after HF etching, which leads to decreasing contact area thus to increasing contact resistance eventually. Hereafter we discuss the second and third aspects.

## APPLICABILITY OF HF CLEANING FOR SUBMICRON CONTACT HOLES

Wet cleaning process in a narrow hole with hydrophilic surface (in our case, contact hole or via hole being opened in a SiO<sub>2</sub> ILD layer) can be divided the following 3 steps: (1) advancing wetting inside the hole, (2) transport of chemical species inside and outside the hole, and (3) etchant removal by rinsing and drying. General theoretical analysis of these phenomena and estimation of the characteristic time of each step were recently carried out by Olim [7]. It was shown that the time scales of these steps are very short and that it is imperative only to minimise the time required to replace the liquid at the hole opening. This conclusion is in agreement with the numerical results by Nakao et al. [8], in which stationary exchange of a solution between contact holes and bath was considered. All those calculations allow us to conclude that the use of liquid solutions for the cleaning of very narrow holes is not problematic, as long as the bath is being mixed intensively so as to produce a rapid exchange of chemicals at the hole opening. However, this conclusion contradicts to technological experience (e.g. see Fig. 4), and there have been no explicit explanations for these phenomena in the extent of the authors' knowledge. In the theoretical analyses, the diffusion coefficients of chemicals in bulk water were used to describe mass transport inside holes, while specific effects arising from small geometry, namely size effects, were not taken into account. We propose that the HF consumption on the ILD sidewall (SiO<sub>2</sub>) and the formation of colloid-like silica [9] are primary reasons for the decrease of cleaning efficiency in narrow contact holes.

In order to analyse the applicability of HF solutions to narrow holes, the contact hole cleaning efficiency were studied by using a test structure specially designed for this purpose (Fig. 5) [10]. The line resistance is constant during SiO<sub>2</sub> etching (discussed above) but starts to increase with silicide consumption at the hole bottom. The amount of silicide consumption can be determined from the line resistance. Measurements by using this structure are useful, because results on blanked wafers cannot be always applied to describe the processes inside contact hole where the dependence of free radical reactions on area/volume (S/V) ratio becomes significant.

In our experiments, TiSi<sub>2</sub> etching rate at the bottom of contact hole was determined first. Next, from the etching rate data, HF concentration near at the contact hole bottom was conversely estimated. The test structures were fabricated under optimised dry etching conditions, and then, were cleaned up by oxygen plasma and SPM solution. All the contact holes were slightly overetched, which was observed as an increase in the line resistance; this means that we can exclude the possibility of *nonetch-through* of holes, which could be caused by a microloading effect during plasma etching. We assume that the process dependence of contact resistance was related to the thin SiO<sub>2</sub> layer on the silicide surface formed during oxygen plasma and SPM treatments. Figure 6 shows the change of the silicide thickness measured after dipping the wafer in a HF solution for different times. The etch rate of silicide in large contact

holes is higher than that in small holes. There can be seen no significant size dependence above 0.8  $\mu\text{m}$ . From this reason, the HF concentration near the bottom of a smaller contact hole (< 0.8  $\mu\text{m}$ ) is supposed to be lower than that of the bath.

Let us now discuss which is most important among the above mentioned steps.

*Wetting* — The driving force of wetting is a pressure gradient that arises from hydrophilic nature of  $\text{SiO}_2$  surface and is described by Pascal equation,

$$\Delta P = 2 \gamma \cos \theta / w \quad (1)$$

where  $\Delta P = P_{\text{gas}} - P_{\text{liquid}}$  is the pressure difference across the interface,  $\gamma$  is the surface tension,  $\theta$  is the contact angle, and  $w$  is the gap width. Analysis of this equation shows that, for a 0.5  $\mu\text{m}$ -wide capillary of  $\text{SiO}_2$ , the wetting time is less than 1000  $\mu\text{s}$  [10]. From contact angle measurements, we have confirmed that  $\text{SiO}_2$  surface becomes more hydrophilic after the sequence of oxygen plasma and SPM treatments. Another important point is that  $\Delta P$  increases with decreasing gap width. Therefore, in the case of deep submicron contact holes, wetting time should be less than the value shown in reference 10. These analyses convince us that the wetting can be excluded as a possible reason for the problems of narrow contact hole cleaning.

*Rinse and drying* —  $\text{TiSi}_2$  (over-)etching can proceed by HF which remains in a contact hole during wafer transportation to a rinse bath. Usually, the transportation time is very short ( $\approx 1$  sec). In addition, the estimated HF concentration inside holes is not so high to explain the observed change of the silicide thickness.

*Reagents transport* — From these reasons, only diffusion can be a main issue. Let us estimate the HF concentration at the bottom of a contact hole. HF is consumed on the sidewall through a reaction with  $\text{SiO}_2$ :



In a diluted solution ( $[\text{HF}] < 2 \text{ M}$ ), the etch rate is proportional to HF concentration; i.e., etch rate ( $\text{nm/min}$ ) =  $k_g [\text{HF}]$ . We experimentally obtained  $k_g = 8 \cdot 10^{-13} \text{ m}^4/\text{mole}\cdot\text{s}$  (at room temperature) for a densified  $\text{SiO}_2$  film, grown by a high temperature and low pressure CVD method, under a wide range of experimental conditions. Note that the etch rate is so small that HF etching does not change hole size. The effective rate constant for HF consumption ( $k$ ) depends on the geometry of the contact hole. In our case, the contact hole has a rectangular cross-section (see Fig. 5), thus the rate constant of the HF consumption is written as

$$k = k_g S/V = 2(x+y)/xy k_g \quad (3)$$

where  $x$  and  $y$  are width and length of the cross-section. Since  $y$  is constant,  $k$  increases with decreasing  $x$ , leading to the increase in HF consumption inside narrow holes. It is apparent that cylindrical contact holes has a similar behaviour where  $S/V$  is given by  $2/R$  ( $R$  = hole radius). The next important factor is the rate of HF diffusion inside the contact hole. The special distribution of HF concentration inside the hole depend both on the rate constant  $k$  and on the diffusion coefficient.

Taking into account reaction (2), one-dimensional diffusion-chemical equation is given as follows.

$$\frac{d^2C}{dz^2} - kC = 0 \quad (4)$$

Here, C is the HF concentration and z is the longitudinal axis. Applying boundary conditions,  $C = C_0$  at  $z = 0$  and  $C = 0$  at  $z = \infty$ , the solution of equation (4) becomes

$$C = C_0 \exp\left(-\sqrt{\frac{k}{D}} z\right) \quad (5)$$

This equation permits to estimate the dependence of the HF concentration in a contact hole on its size. Results shown in Fig. 7 demonstrate that there is no significant change in the HF concentration when the diffusion coefficient inside the contact hole is close to the value of bulk water ( $D \approx 1 \cdot 10^{-9} \text{ m}^2/\text{s}$ ). In this case, cleaning efficiency (in our experiments, TiSi<sub>2</sub> etch rate) should be independent of contact hole size. Clearly, this conclusion contradicts to the experimental observations (Fig. 6). Comparative analysis of TiSi<sub>2</sub> etching rate and equation (5) shows that the diffusion coefficient in a contact hole should be two orders of magnitude smaller than that in bulk water.

Extremely small diffusion coefficients inside narrow contact/via holes can be explained by abnormal behaviours of water in fine quartz capillaries. Physical-chemistry studies on the abnormality started in 1920's [11] and had been extensively carried out. It was established that the water condensed in a fine capillary has a lower vapour pressure than the value predicted by Kelvin law, higher viscosity, and lower melting point than those of water. There were proposed different explanations of these phenomena: for example, ordering effects of water molecules due to long term forces (up to 100 - 200 nm), effects of impurities, a new state of water (anomalous water [9,12]). This dramatic story of anomalous water had almost ceased in 1970's. Finally, the majority of researchers concluded that the change of water properties in fine capillaries is caused by the reaction between water and silica surface that forms certain silica/water complexes. All these observations were analysed extensively; one will find a work by Everett *et al.* as a good reference publication [9].

SiO<sub>2</sub>-based ILDs are used in current technologies, where contact and via holes can be regarded as silica capillaries. Diluted HF solutions accelerate to form silicon containing ions SiF<sub>6</sub><sup>2-</sup> (see eq. (2)) which are stable only in an acid media. Since HF consumption will increase the pH value of the solution inside the contact hole, the SiF<sub>6</sub><sup>2-</sup> ions will consequently react with water, resulting in a colloid-like silica solution. Additionally, the change of the solution properties in a contact hole can be related to the reaction products of HF and TiSi<sub>2</sub> of which formation is very sensitive to the pH of the solution. We believe that this is the problem in applying HF-water solutions to the cleaning of contact/via holes being opened in a SiO<sub>2</sub>-based ILD layer. Similar behaviour can be expected for polar organic solvents. The mechanism we examined in this paper is the first explanation giving a theoretical support for the difficulty in employing wet chemistries for contact/via hole cleaning. Undoubtedly, the application of conventional wet chemistry is facing a turning point in the deep-submicron era.

## CONCLUSIONS

Problems of the cleaning of contact holes on titanium silicide are discussed. During dry etching both teflon-like polymer and metal fluorides are formed on the

silicide surface. This protective film provides the etch selectivity of ILD towards silicide during dry etching, however, should be removed before metal-plug deposition to decrease the electrical contact resistance. Although oxygen plasma and SPM remove this protective film, thin SiO<sub>2</sub> film (3 - 5 nm) is formed on the silicide surface. Therefore, the contact holes must be cleaned furthermore. Two cleaning procedures are studied: *In situ* low energy ion etching has shown low contact resistance values and less hole-size dependence, while the conventional cleaning by using HF solutions shows a large increase in the contact resistance for narrow holes (< 0.45 μm). The later problem, particularly in the case of contact hole cleaning on top of TiSi<sub>2</sub>, is related to the etching of silicide and to the transport of reagents in narrow hydrophilic holes. HF molecules attack the sidewall of contact holes and form hexafluorosilicate ions. SiO<sub>2</sub>, which is a major reaction by-product and is in equilibrium with SiF<sub>6</sub><sup>2-</sup> and water, can form a colloid like solution that has a extremely higher viscosity than that ordinary bulk water. As a result, the mass transport of active species in the contact hole is limited.

### ACKNOWLEDGEMENTS

The authors would like to thank J. Wouters, W. Storm and E. Vranken for their supports for the experiments. We are thankful to R. Donaton for XRD analysis and M. DePotter for electrical evaluations. K. Maex is a research director of the National fund for scientific research - Flanders (FWO).

\* Corresponding author. On leave from Institute of Semiconductor Physics, SB RAS, Novosibirsk, 630090 Russia.

### REFERENCES

1. S. W. Robey, M. A. Jaso, G. S. Oehrlein, *J. Appl. Phys.*, **65**, 1989, 2951
2. M. R. Baklanov, S. Vanhaelemeersch, W. Storm, Y.-B. Kim, W. Vandervorst, K. Maex, submitted to *J. Vac. Sci. Technol.*
3. M. R. Baklanov, S. Vanhaelemeersch, W. Storm, W. Vandervorst, K. Maex, *J. Vac. Sci. Technol.*, in printing.
4. M. R. Baklanov, I. A. Badmaeva, R. A. Donaton, L. L. Sveshnikova, K. Maex, *J. Electrochem. Soc.* **143**, 10, 1996, 3245
5. K. Maex, *Mater. Sci. Eng.*, **R11**, 2-3, 1993, 53
6. M. R. Baklanov, S. Vanhaelemeersch, K. Maex, Abstracts of European Workshop on "Materials for Advanced Metallization", Villard-de-Lans, 1997, p.110;
7. M. Olim, Proc. of the 3 Intern. Symp. on Ultra Clean Processing of Silicon Surfaces (UCPSS'96), eds, M. Heyns, M. Meuris, P. Mertens, Acco Press, Leuven, Belgium, 1996, p.213
8. I. Nakao, H. Umiimoto, S. Onodaka, T. Ohzone, H. Esaki, *J. Electrochem. Soc.*, **137**, 1990,
9. D. H. Everett, J. M. Haynes, P. J. McElroy, *Sci. Prog. Oxf.*, **59**, 1971, 279
10. Q. F. Wang, S. Fransilla, K. Maex, IMEC internal report (unpublished).
11. J. L. Shereshevsky, C. P. Carter, *J. Am. Chem. Soc.*, **72**, 1928, 2966
12. B. V. Derjagin, *Disc. Faraday Soc.*, **42**, 1966, 109

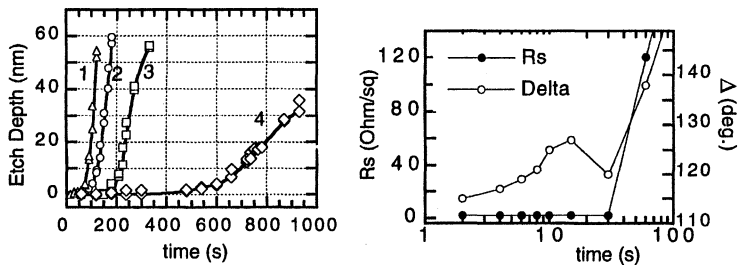
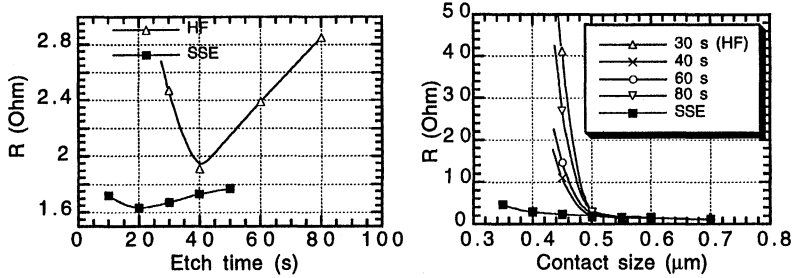


*Fig.1 Kinetic curves of TiSi<sub>2</sub> etching in HF solutions (1: 0.4%; 2: 0.3%; 3: 0.2%; 4: 0.1%).*

*Fig.2 Change of ellipsometric angle  $\Delta$  and sheet resistance of TiSi<sub>2</sub> ( $R$ ) during the etching in a HF solution (0.5%).*



*Figs.3, 4. Dependence of the contact resistance on etch time and contact hole size.*

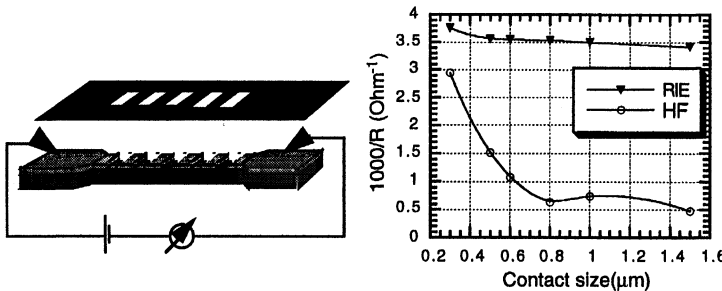


*Fig. 5 Test structure for the measurements of silicide consumption in contact holes.*

*Fig. 6 Change of  $TiSi_2$  thickness after RIE and HF etching as a function of contact hole size.*

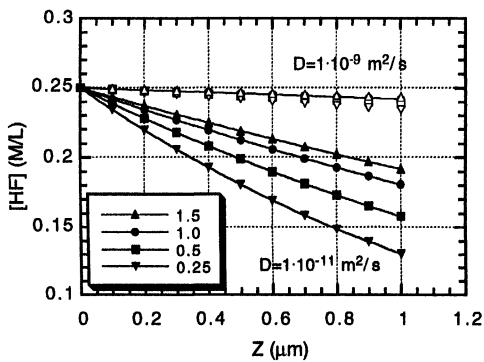


*Fig.7. Numerical analysis of equation 5, showing HF concentration distribution in a contact hole for different HF diffusion coefficients and contact hole sizes (0.25 - 1.5  $\mu m$ ).*

# THE FORMATION AND REMOVAL OF RESIDUE FORMED DURING TiN FLUOROCARBON PLASMA ETCHING

Y.B. Kim, T. Conard, D. Vanhaeren, M. Baklanov,  
S. Vanhaelemersch, W. Vandervorst, K. Maex

IMEC, Kapeldreef 75, B3001 Leuven, Belgium

The composition of the overlayer formed on TiN in a fluorocarbon plasma etch has been studied. XPS and AFM were used to detect changes in chemical bonding and surface roughness after plasma etching, conventional cleaning and Ar sputtering. The residue layer formed on TiN surface in the fluorocarbon plasma contains Teflon-like fluorocarbon polymer, titanium fluoride and oxyfluoride. The composition of the residue and the thickness of the polymer are a function of etch time. The residue layer has the structure of  $\text{CF}_x$  (including C-C, C-H)/ $\text{TiF}_x/\text{TiO}_x\text{F}_y$ , qualitatively. The carbon and fluorine contamination induced in fluorocarbon RIE has been removed from the TiN surface by a cleaning procedure composed of Microstrip, oxygen plasma and HF treatment. In addition, The cleaning procedure also reduces the TiN RMS surface roughness. The Argon sputtering of the TiN surface removes the carbon rich layer first followed by the removal of  $\text{TiF}_x$  and finally  $\text{TiO}_x\text{F}_y$ .

## INTRODUCTION

Titanium nitride(TiN) is widely used in industry due to its high melting point, thermodynamic stability, low resistivity and high electrical conductivity. Especially in the IC industry TiN has been used as an anti-reflective coating layer and as a diffusion barrier. As the device is miniaturized, the understanding of the surface properties of TiN is crucial. Therefore, extensive studies have been done to understand not only the electrical and optical properties of bulk material[1][2] but also the surface modification after air exposure[3], thermal oxidation[3]-[5] and plasma treatment[6]. However, there are still many questions concerning the properties of residue formed on the TiN by fluorocarbon plasma and the mechanism of removal.

## EXPERIMENTAL

A 150nm titanium nitride film was sputter deposited at 300°C on a 500nm silicon dioxide film on a (100) silicon substrate. Before TiN etching, the TiN surface was treated with diluted wet HF. Reactive ion etching(RIE) was done in a LAM Rainbow 4520 etch system at 400KHz with  $\text{CF}_4$  using a mixture of Ar and nitrogen. The electrode gap during etch was 1.15cm. Angle resolved XPS was performed on the sample after etch in

order to extract structural information of the residue layer as a function of depth. The XPS measurements were performed on an SSX-100 spectrometer(Fisons) equipped with a monochromated Al K<sub>α</sub> source and a concentric hemispherical analyzer. The behavior of the composition of the residue layer was also studied as a function of etch process time. The plasma etched samples were treated in different cleaning processes of organic solvent of Microstrip2001, oxygen plasma and HF wet treatment. XPS and AFM measurements were completed after each cleaning steps. Argon sputtered depth profiling using the XPS system was used to study the change of the structure of the residue during sputter cleaning.

## RESULTS AND DISCUSSION

### Analysis of Residue Layer

Typical F 1s spectra of XPS for TiN surface are shown in Fig. 1. The spectra are well resolved by two peaks at about 685 eV and 688 eV, which can be assigned to titanium fluoride(TiF<sub>x</sub>) and Teflon like polymer(CF<sub>x</sub>). The non-volatile residue of metal fluoride is mainly formed by the reaction of the Ti with highly reactive F atoms formed by the dissociation of CF<sub>4</sub>. The Teflon like polymer is formed on the wafer surface by the polymerization reaction of CF<sub>x</sub> radicals which is also formed by the dissociation of the fluorocarbon chemistry.

Angle resolved XPS measurements were performed to characterize the residue layer on the TiN sample after plasma etching (CF<sub>4</sub> = 90 sccm, RF power = 1050 Watts, pressure = 300 mTorr). The normalized intensities of TiF<sub>x</sub> and CF<sub>x</sub> for different take-off angles are plotted in Fig.2. The data indicates that the higher the take-off angle, the higher the TiF<sub>x</sub> concentration and the lower the CF<sub>x</sub> concentration; this indicates that the CF<sub>x</sub> polymer layer is located at the upper part of the residue layer and TiF<sub>x</sub> is located at the lower part in depth. Therefore, it can be said from this ARXPS study that there are two distinct overlayers, TiF<sub>x</sub> and CF<sub>x</sub> on TiN, which is clearly seen in Fig.2.

A conceptual model is suggested to explain this arrangement of the residue and its role in plasma etching. TiN etching is accomplished by forming the volatile TiF<sub>4</sub> on TiN and removing it from TiN surface. Both chemical reaction and physical ion bombardment are involved in the formation of the volatile compound. The TiN surface contains mostly F bonds during the fluorocarbon plasma etch. The fluorine atom which is the predominant chemical etching precursor in CF<sub>4</sub> reactive ion etching reacts with TiN to form TiF<sub>4</sub>; later, the TiF<sub>4</sub> desorbs from the surface. The ion bombardment helps these reactions. Of course, the etching can be also done by physical sputtering of TiN or TiF<sub>x</sub>. The C-F bonds(CF<sub>x</sub> polymer) are located on the Ti-F; the polymerization reaction occurs on the Ti-F bonds. Therefore, the physical ion bombardments and the chemical reactions that form TiF<sub>x</sub> on TiN are affected by the quantity of C-F bonds i.e., thickness of polymer. This can be explained as follows; The ion energy decreases via the scattering in the polymer, which reduces physical etching and ion enhanced chemical etching. In addition, the in-diffusion of chemical etching precursor and out-diffusion of volatile compound depend on the polymer thickness. When the RF power and process gases are off, the chaos by ion bombardment will stop leaving chemical surface reactions - until the remaining gas on the surface is pumped out. The structure of the residue layer may be

completely formed during the time due to the re-distribution of fluorine atoms. First, The unoccupied active sites on TiN are occupied by highly reactive fluorine atoms which are closed to TiN surface. Second, the fluorine atom that was distributed on the top surface of  $\text{CF}_x$  polymer reacts with active  $\text{CF}_x$ . This fluorine re-distribution which occurs after the etch stops can explain why the upper part of the  $\text{CF}_x$  layer is fluorine rich. The fluorine rich layer was confirmed by angle resolved XPS analysis of the residue(the data is not shown in this paper).

### Time Dependence of the Composition of the Residue Layer

The time dependence of the concentration of titanium fluoride( $\text{Ti}-\text{F}$ ) and polymer( $\text{C}-\text{F}$ ) is shown in Fig. 3. The samples were etched by the conditions of  $\text{CF}_4 = 90 \text{ sccm}$ , pressure = 90 mTorr and RF power = 1050 Watts. Clearly, for times less than 20 seconds the concentration ratio of  $\text{CF}_x$  to  $\text{TiF}_x$  is nearly constant. However, after 40 seconds it is changed significantly. The maximum intensity of  $\text{CF}_x$  is at 50 sec for this experimental condition. The intensity is significantly decreased at 60 seconds, increased at 70, and decreased again next. The composition of the residue and the thickness of the polymer are a function of time. The intensity of the  $\text{TiF}_x$  shows similar behavior. When the  $\text{CF}_x$  is increased,  $\text{TiF}_x$  is decreased and when  $\text{CF}_x$  is decreased  $\text{TiF}_x$  is increased.

The abrupt change of composition of polymer composition can be explained by the reaction between carbon or  $\text{CF}_x$  polymer and oxygen released by dissociation during the etching of titanium oxide and titanium oxynitride layer which had been formed during air exposure on the TiN surface. The similar role of the oxygen in the case of  $\text{SiO}_2$  etching has been reported[7]. The oxygen rich Ti and TiN top layer has been reported[8,9]. We can suggest that the oxygen released during the etching of titanium oxide or oxynitride reacts with deposited carbon to form  $\text{CO}$ ,  $\text{CO}_2$  or  $\text{COF}_2$ , which are volatile compounds, and the formation of the  $\text{CF}_x$  polymer is suppressed at the initial stage of TiN etching. However, when the supply of the oxygen for the formation of the volatile compounds is cut off, carbon contributes to the formation of the fluorocarbon polymer, which is clearly shown in Fig. 3. Therefore, the intensity of  $\text{CF}_x$  increases after the first stage. The reason that the intensity of  $\text{TiF}_x$  decreases when  $\text{CF}_x$  increases and vice versa is predominantly due to the electron screening effect of the  $\text{CF}_x$  layer. The  $\text{CF}_x$  layer is located on the top of the  $\text{TiF}_x$ , as is discussed in previous section. Therefore, the intensity of the electron that comes from  $\text{TiF}_x$  is reduced due to  $\text{CF}_x$ . The thicker the thickness of the polymer, the higher the reduction of  $\text{TiF}_x$  intensity.

### Cleaning of the Residue Layer

The cleaning procedure of ‘Microstrip+O-Plasma+HF’ and ‘O-Plasma+HF’ was tested to determine the qualitative change of the polymer composition. C 1s and F 1s spectra of XPS after each cleaning steps are shown in Fig.4 and Fig.5, respectively. Fig.4(a) and Fig.5(a) are the spectra before  $\text{CF}_4$  plasma etching, and Fig.4(b) and Fig.5(b) are after etch( $\text{CF}_4 = 90 \text{ sccm}$ , and RF power = 1050 Watts, 60 sec). The TiN wafer was treated in 2% HF for 1 minute before the RIE. The Ti-F bonds shown in Fig.5(a) were formed by HF treatment. The carbon bonds shown in Fig.4(a) came during air exposure before the XPS analysis. The peak at about 285.2 eV is assigned to polymeric hydrocarbons and the peak at about 286.0 and 289.2 eV are different oxidized carbon species[10]-[12]. The peaks at about 287.1, 291.4 and 294.8 eV in Fig. 4(b)

which were formed after fluorocarbon plasma etching can be assigned to  $\text{CF}_1$ ,  $\text{CF}_2$  and  $\text{CF}_3$ , respectively. The  $\text{C}-\text{CF}_x$  peak is at about 286 eV which is similar to the oxidized carbon states. Those two peaks are not clearly resolved. The two peaks that are assigned to metal fluoride and fluorocarbon polymer are shown in Fig.5(b) as is discussed in the previous section. Fig.4(c) and Fig.5(c) are the C1s and F1s spectra, respectively, after the plasma etching followed by organic solvent cleaning. It is shown that  $\text{CF}_2$  and  $\text{CF}_3$  were removed, but fluorine bonded in  $\text{CF}_1$  and/or  $\text{C}-\text{CF}_x$  and  $\text{TiF}_x$  are not removed completely from the surface. Fig.4(d) and Fig.5(d) are the spectra after the plasma etch followed by organic solvent and oxygen RIE. The fluorocarbon polymer was removed, but metal fluoride was not. The plasma etched TiN surface treated with only oxygen plasma without organic solvent had similar spectra to Fig.4(d) and Fig.5(d). By adding HF process(Fig.4(e) and Fig.5(e)), the amount of Ti-F bonds was reduced down to the initial level by only HF wet treatment. It can be concluded that the cleaning procedure of oxygen plasma followed by wet HF cleaning removed the carbon and fluorine contamination formed by fluorocarbon RIE on the blanket wafer. The organic solvent is effective on patterned wafer because it is isotropic process.

Table 1. shows measured RMS roughness after plasma etch and subsequent cleaning steps. Fluorocarbon plasma etching increases surface roughness and following organic solvent and oxygen plasma reduces the roughness. Finally, the surface roughness drops to 1.03 nm which is significantly lower than initial roughness when the HF treatment is followed. The increase of surface roughness by the plasma etching is due to the non-uniform formation of the residue on TiN and non-uniform TiN etching. The decrease of the roughness by organic solvent followed by oxygen plasma could be explained by the fact that it removes the non-uniform fluorocarbon polymer and oxygen plasma oxidize the rough TiN top surface. By removing the oxide by HF, surface roughness decreases significantly.

The change of the C 1s, F 1s, and Ti 2p spectra during Ar sputtering are shown in Fig. 6(a), (b) and (c), respectively. The surface spectrum is in front in Fig.6 (c), and in back in Fig.6 (a) and (b). It is shown from Fig.6(a) and Fig.6(b) that carbon compounds including  $\text{CF}_x$  is removed easily by Ar sputtering. In contrast with  $\text{CF}_x$  residue,  $\text{TiF}_x$  or  $\text{TiO}_x\text{F}_y$  remains even after long sputtering time. However, it appears that Ti-C bond at about 282.2 eV was formed during Ar sputtering because the intensity of the peak was slightly increased as the sputtering time increased. Ti2p spectra is also shown in Fig.6(c). As the sputtering time is increased, the intensity of TiN peaks at about 455.6 eV(Ti2p3/2) and 461.4 eV(Ti2p1/2) is increased and the peaks at 459.7 eV(Ti2p3/2) and 465.5 eV(Ti2p1/2) assigned to  $\text{TiF}_x$  is decreased. The intermediate peak between TiN and  $\text{TiF}_x$ , which is increased after one or two sputtering cycles and decreased afterward, is assigned to a peak for  $\text{TiO}_x\text{F}_y$ .

## CONCLUSION

We can conclude that the residue layer formed on TiN surface in  $\text{CF}_4$  plasma contains fluorocarbon polymer, titanium fluoride and titanium oxyfluoride. The composition of the residue and the thickness of the polymer are a function of process etch time. The proposed structure of the residue layer is  $\text{CF}$ (including C-C, C-H)/ $\text{TiF}_x/\text{TiO}_x\text{F}_y$ . The carbon and fluorine contamination induced in fluorocarbon RIE has been removed from the TiN surface by a cleaning procedure composed of organic solvent, oxygen plasma and HF treatment. The surface micro-roughness has also been reduced lower than initial

level before plasma etching by the cleaning procedure. The Argon sputtering of the TiN surfaces removes the carbon rich layer first followed by the removal of  $TiF_x$  and finally  $TiO_xF_y$ .

#### REFERENCES

1. T.P. Thorpe, S.B. Qadri, S.A. Wolf, and J.H. Claassen, *Appl. Phys. Lett.* 49(19), 1239(1986)
2. N. Savvides and B. Window, *J. Appl. Phys.* 64(1), 225(1988)
3. Harland G. Tompkins, *J. Appl. Phys.* 70, 3876(1991)
4. I. Milosev, H.-H. Strehblow, B. navinsek, and M. metikos-Hukovic, *Surface and Interface Anal.* 23, 529(1995)
5. M. Wittmer, J. Noser, and H. Melchior, *J. Appl. Phys.* 52, 6659(1981)
6. F. Fracassi, R. d'Agostino, R. Lamendola, and I. Mangieri, *J. Vac. Sci. Technol. A* 13(2), 335(1995)
7. S. Fang, C. Chiang, and D. Fraser, B. Lee, P. Keswick, M.Chang, and K.Fung, *J. Vac. Sci. Technol. A14*, 1996 (1985)
8. I. Milosev, H.-H. Strehblow, B. navinsek, and M. metikos-Hukovic, *Surface and Interface Anal.* 23, 529(1995)
9. C. Ernberger, J. Nickerson A.E. Miller and J. Moulder, *J. Vac. Sci. Technol. A3*, 2415(1985)
10. Tery L. Barr and Mengping Yin, *J. Vac. Sci. Technol. A10*, 2788 (1992)
11. Tery L. Barr and Sudipta Seal, *J. Vac. Sci. Technol. A13*, 1239 (1995)
12. G. Barth, R. Linden, and C. Bryson, *Surface Interface Anal.* 11, 207(1988)

Table 1. Change of surface roughness by plasma etching and subsequent cleaning.

process	RSM[nm]
no process	3.44
plasma etch	4.26
plasma etch + organic solvent + oxygen plasma	3.14
plasma etch + organic solvent + oxygen plasma + HF	1.03

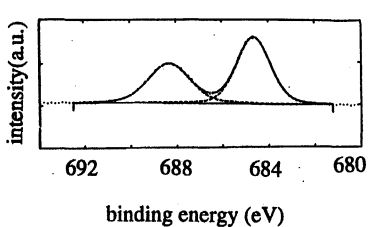


FIG.1 Typical F1s spectra of the residue after fluorocarbon plasma etch on TiN.

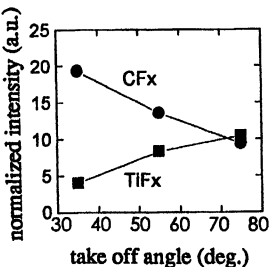


FIG.2 The atomic concentration of the fluorine bonded to TiFx and CFx for different take-off angles.

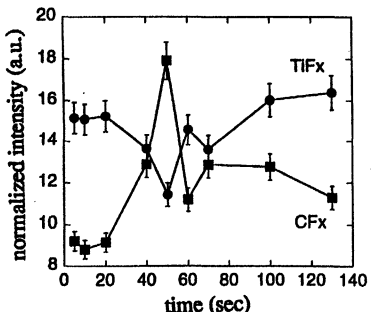


FIG.3 The time dependence of the concentration of titanium fluoride(TiFx) and polymer(CFx). The concentration was calculated from F1s spectra.

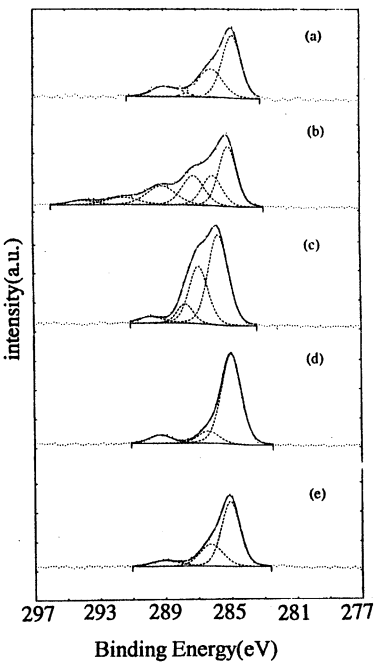


FIG.4 Photoelectron spectroscopy of C1s  
 (a) before CF4 RIE (b) after the etching  
 (c) after the etching followed by organic solvent  
 (d) after the etching followed by organic solvent and oxygen RIE  
 (e) after the etching followed by organic solvent, oxygen RIE and HF wet etching.

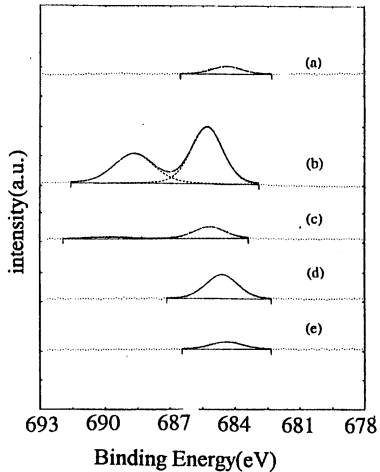


FIG.5 Photoelectron spectroscopy of F1s  
 (a) before CF4 RIE (b) after the etching  
 (c) after the etching followed by organic solvent  
 (d) after the etching followed by organic solvent and oxygen RIE  
 (e) after the etching followed by organic solvent, oxygen RIE and HF wet etching.

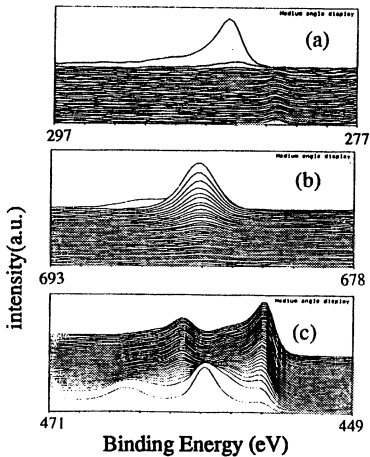


FIG.6 XPS depth profile : (a) C1s (b)  
 F1s (c) Ti2p

A UNIQUE CHEMISTRY TO CLEAN SIDEWALL POLYMERS  
FORMED BY PLASMA ETCHING OF VIA AND METAL  
LAYERS OF INTEGRATED CIRCUIT FABRICATION

Kenji Honda, Donald Perry

Olin Microelectronic Materials, 200 Massasoit Avenue, East Providence, RI 02914

James O'Neil\*, Richard Molin, Gale Hansen, Vincent Leon, Doug Petersen

Olin Microelectronic Materials, 1025 S. 52nd Street, Tempe, AZ 85281

\*Currently at Hewlett Packard, Corvallis, OR

Larry Roberson

Atmel Corporation, 1150 E. Cheyenne Mountain Blvd., Colorado Springs, CO 80906

ABSTRACT

Microstrip® 5002, an aqueous based cleaner solution, has been developed to remove post plasma etch residue with minimum corrosion of exposed metal surfaces. The development of the cleaner solution was based on guidelines that included the requirements that the solution must be more environmentally friendly, eliminate the isopropyl alcohol rinsing step, and work at lower temperatures for a longer bath life. Microstrip® 5002 has met these requirements for removing residues created during plasma etching of contact holes and metal interconnect lines after removing photoresist by oxygen plasma ashing.

INTRODUCTION

Recent trends in plasma etch processing used in semiconductor device manufacturing have resulted in significant impact to polymer strip processes designed to remove sidewall polymer residues from metal and metal interconnect patterned layers. More aggressive chemistries and more aggressive process conditions must be used in the plasma etch process to achieve tighter control of pattern replication for shrinking device geometries in the patterned film with high selectivity to underlying films. Such aggressive conditions produce etch polymer residues deposited on the sidewalls that are high in inorganic material content (Al, TiN, Ti, TiW, Si, chlorides, fluorides, etc.). Such sidewall polymer residues with high composition of inorganics are very difficult to remove using traditional solvent type chemistries designed to simply dissolve residues.

In part due to these difficulties, it is becoming increasingly more common to treat photoresist strip and polymer removal as separate process steps. Common high

temperature oxygen plasma processing used to remove resist residues after etch further aggravate the polymer removal problem by oxidizing these inorganic compounds and making their removal more problematic.

Additionally, due to the accelerating reduction in the size of device patterns, failure to remove these sidewall polymer residues completely can result in major negative impacts to yield and device performance. As these sidewall polymer residues are often difficult to detect using standard quality inspection techniques, it is critical to have a residue removal process that is capable of fully removing all residues across a wide range of process conditions and treatments with extreme reliability.

More aggressive chemistries have been designed in recent years and are used extensively in the semiconductor manufacturing industry today to deal with these tougher polymers. Unfortunately, these chemistries often contain environmentally unfriendly components that can present a significant issue in managing exposure of personnel, equipment, and product, as well as pose challenges and costs associated with waste disposal. Additionally, elevated temperatures required to achieve effective polymer removal present additional safety concerns as well as accelerate any change in chemical composition and strip effectiveness of the chemical. Thus, the effective lifetime of these expensive specialty chemicals is often measured in hours.

From a semiconductor manufacturing standpoint, it is highly desirable to utilize a chemistry that can accomplish several critical (and often contradictory in terms of design of the chemical mechanisms) goals: complete polymer removal, little to no attack of underlying films and device features, minimal process times, a stable and repeatable process over time and process variations, at a minimal cost for sustaining the chemical process, while maximizing safety and minimizing environmental impact.

## EXISTING STRIPPER CHEMISTRY

A number of different chemistries are currently being used for the removal of etching residues. These chemistries include: alkaline based positive resist developers; buffered hydrofluoric acid (HF) with ethylene glycol; a mixture of nitric acid; acetic acid and HF; a combination of HF wet cleaning and NF<sub>3</sub>/hydrogen dry etc.; vapor HF; and solvent/amine based chemistries. A description of each chemistry and its limitations are discussed below.

Alkaline positive resist developers, which include components such as sodium hydroxide, tetramethylammonium hydroxide (TMAH) and choline, are effective at removing aluminum residues but ineffective at removing residues created from etching aluminum alloys, such as Al/Si/Cu. Although experimental results obtained at Olin Microelectronic Materials showed complete removal of the Al/Si/Cu residue using a

TMAH solution, removal is thought to be due undercutting by way of complete corrosion of the underlying aluminum layer. Therefore, removing aluminum residues using positive resist developer requires extreme process control to prevent overetch of exposed aluminum layers.

Buffered HF solutions with ethylene glycol and nitric/acetic/hydrofluoric acids can be used to clean via and metal interconnect residues. The active species in these mixtures are hydrogen ions [ $H^+$ ], fluoride ions [ $F^-$ ], and acetate ions [ $CH_3COO^-$ ]. The major limitation of these chemistries is their non-selective nature -- undue process control is necessary to minimize attack on exposed oxide and metal layers. In some processes the non-selective nature makes them unusable.

The combination of HF wet cleaning and  $NF_3$ /hydrogen dry etch has been used to remove via etch residues. The wafers are dipped in HF and then exposed to a  $NF_3$ /hydrogen dry etch. Although this method is effective, it is a multi-step process. Vapor HF has also been described to effectively remove via hole etch residues.

Solvent/amine based chemistry is currently the most sufficient method of residue removal. This is accomplished by dissociating the aluminum and other metals from the residue. Amines react with water to generate an ion pair of protonated ammonium cation and hydroxide anion in equilibrium. Thus formed hydroxide can further react with metal or metal oxide such as Al or  $Al_2O_3$  to form soluble species. This is a driving force of the plasma-etch residue cleaning. However, hydroxide also attacks substrates such as  $SiO_2$  and Al/Si/Cu to cause a metal corrosion. These two reactions usually take place randomly. Therefore, it is critical to add a corrosion inhibitor which should inhibit the metal attack with hydroxide ions but should not prevent the reaction of plasma-etch residues with hydroxide ions. This approach is currently most popular in this field and a lot of patents have been filed with various compositions of alkylamines, water and proprietary corrosion inhibitors. Table 1 shows a summary of features of various types corrosion inhibitors so far disclosed in patents applied. Some types of corrosion inhibitors tend to inhibit both of the corrosion and plasma-etch residue cleaning. It is thus important in this case to choose an appropriate type of corrosion inhibitor.

#### NEW CHEMISTRY DEVELOPED

The present authors have developed a unique chemistry by using guidelines based on the limitations of the existing stripper technologies. The new chemistry must eliminate the use of any toxic component like catechol as a known carcinogen, and also eliminate the post-strip rinse process with an organic solvent like isopropyl alcohol so that we can minimize amount of wastes, especially organic wastes. The new chemistry is thus an aqueous-based formulation using a weakly acidic buffered solution consisting of amine salts, while the current existing technology is based on an alkaline pH-based formulation,

as mentioned above. It is more possible to make a selective dissolution of plasma-etch residues against the substrate metal attack if the most appropriate pH is applied. In other words, the pH effect on the selective dissolution of plasma etch residues is critical. In addition, a weakly acidic solution is more environmentally friendly, especially for disposing of waste chemicals.

## PERFORMANCE OF MICROSTRIP® 5002

### Characterization of Plasma-Etching Residue

Figure 1 shows the analytical results of contact via and metal lines after photoresist removal by an oxygen plasma ashing process. EDX spectra for the before and after residue removal condition, for the contact via case, are shown in (c) and (e) respectively. These two spectra in contrast, show the loss of the Al signature energy spectra and reduction of intensity of the oxygen energy spectra. This indicates the predominant composition of this residue to be  $\text{Al}_x\text{O}_y$ .

The EDX spectra for the before and after residue removal condition, for the metal line case, are shown in (h) and (j) respectively. Comparing these two spectra in contrast, show the loss of the Si signature energy spectra and reduction of intensity of the oxygen energy spectra. This indicates the predominant composition of this residue to be  $\text{Si}_x\text{O}_y$ . It should be noted that residue compositions are specific to plasma chemistries and reactors that produce them. Therefore, variation of residue is quite expansive.

Illustrations of cross-section layers of the actual device structure of contact via and metal lines are shown in (a) and (f) respectively. The contact via is a structure of thin films consisting of  $\text{SiO}_2/\text{TiN}/\text{Al}-\text{Cu}$  with a residue mainly composed of  $\text{Al}_x\text{O}_y$ . The metal line is a structure consisting of  $\text{Al}-\text{Cu}$  with a residue composition where  $\text{Si}_x\text{O}_y$  is most prevalent.

It is an observed response with sidewall polymer residues, that with increase time, exposure to atmosphere renders these residues to be increasingly difficult to remove and exhibit a decrease in metal selectivity. Atmospheric oxidation and moisture absorption result in increased residue densification and surface binding energies resulting in residues that are difficult or in extreme cases impossible to remove. Increased metal corrosion also results from absorbed halides migrating into the metal sidewalls over time. Upon contact with water these rapidly form corrosive acids. This forces the requirement that functional testing be performed on wafers that are characteristic of the in-situ process timelines of production.

## Process Dependency

The process time requirement for complete removal of residue will have a great dependency on the process that produces them. Typically, a production application would incorporate a process temperature envelope of 55°C and 65°C and a time process envelope of 15 to 30 minutes as shown in Figure 2. Maximum strip time specifically applicable to this sample is demonstrated to be 30 minutes. At this temperature range, a process time of less than 15 minutes is inadequate, as residue is still present, but a 20-minute process time allows for the complete removal of residue. Recommended baseline process conditions for the removal of contact via residue are: 1.) a bath temperature within 55-65°C; 2.) a process time within 20-30 minutes. Residues produced from the dry plasma etching of metal lines (not shown) have a shorter process time requirement than contact via residues. Recommended baseline process conditions for the removal of metal line residue are: 1.) a bath temperature within 55-65°C; 2.) a process time within 10-15 minutes. It should be noted that these are recommended baseline process conditions and that there may be significant deviation from these process conditions due to the varying compositional issues specific to each residue.

## Bath Life

Figure 3 show the results of a 12 hour bath life study at recommended process parameters (60°C, 30 minutes). This test was performed on a temperature controlled laboratory hotplate utilizing 1000 ml beakers as bath reservoirs. The focus of this test was to determine any performance reduction due to the competitive evaporation rates of the various bath components. Bath loading effects associated with production wafer processing, was not evaluated by this method.

Bath life was evaluated in a production environment in a major U.S. wafer FAB facility. This evaluation concentrated on the first 24 hours of bath life. Devices were analyzed at 0, 12, and 24 hours. Bath samples were collected every 4 - 6 hours and analyzed for compositional change and trace metal contamination. The results indicate that there was no observable degradation of bath performance and no significant increase in trace metal contaminants for a period of 24 hours. The water content and pH decreased significantly, however the functionality exhibited excellent stability. The mechanism presumed to allow this enhanced bath performance is the buffered action of Microstrip® 5002 upon heating.

## Performance Comparison with Competitors

The most important requirement for the removal of sidewall polymer residues is high selectivity of residue to metals. When adequate selectivity is not achieved, unwanted etching of metals results. In the case of contact vias, "undercut" of the metal layer will be

observed. In the case on metal lines, excessive sidewall metal attack results. Figure 4 represents the preferred contact via case with Microstrip® 5002 and the related "undercut" resulting from the competitive chemical processing. Observed in the competitor case is the excessive etching of the TiN and Al-Cu metal layer under the SiO<sub>2</sub> layer. The mechanism proposed allowing for the elimination of the corrosion ("undercutting") response is the slightly acidic pH of Microstrip® 5002 as compared to the highly basic pH of the competitor.

#### ACKNOWLEDGMENTS

The present authors would like to acknowledge the following individuals for their contributions to this project through their technical support and discussions:

Dr. E. Rothgery and Dr. K. Knollmueller at Olin Research Center, Cheshire, CT;  
 Dr. Y. Torban for X-ray analysis at Olin Metal Research Laboratory, New Haven, CT;  
 Dr. S. Beaudoin and Mr. B. Wright at Arizona State University, Tempe, AZ; and  
 Mr. M. Towner and Mr. L. Love, Jr. at Olin Microelectronic Materials, Tempe, AZ.

Type	Example	Inventor	Assignee	Patent Application	Base Formulation
Reducing	Hydroxylamine	W.M.Lee	EKC	USP 5,279,771 ('94) USP 5,334,332 ('94)	Amine/Water /Catechol
	Hydrazine			EP 0647 884 A-1 ('94)	Amine
	Ascorbic Acid	G.Schwartzkopf	J.T.Baker		/Organic Solvent
Phenolic	Gallic Acid			USP 5,597,420 ('97)	
	Pyrogallop	I.E.Ward	Ashland	USP 5,563,119 ('96)	Amine/Water
Chelating	8-Hydroxyquinoline	I.E.Ward	Ashland	USP 5,417,877 ('95)	
	Succinic Acid Deriv.	K. Honda	OMM	USP 5,545,353 ('96)	Amine /Organic Solvent
	Polymeric Chelating			USP 5,597,678 ('97)	
Acidic	Acetic Acid			USP 5,308,745 ('94)	
	Phthalic Acid	G.Schwartzkopf	J.T.Baker	USP 5,472,830 ('95)	Amine /Organic Solvent
Alcoholic	Amino Acids	K.Honda	OMM		
		M.Miyazaki	Kanto	JP 7-028254 ('93)	Amine/Water
		R.Hasemi	MGC	JP 8-202051 ('95)	
	Sugar Alcohol	K.Honda	OMM	JP 9-054442 ('95)	Amine /Organic Solvent
		H.Tanka	TOK	JP 64-073348 ('87)	Amine/Organic Solvent/Water
	Acetylenic Alcohol	M.Sugita	Nagase	JP 64-088548 ('87)	
Phosphate	Phosphate/PEO	K.Wakiya	TOK	JP 4-124668 ('90)	Amine /Organic Solvent

Table 1  
 Summary of Patents Applied to Various Types of Corrosion Inhibitors for the  
 Plasma-Etch Residue Cleaning

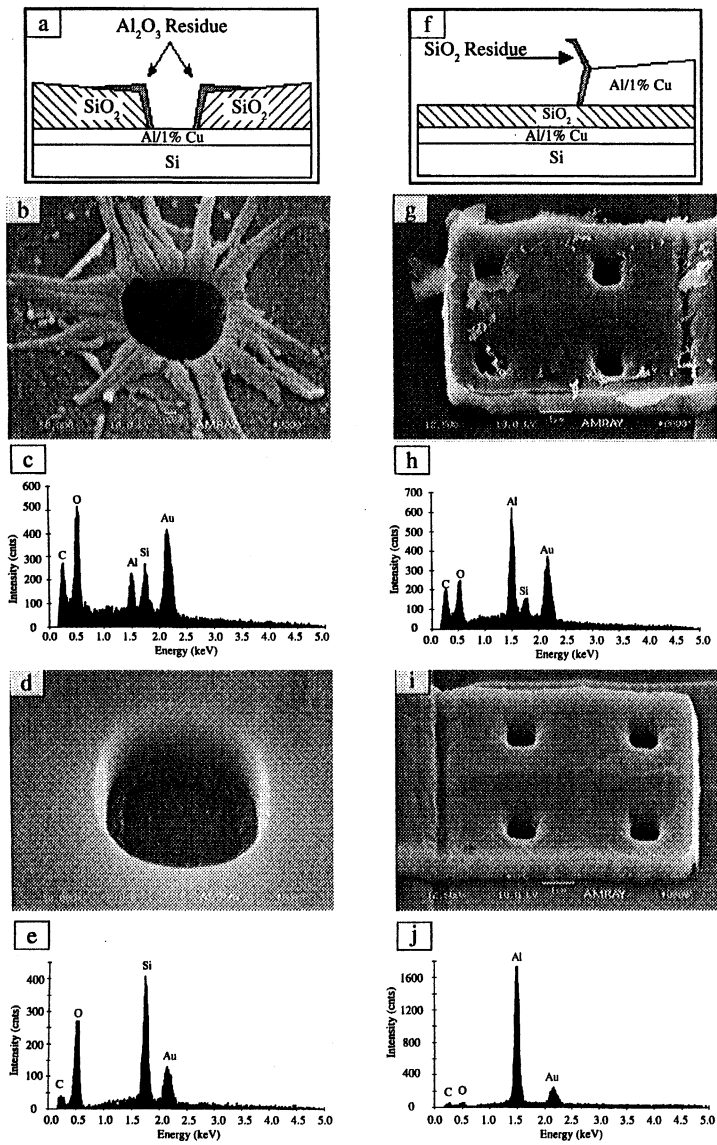


Figure 1  
SEM and EDX Analyses of Plasma-Etch Residues of Via-hole (left) and Metal-line (right)

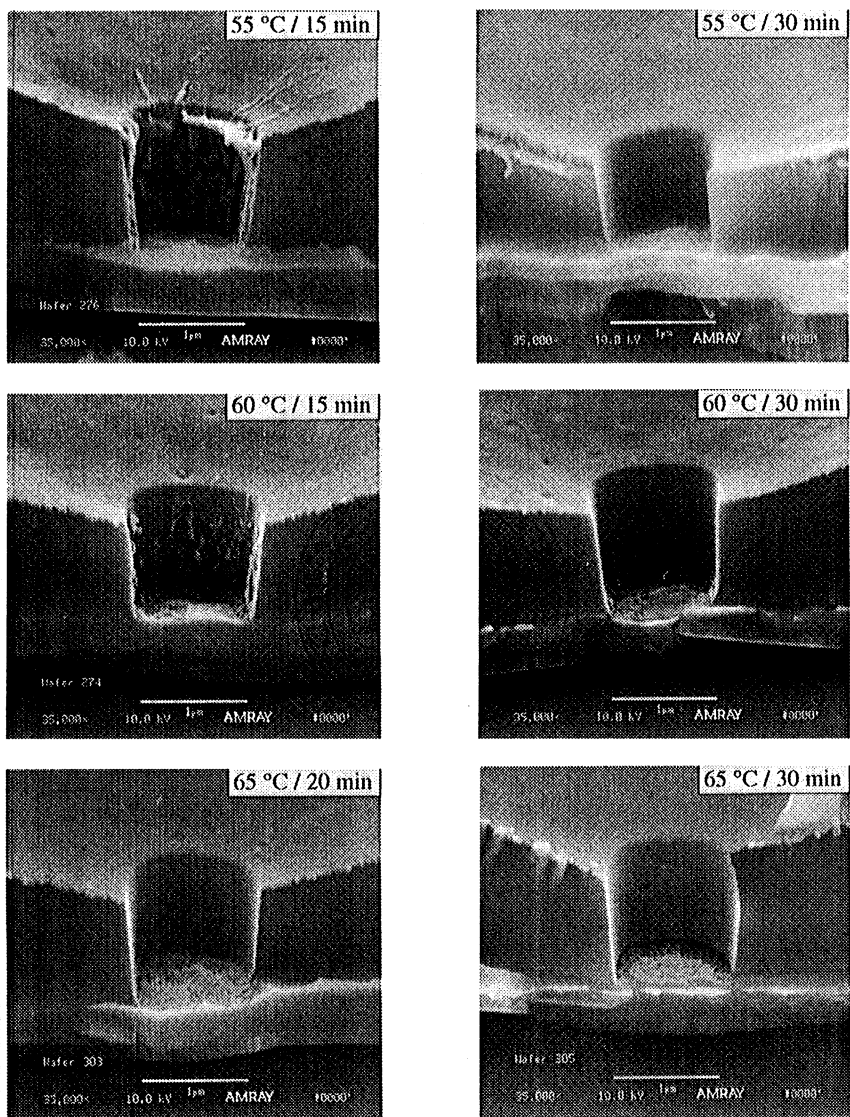
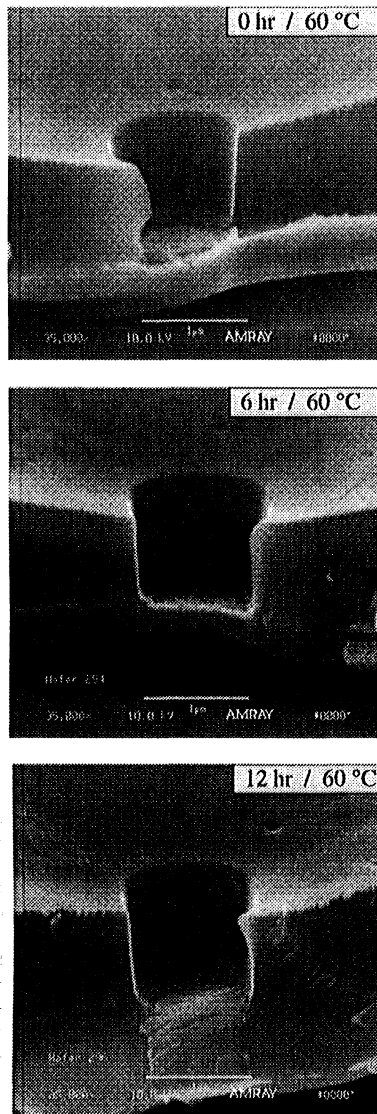
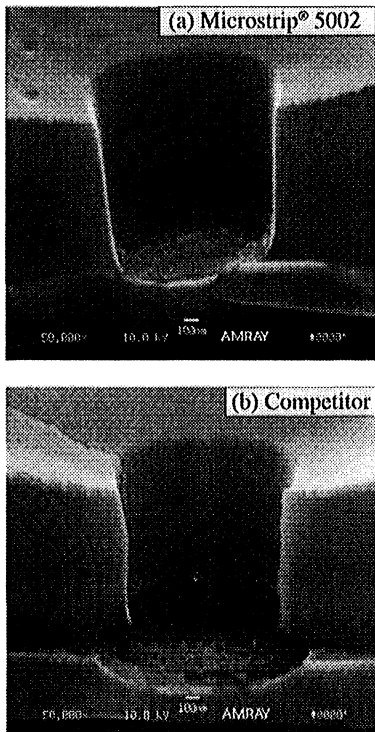


Figure 2  
Process Dependency of Plasma-Etch Residue Cleaning with Microstrip® 5002



**Figure 3**  
Bath-life Test of Microstrip® 5002



**Figure 4**  
Comparison of the Performance of  
Microstrip® 5002 with a Competitor's  
Product under Each Recommended  
Condition without IPA Rinse:  
(a) 60 °C @ 30 min;  
(b) 75 °C @ 30 min.

## POST W CMP CLEANING

I. Constant , S. Marthon ,T. Lardin,  
C. David, M.N Jacquemond and F. Tardif

Gressi-Leti-CEA/G, 17 rue des Martyrs , 38054 Grenoble Cedex 09, France

Chemical Mechanical Polishing (CMP) leaves a lot of residual particles and metals and induces a heavily damaged zone. In this study two different cleaning processes after W CMP are compared on both  $\text{SiO}_2$  and  $\text{Si}_3\text{N}_4$  : conventional wet processes and scrubbing. Finally if the wafer backside can be protected by an oxide or a nitride layer the most suitable cleaning after W CMP consists in using a megasonic diluted ammonia based process. This treatment leaves an acceptable metallic contamination level and leads to better electrical results. The other solution consists in using a scrubber in the first stage and then a final diluted HF wet treatment in order to remove the damaged zone and transported tungsten.

## INTRODUCTION

Chemical Mechanical Polishing (CMP) of tungsten performed to planarize integrate circuit topologies uses alumina colloids in acidic media<sup>(1)</sup>. Unfortunately this kind of process leaves a large amount of particles called slurries, a parasitic metallic contamination and a damaged layer at the surface of the dielectrics<sup>(1),(2)</sup>. A powerful new cleaning is therefore now necessary. The residual slurries must be removed before the wafer proceeds to the next process step because particles cause functional defects and decrease yields in the finished integrated circuits<sup>(2)</sup>. Residual metals induce shorts on the dielectric surfaces leading to parasitic conductances by percolation phenomena. This study uses Damascene structure tests presenting at the top surface PECVD TEOS  $\text{SiO}_2$  or a PECVD  $\text{Si}_3\text{N}_4$  stopping layer. Particles can be removed by an underetching mechanism in wet processes or by the mechanical effects of scrubbing. As demonstrated earlier<sup>(3)</sup> the most efficient chemistry to remove particles is still alkaline mixtures which can be used in this case as they are compatible with the presence of W plugs. Scrubbing and wet processes are compared here in terms of particle and metallic removal efficiency W line transports and electrical results on actual devices.

## EXPERIMENTALS

### Sample preparation

All the tests were performed on 200 mm p type wafers CZ, 14-22 Ohm.cm. The particle removal tests are performed on full sheet wafers covered with silicon PECVD TEOS oxide or silicon PECVD nitride. For electrical tests a 0.18  $\mu\text{m}$  specific test vehicle including

Damascene structures is used. A model ITEC 676 CMP system consisting of a Thomas West pad is used for the polishing with Baikovsky.

### Sample cleaning

The wafers are scrubbed with a 1% NH<sub>4</sub>OH solution necessary in the case of alumina slurries and PVA brushes for Zeta potential driving forces. The cleaning processes are performed on a conventional wet bench from Submicron System including a high megasonic power source (1600W).

### Sample characterization

The metallic contamination is measured with a RIGAKU Model 3726A TXRF equipped with a W cathode or with a VPD-ICPMS 4500 from Hewlett Packard and residual particles by a Tencor 6420. The damaged layer thickness is determined by spectroscopic ellipsometry (SE) or X-ray specular reflectivity (XRSR). Ellipsometric measurements are performed on a modified ES4G ellipsometer from SOPRA. The incident angle is 75°. This method is used to confirm analysis from X-ray specular reflectivity on a D5000 goniometer from Siemens. The electrical parameters are measured by means of a Keithley Model 400 with a KLA 1201 prober.

## ETCHING RATE OF W

As the cleaning solutions have to respect the W presence the etching rates of a full sheet wafer of W deposited on a Ti/TiN barrier are studied in figure 1. The acceptable maximum etching was arbitrarily limited to 5 nm for an industrial process time of 10 min. It can be seen that W is not very corroded by all the non-oxidant tested mixtures. SC1 which contains the strong oxidant H<sub>2</sub>O<sub>2</sub> is all the same studied for its obvious manufacturing interest : it is not necessary to protect the Silicon of the backside of the wafers from roughening effects. Furthermore from the particle removal efficiency point of view the SC1 mixture can be diluted if the ratio between H<sub>2</sub>O<sub>2</sub> and NH<sub>4</sub>OH is kept constant<sup>(2)</sup> and if strong megasonics are used. As shown in figure 2 the conventional SC1 [0.25,1,5] performed at 70°C during 10 minutes can not be used because of its too high etching rate even when used very diluted. On the other hand NH<sub>4</sub>OH [0.25,6] 70°C 10 minutes (dNH<sub>3</sub>) represents an acceptable solution with an etching rate below 0.5 nm/min. Unfortunately as the oxidant agent can not be used, the backside of the wafer has to be protected from etching effects.

After scrubber HF or dNH<sub>3</sub> cleanings no parasitic corrosion effect is detected at the edges of the actual structures (W/Ti) by SEM observations. As an example figure 3 presents a W plug after dNH<sub>3</sub> bath. The top W consumption is only due to dishing phenomena.

## PARTICLE REMOVAL

Full sheet wafers of both oxide and nitride are intentionally polluted with alumina slurries in order to simulate the particulate contamination left by the CMP. About 30,000 particles greater than 0.2 μm are deposited on PECVD TEOS oxide and about 700 particles greater than 0.3 μm on PECVD nitride. In order to remove the particles a 50 Å underetching is necessary on both silicon nitride and oxide which corresponds to a 0.5 nm/min. etching rate for an industrial 10 min. process<sup>(4)</sup>. We earlier demonstrated that HF based chemistries

even with surfactants did not lead to results as good as alkaline mixtures<sup>(4)</sup>. Therefore only alkaline media are tested in terms of particle removal.

The particle removal efficiency with the scrubber and the dNH<sub>3</sub> bath for each dielectric is tested in figures 4 and 5. The results are comparable in both cases. The dNH<sub>3</sub> with megasonics cleaning usually leads to the best results (residual particles <30 for SiO<sub>2</sub> and <50 for Si<sub>3</sub>N<sub>4</sub>). When a scrubber is used the 0.1% HF dip necessary to remove the damaged zone participates in the final particle level. This treatment is more efficient before the scrubbing. Finally dNH<sub>3</sub> seems to be the most promising cleaning after W CMP as its cost of ownership is about 3 times lower than for this scrubber.

## DEPOSITED METALS ON DIELECTRICS

The CMP leaves metallic contamination on the dielectrics. At the interconnection level these charges can disturb the electrical information transfer<sup>(3)</sup>. The proposed cleanings have to remove this contamination as well. So the scrubber and the dNH<sub>3</sub> bath are compared in terms of residual contaminants after cleaning on oxide and nitride. Figure 6 shows that both processes leave nearly the same acceptable quantities of foreign metals.

## POST SCRUBBER TREATMENT

### Metal line transportations

The metal line transportations during the cleanings can cause shorts between 2 conductive lines. In order to simulate this effect a full sheet W wafer is scrubbed between two clean oxide or nitride wafers. Figure 7 shows that scrubbing leaves a large amount of W essentially on oxide. This dangerous W transportation has to be removed.

As far as dNH<sub>3</sub> performances are concerned, a full sheet of 100 mm wafer covered with W deposited on a Ti/TiN barrier is fixed at the centre of a 200 mm wafer of oxide or nitride during the wet cleaning. The 200 mm wafers are then analyzed out of the mark left by the 100 mm wafer by VPD-ICPMS. Figure 7 shows that W contamination transportation is negligible after dNH<sub>3</sub> cleaning.

The EDX did not allow us to observe the phenomenon because of its too low limit detection.

### Dielectric cleaning

As previously demonstrated a post scrubber treatment is therefore necessary to remove the transported W. Several wafers with PECVD oxide and nitride are intentionally polluted at 10<sup>13</sup> at/cm<sup>2</sup> by a W solution using a spin drier technique. Two kinds of cleaning are tested : 0.1% HF or room temperature H<sub>2</sub>O<sub>2</sub> [1/5] presenting a very low W etching rate (see figures 8 and 9). Even though the particulate cleaning recommends an HF dip before the scrubbing, a post scrubber HF treatment during 3 min is also required in order to remove W contamination on oxide. Relating to nitride a H<sub>2</sub>O<sub>2</sub> treatment is more appropriate but not *a priori* necessary.

### Damaged zone removal

The mechanical effects of CMP damages the top dielectric layers. The thickness of the damaged zone can be determined by a succession of short dips in diluted 0.1%HF (see figure 10) or in hot ammonia.

The RX specular reflectivity and ellipsometry are also useful methods to determine the damaged layer. The thickness is extracted from the measured data by means of a modelling and fitting process using the Refsim software from Siemens. RXSR and SE are based on the reflective wave properties. The measures are deduced from the difference between the behaviour of polished layers and reference layers.

The reflectivity diagram shown in figure 11 presents oxide layer interferences which lead to determination of the damaged layer. The SE measures the change of wave polarization as a function of the wavelength. The reflective wave polarization is elliptic and is determined with two parameters:  $Tg\gamma$  and  $\cos\Delta$  which depend on the thickness (see figures 12 and 13). This method is used to confirm the previous measures.

Finally the results obtained are similar to those measured on  $SiO_2$  with the HF dip technique : the damaged zone is about 1 nm .For the nitride the thickness is about 6 nm. Therefore the proposed  $dNH_3$  cleaning enables this damaged layer on the oxide to be removed without any other treatment. Related to nitride this process has to last around 15 minutes.(figure 2).

## ELECTRICAL TESTS

Different tests are performed on several patterned structures of wafers with nitride oxide as the dielectric only. The connections are tested (see figure 14). Cleaning after CMP is necessary since without any cleaning patterned wafers present a high leakage current. Scrubber cleaning is not enough and an HF bath improves the yield. However  $dNH_3$  followed by HF cleaning leads to the best results with regard to yield and leakage current.

## CONCLUSION

CMP used to planarize IC topologies leaves a large amount of particles, parasitic metallic contaminations, and a damaged layer at the top surface of the dielectrics. Particles can be removed adequately from silicon and nitride oxides by diluted megasonic hot ammonia [0.25/6] or scrubber in conjunction with 0.1% HF. These solutions respect the W line, leave an acceptable metallic contamination level, and enable the damaged zone left by CMP to be removed. In spite of the obvious manufacturing interest for SC1 this cleaning solution can not be used because of its too high etching rate. In this case the backside of the wafer has to be protected from the etching. After comparison between  $dNH_3$  and scrubber results show that the most suitable cleaning after W CMP consists in using the ammonia process for the particles and the damaged layer as well. This solution does not lead to a metal line transportation which can induce shorts on the dielectric surface. The scrubber method requires an HF bath before the scrubbing to increase the particle removal efficiency and one more HF post-treatment in order to remove the W line transportation contaminations.

## **ACKNOWLEDGEMENTS**

The authors would like to acknowledge the contributions of H.Banville for polishing patterned nitride wafers and A. Chabli for analyzing the damaged zone by X-rays.

## **REFERENCES**

- (1) I Malik et al, (SPRING) MRS 1995
- (2) T.L. Myers et al, Solid State Technology-Oct 5-59
- (3) Chi Web Liu et al, Applied Surface Science- 92 (1996), 176-179
- (4) F. Tardif et al, MAM'97, Villard de Lans
- (5) P. Boelen et al, MRS'97, Paris
- (6) F. Tardif et al, Microelectronic Engineering 33 (1997) 195-201

This work was carried out within the GRESSI consortium between CEA-LETI and France Télécom-CNET

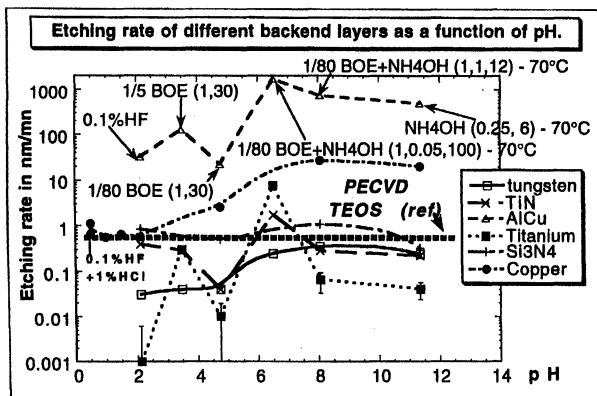


Figure 1 : Etching rate of different back-end layers

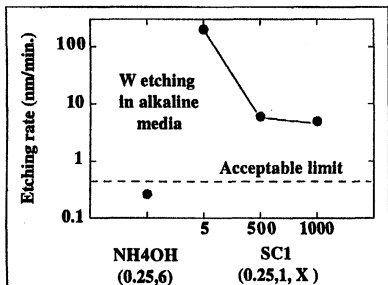


Figure 2 : Etching rate of W by alkaline mixtures

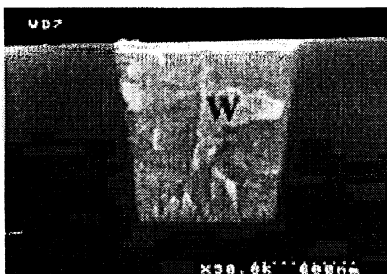


Figure 3 : SEM view of W plug after cleanings

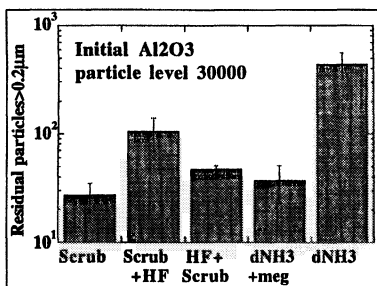


Figure 4 : Particle removal on PECVD TEOS oxide

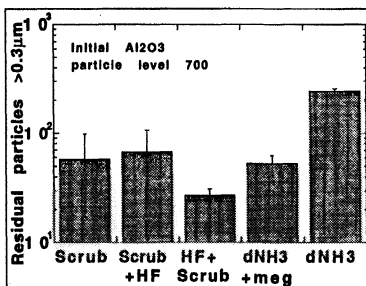


Figure 5 : Particle removal on PECVD nitride

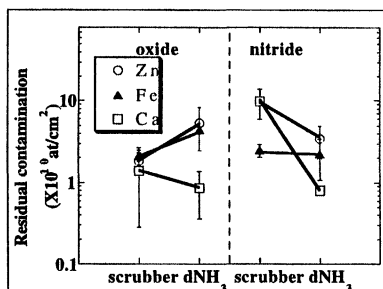


Figure 6 : Deposited metals on dielectrics

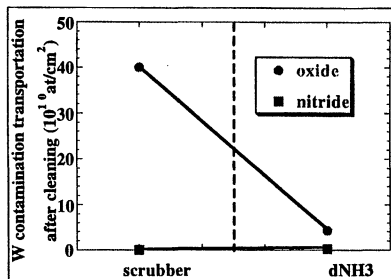


Figure 7 : Metal line transportation

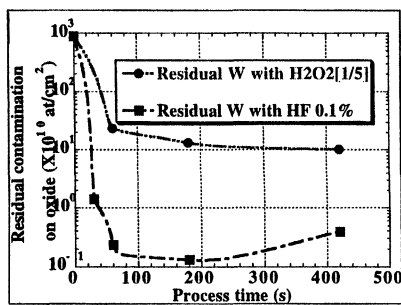


Figure 8 : Oxide cleaning

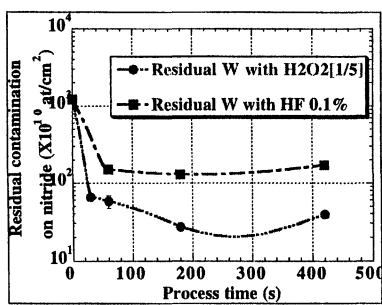


Figure 9 : Nitride cleaning

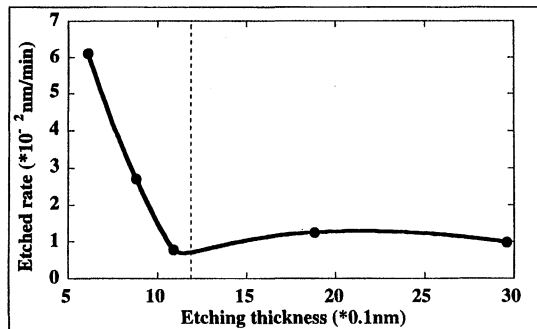


Figure 13 : Damaged zone removal by HF method on oxide

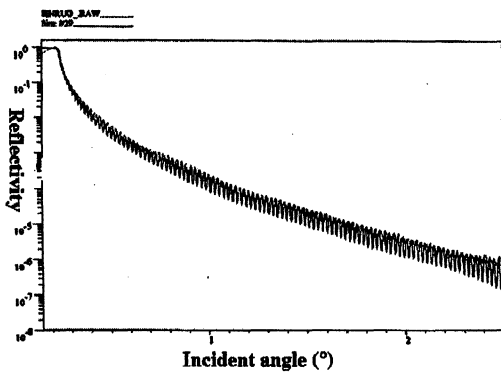


Figure 10: nitride XRSR spectrum

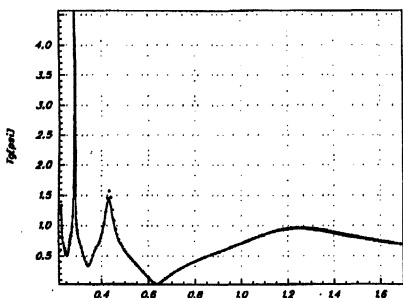


Figure 11 : nitride SR tangent  $\psi$  diagram

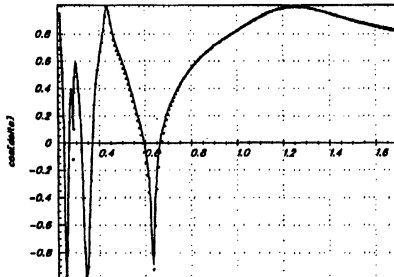


Figure 12 : nitride SR cosine  $\Delta$  diagram

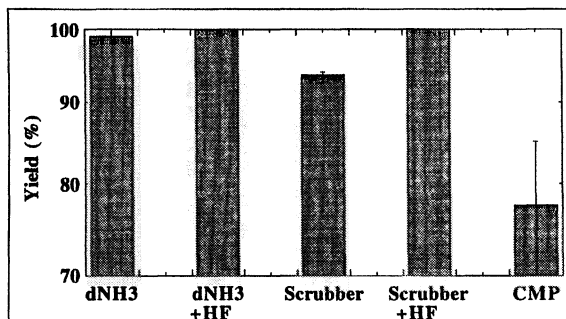


Figure 14 : Contact yield after cleanings

# **EVALUATION OF NON-CONTACT POST-CMP CLEANING PROCESS UTILIZING SPLIT-LOT POLISHING AND CLEANING COMPARISONS**

Brian Fraser, Michael B. Olesen, Tu Phan

VERTEQ, Inc.

1241 E. Dyer Rd. Suite 100

Santa Ana, CA 92705

Bill Morrison

Texas Instruments

13353 Floyd Road 75243 M/S 374

Dallas, TX 75263

A non-contact, post-chemical mechanical planarization (CMP) cleaning method is presented as an alternative to the commonly used physical scrubbing method. This cleaning method uses one tank for aqueous ammonia cleaning and rinsing with megasonic energy, and a second tank for HF processing. Since the planarization and cleaning processes are interdependent, truly useful evaluation of different cleaning methods dictates the use of wafers from the same polish lot. The production environment split-lot testing reviewed in this paper shows the non-contact cleaner ( $40 \pm 24$  defects  $\geq 0.20\mu\text{m}$ ) to be a viable alternative to the contact cleaner ( $88 \pm 112$  defects  $\geq 0.20\mu\text{m}$ ). It should be considered that both types of cleaners have independently shown better net results, but the data presented in this paper represents split lot testing using the same polished wafer for both cleaners.

## **Introduction**

Chemical mechanical planarization (CMP) is rapidly developing due to the inherent advantages of global planarization. The importance of step coverage prior to CMP is practically eliminated and concern for lithographic depth of field following CMP is greatly reduced [1]. As CMP prevalence grows, the importance of post-process cleanup grows as well. Due to the use of silica (for dielectric layers) and alumina (for metal layers) to mechanically remove films during polishing, these

materials pose significant contamination potential in subsequent manufacturing steps, and must be removed afterwards [2].

As a relatively new process, a high degree of standardization does not exist for CMP, and consequently, evaluation is difficult. Standardization has shown to be especially important for this application because of the co-dependence of the polishing and cleaning steps on the overall cleaning results. Performance claims for either the CMP or post-CMP clean steps must be considered with both steps well defined. This paper presents test results where multiple polish and clean processes were performed at a common site.

Scrubbers have been widely used for the post-CMP cleaning application[3]. They consist of PVA brushes which rotate and press against the wafer in order to mechanically remove particles from the surface. Chemical solutions can be used in the brush stations and deionized water is flowed through the brush core to flush the PVA. Additionally, a megasonic spray nozzle can be used and in conjunction, and wafers can be treated with HF acid.

### **Non-Contact Cleaning**

Introduced here is a non-contact cleaning method which has been used in production for post-CMP cleanup. The *VERTEQcleanSYSTEM™* (VcS), consists of (1) a VcS tank in which dilute SC1 (or other chemical) processing and rinsing are done in the presence of megasonic energy, and (2) a recirculation tank in which HF processing is executed. Chemicals and DI water are injected into the VcS tank as needed, and rinsing is performed by dump paddle in the tank bottom.

Megasonic energy is the non-contact method of physically removing particles. This particle removing ability has been well documented[4]. A spin-rinse dryer (SRD) is used following wet processing. A schematic of the system configuration is shown in Figure 1.

The patented method of chemical delivery and system design, though beyond the scope of this paper to explore in depth, are important features of the VcS for the following reasons: (1) chemical concentrations and solution temperatures can be controlled and easily changed; (2) megasonic energy can be applied to the wafers during the filling and dumping of the VcS tank.

Control of the ammonium hydroxide concentration is necessary to control the solution pH. This is important because both the rate at which water dissolves

silicon dioxide and the zeta potential of the solution constituents are functions of the pH. The etching reaction influences the amount of particle removal [5] and the zeta potential determines whether particle attachment or reattachment is electrostatically favored [6]. The optimal amount of etching is process specific, but can be adjusted by changing the ammonium hydroxide concentration or solution temperature. It should also be noted that the amount of etching required for particle removal has been shown to be significantly reduced when megasonic energy is used in the process [7].

Following particle removal, and prior to initial attachment, electrostatic forces can be used so that particles are not attracted to the surface and are unable to approach within distances needed for van der Waal interactions. Ideally, cleaning should done at a pH where the particles and film have the same sign zeta potential. For oxide CMP, this seems relatively simple because the film and the typical slurry are both  $\text{SiO}_2$ . However, the zeta potential is strongly a function of surface condition and impurities [8]. Consequently, the film and particles are not necessarily electrostatically repelled at all pH values. Above pH 8, silica particle and film zeta potentials approach fairly large negative values and are repelled. Therefore, use of basic pH solutions for post oxide CMP cleaning is electrostatically favorable.

Alumina slurry is typically used for tungsten CMP, and therefore it is desirable for the slurry to be electrostatically repelled from the tungsten and oxide films. Only above pH 8 does the zeta potential of alumina have the same sign (negative) as that of tungsten and  $\text{SiO}_2$ . Consequently, basic solutions are generally used for post-tungsten-CMP cleaning.

Megasonic energy (700–1500 kHz) used during cleaning has been established as a method of obtaining cleaner films than otherwise possible [4]. Unlike with ultrasonic energy (20–40 kHz), megasonic energy is not known to cause surface damage. It has been shown that bubble cavitation is the cause of ultrasonic energy damaging wafer surfaces [9]. However, the mechanism of megasonic energy in particle removal is not yet well understood, though acoustic streaming, cavitation and acoustic pressure are currently being investigated as contributors to particle removal [10]. It has also been suggested that megasonic energy reduces the boundary layer thickness, and therefore transfer of cleaning chemicals and particles through this layer is achieved more easily [11]. Other investigation of the effect of megasonic energy on wafer cleaning includes megasonic induced chemical reactions, specifically creation of radical species [12].

The efficiency of megasonic cleaning within the VcS is enhanced by the use of a patented transducer which has a curved design in order to produce a radially

dispersed wave pattern. Traditional transducers have produced perpendicular megasonic wave patterns requiring that either the transducer or wafers be moved during processing. This causes reduced contaminant removal efficiency, increased processing time, and typically causes particle generating damage to cassettes.

Experiments have indicated that better contamination removal and more efficient rinsing are obtained if megasonic power is applied to the wafers as the chemical or rinsing solution is filling the tank[13]. The improvement upon switching from the traditional full tank megasonic processing to the "fill-megasonic" method could be due to a different primary megasonic mechanism at the air/liquid/wafer interface as compared with the liquid/wafer interface. Application of megasonic energy during the entire cleaning and rinsing cycles also increases the exposure time to megasonic energy resulting in decreased cycle time.

### **Polisher Cleaner Co-Dependence**

Although the post CMP cleanup is crucial to final wafer cleanliness, the polisher has also been shown to be an extremely important part of the cleanup process. The polisher and cleaner should be considered co-dependent. The final cleanliness is a function of the history of the surface state, and the wafer surface is altered on the polisher in manners similar to the cleaning process. Specifically, the post polish buff and rinse have been shown to be critical steps in achieving low particle contamination[14].

This co-dependence has been discussed before, but is reiterated because of the importance for meaningful evaluation and comparisons between post CMP cleaning methods. An example is shown in Figure 2. Blanket PE-TEOS polish experiments are shown in which the post-CMP cleaning for all wafers (200mm) was identical. The only difference is in the polish recipe. Experiments were done with (1) a single platen, (2) two platens including a 2nd platen, 30-second rinse, and (3) two platens including a modified, 2nd-platen process. The difference in particle performance is due solely to the polisher process and shows the importance of considering the polisher in the evaluation of any post CMP clean[15]. The improved performance upon using a second platen rinse or buff has been shown [16] including the effect of platen downforce and chemistry [17]. The second platen is essentially the beginning of the cleaning process even if it does occur on the polisher.

Considering the significance of the polisher to cleaning performance, this variable must be known for any meaningful comparisons between post CMP cleaning methods. Experiments were performed to evaluate if the VcS could give particle results comparable to that of a scrubber. First, blanket PE-TEOS oxide wafers were polished to 8500Å thickness using a two-platen process including a 2nd-platen, 30-second rinse. All wafers were processed under identical polish conditions each time. Then, wafers were processed through either the VcS or scrubber (DNS-SP-W813-AS). The 150 wafers were analyzed with a Tencor 6420 at 0.20 $\mu$ m size and larger. The results are shown in Figure 3. The sum of all defects for the VcS and scrubber were 40  $\pm$ 24, and 88  $\pm$ 112, respectively. Also shown is the chart showing the performance with the same polish conditions and VcS cleanup over a 60-day period (Figure 4).

It is important to note that the polish process was not optimized and consequently the presented results are not as good as independent tests for many types of cleaning. Still, the polish process was held constant for cleaning evaluative purposes.

Another important evaluation parameter is surface-metal contamination following cleaning. In the VcS as well as with scrubbers, this is very dependent on the chemical treatment used. Following removal of the slurry particles with a dilute SC1-like solution, HF is used to etch approximately 100Å of oxide in order to greatly reduce the metal contamination. Following this treatment, surface metal concentration levels are below 10<sup>10</sup> atoms/cm<sup>2</sup>. Figure 5 shows these levels with and without HF treatment. Measurements were made with TXRF with verification by SIMS.

## Conclusions

Based on production environment, split-lot testing, non-contact cleaning has shown to be a viable alternative to post-chemical-mechanical-planarization (post-CMP) cleaning via brush scrubbing. Sum of defect results for the non-contact and contact methods were 40  $\pm$ 24 and 88  $\pm$ 112  $\geq$ 0.20 $\mu$ m, respectively. The non-contact surface metal concentration levels were below 10<sup>10</sup> atoms/cm<sup>2</sup>. The non-contact cleaner has one tank for aqueous ammonia cleaning and rinsing with megasonic energy and a second tank for HF processing.

## References

1. (a) F.B. Kaufman, D.B. Thompson, R.E. Broadie, M.A. Jaso, W.L. Guthrie, D.J. Pearson and M.B. Small, *J. Electrochem. Soc.*, 138 (1991) 3460. (b) M. Fury, *Solid State Tech.*, April (1995) 47. (c) M. Martinez, *Solid State Tech.*, Sept (1995) 44. (d) P. Burggraaf, *Semiconductor Intl.*, Nov (1995) 74.
2. T. Myers, M. Fury and W. Krusell, *Solid State Tech.*, Oct (1995) 59.
3. (a) W. Krusell, J. de Larios and J. Zhang, *Solid State Tech.*, June (1995), 109. (b) D. Hymes and I. Malik, *Micro*, Oct (1996) 55.
4. (a) A. Mayer and S. Schwartzman, *J. Electron. Mater.*, 8 (1979) 885. (b) S. Schwartzman, A. Mayer and W. Kern, *RCA Review*, 46 (1985) 81. (d) S. Cohen, D. Rath, G. Lee, B. Furman, K. Pope, R. Tsai, W. Syverson, C. Gow and M. Liehr, *MRS Symp. Proc.*, 386 (1995) 13. (e) P. Resnick, C. Adkins, P. Clews, E. Thomas and N. Korbe, *MRS Symp. Proc.*, 386 (1995) 21.
5. S. Verhaverbeke, M. Meuris, P. Mertens, H. Schmidt and M.M. Heyns, *Semicon Japan* (1993).
6. J. de Larios, M. Ravkin, D. Hetherington and J. Doyle, *Semiconductor Intl.*, May (1996) 121.
7. S. Cohen, D. Rath, G. Lee, B. Furman, K. Pope, R. Tsai, W. Syverson, C. Gow and M. Liehr, *MRS Symp. Proc.*, 386 (1995) 177.
8. C. Raghunath, D. Jan and S. Raghavan, *Microcontamination Conf. Proc.* (1994) 164.
9. K. Suslick, *Sci. American*, 260 (1989) 80.
10. D. Kittelson, T. Kuehn and Y. Wu, *Spring '97 MRS Conf.*
11. R.M. Hall, T. Jarvis, T. Parry, L. Li and R. Hawthorne, *Micro*, (July 1996) 81.
12. T. Ohmi and M. Toda, *Ohmi*, *Spring '97 MRS Conf.*
13. Unpublished results, VERTEQ (part of VcS patent).
14. S.R. Roy, I. Alli, G. Shinn, N. Furusawa, R. Shah, S. Peterman, K. Witt, S. Eastman, P. Kumar, *J. Electrochem. Soc.*, 142 (1995) 216.
15. These experiments and all other experiments described were performed at Texas Instruments with an IPEC/Westech polisher, semi-automated VcS and DNS-SP-W813-AS scrubber.
16. M. Horn, *Solid State Tech.*, (1991) 57.
17. I. Ali, S. Roy, G. Shinn, S. Raghavan, R. Shah and S. Peterman, *Microcontamination Conf. Proc.* (1994) 196.

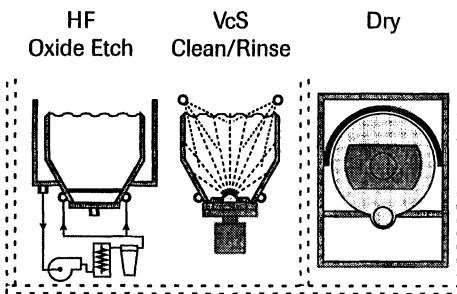


**Figure 1.** Schematic of Non-Contact Cleaning System

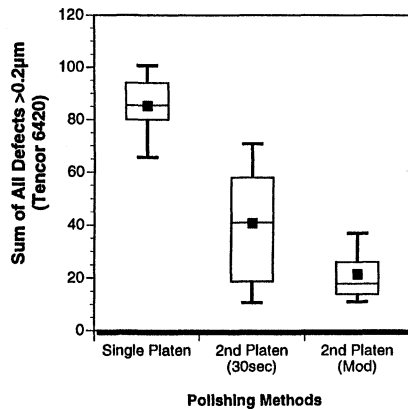


**Figure 2.** Effects of Various Polish Processes Using the Same VcS Clean Process

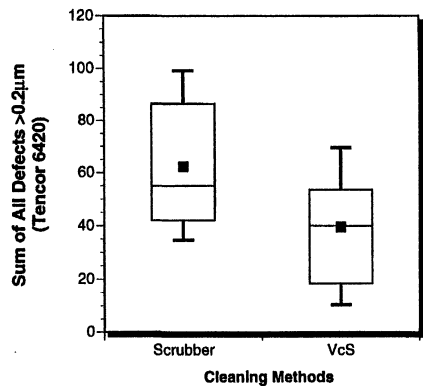


**Figure 3.** Results of Scrubber and VcS Cleaners Utilizing the Same Polish Process

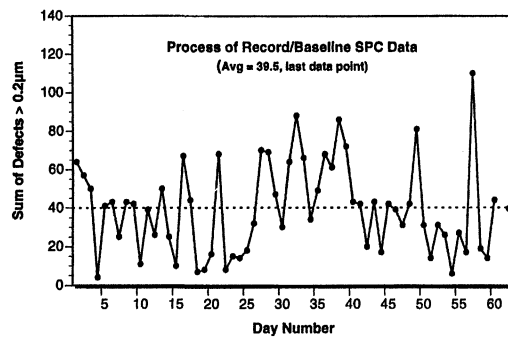


**Figure 4.** 60-Day SPC Chart of Polish and Clean Process

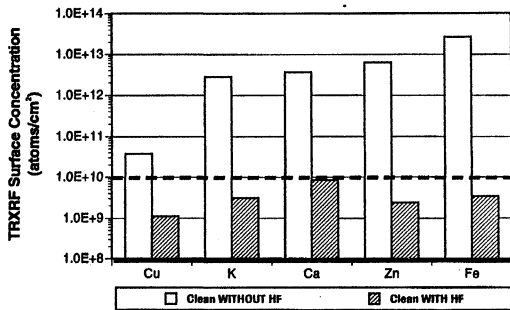


**Figure 5.** Metals Contamination Comparison With and Without HF Process Sequence



## AUTHORS INDEX

Abe, N.	513	Fakhouri, S.	315, 408
Adkins, C.L.J.	23	Fayfield, T.	299
Aldrich, D.B.	322	Flietner, H.	46
Alessandri, M.	207, 239, 523	Fowler, B.	62
Andoh, E.	536, 560	Fraser, G.	634
Angermann, H.	46	Froeschle, B.	415
Appel, C.	105, 322, 346	Frystak, D.C.	62
<b>B</b> adowski, A.A.	336	Fujimura, S.	97
Baeyens., M.	176	Fukazawa, Y.	264
Baklanov, M.	602, 610	<b>G</b> ale, G.W.	31
Bakovets, V.V.	463	Geomini, M.	207
Barnett, J.	62	George, M.A.	336
Bauer, A.	415	Gilton, T.	272
Beck, S.E.	336	Glick, J.S.	195
Bellandi, E.	207, 239, 523	Glowacki, F.	415
Bertagna, V.	128	Gonzalez, F.	272, 392
Boelen, P.	15, 161	Graf, D.	455
Bohling, D.A.	336	Graham, S.W.	587
Boone, T.	552	Grant, R.	168
Brause, E.	168	Grothe, R.P.	62
Brigante, J.A.	31	Gupta, P.	113, 136
Brown, G,	344	<b>H</b> an, J.-H.	231
Brubaker, M.	315, 418	Han, Y.-P.	423, 431
Carpio, R.	62	Hansen, G.	617
Caymax, M.	455	Harada, Y.	77
Chemla, M.	128	Hatcher, Z.	176, 569
Cheng, A.	365	Hattori, T.	1, 256
Chiarello, R.P.	113, 136	Hayami, Y.	87
Chiyokawa, A.	71	Henrion, W.	46
Christenson, K.	480, 544	Helms, C.R.	113, 136
Clews, P.	23	Heyns, M.	176, 221, 247, 455, 569
Conard, T.	610	<b>H</b> igashi, G.S.	552
Constant, I.	626	Hiraoka, N.	77
Crivelli, B.	523	Honda, K.	617
<b>D</b> anel, A.	400	Horiguchi, H.	536
David, C.	626	Hwang, K.-H.	307
De Gendt, S.	176, 247	Hu, J.C.	344
De Waele, R.	176	Hub, W.	176
Dhanda, S.	113, 136	Hurd, T.Q.	105

Ito, T.	291, 328	Meuris, M.	176, 247, 569
Jacquemond, M.	626	Misra, A.	105
Jafarpour, A.	195	Miyazaki, K.	264
Jeon, J.S.	195, 37	Molin, R.	617
Jizaimaru, T.	488	Moniot, D.A.	336
Joo, J.-D.	151	Morita, H.	143, 151, 280, 528
Jungblut, H.	439	Morrison, B.	634
Kamarinos, G.	400	Moyaerts, G.	176
Kamieniecki, E.	400	Murota, J.	213
Kanno, I.	54	Nakamori, K.M.	528
Kashkoush, I.	15, 161, 168, 471	Narayanswami, N.	350, 357
Kasko, I.	415	Nast, O.	439
Kawada, K.	143, 528	Nelson, G.C.	23, 480
Kawai, A.	536, 560	Nelson, S.L.	38, 480
Kenens, C.	247	Nitta, T.	528
Kenis, K.	45	Novak, R.	15, 161, 168, 471
Kim, J.-S.	143, 151, 1280	O'Brien, S.	579
Kim, Y.-B.	610	Oechsner, R.	415
Kinoshita, H.	77	Ogawa, H.	97
Kneer, E.A.	277	Ogawa, Y.	264
Knoller, M.	176, 247	Ogle, B.	195
Kondoh, E.	221, 602	Ohkubo, S.	291
Kraft, R.	344	Ohmi, T.	143, 151, 280, 488,
Kuniyasu, H.	256	Ohnishi, A.	528
Kunz, S.	120	Ojima, S.	71, 77
Kwakman, L.F.T.	207	Okamoto, A.	488
Lardin, T.	15, 161, 626	Okano, S.	256
Lawing, A.	299, 423, 431	Okorn-Schmidt, H.	532
Lee, C.	552	Okui, Y.	176
Lee, W.	392	Olesen, M.B.	97, 291, 328
Leon, V.	617	Olim, M.	634
Lewerenz, H.J.	439	Ollier, E.	385, 480
Li, L.	272	Omae, S.	447
Liu, J.Q.	552	O'Neil, J.	488
Loewenstein, L.M.	89, 247	Osaka, T.	617
Maex, K.	221, 602, 610	Palsulich, D.	207, 523
Marthon, S.	120, 447, 626	Park, J.-G.	392
Matlock., C.	23, 505	Park, J.-W.	231
Matsuura, T.	213	Parker, J.	307
Matthews, R.	15, 161, 471	Phan, T.	184
Mautz, K.	594	Perry, D.	634
Mertens, P.W.	89, 176, 455, 569	Petersen, D.	617
Messoussi, R.	143	Pipia, F.	617

Quagliotti, G.	447	Tada, Y.	328
Raghavan, S.	377	Takasaki, K.	291
Rauscher, S.	439	Tanishima, M.	513
Reagen, B.	365	Tardif, F.	15, 120, 161, 400, 447, 626
Rebien, M.	46	Tatehaba, Y.	546, 560
Resnick, P.	23, 505	Tomozawa, A.	71, 77
Roberson, L.	617	Tonti, A.	207
Robertson, E.A.	336	Torek, K.	392
Roman, P.	315, 408	Trauwaert, M.-A.	221, 455
Rosamilia, J.M.	552	Vandervorst, W.	247, 610
Roseler , A.	46	Vanhaelemeersch, S.	602, 610
Rotondaro, A.L.P.	105, 322, 344	Vanhaeren, D.	610
Rouelle, F.	128	Vanherlemont, J.	455
Ruzylo, J.	315, 408	Verhaverbeke, S.	184, 496
Sakata, Y.	77	Vos, R.	176, 569
Sakuma, J.	328	Wagner, P.	455
Sakuraba, M.	213	Waskiewicz, J.L	336
Sandrier, B.	15, 161	Wei, J.	496
Satoh, K.	54	Whang, K.-W.	307
Sawin, H.	299, 423, 431	Wise , R.	62
Schenkl, M.	207, 239, 523	Weston, L.	392
Schneider, C.	415	Wolke, K.	207, 239, 523
Sees, J.	105	Yang, H.	344
Shigeno, M.	291	Yokoi, N.	54
Shimada, K.	536, 560	Yoon, E.	307
Smith, P.B.	322	Young, K.M.	336
Smith, S.M.	544	Yuh, H-K.	307
Staffa, J.	315, 408	Zazzera, L.	365
Straube, U.	400	Zettler, J.T.	46
Sugino, R.	291, 328		
Syverson, W.A.	31		



## SUBJECT INDEX

Absorption peaks, 218  
AC polarization resistance, 378  
ac-surface photovoltaic (ac-SPV), 392  
acitic solution, 235  
adhesion theory, 560  
aerosol cluster formation, 357  
aliphatic hydrocarbons, 10  
alkali ion contamination, 594  
alkaline solution, 235  
aluminum alloys, 570  
ammonium hydroxide, 186, 561, 627  
anhydrous HF, 64, 411, 423, 432  
argon aerosol formation, 359  
aspect ratio, 326  
atomic force microscopy (AFM), 536

Back surface, 58, 80  
boron deactivation, 403  
BPSG, 426, 489, 596  
buffered oxide etchant (BOE), 597  
bulk carrier lifetime, 401  
bulk layers, 328

Caro's acid, 496  
carry-over layer, 213  
cavitation energy, 73  
chelating agent, 6  
chelation compounds, 338  
chemical oxide, 277, 340  
chlorine dissociation, 303  
chlorine radicals, 296, 341  
cluster tool, 65, 408, 431  
Co etching, 582  
condensed phase etching, 423  
constant current stress, 201  
contact angle, 226, 235, 252, 275  
copper deposition, 201  
copper oxide, 338  
corner damage, 347  
corrosion, 588

CoSi<sub>x</sub> etching, 582  
cryogenic aerosol, 357

Dangling bond, 217  
decomposition kinetics, 180  
degassification, 394  
depletion layer, 226  
depletion width, 393  
diffraction pattern, 310  
diffusion, 481  
dilute HF, 98, 144, 259, 400, 523, 635  
dilute NH<sub>3</sub>, 628  
diluted clean, 17  
dimer structure, 217  
diode yield, 67  
dissociation constant, 187  
di-2-ethylhexyl phthalate (DOP), 514  
DMT theory, 538  
drying stains, 35

ECR plasma, 310  
electrochemical potential, 202, 377  
electrochemical methods, 129  
emissions monitoring, 367  
energy dispersive spectroscopy, 309  
Environmental Protection Agency, 365  
epitaxy, 64  
equimolar mixtures, 90  
etching rate, 423  
etching uniformity, 209  
evaporation, 385  
exhaust gases, 366

Fan filter unit, 513  
fluorinated chemistries, 325, 344, 439, 528, 588  
Fourier Transform Infrared Spectroscopy (FTIR), 366  
FPMS, 528  
free expansion, 358, 359

**G**as chromatograph, 368  
gas-phase etching, 423  
gas-phase photolysis, 301  
gate oxide, 20  
gettered metals, 330  
gettering effects, 332  
Gibbs free energy, 43  
global warming, 370

**H**alogen lamp, 331  
hazardous air pollutant compounds, 366  
heat of formation, 284  
hexafluorethane, 325  
HF partial pressure, 424  
high density plasma etching, 431  
hot wafer rinse (HWR), 544  
hydrocarbons, 18, 448  
hydrochloric acid, 108, 137, 525, 574  
hydrogen peroxide, 116, 144, 186, 496,  
    580  
hydrogen plasma, 34  
hydrogen termination, 48, 458  
hydrolysis, 66  
hydrolysis mechanism, 251  
hydrophilization, 234, 242  
hydroxyl groups, 93, 107

**I**AP method, 98  
immersion cleaning, 5  
implanted silicon, 225  
incident angle, 81  
inductive sensor, 214  
inductively coupled plasma, 324  
interface traps, 199  
interlevel dielectric, 325  
ion mobility spectroscopy, 447  
IPA drying, 8, 33, 569  
iron oxide, 294  
isopropyl alcohol (IPA), 525

**J**et scrubber, 56

**L**angmuir-Hinshelwood mechanism, 425  
LPD, 41, 409

**M**arangoni drying, 8, 244, 569  
mass balance, 179  
mass transport, 424, 481, 605  
megasonic agitation, 180, 482, 508, 552,  
    635  
megasonic scrubber, 57  
mercury lamp, 294  
metal particles, 282  
metal surface concentration, 90  
metallic contamination, 89, 115, 144,  
    377, 408, 475, 507, 545, 628, 638  
metallic ions, 200  
metal-silicide etching, 602  
microwave photoconductance decay  
( $\mu$ -PCD), 400  
microwave reflectivity, 439  
mobile ion contamination, 378, 594

**N**ative oxide, 268  
neutral pH water, 89  
nitric acid, 90, 98  
noble metals, 199, 400  
nucleation, 358  
nucleophilic reaction, 339  
Nyquist plots, 378

**O**rganic adsorption, 10  
organic complex, 331  
organic surface coverage, 250, 507, 513  
oscillation phenomena, 439  
oxidation power, 473  
oxygen clusters, 312  
oxygen passivation, 40  
oxygen plasma, 324, 432, 612  
ozonated water, 144, 448, 480, 524, 590  
ozonator, 276  
ozone decomposition, 239  
ozone dissolution, 248  
ozone generator, 243, 416, 480  
ozone saturation, 251  
ozone solubility, 233

**P**article contamination, 508, 637, 627  
PECVD chamber cleaning, 366

- perfluorocompounds (PFCs), 365  
piranha clean, 26, 236  
pH, 91, 94, 105, 144  
photochemical reduction, 301  
photon stimulated desorption, 305  
plasma etch processing, 617  
plasticizer, 98  
point-of-use-purification, 123  
polymer residue, 324, 432, 602, 617  
post-silicide formation stripping, 579  
potassium fluoride, 489  
primary oxidant, 188  
process monitoring, 392, 400, 408, 415  
PSG, 596  
pulsed process, 304
- R**amp voltage breakdown, 345  
rapid thermal oxidation (RTO), 416  
RCA-type cleans, 113, 506  
reactive ion etching (RIE), 488  
redox potential, 235, 282  
residual polymer removal, 587  
resistance, 571
- Scanning Auger Microprobe, 283  
Scanning Electron Microscopy, 283, 323  
scrubbing, 7, 628  
SC-1, 90, 377, 544, 580, 635  
processing time, 553  
temperature, 553  
position in bath, 554  
SC-2, 90, 98, 114, 545, 580  
seed crystals, 358  
selectivity, 188  
shear modulu, 83  
silanol groups, 250  
SIMS, 594  
soft sputtering etching, 603  
spherical particle, 59  
spectroscopic ellipsometry, 424  
spin cleaning, 7, 528  
spin dryer, 33
- spray cleaning, 597, 544, 588  
staging time, 277  
storage effects, 9  
sulfur contamination, 26  
sulfuric peroxide mixtures (SPM), 506, 545  
sulfuric nitric mixtures (SNM), 506  
sulfuric/ozone mixtures (SOM), 497  
surface charge, 223, 401, 455  
Surface Charge Imaging (SCI), 400  
Surface Charge Profiling (SCP), 225, 393, 408, 455  
surface dopant concentration, 401, 459  
surface energy, 42  
surface photovoltage, 226, 392, 400  
surface photolysis, 304  
surface recombination lifetime, 401, 411, 455  
surface recombination velocity, 401  
surface relaxation, 227  
surface roughness, 20, 122, 442, 499, 545, 613  
surface state density, 50
- T**EOOS, 596  
thermal budget, 65  
TiN etching, 581, 582  
TiSi<sub>2</sub> etching, 581  
titanium etching, 186  
transfer time, 210  
transmission electron spectroscopy, 34  
trimethylsilanol, 515
- U**CT cleaning, 193, 528  
ultrathin oxide, 72  
ultrasonic agitation, 324  
ultrasonic bath, 81  
ultrasonic damage, 72  
ultrasonic wave, 82  
UV chlorine, 411, 433  
UV irradiation, 294

**V**an der Pauw structure, 324  
Van der Waals force, 60, 536, 580  
via resistance, 325

**W**wavelength dependance, 302  
Weibull distribution, 346  
wet etch, 343  
wetting, 605  
wetting angle method, 463  
work function, 343

**X**-Ray Photoelectron Spectroscopy  
(XPS), 416, 433

**Y**oung-Neumann equation, 463

**Z**eta potential, 266